



Ruddell, Stuart (2019) *Investigations into ivermectin resistance mechanisms in parasitic nematodes and the development of PROTAC technology towards the selective degradation of HIV Capsid protein*. PhD thesis.

<https://theses.gla.ac.uk/75081/>

Copyright and moral rights for this work are retained by the author

A copy can be downloaded for personal non-commercial research or study, without prior permission or charge

This work cannot be reproduced or quoted extensively from without first obtaining permission from the author

The content must not be changed in any way or sold commercially in any format or medium without the formal permission of the author

When referring to this work, full bibliographic details including the author, title, awarding institution and date of the thesis must be given

Enlighten: Theses  
<https://theses.gla.ac.uk/>  
[research-enlighten@glasgow.ac.uk](mailto:research-enlighten@glasgow.ac.uk)

**Investigations into Ivermectin Resistance  
Mechanisms in Parasitic Nematodes and the  
Development of PROTAC Technology Towards  
the Selective Degradation of HIV Capsid Protein**

**Stuart Ruddell, MSci**

A thesis submitted in part fulfilment of the requirements of the degree of Doctor of Philosophy



University  
of Glasgow

School of Chemistry

College of Science and Engineering

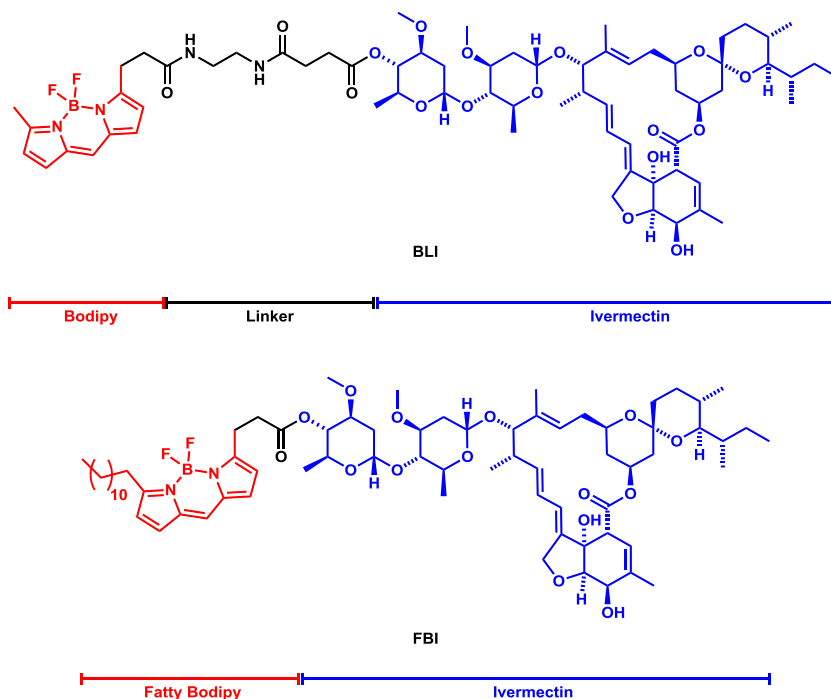
University of Glasgow

August 2019

## Abstract

This thesis comprises two projects detailing the synthesis and testing of bifunctional molecules. The projects were aimed at addressing the key biological problems of combating drug resistance and the requirement for novel therapeutic strategies.

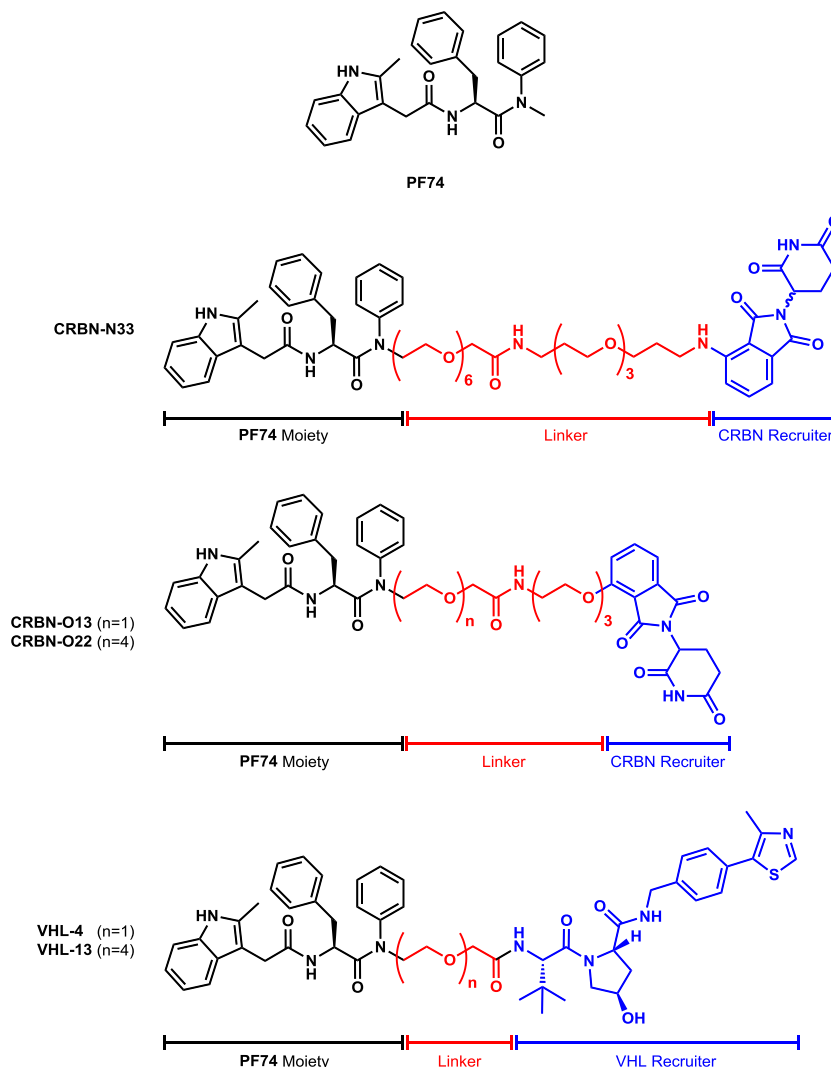
Chapter one details the first of these projects, which was concerned with elucidating the mechanism(s) of drug resistance in parasitic nematodes by using bifunctional fluorescent chemical probes based on the anthelmintic drug **ivermectin**. The first section presents the relevant background information for the project including information regarding the mechanism of action of **ivermectin** and the basic anatomy of nematodes, which were used to guide the design of the probes, **BLI** and **FBI**.



The second section discusses the synthesis of each of the probes as well as their biological assaying used to assess the utility of the probes for the purposes of studying ivermectin resistance. The **FBI** probe was then administered to both free-living and parasitic nematode strains, which when assessed with fluorescence microscopy, successfully identified the route of **ivermectin** uptake. Furthermore, the data generated was consistent with impaired drug uptake as an operative mechanism of **ivermectin** resistance.

The final section comprises experimental data regarding the preparation and characterisation of the discussed compounds as well as biological assay data.

Chapter two details a project aimed at developing heterobifunctional PROTAC molecules towards the selective degradation of HIV capsid protein in human cells. The first section presents the relevant background information for the project including information on the chosen protein targets, which was used to guide the design of the PROTAC molecules. These molecules are based on the HIV capsid inhibitor **PF74**.



The second section discusses the synthesis of each of the PROTAC molecules. Additionally, the synthesis of (*S*)- and (*R*)-**PF74** and an epimerisation study of **PF74** are discussed.

The third section discusses the biological assaying of the enantiomers of **PF74**, which successfully identified (*S*)-**PF74** as significantly more active than (*R*)-**PF74**. In addition, the testing of each of the synthesised PROTACs is presented, which successfully demonstrated inhibition of HIV replication and answered fundamental questions regarding PROTAC target engagement.

The final section comprises experimental data regarding the preparation and characterisation of the discussed compounds as well as biological assay data.

# Contents

<b>Chapter 1. Development of Fluorescent Chemical Probes to Investigate Ivermectin Resistance in Nematodes</b> .....	15
<b>1.1 Introduction</b> .....	15
1.1.1 Background .....	15
1.1.2 Current Anthelmintics .....	16
1.1.3 <b>Ivermectin</b> Mechanism of Action .....	17
1.1.4 <b>Ivermectin</b> Resistance .....	20
1.1.5 Basic Nematode Anatomy.....	21
1.1.6 Hypotheses and Project Aims .....	22
1.1.7 Probe Design .....	23
<b>1.2 Results and Discussion</b> .....	24
1.2.1 Synthesis of Bodipy Fragment <b>1.1</b> .....	24
Synthesis of Bodipy Core.....	24
Attempted <b>Pathway A</b> .....	26
Attempted <b>Pathway B</b> .....	28
Attempted <b>Pathway C</b> .....	29
Attempted <b>Pathway D</b> .....	29
1.2.2 Synthesis of Ivermectin Fragment <b>1.11</b> .....	31
1.2.3 Completion of <b>BLI</b> synthesis .....	33
<b>1.3 BLI Biological Assaying</b> .....	36
1.3.1 Materials and Methods .....	36
Nematode Strains and Culture.....	36
Nematode Microscopy Preparation.....	36
<b>DiI</b> Staining Procedure.....	36
Free Swimming Assay .....	37
Plate-Based Assay .....	37
1.3.2 <b>BLI</b> Study.....	37
Establishing <b>BLI</b> Efficacy.....	37

<b>1.4 Probe Redesign</b> .....	40
1.4.1 Troubleshooting .....	40
1.4.2 Lipophilicity Calculations .....	41
1.4.3 New Probe Proposal .....	43
<b>1.5 FBI Synthesis</b> .....	44
1.5.1 Synthetic Strategy .....	44
1.5.2 Fatty Bodipy Fragment Synthesis .....	44
1.5.3 Completion of <b>FBI</b> Synthesis.....	46
<b>1.6 FBI Biological Assaying</b> .....	48
1.6.1 Materials and Methods .....	48
Nematode Strains and Culture.....	48
Nematode Microscopy Preparation .....	48
<b>DiI</b> staining Procedure .....	48
Plate-Based Assay .....	48
1.6.2 <b>FBI</b> Study in Non-Parasitic Nematodes.....	49
Establishing <b>FBI</b> Efficacy .....	49
Establishing <b>Ivermectin</b> Route of Uptake .....	50
Elucidating <b>Ivermectin</b> Resistance Mechanism .....	52
1.6.3 <b>FBI</b> Study in Clinically Relevant Parasitic Nematodes .....	54
Adaptation of Assay Conditions .....	54
Establishing Comparable Efficacy of <b>FBI</b> and <b>Ivermectin</b> .....	55
Establishing <b>Ivermectin</b> Route of Uptake in Parasitic Nematodes .....	56
Probing <b>Ivermectin</b> Resistance Mechanism in Parasitic Nematodes .....	56
<b>1.7 Conclusions</b> .....	59
<b>1.8 Future Work</b> .....	61
<b>1.9 Experimental</b> .....	62
1.9.1 General Methods .....	62
1.9.2 Preparation of Compounds.....	63

<b>Chapter 2. Synthesis of PROTAC Molecules Towards <i>in vivo</i> Degradation of HIV Capsid Protein</b> .....	86
<b>2.1 Introduction</b> .....	86
2.1.1 Human Immunodeficiency Virus .....	86
2.1.2 Occupancy-Based Drug Paradigm .....	86
2.1.3 Targeted proteolysis .....	88
2.1.4 Natural Degradation of Endogenous Proteins .....	89
2.1.5 Proteolysis Targeting Chimeras (PROTACs) .....	90
2.1.6 E3 Ligase Ligand .....	91
2.1.7 Linker .....	93
2.1.8 Targeting HIV .....	94
2.1.9 <b>PF74</b> and Capsid Protein.....	96
2.1.10 First generation probe design .....	96
2.1.11 Synthetic Strategy .....	98
<b>2.2 Results and Discussion</b> .....	99
2.2.1 Protected <b>PF74</b> -Linker Fragment Synthesis .....	99
Aniline Linker Fragment Synthesis.....	99
<b>PF74</b> Fragment Synthesis .....	101
Completion of <b>PF74</b> -Linker Fragment .....	102
2.2.2 Protected CRBN-Linker Fragment Synthesis .....	106
2.2.3 Synthesis of PROTAC <b>CRBN-N33</b> .....	107
2.2.4 VHL-Linker Fragment Synthesis .....	107
2.2.5 Attempted Synthesis of PROTAC <b>VHL-38</b> .....	109
2.2.6 Redesigning the Route .....	110
2.2.7 Attempted Synthesis of Proposed Complete- <b>PF74</b> Fragment <b>2.24</b> .....	111
Alcohol Terminating <b>PF74</b> Fragment <b>2.27</b> Synthesis.....	112
Model Fragment Synthesis.....	114
Model Fragment Oxidation .....	115
Model Fragment Alkylation .....	115

2.2.8 Synthesis of Short Linker PROTACs.....	118
Completion of Short VHL-Based PROTAC.....	121
Completion of Short CRBN-Based PROTAC .....	122
2.2.9 Synthesis of medium length PROTACs.....	123
Completion of Medium Length VHL-Based PROTAC.....	125
Completion of Medium Length CRBN-Based PROTAC .....	126
2.2.10 PROTAC Synthesis Summary .....	126
2.2.11 <b>PF74</b> synthesis and epimerisation study .....	128
Natural <b>PF74</b> Synthesis and Analysis.....	128
Unnatural <b>PF74</b> Synthesis and Analysis.....	131
Racemic <b>PF74</b> Synthesis and Analysis.....	132
Collection of Enantiomerically Pure <b>PF74</b> .....	133
<b>2.3 Biological Assays</b> .....	136
2.3.1 Materials and Methods .....	136
Cell Lines and Culture.....	136
Viral Vector Preparation .....	136
Cell Counting .....	136
Cell preparation for flow cytometry.....	137
Viral Vector Titration.....	137
Compound Fixed Dose (Viral Vector Titration) Assay .....	137
Compound Dose Response (Fixed Viral Vector Titre) Assay .....	137
E3 Ligase Ligand Titration (Fixed Compound Dose, Fixed Viral Vector Titre)	
Competition Assay .....	138
2.3.2 <b>PF74</b> Study.....	138
Establishing Control Experiments.....	138
Synthetic and Commercial <b>PF74</b> Comparison.....	139
Enantiomerically Enriched ( <i>S</i> )- <b>PF74</b> and ( <i>R</i> )- <b>PF74</b> Comparison .....	140
( <i>S</i> )- <b>PF74</b> and ( <i>R</i> )- <b>PF74</b> IC <sub>50</sub> Determination.....	141
( <i>S</i> )- <b>PF74</b> and ( <i>R</i> )- <b>PF74</b> Docking Study .....	142

2.3.3 PROTAC Testing .....	144
Establishing PROTAC Efficacy .....	144
Confirming HIV-Specific Binding.....	146
Confirming Correct Target Engagement.....	147
Investigating Proteasome Dependence.....	149
Investigating E3 Ligase Recruitment .....	149
2.3.4 Summary of Biological Assaying .....	151
<b>2.4 Future Work .....</b>	<b>152</b>
<b>2.5 Experimental.....</b>	<b>155</b>
2.5.1 General Methods .....	155
2.5.2 Preparation of Compounds.....	157
<b>References .....</b>	<b>220</b>

## Acknowledgements

I would like to thank Dr David France for his unwavering support and wisdom throughout the past four years, in matters of both science and life. I am grateful for the opportunity to have worked within his research group and to have studied under the tutelage of a true master of molecular manipulation.

I would also like to thank our collaborators Prof Tony Page, Dr Sam Wilson and Dr Elena Sugrue for their knowledge, patience and assistance in bridging the divide. I am grateful to all the staff at the School of Chemistry for their support. I would also like to gratefully acknowledge financial support from the University of Glasgow, EPSRC, BBSRC, RSC and WestChem.

I would also like to extend my thanks to all the past members of the France Research Group, for all their assistance and intellectual discussions through the years. Dr Lewis Williams, Dr Craig Smith and Dr David Phillips are partly responsible for crafting me into the Man I have become today. The power of bad examples should never be underestimated in the pursuit of greatness. I am very grateful to all the present members of the France group also, to Glen, Sarah and Claire for your useful insights, camaraderie and our shared good times. I would like to thank you guys, along with the present and past members of the Clark and Boyer research Groups for providing a truly enjoyable working atmosphere utterly devoid of intellectual conversation. The ever-present awareness that you are never truly safe in office C4.06 will remain with me as a fond memory to accompany the memories of laughter and joy. Thanks also go to Dr Alistair Boyer for his useful discussions, helpful contraptions and all-round indispensable presence in the lab; he is truly the HendoFurze. Here! Big Kev should be proud. Particular thanks also to Dan and Glen “GleBro” Brodie for accompanying me when climbing both the literal (plastic) rocks of TCA, and the figurative rocks of friendship and life. Dr. Michael Popadyneec has been a truly negative influence, in the greatest of ways. Dr Gregor Meier, a man and brother, a first class Kung Fu man and expert. His wisdom and eccentricity have demonstrated to me that scientific endeavour and artistic creativity are but two sides of the same coin, separated only by the boundary of our self-imposed limitations.

I must also thank my family for their moral and financial backing throughout my long and arduous journey of education, without whom, none of this would have been possible. And particular thanks to Megasaurus Rex for your ludicrous shenanigans and much needed distractions.

To Marie, my light in the darkness. A single grain of rice can tip the balance, and you frequently added sacks to keep me on track. When adversity seemed unending you were always there to remind me that Alles hat ein Ende, nur die Wurst hat zwei. My deepest gratitude and unending thanks for all your support.

I shall end with a quote that has come to embody my time in the Henderson Lab and encompasses the idea that no matter how challenging and insurmountable a task appears; the motivation to succeed comes from within.

*“A hungry pig will eat through bone like butter”*

## **Authors Declaration**

This thesis represents the original work of Stuart Ruddell, unless otherwise explicitly stated in the text. The research was conducted primarily at the University of Glasgow School of Chemistry in the Henderson and Connolly Lab under the supervision of Dr David France during the period of October 2015 to March 2019. During this time, research was also conducted as at the University of Glasgow Institute of Biodiversity Animal Health & Comparative Medicine in the lab of Prof Tony Page and at the University of Glasgow Centre for Virus Research in the lab of Dr Sam Wilson.

## Abbreviations

Å	Angstrom(s)
Ac	acyl
AIDS	acquired immunodeficiency syndrome
aq.	aqueous
Ar	aryl
ART	anti-retroviral treatment
ATP	adenosine triphosphate
BET	bromodomain and extraterminal domain
BLI	bodipy-linker-ivermectin
Bn	benzyl
Boc	<i>tert</i> -butyl carbamate
br	broad
<i>C. elegans</i>	<i>Caenorhabditis elegans</i>
CA	HIV capsid protein
cat.	catalytic
conc.	concentration
COSY	correlated spectroscopy
CRBN	cereblon
CVR	Centre for Virus Research, University of Glasgow
d	doublet
DALY	disability-adjusted life year
DEPT	distortionless enhancement by polarisation transfer
DIC	differential interference contrast
DMAP	4-dimethylaminopyridine
DMF	<i>N,N</i> -dimethylformamide
DMP	Dess–Martin periodinane
DMSO	dimethyl sulfoxide
DNA	deoxyribonucleic acid
dyf	dye-filling defective
DMEM	Dulbecco's modified eagle medium

<i>E. coli</i>	<i>Escherichia coli</i>
EDC	1-ethyl-3-(3-dimethylaminopropyl)carbodiimide
EDTA	ethylenediaminetetraacetic acid
EI	electron ionisation
EMS	ethyl methanesulfonate
equiv.	equivalent(s)
ESI	electrospray ionisation
Et	ethyl
<i>et al.</i>	<i>et alii</i>
FBI	fatty bodipy-ivermectin
FCS	fetal calf serum
FRET	fluorescence resonance energy transfer
GABA	$\gamma$ -aminobutyric acid
GFP	green fluorescent protein
GluCl	glutamate-gated chloride channel
h	hour
[H]	reduction
<i>H. contortus</i>	<i>Haemonchus contortus</i>
HAART	highly active anti-retroviral treatment
HATU	1-[Bis(dimethylamino)methylene]-1 <i>H</i> -1,2,3-triazolo[4,5- <i>b</i> ]pyridinium 3-oxid hexafluorophosphate
HBA	hydrogen-bond acceptor
HBD	hydrogen-bond donor
HBTU	<i>O</i> -(Benzotriazol-1-yl)- <i>N,N,N',N'</i> -tetramethyluronium hexafluorophosphate
HEK	human embryonic kidney
HIF	hypoxia-inducible factor
HIV	human immunodeficiency disease
HMBC	heteronuclear multiple bond correlation spectroscopy
HMDS	hexamethyldisilazane
HPLC	high-performance liquid chromatography
HSQC	heteronuclear single quantum coherence spectroscopy

<i>i</i> -Pr	isopropyl
IAP	inhibitor of apoptosis protein
IR	infrared
IVM	ivermectin
LCMS	liquid chromatography-mass spectrometry
lit.	literature
M	molar
m	multiplet
MDM2	mouse double minute 2 homolog
Me	methyl
min	minute
MLV	murine leukaemia virus
mol	mole
NGM	nematode growth media
NHA	non hydrogen atom
THF	tetrahydrofuran
NHS	<i>N</i> -hydroxysuccinimide
NIR	near infrared
NMR	nuclear magnetic resonance
NOESY	nuclear Overhauser enhancement spectroscopy
Nu	nucleophile
[O]	oxidation
PEG	polyethylene glycol
Ph	phenyl
POI	protein of interest
PPI	protein-protein interaction
ppm	parts per million
PROTAC	proteolysis targeting chimera
PyBOP	(Benzotriazol-1-yloxy)tripyrrolidinophosphonium hexafluorophosphate
q	quartet
R	generic alkyl/aryl group

R <sub>f</sub>	retention factor
RNA	ribonucleic acid
Rpm	revolutions per minute
rt	room temperature
s	singlet
SAR	structure-activity relationship
t	triplet
TBAI	tetrabutylammonium iodide
TBS	<i>tert</i> -butyldimethylsilyl
<sup>t</sup> Bu	<i>tert</i> -butyl
temp.	temperature
TFA	trifluoroacetic acid
TLC	thin layer chromatography
TP	target protein
tPSA	topological polar surface area
Ts	toluenesulfonyl (tosyl)
Ub	ubiquitin
UPP	ubiquitin-proteasome pathway
UV	ultraviolet
VDW	van der Waals
VHL	von Hippel-Lindau
Vis	visible
VSV-G	vesicular stomatitis virus envelope glycoprotein
X	leaving group

# Chapter 1. Development of Fluorescent Chemical Probes to Investigate Ivermectin Resistance in Nematodes

## 1.1 Introduction

### 1.1.1 Background

Helminths (parasitic worms) are ubiquitous in nature, inhabiting every known ecosystem on the planet.<sup>[1]</sup> They comprise two major phyla; platyhelminths (flat worms) and nematodes (round worms) however, for the purposes of this thesis, only nematodes are discussed. While not all nematode species are parasitic, those that are infect vertebrates, invertebrates and plants and in doing so, represent a major global healthcare and economic burden. While over 340 species of helminth are known to parasitise humans, the five species of greatest medical importance are all members of phylum Nematoda. Collectively these five nematode species are responsible for infection of more than half of the global population.<sup>[2][3][4]</sup> While the majority of human nematode infections are asymptomatic, those that aren't can cause debilitating disfigurement, permanent paralysis, blindness and death. Nematode infection results in approximately 125 thousand deaths per annum, but with an estimated 3.5 billion people infected globally the number of deaths attributed to these infections seems comparatively low.<sup>[2][3][4]</sup> However, the true cost of nematode infection is the loss of 39 million disability-adjusted life years (DALYs) which when compared with malaria for example (loss of 36 million DALYs), highlights the scale of the burden of nematode infection.<sup>[2][4]</sup> The vast majority of human infection occurs in tropical and subtropical regions, and typically in developing countries with poor sanitation and limited access to quality healthcare.<sup>[4]</sup>

While human infection is still present in more developed nations, the impact of nematode infections manifests primarily as an economic burden to the agricultural industry. Over 4100 plant-parasitic nematodes species are known, which constitute a serious menace to global food supply and sustainable agriculture.<sup>[5]</sup> While it is difficult to accurately measure the worldwide economic impact, estimates of nematode-induced losses range from 80–160 billion US dollars which represents 6–12% of global crop yield.<sup>[5][6][7][8]</sup> In the UK, two nematodes species are responsible for the potato cyst nematode problem which contributes to a loss of approximately 9% of UK potato production.<sup>[7][8]</sup>

In addition to plant-parasitic nematodes, and of paramount importance to this project, is nematode parasitism of economically important livestock. Nematode infections of livestock manifest in various different symptoms including reduced weight gain, milk yields, wool growth, reproductive performance and high mortality rates.<sup>[9][10]</sup> *Haemonchus contortus* for example, is one of the most pathogenic parasites of small ruminants such as sheep and goats. It can have a devastating effect on entire herds in a relatively short period of time, by causing severe anaemia, emaciation and death.<sup>[10]</sup> These factors can be significantly detrimental to farmers' and producers' already slim profit margins, and impact the long term viability of individual farms.<sup>[11]</sup> In an attempt to lessen the globally present detrimental socio-economic impact of helminth infections, many chemotherapeutic treatments have been developed which are known as anthelmintics.

### 1.1.2 Current Anthelmintics

Several classes of anthelmintic exist, each with different mechanisms of action and targets. The first class to be widely adopted were the broad-spectrum benzimidazoles, and the first of its class, **thiabendazole** (released in 1961), launched the golden age of anthelmintic research and development (Figure 1.1).<sup>[12][13]</sup> Benzimidazoles have been shown to bind selectively to parasitic  $\beta$ -tubulin, inhibiting the formation of microtubules. As microtubules form the cytoskeleton of the cell, impaired microtubule formation leads to destruction of the cell structure and subsequent death of the parasite.<sup>[14][15]</sup>



Figure 1.1. General structure of benzimidazoles and the structure of **thiabendazole**.

Following the success of the benzimidazoles was the discovery of the avermectins (Figure 1.2), which are the class of anthelmintic most relevant to this project. The broad-spectrum avermectins are 16-membered macrocyclic lactones that were originally isolated from the fermentation broth of soil-dwelling *Streptomyces avermitilis* bacteria. The first of the avermectin class and by far the most widely used of the avermectins, is the semi-synthetic **ivermectin**, which is sold as a mixture of 22,23-dihydroavermectin **B1a** and **B1b** (Figure 1.2).

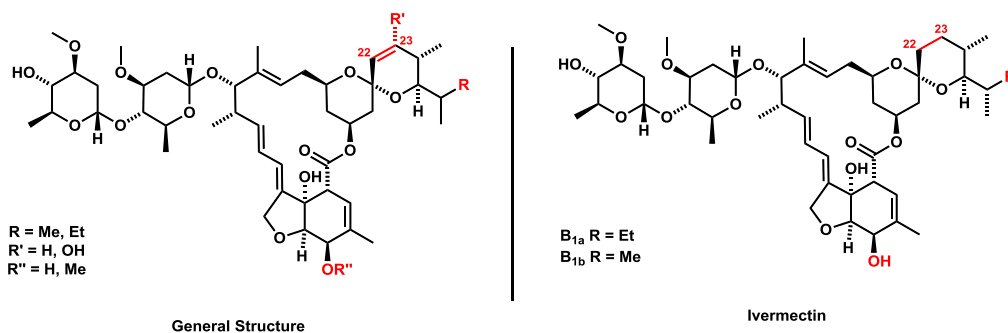


Figure 1.2. General structure of the avermectins and the structure of **ivermectin**, a mixture of 22,23-dihydroavermectins **B1a** and **B1b**.

Released in 1981, **ivermectin** started clinical use as a veterinary medicine before being adopted for use in human medicine and it has since been a front line anthelmintic treatment in both clinical areas.<sup>[16]</sup> The global significance of **ivermectin** is exemplified by its inclusion in the World Health Organisations 'list of essential medicines for a basic healthcare system'. Furthermore, the 2015 Nobel prize for medicine was in part, jointly awarded to Satoshi Ōmura and William Campbell for their discovery and development of **ivermectin**.<sup>[16][17]</sup> As with most chemotherapeutics designed to kill human pathogens and pest species, nematode resistance to available anthelmintic treatments has become a major global problem.

### 1.1.3 Ivermectin Mechanism of Action

Despite **ivermectin** being released almost 40 years ago, both its mechanism of action in parasitic species, and the mechanism of resistance to **ivermectin** are still not fully understood.<sup>[16]</sup> Indeed **ivermectin** has been shown to interact with several targets including GABA gated chloride channels, histamine gated chloride channels and glutamate gated chloride channels.<sup>[18]</sup> However, while it is not certain, there is strong evidence to suggest that the primary nematicidal activity of **ivermectin** (and all the avermectins) is due to its interaction with invertebrate-specific glutamate gated chloride channels (GluCl).<sup>[16][19][20][21][22]</sup>

These chloride channels are located in invertebrate nerve cells and are an integral part of the nervous system. Glutamate-gated chloride channels are partly responsible for repolarising nerve cells back to the neuronal resting potential after normal neuron excitation.<sup>[20]</sup> **Ivermectin** is an allosteric agonist of GluCl, whereby the binding of **ivermectin** causes a global conformational change in the channel, which stabilises the active state while still allowing further activation by the endogenous glutamate ligand.<sup>[20]</sup> When **ivermectin** contacts a nerve cell, it partly embeds in the outer layer of the phospholipid bilayer and diffuses along it until it meets and binds to the GluCl

(Figure 1.3 A).<sup>[21]</sup> The binding is extremely potent (with inhibitory effects seen at 0.29 nM) and causes the channel to open, which results in an influx of chloride ions and hyperpolarisation of the nerve cell (Figure 1.3 B).<sup>[23]</sup> This hyperpolarisation causes spastic paralysis of the nematodes, producing an inability to move or feed which subsequently results in their rapid expulsion from the host organism.<sup>[23]</sup>

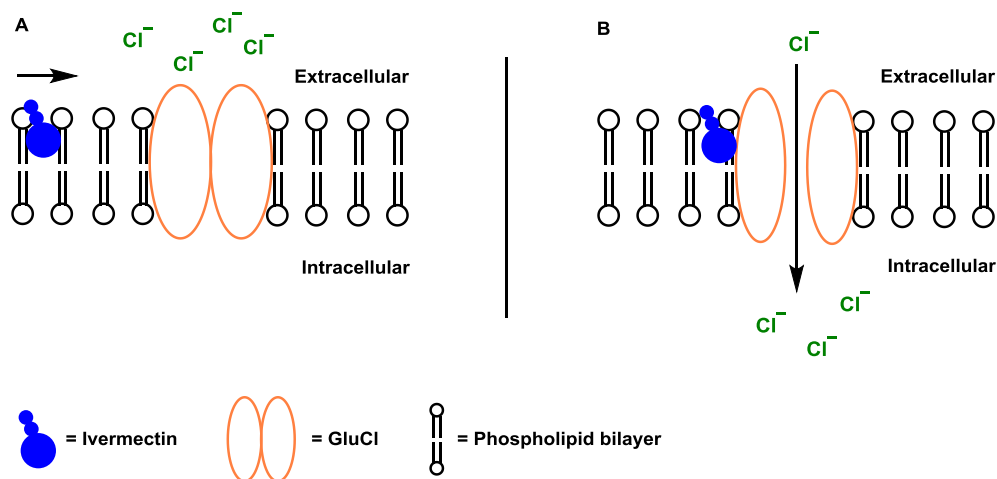


Figure 1.3. Basic overview of **ivermectin** interaction with glutamate gated chloride channel.

As mentioned above, **ivermectin** diffuses along the outer layer of the phospholipid bilayer without crossing the cell membrane, indicating the **ivermectin** site of action on the GluCl to be located extracellularly.<sup>[21]</sup> This is based on a study conducted by Martin *et al.* in which a bodipy labelled **ivermectin** probe (Figure 1.4) was utilised to study the distribution of **ivermectin** in isolated nematode muscle cell vesicles.

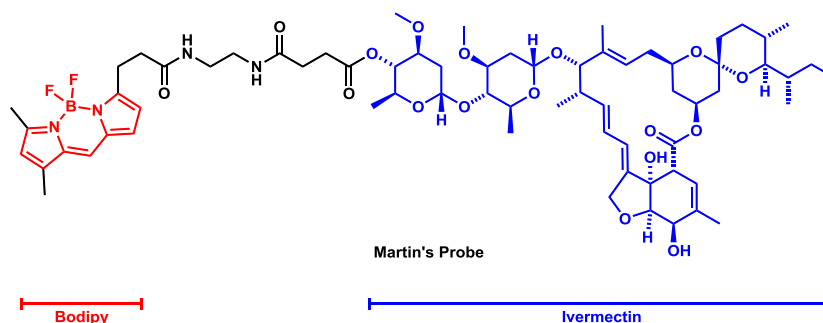


Figure 1.4. Structure of Martin *et al.* bodipy labelled **ivermectin** probe.

The crystal structure of **ivermectin** bound to the target GluCl in combination with structure-activity relationship (SAR) studies, allowed the biologically active moieties of **ivermectin** to be elucidated (Figure 1.4).<sup>[20][22]</sup> As can be seen in the crystal structure (Figure 1.5 A) **ivermectin** binds between the M1 loop of the (−) subunit and the M3 loop of the adjacent (+) subunit. This binding causes the two subunits to splay slightly, which induces the aforementioned global conformational change of the channel.<sup>[20]</sup> The

key binding interactions that produce the high binding affinity are primarily located around the macrocyclic core of **ivermectin** (Figure 1.5 B). There are six interactions around the macrocycle which consist of three H-bonding interactions and three van der Waals interactions. Additionally, two van der Waals interactions are present on the saccharide moiety directly attached to the macrocyclic core, but no interactions are present on the terminal saccharide moiety.

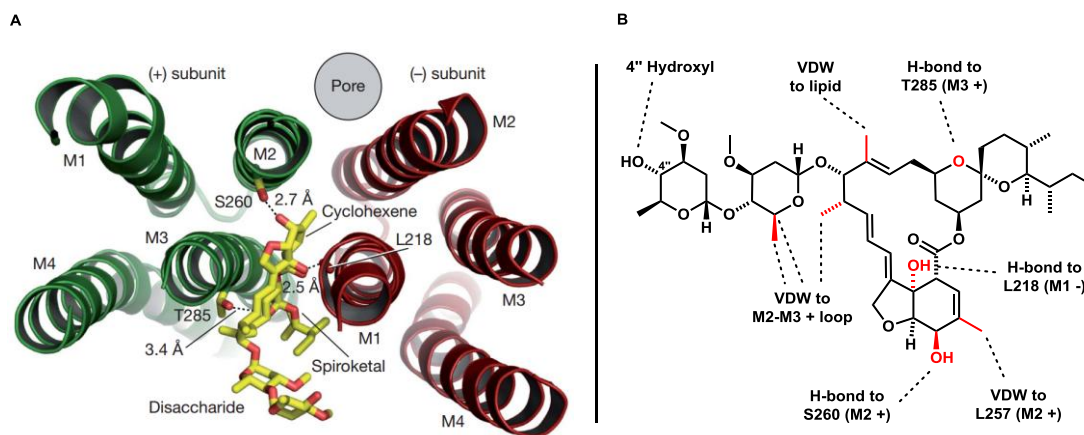


Figure 1.5. A) Crystal structure of **ivermectin** bound to GluCl.<sup>[20]</sup> B) Key binding interactions highlighted.<sup>[20]</sup>

The lack of binding at the terminal disaccharide moiety is corroborated by an SAR study conducted by Mrozik *et al.* that showed functionalisation of the terminal 4'' hydroxyl does not hinder binding.<sup>[22]</sup> The SAR study utilised **avermectin B1<sub>a</sub>** (Figure 1.6), a structurally similar analogue of **ivermectin** (a mixture of 22,23-dihydro avermectin B1<sub>a</sub> and B1<sub>b</sub>; Figure 1.2, page 17). In the study, the 4'' hydroxyl of **avermectin B1<sub>a</sub>** was functionalised *via* an ester linkage with a variety of moieties (Figure 1.6).<sup>[22]</sup> With all of these modifications, the *in vivo* efficacy of the modified compound was comparable to that of the parent **avermectin B1<sub>a</sub>**. Furthermore, the aforementioned **Martin's Probe** (Figure 1.4, page 18), featured a bodipy fluorophore linked *via* an amide containing linker to **ivermectin** at the 4'' position. While this probe was not assayed *in vivo*, it was determined to maintain *in vitro* activity against the target GluCl.<sup>[21]</sup> In contrast to the tolerated 4'' modifications, functionalisation of the secondary allylic alcohol, the tertiary alcohol or destruction of the spiroketal moiety (which possess the strongest binding interactions) was shown to greatly reduce the efficacy of the drug.<sup>[22]</sup>

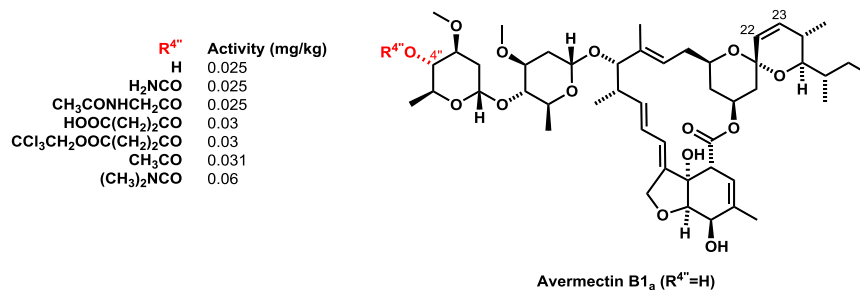


Figure 1.6. Structure of **avermectin B<sub>1a</sub>** 4'' derivatives that maintain anthelmintic activity.<sup>[22]</sup>

### 1.1.4 Ivermectin Resistance

For the purpose of this project, anthelmintic resistance will be studied using **ivermectin** as a model; however, the factors that have led to **ivermectin** resistance are common to the resistance observed in every class of anthelmintic. Since the inception of **ivermectin** almost 40 years ago, reports of nematode resistance to the drug have been steadily increasing in both frequency and severity.<sup>[24][25][26][27][28]</sup> There are several factors that have contributed to the prevalence of this resistance, but as is the case with the vast majority of pathogen-targeting pharmaceuticals, selection for drug resistance is unavoidable.

A major factor in the rise of **ivermectin** resistance in nematodes was paradoxically the outstanding efficacy of the drug. Due to its high potency, low host-toxicity and broad spectrum utility, the tremendous success of **ivermectin** halted novel anthelmintic research due to the unfavourable economics of developing more effective alternatives. This resulted in an overreliance on available anthelmintics, especially **ivermectin** and the avermectins. Furthermore, there was a concomitant shift in treatment practices from the clinical treatment of individually infected livestock (or humans) towards the prophylactic mass administration of anthelmintics to entire herds (and human populations).<sup>[11][29]</sup> While this has undoubtedly significantly reduced the damage caused by nematode infections, this same paradigm shift in treatment, unfortunately also contributed significantly to the emergence of resistance.<sup>[11][29][30][31][32]</sup> Additionally, the nature of nematodes themselves plays a large part in the emergence of **ivermectin** resistance. They demonstrate an exceptional ability to adapt to environmental change, which is due in part to their rapid reproductive rates and extremely large population sizes. These factors combined gives nematodes a high level of genetic diversity, and this high gene flow greatly increases their potential to respond to chemical attack.<sup>[24]</sup>

In general, there are several possible mechanisms of resistance. These include mutation of the drug target protein, mutations preventing or hindering drug uptake or processes such as efflux and metabolic inactivation or destruction. Studies to elucidate the biochemical basis of **ivermectin** resistance have been conducted using the free-living (non-parasitic) nematode *Caenorhabditis elegans* (*C. elegans*) as a model organism. These studies identified the main genes of GluCl receptors, and reported that concomitant mutation of three of these genes conferred high levels of **ivermectin** resistance.<sup>[33][34][35]</sup> While the use of the free-living *C. elegans* nematode as a model organism has questionable relevance to the study of parasitic species, the GluCl subunits of *C. elegans* are known to be homologous to parasitic species.<sup>[25][28][36][37]</sup> Despite the use of a good model organism, to date, no GluCl mutation has been directly linked to **ivermectin** resistance in any field isolates of parasitic nematodes.<sup>[35]</sup> Additionally, mutations to GluCl that confer **ivermectin** resistance, cannot account for the existence of resistance to multiple drug classes. Instead of drug target mutation, the hypothesis for this project is that a primary operative mechanism of **ivermectin** resistance is due to impaired drug uptake, which could also explain the observation of multidrug resistance. In order to investigate this hypothesis it is necessary to have a basic understanding of nematode anatomy.

#### 1.1.5 Basic Nematode Anatomy

Despite the huge biodiversity within the phylum Nematoda, the anatomy of nematodes is remarkably well conserved.<sup>[38]</sup> They all feature a cylindrical body coated in a cuticle, with a mouth like organ known as the pharynx which includes a grinder located in the terminal bulb (Figure 1.7). This then leads into the digestive tract known as the lumen, which is lined with gut granules that are responsible for aiding digestion.

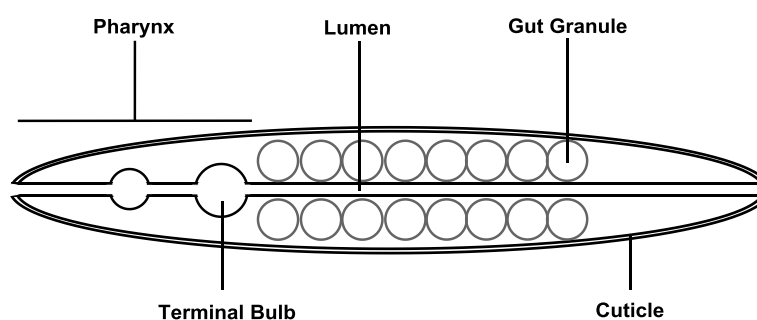


Figure 1.7. Basic depiction of generic nematode anatomy.

The central nervous system of nematodes consists of a circular bundle of nerves around the pharyngeal muscle known as the nerve ring (Figure 1.8). Of importance to this project are the sensory organs connected to the nerve ring known as the amphids. These

bilaterally symmetrical organs run parallel to the pharynx and are common to all nematodes. They are responsible for chemosensation as well as osmotic, touch and thermosensation.<sup>[38]</sup> Being comprised of nerve cells, both the nerve ring and the amphids contain glutamate gated chloride channels.

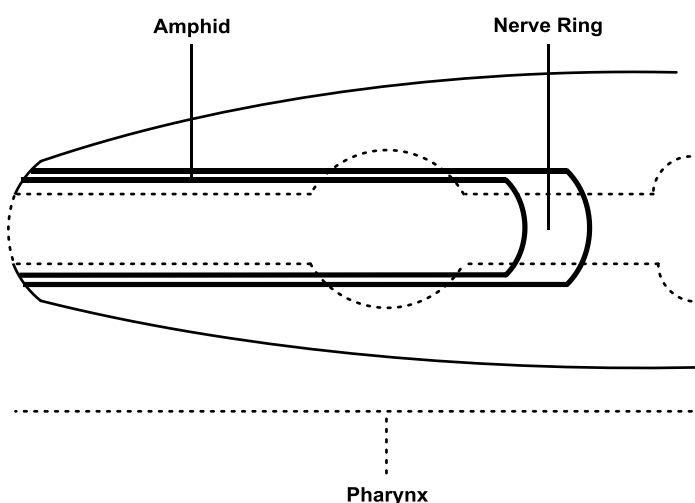


Figure 1.8. Simplified depiction of the nerve ring and chemosensory amphids.

Dye-filling experiments have been conducted in which *C. elegans* has been treated with lipophilic fluorescent dyes such as **DiI** (Figure 1.9 A) and when imaged with fluorescent microscopy, the amphids and nerve rings are heavily stained (Figure 1.9 B). However, amphid-defective mutants are known whose amphids are not stained during these dye-filling assays (Figure 1.9 C). These dyf (dye filling defective) mutants are also resistant to **ivermectin**. It is interesting to note that these dyf genes are unrelated to *GluCl* and instead are necessary for forming sensory endings such as in the amphids.<sup>[33]</sup>

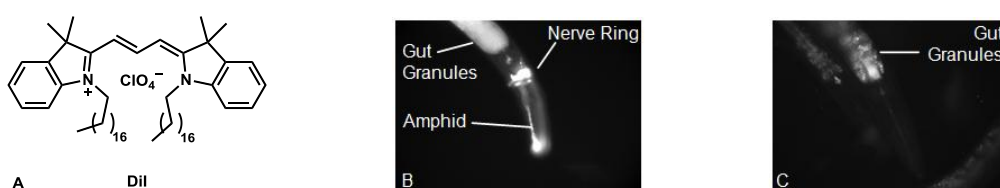


Figure 1.9. A) Structure of the commercial lipophilic dye, **DiI**. B) Fluorescence microscopy of **ivermectin**-sensitive *C. elegans* treated with **DiI**. C) Fluorescence microscopy of **ivermectin**-resistant *C. elegans* treated with **DiI**.

### 1.1.6 Hypotheses and Project Aims

For this project, a direct link between amphidal defects and **ivermectin** resistance is proposed. The hypothesis is that the route of **ivermectin** uptake is *via* the amphids, and that an operative mechanism of **ivermectin** resistance in nematodes is impaired drug uptake due to loss-of-function amphid mutations. In order to investigate this, a

fluorescent probe based on **ivermectin** was designed to study the route of **ivermectin** uptake.

### 1.1.7 Probe Design

The probe designed for studying the uptake route of **ivermectin** and thus also for investigating possible resistance mechanisms, is called **BLI** (bodipy-linker-**ivermectin**) (Figure 1.10). It is structurally similar to the aforementioned **Martin's Probe** (Figure 1.4, page 18) and is composed of **ivermectin** covalently linked *via* an amide containing linker to a bodipy fluorophore. The linker is attached at the 4'' hydroxyl of **ivermectin** as this position is known not to have any key binding interactions, and functionalisation is known not to hinder the efficacy of the drug as was previously discussed (1.1.3 **Ivermectin** Mechanism of Action, page 17).<sup>[20][22]</sup> Strategically, a straightforward amide disconnection was proposed which split the probe into two fragments, an amine terminal bodipy fragment and an acid terminal ivermectin fragment.

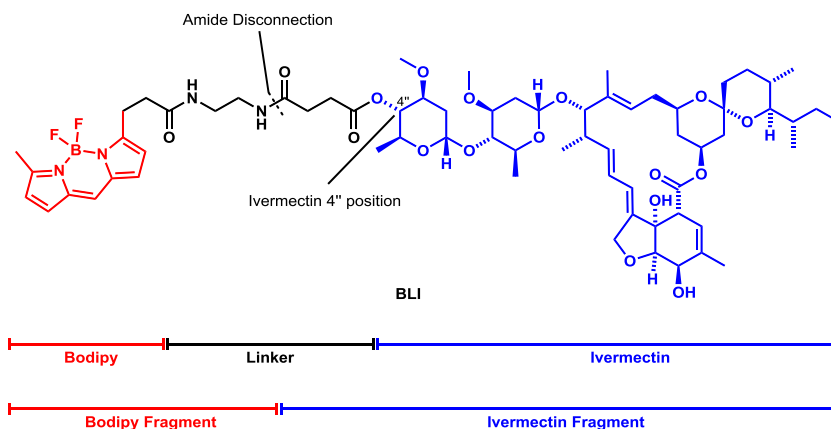


Figure 1.10. Structure of proposed **BLI** probe.

## 1.2 Results and Discussion

### 1.2.1 Synthesis of Bodipy Fragment 1.1

#### Synthesis of Bodipy Core

To begin the synthesis of **BLI** (Bodipy-Linker-**Ivermectin**), the abovementioned bodipy fragment was targeted (Figure 1.10, page 23). Bodipy fragment **1.1** consisted of the core bodipy moiety covalently linked to a section of the linker which terminates with an amine. (Figure 1.11).

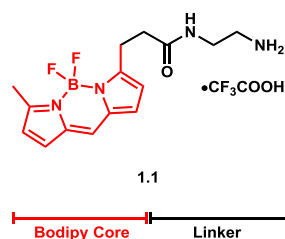
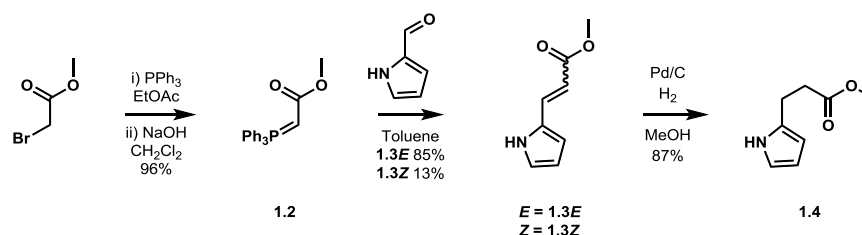


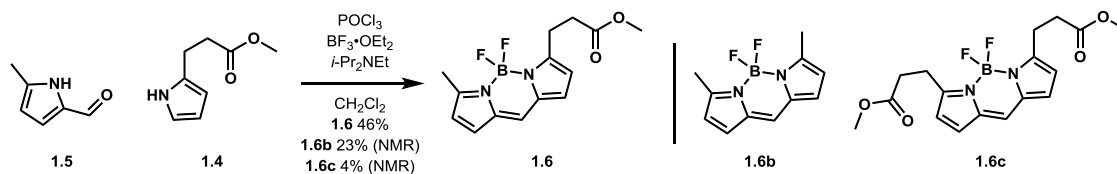
Figure 1.11. Structure of bodipy fragment **1.1**.

The synthesis of bodipy fragment **1.1** began with the synthesis of the core bodipy moiety. To achieve this, methyl bromoacetate was converted to the corresponding phosphonium ylide **1.2** which proceeded with a 96% yield (Scheme 1.1).<sup>[39]</sup> Following this, Wittig olefination between phosphonium ylide **1.2** and pyrrole-2-carboxaldehyde was conducted, which generated the (*E*)-alkene **1.3E** with an 85% yield and the (*Z*)-alkene **1.3Z** with a 13% yield.<sup>[40]</sup> Subsequent hydrogenation of the unsaturated methyl ester **1.3** gave access to the methyl ester pyrrole **1.4** with an 87% yield.<sup>[41]</sup>



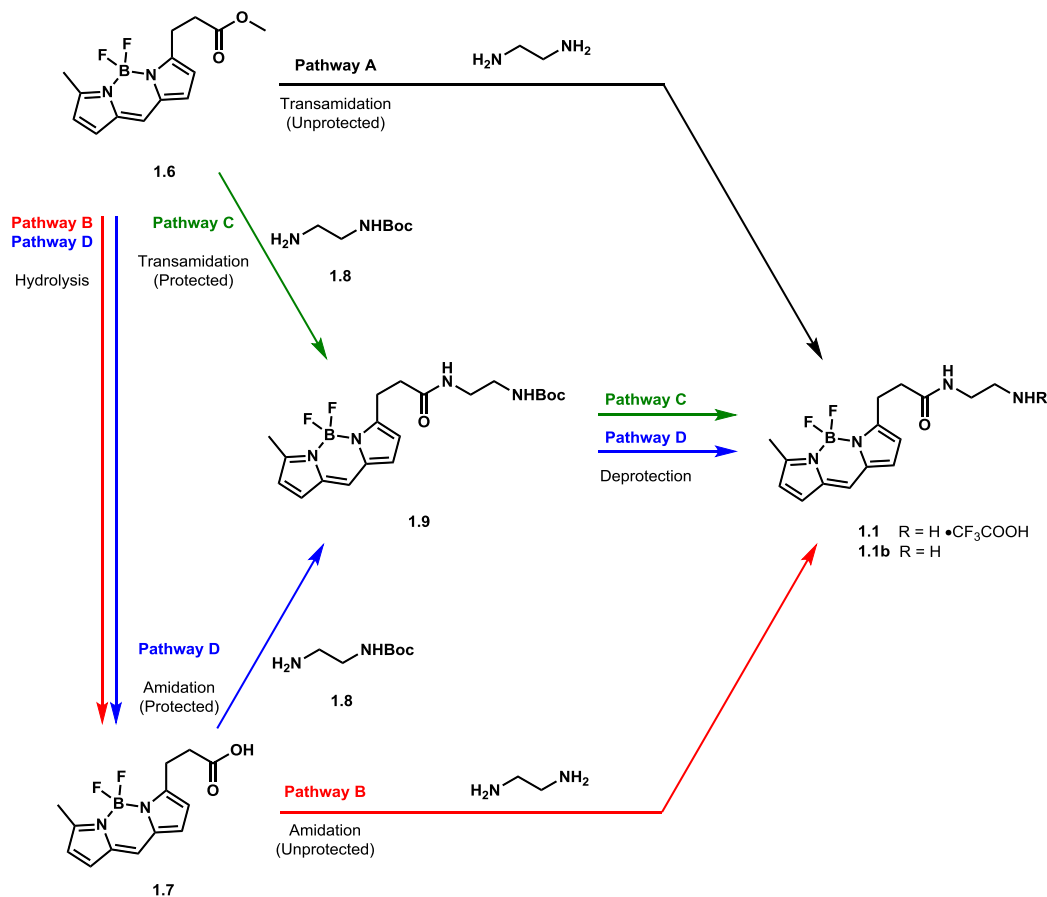
Scheme 1.1. Generation of phosphonium ylide **1.2**, followed by Wittig olefination to alkenes **1.3E** and **1.3Z** and subsequent reduction to saturated methyl ester **1.4**.

Methyl ester pyrrole **1.4** was then coupled with pyrrole **1.5** in the presence of phosphorus (V) oxychloride and boron trifluoride diethyl etherate, which successfully generating the desired bodipy **1.6** with a yield of 46% (Scheme 1.2).<sup>[42]</sup> Additionally, two ‘homo dimer’ side products were observed, the dimethyl bodipy **1.6b** in a 23% yield (determined by NMR spectroscopy) and the diester bodipy **1.6c** with a 4% yield (determined by NMR spectroscopy).



Scheme 1.2. Coupling of pyrroles **1.4** and **1.5** to form bodipy **1.6** and the homo dimer side products **1.6b** and **1.6c**.

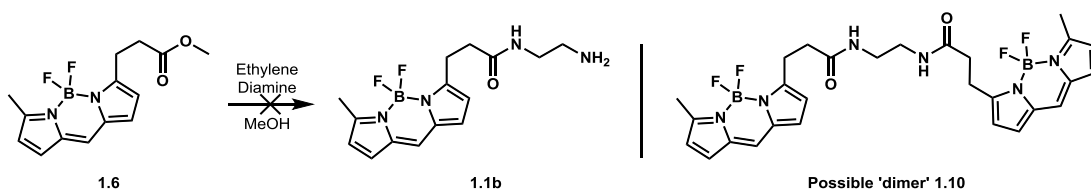
With the successful synthesis of the bodipy core complete, the next step was to append the linker and thus generate bodipy fragment **1.1** (Figure 1.11, page 24). To generate fragment **1.1** from methyl ester bodipy **1.6**, several possible routes were envisioned (Scheme 1.3). **Pathway A** was the most direct route, involving a single step of direct transamidation of methyl ester **1.6** with ethylene diamine to generate the free amine bodipy fragment **1.1b**. The two-step **Pathway B** entailed the initial hydrolysis of methyl ester **1.6** to acid **1.7**, followed by amidation of acid **1.7** with ethylene diamine to generate the free amine bodipy fragment **1.1b**. An alternative two-step sequence, **Pathway C**, involved transamidation of methyl ester **1.6** with *tert*-butyl carbamate protected amine **1.8** to generate the protected bodipy fragment **1.9**, followed by deprotection to bodipy fragment **1.1**. Finally, the three-step **Pathway D** involved an initial hydrolysis of methyl ester **1.6** to acid **1.7**, followed by the amidation of acid **1.7** with protected amine **1.8** to generate the protected bodipy fragment **1.9** and subsequent deprotection to bodipy fragment **1.1**.



Scheme 1.3. Possible pathways from methyl ester **1.6** to bodipy fragment **1.1(b)**.

### Attempted Pathway A

Initial efforts were targeted towards the route with the best step economy, **Pathway A**, which involved the direct transamidation of methyl ester **1.6** with ethylene diamine (Scheme 1.4). To reduce the likelihood of ‘dimer’ **1.10** formation, resulting from transamidation between the desired product amine **1.1b** and the methyl ester starting material **1.6**, 50 equivalents of ethylene diamine were utilised. The reaction however, did not produce any of the free amine bodipy fragment **1.1b**. Furthermore, no aromatic peaks corresponding to the bodipy core were observed by NMR spectroscopy which indicated decomposition of the bodipy core.



Scheme 1.4. Attempted transamidation of methyl ester **1.6** to amine **1.1b** and the structure of the possible side product, ‘dimer’ **1.10**.

In an attempt to monitor how the reaction was proceeding, and to gain some information regarding why no desired amine **1.1b** had been observed, the reaction was

repeated in an NMR tube to allow direct NMR spectroscopy at various time points. Utilising this method required changing the solvent from methanol to deuterated methanol. Furthermore, to facilitate the analysis of the NMR spectra, the number of equivalents of ethylene diamine were reduced from 50 to 5.

The spectra, recorded at various time points during the reaction, are displayed with the key peaks of methyl ester **1.6**, the methoxy group (-OCH<sub>3</sub>), the two methylene groups (-CH<sub>2</sub>) and the bodipy methyl group (Ar-CH<sub>3</sub>) labelled (Figure **1.12**). The first spectrum shows the reaction mixture before the addition of ethylene diamine, for clarity of the peaks of the starting material. The spectrum recorded at T=15 minutes already shows significant degradation of the bodipy methyl signal. The spectrum recorded at T=45 minutes showed that the signal corresponding to the bodipy methyl group (Ar-CH<sub>3</sub>) had completely degraded and further depicts partial degradation of the methyl ester (-OCH<sub>3</sub>) signal. The spectrum at T=2 hours 15 minutes indicates decomposition of the two methylene (-CH<sub>2</sub>) groups, and further splitting of the ester (-OCH<sub>3</sub>) signal. The spectra recorded at T=24 and 96 hours indicate further degradation, followed by disappearance of the methyl ester (-OCH<sub>3</sub>) signal. Due to the decomposition observed, this route was abandoned in favour of attempting the aforementioned **Pathway B**. (Scheme **1.3**, page 26).

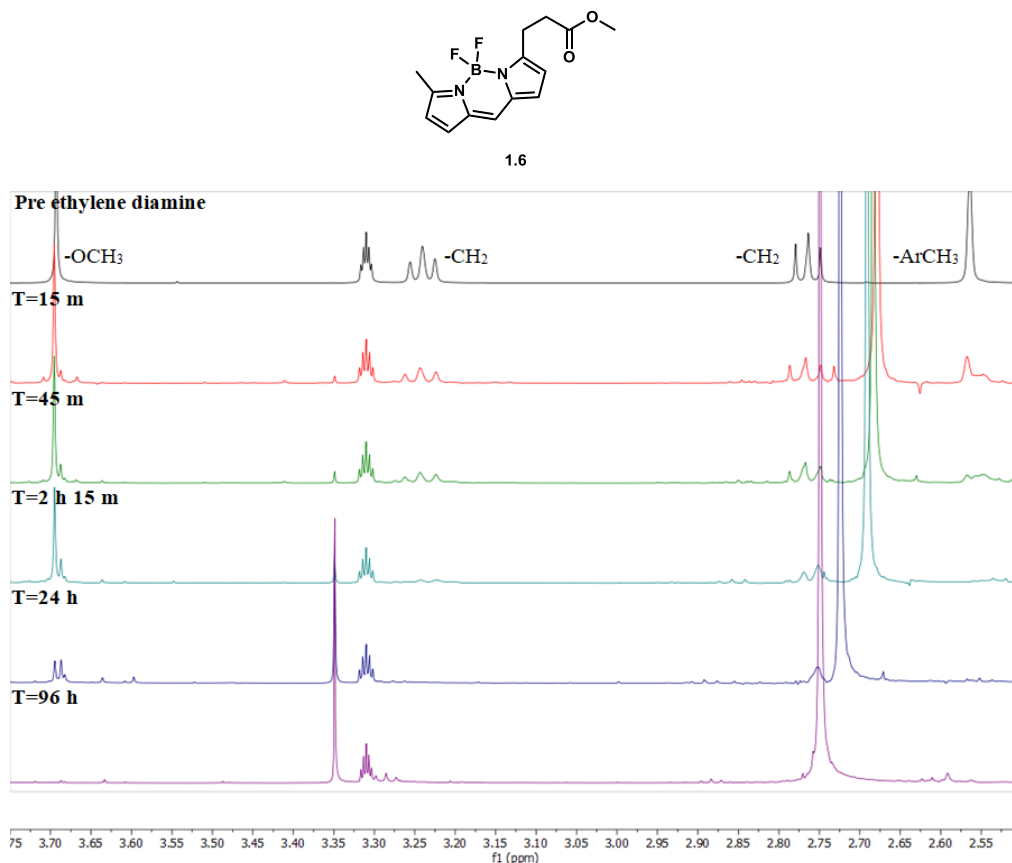
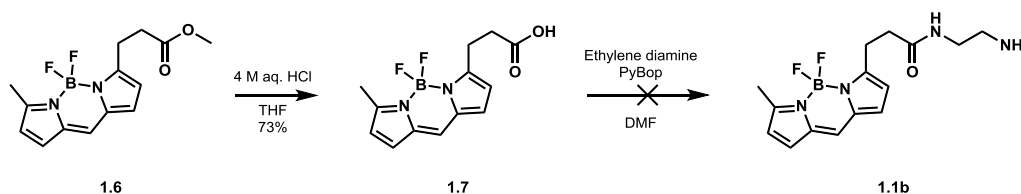


Figure 1.12. Structure of methyl ester **1.6** and  $^1\text{H}$  NMR spectra showing decomposition of bodipy methyl ester **1.6**.

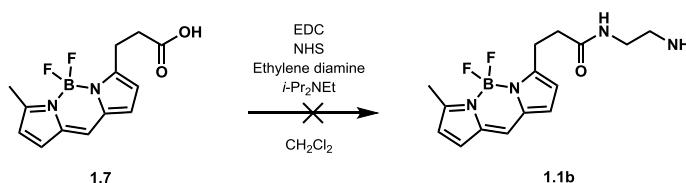
### Attempted **Pathway B**

To continue efforts toward synthesising bodipy fragment **1.1b**, the aforementioned **Pathway B** was attempted, which involved the two-step ester hydrolysis-amidation (unprotected) sequence (Scheme 1.3, page 26). Methyl ester **1.6** was successfully hydrolysed under acidic conditions to the corresponding acid **1.7** with a 73% yield (Scheme 1.5). Following this, a PyBop mediated amide coupling between acid **1.7** and ethylene diamine was attempted. Due to the possibility of dimerisation to amide **1.10** (Scheme 1.4, page 26) between the free amine of the desired product **1.1b** and the starting material acid **1.7**, ten equivalents of ethylene diamine were utilised. However, this attempted amidation did not result in the desired amide **1.1b**. Inspection of the crude material by  $^1\text{H}$  NMR spectroscopy revealed similar decomposition to that observed in the **Pathway A** attempts (Attempted Pathway A, page 26).



Scheme 1.5. Acid hydrolysis of methyl ester **1.6** to acid **1.7**, followed by the attempted amidation of acid **1.7** to amine **1.1b**.

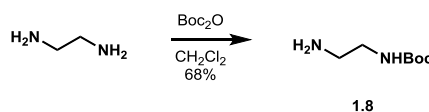
The amidation reaction between acid **1.7** and ethylene diamine was attempted again, this time with alternate coupling conditions (Scheme **1.6**). Acid **1.7** was activated with 1-Ethyl-3-(3-dimethylaminopropyl)carbodiimide (EDC) and *N*-hydroxysuccinimide (NHS) to form the activated NHS-ester *in situ*. Subsequent coupling with ethylene diamine (10 equivalents to minimise the risk of unwanted coupling between the product amine **1.1b** with acid **1.7**) failed to produce any of the desired amine **1.1b**. Similarly to the previous attempts, <sup>1</sup>H NMR spectroscopy revealed decomposition of the bodipy core. A plausible explanation for the decomposition of both acid **1.7** and methyl ester **1.6** could be decomplexation of the BF<sub>2</sub> moiety from the bodipy core by ethylene diamine, as bodipy is known to be unstable in strongly basic environments.<sup>[43]</sup> While ethylene diamine is not a particularly strong base, the bidentate nature of the compound may have been sufficient to cause decomplexation, and thus decomposition of the bodipy core.



Scheme **1.6**. Attempted amid coupling of acid **1.7** to amine **1.1b**.

### Attempted Pathway C

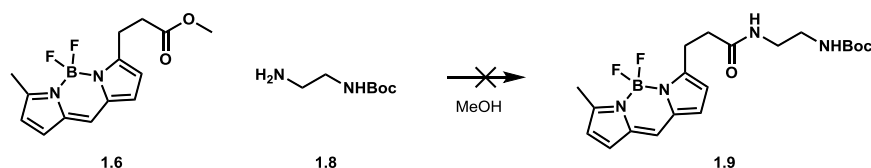
With both **Pathway A** and **Pathway B** resulting in decomposition of methyl ester **1.6** and acid **1.7** respectively, attention turned to **Pathway C** (Scheme **1.3**, page 26). **Pathway C** involved the transamidation of methyl ester **1.6** with protected amine **1.8** to generate the protected bodipy fragment **1.9** followed by deprotection to bodipy fragment **1.1** (Scheme **1.3**, page 26). The use of mono protected ethylene diamine would decrease the bidentate nature of the (unprotected) diamine and would thus be likely to decrease the possibility of decomplexation of the BF<sub>2</sub> moiety from the bodipy core. To generate the required mono protected amine **1.8**, ethylene diamine was reacted with di-*tert*-butyl dicarbonate to afford the *tert*-butyl carbamate protected amine **1.8** in a 68% yield (Scheme **1.7**).<sup>[44]</sup>



Scheme **1.7**. Mono protection of ethylene diamine to *tert*-butyl carbamate **1.8**.

Following the synthesis of protected amine **1.8**, the transamidation with methyl ester **1.6** was attempted (Scheme **1.8**). Although the reaction did not result in the desired

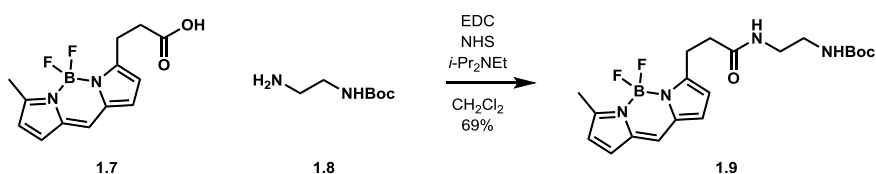
amide **1.9**, no decomposition was observed and methyl ester **1.6** was recovered. This lack of decomposition is consistent with the assumption that the presence of the bidentate ethylene diamine was responsible for the previously observed decomposition.



Scheme **1.8**. Attempted transamidation of methyl ester **1.6** with amine **1.8** to generate the protected bodipy fragment **1.9**.

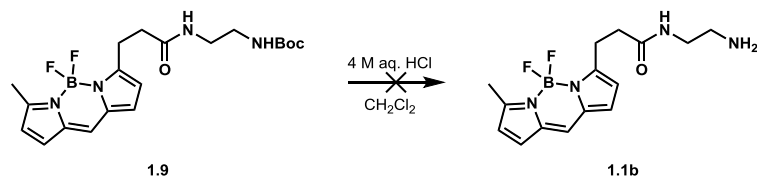
### Attempted **Pathway D**

As the desired bodipy fragment **1.1(b)** was not observed when utilising the three pathways with the shortest step-count (**Pathways A, B** and **C**), attention was shifted toward the three-step **Pathway D** (Scheme **1.3**, page 26). The first step of this sequence was the aforementioned hydrolysis of ester **1.6** to acid **1.7** (Scheme **1.5**, page 28). Following this, an EDC/NHS mediated coupling of acid **1.7** with *tert*-butyl carbamate protected amine **1.8** was attempted which successfully generated the protected bodipy fragment **1.9** with a 69% yield (Scheme **1.9**).<sup>[45]</sup>

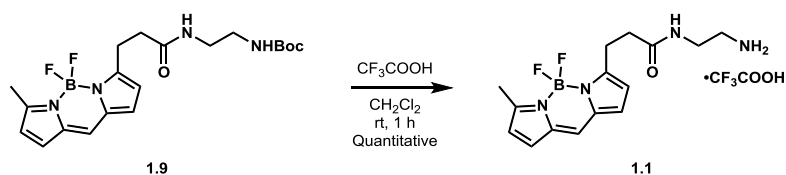


Scheme **1.9**. Coupling of acid **1.7** with protected amine **1.8** to generate *tert*-butyl carbamate protected amide **1.9**.

With the protected bodipy fragment **1.9** in hand, deprotection to generate the desired bodipy fragment **1.1** was attempted (Scheme **1.10**). Due to the reported sensitivity of the bodipy moiety to strong Brønsted acids and bases,<sup>[43][46]</sup> deprotection of *tert*-butyl carbamate **1.9** was attempted using 2 M hydrochloric acid.<sup>[47]</sup> After eight hours however, no reaction had taken place and so the concentration of acid was increased to 4 M. After 16 hours, no conversion had been observed, however some decomposition was evident and so the reaction was terminated and *tert*-butyl carbamate **1.9** was recovered.



Scheme **1.10**. Attempted acidic deprotection of *tert*-butyl carbamate **1.9** to amine **1.1b**. Following the attempts to deprotect *tert*-butyl carbamate **1.9** using hydrochloric acid, the use of trifluoroacetic acid was trialled. While this is the most commonly used reagent to effect *tert*-butyl carbamate deprotection, it was not initially attempted due to a study in which trifluoroacetic acid was reported to efficiently decomplex the BF<sub>2</sub> moiety from the bodipy core within one hour of reaction time.<sup>[46]</sup> Due to this report, the reaction was attempted with careful regular observation. *Tert*-butyl carbamate **1.9** was treated with trifluoroacetic acid at room temperature for one hour which successfully yielded amine TFA salt **1.1**, completing the synthesis of the bodipy fragment (Scheme **1.11**).<sup>[48]</sup>



Scheme **1.11**. Acidic deprotection of *tert*-butyl carbamate **1.9** to bodipy fragment **1.1**.

### 1.2.2 Synthesis of Ivermectin Fragment 1.11

With the synthesis of the bodipy fragment complete, focus was shifted toward the synthesis of the ivermectin fragment **1.11** (Figure **1.13**). This consisted of **ivermectin** covalently bound *via* an ester linkage to a section of linker with a terminal acid moiety.

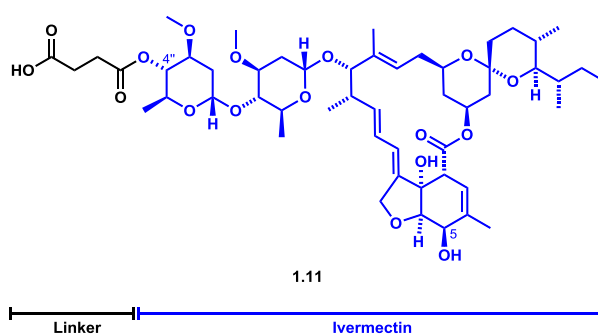
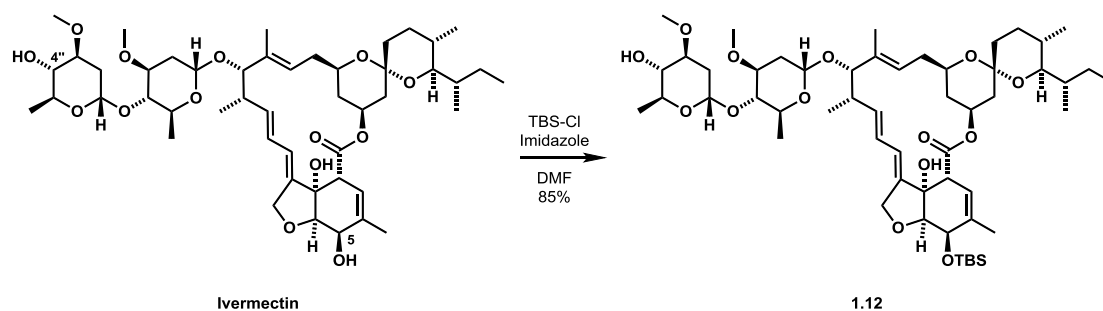


Figure **1.13**. Structure of acid terminal ivermectin fragment **1.11**.

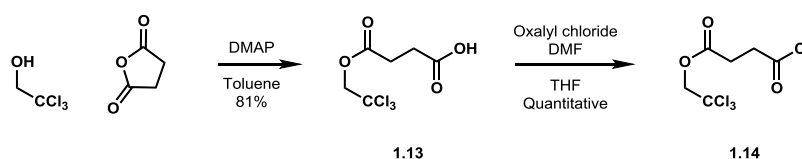
In order to selectively functionalise the desired secondary 4'' alcohol of **ivermectin**, the more reactive secondary allylic 5 alcohol had to be protected (Figure **1.13**).<sup>[22]</sup> This was achieved by reacting **ivermectin** with *tert*-butyldimethylsilyl chloride in the presence of imidazole, which generated silyl ether **1.12** in an 85% yield (Scheme **1.12**).<sup>[22]</sup> The

reaction was terminated after two hours as this marked the point at which the formation of undesired diprotected material could be observed.



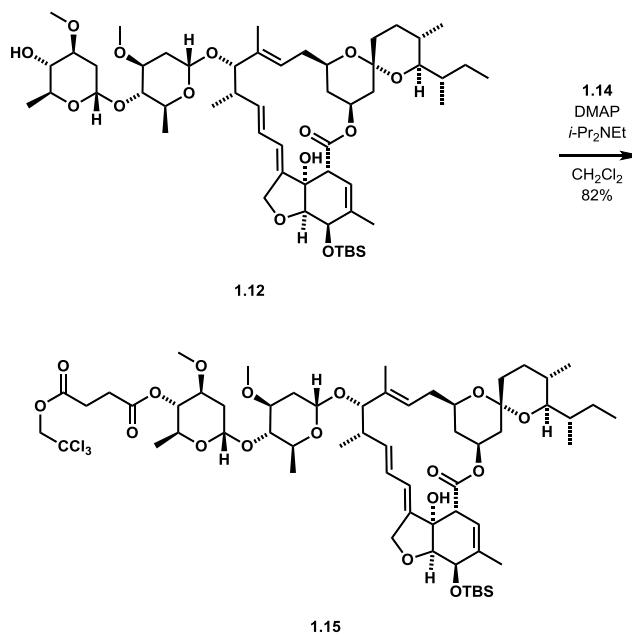
Scheme 1.12. Mono *tert*-butyldimethylsilyl protection of **ivermectin** to silyl ether **1.12**.

The next steps involved the synthesis of the linker fragment that features in ivermectin fragment **1.11** (Figure 1.13, page 31). This was achieved in two steps, beginning with the ring opening of succinic anhydride with trichloroethanol in the presence of the nucleophilic catalyst 4-dimethylaminopyridine (Scheme 1.13).<sup>[22]</sup> This afforded the trichloroethanol protected acid **1.13** in an 81% yield. Acid **1.13** was subsequently activated to the corresponding acyl chloride **1.14** using oxalyl chloride and catalytic *N,N*-dimethylformamide.<sup>[22]</sup>



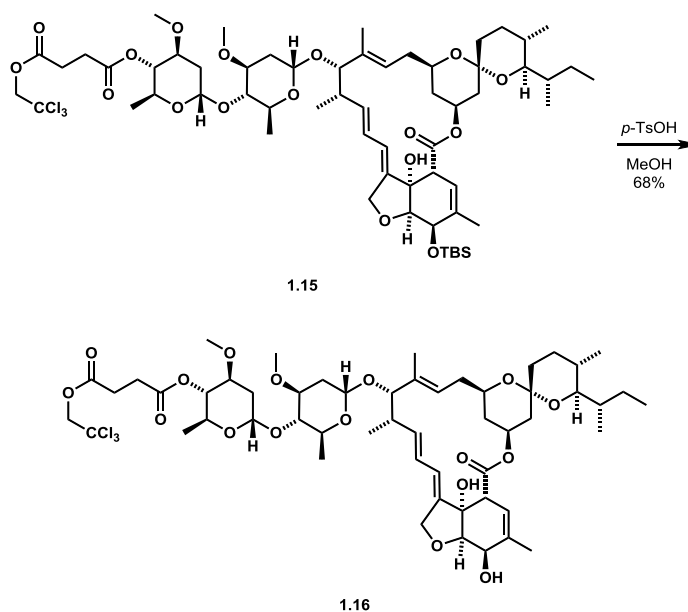
Scheme 1.13. Ring opening of succinic anhydride with trichloroethanol to generate acid **1.13** followed by the activation of acid **1.13** to acyl chloride **1.14**.

Due to the susceptibility of acyl chloride **1.14** to hydrolysis, it was immediately coupled with the free secondary 4'' hydroxyl of silyl ether **1.12**. The coupling was conducted in the presence of catalytic 4-dimethylaminopyridine and Hünig's base which afforded the desired ester **1.15** with an 82% yield (Scheme 1.14).<sup>[22]</sup>



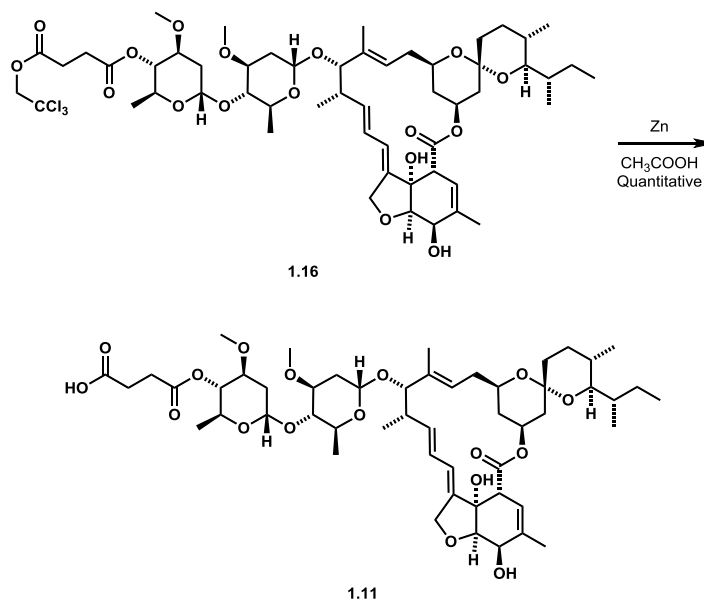
Scheme 1.14. Coupling of silyl ether **1.12** with acyl chloride **1.14** to ester **1.15**.

With the doubly protected ivermectin fragment **1.15** now complete, the following step was the deprotection of the *tert*-butyldimethylsilyl protecting group. Acidic deprotection of silyl ether **1.15** using *p*-toluenesulfonic acid in methanol afforded the free secondary allylic alcohol **1.16** with a 68% yield (Scheme 1.15).<sup>[22]</sup>



Scheme 1.15. Acidic deprotection of silyl ether **1.15** to secondary allylic alcohol **1.16**.

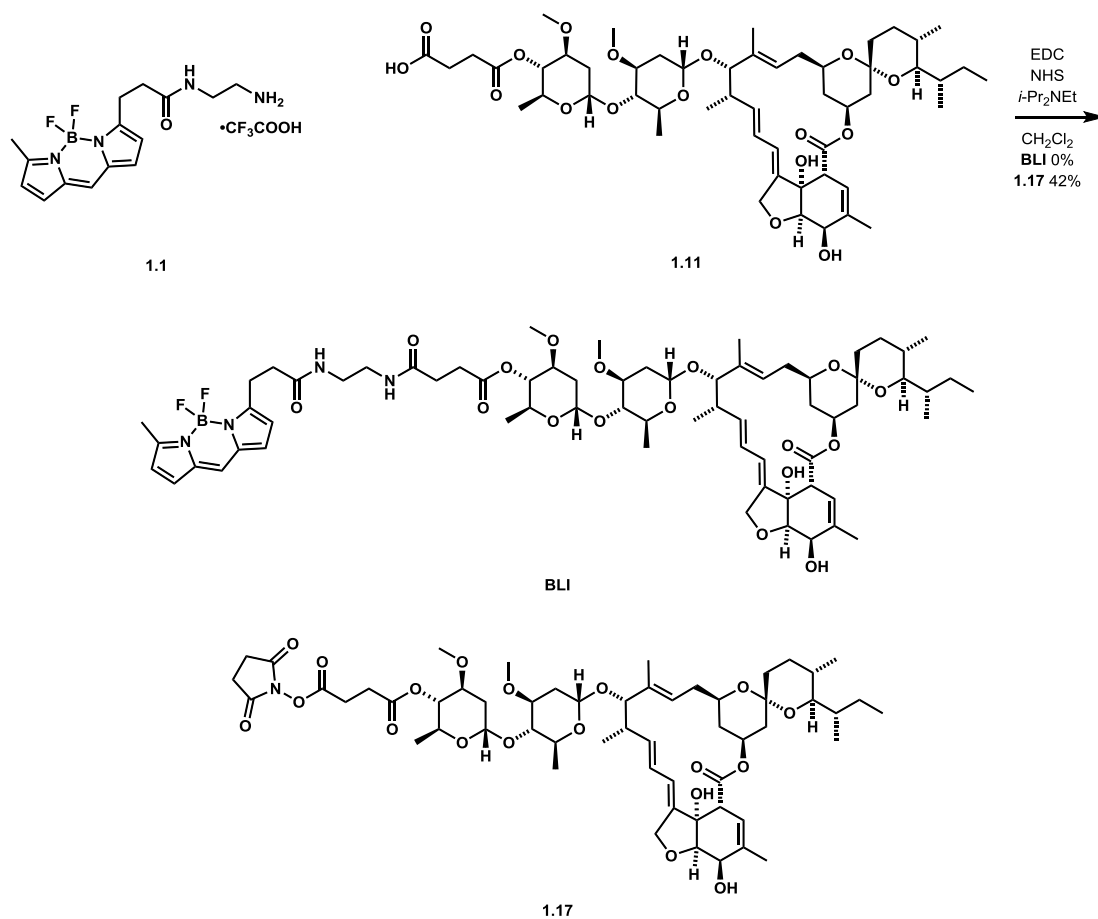
The final step in the synthesis of ivermectin fragment **1.11** involved the reductive deprotection of the trichloroethyl group from ester **1.16**. To achieve this, ester **1.16** was treated with metallic zinc in acetic acid, which successfully generated the corresponding free acid **1.11** with a quantitative yield and completed the synthesis of the ivermectin fragment (Scheme 1.16).<sup>[22]</sup>



Scheme 1.16. Reductive deprotection of ester **1.16** to acid **1.11**.

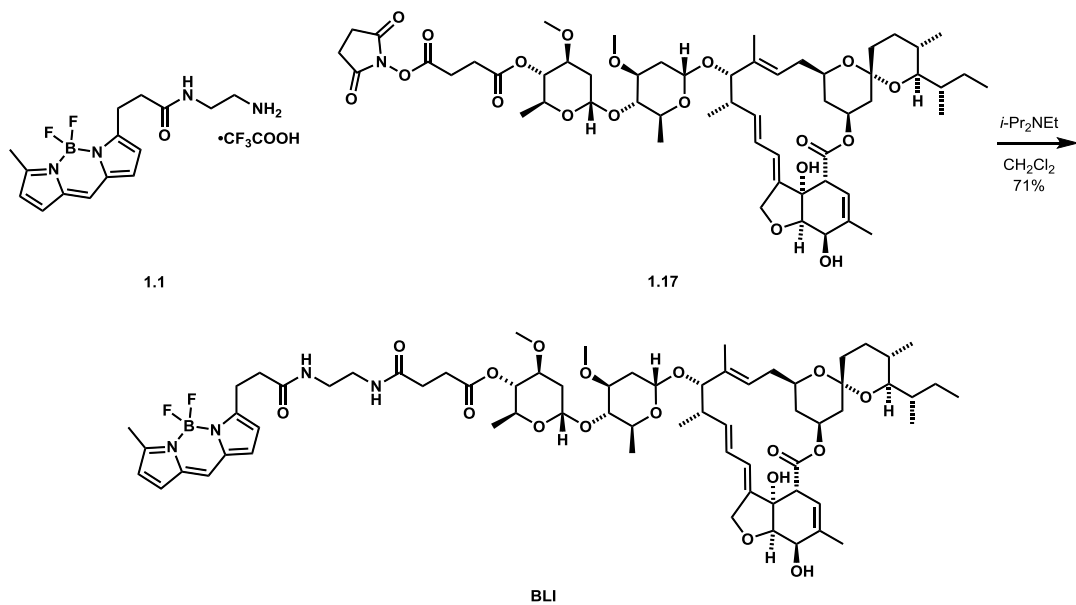
### 1.2.3 Completion of **BLI** synthesis

With both bodipy fragment **1.1** and ivermectin fragment **1.11** in hand, coupling of these fragments to generate the **BLI** (Bodipy-Linker-Ivermectin) probe was attempted. Initially, an EDC/NHS mediated amide coupling was attempted between amine TFA salt **1.1** and acid **1.11** (Scheme 1.17).<sup>[45]</sup> This did not result in any of the desired **BLI** probe; however, full consumption of starting material was observed, resulting in the formation of several side products. Upon inspection of these side products, it was determined that the major product was the NHS activated ester **1.17**. This indicated that either the reaction had not reached completion, or the batch of amine TFA salt **1.1** was impure, or had degraded.



Scheme **1.17**. Attempted coupling of amine TFA salt **1.1** and acid **1.11** to generate **BLI** probe and the structure of the major isolated side product, activated NHS ester **1.17**.

Having isolated the activated NHS ester **1.17**, another batch of amine TFA salt **1.1** was generated (Scheme **1.11**, page 31), and the coupling to form the **BLI** probe was attempted. The coupling was conducted under basic conditions and successfully generated the **BLI** probe with a 71% yield (Scheme **1.18**). With the probe successfully generated, biological assaying was conducted.



Scheme **1.18**. Coupling of amine TFA salt **1.1** with the activated NHS ester **1.17** to generate probe **BLI**.

## 1.3 BLI Biological Assaying

### 1.3.1 Materials and Methods

#### Nematode Strains and Culture

For the testing of **BLI**, only the N2 (wild type) *Caenorhabditis elegans* strain was utilised which was supplied by the *C. elegans* Genetics Centre (USA). They were maintained on nematode growth media Petri plates which were supplemented with 50–100  $\mu\text{L}$  *Escherichia coli* OP50-1 liquid culture (a non-pathogenic, slow growing *E. coli* strain).<sup>[49]</sup> The nematode growth media Petri plates were prepared with 3 g NaCl, 17 g agar, 2.5 g peptone and 975 mL H<sub>2</sub>O which were combined and autoclaved for 50 minutes. After cooling at 55 °C for 15 minutes, 1 mL 1 M CaCl<sub>2</sub>, 1 mL 5 mg/mL ethanolic cholesterol, 1 mL 1 M MgSO<sub>4</sub> and 25 mL KPO<sub>4</sub> buffer were added and mixed before being added under sterile conditions to Petri dishes and allowed to cool.

#### Nematode Microscopy Preparation

Nematodes were viewed directly on the assay plates using a Zeiss benchtop microscope fitted with a Canon sureshot camera. For viewing under differential interference contrast (DIC) and fluorescence microscopy, nematodes were picked using a 32 gauge platinum wire (flamed before and after each use) from the assay plates. The picked nematodes were then mounted on slides with a pad of 2% agarose in M9 buffer (3 g KH<sub>2</sub>PO<sub>4</sub>, 6 g Na<sub>2</sub>HPO<sub>4</sub>, 5 g NaCl, 1 mL 1 M MgSO<sub>4</sub>, H<sub>2</sub>O to 1 L and autoclave sterilisation) which were supplemented with 10 mM NaN<sub>3</sub> (to immobilize nematodes). The slide was then covered with petroleum jelly edged cover slips and stored in a dark and moistened atmosphere before viewing. Nematodes were viewed using DIC or fluorescence optics on a Zeiss Axioscop2 microscope and imaged using a mounted Zeiss AxioCam camera with Axiovision software.<sup>[35]</sup>

#### DiI Staining Procedure

In addition to drug exposure, nematodes were also treated with the lipophilic dye **DiI** (Figure 1.7, page 22) to assess the integrity of the amphid sensory structures. Nematodes stained with **DiI** were suspended in 1 mL M9 buffer and centrifuged at 2500 rpm. The supernatant was removed, the pellet resuspended in 1 mL M9 containing 5  $\mu\text{L}$  of **DiI** stock solution (2 mg/mL in dimethylformamide) and the suspension was placed in the dark at ambient temperature for three hours. The nematodes were then centrifuged and washed with M9 solution twice before being transferred to NGM plates seeded with 50  $\mu\text{L}$  OP50-1 liquid culture and incubated at

20 °C overnight. Following this, nematodes were prepared and imaged as per the aforementioned procedure (1.3.1.2 Nematode Microscopy Preparation, page 37).

### Free Swimming Assay

To measure the acute (short term) effects of the test compounds on nematodes, the free swimming assay was utilised. Using sterile conditions, either 99 µL of M9 buffer or 94 µL of M9 buffer and 5 µL of *E. coli* OP50-1 liquid culture were added to each lane of a 96 well plate. To this, 1 µL of the test compound in a methanolic stock solution (generating a final concentration of 1% methanol) was added. Finally, 25 adult nematodes (for **BLI** testing only N2 (wild type) *C. elegans* strain was utilised) were added to the wells, and the plates were incubated at 20 °C for 24 hours with images taken at one, four and 24 hours.

### Plate-Based Assay

To measure the long term effects of the test compounds on nematode populations, the plate-based assay was utilised. Using sterile conditions, 5 mL of NGM was added to a Petri plate and allowed to set. The plates were then seeded with 50 µL of *E. coli* OP50-1 liquid culture followed by 50 µL methanolic solution of the desired compound (generating a final concentration of 1% methanol). Five adult N2 *C. elegans* were then transferred to the plate using a flamed 32 gauge platinum wire before the plates were incubated at 20 °C in the dark for 48 h with images taken at five, 24 and 48 hours.

### 1.3.2 BLI Study

For the testing of the **BLI** probe, *C. elegans* was utilised as a model organism as the free-living nematode is significantly easier to work with than parasitic species. While the extensively studied *C. elegans* is not parasitic, and thus has questionable relevance in studying clinically relevant parasitic species, the first aim of this project was to establish the primary route of uptake of **ivermectin**. The hypothesis, for which this project attempted to generate evidence, is that the uptake route of **ivermectin** is *via* the amphids. With this in mind, *C. elegans* is an acceptable model organism as the amphids are known to be homologous throughout the phylum Nematoda.<sup>[50]</sup>

### Establishing BLI Efficacy

The initial testing with **BLI** was to establish if the probe had comparable efficacy to the parent drug, or if the modifications that were made hamper its nematicidal activity. This was important as a substantial loss of efficacy would destroy any confidence that the probe was acting in a similar manner as the parent drug, thus nullifying any results. As some loss of efficacy is expected when modifying an already optimised and

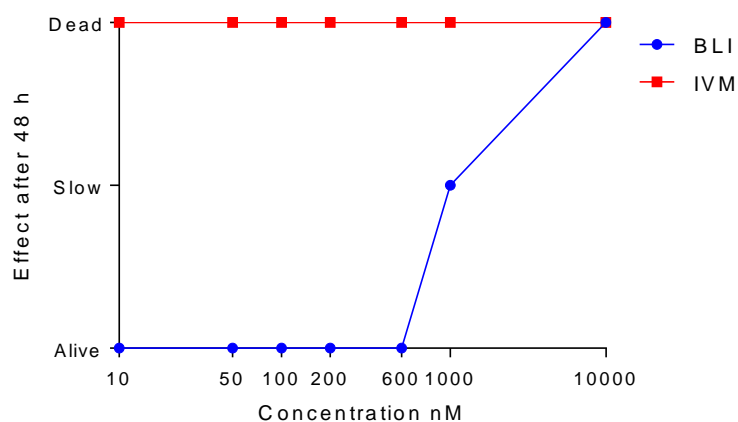
extremely potent drug, a self-imposed maximum limit of efficacy loss was set at one order of magnitude. Efficacy loss beyond this limit was deemed to be too great, and likely indicated a poor chemical probe for the purposes of this project.

With that in mind, the free swimming assay (Free Swimming Assay, page 38) was developed and utilised to establish the efficacy of **BLI**, using **ivermectin** as a positive control. As the compounds were in methanolic stock solutions, the assay contained a final concentration of 1% methanol. To ensure that this did not interfere with the health of the nematodes, a 1% methanol negative control was included in the assay. Interestingly, when utilising this assay the positive control **ivermectin** was not efficacious at its normal effective concentration (10 nM) against *C. elegans*. With the positive control not functioning reliably, the results obtained were nullified and an alternative assay was utilised.

The next assay to be conducted was the plate-based assay (Plate-Based Assay, page 38). With this assay, positive nematicidal activity is determined by reduction of the nematode population to zero. Treatment with sub-lethal concentrations of nematicidal compounds results in lowered motility of individual nematodes, as well as a reduced population (compared to wild type population). Treatment with non-nematicidal compounds (and nematicidal compounds at concentrations too low to produce detectable efficacy) results in normal motility of individual nematodes, and a normal population size when compared with wild type nematodes.

With that in mind, **BLI** was tested and once more, the purpose was to establish whether the efficacy of **BLI** was within an order of magnitude of that of the parent drug **ivermectin**. **Ivermectin** was utilised as the positive control and the two negative controls, no compound and 1% methanol were again employed. Upon completion of the assay after 48 hours, the 1% methanol control had no discernible detrimental effect on the health or reproduction of the nematodes. The **ivermectin** control however, had successfully destroyed the population from a concentration of 10 nM and upwards (Graph 1.1). As this was the expected lethal concentration of **ivermectin** for this assay, the control functioned as intended and the results of this assay were deemed reliable. Upon observation of the **BLI** treated plates, thriving populations were noted for concentrations up to and including 600 nM. At 1  $\mu$ M **BLI**, some efficacy was observed as the nematodes were noticeably less motile and the population was somewhat reduced compared to the no compound control. At 10  $\mu$ M **BLI**, full efficacy was observed and the population was completely destroyed. This represented a three orders of magnitude loss of efficacy for **BLI** compared to **ivermectin**, which was well beyond

the self-imposed maximal limit of one order of magnitude. With these results, **BLI** was determined to be a poor probe for the purposes of this project and therefore the probe design needed to be readdressed.



Graph 1.1. Graph showing efficacies of **ivermectin** and **BLI**.

While the probe was not as efficacious as **ivermectin**, fluorescent microscopy was conducted regardless in an attempt to rationalise why such a large decrease in efficacy had occurred (Figure 1.14). At 10 nM **BLI**, no fluorescence was observed, which correlated with the observed lack of efficacy. At 100 nM and 600 nM **BLI**, some fluorescence was observed which stained the pharynx (mouth) and the lumen (digestive tract). This indicated that the nematodes ingested the probe, however as no lethality was observed in the assay, it implied that ingestion of the drug is not the primary route of uptake. As no fluorescence was observed in the amphids, the probe likely did not enter the amphids which, when correlated with the lack of lethality at these concentrations, is indirectly consistent with an amphidal uptake mechanism. However, due to the significantly reduced efficacy of **BLI** compared to **ivermectin** the probe needed to be redesigned with the aim of improving the efficacy.

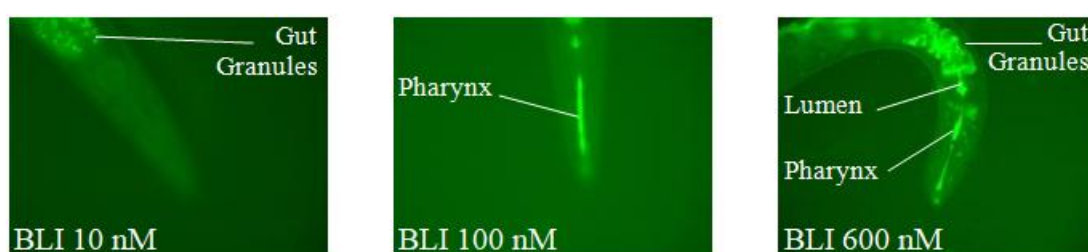


Figure 1.14. Fluorescence microscopy of **BLI** treated *C. elegans*.

## 1.4 Probe Redesign

### 1.4.1 Troubleshooting

With the probe not functioning as intended, troubleshooting was conducted in an attempt to establish the cause(s) of the loss of efficacy. When designing **BLI**, two structural modifications were made to **ivermectin**; the addition of the linker, and the addition of the bodipy moiety. It was evident therefore, that the loss of efficacy of **BLI** was a result of either one, or both, of these structural modifications.

The first of the possible issues was with regard to the linker, which contained two potential sources of efficacy loss; the site of the linker attachment and the composition of the linker. However, when designing **BLI**, a core publication by Mrozik *et al.* was utilised to guide both the site of linker attachment and the linker composition.<sup>[22]</sup> The aforementioned structure-activity relationship (SAR) study of **avermectin B1<sub>a</sub>** (Figure 1.6, page 20), showed minimal loss of *in vivo* efficacy of the 4'' derivatives. This therefore provided some rationale that neither the linker attachment site, nor the composition of the linker chosen for **BLI** is likely to be the source of the observed loss of efficacy.

With this in mind, it therefore seemed likely that the addition of the bodipy moiety was somewhat responsible for the lack of efficacy. When designing **BLI**, the aforementioned publication by Martin *et al.* was utilised to guide the design of the linker and fluorophore moiety.<sup>[21]</sup> In this study, **Martin's Probe** (Figure 1.4, page 18), which is structurally similar to **BLI**, was utilised to study the diffusion of **ivermectin** along cell membranes. For this study, the probe was administered *in vitro* to isolated muscle cell vesicles and not administered *in vivo* to either live nematodes or infected host organisms. Martin *et al.* demonstrated that their bodipy-containing **ivermectin**-based probe maintained efficacy against the Glutamate gated chloride channel (GluCl) target.<sup>[21]</sup> This therefore provided a good rationale that the **BLI** probe from this project could likely still engage the GluCl target.

The difference between the *in vitro* isolated muscle cell assay employed by Martin *et al.* and the assay employed in this project was the *in vivo* administration of **BLI** to live nematodes. This therefore required **BLI** to enter the nematodes, and make its way to the GluCl target. With the abovementioned knowledge that **BLI** can likely still bind to the GluCl and maintain efficacy, the loss of efficacy of **BLI** could have been due to **BLI** not being able to reach GluCl target. As no staining was observed in the

nematodes during the **BLI** assay, the likely cause of this low target engagement was a lack of **BLI** probe uptake.

As the hypothesis for this project is an amphidal route of **ivermectin** uptake, the properties of the commercially available **DiI** dye were scrutinised. **DiI** is frequently used to stain nematode amphids and nerve rings and is thus known to have an amphidal route of uptake. As the dye is designed to stain membranes, it is extremely lipophilic featuring two C<sub>18</sub> alkyl chains and a hydrocarbon backbone (Figure 1.15).

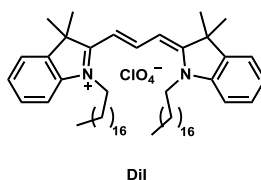


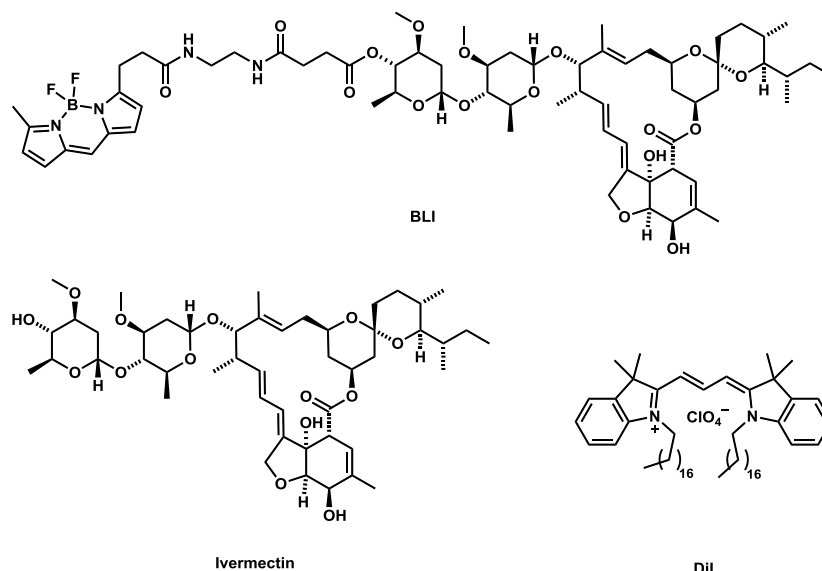
Figure 1.15. Structure of commercially available lipophilic dye **DiI**.

Additionally, it is known that **ivermectin** partially embeds in the outer layer of nerve cell membranes and diffuses along the outer membrane (without crossing it) until it meets and binds to the GluCl.<sup>[21]</sup> A high degree of lipophilicity is required to allow this membrane interaction to occur, as is present in the membrane staining **DiI** dye. Therefore, it was deemed possible that the addition of the linker, the bodipy or a combination of the two, reduced the lipophilicity of the probe enough to prevent this necessary lipophilic membrane interaction for occurring.

#### 1.4.2 Lipophilicity Calculations

In an attempt to generate values for the lipophilicity with which to be able to compare **ivermectin**, **DiI** and **BLI**, some parameters were calculated using the OSIRIS DataWarrior software. The values chosen to represent lipophilicity were the calculated partition coefficient between octanol and water (cLogP), the surface sum of all polar atoms known as topological polar surface area (tPSA), and a count of the hydrogen-bond acceptors and donors. While these calculated values are of course not quantitative empirical data, they were useful for generating an estimation of the lipophilicity of each compound. The cLogP for **ivermectin** was calculated to be five which is the upper limit of ‘Lipinski’s rule of fives’ for orally administered drugs (Figure 1.16).<sup>[51]</sup> The cLogP for **BLI** was six which was close to that of **ivermectin**. For comparison, the lipophilic **DiI** had a cLogP of 20, which is significantly higher than **ivermectin** and **BLI** and was unsurprising based on its structure. A look at the topological surface areas (tPSA) however, indicated a more significant difference between the compounds. For reference, a tPSA value of more than 140 Å<sup>2</sup> typically indicates low lipophilicity at

which point the membrane diffusion of a compound is hindered.<sup>[52]</sup> The tPSA value for **ivermectin** was calculated to be 170 Å<sup>2</sup> (Figure 1.16). The tPSA of the **BLI** probe however, was calculated to be 250 Å<sup>2</sup> which is significantly higher than that of **ivermectin** and thus indicates a significant drop in lipophilicity. Conversely and as expected, the tPSA of **DiI** was extremely low with a value of 6 Å<sup>2</sup>, indicating significantly increased lipophilicity compared to **ivermectin**. The hydrogen bond acceptor count for **ivermectin** was 14 (Figure 1.16). For **BLI** however, this value was 21 which indicated a much lower degree of lipophilicity compared to **ivermectin**. As expected the lipophilic dye **DiI** had a lower count of one hydrogen-bond acceptor. And finally the hydrogen-bond donor count for **ivermectin** was three and for **BLI** was four, indicating a slight decrease in lipophilicity compared to **ivermectin**. The lack of any hydrogen bond donors for **DiI** again contributed to its high lipophilicity.



	<b>Ivermectin</b>	<b>BLI</b>	<b>DiI</b>
cLogP	5	6	20
tPSA (Å <sup>2</sup> )	170	250	6
HBA	14	21	1
HBD	3	4	0

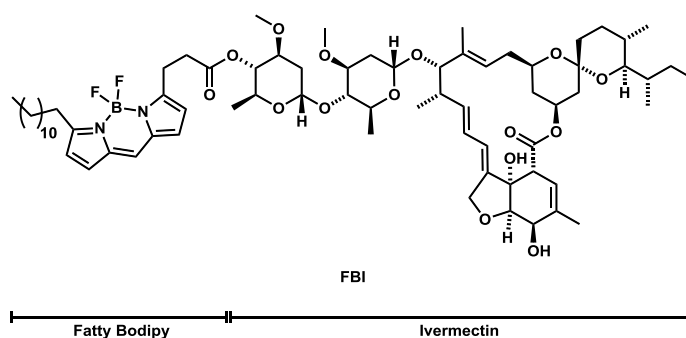
Figure 1.16. Structures of **BLI** probe, **ivermectin** and commercial lipophilic dye **DiI** and the table of calculated lipophilicity measurements.

With these values, it was clear that the addition of the amide-based linker and bodipy moiety significantly decreased the lipophilicity of the **BLI** probe compared to that of **ivermectin**. This decreased lipophilicity in combination with the observed lack of **BLI**

uptake is consistent with the hypothesis that the lipophilicity of the **BLI** probe was too low to allow the necessary lipophilic membrane interactions to occur.

### 1.4.3 New Probe Proposal

In an attempt to increase the probes lipophilicity, two modifications to the structure of **BLI** were made. Firstly, the hydrophilic linker which contributed two hydrogen bond donors and five hydrogen bond acceptors was removed. Secondly, the methyl group affixed to the bodipy core was increased in length to a dodecyl chain to mimic the commercial lipophilic dye **DiI** (Figure 1.9, page 22). These modifications resulted in the design of the new probe named **FBI** (Fatty-Bodipy-Ivermectin) (Figure 1.17). With these modifications, the cLogP was increased to 12, a value between that of **ivermectin** and **DiI** (Figure 1.17). The tPSA was lowered (relative to **BLI**) to 190 Å<sup>2</sup> which, while still above the desired lipophilic lower limit of 140 Å<sup>2</sup>, was much closer to the value of **ivermectin** than the **BLI** probe was. And finally the hydrogen bond acceptor and donor counts of **FBI** are much closer to **ivermectin** than those of **BLI**. With the modifications proposed and validated by the calculations, efforts were focussed on the synthesis of **FBI**.



	Ivermectin	BLI	FBI
cLogP	5	6	12
tPSA (Å <sup>2</sup> )	170	250	190
HBA	14	21	17
HBD	3	4	2

Figure 1.17. Structure of redesigned lipophilic probe **FBI** and tabulated comparison of calculated lipophilicity values.

## 1.5 FBI Synthesis

### 1.5.1 Synthetic Strategy

While the design of **FBI** was primarily to increase the lipophilicity, it was also designed to incorporate stock intermediates from the **BLI** synthesis such as silyl ether protected ivermectin **1.12** (Scheme **1.12**, page 32) and the methyl ester functionalised pyrrole **1.4** (Scheme **1.1**, page 24). With this in mind, the synthetic strategy to generate **FBI** was a straightforward ester disconnection to generate an acid terminal fatty bodipy fragment, and a hydroxyl terminal ivermectin fragment (Figure **1.18**).

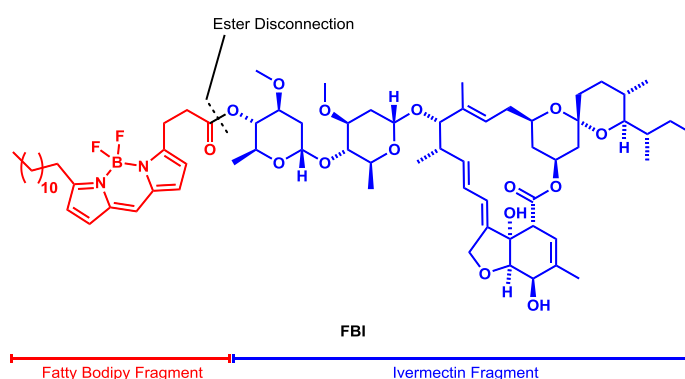


Figure **1.18**. Structure of **FBI** and the constituent fragments.

### 1.5.2 Fatty Bodipy Fragment Synthesis

As a design feature of **FBI** was to take advantage of common intermediates from the **BLI** synthesis, the ivermectin fragment that was to be used for coupling to the fatty bodipy fragment was the previously synthesised silyl ether **1.12** (Scheme **1.12**, page 32). With this in mind, the synthesis of **FBI** began with the targeting of the acid terminal fatty bodipy fragment **1.18** (Figure **1.19**).

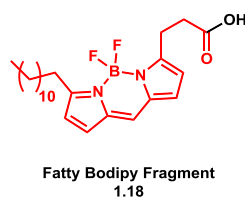
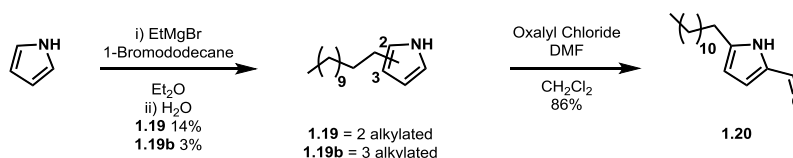


Figure **1.19**. Structure of fatty bodipy fragment **1.18**.

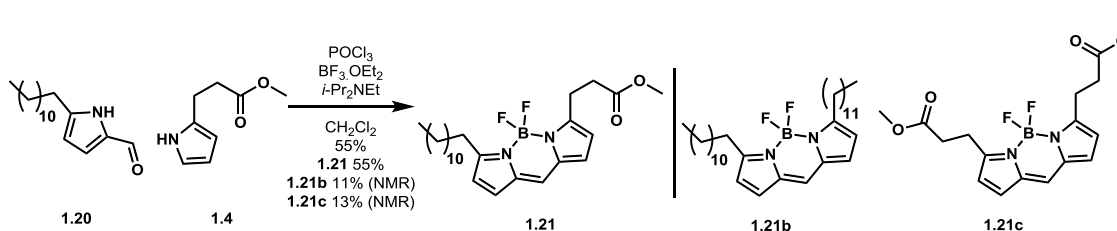
The synthesis of the fatty bodipy fragment **1.18** was analogous to that of the methyl bodipy acid **1.7** (1.2.1 Synthesis of Bodipy Fragment **1.1**, page 24). Initially, pyrrole was alkylated with dodecyl bromide which produced a complex mixture of alkylated products that resulted in a difficult purification (Scheme **1.19**).<sup>[53]</sup> Multiple successive purification attempts were required; however, two mono alkylated products were

isolated. These were the desired 2-alkylated pyrrole **1.19** and the undesired 3-alkylated pyrrole **1.19b** in a 14% and 3% yield respectively. In addition to the isolated mono alkylated products, m/z ratios consistent with a mixture of di-, tri- and tetra-alkylated pyrroles were observed by LCMS analysis. Following the synthesis of the desired 2-alkylated dodecyl pyrrole **1.19**, it was subjected to Vilsmeier–Haack formylation conditions generating pyrrole carboxylate **1.20** with an 86% yield.<sup>[54]</sup>



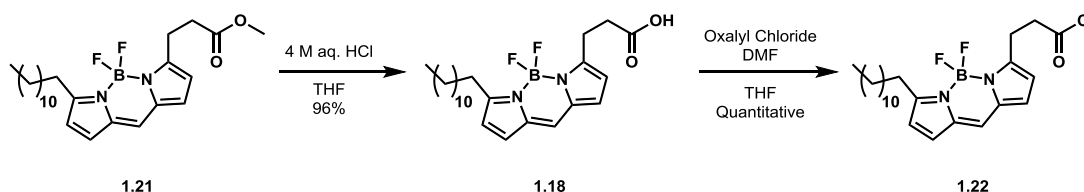
Scheme **1.19**. Alkylation of pyrrole to dodecyl pyrroles **1.19** and **1.19b**, followed by the Vilsmeier–Haack formylation of pyrrole **1.19** to pyrrole carboxylate **1.20**.

With pyrrole carboxylate **1.20** in hand, it was coupled with the previously synthesised pyrrole **1.4** (Scheme **1.1**, page 24) in the presence of phosphorus oxychloride and boron trifluoride generating the desired hetero bodipy **1.21** with a 55% yield (Scheme **1.20**).<sup>[42]</sup> In addition, the undesired dialkyl bodipy **1.21b** and diester bodipy **1.21c** were detected by NMR spectroscopy in 11% and 13% yields respectively.



Scheme **1.20**. Coupling of pyrroles **1.20** and **1.4** to generate the desired hetero bodipy **1.21** and the undesired homo bodipys **1.21b** and **1.21c**.

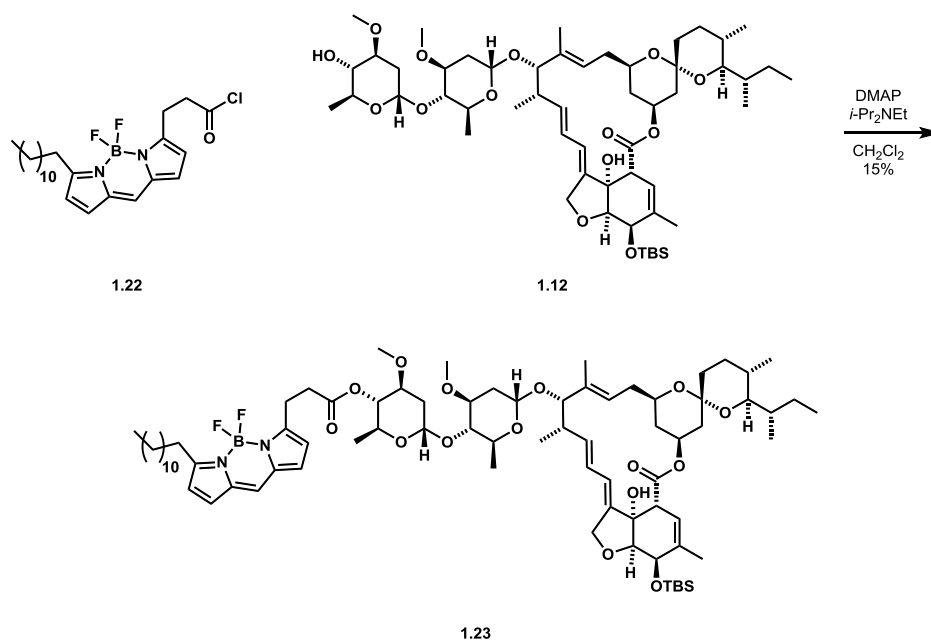
To complete the fatty bodipy fragment synthesis, bodipy methyl ester **1.21** was hydrolysed under acidic conditions to the corresponding bodipy acid **1.18** in a 96% yield (Scheme **1.21**). With the completion of the fatty bodipy fragment **1.18**, subsequent activation of acid **1.18** with oxalyl chloride and catalytic dimethylformamide to acyl chloride **1.22** prepared the fragment for coupling.<sup>[22]</sup>



Scheme **1.21**. Acidic hydrolysis of methyl ester **1.21** to acid **1.18** and the subsequent activation to acyl chloride **1.22**.

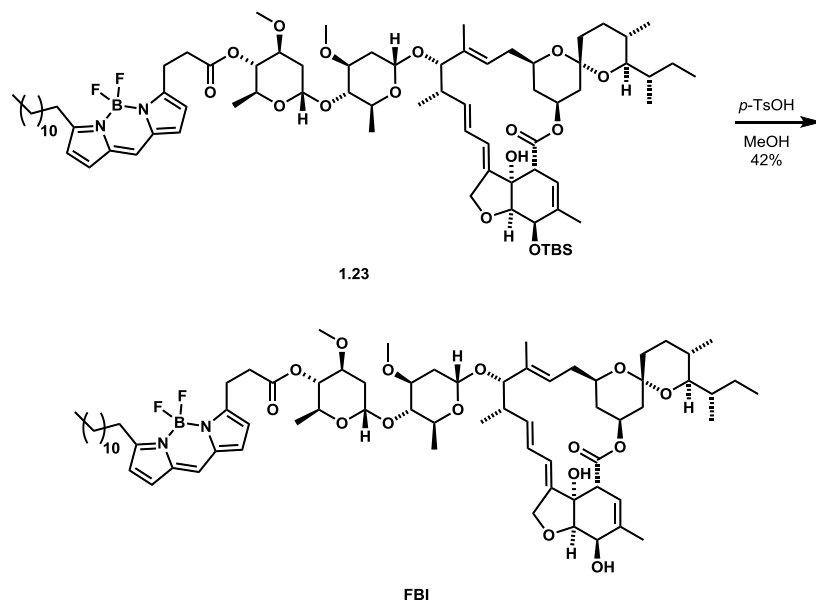
### 1.5.3 Completion of **FBI** Synthesis

To complete the synthesis of **FBI**, the bodipy acyl chloride **1.22** was coupled with the previously synthesised silyl ether **1.12** (Scheme 1.12, page 32) *via* an ester linkage. The coupling was achieved with the use of nucleophilic catalyst 4-dimethylaminopyridine under basic conditions, which afforded *tert*-butyldimethylsilyl ether **1.23** in a 15% yield (Scheme 1.22).<sup>[22]</sup>



Scheme 1.22. Coupling of acyl chloride **1.22** and silyl ether **1.12** to generate *tert*-butyldimethylsilyl ether **1.23**.

The final step in the synthesis of **FBI** was the deprotection of silyl ether **1.23** to the corresponding alcohol. To achieve this, silyl ether **1.23** was subjected to acidic deprotection conditions which successfully resulted in the generation of the lipophilic **FBI** probe with a 42% yield (Scheme 1.23).<sup>[22]</sup> With the synthesis of **FBI** complete, focus shifted to the biological testing of the lipophilic probe.



Scheme 1.23. Acidic deprotection of silyl ether **1.23** to generate lipophilic probe **FBI**.

## 1.6 FBI Biological Assaying

### 1.6.1 Materials and Methods

#### Nematode Strains and Culture

For the testing of **FBI**, the *Caenorhabditis elegans* strains utilised in the study were N2 (wild type, **ivermectin**-sensitive), *Dyf-7* (Dye filling defective, **ivermectin**-resistant) and *TP-238* (**ivermectin**-resistant). N2 and *Dyf-7* were supplied by the *C. elegans* Genetics Centre (USA). *TP-238* was generated by random ethyl methanesulfonate (EMS) mutagenesis and selection for **ivermectin** resistance by collaborator Prof Tony Page, Institute of Biodiversity, Animal Health and Comparative Medicine, University of Glasgow.<sup>[35]</sup> All strains were maintained on nematode growth media Petri plates supplemented with 50  $\mu$ L *Escherichia coli* OP50-1 liquid culture as described above (Nematode Strains and Culture, page 37).<sup>[49]</sup>

The field isolated strains of the parasitic nematode *Haemonchus contortus* (*H. contortus*) used in this study were MHco3 (**ivermectin**-sensitive), MHco17 (**ivermectin**-resistant) and MHco18 (**ivermectin**-resistant), which were kindly donated by Dave Bartley and Alison Morrison, Moredun Research Institute, UK. The supplied embryos were purified *via* saturated salt floatation from faecal samples derived from mono-specifically infected donor lambs. The purified eggs were then hatched to L1 larvae and allowed to develop to L2 and L3 larvae by culturing on NGM plates containing 5% whole sheep blood and supplemented with *E. coli* OP50-1.<sup>[35]</sup>

#### Nematode Microscopy Preparation

Same procedure as that utilised for the testing of **BLI** (Nematode Microscopy Preparation, page 37).

#### Dil staining Procedure

Same procedure as that utilised for the testing of **BLI** (**DiI** Staining Procedure, page 37).

#### Plate-Based Assay

Using sterile conditions either 5 mL of NGM or 4.95 mL of NGM and 50  $\mu$ L of whole sheep blood was added to a Petri plate and allowed to set. The plates were then seeded with 50  $\mu$ L of *E. coli* OP50-1 liquid culture followed by 50  $\mu$ L methanolic solution of the desired compound (generating a final concentration of 1% methanol). For assays utilising the free living nematode *C. elegans*, five adult N2 *C. elegans* were transferred to either NGM or 5% whole sheep blood NGM plates using a flamed 32 gauge

platinum wire before the plates were incubated at 20 °C in the dark with images taken at various time points over 96 hours. For assays involving the parasitic nematode *H. contortus*, L1 larvae were washed onto either NGM or 5% whole sheep blood NGM plates with a minimal amount of M9 buffer. The plates were then incubated at 20 °C in the dark with images taken at various time points over 96 hours.

### 1.6.2 FBI Study in Non-Parasitic Nematodes

#### Establishing FBI Efficacy

Similarly to the testing of **BLI** (1.3.2 **BLI** Study, page 38), the initial testing of **FBI** focussed on establishing if the nematicidal activity was comparable to the parent drug **ivermectin**, and thus to determine if **FBI** is a suitable probe for the purposes of this project. For this initial testing, the N2 strain (**ivermectin**-sensitive wild type) of the free-living *C. elegans* nematode was selected and the NGM plate-based assay described above (Plate-Based Assay, page 49) was utilised. With this assay, the positive indication of nematicidal activity was a complete elimination of the nematode population. A sub lethal concentration of a nematicidal compound produced a state of lethargy in the nematodes, with clearly reduced motility and a diminished population when compared to the population of nematodes treated with no compounds. When the concentration of a nematicidal compound is too low to produce any discernible effects (or when a non nematicidal control compound is administered) the negative readout from the assay is a thriving population with individuals displaying a normal motility rate.

With this in mind, N2 *C. elegans* were treated with various concentrations of **FBI**, **ivermectin** (positive control), 1% methanol (negative control) and no compounds (negative control). The controls performed as expected with no discernible difference between the nematodes treated with no compounds and those treated with 1% methanol (Figure 1.20). As expected, **ivermectin** displayed an effective lethal concentration of 10 nM which was indicated by a lack of any nematode population in the image of the assay plate (Figure 1.20). Interestingly, **FBI** produced a strong reduction in nematode motility and a slight reduction in the population size (when compared to the 1% methanol control) at a concentration of 10 nM and displayed an effective lethal concentration of 50 nM. As the observed lethal concentration of **FBI** compared to **ivermectin** was within the one order of magnitude self-imposed limit of efficacy loss, this positive result provided confidence that **FBI** was a suitable probe for studying the uptake route of **ivermectin**.

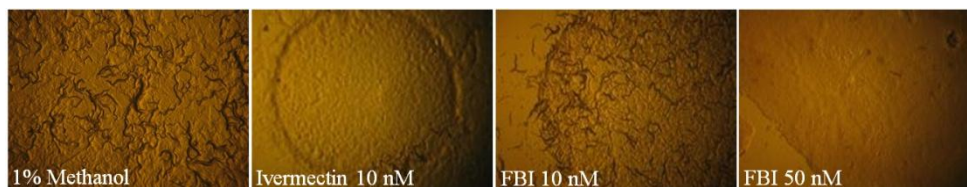
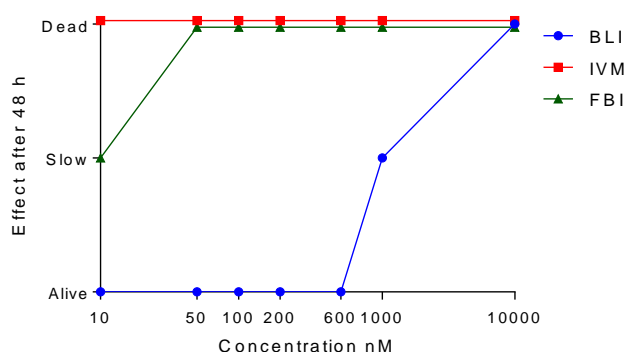


Figure 1.20. Plate images of nematode populations after treatment with 1% methanol, **ivermectin** and **FBI**.

A comparison of the efficacy of **FBI** with that of the original **BLI** probe shows how effective the lipophilic modifications to the original probe design were to the efficacy of **FBI** (Graph 1.2). The new lipophilic **FBI** has an effective lethal concentration of 50 nM, while the original **BLI** probe had an effective lethal concentration of 10  $\mu$ M.



Graph 1.2. Graph comparing the nematicidal efficacies of **ivermectin**, **FBI** and **BLI**.

### Establishing Ivermectin Route of Uptake

With the nematicidal efficacy of **FBI** established, fluorescence microscopy was conducted in an effort to elucidate the route of uptake of **ivermectin** in *C. elegans*. Included as a fluorescence negative control (but nematicidal positive control) is **ivermectin**, which at the lethal concentration of 10 nM clearly displays only gut granule autofluorescence with no amphid or nerve ring staining (Figure 1.21). Importantly however, **FBI** is shown to clearly stain the amphids and nerve ring of *C. elegans* nematodes at the lethal concentrations of 50 nM and 100 nM. The combination of lethality with the observed amphid and nerve ring staining constitutes strong evidence consistent with an amphidal route of uptake of **ivermectin**.

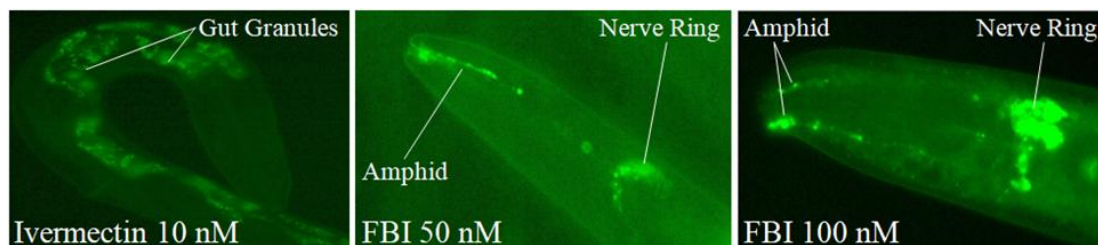


Figure 1.21. Fluorescence microscopy of *C. elegans* treated with **FBI** and **ivermectin**.

In order to corroborate this finding, the experiment was repeated with an additional control compound, bodipy methyl ester **1.21** (Figure 1.22). There were three main reasons for this negative control compound. The first was to ensure that the amphid and nerve ring staining was due to **ivermectin** induced selectivity and not merely non-specific staining with a lipophilic dye. The fact that amphid and nerve ring staining is observed concomitantly with nematode lethality is already strong evidence that the staining is not non-specific; however, this control served to further substantiate the claim. The second reason for this control was to ensure that the lethality observed was due to the **ivermectin** moiety of **FBI**, and not due to unanticipated bodipy-induced toxicity. And finally, this control served to probe the possibility of *in vivo* hydrolysis of the ester bond that connects the bodipy moiety of **FBI** to **ivermectin**. While the ester is significantly hindered and thus somewhat resistant to esterase hydrolysis, it could still be possible for hydrolysis to occur. If enzyme catalysed hydrolysis was occurring, it would be releasing the toxic **ivermectin** and a dodecyl bodipy fragment (Figure 1.22). With these two species present, it would have been possible that the **ivermectin** was causing the toxicity and that the lipophilic bodipy was causing the amphid and nerve staining. Therefore to address these three issues, bodipy **1.21** was administered to the **ivermectin**-sensitive N2 *C. elegans* strain as a negative control. Additionally an assay involving co-administration of bodipy **1.21** and **ivermectin** was administered to N2 *C. elegans* to simulate the effect of hydrolysis and to probe what how result of that possibility would manifest in the utilised assay conditions.

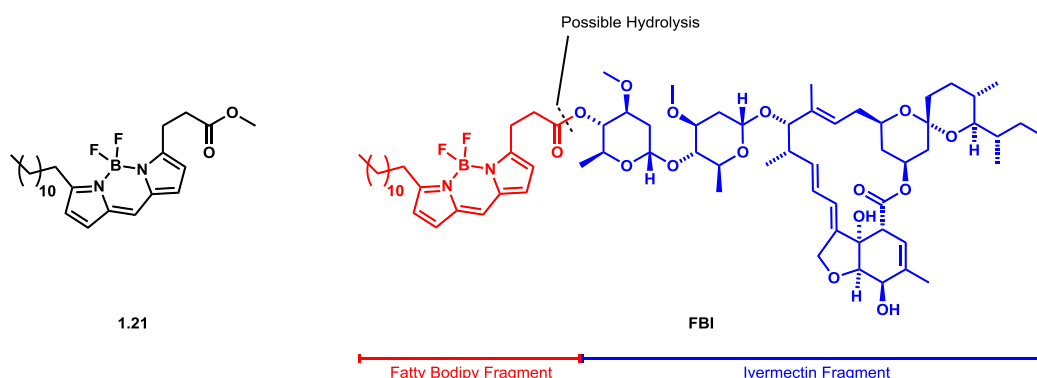


Figure 1.22. Structures of bodipy **1.21** and lipophilic probe **FBI**.

The ideal result of the bodipy **1.21** administration assay would be for bodipy **1.21** to produce no amphid or nerve ring staining in the **ivermectin**-sensitive N2 *C. elegans*, and additionally be non toxic to the nematodes. Indeed, it was observed that administration of 100 nM and 20  $\mu$ M (significantly higher than the 50 nM effective lethal concentration of **FBI**) bodipy **1.21** produced no discernible detrimental effect to the health, motility or population of N2 *C. elegans* when compared to the no compound and 1% methanol negative controls. Furthermore, when the nematodes were viewed under fluorescence microscopy, slight pharynx staining was observed (indicating ingestion). Importantly however, no staining of the amphids or nerve ring was observed at either 100 nM or 20  $\mu$ M (Figure **1.23**). This indicated that the lipophilic bodipy methyl ester **1.21** is non-nematicidal and does not accumulate in the amphids and thus the **FBI**-induced nematicidal activity and amphid and nerve ring staining of N2 *C. elegans* is likely a result of **ivermectin** dependant specificity.

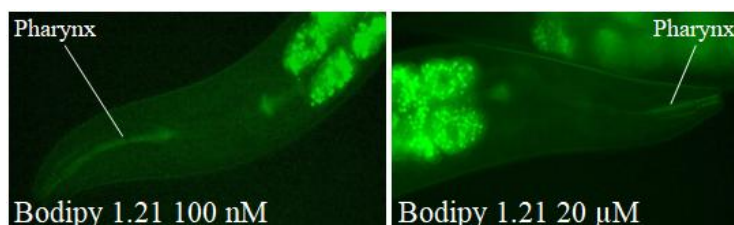


Figure **1.23**. Fluorescence microscopy of N2 *C. elegans* treated with 100 nM and 20  $\mu$ M bodipy **1.21**.

The ideal result from the co-administration of bodipy **1.21** and **ivermectin** would be to see **ivermectin** induced lethality of the nematodes, while simultaneously not observing bodipy **1.21** induced staining of the amphids or nerve ring. As expected after the abovementioned lack of bodipy **1.21** induced amphid or nerve ring staining, the co administration of bodipy **1.21** and **ivermectin** displayed nematicidal activity at 10 nM (expected from **ivermectin**) but resulted in no amphid or nerve ring staining at either 10 nM or 100 nM. This result generated a high degree of confidence that the ester linkage connecting the bodipy moiety to **ivermectin** in the lipophilic probe **FBI** was likely intact for the duration of the assay. These assays successfully provided additional evidence consistent with an amphidal route of uptake of **ivermectin** in *C. elegans*.

### Elucidating **Ivermectin** Resistance Mechanism

Having established the amphidal route of **ivermectin** uptake in the wild type (**ivermectin**-sensitive) N2 *C. elegans*, the next step was to investigate the primary operative mechanism of resistance. As stated above (1.1.6 Hypotheses and Project Aims, page 22), the hypothesis for this project is that a primary operative **ivermectin**

resistance mechanism is impaired drug uptake, due to mutation(s) causing loss-of-function of the amphid sensory structures. In order to probe this hypothesis, two **ivermectin**-resistant *C. elegans* strains were selected. The first strain chosen was the dye filling defective *Dyf-7* which is characterised by an inability to uptake lipophilic dyes (such as **DiI**) due to defective amphids. The second strain chosen was *TP-238* which is an **ivermectin**-resistant strain developed through random chemical mutagenesis (ethyl methanesulfonate) and selection for **ivermectin** resistance by collaborator Prof Tony Page. Both *Dyf-7* and *TP-238* exclude lipophilic dyes (such as **DiI**) thus indicating defective amphids. To confirm the hypothesis of a link between these defective amphids and **ivermectin** resistance, both these **ivermectin**-resistant strains were treated with **FBI**. Initially, it was important to establish whether the **ivermectin**-resistant *Dyf-7* and *TP-238* strains were also resistant to **FBI**. If this was not the case, it would imply that **ivermectin** and **FBI** do not share the same mechanism of action which would indicate **FBI** to be a poor chemical probe for this study.

Upon treatment of both **ivermectin**-resistant *C. elegans* strains *Dyf-7* and *TP-238* with 100 nM **FBI** (twice the effective lethal concentration in **ivermectin**-sensitive N2 *C. elegans*), no lethality was observed (Figure 1.24). The pictures of the NGM plates that the assay was conducted on shows that both the population and motility of *Dyf-7* and *TP-238* were unaffected by the administration of 100 nM **FBI**. Included for reference, is the administration of **FBI** to the **ivermectin**-sensitive N2 *C. elegans* strain for which 100 nM is a sufficiently lethal concentration to reduce to population to zero. This established that **ivermectin**-resistant *C. elegans* are also resistant to the **ivermectin**-based **FBI** probe, thus further validating **FBI** as a suitable probe to study **ivermectin** resistance in nematodes.

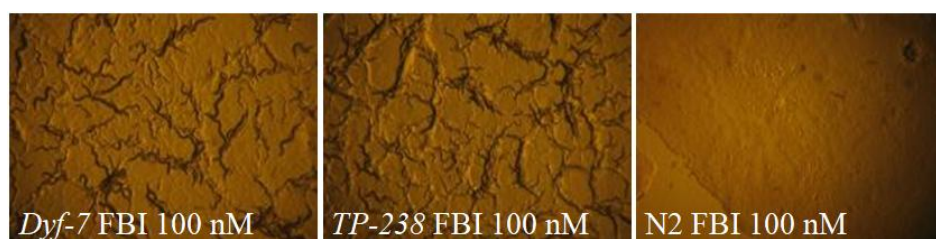


Figure 1.24. Treatment of **ivermectin**-resistant *Dyf-7* and *Tp-238* and **ivermectin**-sensitive N2 *C. elegans* with 100 nM **FBI**.

Having established **FBI** resistance in *Dyf-7* and *TP-238*, fluorescence microscopy was conducted which displayed no amphid or nerve ring staining (Figure 1.25). Included for reference is the **ivermectin**-sensitive N2 strain treated with 100 nM **FBI**. The observation of a lack of nematicidal activity combined with the lack of amphid or nerve

ring staining constitutes strong evidence consistent with an amphidal route of uptake of **ivermectin** in the free-living nematode *C. elegans*. Furthermore, these results have established a primary operative **ivermectin** resistance mechanism of impaired drug uptake due to mutations resulting in amphid loss-of-function.

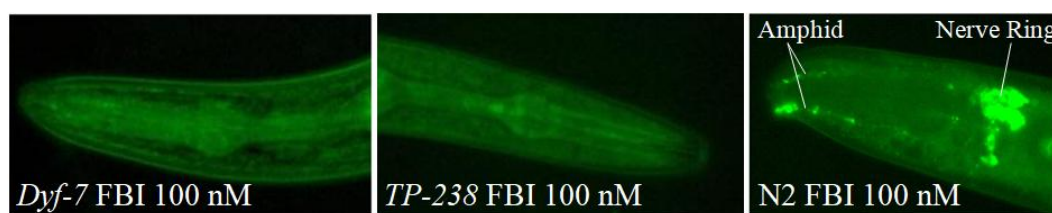


Figure 1.25. Fluorescent microscopy of **ivermectin**-resistant *Dyf-7* and *Tp-238* and **ivermectin**-sensitive N2 *C. elegans* with 100 nM **FBI** administration.

### 1.6.3 FBI Study in Clinically Relevant Parasitic Nematodes

With the establishment of an amphidal route of **ivermectin** uptake and an impaired drug uptake resistance mechanism in the non-parasitic *C. elegans* nematode, testing of **FBI** became focussed on elucidating the route of **ivermectin** uptake in clinically relevant parasitic nematodes. For this purpose, the ruminant parasite *Haemonchus contortus* (*H. contortus*) was selected as it is one of the most economically significant livestock parasites worldwide.<sup>[55]</sup>

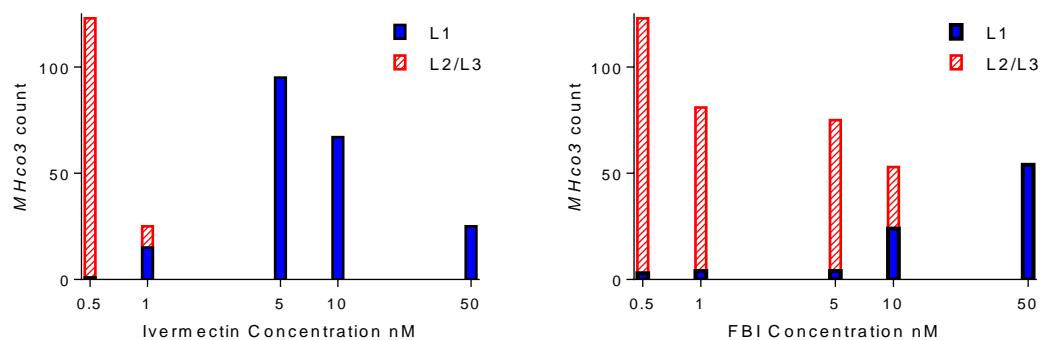
#### Adaptation of Assay Conditions

In the absence of a nematicidal compound, *H. contortus* eggs naturally hatch to L1 (larval stage 1) before progression to L2 (larval stage 2) and then L3 (larval stage 3) at which point they would either naturally infect a host and progress to L4 (larval stage 4) and subsequent adulthood, or enter a coiled L3 state in which they lay dormant until ingested by a host organism. Due to the difficulty of culturing parasitic nematodes in the absence of a host, 5% whole sheep blood was added to the nematode growth media agar plates in the assays, which appeared to have a positive effect on the health and development of the *H. contortus* larvae. As the assays were conducted on this 5% sheep blood infused nematode growth media and in the absence of a host organism, the terminus of the assay was the appearance of the coiled L3 state. Control assays of N2 *C. elegans* (**ivermectin**-sensitive) grown on nematode growth media containing 5% whole sheep blood were conducted to ensure that the addition of sheep blood to the assay did not interfere with the operation of **FBI** or any of the controls. The results from these assays were indistinguishable from the results of the NGM plates without 5% sheep blood, thus determining the addition of sheep blood to have no detrimental effect on the operation of any of the tested compounds.

Additionally, in previous testing with the non-parasitic nematode *C. elegans* the indication of positive nematicidal activity was complete elimination of the population. However, the *H. contortus* larvae used in the following assays were not sexually mature and thus could not reproduce or grow the population. With this in mind, a different approach to measure the nematicidal efficacy of compounds was utilised. Instead of lethality and population monitoring, the metric used to determine efficacy was to monitor the larval stage progression of the parasitic *H. contortus*. In the absence of a nematicidal compound, or in the presence of sub-lethal concentrations of a nematicidal compound, the larval stage of *H. contortus* progressed naturally from egg to L1 to L2 to L3. In the presence of an efficacious concentration of a nematicidal compound, the larval progression of the parasitic *H. contortus* was arrested at the L1 larval stage. Thus nematicidal efficacy of compounds for these parasitic nematode assays was determined by the percentage of the population that was arrested at the L1 larval stage.

#### Establishing Comparable Efficacy of **FBI** and **Ivermectin**

The initial testing was to establish if the **ivermectin**-based lipophilic probe **FBI** was as effective at arresting the development of *H. contortus* larvae as the parent drug **ivermectin**. As with previous testing, this was to establish the utility of **FBI** as a chemical probe for studying **ivermectin** resistance in parasitic species of nematode. With this in mind, *MHco3* (**ivermectin**-sensitive *H. contortus*) eggs were treated with **ivermectin** (positive control), **FBI**, 1% methanol (negative control) and no compound (negative control). As with the non-parasitic *C. elegans*, treatment of the parasitic larvae with 1% methanol did not result in any discernible effect in comparison to the no compound negative control. Measurements of larval stage progression of the **ivermectin**-sensitive *MHco3* parasites were taken at 24 and 94 hours (at which point the assay was terminated) which determined the effective concentration of **ivermectin** (that which was required to arrest the development of the population at the L1 larval stage) against *H. contortus* to be 5 nM (Graph 1.3). The effective concentration of **FBI** was determined to be 50 nM which was within the limit of acceptable efficacy loss of one order of magnitude.



Graph 1.3. Graphs showing the counts of each *MHco3* larval stage after 96 hours of treatment with varying concentrations of **ivermectin** and **FBI**.

### Establishing Ivermectin Route of Uptake in Parasitic Nematodes

Fluorescence microscopy of the **FBI** treated nematodes was then conducted to establish the route of **ivermectin** uptake in **ivermectin**-sensitive parasitic nematodes. Intriguingly, the **ivermectin**-sensitive *MHco3* that was effectively arrested at the L1 larval stage by 50 nM **FBI** showed no sign of amphid or nerve ring staining (Figure 1.26). Instead of amphid uptake, there was heavy staining of the parasites' pharynx (mouth) and lumen (digestive tract) indicating ingestion of the probe. To ensure the amphids were functional, the *MHco3* larvae were also stained with the commercial dye **DiI** which showed strong amphid and nerve ring staining, indicating the integrity of the amphid sensory structures to be intact. With the correlation of effective **FBI**-induced arrested development of larval progression and the observed pharynx and lumen staining at the effective concentration, it appeared evident that the primary route of **ivermectin** uptake in the parasitic *H. contortus* is pharyngeal and not amphidal (as was the case with the non-parasitic *C. elegans* model).

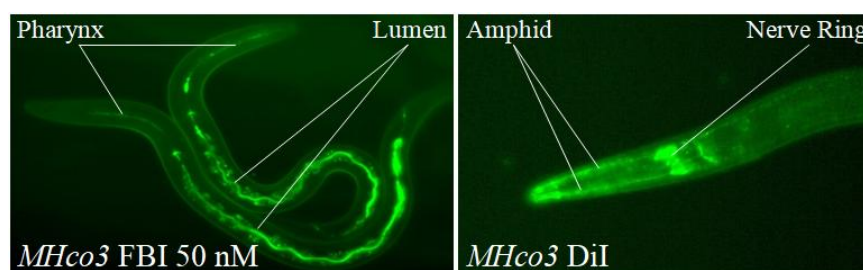


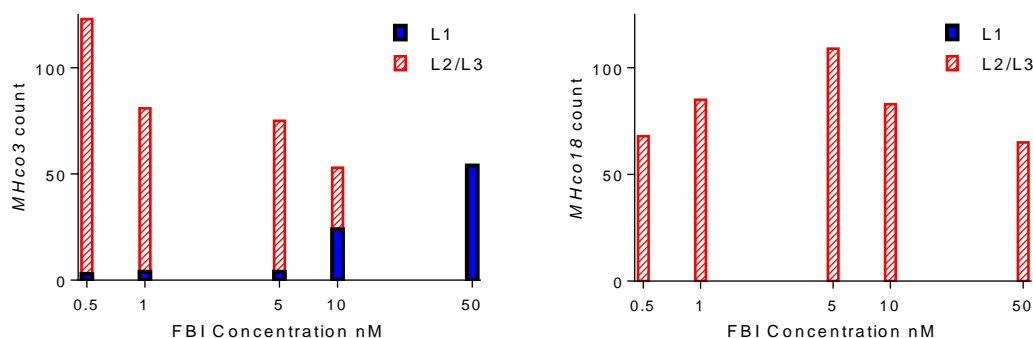
Figure 1.26. Fluorescent microscopy of **ivermectin**-sensitive *MHco3* parasites treated with 50 nM **FBI** and the lipophilic dye **DiI**.

### Probing Ivermectin Resistance Mechanism in Parasitic Nematodes

With the unexpected discovery of an alternative pharyngeal route of **ivermectin** uptake in parasitic nematodes (compared to the non-parasitic amphidal route of **ivermectin**

uptake), testing was conducted in **ivermectin**-resistant *H. contortus* parasites in an effort to elucidate possible operative **ivermectin** resistance mechanisms in parasitic species. For this testing, the **ivermectin**-resistant *MHco18* strain of *H. contortus* was utilised, which is a clinically-relevant multi drug resistant strain.<sup>[56][57]</sup> *MHco18* was originally isolated from sheep and is a triple-resistant field-isolate, resistant to **ivermectin**, **levamisole** and the benzimidazoles.<sup>[56]</sup>

For the testing, *MHco18* was treated with **FBI**, **ivermectin** (positive control), 1% methanol (negative control) and no compounds (negative control). As expected, the 1% methanol had no detrimental effect to the nematodes compared to that of the no compound negative control. As established above, the **ivermectin**-sensitive *MHco3* strain, a concentration of 50 nM **FBI** was sufficient to effectively arrest the development of the larvae at the L1 larval stage (Graph 1.4). This same concentration of **FBI** against the **ivermectin**-resistant *MHco18* strain failed to effectively arrest the development of the larvae at the L1 larval stage, thus demonstrating that **ivermectin**-resistant *H. contortus* are also resistant to **FBI**. **FBI** was therefore determined to be a suitable probe to study **ivermectin** resistance in this parasitic strain.



Graph 1.4. Comparison of nematode larval stage counts from *MHco3* and *MHco18* after treatment with varying concentrations of **FBI**.

Fluorescence microscopy of the **FBI** treated **ivermectin**-resistant *MHco18* nematodes showed no probe-induced staining of the amphids, nerve ring, pharynx or lumen (Figure 1.27). The lack of amphid and nerve ring staining was expected after the lack of staining observed in the **ivermectin**-sensitive parasite *MHco3*. The lack of pharynx and lumen staining in the **ivermectin**-resistant *MHco18* coupled with the effective arrested larval development further corroborates the abovementioned establishment of a pharyngeal route of **ivermectin** uptake in the parasitic *H. contortus*.

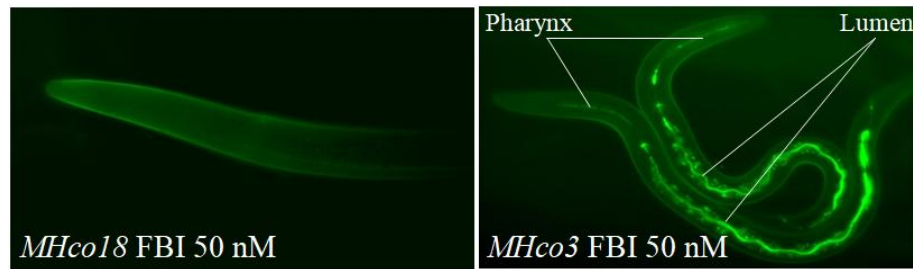


Figure 1.27. Fluorescence microscopy of **ivermectin**-resistant *MHco18* and **ivermectin**-sensitive *MHco3* parasites with 50 nM **FBI**.

With the discovery of a pharyngeal route of **ivermectin** uptake in the **ivermectin**-sensitive parasitic *H. contortus* and a lack of **FBI** accumulation in the **ivermectin**-resistant *H. contortus*, several possibilities exist as to the operative mechanism of **ivermectin** resistance in parasitic species. In order to elucidate the primary operative mechanism(s) of **ivermectin** resistance in parasitic nematodes, further biological investigation is required as the utility of the **FBI** probe has reached its limit.

## 1.7 Conclusions

The initial fluorescent **ivermectin**-based probe **BLI** (Bodipy-Linker-Ivermectin) (Figure 1.28) was successfully synthesised and tested against **ivermectin**-sensitive *C. elegans*. For the testing of **BLI**, the initially attempted and ineffective free-swimming assay (Free Swimming Assay, page 38) produced inconsistent results from the control compounds. With this in mind, an alternative plate-based assay was successfully developed which produced consistent and expected results for the utilised control compounds. This assay subsequently revealed **BLI** to be a poor probe for studying **ivermectin** resistance due to a 1000-fold loss of efficacy compared to the parent drug **ivermectin**.

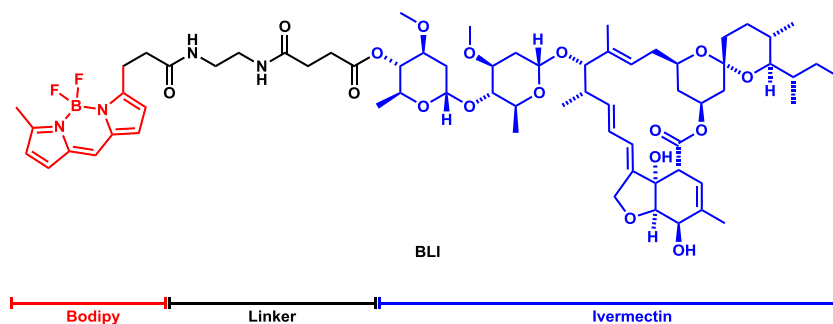


Figure 1.28. Structure of the ineffective **BLI** probe.

Using calculated physical chemistry parameters, the probe was successfully redesigned with the aim of increased lipophilicity. The new lipophilic probe **FBI** (Figure 1.29) was then successfully synthesised utilising common intermediates from the synthesis of the ineffective **BLI** probe.

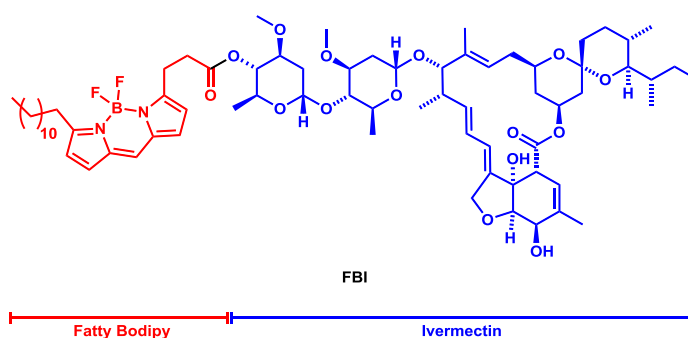


Figure 1.29. Structure of redesigned lipophilic **FBI** probe.

Testing of **FBI** was conducted using the non-parasitic *C. elegans* nematode as a model organism. Using the **ivermectin**-sensitive N2 (wild type) strain of *C. elegans*, **FBI** was shown to be taken up through the amphid sensory structures. This observation, when correlated with concomitant lethality, generated evidence consistent with an amphidal route of **ivermectin** uptake in *C. elegans*. Having achieved the first aim of establishing

the route of uptake of **ivermectin**, the second aim of establishing a primary operative mechanism of resistance was addressed. To achieve this, **ivermectin**-resistant *C. elegans* were treated with **FBI** and were determined to also be resistant to **FBI**. Fluorescence microscopy was utilised which showed a lack of amphidal uptake of **FBI** which was concomitant with an observed lack of nematicidal activity. With these results, impaired drug uptake *via* loss-of-function amphid mutations was established as a primary mechanism of **ivermectin** resistance in the non-parasitic *C. elegans* nematode.

With the successful testing of **FBI** in the non-parasitic *C. elegans* nematode complete, **FBI** was administered to the clinically relevant parasitic nematode *H. contortus*. Administration of **FBI** to **ivermectin**-sensitive *H. contortus* indicated an alternative pharyngeal route of **ivermectin** uptake compared to the amphidal route in the non-parasitic *C. elegans*. This finding was intriguing due to the known homology between *C. elegans* and *H. contortus* amphid structure.<sup>[50]</sup> With this information, testing of **FBI** was conducted in **ivermectin**-resistant *H. contortus* which showed a complete exclusion of the probe from the organism. While this was consistent with the impaired drug uptake resistance mechanism, several possible explanations of this observation exist. As the practical limit of the lipophilic **FBI** probe has been reached, further biological investigation is required to elucidate the exact operative resistance mechanism(s).

## 1.8 Future Work

Future chemical biology work for this project could involve optimisation of the route to **FBI** or a slight adjustment of the structure of **FBI** to allow a more facile synthesis. The current synthesis involves the alkylation of pyrrole to dodecyl pyrrole **1.19** (Scheme **1.19**, page 46), which produced a complex mixture of mono- and polyalkylated isomers that resulted in a difficult and time consuming purification process. Additionally, the synthesis of unsymmetrical bodipy moieties in the synthesis of both **BLI** (Scheme **1.2**, page 25) and **FBI** (Scheme **1.20**, page 46) resulted in the generation of undesired homo ‘dimer’ bodipys in addition to the desired hetero ‘dimer’ bodipy. These undesired side products significantly lowered the yield of the desired bodipy and in the process, wasted valuable starting materials. By redesigning **FBI** to include a symmetrical bodipy linked to **ivermectin** at the 8 position of the bodipy core (Figure **1.30**) instead of the 3 position currently utilised, the synthesis would remove the possibility of homo dimer formation. Furthermore, this adaptation would allow the bodipy synthesis to be conducted using commercially available materials, thus streamlining the synthesis.

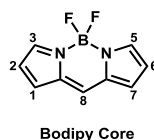


Figure **1.30**. Structure of bodipy core with position numbering.

Additionally, fluorescent probes should be developed based on anthelmintic drugs of different classes, such as **albendazole** from the benzimidazole class (Figure **1.31**). Using fluorescent probes of different drug classes, it would be possible to further investigate the resistance mechanisms in regards to multi drug class resistance. Mutation to the target of a drug class may confer resistance to a particular drug but is unlikely to confer resistance to different classes of anthelmintics that do not inhibit that particular target. As **FBI** has established a target-independent resistance mechanism in *C. elegans*, it would be interesting to investigate if the benzimidazole drug class also has an amphidal uptake mechanism, and if so, if defective amphids also confer benzimidazole resistance.

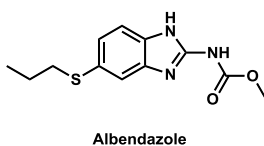


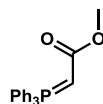
Figure **1.31**. Structure of the benzimidazole **Albendazole**.

## 1.9 Experimental

### 1.9.1 General Methods

All reagents were purchased from commercial suppliers and used without further purification unless otherwise stated. Reactions involving air-sensitive agents and dry solvents were performed in glassware that had been dried in an oven (150 °C) or flame-dried *in vacuo* and allowed to cool *in vacuo* before being flushed with argon. These reactions were carried out with the exclusion of air using an argon atmosphere. Reactions were monitored by thin layer chromatography (TLC) on Merck silica gel 60 covered aluminium sheets. TLC plates were developed under UV-light and/or with an acidic ethanolic anisaldehyde solution or a KMnO<sub>4</sub> solution. NMR spectra were recorded on a Bruker DPX-400 spectrometer (<sup>1</sup>H NMR at 400 MHz, <sup>13</sup>C NMR at 100 MHz, <sup>19</sup>F NMR at 377 MHz and <sup>11</sup>B NMR at 128 MHz) or a Bruker DPX-500 spectrometer (<sup>1</sup>H NMR at 500 MHz and <sup>13</sup>C NMR at 125 MHz). Chemical shifts are reported in ppm. <sup>1</sup>H NMR spectra were recorded with CDCl<sub>3</sub> or CD<sub>3</sub>OD as the solvent using residual CHCl<sub>3</sub> (δ = 7.26) or CHD<sub>2</sub>OD (δ = 3.31) as internal standard, and for <sup>13</sup>C NMR spectra the chemical shifts are reported relative to the central resonance of CDCl<sub>3</sub> (δ = 77.16) or CD<sub>3</sub>OD (δ = 49.00). Signals in NMR spectra are described as singlet (s), doublet (d), triplet (t), quartet (q), multiplet (m), broad (br) or a combination of these, which refers to the spin-spin coupling pattern. Spin-spin coupling constants are reported in Hertz (Hz) and are uncorrected. Two-dimensional NMR spectroscopy (COSY, HSQC, HMBC, NOESY) and <sup>13</sup>C DEPT NMR spectroscopy were used where appropriate to assist the assignment of signals in the <sup>1</sup>H and <sup>13</sup>C NMR spectra. IR spectra were obtained employing a Shimadzu FTIR-8400 instrument with a Golden Gate™ attachment that uses a type IIa diamond as a single reflection element so that the IR spectrum of the compound (solid or liquid) could be detected directly (thin layer). Melting point ranges were collected using a Barnstead Electrothermal 9100 melting point apparatus. High resolution mass spectra were recorded under ESI or EI conditions by the analytical services at the University of Glasgow. Liquid chromatography-mass spectrometry was conducted using a Thermo Scientific Dionex UltiMate 3000 LC system coupled with a Thermo Scientific LCQ Fleet ion trap mass spectrometer. A Dr Maisch GmbH Reprosil Gold 120 C18 3µm 150x4 mm column was used with UV absorption detected at 214 nm. A linear gradient of 5%–95% HPLC grade acetonitrile in ultra pure water with 0.1% trifluoroacetic acid over 10 or 40 minutes was utilised with a flow rate of 1 mLmin<sup>-1</sup>. UV-Vis-NIR absorbance spectra were recorded using a Perkin Elmer LAMBDA 1050 spectrophotometer.

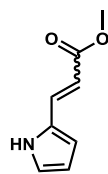
### 1.9.2 Preparation of Compounds



1.2

**1.2.** Prepared according to a modified literature procedure.<sup>[39]</sup> To a stirred solution of triphenylphosphine (4.10 g, 15.6 mmol, 1.1 equiv.) in ethyl acetate (24 mL, 0.65 M) was added a solution of 2-bromoacetate (1.40 mL, 14.9 mmol, 1.0 equiv.) in ethyl acetate (4.5 mL, 3.3 M) and the resulting solution was stirred at room temperature for 18 hours. The resulting white precipitate was collected by filtration, washed with diethyl ether and dried under vacuum. The white solid was dissolved in dichloromethane (34 mL) and a solution of sodium hydroxide (1.31 g, 32.7 mmol, 2.2 equiv.) in water (33 mL, 1 M) was added and stirred at room temperature for 15 minutes. The aqueous phase was extracted with dichloromethane (2 x 30 mL) and the combined organic extracts were dried with magnesium sulphate, filtered and concentrated in vacuo yielding title compound **1.2** (4.80 g, 14.4 mmol, 96%) as a white solid. Analytical data observed were in accordance with literature values.<sup>[39]</sup>

<sup>1</sup>H NMR (400 MHz, CDCl<sub>3</sub>) δ 7.68–7.63 (6H, m, 6 x Ar-CH), 7.57–7.53 (3H, m, 3 x Ar-CH), 7.48–7.44 (6H, m, 6 x Ar-CH), 3.56 (3H, br s, -OCH<sub>3</sub>), 2.92 (1H, br s, -COCH). HRMS (ESI) exact mass calculated for C<sub>21</sub>H<sub>20</sub>PO<sub>2</sub>Na [M+Na]<sup>+</sup> m/z 335.1195, found m/z 335.1194. IR (thin film) 2961, 1616, 1566. Melting point 165–167 °C (lit. 167-168 °C).<sup>[39]</sup> Elemental analysis calculated for C<sub>21</sub>H<sub>19</sub>O<sub>2</sub>P: C, 75.44%, H, 5.73%. Found C, 75.43%, H, 5.79%.

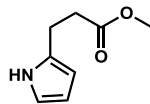


*E* = 1.3*E*  
*Z* = 1.3*Z*

**1.3*E*** and **1.3*Z***. Prepared according to a modified literature procedure.<sup>[40]</sup> To a stirred solution of ylide **1.2** (4.80 g, 14.4 mmol, 1.2 equiv.) in toluene (50 mL, 0.3 M) was added pyrrole-2-carboxaldehyde (1.11 g, 11.7 mmol, 1 equiv.) and the resulting solution was stirred at reflux for 18 hours forming a dark yellow/brown solution. The solvent was removed *in vacuo* and the resulting dark brown oil dissolved in diethyl ether. The resulting suspension was filtered and the filtrate was concentrated *in vacuo* yielding a crude mixture of **1.3** as *E* and *Z* isomers (6.7 *E*:1 *Z*). Purification by column chromatography on silica gel with an eluent of 30% diethyl ether in petroleum ether afforded **1.3*E*** (1.44 g, 9.54 mmol, 85%), and **1.3*Z*** (0.220 g, 1.46 mmol, 13%). Analytical data observed were in accordance with literature values.<sup>[58]</sup>

**1.3*E***.  $R_f = 0.33$  in 40% diethyl ether in petroleum ether.  $^1\text{H NMR}$  (400 MHz,  $\text{CDCl}_3$ )  $\delta$  8.68 (1H, br s, -NH), 7.56 (1H, d,  $J = 15.9$ , -CH), 6.93 (1H, ddd,  $J = 2.7, 2.7, 1.4$ , Ar-CH), 6.57 (1H, ddd,  $J = 3.8, 2.5, 1.4$ , Ar-CH), 6.29 (1H, ddd,  $J = 3.7, 2.6, 2.6$ , Ar-CH), 6.00 (1H, d,  $J = 15.9$ , -CH), 3.78 (3H, s, -OCH<sub>3</sub>).  $^{13}\text{C NMR}$  (101 MHz,  $\text{CDCl}_3$ )  $\delta$  168.4 (-COOR), 134.7 (-CH), 128.5 (Ar-C), 122.6 (Ar-CH), 114.6 (-CH), 111.1 (Ar-CH), 110.9 (Ar-CH), 51.7 (-OCH<sub>3</sub>). HRMS (ESI) exact mass calculated for  $\text{C}_8\text{H}_9\text{NO}_2\text{Na}$   $[\text{M}+\text{Na}]^+$   $m/z$  174.0525, found  $m/z$  174.0520.

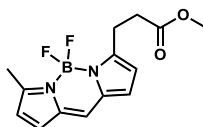
**1.3*Z***.  $R_f = 0.74$  in 40% diethyl ether in petroleum ether.  $^1\text{H NMR}$  (400 MHz,  $\text{CDCl}_3$ )  $\delta$  12.21 (1H, br s, -NH), 7.01 (1H, ddd,  $J = 2.7, 2.7, 1.4$ , Ar-CH), 6.78 (1H, d,  $J = 12.4$ , -CH), 6.52 (1H, ddd,  $J = 3.7, 2.6, 1.5$ , Ar-CH), 6.27 (1H, ddd,  $J = 3.6, 2.6, 2.5$ , Ar-CH), 5.54 (1H, d,  $J = 12.4$ , -CH), 3.77 (3H, s, -OCH<sub>3</sub>).  $^{13}\text{C NMR}$  (101 MHz,  $\text{CDCl}_3$ )  $\delta$  169.8 (-COOR), 135.0 (-CH), 129.2 (Ar-C), 123.1 (Ar-CH), 118.9 (-CH), 110.3 (Ar-CH), 107.3 (Ar-CH), 51.7 (-OCH<sub>3</sub>). HRMS (ESI) exact mass calculated for  $\text{C}_8\text{H}_9\text{NO}_2\text{Na}$   $[\text{M}+\text{Na}]^+$   $m/z$  174.0525, found  $m/z$  174.0527.



1.4

**1.4.** Prepared according to a modified literature procedure.<sup>[41]</sup> To a stirred suspension of 10% palladium on carbon (99 mg, 0.093 mmol, 10 mol%) in methanol (30 mL, 0.03 M) under argon atmosphere at room temperature was added a solution of olefin **1.3E** (1.4 g, 9.3 mmol, 1 equiv.) in methanol (20 mL, 0.5 M). The flask was then evacuated and the suspension sparged with hydrogen gas for 5 minutes and then stirred at room temperature under a hydrogen atmosphere for 18 hours. The hydrogen was then removed under reduced pressure and the suspension sparged with argon (x 3). The suspension was then filtered through a pad of celite (300 g) in dichloromethane (200 mL) and the celite washed with dichloromethane (500 mL). The organic phase was then concentrated *in vacuo* generating title compound **1.4** (1.3 g, 0.85 mmol, 87%) as a pale yellow oil. Analytical data observed were in accordance with literature values.<sup>[59]</sup>

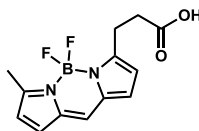
<sup>1</sup>H NMR (400 MHz, CDCl<sub>3</sub>) δ 8.53 (1H, br s, -NH), 6.67 (1H, ddd, *J* = 2.6, 2.6, 1.6, Ar-CH), 6.11 (1H, ddd, *J* = 2.7, 2.7, 2.7, Ar-CH), 5.94–5.91 (1H, m, Ar-CH), 3.70 (3H, s, -OCH<sub>3</sub>), 2.92 (2H, t, *J* = 6.9, -CH<sub>2</sub>), 2.65 (2H, t, *J* = 6.8, -COCH<sub>2</sub>). <sup>13</sup>C NMR (101 MHz, CDCl<sub>3</sub>) δ 174.6 (-COOR), 131.1 (Ar-C), 116.9 (Ar-CH), 108.2 (Ar-CH), 105.6 (Ar-CH), 51.9 (-OCH<sub>3</sub>), 34.5 (-COCH<sub>2</sub>), 22.7 (-CH<sub>2</sub>). HRMS (ESI) exact mass calculated for C<sub>8</sub>H<sub>11</sub>NO<sub>2</sub>Na [M+Na]<sup>+</sup> *m/z* 176.0682, found *m/z* 176.0683. IR (thin film) 2951, 1721, 1674, 1570.



1.6

**1.6.** Prepared according to a modified literature procedure.<sup>[42]</sup> To a stirred solution of pyrrole **1.4** (0.30 g, 2.0 mmol, 1 equiv.) and aldehyde **1.5** (0.23 g, 2.2 mmol, 1.1 equiv.) in anhydrous dichloromethane (6 mL, 0.3 M) at 0 °C was added dropwise POCl<sub>3</sub> (0.20 mL, 2.2 mmol, 1.1 equiv.) and the resulting solution was stirred at 0 °C for 30 minutes, warmed to room temperature and stirred for six hours. The reaction mixture was cooled to 0 °C and *N,N*-diisopropylethylamine (1.4 mL, 8.2 mmol, 4.2 equiv.) and BF<sub>3</sub>•OEt<sub>2</sub> (0.97 mL, 7.9 mmol, 4 equiv.) were added and the reaction was warmed to room temperature and stirred for 12 hours. To the reaction mixture was added water (10 mL) and the aqueous phase was extracted with dichloromethane (3 x 10 mL). The combined organic extracts were washed with brine (1 x 10 mL), dried with magnesium sulphate, filtered and concentrated *in vacuo*. Purification by column chromatography on silica gel with an eluent of 10% to 40% diethyl ether in petroleum ether afforded title compound **1.6** (0.26 g, 0.89 mmol, 46%) as a red/green solid.

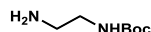
R<sub>f</sub> = 0.38 in 40% diethyl ether in petroleum ether. <sup>1</sup>H NMR (400 MHz, CDCl<sub>3</sub>) δ 7.09 (1H, s, Ar-CH), 6.97 (1H, d, *J* = 4.2, Ar-CH), 6.94 (1H, d, *J* = 4.2, Ar-CH), 6.31 (1H, d, *J* = 4.1, Ar-CH), 6.29 (1H, d, *J* = 4.2, Ar-CH), 3.70 (3H, s, -OCH<sub>3</sub>), 3.32 (2H, t, *J* = 7.6, -CH<sub>2</sub>), 2.78 (2H, t, *J* = 7.6, -COCH<sub>2</sub>), 2.62 (3H, s, -CH<sub>3</sub>). <sup>13</sup>C NMR (100 MHz, CDCl<sub>3</sub>) δ 172.9 (-COOR), 159.7 (Ar-C), 159.6 (Ar-C), 135.3 (Ar-C), 134.5 (Ar-C), 131.0 (Ar-CH), 129.9 (Ar-CH), 127.5 (Ar-CH), 120.4 (Ar-CH), 118.0 (Ar-CH), 51.9 (-OCH<sub>3</sub>), 33.3 (-COCH<sub>2</sub>), 24.2 (-CH<sub>2</sub>), 15.6 (-CH<sub>3</sub>). <sup>19</sup>F NMR (377 MHz, CDCl<sub>3</sub>) δ -145.9 (2F, 1:1:1:1 q, *J* = 32.8, -BF<sub>2</sub>). <sup>11</sup>B NMR (128 MHz, CDCl<sub>3</sub>) δ 0.95 (1B, t, *J* = 32.9, -BF<sub>2</sub>). HRMS (ESI) exact mass calculated for C<sub>14</sub>H<sub>15</sub>BF<sub>2</sub>N<sub>2</sub>O<sub>2</sub>Na [M+Na]<sup>+</sup> m/z 315.1087, found m/z 315.1085. IR (thin film) 2928, 1726, 1593, 1487. Melting point 104–105 °C.



1.7

**1.7.** To a stirred solution of methyl ester **1.6** (0.17 g, 0.58 mmol, 1 equiv.) in tetrahydrofuran (23 mL, 0.03 M) was added 4 M aqueous hydrochloric acid (27 mL) and the resulting solution was stirred at room temperature for 30 hours. To the reaction mixture was added dichloromethane (30 mL) and the phases were separated. The aqueous phase was extracted with dichloromethane (3 x 30 mL) and the combined organic extracts were washed with brine (1 x 20 mL), dried with magnesium sulphate, filtered and concentrated *in vacuo*. Trituration in dichloromethane afforded title compound **1.7** (117 mg, 0.241 mmol, 73%).

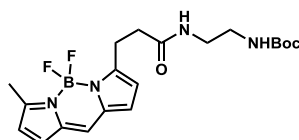
$^1\text{H}$  NMR (400 MHz,  $\text{CD}_3\text{OD}$ )  $\delta$  7.36 (1H, s, Ar-CH), 7.10 (1H, d,  $J = 4.2$ , Ar-CH), 7.06 (1H, d,  $J = 4.2$ , Ar-CH), 6.39 (1H, d,  $J = 4.2$ , Ar-CH), 6.36 (1H, d,  $J = 4.2$ , Ar-CH), 3.24 (2H, t,  $J = 7.7$ ,  $-\text{CH}_2$ ), 2.73 (2H, t,  $J = 7.7$ ,  $-\text{COCH}_2$ ), 2.57 (3H, s,  $-\text{CH}_3$ ).  $^{13}\text{C}$  NMR (100 MHz,  $\text{CD}_3\text{OD}$ )  $\delta$  176.0 ( $-\text{COOH}$ ), 160.9 (Ar-C), 160.4 (Ar-C), 136.6 (Ar-C), 136.0 (Ar-C), 132.3 (Ar-CH), 131.3 (Ar-CH), 129.2 (Ar-CH), 121.1 (Ar-CH), 118.8 (Ar-CH), 33.9 ( $-\text{COCH}_2$ ), 25.1 ( $-\text{CH}_2$ ), 14.9 ( $-\text{CH}_3$ ).  $^{19}\text{F}$  NMR (377 MHz,  $\text{CDCl}_3$ )  $\delta$  -147.1 (2F, 1:1:1:1 q,  $J = 32.5$ ,  $\text{BF}_2$ ).  $^{11}\text{B}$  NMR (128 MHz,  $\text{CDCl}_3$ )  $\delta$  0.95 (1B, t,  $J = 32.2$ ,  $\text{BF}_2$ ) HRMS (ESI) exact mass calculated for  $\text{C}_{13}\text{H}_{13}\text{BF}_2\text{N}_2\text{O}_2\text{Na}$   $[\text{M}+\text{Na}]^+$   $m/z$  301.0930, found  $m/z$  301.0928. IR (thin film) 2920, 1717, 1601, 1545.



1.8

**1.8.** Prepared according to a modified literature procedure.<sup>[44]</sup> To a stirred solution of ethylene diamine (0.92 mL, 14 mmol, 1 equiv.) in dichloromethane (50 mL, 0.3 M) at 0 °C was added dropwise a solution of di-*tert*-butyl dicarbonate (3.0 g, 14 mmol, 1 equiv.) in dichloromethane (50 mL, 0.3 M). The resulting colourless solution was stirred at room temperature for 24 hours. The solvent was removed under reduced pressure and the residue dissolved in saturated aqueous calcium carbonate solution which was then extracted with dichloromethane (3 x 50 mL), dried with magnesium sulphate, filtered, and concentrated *in vacuo*. Purification by column chromatography on silica gel with an eluent of 2.4% methanol and 0.1% aqueous ammonium hydroxide to 9% methanol and 1% aqueous ammonium hydroxide in dichloromethane afforded title compound **1.8** (1.5 g, 9.4 mmol, 68%) as a white solid. Analytical data observed were in accordance with literature values.<sup>[44]</sup>

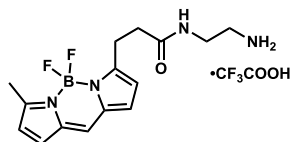
<sup>1</sup>H NMR (400 MHz, CDCl<sub>3</sub>) δ 5.28 (1H, s, -CONH), 3.08 (2H, dt, *J* = 6.0, 5.9, -NCH<sub>2</sub>), 2.70 (2H, t, *J* = 5.9, -NCH<sub>2</sub>), 1.66 (2H, s, -NH<sub>2</sub>), 1.34 (9H, s, -C(CH<sub>3</sub>)<sub>3</sub>). <sup>13</sup>C NMR (101 MHz, CDCl<sub>3</sub>) δ 156.3 (-NCOOR), 79.0 (-OCR<sub>3</sub>), 43.2 (-NCH<sub>2</sub>), 41.7 (-NCH<sub>2</sub>), 28.4 (3C, -C(CH<sub>3</sub>)<sub>3</sub>). HRMS (ESI) exact mass calculated for C<sub>7</sub>H<sub>16</sub>O<sub>2</sub>N<sub>2</sub>Na [M+Na]<sup>+</sup> *m/z* 183.1104, found *m/z* 183.1100. IR (thin film) 2934, 1681, 1593.



1.9

**1.9.** Prepared according to a modified literature procedure.<sup>[60]</sup> To a stirred solution of acid **1.7** (30 mg, 0.11 mmol, 1 equiv.) in dichloromethane (5 mL, 0.02 M) was added *N*-hydroxysuccinimide (48 mg, 0.42 mmol, 3.8 equiv.) and EDC•HCl (72 mg, 0.38 mmol, 3.5 equiv.) and the resultant solution was stirred at room temperature for 16 hours. To the reaction mixture was added *N,N*-diisopropylethylamine (57  $\mu$ L, 0.32 mmol, 3 equiv.) and *tert*-butyl carbamate protected amine **1.8** (23 mg, 0.14 mmol, 1.3 equiv.) and the resulting solution was stirred at room temperature for six hours. To the reaction mixture was added water (10 mL) and the aqueous phase was extracted with dichloromethane (3 x 10 mL). The combined organic extracts were dried with magnesium sulphate, filtered and concentrated *in vacuo*. Purification by column chromatography on silica gel using an eluent of 1% methanol in dichloromethane afforded title compound **1.9** (32 mg, 0.076 mmol, 69%) as a red solid.

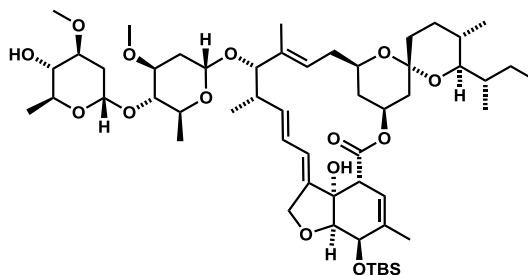
<sup>1</sup>H NMR (400 MHz, CDCl<sub>3</sub>)  $\delta$  7.10 (1H, s, Ar-CH), 6.99 (1H, d, *J* = 4.2, Ar-CH), 6.95 (1H, d, *J* = 4.2, Ar-CH), 6.34 (1H, d, *J* = 4.2, Ar-CH), 6.31 (1H, d, *J* = 4.2, Ar-CH), 6.10 (1H, br s, -CONH), 4.85 (1H, br s, -OCONH), 3.31 (2H, td, *J* = 5.4, 5.4, -NCH<sub>2</sub>), 3.30 (2H, t, *J* = 7.5, -CH<sub>2</sub>), 3.18 (2H, td, *J* = 5.4, 5.4, -NCH<sub>2</sub>), 2.65 (2H, t, *J* = 7.5, -COCH<sub>2</sub>), 2.62 (3H, s, -CH<sub>3</sub>), 1.42 (9H, s, -C(CH<sub>3</sub>)<sub>3</sub>). <sup>13</sup>C NMR (100 MHz, CDCl<sub>3</sub>)  $\delta$  172.3 (-CONH), 159.8 (Ar-C), 159.5 (Ar-C), 156.6 (-NCOOR), 135.2 (Ar-C), 134.5 (Ar-C), 131.0 (Ar-CH), 130.0 (Ar-CH), 127.4 (Ar-CH), 120.4 (Ar-CH), 118.7 (Ar-CH), 79.6 (-OCR<sub>3</sub>), 40.6 (-NCH<sub>2</sub>), 40.3 (-NCH<sub>2</sub>), 35.8 (-COCH<sub>2</sub>), 28.5 (3C, -C(CH<sub>3</sub>)<sub>3</sub>), 25.0 (-CH<sub>2</sub>), 15.1 (-CH<sub>3</sub>). <sup>19</sup>F NMR (377 MHz, CDCl<sub>3</sub>)  $\delta$  -145.1 (2F, 1:1:1:1 q, *J* = 33.2, -BF<sub>2</sub>). <sup>11</sup>B NMR (128 MHz, CDCl<sub>3</sub>)  $\delta$  0.95 (1B, t, *J* = 33.0, -BF<sub>2</sub>). HRMS (ESI) exact mass calculated for C<sub>20</sub>H<sub>27</sub>BF<sub>2</sub>N<sub>4</sub>O<sub>3</sub>Na [M+Na]<sup>+</sup> *m/z* 443.2036, found *m/z* 443.2030. IR (thin film) 2930, 1701, 1612, 1494. Melting point 147–151 °C.



1.1

**1.1.** Prepared according to a modified literature procedure.<sup>[48]</sup> To a stirred solution of *tert*-butyl carbamate **1.9** (15 mg, 0.036 mmol, 1 equiv.) in dichloromethane (5 mL, 7 mM) was added trifluoroacetic acid (0.5 mL) and the resulting solution was stirred at room temperature for two hours. Volatiles were removed *in vacuo* and dichloromethane (2 mL) was added, followed by *in vacuo* concentration (x 3) generating the title compound **1.1** as a dark red solid. The crude material was used without further purification.

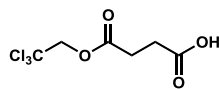
<sup>1</sup>H NMR (400 MHz, CDCl<sub>3</sub>) δ 7.09 (1H, s, Ar-CH), 6.99 (1H, d, *J* = 4.1, Ar-CH), 6.95 (1H, d, *J* = 4.1, Ar-CH), 6.34 (1H, d, *J* = 4.2, Ar-CH), 6.30 (1H, d, *J* = 4.2, Ar-CH), 6.14 (1H, br s, -CONH), 3.30 (2H, t, *J* = 7.5, -CH<sub>2</sub>), 3.27 (2H, td, *J* = 5.8, 5.8, -NCH<sub>2</sub>), 2.75 (2H, t, *J* = 5.8, -NCH<sub>2</sub>), 2.66 (2H, t, *J* = 7.5, -COCH<sub>2</sub>), 2.62 (3H, s, -CH<sub>3</sub>).  
<sup>19</sup>F NMR (377 MHz, CDCl<sub>3</sub>) δ -77.0 (3F, s, -CF<sub>3</sub>), -146.6 (2F, 1:1:1:1 q, *J* = 32.5, -BF<sub>2</sub>).  
<sup>11</sup>B NMR (128 MHz, CDCl<sub>3</sub>) δ 0.95 (1B, t, *J* = 32.6, -BF<sub>2</sub>).



1.12

**1.12.** Prepared according to a modified literature procedure.<sup>[22]</sup> To an oven dried flask charged with argon was added anhydrous *N,N*-dimethylformamide (5 mL, 0.06 M), **ivermectin** (0.250 g, 0.286 mmol, 1 equiv.), imidazole (0.117 g, 1.72 mmol, 6 equiv.) and *tert*-butyldimethylsilyl chloride (0.130 g, 0.854 mmol, 3 equiv.) and the resulting colourless solution was stirred at ambient temperature for two hours. To the reaction mixture was added water (15 mL) and the aqueous phase was extracted with diethyl ether (3 x 20 mL). The combined organic extracts were washed with water (6 x 20 mL), dried with magnesium sulphate, filtered and concentrated *in vacuo* yielding a viscous oil (0.387 g). Purification by column chromatography on silica gel with an eluent of 5% tetrahydrofuran in dichloromethane afforded title compound **1.12** (0.244 g, 0.247 mmol, 85%) as a white solid.

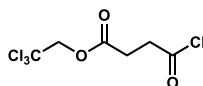
<sup>1</sup>H NMR (400 MHz, CDCl<sub>3</sub>) δ 5.85–5.79 (1H, m), 5.74–5.70 (2H, m), 5.40 (1H, d, *J* = 3.8), 5.37–5.30 (2H, m), 5.02–4.95 (1H, m), 4.77 (1H, d, *J* = 3.8), 4.68 (1H, dd, *J* = 14.5, 2.4), 4.58 (1H, dd, *J* = 14.6, 2.3), 4.46–4.41 (1H, m), 4.22 (1H, s), 3.94 (1H, br s), 3.83 (1H, d, *J* = 5.6), 3.86–3.79 (1H, m), 3.69–3.58 (2H, m), 3.52–3.45 (1H, m), 3.43 (3H, s), 3.42 (3H, s), 3.40–3.36 (1H, m), 3.24 (1H, t, *J* = 9.0), 3.24–3.19 (1H, m), 3.17 (1H, td, *J* = 9.1, 1.8), 2.56–2.48 (1H, m), 2.47 (1H, d, *J* = 1.9), 2.37–2.18 (4H, m), 1.98 (1H, dd, *J* = 12.1, 4.9), 1.79 (3H, s), 1.77–1.71 (1H, m), 1.70–1.58 (2H, m), 1.55 (3H, s), 1.53–1.31 (11H, m), 1.28 (3H, d, *J* = 6.3), 1.26 (3H, d, *J* = 6.3), 1.16 (3H, d, *J* = 6.9), 0.93 (9H, s), 0.93 (3H, t, *J* = 7.3), 0.85 (3H, d, *J* = 6.6), 0.78 (3H, br d, *J* = 5.3), 0.13 (6H, s). <sup>13</sup>C NMR (100 MHz, CDCl<sub>3</sub>) δ 174.3, 140.5, 137.7, 135.2, 125.0, 119.5, 118.5, 117.4, 98.7, 97.7, 95.0, 82.0, 80.6, 80.4, 80.2, 79.5, 78.4, 76.3, 69.7, 68.9, 68.3, 68.1, 67.4, 56.7, 56.6, 46.0, 41.4, 39.8, 37.1, 35.9, 35.7, 34.7, 34.3, 31.4, 28.3, 27.5, 26.1, 20.5, 20.2, 18.6, 17.8, 17.6, 15.4, 12.6, 12.3, 5.3, –4.4, –4.7. HRMS (ESI) exact mass calculated for C<sub>54</sub>H<sub>88</sub>O<sub>14</sub>SiNa [M+Na]<sup>+</sup> *m/z* 1011.5836, found *m/z* 1011.5816. IR (thin film) 2930, 1713, 1674. Melting point 139–145 °C (not lit. reported).



1.13

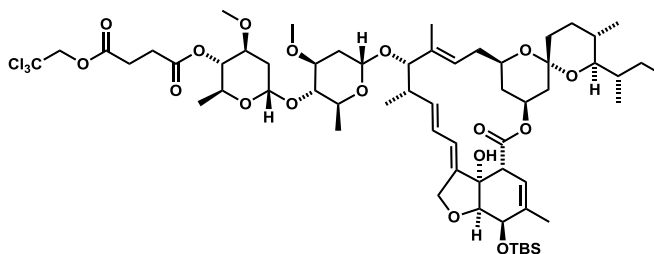
**1.13.** Prepared according to a modified literature procedure.<sup>[22]</sup> To a suspension of succinic anhydride (0.60 g, 6.0 mmol, 1 equiv.) in anhydrous toluene (10 mL, 0.6 M) was added trichloroethanol (0.58 mL, 6.0 mmol, 1 equiv.) and 4-dimethylaminopyridine (10 mg, 1 mol%). The resulting white suspension was stirred at 60 °C for 16 hours. The solvent was removed under reduced pressure and the resultant white solid was dissolved in dichloromethane and extracted with 1 M aqueous sodium hydrogen carbonate solution (3 x 20 mL). The aqueous extracts were acidified to pH 1 and extracted with dichloromethane (3 x 15 mL). The combined organic extracts were washed with brine (1 x 20 mL), dried with magnesium sulphate, filtered and concentrated *in vacuo* to afford title compound **1.13** (1.2 g, 4.9 mmol, 81%) as a white solid. Analytical data observed were in accordance with literature values.<sup>[61]</sup>

<sup>1</sup>H NMR (400 MHz, CDCl<sub>3</sub>) δ 11.43 (1H, s, -COOH), 4.77 (2H, s, -OCH<sub>2</sub>), 2.83–2.73 (4H, m, 2 x -COCH<sub>2</sub>). HRMS (ESI) exact mass calculated for C<sub>6</sub>H<sub>7</sub>O<sub>2</sub><sup>35</sup>Cl<sub>3</sub>Na [M+Na]<sup>+</sup> m/z 270.9302, found m/z 270.9293. IR (thin film) 2969, 1749, 1699. Melting point 88–89 °C (not lit. reported). Elemental analysis calculated for C<sub>6</sub>H<sub>7</sub>O<sub>4</sub>Cl<sub>3</sub>: C, 28.89%, H, 2.83%. Found C, 28.81%, H, 2.80%.



1.14

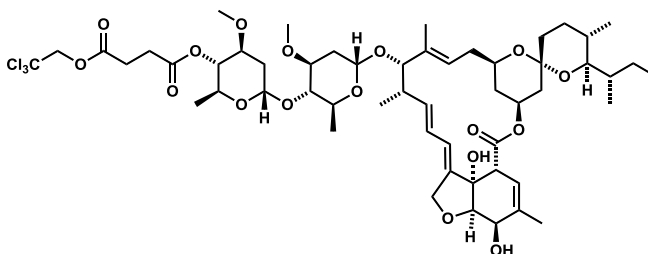
**1.14.** Prepared according to a modified literature procedure.<sup>[22]</sup> To a solution of acid **1.13** (0.25 g, 1.0 mmol, 1.0 equiv.) in anhydrous tetrahydrofuran (1 mL, 1 M) was added anhydrous *N,N*-dimethylformamide (1 drop) and oxalyl chloride (0.13 mL, 1.5 mmol, 1.5 equiv.) and the solution was stirred at room temperature for one hour. The solvent was evaporated under reduced pressure and the resulting residue was dissolved in anhydrous tetrahydrofuran (5 mL) and concentrated *in vacuo* (x 3) affording title compound **1.14** as a dark yellow clear oil, which was used without further purification.



1.15

**1.15.** Prepared according to a modified literature procedure.<sup>[22]</sup> To a stirred solution of silyl ether **1.12** (0.20 g, 0.20 mmol, 1 equiv.), 4-dimethylaminopyridine (98 mg, 0.80 mmol, 4 equiv.) and *N,N*-diisopropylethylamine (0.14 mL, 0.81 mmol, 4 equiv.) in anhydrous dichloromethane (5 mL, 0.04 M) at 0 °C was added a solution of acyl chloride **1.14** (0.16 g, 0.60 mmol, 3 equiv.) in anhydrous dichloromethane (1 mL, 0.6 M) and the resulting solution was stirred at 0 °C for four hours. To the reaction was added ice and the aqueous phase was extracted with dichloromethane (3 x 10 mL) giving a crude mass of 0.32 g as a red/brown oil. Purification by column chromatography on silica gel with an eluent of 0% to 4% tetrahydrofuran in dichloromethane afforded title compound **1.15** (0.20 g, 0.16 mmol, 82%) as a clear glass that upon crushing formed a colourless solid. Analytical data observed were in accordance with literature values.<sup>[22]</sup>

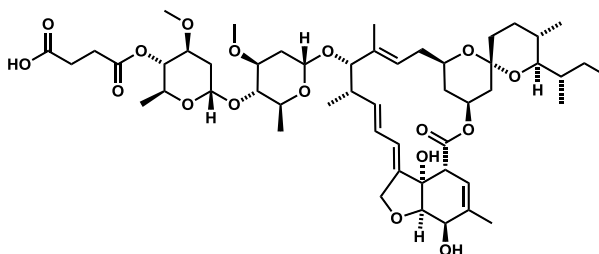
<sup>1</sup>H NMR (400 MHz, CDCl<sub>3</sub>) δ 5.85–5.80 (1H, m), 5.75–5.70 (2H, m), 5.39 (1H, d, *J* = 3.7), 5.39–5.26 (2H, m), 4.98 (1H, br d, *J* = 10.8), 4.78 (1H, d, *J* = 12.0), 4.78 (1H, d, *J* = 4.0), 4.74 (1H, d, *J* = 12.0), 4.70 (1H, t, *J* = 9.4), 4.68 (1H, dd, *J* = 14.4, 2.4), 4.58 (1H, dd, *J* = 14.5, 2.3), 4.46–4.42 (1H, m), 4.24 (1H, s), 3.94 (1H, br s), 3.89–3.81 (3H, m), 3.68–3.58 (3H, m), 3.43 (3H, s), 3.40–3.35 (1H, m), 3.37 (3H, s), 3.23 (2H, t, *J* = 9.0), 2.90–2.79 (2H, m), 2.76–2.71 (2H, m), 2.55–2.49 (1H, m), 2.37–2.19 (4H, m), 1.98 (1H, dd, *J* = 12.2, 4.9), 1.79 (3H, br s), 1.77–1.71 (1H, m), 1.70–1.61 (4H, m), 1.61–1.30 (11H, m), 1.25 (3H, d, *J* = 6.2), 1.17 (3H, d, *J* = 7.0), 1.15 (3H, d, *J* = 7.0), 0.96–0.90 (3H, m), 0.93 (9H, s), 0.85 (3H, d, *J* = 6.6), 0.78 (3H, d, *J* = 5.3), 0.13 (6H, s). HRMS (ESI) exact mass calculated for C<sub>60</sub>H<sub>93</sub>O<sub>17</sub>Si<sub>35</sub>Cl<sub>3</sub>Na [M+Na]<sup>+</sup> *m/z* 1241.5140, found *m/z* 1241.5160. IR (thin film) 2931, 1743, 1450. Melting point 140–143 °C (not lit. reported).



1.16

**1.16.** Prepared according to a modified literature procedure.<sup>[22]</sup> To a stirred solution of 4-toluenesulfonic acid (1 mol%) in methanol (16 mL, 0.01 M) was added silyl ether **1.15** (0.20 g, 0.16 mmol, 1 equiv.) and the resulting solution was stirred at room temperature for six hours. The reaction mixture was quenched with saturated aqueous sodium hydrogen carbonate solution (15 mL) and the aqueous phase was extracted with ethyl acetate (3 x 15 mL). The combined organic extracts were washed with water (3 x 10 mL), dried with magnesium sulphate, filtered and concentrated *in vacuo*, yielding 0.21 g of pale yellow viscous oil. The crude material was purified using column chromatography on silica gel with an eluent of 2.5% methanol in dichloromethane affording title compound **1.16** (0.12 g, 0.11 mmol, 68%) as a colourless solid. Analytical data observed were in accordance with literature values.<sup>[22]</sup>

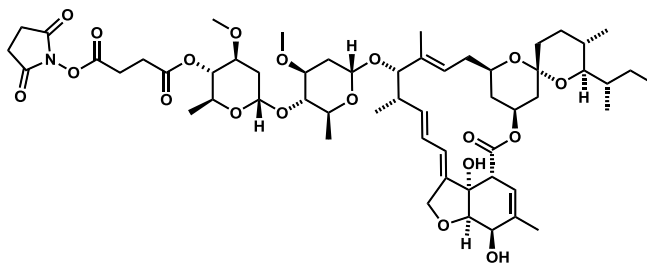
<sup>1</sup>H NMR (400 MHz, CDCl<sub>3</sub>) δ 5.82 (1H, dt, *J* = 10.4, 2.4), 5.76–5.64 (2H, m), 5.38 (1H, s), 5.36–5.33 (1H, m), 5.26 (2H, s), 4.99–4.92 (1H, m), 4.73 (1H, d, *J* = 12.0), 4.73 (1H, d, *J* = 3.5), 4.70 (1H, d, *J* = 12.0), 4.67–4.58 (3H, m), 4.27–4.21 (1H, m), 4.12 (1H, s), 3.93–3.89 (2H, m), 3.85–3.76 (2H, m), 3.67–3.53 (2H, m), 3.39 (3H, s), 3.32 (3H, s), 3.26–3.22 (1H, m), 3.21–3.15 (2H, m), 2.84–2.74 (2H, m), 2.73–2.66 (2H, m), 2.51 (1H, d, *J* = 8.3), 2.49–2.44 (1H, m), 2.34–2.15 (4H, m), 1.98–1.91 (1H, m), 1.85–1.80 (3H, br s), 1.76–1.68 (1H, m), 1.65–1.57 (2H, m), 1.57–1.26 (12H, m), 1.21 (3H, d, *J* = 6.1), 1.14 (3H, d, *J* = 7.0), 1.10 (3H, d, *J* = 6.3), 0.89 (3H, t, *J* = 7.3), 0.81 (3H, d, *J* = 6.7), 0.78–0.71 (4H, m). HRMS (ESI) exact mass calculated for C<sub>54</sub>H<sub>79</sub>O<sub>17</sub><sup>35</sup>Cl<sub>3</sub>Na [M+Na]<sup>+</sup> *m/z* 1127.4275, found *m/z* 1127.4305. IR (thin film) 2924, 1751, 1434. Melting point 118–122 °C (not lit. reported).



1.11

**1.11.** Prepared according to a modified literature procedure.<sup>[22]</sup> To a stirred solution of trichloroethyl ester **1.16** (40 mg, 0.036 mmol, 1 equiv.) in acetic acid (2.5 mL) was added zinc powder (0.32 g, 4.9 mmol, 137 equiv.) and the resulting suspension was stirred at room temperature for 3 hours. The reaction mixture was filtered and the solid washed with dichloromethane. The filtrate was washed with 1 M aqueous hydrochloric acid (10 mL) and water (10 mL) and the aqueous layer extracted with dichloromethane (3 x 20 mL). The combined organic extracts were dried with magnesium sulphate, filtered and concentrated *in vacuo* affording title compound **1.11** (55 mg crude) as a white solid. The crude material was used without further purification. Analytical data observed were in accordance with literature values.<sup>[22]</sup>

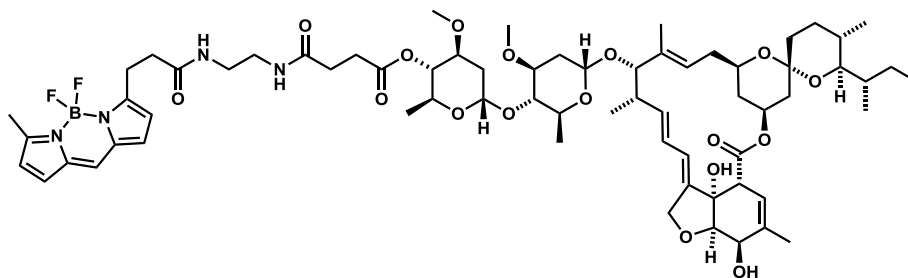
<sup>1</sup>H NMR (400 MHz, CDCl<sub>3</sub>) δ 5.89–5.83 (1H, m), 5.78–5.67 (2H, m), 5.42 (1H, br s), 5.40–5.38 (1H, m), 5.37–5.28 (1H, m), 4.98 (1H, d, *J* = 11.0), 4.79–4.76 (1H, m), 4.73–4.62 (3H, m), 4.30 (1H, d, *J* = 6.2), 3.97 (1H, d, *J* = 6.2), 3.94 (1H, br s), 3.89–3.80 (2H, m), 3.73–3.55 (3H, m), 3.42 (3H, s), 3.35 (3H, s), 3.30–3.26 (1H, m), 3.25–3.19 (2H, m), 2.77–2.61 (4H, m), 2.55–2.47 (1H, m), 2.37–2.16 (4H, m), 2.02–1.95 (1H, m), 1.86 (3H, br s), 1.79–1.72 (1H, m), 1.71–1.60 (2H, m), 1.61–1.29 (12H, m), 1.27–1.22 (5H, m), 1.16 (3H, d, *J* = 7.0), 1.13 (3H, d, *J* = 6.3), 0.92 (3H, t, *J* = 7.4), 0.85 (3H, d, *J* = 6.7), 0.78 (3H, d, *J* = 4.6). <sup>13</sup>C NMR (126 MHz, CDCl<sub>3</sub>) δ 177.4, 174.0, 171.6, 139.6, 138.2, 138.0, 135.1, 129.2, 124.9, 120.6, 118.2, 98.5, 97.7, 95.0, 82.0, 80.9, 80.5, 79.4, 79.3, 75.7, 68.9, 68.6, 67.8, 67.4, 67.3, 66.6, 57.0, 56.7, 45.9, 41.3, 39.9, 37.0, 35.9, 35.6, 35.1, 34.6, 34.2, 31.3, 29.8, 29.2, 28.2, 27.4, 22.8, 20.9, 20.4, 20.0, 18.5, 17.6, 17.4, 15.3, 12.6, 12.2. HRMS (ESI) exact mass calculated for C<sub>52</sub>H<sub>77</sub>O<sub>17</sub> [M-H]<sup>-</sup> *m/z* 973.5166, found *m/z* 973.5134. IR (thin film) 2924, 1659.



1.17

**1.17.** Prepared according to a modified literature procedure.<sup>[22]</sup> To a stirred solution of acid **1.11** (30 mg, 0.033 mmol, 1 equiv.) in dichloromethane (0.75 mL, 0.04 M) was added *N*-hydroxysuccinimide (14 mg, 0.12 mmol, 3.5 equiv.) and EDC•HCl (22 mg, 0.12 mmol, 3.5 equiv.) and the resultant solution was stirred at room temperature for three hours. To the reaction mixture was added water (5 mL) and the aqueous phase was extracted with dichloromethane (3 x 5 mL). The combined organic extracts were dried with magnesium sulphate, filtered and concentrated *in vacuo* generating a crude mass of 52 mg. Purification by column chromatography on silica gel using an eluent of 1% to 2% methanol in dichloromethane afforded the title compound **1.17** (13 mg, 0.012 mmol, 36%).

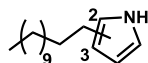
<sup>1</sup>H NMR (500 MHz, CDCl<sub>3</sub>) δ 5.87 (1H, dt, *J* = 10.6, 2.4), 5.79–5.68 (2H, m), 5.43 (1H, br s), 5.41–5.37 (1H, m), 5.38–5.32 (1H, m), 4.99 (1H, d, *J* = 11.4), 4.79–4.76 (1H, m), 4.73–4.63 (3H, m), 4.30 (1H, t, *J* = 6.9), 4.14 (1H, s), 3.97 (1H, d, *J* = 6.2), 3.94 (1H, br s), 3.90–3.81 (2H, m), 3.72–3.58 (4H, m), 3.46–3.40 (3H, m), 3.35 (3H, s), 3.30–3.27 (1H, m), 3.23 (2H, dd, *J* = 10.3, 7.9), 3.06–2.93 (2H, m), 2.80–2.76 (2H, m), 2.55–2.49 (1H, m), 2.38–2.20 (6H, m), 2.01–1.95 (1H, m), 1.88 (3H, br s), 1.79–1.73 (1H, m), 1.69–1.62 (3H, m), 1.60–1.36 (11H, m), 1.26 (3H, d, *J* = 7.5), 1.20 (3H, d, *J* = 6.2), 1.17 (3H, d, *J* = 6.9), 1.13 (3H, d, *J* = 6.3), 0.93 (3H, t, *J* = 7.4), 0.85 (3H, d, *J* = 6.8), 0.79 (3H, d, *J* = 5.3). <sup>13</sup>C NMR (101 MHz, CDCl<sub>3</sub>) δ 174.0, 170.4, 168.9, 167.8, 139.9, 138.2, 138.1, 135.1, 124.9, 120.6, 118.5, 118.2, 98.5, 97.6, 95.0, 82.0, 80.9, 80.5, 79.4, 79.2, 75.7, 68.8, 68.6, 67.9, 67.4, 67.3, 66.5, 57.0, 56.7, 53.6, 45.9, 41.3, 39.9, 37.1, 35.9, 35.6, 35.1, 34.7, 34.3, 31.4, 29.8, 29.0, 28.2, 27.4, 26.4, 25.7, 20.4, 20.1, 18.6, 17.6, 17.5, 15.3, 12.6, 12.2. HRMS (ESI) exact mass calculated for C<sub>56</sub>H<sub>81</sub>NO<sub>19</sub>Na [M+Na]<sup>+</sup> *m/z* 1094.5295, found *m/z* 1094.5248.



BLI

**BLI**. Prepared according to a modified literature procedure.<sup>[60]</sup> To a stirred solution of NHS ester **1.17** (14 mg, 14  $\mu\text{mol}$ , 1.3 equiv.) in dichloromethane (0.1 mL, 0.14 M) was added a solution of *N,N*-diisopropylethylamine (6.0  $\mu\text{L}$ , 36  $\mu\text{mol}$ , 3.5 equiv.) in dichloromethane (0.1 mL, 0.4 M) and a solution of amine TFA salt **1.1** (4.5 mg, 10  $\mu\text{mol}$ , 1 equiv.) in dichloromethane (0.033 mL, 0.3 M). The resulting solution was stirred at ambient temperature for four hours. The crude mixture was washed with water (2 x 5 mL) and the combined aqueous phases extracted with dichloromethane (3 x 10 mL). The combined organic phases were dried with magnesium sulphate, filtered and concentrated *in vacuo* yielding a crude red oil (19 mg). Purification by column chromatography on silica gel with an eluent of 2% to 4% methanol in dichloromethane afforded title compound **BLI** (9.0 mg, 7.0  $\mu\text{mol}$ , 71%) as a red/green solid.

<sup>1</sup>H NMR (400 MHz, CDCl<sub>3</sub>)  $\delta$  7.11 (1H, s), 6.99 (1H, d, *J* = 4.1), 6.96 (1H, d, *J* = 4.1), 6.35 (1H, d, *J* = 4.1), 6.31 (1H, d, *J* = 4.1), 6.25–6.16 (2H, m), 5.89–5.84 (1H, m), 5.79–5.67 (2H, m), 5.43 (1H, s), 5.41–5.31 (2H, m), 4.98 (1H, d, *J* = 10.7), 4.78 (1H, d, *J* = 3.8), 4.75–4.62 (3H, m), 4.30 (1H, t, *J* = 7.3), 4.13 (1H, s), 3.97 (1H, d, *J* = 6.3), 3.94 (1H, s), 3.83 (2H, dd, *J* = 9.6, 6.2), 3.72–3.56 (2H, m), 3.43 (3H, s), 3.34 (3H, s), 3.33–3.19 (8H, m), 2.70–2.64 (3H, m), 2.62 (3H, s), 2.56–2.49 (1H, m), 2.46–2.37 (2H, m), 2.37–2.19 (4H, m), 1.98 (1H, dd, *J* = 12.0, 4.9), 1.88 (3H, s), 1.76 (1H, d, *J* = 12.5), 1.70–1.61 (2H, m), 1.54–1.48 (11H, m), 1.48–1.27 (4H, m), 1.28–1.22 (4H, m), 1.17 (3H, d, *J* = 7.0), 1.10 (3H, d, *J* = 6.2), 0.93 (3H, t, *J* = 7.3), 0.86 (3H, d, *J* = 6.7), 0.81–0.75 (4H, m). <sup>13</sup>C NMR (100 MHz, CDCl<sub>3</sub>)  $\delta$  174.0, 160.3, 159.7, 159.5, 146.4, 142.0, 139.8, 138.1, 135.1, 131.1, 130.0, 127.5, 125.6, 125.0, 124.9, 121.6, 120.6, 120.5, 118.5, 118.2, 104.9, 104.1, 98.5, 97.6, 95.0, 92.8, 82.5, 82.0, 80.9, 80.5, 79.4, 79.2, 77.7, 75.8, 68.8, 68.7, 67.9, 67.4, 67.3, 66.6, 57.0, 56.7, 45.9, 41.3, 40.2, 39.9, 39.5, 37.1, 35.9, 35.1, 34.7, 31.4, 31.2, 29.9, 28.2, 27.5, 25.0, 22.8, 20.4, 20.1, 20.0, 18.6, 17.6, 17.5, 15.3, 12.6, 12.3. HRMS (ESI) exact mass calculated for C<sub>67</sub>H<sub>95</sub>BF<sub>2</sub>N<sub>4</sub>O<sub>17</sub>Na [M+Na]<sup>+</sup> m/z 1299.6651, found m/z 1299.5962.

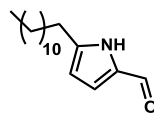


**1.19** = 2 alkylated  
**1.19b** = 3 alkylated

**1.19** and **1.19b**. Prepared according to a modified literature procedure.<sup>[53]</sup> To an oven dried flask cooled under vacuum and charged with argon was added pyrrole (2.06 mL, 30 mmol, 1 equiv.) and anhydrous diethyl ether (15 mL, 2 M). To this stirred solution was added ethylmagnesium bromide (16 mL, 2 M, 33 mmol, 1.1 equiv.) slowly over one hour at 0 °C and stirred at 0 °C for one hour forming a very dark green solution. To this solution was slowly added dodecyl bromide (7.1 mL, 45 mmol, 1.5 equiv.) at 0 °C over three hours. The solution was then warmed to ambient temperature and stirred for a further 16 hours. To the reaction mixture was added saturated aqueous sodium hydrogen carbonate solution (60 mL) and the solids removed by vacuum filtration. The filtrate was extracted with diethyl ether (3 x 60 mL) and combined organic fractions dried with magnesium sulphate, filtered and concentrated *in vacuo* yielding a brown oil (7.76 g). Purification by column chromatography on silica gel with an eluent of 1.5% ethyl acetate in petroleum ether afforded title compounds **1.19** (1.00 g, 4.25 mmol, 14%) and **1.19b** (210 mg, 0.89 mmol, 3%).

**1.19**.  $R_f$  0.68 in 1.5% ethyl acetate in petroleum ether.  $^1\text{H}$  NMR (400 MHz,  $\text{CDCl}_3$ )  $\delta$  7.89 (1H, br s, -NH), 6.67 (1H, ddd,  $J = 2.6, 2.6, 1.6$ , Ar-CH), 6.13 (1H, ddd,  $J = 2.8, 2.8, 2.8$ , Ar-CH), 5.95–5.88 (1H, m, Ar-CH), 2.60 (2H, t,  $J = 7.7$ , - $\text{CH}_2$ ), 1.62 (2H, tt,  $J = 7.7, 7.5$ , - $\text{CH}_2$ ), 1.41–1.19 (18H, m, 9x - $\text{CH}_2$ ), 0.89 (3H, t,  $J = 6.7$ , - $\text{CH}_3$ ).  $^{13}\text{C}$  NMR (100 MHz,  $\text{CDCl}_3$ )  $\delta$  133.0 (Ar-C), 116.1 (Ar-CH), 108.4 (Ar-CH), 105.0 (Ar-CH), 32.1 (- $\text{CH}_2$ ), 29.8 (4 x - $\text{CH}_2$ ), 29.7 (- $\text{CH}_2$ ), 29.6 (2 x - $\text{CH}_2$ ), 29.5 (- $\text{CH}_2$ ), 27.9 (- $\text{CH}_2$ ), 22.9 (- $\text{CH}_2$ ), 14.3 (- $\text{CH}_3$ ). HRMS (ESI) exact mass calculated for  $\text{C}_{16}\text{H}_{29}\text{N}$   $[\text{M}]^+$   $m/z$  235.2300, found  $m/z$  235.2297. IR (thin film) 3356, 2916, 1705, 1566.

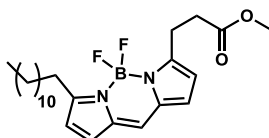
**1.19b**.  $R_f$  0.33 in 1.5% ethyl acetate in petroleum ether.  $^1\text{H}$  NMR (400 MHz,  $\text{CDCl}_3$ )  $\delta$  7.98 (1H, br s, -NH), 6.72 (1H, ddd,  $J = 2.6, 2.5, 2.2$ , Ar-CH), 6.58 (1H, ddd,  $J = 1.9, 1.9, 1.7$ , Ar-CH), 6.10 (1H, ddd,  $J = 2.7, 2.7, 1.6$ , Ar-CH), 2.48 (2H, t,  $J = 7.7$ , - $\text{CH}_2$ ), 1.59 (2H, tt,  $J = 7.7, 7.7$ , - $\text{CH}_2$ ), 1.39–1.23 (18H, m, 9 x - $\text{CH}_2$ ), 0.89 (3H, t,  $J = 7.0$ ,  $\text{CH}_3$ ).  $^{13}\text{C}$  NMR (101 MHz,  $\text{CDCl}_3$ )  $\delta$  124.9 (Ar-C), 117.7 (Ar-CH), 114.9 (Ar-CH), 108.7 (Ar-CH), 32.1 (- $\text{CH}_2$ ), 31.4 (- $\text{CH}_2$ ), 29.9 (2 x - $\text{CH}_2$ ), 29.8 (2 x - $\text{CH}_2$ ), 29.7 (2 x  $\text{CH}_2$ ), 29.5 (- $\text{CH}_2$ ), 27.1 (- $\text{CH}_2$ ), 22.9 (- $\text{CH}_2$ ), 14.3 (- $\text{CH}_3$ ).



1.20

**1.20.** Prepared according to a modified literature procedure.<sup>[54]</sup> To an oven dried flask cooled under vacuum and flushed with argon was added anhydrous dichloromethane (1.8 mL, 2 M) and oxalyl chloride (0.30 mL, 3.5 mmol, 1.1 equiv.) and the resulting stirred solution was cooled to 0 °C. To this solution was added slowly *N,N*-dimethylformamide (0.27 mL, 3.5 mmol, 1.1 equiv.) and the resulting solution was stirred at 0 °C for one hour. To this was quickly added a solution of pyrrole **1.19** (750 mg, 3.2 mmol, 1 equiv.) in anhydrous dichloromethane (1.8 mL, 2 M) in one portion and the resulting solution was stirred under reflux for three hours. The reaction was quenched with a 5 M aqueous solution of sodium acetate (1.84 g, 22.4 mmol, 7 equiv.) and the resulting biphasic mixture was refluxed for one hour, after which it was neutralised using 1 M aqueous hydrochloric acid, and the aqueous phase was extracted with dichloromethane (3 x 10 mL). The combined organic extracts were dried with magnesium sulphate, filtered and concentrated *in vacuo* yielding a light brown solid (0.758 g). Purification by column chromatography on silica gel with an eluent of 6% ethyl acetate in petroleum ether afforded title compound **1.20** (0.723 g, 2.74 mmol, 86%).

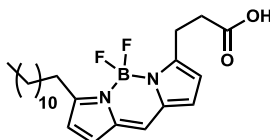
<sup>1</sup>H NMR (400 MHz, CDCl<sub>3</sub>) δ 9.37 (1H, s, -CHO), 9.34 (1H, br s, -NH), 6.89 (1H, dd, *J* = 3.8, 2.5, Ar-CH), 6.07 (1H, dd, *J* = 3.8, 2.6, Ar-CH), 2.65 (2H, t, *J* = 7.7, -CH<sub>2</sub>), 1.65 (2H, tt, *J* = 7.6, 7.6, -CH<sub>2</sub>), 1.37–1.23 (18H, m, x9 -CH<sub>2</sub>), 0.88 (3H, t, *J* = 6.7, -CH<sub>3</sub>). <sup>13</sup>C NMR (100 MHz, CDCl<sub>3</sub>) δ 178.2 (-CHO), 132.0 (Ar-C), 122.4 (Ar-C), 109.6 (Ar-CH), 109.5 (Ar-CH), 32.1 (-CH<sub>2</sub>), 29.8 (3 x -CH<sub>2</sub>), 29.6 (-CH<sub>2</sub>), 29.5 (2 x -CH<sub>2</sub>), 29.4 (-CH<sub>2</sub>), 29.1 (-CH<sub>2</sub>), 28.1 (-CH<sub>2</sub>), 22.8 (-CH<sub>2</sub>), 14.3 (-CH<sub>3</sub>). HRMS (ESI) exact mass calculated for C<sub>17</sub>H<sub>29</sub>NONa [M+Na]<sup>+</sup> *m/z* 286.2141, found *m/z* 286.2138. IR (thin film) 2916, 1637, 1497.



1.21

**1.21.** Prepared according to a modified literature procedure.<sup>[42]</sup> To an oven dried flask cooled under vacuum and charged with argon was added anhydrous dichloromethane (4.2 mL, 0.3 M), pyrrole **1.4** (0.196 g, 1.30 mmol, 1 equiv.) and aldehyde **1.20** (0.370 g, 1.4 mmol, 1.1 equiv.) and the resulting stirred solution was cooled to 0 °C. To this was added dropwise POCl<sub>3</sub> (0.13 mL, 1.3 mmol, 1 equiv.) at 0 °C over 30 minutes and the resulting solution then warmed to ambient temperature and stirred for an additional six hours. The mixture was cooled again to 0 °C and *N,N*-diisopropylethylamine (0.89 mL, 5.2 mmol, 4 equiv.) and BF<sub>3</sub>•OEt<sub>2</sub> (0.66 mL, 5.5 mmol, 4.2 equiv.) were added and the reaction allowed to warm to ambient temperature and stirred for 12 hours. To the reaction mixture was added water (15 mL) and the aqueous phase was extracted with dichloromethane (3 x 20 mL). The combined organic fractions were washed with brine (1 x 20 mL), dried with magnesium sulphate, filtered and concentrated *in vacuo* to a dark red/green oil (0.918 g). Purification by column chromatography, on silica gel with an eluent of dichloromethane afforded title compound **1.21** (0.317 g, 0.710 mmol, 55%).

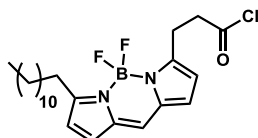
<sup>1</sup>H NMR (400 MHz, CDCl<sub>3</sub>) δ 7.07 (1H, s, Ar-CH), 6.98 (1H, d, *J* = 4.3, Ar-CH), 6.92 (1H, d, *J* = 4.1, Ar-CH), 6.35 (1H, d, *J* = 4.3, Ar-CH), 6.30 (1H, d, *J* = 4.1, Ar-CH), 3.69 (3H, s, -OCH<sub>3</sub>), 3.31 (2H, t, *J* = 7.6, -CH<sub>2</sub>), 2.99 (2H, t, *J* = 7.9, -CH<sub>2</sub>), 2.78 (2H, t, *J* = 7.6, -COCH<sub>2</sub>), 1.73 (2H, tt, *J* = 7.9, 7.5, -CH<sub>2</sub>), 1.42 (2H, tt, *J* = 7.9, 7.5, -CH<sub>2</sub>), 1.37–1.18 (16H, m, x8 -CH<sub>2</sub>), 0.88 (3H, t, *J* = 6.7, -CH<sub>3</sub>). <sup>13</sup>C NMR (100 MHz, CDCl<sub>3</sub>) δ 172.8 (-COOR), 164.7 (Ar-C), 159.1 (Ar-C), 134.9 (Ar-C), 134.2 (Ar-C), 130.9 (Ar-CH), 129.4 (Ar-CH), 127.3 (Ar-CH), 118.7 (Ar-CH), 117.7 (Ar-CH), 51.7 (-OCH<sub>3</sub>), 33.1 (-COCH<sub>2</sub>), 31.9 (-CH<sub>2</sub>), 29.7 (-CH<sub>2</sub>), 29.6 (3 x -CH<sub>2</sub>), 29.5 (-CH<sub>2</sub>), 29.4 (-CH<sub>2</sub>), 29.3 (-CH<sub>2</sub>), 29.0 (-CH<sub>2</sub>), 28.5 (-CH<sub>2</sub>), 24.1 (-CH<sub>2</sub>), 22.7 (-CH<sub>2</sub>), 14.1 (-CH<sub>3</sub>). HRMS (ESI) exact mass calculated for C<sub>25</sub>H<sub>37</sub>BF<sub>2</sub>N<sub>2</sub>O<sub>2</sub>Na [M+Na]<sup>+</sup> *m/z* 469.2808, found *m/z* 469.2796. IR (thin film) 2916, 1736, 1605, 980, 679.



1.18

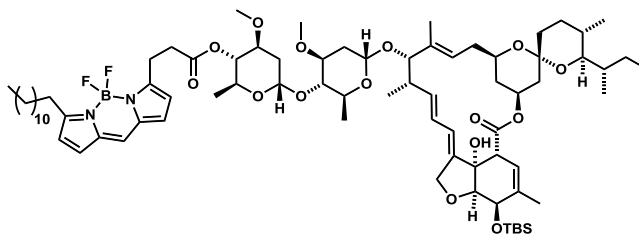
**1.18.** To a stirred solution of ester **1.21** (32 mg, 0.072 mmol, 1 equiv) in tetrahydrofuran (2.5 mL, 0.03 M) was added 4 M aqueous hydrochloric acid (2.5 mL) and the resulting mixture was stirred for 48 hours. To the reaction mixture was added dichloromethane (10 mL) and the phases separated. The aqueous phase was extracted with dichloromethane (3 x 10 mL) and the combined organic fractions were washed with brine (1 x 10 mL), dried with magnesium sulphate, filtered and concentrated *in vacuo* yielding a red/green solid (34 mg). Purification by column chromatography on silica gel with an eluent of 5% methanol in dichloromethane afforded title compound **1.18** (30 mg, 69  $\mu$ mol, 96%) as a red/green solid.

$^1\text{H}$  NMR (400 MHz,  $\text{CDCl}_3$ )  $\delta$  11.27 (1H, br s, -COOH), 7.09 (1H, s, Ar-CH), 7.00 (1H, d,  $J = 4.2$ , Ar-CH), 6.93 (1H, d,  $J = 4.1$ , Ar-CH), 6.37 (1H, d,  $J = 4.2$ , Ar-CH), 6.32 (1H, d,  $J = 4.1$ , Ar-CH), 3.32 (2H, t,  $J = 7.5$ , -CH<sub>2</sub>), 2.99 (2H, t,  $J = 7.8$ , -CH<sub>2</sub>), 2.84 (2H, t,  $J = 7.5$ , -COCH<sub>2</sub>), 1.74 (2H, tt,  $J = 7.8, 7.8$ , -CH<sub>2</sub>), 1.46–1.39 (2H, m, -CH<sub>2</sub>), 1.37–1.22 (16H, m, x8 -CH<sub>2</sub>), 0.87 (3H, t,  $J = 6.8$ , -CH<sub>3</sub>).  $^{13}\text{C}$  NMR (101 MHz,  $\text{CDCl}_3$ )  $\delta$  178.3 (-COOH), 165.1 (Ar-C), 158.7 (Ar-C), 135.1 (Ar-C), 134.4 (Ar-C), 131.2 (Ar-CH), 129.6 (Ar-CH), 127.6 (Ar-CH), 119.0 (Ar-CH), 117.8 (Ar-CH), 33.1 (-COCH<sub>2</sub>), 32.1 (-CH<sub>2</sub>), 29.8 (4 x -CH<sub>2</sub>), 29.7 (-CH<sub>2</sub>), 29.6 (-CH<sub>2</sub>), 29.5 (-CH<sub>2</sub>), 29.1 (-CH<sub>2</sub>), 28.6 (-CH<sub>2</sub>), 23.9 (-CH<sub>2</sub>), 22.8 (-CH<sub>2</sub>), 14.3 (-CH<sub>3</sub>). HRMS (ESI) exact mass calculated for  $\text{C}_{24}\text{H}_{35}\text{BF}_2\text{N}_2\text{O}_2\text{Na}$  [ $\text{M}+\text{Na}$ ]<sup>+</sup>  $m/z$  455.2652, found  $m/z$  455.2633. IR (thin film) 2924, 1705, 1612, 1157, 972, 687. Melting point 94–98 °C.



1.22

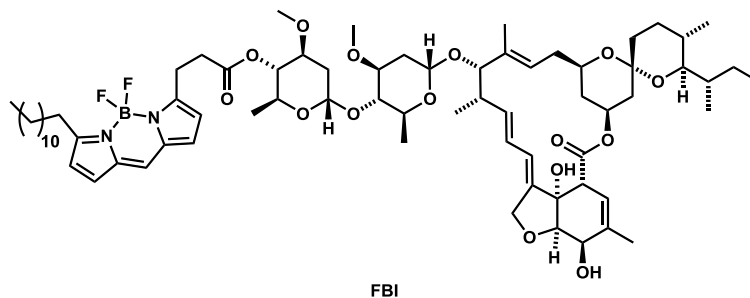
**1.22.** Prepared according to a modified literature procedure.<sup>[22]</sup> To an oven dried flask cooled under vacuum and charged with argon was added anhydrous tetrahydrofuran (0.40 mL, 0.15 M), acid **1.18** (28 mg, 65  $\mu$ mol, 1 equiv.) and one drop of *N,N*-dimethylformamide and the resulting solution was stirred at ambient temperature. To this was added oxalyl chloride (22  $\mu$ L, 0.26 mmol, 4 equiv.) and the resulting solution was stirred at ambient temperature for two hours. The solvent was removed *in vacuo* and the residue dissolved in tetrahydrofuran (5 mL) and repeated (3 x 5 mL) affording title compound **1.22**. The crude material was used immediately without further purification.



1.23

**1.23.** Prepared according to a modified literature procedure.<sup>[22]</sup> To an oven dried flask cooled under vacuum and charged with argon was added silyl ether **1.12** (49 mg, 49  $\mu\text{mol}$ , 1 equiv.), dichloromethane (0.1 mL, 0.5 M), 4-dimethylaminopyridine (7.6 mg, 49  $\mu\text{mol}$ , 1 equiv.) and *N,N*-diisopropylethylamine (9.0  $\mu\text{L}$ , 49  $\mu\text{mol}$ , 1 equiv.) and the resulting stirred solution was cooled to 0 °C. To this was added a solution of acyl chloride **1.22** (29 mg, 65  $\mu\text{mol}$ , 1.3 equiv.) in anhydrous dichloromethane (0.1 mL, 0.65 M) and the resulting solution was stirred at 0 °C for two hours. To the reaction mixture was added ice and the aqueous phase was extracted with dichloromethane (3 x 5 mL). The combined organic extracts were dried with magnesium sulphate, filtered and concentrated *in vacuo* yielding a red oil (79 mg). Purification by column chromatography on silica gel with an eluent of 15% ethyl acetate in petroleum ether afforded title compound **1.23** (10 mg, 7.1  $\mu\text{mol}$ , 15%) as a red solid.

<sup>1</sup>H NMR (400 MHz, CDCl<sub>3</sub>)  $\delta$  7.08 (1H, s), 6.99 (1H, d, *J* = 4.2), 6.92 (1H, d, *J* = 4.1), 6.37 (1H, d, *J* = 4.2), 6.35 (1H, d, *J* = 4.2), 5.84–5.78 (1H, m), 5.72 (1H, d, *J* = 4.2), 5.70 (1H, s), 5.39 (1H, d, *J* = 3.8), 5.37–5.27 (2H, m), 5.02–4.94 (1H, m), 4.77 (1H, d, *J* = 3.8), 4.70 (1H, t, *J* = 9.4), 4.67 (1H, dd, *J* = 14.4, 2.4), 4.57 (1H, dd, *J* = 14.4, 2.3), 4.45–4.41 (1H, m), 4.22 (1H, s), 3.93 (1H, br s), 3.88–3.78 (2H, m), 3.82 (1H, d, *J* = 5.6), 3.72–3.54 (3H, m), 3.42 (3H, s), 3.39–3.34 (3H, m), 3.32 (3H, s), 3.25–3.18 (2H, m), 2.98 (2H, t, *J* = 7.8), 2.81 (2H, t, *J* = 7.2), 2.55–2.46 (1H, m), 2.37–2.27 (3H, m), 2.26–2.18 (1H, m), 2.03–1.94 (1H, m), 1.80–1.77 (3H, m), 1.77–1.60 (6H, m), 1.59–1.20 (34H, m), 1.15 (3H, d, *J* = 6.9), 1.10 (3H, d, *J* = 6.2), 0.92 (11H, s), 0.88–0.83 (6H, m), 0.78 (3H, d, *J* = 4.9), 0.13 (6H, s). <sup>13</sup>C NMR (100 MHz, CDCl<sub>3</sub>)  $\delta$  174.3, 171.8, 164.7, 161.0, 160.9, 140.5, 140.4, 137.7, 137.6, 137.5, 135.1, 134.5, 134.4, 131.0, 130.6, 129.8, 129.6, 127.4, 127.3, 125.0, 124.9, 119.5, 118.5, 118.1, 117.4, 98.5, 98.4, 97.6, 95.0, 82.1, 80.8, 80.4, 80.2, 79.4, 57.8, 57.5, 69.7, 68.9, 68.1, 67.3, 67.2, 66.6, 66.2, 57.0, 56.9, 56.7, 56.6, 45.9, 41.3, 39.8, 37.3, 37.0, 35.9, 35.7, 35.6, 35.2, 34.7, 34.3, 33.5, 32.1, 3 x 29.8, 29.7, 29.6, 29.5, 26.0, 22.8, 20.2, 18.6, 17.6, 14.3, 12.6, 12.3, -4.4, -4.7. HRMS (ESI) exact mass calculated for C<sub>78</sub>H<sub>121</sub>BF<sub>2</sub>N<sub>2</sub>O<sub>15</sub>SiNa [M+Na]<sup>+</sup> *m/z* 1425.8490, found *m/z* 1425.8482. IR (thin film) 2928, 1734, 1701, 1609. Melting point 46–49 °C.



**FBI.** Prepared according to a modified literature procedure.<sup>[22]</sup> To a stirred solution of silyl ether **1.23** (18 mg, 13  $\mu\text{mol}$ , 1 equiv.) in methanol (1.4 ml, 0.01 M) at ambient temperature was added 4-toluenesulfonic acid (14 mg, 1 mol%) and the resulting solution was stirred for five hours. To the reaction mixture was added saturated aqueous sodium hydrogen carbonate solution (15 mL) and the aqueous phase was extracted with ethyl acetate (3 x 10 mL). The combined organic extracts were washed with water (3 x 10 mL), dried with magnesium sulphate, filtered and concentrated *in vacuo* yielding a red oil. Purification by column chromatography on silica gel with an eluent of 20% ethyl acetate in petroleum ether afforded title compound **FBI** (7.0 mg, 5.4  $\mu\text{mol}$ , 42%).

$^1\text{H}$  NMR (400 MHz,  $\text{CDCl}_3$ )  $\delta$  7.08 (1H, s), 6.99 (1H, d,  $J = 4.2$ ), 6.93 (1H, d,  $J = 4.2$ ), 6.37 (2H, d,  $J = 4.2$ ), 6.35 (1H, d,  $J = 4.2$ ), 5.89–5.83 (1H, m), 5.79–5.66 (2H, m), 5.42 (1H, br s), 5.39 (1H, d,  $J = 3.7$ ), 5.37–5.31 (1H, m), 4.98 (1H, br d,  $J = 11.1$ ), 4.77 (1H, d,  $J = 3.8$ ), 4.74–4.63 (3H, m), 4.29 (3H, t,  $J = 7.0$ ), 4.13 (1H, s), 3.97 (1H, d,  $J = 6.2$ ), 3.94 (1H, br s), 3.87–3.79 (2H, m), 3.72–3.55 (3H, m), 3.43 (3H, s), 3.36 (1H, dd,  $J = 7.3, 2.1$ ), 3.32 (3H, s), 3.30–3.27 (1H, m), 3.22 (2H, t,  $J = 9.0$ ), 2.98 (2H, t,  $J = 7.9$ ), 2.81 (2H, t,  $J = 7.2$ ), 2.54–2.48 (1H, m), 2.37–2.18 (5H, m), 1.97 (1H, dd,  $J = 12.5, 4.5$ ), 1.88 (3H, s), 1.80–1.70 (3H, m), 1.69–1.61 (3H, m), 1.60–1.21 (32H, m), 1.16 (3H, d,  $J = 6.9$ ), 1.10 (3H, d,  $J = 6.2$ ), 0.93 (3H, t,  $J = 7.3$ ), 0.90–0.84 (5H, m), 0.79 (3H, d,  $J = 5.7$ ).  $^{13}\text{C}$  NMR (100 MHz,  $\text{CDCl}_3$ )  $\delta$  174.0, 171.9, 139.8, 138.2, 138.1, 135.1, 131.0, 129.6, 127.5, 124.9, 120.6, 118.8, 118.5, 118.2, 118.1, 98.5, 97.6, 95.0, 81.9, 80.8, 80.5, 79.4, 79.2, 76.6, 75.8, 68.8, 68.7, 67.9, 67.4, 67.3, 66.6, 57.1, 56.7, 45.9, 41.3, 39.9, 37.1, 35.9, 35.6, 35.2, 34.7, 34.3, 33.5, 32.1, 31.6, 31.4, 30.5, 30.3, 29.9, 6 x 29.8, 29.7, 29.6, 29.5, 29.1, 28.6, 28.2, 27.5, 24.1, 22.9, 20.4, 20.2, 18.6, 17.6, 15.3, 14.3, 12.6, 12.3. HRMS (ESI) exact mass calculated for  $\text{C}_{72}\text{H}_{107}\text{BF}_2\text{N}_2\text{O}_{15}\text{Na}$   $[\text{M}+\text{Na}]^+$   $m/z$  1311.7625, found  $m/z$  1311.7575. IR (thin film) 2956, 1742, 1716, 1608, 965, 699. UV (MeOH) Absorption  $\lambda_{\text{max}}$  509 nm ( $\epsilon$  60700  $\text{cm}^{-1}\text{M}^{-1}$ ), Emission  $\lambda_{\text{max}}$  514 nm.

## Chapter 2. Synthesis of PROTAC Molecules Towards *in vivo* Degradation of HIV Capsid Protein

### 2.1 Introduction

#### 2.1.1 Human Immunodeficiency Virus

Human immunodeficiency virus (HIV) is a pathogenic retrovirus that infects cells of the human immune system. If the infection is left untreated, it can develop into acquired immunodeficiency syndrome (AIDS). An estimated 50 million people worldwide are infected with HIV and an estimated 35 million have died from AIDS related diseases since the beginning of the HIV/AIDS epidemic in 1981.<sup>[62][63]</sup>

Although no cure for HIV infection exists, treatments are available that suppress viral replication, enabling partial recovery of the host immune system. Such viral suppression almost completely eliminates the risk of HIV infection developing into AIDS and greatly reduces the risk of transmission to uninfected individuals.<sup>[64][65]</sup> These existing treatments (known as antiretroviral treatment (ART)), are small molecule drugs of various classes which target either viral proteins, or host cell proteins key to HIV replication.<sup>[66]</sup>

The hallmarks of retroviral (and therefore HIV) replication are reverse transcription of viral RNA into DNA, and subsequent integration of the viral DNA into the host cell genome.<sup>[67]</sup> However, these processes are inherently inefficient and result in mutations which inevitably lead to ART resistance.<sup>[62]</sup> In recent years, combinations of ART drugs have been administered in an effort to reduce the likelihood of developing resistance. This approach, known as highly active antiretroviral therapy (HAART), is the combination of three or more ART drugs of different classes. While it is an effective strategy to limit retroviral drug resistance, resistance is still prevalent.<sup>[68][69][70][71][72]</sup> Ultimately, when killing or suppressing the reproduction/replication of any pathogen, selection for drug resistance is unavoidable. For this reason, novel drug targets and particularly novel therapeutic strategies are attractive targets for future research.<sup>[62]</sup>

#### 2.1.2 Occupancy-Based Drug Paradigm

At present, the majority of small molecule pharmaceuticals, including HIV therapies, rely on the occupancy of an inhibitor in a specific binding site of a target protein (Figure 2.1). In the case of competitive inhibition for example, the binding of the

inhibitor to the same site as the proteins endogenous ligand prevents the ligand from binding, which consequently inhibits the natural function(s) of the protein.

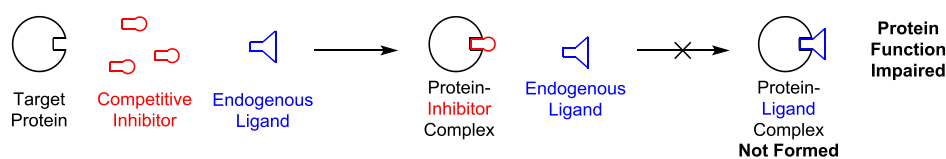


Figure 2.1. Basic concept behind the occupancy based inhibitor paradigm.

While current medical technology is the most effective it has ever been, the occupancy-based drug paradigm that is the cornerstone of modern medicine has several drawbacks. The requirement of one drug molecule per protein necessitates a high systemic concentration of the drug, which increases the likelihood of off-target side effects (Figure 2.2).<sup>[73]</sup> Furthermore, the instant the drug is no longer bound to the protein, for example *via* drug metabolism, the protein regains its function.<sup>[73]</sup> In an attempt to mitigate possible off-target side effects and prolong drug-protein binding, high binding affinities are sought. This requires extensive structure activity relationship (SAR) studies and optimisation, leading to a high attrition rate of potential pharmaceuticals. While this high attrition rate results in safer drug compounds and is thus not necessarily a drawback in itself, it has resulted in the lowest level of approved drugs in a generation.<sup>[74]</sup>

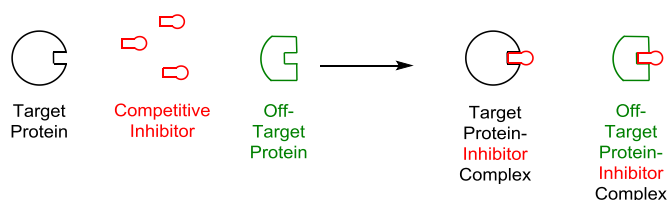


Figure 2.2. Basic depiction of off-target engagement.

Additionally, small molecule inhibitors typically inhibit only one domain of multidomain proteins (Figure 2.3). This leaves their scaffolding functions and interactions with other proteins unperturbed.<sup>[75]</sup>

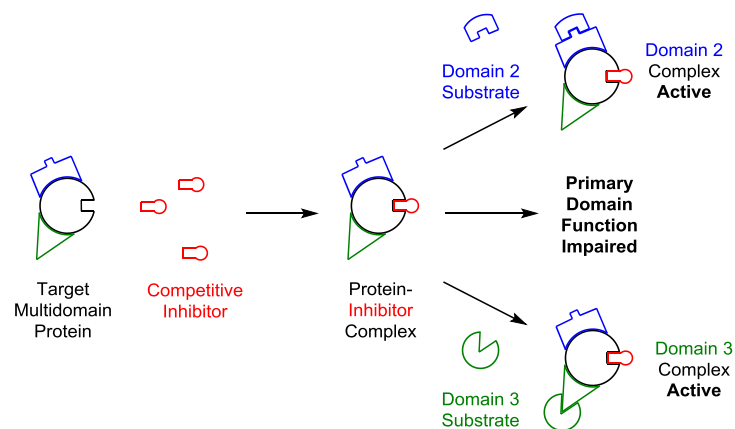


Figure 2.3. Depiction of single domain inhibition of multidomain proteins.

Furthermore, the use of small molecule inhibitors requires the target protein to possess a binding site for the drug. While this is common in proteins that interact with endogenous small molecule ligands such as enzymes and ion channels, many disease-causing proteins interact with other proteins *via* protein-protein interactions (PPI).<sup>[76]</sup> The proteins that interact solely *via* PPI typically lack these well defined binding sites and are not currently amenable to small molecule inhibition, and have thus been termed “undruggable” (Figure 2.4). With 80% of the proteome classified as “undruggable”<sup>[76]</sup>, it is evident that novel therapeutic strategies and novel drug discovery paradigms are required to advance medical care.

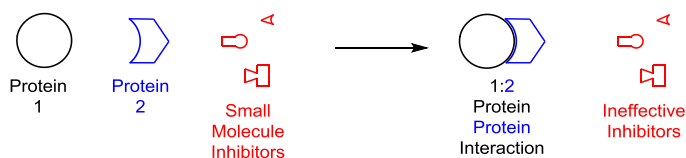


Figure 2.4. Depiction of inability of small molecule inhibitors to interfere with protein-protein interactions.

### 2.1.3 Targeted proteolysis

A recently emerging therapeutic avenue that avoids the occupancy-based drug paradigm, is targeted proteolysis. Instead of small molecule inhibition of a target protein, targeted proteolysis utilises a small molecule to direct the degradation of a protein of interest *via* the endogenous cellular degradation machinery (Figure 2.5). These small molecules, referred to as proteolysis targeting chimeras (PROTACs), have the potential to circumvent many of the drawbacks inherent with the traditional occupancy-based drug approach. However, before PROTAC technology is discussed in greater detail, it is important to have an understanding of natural protein degradation.

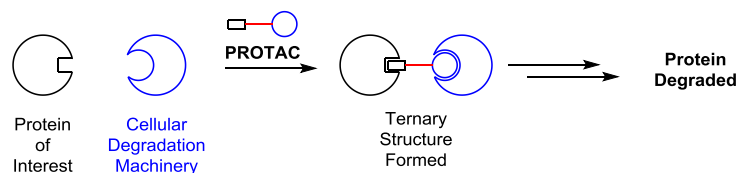


Figure 2.5. Basic concept of PROTAC technology.

#### 2.1.4 Natural Degradation of Endogenous Proteins

The natural cellular degradation of endogenous proteins is an extremely important process which occurs for a variety of reasons. Regulatory proteins such as transcription factors and proteins that respond to specific stimuli require rapid degradation to help regulate intracellular enzyme activity.<sup>[77][78]</sup> Additionally, to eliminate the consequences of errors in protein translation, faulty and damaged proteins are also signalled for rapid degradation.<sup>[77][78]</sup> Two major pathways of protein degradation exist in eukaryotic cells, the ubiquitin-proteasome pathway (UPP) and lysosomal proteolysis.<sup>[77][78]</sup> For the purposes of this thesis, only the UPP is of relevance. The UPP is the major pathway of selective proteolysis in eukaryotic cells.<sup>[77]</sup> In essence, an enzyme cascade tags a protein with ubiquitin (a 76 residue polypeptide cofactor) which signals the protein for degradation by the proteasome (a multisubunit complex of proteases) (Figure 2.6).<sup>[77][79]</sup> The enzyme cascade of the UPP is composed of enzymes E1, E2 and E3. The E1 enzyme is responsible for the activation of ubiquitin by reaction of the C-terminal carboxylate with ATP to form the corresponding ubiquitin adenylate. The ubiquitin adenylate then reacts with a catalytic cysteine residue of the E1, forming a thioester and generating the E1-ubiquitin complex.<sup>[79]</sup> Following this, the ubiquitin is transferred to the E2 enzyme, forming an E2-ubiquitin conjugate *via* transthioesterification. Finally, the E3 enzyme allows for the transfer of ubiquitin from the E2-ubiquitin conjugate, to the target protein *via* the formation of an amide bond to an available lysine residue. This process happens several times, forming a poly-ubiquitinated protein which is recognised by the proteasome, and subsequently degraded.<sup>[79]</sup>

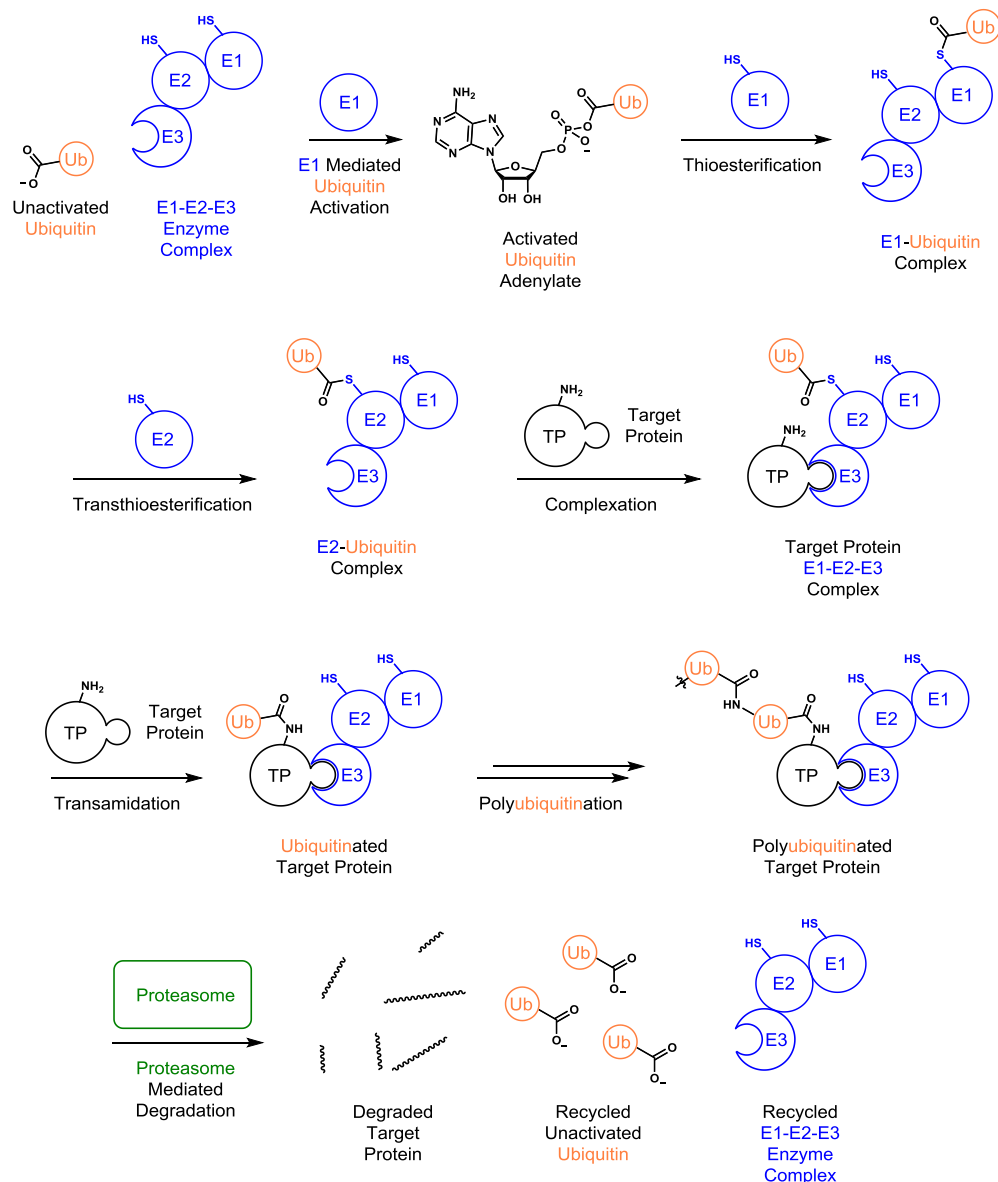


Figure 2.6. Basic concept of natural cellular degradation of endogenous proteins.

For this project, the most important of these enzymes is the E3 ligase of which over 1000 are coded for in the human genome as it is the E3 ligases that are responsible for conferring specificity for the target protein.<sup>[78]</sup> Combining known ligands of different E3 ligases with small molecule inhibitors allows for the targeted degradation of proteins of interest. This hijacking of the cellular degradation machinery is the core concept of PROTAC technology.

### 2.1.5 Proteolysis Targeting Chimeras (PROTACs)

PROTACs, as mentioned briefly above, are heterobifunctional small molecules that comprise an E3 ligase ligand connected *via* a linker to a ligand that binds a protein of interest. They act as a molecular adapter to connect a disease-causing protein to a chosen E3 ligase, which would otherwise not have been recognised by the ligase (Figure 2.7). This proximity to the E1-E2-E3 enzyme cascade allows the natural

cellular degradation process to effect ubiquitination and subsequent degradation of the target protein. This strategy has the potential to address many of the drawbacks of traditional occupancy-based protein inhibition which were outlined above (2.1.2 Occupancy-Based Drug Paradigm, page 87).

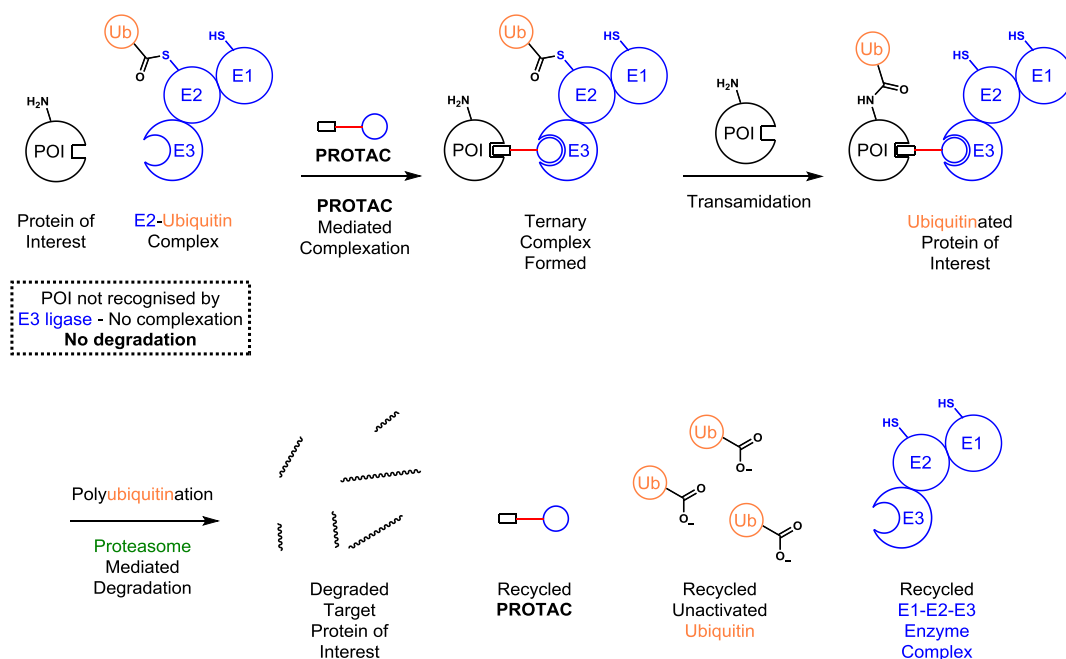


Figure 2.7. Basic concept of PROTAC mediated degradation.

PROTACs have been shown to act catalytically as they are not degraded by the proteasome, allowing one PROTAC molecule to degrade multiple protein copies. This allows for a lower systemic concentration of the compound and subsequently reduces the likelihood of off-target engagement and side effects.<sup>[41]</sup> As discussed previously, traditional inhibition of multidomain proteins only inhibits the function of one domain. In contrast, the degradation of multidomain proteins induced by PROTACs eliminates all of the proteins' functions such as scaffolding, interaction with other proteins and downstream signalling cascades.<sup>[75][80]</sup> Furthermore, the protein is degraded rapidly and the low cellular protein levels are often sustained for up to 48 hours after the removal of the PROTAC.<sup>[75][41][81]</sup> Perhaps one of the strongest potential advantages to PROTAC technology, lies in its ability to induce degradation with only transient binding.<sup>[75][82][83]</sup> This introduces the possibility to target the so-called "undruggable" 80% of the proteome. The degradation of proteins, allows for the disruption of PPIs, something that traditional inhibitors have notoriously struggled to achieve.<sup>[82]</sup>

### 2.1.6 E3 Ligase Ligand

A vast number of E3 ligases exist and the choice of which E3 ligase to recruit in PROTAC design can be highly influential to its efficacy. Research has primarily

focussed on a limited number of these ligases and several small molecule ligands that bind the ligases have been identified. Successful PROTACs to date have incorporated ligands for four particular E3 ligases: MDM2, IAP, VHL and CRBN.<sup>[75]</sup> Since 2015, over 30 PROTACs have been reported in literature, the vast majority of which incorporate ligands for the exploitation of VHL (von Hippel-Lindau) and CRBN (Cereblon).<sup>[75]</sup>

The primary endogenous substrate of the VHL E3 ligase is hypoxia-inducible factor 1 $\alpha$  (HIF-1 $\alpha$ ). This transcription factor is important in the upregulation of several genes and as such its intracellular protein levels are maintained at a low level by VHL-mediated degradation.<sup>[84]</sup> Hydroxylation of a proline residue of HIF-1 $\alpha$  allows for its recognition by VHL and with this knowledge, inhibitors of the HIF-1 $\alpha$ :VHL interaction were developed (Figure 2.8).<sup>[84][85]</sup> Using these inhibitors as VHL-targeting ligands, several PROTACs have been developed that target various different classes of proteins. These include GFP-halotag fusion proteins, kinases, estrogen receptors and bromodomain containing proteins.<sup>[75][84]</sup>

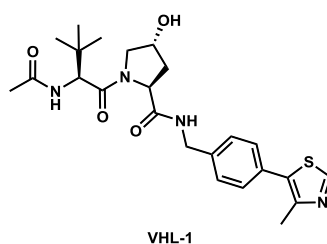


Figure 2.8. Structure of **VHL-1**, a known inhibitor of the VHL E3 ligase.

The CRBN E3 ligase has been shown to bind the phthalimide-based immunomodulatory drugs **thalidomide**, **pomalidomide** and **lenalidomide** (Figure 2.9).<sup>[75][86][87]</sup> This discovery was made after years of research directed towards elucidating the teratogenicity-causing target of **thalidomide** after the infamous disaster in the late 1950's.<sup>[86][87]</sup> While (*S*)-**thalidomide** was responsible for the teratogenic effects observed in the 50's/60's, rapid *in vivo* racemisation of the phthalimide-based drugs (**thalidomide**, **pomalidomide** and **lenalidomide**) is known and both (*S*)- and (*R*)-**thalidomide** were found to bind to the same CRBN E3 ligase target.<sup>[88][89]</sup> Since the discovery of the CRBN E3 ligase target, the phthalimide-based drugs have been incorporated as E3 ligase ligands into numerous CRBN recruiting PROTACs. Similarly to the VHL-based PROTACs, CRBN-based PROTACs have been reported that degrade a variety of different protein classes including bromodomain and extra terminal (BET) proteins, kinases and the epigenetic eraser protein Sirt2.<sup>[75][90][91][92]</sup>

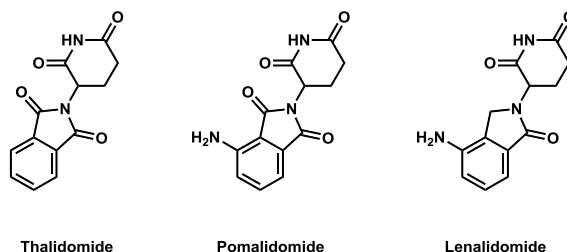


Figure 2.9. Structures of **thalidomide**, **pomalidomide** and **lenalidomide**, known ligands of the CRBN E3 Ligase

Due to the modular character of PROTACs, research has highlighted the importance of E3 ligase ligand selection toward the efficacy of the PROTAC. When the ternary structure of POI-PROTAC-E3 Ligase is formed, key interactions form between each member which stabilises the structure and increases the likelihood of successful degradation.<sup>[83]</sup> The selection of which E3 ligase to target (and thus the selection of E3 ligase ligand utilised in the PROTAC) can either increase or decrease the number of these favourable interactions.<sup>[83]</sup> The selection of E3 ligase ligand is therefore extremely important; however, all constituents of the PROTAC can have a large effect on its efficacy, including the linker.

### 2.1.7 Linker

While the primary function of the linker is to connect the two protein binding ligands, it also plays an important role in stabilising the ternary structure, and can be used to modulate various physicochemical properties of the PROTAC such as solubility and cell permeability.<sup>[83][93][94][95]</sup> As an example, using molecular dynamics modelling it was shown that a poly ethylene glycol (PEG) based linker adopted a kinked conformation allowing key PPI to occur between the E3 ligase and the POI.<sup>[93]</sup> Furthermore, this kinked conformation allowed the formation of key hydrophobic interactions between the E3 ligase and the linker itself.<sup>[93]</sup> While this highlighted the importance of linker composition, it was also shown that linker lengths long enough to allow the formation of the kinked conformation were necessary for the stabilisation of the ternary structure. However, linker lengths exceeding this optimal length by even a single ethylene glycol unit, almost completely destroyed the activity of the PROTAC.<sup>[93]</sup> In contrast to this, studies to determine optimal linker lengths have been performed which have concluded that longer linker lengths of around 12 and above non-hydrogen atoms (NHA) are generally more desirable.<sup>[96]</sup> Ultimately, optimal linker length appears to be highly dependent on the system in which it is required, and thus prudent PROTAC design should be modular to allow for facile incorporation of multiple diverse linkers.

### 2.1.8 Targeting HIV

A basic schematic of the structure of HIV is shown below, highlighting some important structural components of HIV (Figure 2.10).<sup>[97]</sup> The viral genome is encoded on two identical copies of RNA which is later reverse transcribed into double stranded DNA by the viral reverse transcriptase (RT).<sup>[98]</sup> As with all viruses, the genome materials are encased within the capsid, a proteinaceous shield composed of capsid protein (CA).<sup>[99]</sup> This in turn is encased within the viral envelope upon the surface of which, envelope glycoproteins are expressed that are involved in host cell recognition and entry.<sup>[99][100]</sup>

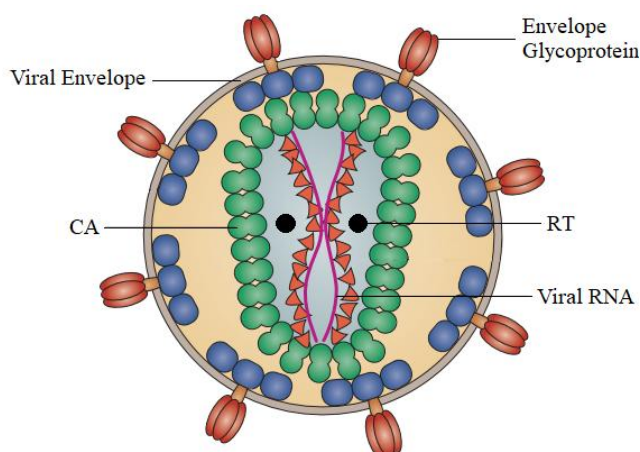


Figure 2.10. Basic structure of HIV-1 virion.<sup>[97]</sup>

While a peptidic Hepatitis B-targeting PROTAC has been developed, until recently no small molecule PROTAC-induced degradation of viral proteins had been reported.<sup>[101]</sup> In the past month a small molecule PROTAC that degrades the Hepatitis C protease was published, but small molecule PROTACs that degrade non-hepatitis viral proteins are hitherto unreported.<sup>[102]</sup> However, several small molecule inhibitors of HIV replication are known which inhibit different key proteins important in HIV replication.<sup>[66][67]</sup> Fuelled by the rapid replication and the high mutation rate of the virus, antiviral drug resistance is prevalent.<sup>[68][69][70][71][72]</sup> This widespread resistance necessitates a relentless search for novel drug targets. One such promising candidate that has emerged from the search for new targets is the capsid. This conical structure is composed of capsid protein (CA) arranged in a lattice of predominantly hexameric CA subunits (orange) with some pentameric CA subunits (yellow) responsible for the increased curvature of the conical shape (Figure 2.11).<sup>[97][103]</sup>

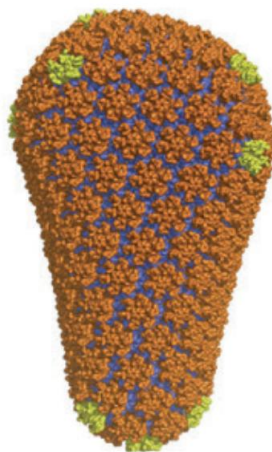


Figure 2.11. Conical structure of the assembled capsid core consisting of hexameric CA (orange) and pentameric CA (yellow).<sup>[97]</sup>

After viral entry to the host cell, the capsid disassembles in a highly controlled manner. This process, known as uncoating, is extremely important to the infectivity of the virus and perturbation of the process results in failed replication.<sup>[103]</sup> This makes the capsid a desirable drug target, and an HIV inhibitor known as **PF74** was developed by Pfizer which binds to the capsid and disrupts the uncoating process (Figure 2.12).<sup>[103][104]</sup>

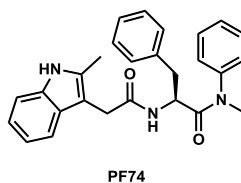


Figure 2.12. The HIV capsid-targeting inhibitor **PF74**.

As is often the case with small molecule inhibitors of viral targets, resistance to **PF74** has been reported.<sup>[105]</sup> This resistance is complex and requires four amino acid mutations in the vicinity of the **PF74** binding site. Interestingly however, the **PF74**-resistant mutant does not prevent the binding of **PF74** to its binding site. This serves to highlight another possible advantage of PROTAC technology over small molecule inhibition. As PROTAC technology requires only binding (and not the typically associated inhibition), a PROTAC based on **PF74** would likely still degrade the **PF74**-resistant CA protein. Furthermore, **PF74** as an inhibitor has a relatively high reported  $EC_{50}$  of 473 nM (although this has recently been improved through extensive MedChem optimisation).<sup>[106]</sup> This is less potent than most effective inhibitors, but is potent enough to achieve the transient binding required for PROTAC efficacy. These factors make capsid protein an attractive target for **PF74**-based PROTAC-induced degradation.

### 2.1.9 PF74 and Capsid Protein

The crystal structure of **PF74** bound to capsid protein (CA) has been determined, which revealed the binding site to be located approximately 30 Å into the interface between two monomer CA subunits of a single hexameric CA complex (Figure 2.13).<sup>[105][107][108]</sup> Important amino acid residues are highlighted by their representation as ‘sticks’ and favourable hydrogen bond interactions are denoted by dashed lines.<sup>[107][108]</sup> **PF74** has been shown to have an affinity for the assembled CA hexamer that is over tenfold greater than the affinity for unassembled CA monomers due to additional favourable interactions in the binding site of the assembled protein.<sup>[105][108]</sup> Of particular interest to this project, is the solvent exposed tertiary amide *N*-methyl group (highlighted by a red circle). The solvent exposure at this position and the lack of key binding interactions make it an ideal site for linker attachment. With these factors in mind, PROTACs based on **PF74** (as the POI ligand) were designed toward the aim of capsid protein degradation.

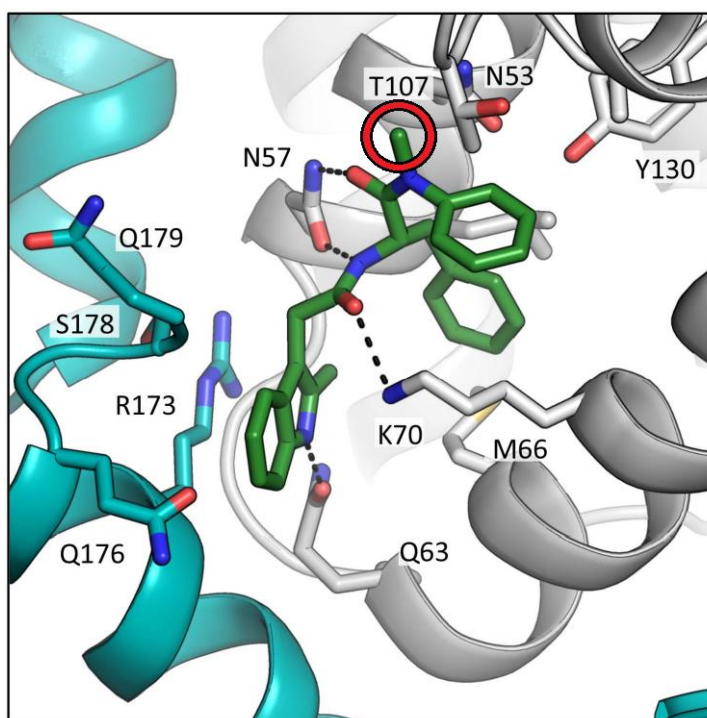


Figure 2.13. **PF74** bound to interface between two CA subunits (teal and grey) of hexameric CA.<sup>[107]</sup> The solvent exposed *N*-methyl is highlighted (red circle).

### 2.1.10 First generation probe design

For the design of the first generation of capsid targeting PROTACs, two PROTACs were designed which are outlined below (Figure 2.14). Both incorporate **PF74** as the capsid protein ligand. The PROTACs are named **VHL-38** and **CRBN-N33** and the names indicate the particular E3 ligase that is to be recruited (VHL or CRBN),

followed by the length of the linkers (expressed as the number of non-hydrogen atoms, 38 or 33) utilised by each PROTAC.

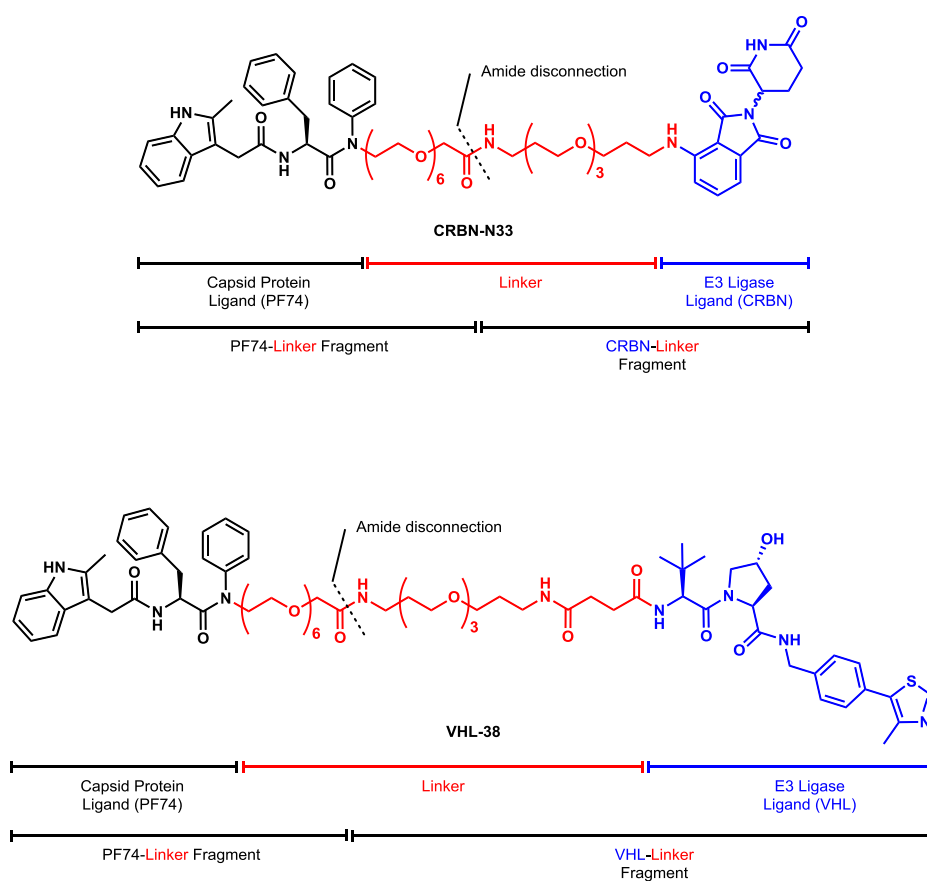


Figure 2.14. Design and composition of first generation PROTACs.

The linkers are composed of polyethylene glycol (PEG) chains and are connected to the **PF74** moiety at the *N*-methyl group of the tertiary amide due to the aforementioned solvent exposure of this position. (Figure 2.13, page 97). The primary rationale behind the selection of hydrophilic PEG-based linkers was to improve the solubility of the lipophilic protein ligand moieties in aqueous media.<sup>[95]</sup> Furthermore, PEG chains are readily available in various lengths, facilitating the synthetic tractability of structural analogues. These lengths were chosen as they are beyond 30 Å in length which was the approximate calculated depth of the **PF74** binding site into the interface between two CA subunits. The major difference between **VHL-38** and **CRBN-N33** is the choice of E3 ligase ligands. **VHL-38** incorporates **VHL-1** (Figure 2.8, page 93) and **CRBN-N33** incorporates **pomalidomide** (Figure 2.9, page 94). The decision to incorporate both ligands was simply to increase the likelihood of successful degradation, and to have a comparison between the efficacies of the two ligands that would help guide the design of the second generation PROTACs.

To increase convergence of the synthesis, it was proposed to generate the PROTACs from three roughly equal sized fragments (Figure 2.14). A **PF74**-linker fragment (which is common to both PROTACs and terminates in an acid), a **CRBN**-linker fragment (for use in **CRBN-N33** and which terminates in an amine) and a **VHL**-linker fragment (for use in **VHL-38** and which also terminates in an amine).

### 2.1.11 Synthetic Strategy

Strategically, the proposed synthetic route involved adopting a modular and thus convergent approach. It was envisioned that protected versions of the abovementioned fragments could be constructed from smaller fragments (Figure 2.15). The protected **PF74**-linker fragment could be accessed from a tertiary amide coupling between the acid terminating **PF74** fragment and the aniline linker fragment. The protected **CRBN**-linker fragment could be accessed from a  $S_NAr$  alkylation of an electrophilic **CRBN** fragment and the nucleophilic amine linker fragment. Finally, the protected **VHL**-linker fragment could be generated by amide coupling between the acid linker fragment and the terminal amine of **VHL-1**.

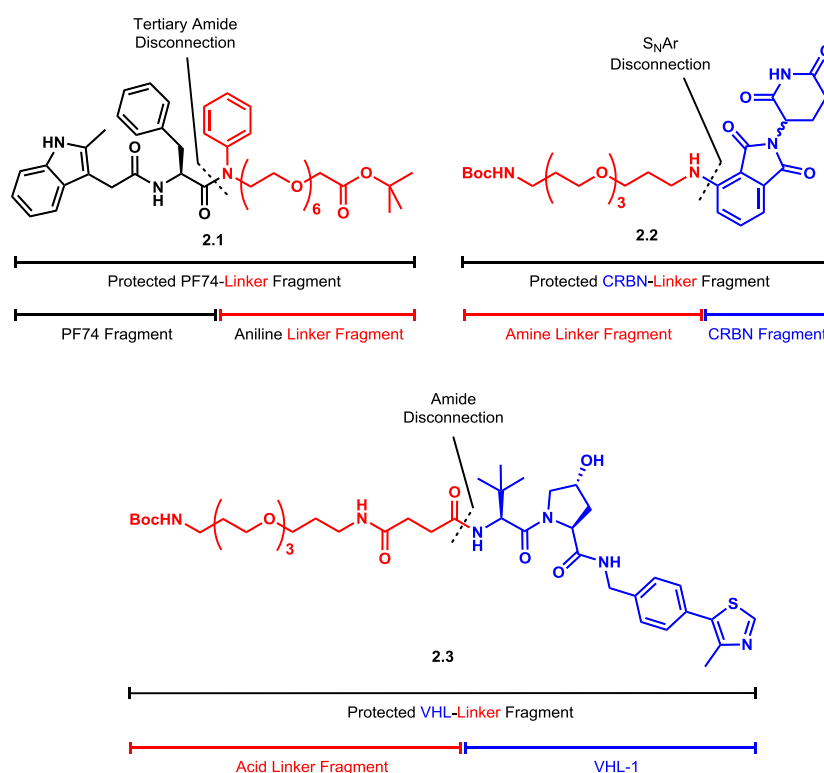


Figure 2.15. Schematic of PROTAC fragments and their constituent fragments.

## 2.2 Results and Discussion

### 2.2.1 Protected PF74-Linker Fragment Synthesis

Initial efforts were focussed on the synthesis of the protected **PF74**-linker fragment **2.1**, as this fragment is common to both of the proposed PROTACs (Figure 2.16). To begin with, the aniline linker fragment was targeted which comprised a protected terminal acid (for coupling to an amine of the E3 ligase fragment) and a terminal secondary aniline (for coupling to an acid of the **PF74** fragment).

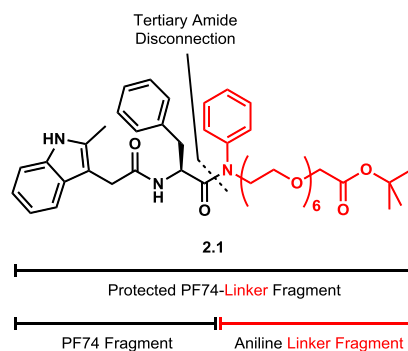
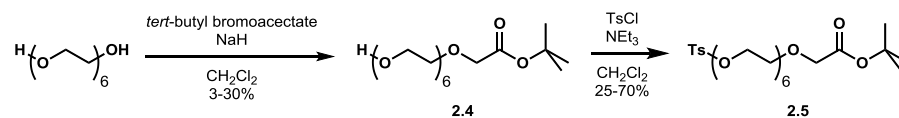


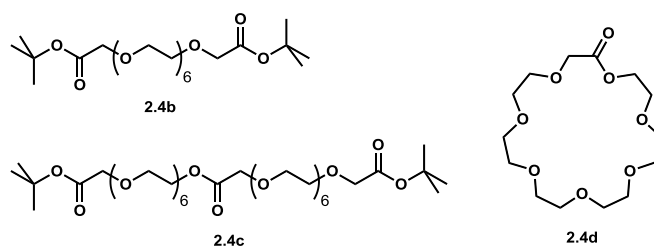
Figure 2.16. Protected **PF74**-linker fragment.

### Aniline Linker Fragment Synthesis

In order to generate such a linker, direct mono alkylation of hexaethylene glycol with *tert*-butyl bromoacetate was attempted (Scheme 2.1).<sup>[109]</sup> This initial attempt however, was largely unsuccessful. While some ester **2.4** was observed, the yield was low and the presence of various side products resulted in a difficult purification. Using LCMS analysis, the plausible identities of the aforementioned side products were determined. The *m/z* ratios attained from the analysis were consistent with that of dialkylated product **2.4b**, diester **2.4c** and macrocyclic ester **2.4d**. Diester **2.4c** likely formed as a result of two molecules of desired ester **2.4** reacting *via*  $S_N2$  displacement and transesterification with *tert*-butyl bromoacetate. The macrocyclic product **2.4d** is presumably a result of intramolecular transesterification of the desired ester **2.4**. Despite the drawbacks, enough material of ester **2.4** was generated to attempt the following tosyl activation (Scheme 2.1).<sup>[110]</sup> While the tosyl activation did produce the desired tosylate **2.5**, the yield of the reaction suffered from irreproducibility. The most likely cause of this was inconsistent starting material purity. Upon concentration of the isolated ester **2.4**, spontaneous degradation of the sample was observed. With all of these drawbacks, the route was abandoned.

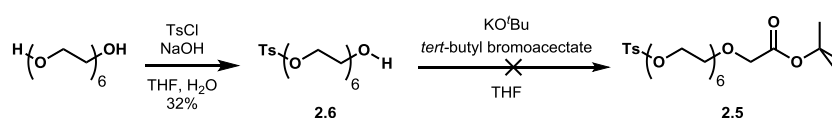


#### 2.4 Side Products



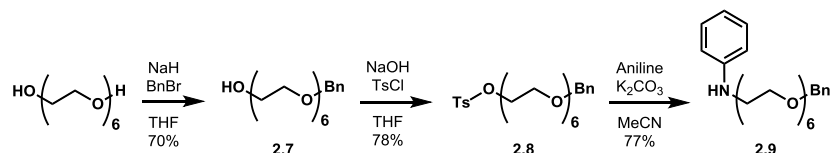
Scheme **2.1**. Alkylation of hexaethylene glycol to ester **2.4** (and side products **2.4b**, **2.4c** and **2.4d**), and subsequent activation to tosylate **2.5**.

The next attempt involved an initial mono tosyl activation of hexaethylene glycol, followed by alkylation of the remaining alcohol with *tert*-butyl bromoacetate (Scheme **2.2**).<sup>[110]</sup> Despite several attempts, the initial tosyl activation suffered from a poor yield and the hexaethylene glycol starting material could not be recovered. Enough of tosylate **2.6** was generated to attempt the subsequent alkylation; however, this reaction did not produce any of the desired ester **2.5**.<sup>[110]</sup> In light of this and the low yielding tosyl activation, this route was terminated.



Scheme **2.2**. Activation of hexaethylene glycol to tosylate **2.6** followed by the failed alkylation to ester **2.5**.

The next attempted route took inspiration from a publication by the Crews group, which involved an additional benzyl protection and deprotection sequence.<sup>[109]</sup> For this reason, the route was not initially attempted, opting instead for the abovementioned brevity-focused routes. Adopting the Crews-type route, an initial mono benzyl protection of hexaethylene glycol generated benzyl ether **2.7** in a 70% yield (Scheme **2.3**).<sup>[109]</sup> Following the successful and reproducible benzylation, the activation of the remaining free alcohol to the corresponding tosylate **2.8** proceeded with an efficient 78% yield which was reproducible at increased scale.<sup>[110]</sup> To complete this sequence, the tosylate group was displaced with aniline to generate secondary aniline **2.9** in a 77% yield.

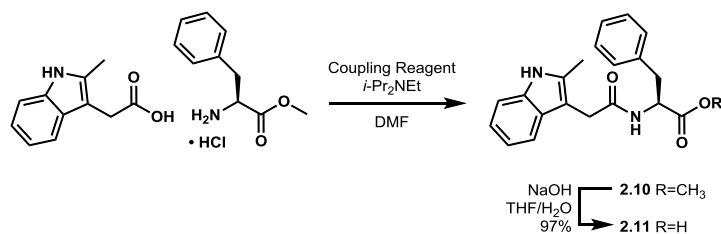


Scheme 2.3. Benzyl protection of hexaethylene glycol to benzyl ether **2.7**, followed by activation to tosylate **2.8** and subsequent displacement generating aniline **2.9**.

One possible option at this point was to remove the benzyl protecting group and alkylate to a *tert* butyl ester. However, this was not attempted as the product would have contained a nucleophilic aniline and an electrophilic *tert*-butyl ester. As this was deemed to be partly responsible for the unwanted side products in the failed initial routes, the next steps were carried out with the benzyl ether in place.

### PF74 Fragment Synthesis

With aniline linker **2.9** in hand, efforts were focused on generating the **PF74** fragment (Figure 2.16, page 100). To generate the **PF74** fragment, a two step synthesis was devised. Initially, 2-methylindole-3-acetic acid was coupled *via* amide bond formation with L-phenylalanine methyl ester hydrochloride generating amide **2.10** (Table 2.1).<sup>[111]</sup> Optimisation of the reaction focussed on testing several different coupling reagents. Equivalents of 2-methylindole-3-acetic acid and L-phenylalanine methyl ester hydrochloride were consistent throughout as 1 and 1.05 respectively. All reactions were carried out with 3 equivalents of diisopropylethylamine and at a concentration of 0.4 M in *N,N*-dimethylformamide. Initial efforts using HBTU produced a low yield of 13% (entry 1, Table 2.1). The reaction utilising HATU was carried out on a reduced scale, due to the high cost of the reagent but resulted in a respectable 59% (entry 2, Table 2.1). Utilising PyBOP as the coupling reagent improved the yield to a moderate 68% (entry 3, Table 2.1), which was deemed acceptable to proceed with. Upon scale up of these conditions (entries 4-6, Table 2.1), the coupling with PyBOP proved to be reproducible with only one errant result, serendipitously generating a quantitative yield at the largest scale. Following the generation of methyl ester **2.10**, the ester protecting group was removed under basic conditions generating acid **2.11** in a 97% yield (Table 2.1).<sup>[111]</sup>



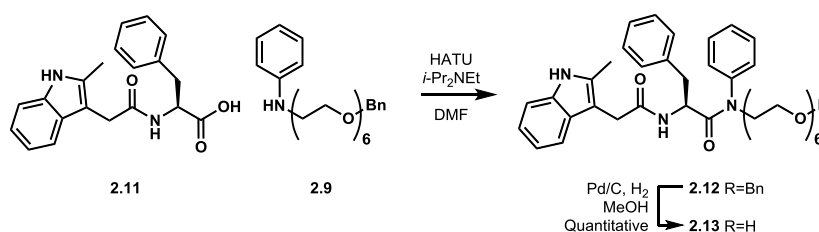
	Coupling reagent	Scale/mmol	<b>2.10</b> yield/%
1	HBTU	1	13
2	HATU	0.1	59
3	PyBOP	1	68
4	PyBOP	3	65
5	PyBOP	9	65
6	PyBOP	30	Quantitative

Table **2.1**. Optimisation of coupling conditions to generate methyl ester **2.10**, followed by saponification to acid **2.11**.

#### Completion of PF74-Linker Fragment

With both the **PF74** fragment and the aniline linker fragment successfully synthesised, efforts were focused on the completion of the protected **PF74**-linker fragment **2.1** (Figure **2.16**, page 100). To begin this, acid **2.11** was coupled to aniline linker **2.9** which required some optimisation (Table **2.2**). Initially, the optimal conditions for the coupling to synthesise methyl ester **2.10** (Entries 3-6 Table **2.1**, page 103) were tested, which resulted in none of the desired tertiary amide **2.12** being observed (not shown in Table **2.2**). Following a literature procedure used for the synthesis of **PF74**, HATU was utilised as the coupling reagent.<sup>[111]</sup> For the optimisation, the equivalents of acid **2.11** was set to 1, the equivalents of HATU to 1.5, the equivalents of secondary aniline coupling partner **2.9** also to 1.5 and the equivalents of *N,N*-diisopropylethylamine to 2. The variable parameters for this optimisation were the concentration and the temperature. The initial reaction was carried out at room temperature with a concentration of 0.3 M in *N,N*-dimethylformamide and resulted in a poor yield of 10% (entry 1, Table **2.2**). However, when the reaction was attempted at an elevated temperature of 60 °C, the yield increased to 20% (entry 2, Table **2.2**). At this point, the concentration was increased from 0.3 M to 0.9 M which boosted the yield to 32% (entry 3, Table **2.2**). This yield was deemed acceptable due to the difficulty of coupling a sterically hindered and electronically deactivated secondary aniline. Furthermore, the valuable aniline linker **2.9** was easily recovered during purification. Upon subsequent scaling of these conditions, the yield was improved to a respectable 57% (entries 4-6,

Table 2.2). During the coupling, when acid **2.11** is activated, there exists the possibility of oxazolone formation due to the presence of the *N*-acyl amino acid. This is known to be a major source of epimerisation in amide couplings, and with the elevated temperatures of this coupling, there was some concern over the stereochemical integrity of the phenylalanine alpha position.<sup>[112][113]</sup> With this in mind, a study was conducted to determine the stereochemical integrity of the alpha position when subjected to these coupling conditions (2.2.11 **PF74** synthesis and epimerisation study, page 128). While it was important to know if epimerisation was likely given the reaction conditions, it was not deemed to be problematic for the project thus the PROTAC synthesis continued. Following the amide coupling, the benzyl ether protecting group was removed under reductive conditions to the corresponding alcohol **2.13** with a quantitative yield (Table 2.2).<sup>[41]</sup>



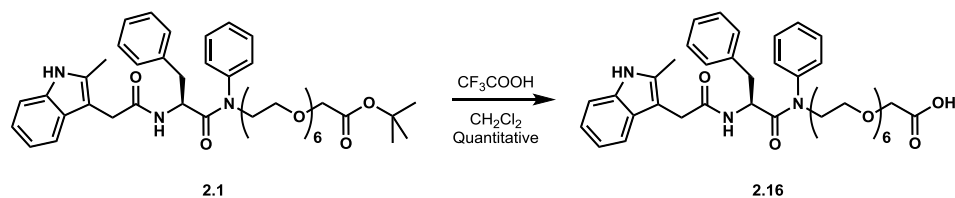
	Temp./°C	Conc./M	Scale/mmol	<b>2.12</b> yield/%
1	rt	0.3	0.09	10
2	60	0.3	0.09	20
3	60	0.9	0.09	32
4	60	0.9	0.27	43
5	60	0.9	0.81	42
6	60	0.9	1.62	57

Table 2.2. Optimisation of the coupling of acid **2.11** and aniline **2.9** to form tertiary amide **2.12**, followed by benzyl deprotection to alcohol **2.13**.

Following the benzyl deprotection to alcohol **2.13** was the alkylation to the corresponding *tert*-butyl ester **2.1** using *tert*-butyl bromoacetate (Table 2.3).<sup>[41]</sup> Attempts at carrying out this reaction consistently produced a mixture of products. These products were the desired *O*-alkylated **2.1**, the undesired *N*-alkylated **2.14** and the *O*- and *N*- dialkylated **2.15**. There was difficulty in differentiating *O*-alkylated **2.1** from *N*-alkylated **2.14** due to their similar NMR spectra (distinction was made using 2D HMBC spectroscopy). Furthermore, the two compounds **2.1** and **2.14** had very similar R<sub>f</sub> values (**2.1** = 0.42, **2.14** = 0.36 in 5% methanol in dichloromethane) making

separation from each other difficult and often requiring multiple purification attempts. Some time was spent optimising this reaction; however, the results were consistently poor (Table 2.3). For the optimisation, one equivalent of alcohol **2.13**, *tert*-butyl bromoacetate and the chosen base was utilised (except where stated). The concentration of the reaction was 0.3 M in the chosen solvent and the reactions were carried out at ambient temperature. Initial attempts with potassium carbonate (entry 1, Table 2.3) proved to be ineffective and only the starting material, alcohol **2.13**, was recovered from the reaction mixture. It is likely that the reaction failed as a result of potassium carbonate not being strong enough to deprotonate alcohol **2.13**. From this, it was surmised that the alcohol itself was not nucleophilic enough to react with the bromide. The reaction was therefore repeated with a catalytic amount of 4-dimethylaminopyridine; however, this also resulted in no reaction (not shown in table). With that in mind, sodium hydride was tested (entry 2, Table 2.3). This resulted in some of the desired *O*-alkylated **2.1** (8%); however, a significantly higher amount of the *N*-alkylated **2.14** (22%) and dialkylated **2.15** (16%) were observed. Due to the difficulties in separating the *O*- and *N*-alkylated products, alternate conditions were sought. As it seemed that sodium hydride was perhaps a stronger base than required, a weaker base was utilised while still being stronger than potassium carbonate. Initial conditions using potassium *tert*-butoxide (entry 3, Table 2.3) used 1.2 equivalents of the base and 1.1 equivalents of the bromide. The result seemed promising with a higher amount of *O*-alkylated **2.1** (12%) but unfortunately still a high level of *N*-alkylated **2.14** (12%) and dialkylated **2.15** (22%). With this in mind, the equivalents of *tert*-butoxide and *tert*-butyl bromoacetate were lowered to 1 (entry 4, Table 2.3). This produced a more desirable reaction profile with the desired *O*-alkylated **2.1** (18%) in a higher yield than the *N*-alkylated **2.14** (9%) for the first time. While this profile was not ideal, it was deemed acceptable for scale up to generate more material. (entry 5, Table 2.3). However, this resulted in an inferior profile with equal amounts of *O*-alkylation (13%) and *N*-alkylation (13%). At this point, with the irreproducibility of the reaction conditions tested, it was decided to continue with the best conditions yet observed. The potassium *tert*-butoxide reaction conditions were scaled up again (entry 6, Table 2.3), this time resulting in a vast improvement of the reaction profile. The desired *O*-alkylated **2.1** (12%) was observed in a much higher yield than the *N*-alkylated **2.14** (2%) which greatly facilitated the purification. The relatively high yield of dialkylated **2.15** (18%) was tolerated due to its more facile separation during purification. With the poor yields, difficult purification, and irreproducibility, this reaction needed further





Scheme 2.5. Acidic deprotection of *tert*-butyl ester **2.1** to acid **2.16**.

### 2.2.2 Protected CRBN-Linker Fragment Synthesis

With the synthesis of the **PF74** fragment complete, the synthesis of the aforementioned E3 ligase fragments were the next targets (Figure 2.15, page 99). The first of these fragments to be targeted was the protected CRBN-linker fragment **2.2** (Figure 2.17).

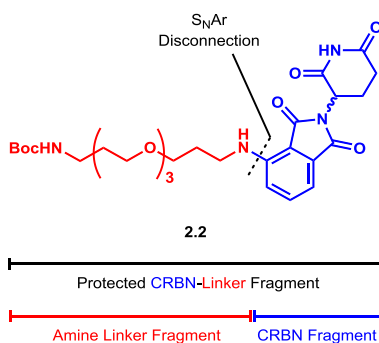
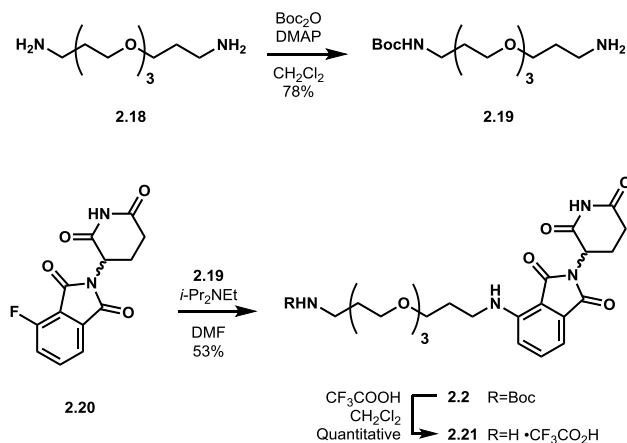


Figure 2.17. Protected CRBN-linker fragment **2.2**.

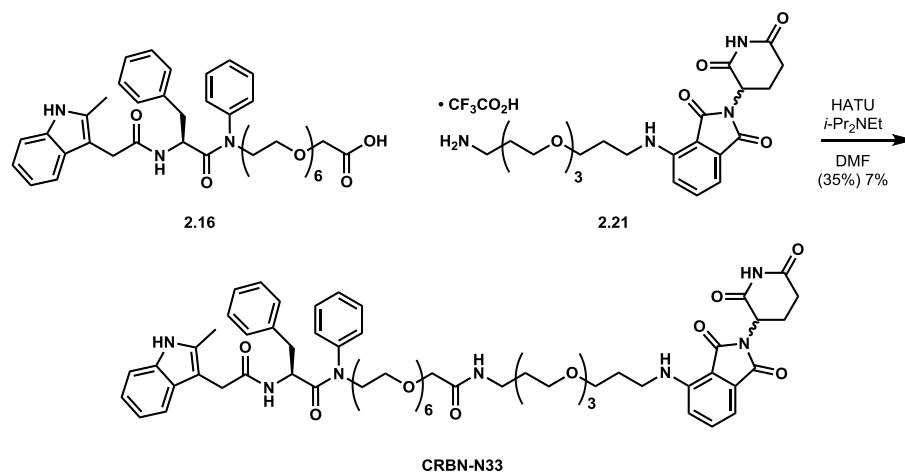
To begin the synthesis of the protected CRBN-linker fragment **2.2**, diamine **2.18** was selectively mono protected to *tert*-butyl carbamate **2.19** with a yield of 78% to form the amine linker fragment (Scheme 2.6).<sup>[48]</sup> As part of a different France group PROTAC project, the fluorinated phthalimide **2.20** was synthesised and coupled with the free amine of *tert*-butyl carbamate **2.19**. This was achieved *via* a  $S_NAr$  alkylation generating the *tert*-butyl carbamate protected phthalimide **2.2** in a 53% yield. It should be noted that although the naturally occurring L-glutamine was used in the synthesis of phthalimide **2.20**, racemisation was likely during the synthesis of **2.20**. However, due to the reported *in vivo* racemisation of phthalimide-based compounds the inclusion of this fragment as a racemate in the final PROTAC was deemed inconsequential.<sup>[88][89]</sup> Enough of *tert*-butyl carbamate **2.2** was generated to allow it to also be utilised for this project. With the protected CRBN-linker fragment **2.2** complete, acidic deprotection of *tert*-butyl carbamate **2.2** afforded the corresponding amine TFA salt **2.21**.<sup>[48]</sup>



Scheme 2.6. Protection of diamine **2.18** to *tert*-butyl carbamate **2.19**, followed by the coupling to fluorinated phthalimide **2.20** and subsequent acidic deprotection to amine TFA salt **2.21**.

### 2.2.3 Synthesis of PROTAC **CRBN-N33**

With both the **PF74**-linker fragment **2.16** and the CRBN-linker fragment **2.21** synthesised, coupling was attempted. A HATU mediated amide coupling between acid **2.16** and amine **2.21** successfully generated PROTAC **CRBN-N33** in a 35% yield (Scheme 2.7). As the compound was required for cellular testing, additional preparative HPLC purification was conducted. These additional purification steps lowered the yield to 7%, which correlated to 3 mg of final product. This provided sufficient amounts of material with which to carry out some cellular assays (2.3.3 PROTAC Testing, page 145). While the route successfully resulted in enough material for testing, significant improvements could be made to increase the efficiency of the synthesis.



Scheme 2.7. Coupling of acid **2.16** and amine **2.21** to PROTAC **CRBN-N33**.

### 2.2.4 VHL-Linker Fragment Synthesis

With the successful synthesis of **CRBN-N33** achieved, focus was shifted to the synthesis of the analogous **VHL-38** (Figure 2.14, page 98). As the **PF74**-linker

fragment **2.16** is common to both PROTACs, the synthesis of the protected VHL-linker fragment **2.3** (Figure **2.18**) was conducted.

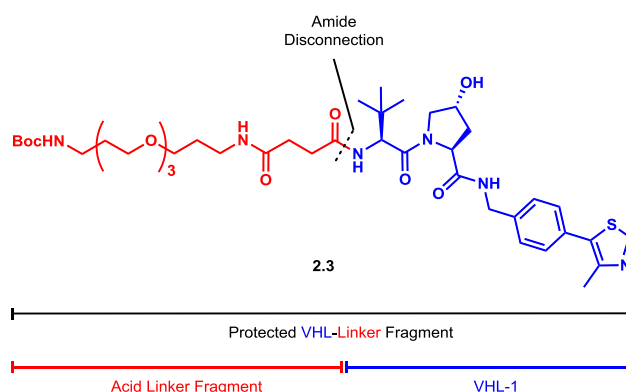
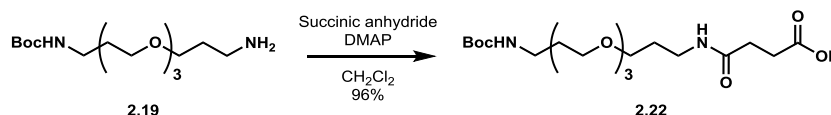


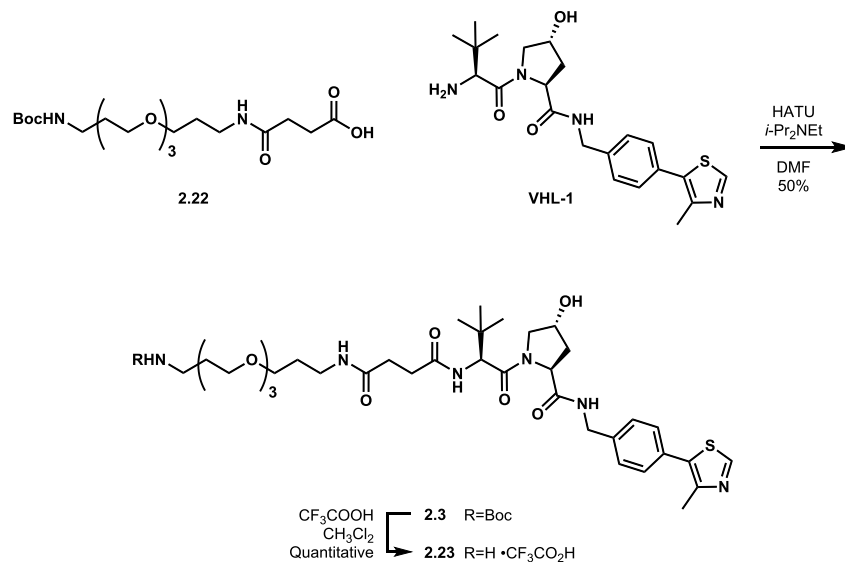
Figure **2.18**. VHL-Linker Fragment **2.3**.

To synthesise the protected VHL-linker fragment **2.3**, an adaption to linker **2.19** was required. As fluorinated phthalimide **2.20** was electrophilic at the site of linker attachment, a nucleophilic terminal amine on linker **2.19** suited well. However as the linker attachment site of **VHL-1** was a nucleophilic terminal amine, it was first required to reverse the reactivity of linker **2.19**. This reactivity reversal was achieved by reaction of the terminal amine of linker **2.19** with succinic anhydride, which successfully yielded 96% of the acid terminating linker **2.22** (Scheme **2.8**).<sup>[114]</sup>



Scheme **2.8**. Ring opening of succinic anhydride with amine **2.19** to form acid **2.22**.

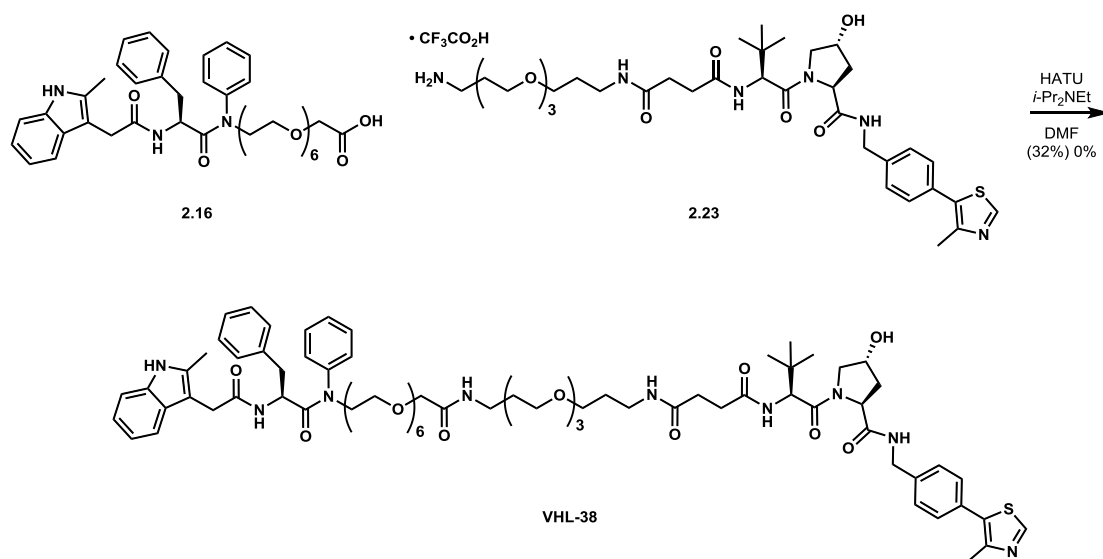
With the reactivity of the linker reversed, acid **2.22** was coupled with the terminal amine of **VHL-1** generating the corresponding amide **2.3** in a 50% yield (Scheme **2.9**).<sup>[109]</sup> Following this, the *tert*-butyl carbamate protecting group was removed under acidic conditions generating the amine TFA salt **2.23**.<sup>[48]</sup>



Scheme 2.9. Coupling of acid **2.22** and amine **VHL-1** to amide **2.3** followed by acidic deprotection to amine TFA salt **2.23**.

### 2.2.5 Attempted Synthesis of PROTAC **VHL-38**

With the **PF74**-linker fragment **2.16** and VHL-linker fragment **2.23** in hand, the coupling of the two fragments to form **VHL-38** was attempted. HATU mediated amide coupling of acid **2.16** and amine **2.23** successfully generated **VHL-38** with a yield of 32% after initial purification by column chromatography (Scheme 2.10). However as with **CRBN-N33**, further purification by preparative HPLC was employed before being utilised for cellular assays. The additional purification steps proved difficult with this substrate and due to the poor mass recovery from each step, no pure sample of the material was recovered.



Scheme 2.10. Coupling of acid **2.16** and amine **2.23** to form amide **VHL-38**.

Although it may have been possible to generate more material and reattempt the synthesis of **VHL-38** on a larger scale, this was not conducted for a number of reasons.

Firstly, the hexaethylene glycol starting material was removed from the market. Secondly, there were various problems with the route including the low yielding alkylation steps (with difficult separations and mixed products), the high step count and the somewhat linear sequence. Ultimately, these factors in combination with the low yield of **CRBN-N33** and the lack of **VHL-38** indicated that the route to these products was inadequate for generating both the number, and structural variety of compounds required for the future success of the project.

### 2.2.6 Redesigning the Route

To improve the route to **CRBN-N33**, the core limitations had to be addressed. These included the low yields of the final products, which could be improved by increasing the convergence of the synthesis. Furthermore, the linear nature of the original **PF74**-linker fragment synthesis hinders the facile incorporation of structural diversity. The linearity of the **PF74**-linker fragment synthesis was derived from the incorporation of the aniline moiety as part of the linker (Figure 2.19). As the aniline moiety is an integral part of **PF74**, a complete-**PF74** fragment **2.24** would be useful for coupling to a variety of generic linkers. This would remove the additional steps required to functionalise generic linkers with an aniline moiety, thus increasing convergence of the synthesis and allowing more structurally diverse linkers to be utilised.

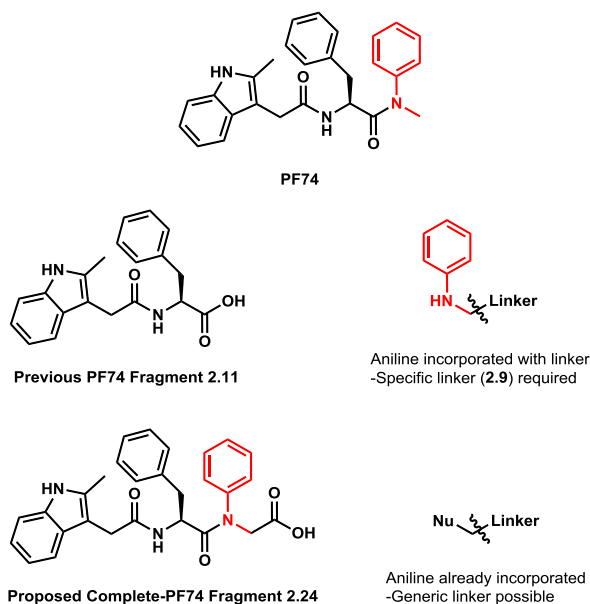


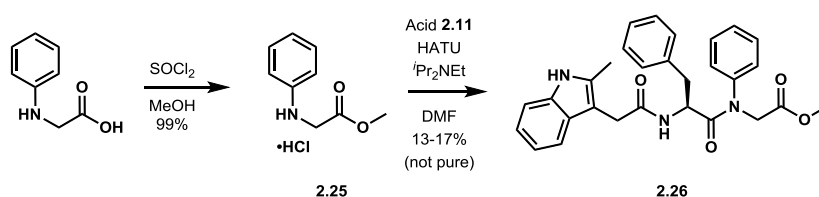
Figure 2.19. Comparison of the previous **PF74** fragment **2.11** with a proposed complete-**PF74** fragment **2.24**.

The France Group is currently working on several PROTAC projects, and as such a library of intermediate fragments common to different projects was created. Part of the motivation to redesign the route to incorporate a complete-**PF74** fragment such as **2.24** was to enable the use of the generic library of linkers and E3 ligases. The generic

linkers that comprise the common library typically terminate with a protected amine and an orthogonally protected acid, allowing selective deprotection and facile amide couplings to the required fragments. Additionally, this proposed strategy would allow the linkers developed for this project to be added to the common library (thus providing other group members access to these valuable compounds), which was not the case with the previously described aniline linker fragment **2.9** (Scheme **2.3**, page 102). For clarity of authorship, any compounds sourced from the common library for use in this project are clearly stated, otherwise any compounds described herein were synthesised as part of this project.

### 2.2.7 Attempted Synthesis of Proposed Complete-PF74 Fragment **2.24**

In an attempt to synthesise the proposed complete-PF74 fragment **2.24** (Figure **2.19**, page 111), the secondary aniline coupling that previously incorporated the linker (Table **2.2**, page 104) was attempted instead with the methyl ester of *N*-phenyl glycine **2.25** (Scheme **2.11**). This required the protection of the acid of *N*-phenyl glycine using thionyl chloride in methanol, which afforded methyl ester **2.25** with a 99% yield.<sup>[115]</sup> Following this, the coupling of secondary aniline **2.25** with the previously synthesised acid **2.11** (Table **2.1**, page 103) was attempted using the previously optimised conditions for these couplings (Entries 3-6, Table **2.2**, page 104). This coupling however, did not proceed as well as anticipated. The reaction was attempted several times with yields ranging from 13-17%. While these yields were poor, they could have been acceptable for generating material as each of the other steps to this point were high yielding. However, in addition to the poor yield the product could not be fully purified due to co-elution with an unidentified impurity. These factors made this route undesirable for the generation of the complete-PF74 fragment **2.24**.

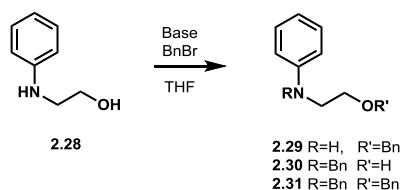


Scheme **2.11**. Protection of *N*-phenyl glycine as methyl ester **2.25** followed by coupling to acid **2.11** to form tertiary amide **2.26**.

Following the *N*-phenyl glycine route, it was decided to install a terminal alcohol which would enable oxidation of alcohol **2.27** to an aldehyde and then to the desired terminal acid **2.24** (Scheme **2.12**). In the event that the final oxidation to the acid fails, the aldehyde could then be used for a Wittig type olefination followed by reduction to install an alkyl chain based linker. If in turn this route were to fail, there would be the



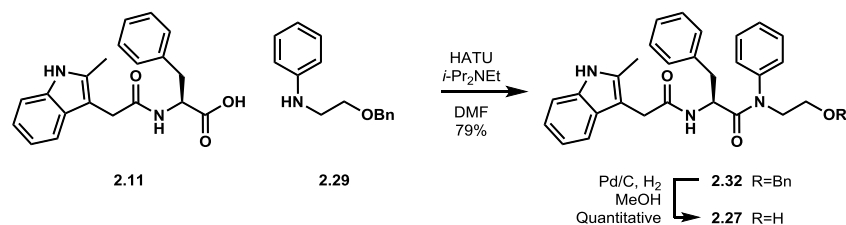
observed, it was determined that a stronger base was required in order to form the alkoxide, which would be more nucleophilic than the aniline. With this in mind, sodium hydride was tested which resulted in a much better profile of 32% *O*-alkylated **2.29** and 32% of dialkylated **2.31** (entry 2, Table **2.4**). With over-alkylation now seeming to be the problem, the equivalents of benzyl bromide were dropped back from 1.1 equivalents to substoichiometric 0.8 equivalents (entry 3, Table **2.4**). The reason for this was that unreacted alcohol **2.28** was easier to separate from the desired **2.29** than either the *N*-alkylated **2.30** or dialkylated **2.31**. This improved the yield of desired **2.29** to 72% with the *N*- and dialkylated **2.30** and **2.31** at 10% and 4% respectively. Finally, in an attempt to lower the percentage of the more difficult to separate *N*-benzyl **2.30**, the concentration of the reaction was lowered from 0.3 M to 0.15 M (entry 4, Table **2.4**). This had the desired effect of decreasing the yield of *N*-alkylated **2.30** to trace quantities; however, it also slightly lowered the yield of the desired *O*-benzyl **2.29** and increased that of dialkylated **2.31**. This was not a problem however, as the dialkylated **2.30** was relatively more facile to separate from the desired *O*-benzyl **2.29** compared to the separation of *N*-benzyl **2.30** from *O*-benzyl **2.29**. These conditions were reproducible upon scale up generating ample quantities of benzyl ether **2.29**.



	Base	BnBr, equiv.	Solvent, Conc./M	Yield (%)		
				<b>2.29</b> / <i>O</i> -	<b>2.30</b> / <i>N</i> -	<b>2.31</b> / Di-
1	K <sub>2</sub> CO <sub>3</sub>	1.1	THF, 0.3	0	66	0
2	NaH	1.1	THF, 0.3	32	3	32
3	NaH	0.8	THF, 0.3	72	10	4
4	NaH	0.8	THF, 0.15	61	2	15

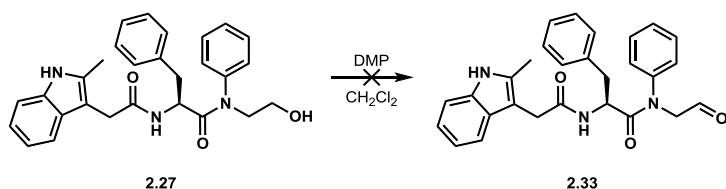
Table **2.4**. Optimisation of the benzyl protection of alcohol **2.28** to benzyl ether **2.29** and side products **2.30** and **2.31**.

The coupling of the benzyl protected linker **2.29** with acid **2.11** was carried out using the previously optimised conditions (Entries 3-6, Table **2.2**, page 104) which generated the desired amide **2.32** in a 77% yield (Scheme **2.14**). Following the coupling, the reductive deprotection of benzyl ether **2.32** to alcohol **2.27** was performed with a quantitative yield.<sup>[41]</sup>



Scheme 2.14. Coupling of acid **2.11** and aniline **2.29** to generate tertiary amide **2.32** followed by benzyl deprotection to alcohol **2.27**.

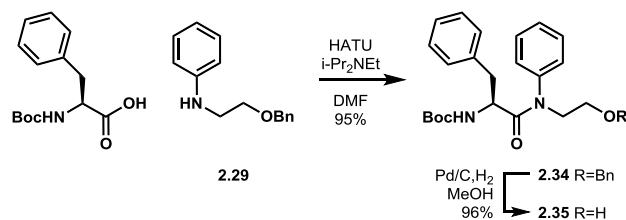
With the terminal alcohol now installed, a sequence of Dess–Martin oxidation to aldehyde **2.33** followed by Pinnick oxidation to acid **2.24** could be attempted. Unfortunately the initial Dess–Martin oxidation to aldehyde **2.33** resulted in a mixture of many compounds, none of which had the mass of the desired aldehyde by LCMS analysis (Scheme 2.15). With the decomposition that was observed from this reaction, it was decided to test these conditions on a less structurally complex system, in an attempt to suppress side reactions.



Scheme 2.15. Attempted Dess–Martin oxidation of alcohol **2.27** to aldehyde **2.33**.

### Model Fragment Synthesis

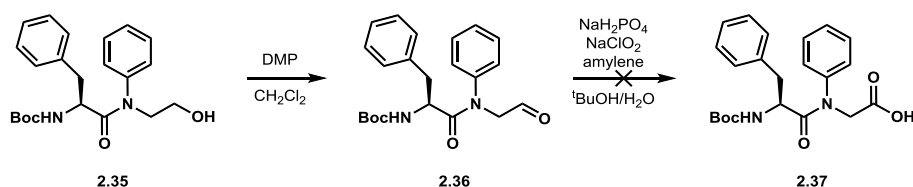
To generate a smaller (indole free) model fragment, Boc-L-phenylalanine was coupled to aniline **2.29** affording amide **2.34** with a 95% yield (Scheme 2.16). This was a very high yield for a secondary aniline coupling compared to the previous couplings of this type, which implied that the presence of the indole group had been detrimental to these couplings. As mentioned previously, these coupling conditions could generate a risk of erosion of stereochemical integrity at the phenylalanine alpha position *via* oxazolone mediated epimerisation. This risk is exacerbated when the acid coupling partner is an *N*-acyl amino acid as is the case with the indole containing acid **2.11**.<sup>[112]</sup> As an additional benefit to this reaction, the risk can be somewhat mitigated when the *N*-acyl amino acid is protected as a *tert*-butyl carbamate, as with the case below (Scheme 2.16).<sup>[112]</sup> Following the coupling, the benzyl ether protecting group was removed under reductive conditions, generating alcohol **2.35** with a 96% yield and affording the model fragment.<sup>[41]</sup>



Scheme 2.16. Coupling of Boc-L-phenylalanine with aniline **2.29** to form tertiary amide **2.34** followed by the benzyl deprotection to alcohol **2.35**.

### Model Fragment Oxidation

With alcohol **2.35** in hand, the previous oxidation sequence of Dess–Martin oxidation to aldehyde **2.36** followed by Pinnick oxidation to acid **2.37** was attempted (Scheme 2.17). The initial Dess–Martin oxidation to aldehyde **2.36** resulted in an inseparable mixture of coeluted compounds, two of which had the correct mass of oxidised product (by LCMS analysis). Before investing time in the optimisation of this reaction, the mixture of oxidised products was subjected to Pinnick oxidation conditions. It was rationalised that if the desired aldehyde **2.36** was present in the mixture, it would be oxidised to acid **2.37** which should then produce a more facile purification. However, the Pinnick reaction failed to produce the desired acid **2.37**. Furthermore, the crude reaction mixture looked identical to that of the mixture used as the starting material (by LCMS analysis), and thus it was surmised that the initial Dess–Martin oxidation had not produced the desired aldehyde **2.36**. With the mixture of products that were observed from this reaction it was decided to abandon the oxidation route.

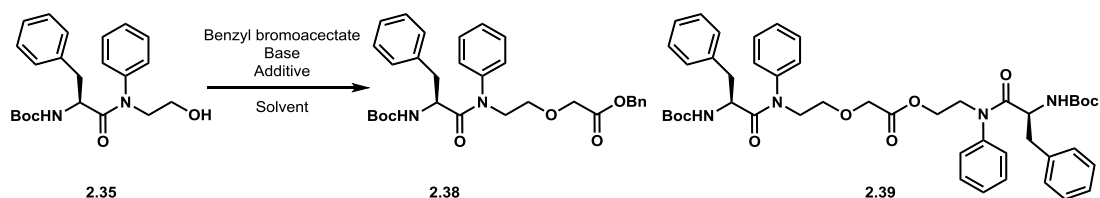


Scheme 2.17. Dess–Martin oxidation of alcohol **2.35** to aldehyde **2.36** followed by the attempted Pinnick oxidation to acid **2.37**.

### Model Fragment Alkylation

With the oxidations not producing the desired results, alcohol **2.35** was used for alkylation in an attempt to install a terminal masked acid residue. Due to the presence of the *tert*-butyl carbamate protecting group, a benzyl ester was chosen as the terminal group as they could be orthogonally deprotected. To achieve this, alcohol **2.35** was alkylated with benzyl bromoacetate in the presence of a base (Table 2.5).<sup>[41]</sup> The reaction produced a mixture of two products, the desired ester **2.38** resulting from a direct S<sub>N</sub>2 displacement of the bromide, and a dialkylated product resulting from a transesterification reaction between a molecule of starting material **2.35**, and the

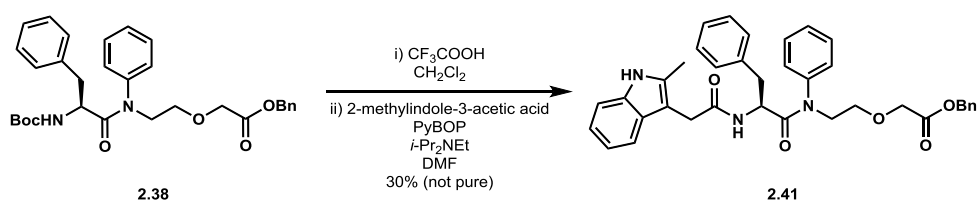
desired ester **2.38** to form what will be referred to as dimer **2.39**. In addition to the two isolated products, LCMS analysis indicated the presence of a direct transesterification product however this was never isolated for confirmation. Several different conditions were tested in an attempt to selectively generate ester **2.38** and suppress the formation of dimer **2.39** (Table 2.5). For the optimisation, one equivalent of alcohol **2.35**, benzyl bromoacetate and the chosen base was utilised, and the reactions were carried out at ambient temperature at a concentration of 0.3 M in the chosen solvent. The bases triethylamine (entry 1, Table 2.5), potassium *tert*-butoxide (entry 2, Table 2.5) and potassium carbonate (entry 3, Table 2.5) all resulted in no reaction occurring, and allowed the recovery of alcohol **2.35**. Interestingly, while potassium carbonate failed, caesium carbonate (entry 4, Table 2.5) did form the product albeit in a meagre 10% yield. A very slight improvement on the yield was obtained with the use of sodium hydride in tetrahydrofuran (entry 5, Table 2.5) which formed the product **2.38** in a 15% yield and the undesired dimer **2.39** with a 16% yield. Several conditions were tested to try and suppress the transesterification and improve the S<sub>N</sub>2 selectivity. These involved adding nucleophilic catalysts 4-dimethylaminopyridine (entry 6, Table 2.5) and tetrabutylammonium iodide (entry 7, Table 2.5) and altering the polarity of the solvents (entries 8 and 9, Table 2.5). However, none of these changes resulted in any reaction and alcohol **2.35** was recovered.



	Base	Additive	Solvent	<b>2.38</b> /%	<b>2.39</b> /%
1	NEt <sub>3</sub>	DMAP	THF	0	0
2	KO <sup>t</sup> Bu	/	<sup>t</sup> BuOH	0	0
3	K <sub>2</sub> CO <sub>3</sub>	/	THF	0	0
4	Cs <sub>2</sub> CO <sub>3</sub>	/	DMF	10	0
5	NaH	/	THF	15	16
6	NaH	DMAP	THF	0	0
7	NaH	TBAI	THF	0	0
8	NaH	/	DMSO	0	0
9	NaH	/	MeCN	0	0

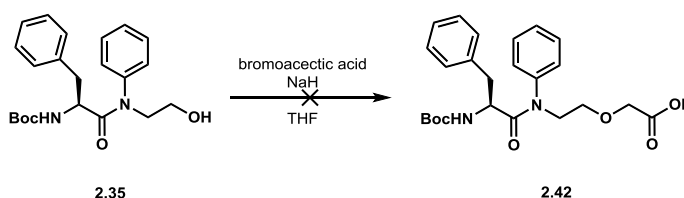
Table 2.5. Optimisation of the alkylation of alcohol **2.35** to ester **2.38** and dimer **2.39**.

With enough of the desired benzyl ester **2.38** generated, the deprotection of the *tert*-butyl carbamate group was performed resulting in amine TFA salt **2.40** (Scheme **2.18**).<sup>[48]</sup> This was used directly in the proceeding amide coupling with 2-methylindole-3-acetic acid generating benzyl ester **2.41**. This step did not work as well as expected, yielding 30% of the desired ester **2.41** (equivalent to 7 mg of product). Furthermore, this product was difficult to purify from the crude reaction mixture due to co-elution with an unidentified impurity. In light of the poor yielding alkylation step, and the poor yielding and difficult to purify amide coupling, this route was abandoned.



Scheme **2.18**. Acidic deprotection of *tert*-butyl carbamate **2.38** followed by coupling with 2-methylindole-3-acetic acid to form amide **2.41**.

With the masked acid alkylation abandoned, the final attempt at alkylation of the model fragment was to alkylate alcohol **2.35** with bromoacetic acid, to directly generate acid **2.42** (Scheme **2.19**). The alkylation was conducted with the use of both sodium hydroxide and sodium hydride, and both reactions produced a compound with a mass consistent with the desired acid **2.42** (by LCMS analysis). In the reaction using sodium hydride, an additional product was detected by LCMS that had a mass consistent with a dialkylated product (presumably as a result of alkylation at both the oxygen of the alcohol and the nitrogen of the carbamate protecting group). Regardless of the base selected for the reaction, acid **2.42** was unable to be purified from the reaction mixture due to co-elution with an unknown impurity.



Scheme **2.19**. Attempted alkylation of alcohol **2.35** to acid **2.42**.

With the failed attempts at generating a complete-**PF74** fragment using *N*-phenyl glycine, oxidation and alkylation, more work is required toward the generation of a stock of complete-**PF74** fragment as ultimately, it will be exceedingly useful in the diversification of later generations of PROTACs. However, due to time constraints no

further time could be invested in the pursuit of this elusive fragment. Focus was therefore necessarily shifted toward the generation of additional PROTAC analogues.

### 2.2.8 Synthesis of Short Linker PROTACs

In an attempt to quickly access further compounds for testing, the synthesis of additional analogues proceeded by mimicking the original successful route. It was decided to include a protecting group for the indole nitrogen in this iteration in an attempt to improve the yield of the *tert*-butyl ester alkylation, which was a major drawback with the original synthesis.

In order to test the efficacy of the planned protecting group, a short linker VHL targeting PROTAC (**VHL-4**) was designed (Figure 2.20). The design of **VHL-4** included the use of the previously synthesised benzyl ether **2.32** (Scheme 2.14, page 115) and the commercially available **VHL-1** (VHL ligase ligand) (Scheme 2.9, page 110). Therefore, the planned protection step, subsequent alkylation (in the presence of the protecting group) and the necessary deprotection step could all be evaluated without investing time in a lengthy synthesis.

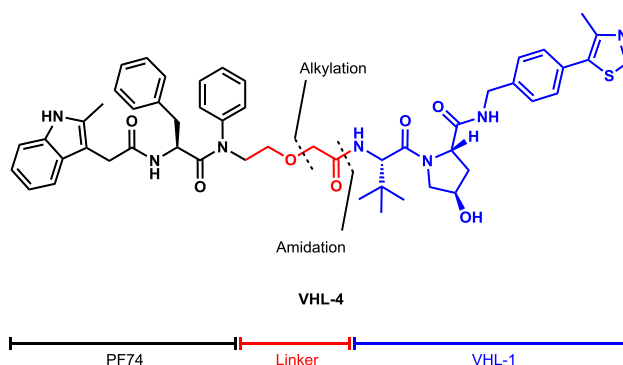
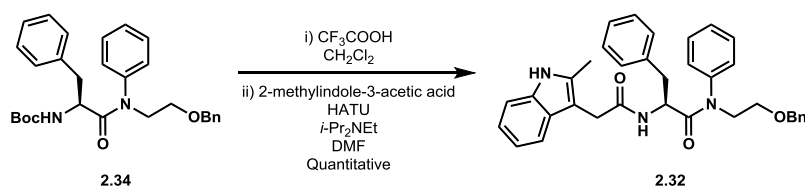


Figure 2.20. Design of PROTAC **VHL-4**.

While the linker of **VHL-4** is a lot shorter than originally planned, the shorter PROTAC could still prove useful. A shorter PROTAC could be a valuable control compound in establishing if it is indeed necessary to have a long linker. The longer linker was originally targeted due to the binding site of **PF74** being located approximately 30 Å into a cleft between two capsid protein (CA) subunits of a CA hexamer. It was therefore hypothesised that the linker would need to span this 30 Å distance to position the E3 ligase binding portion of the PROTAC in an area that is accessible to the required E3 ligase (2.1.10 First generation probe design, page 97). However it is known in the literature that **PF74** also binds to monomeric CA with around a 10-fold reduced affinity than for the hexameric CA.<sup>[108]</sup> As it has also been

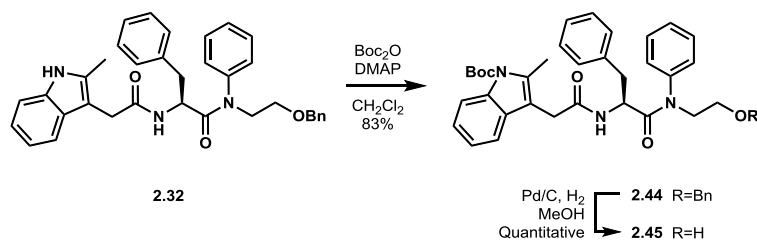
reported that some PROTACs only require transient binding<sup>[82]</sup>, **VHL-4** provided us with an opportunity to investigate this possibility within the boundaries of this project.

Although the synthesis of benzyl ether **2.32** had already been established (Scheme **2.14**, page 115), an improved synthesis was realised during the failed attempts at producing the complete-**PF74** fragment **2.24** (Figure **2.19**, page 111). The improved synthesis began with the acidic deprotection of the previously synthesised carbamate **2.34** (Scheme **2.16**, page 116) to the corresponding amine TFA salt **2.43** (Scheme **2.20**). Following this, amine **2.43** was coupled with 2-methylindole-3-acetic acid using HATU to generate amide **2.32** in a quantitative yield. This alternative synthesis improved the overall yield of benzyl ether **2.32** (95% over three steps), compared to that of the original synthesis (Scheme **2.14**, page 115) (76% over three steps). Furthermore, the synthesis of carbamate **2.34** (Scheme **2.16**, page 116) had a reduced likelihood of stereochemical erosion at the phenylalanine alpha position during the secondary aniline amide coupling. As mentioned above, this was due to the presence of the *tert*-butyl carbamate protecting group of *boc*-L-phenylalanine being less susceptible to epimerisation *via* oxazolone formation (compared with that of the *N*-acyl amino acid present in acid **2.11**).<sup>[112]</sup>



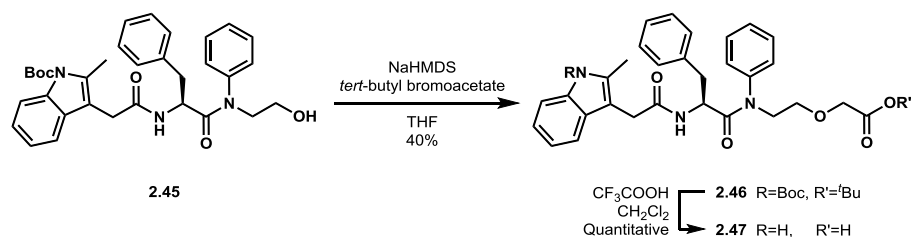
Scheme **2.20**. Acidic deprotection of *tert*-butyl carbamate **2.34** followed by coupling to 2-methylindole-3-acetic acid to form amide **2.32**.

The next step was the protection of the indole moiety as a *tert*-butyl carbamate. This would hopefully assist with increasing the yield of the upcoming alkylation step, by decreasing the possibility of side products. The protection was carried out using di-*tert*-butyl dicarbonate which afforded *tert*-butyl carbamate **2.44** with an 83% yield (Scheme **2.21**).<sup>[48]</sup> Following the protection of the indole moiety, was the reductive deprotection of benzyl ether **2.44** to alcohol **2.45** which proceeded with a quantitative yield.<sup>[41]</sup> It is interesting to note that full conversion was attained after five hours; however, if left for longer than this, an unidentified side product was formed to the detriment of the desired alcohol **2.45**. The deprotection of the analogous non *tert*-butyl carbamate protected benzyl ether **2.12** (Table **2.2**, page 104) was frequently left for 16 hours or longer with no erosion of the desired product yield. This suggested that the *tert*-butyl carbamate protecting group was integral to the undesired reaction.



Scheme 2.21. Protection of indole **2.32** to generate *tert*-butyl carbamate **2.44** followed by benzyl deprotection to alcohol **2.45**.

With the indole moiety protected and the alcohol unmasked, the alkylation of alcohol **2.45** was attempted. It was decided to alkylate with *tert*-butyl bromoacetate to install a *tert*-butyl ester. The rationale for this decision was that both the ester and the carbamate protecting group can be removed concomitantly under acidic conditions, thus reducing the step count and improving the overall yield. Initial attempts at alkylation using sodium hydride as a base gave poor results. The yield was only 8% and consisted of an inseparable mixture of the desired ester **2.46** and an unidentifiable impurity. Following the attempts with sodium hydride, the reaction was conducted using sodium bis(trimethylsilyl)amide as the base (Scheme 2.22). This proceeded with a moderate yield of 40% and a relatively facile purification. In addition to the improved yield over previous similar alkylations, no *N*-alkylation products were observed which contributed to the ease of purification. Furthermore, the reaction was reproducibly scaled up and gave access to 150 mg of the diprotected **2.46**. With the improved alkylation complete, the double deprotection of the *tert*-butyl carbamate and *tert*-butyl ester was attempted. This was conducted under acidic conditions using trifluoroacetic acid and afforded the free-indole containing acid **2.47** with a quantitative yield.<sup>[48]</sup>

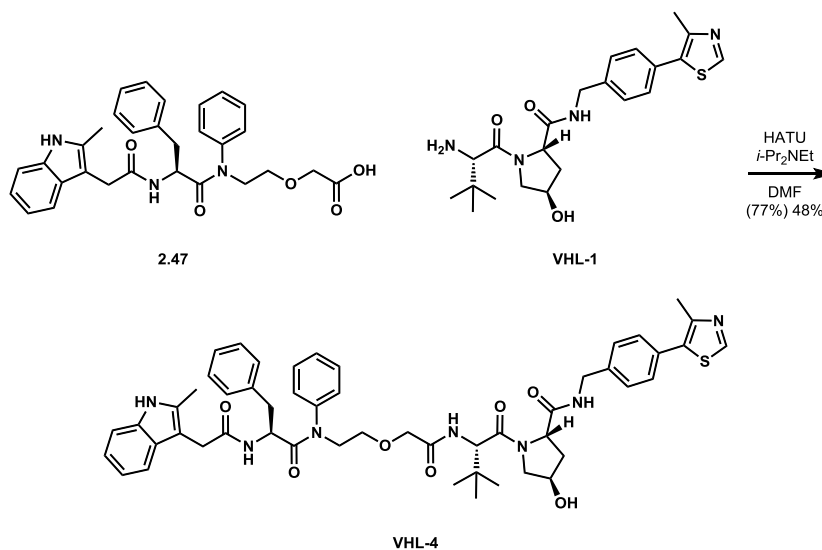


Scheme 2.22. Alkylation of alcohol **2.45** to ester **2.46** followed by acidic double deprotection to acid **2.47**.

### Completion of Short VHL-Based PROTAC

With acid **2.47** in hand, its coupling partner was required. Similar to the original synthesis, the plan was to couple acid **2.47** with a VHL fragment, and a CRBN fragment thus generating two more PROTACs. Firstly the VHL analogue was synthesised, due to the immediate access to commercially available **VHL-1**. HATU mediated coupling of acid **2.47** with the amine of **VHL-1** afforded **VHL-4** with a yield

of 77% after initial purification by column chromatography (Scheme 2.23). However, due to additional purification by preparative HPLC, the yield lowered to 48%. This equated to 26 mg (28  $\mu$ mol) of material, which was ample for biological testing.



Scheme 2.23. Coupling of acid **2.47** and amine **VHL-1** to form PROTAC **VHL-4**.

### Completion of Short CRBN-Based PROTAC

Following the synthesis of **VHL-4**, focus shifted to generating a CRBN targeting analogue. It was observed with **CRBN-N33**, that the compound was fluorescent. While this could potentially be useful in certain applications, it was decided to synthesise a non-fluorescent analogue. This decision was attributed to the planned use of flow cytometry to analyse the results of the biological assays. As flow cytometry measures fluorescence, a fluorescent compound could potentially complicate analysis. Through the synthesis of CRBN targeting PROTACs carried out by another group member, it was discovered that anilinic phthalimide based ligands are fluorescent (as is the case with **CRBN-N33**), while phenolic phthalimide based ligands are not (Figure 2.21).

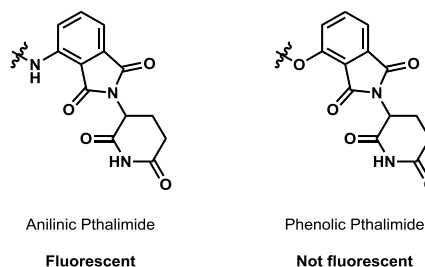
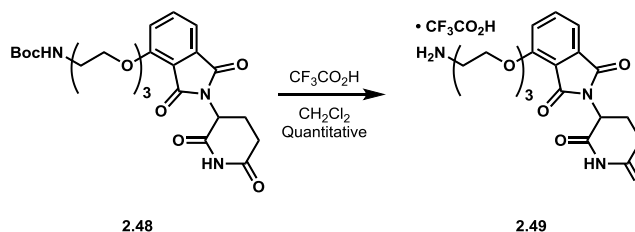


Figure 2.21. Comparison of the effect of substitution on the fluorescence of **thalidomide** derivatives.

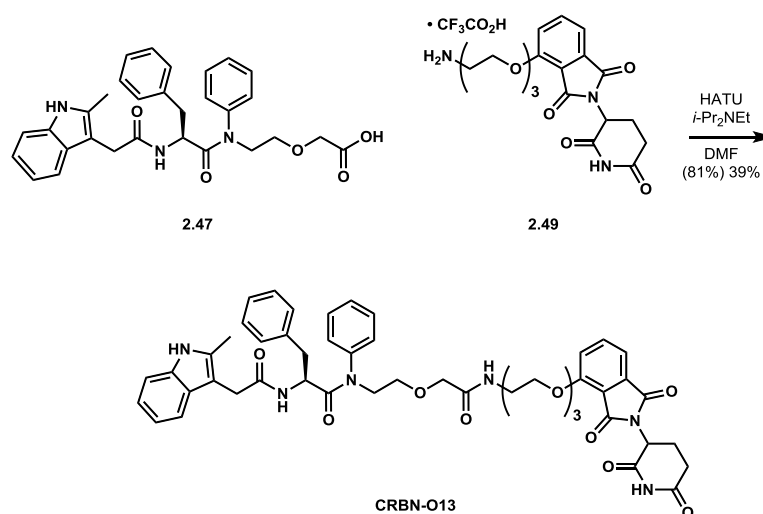
The non-fluorescent phenolic phthalimide **2.48** which featured a section of linker already attached, had been previously synthesised within the France group and added to the communal group library (Scheme 2.24). The synthesis of phthalimide **2.48** was

conducted with racemic starting materials, and thus is itself a racemate. This was determined to be inconsequential due to the aforementioned *in vivo* racemisation of the stereogenic centre of phthalimide-based compounds such as **2.48**.<sup>[88][89]</sup> Taking advantage of the communal material, *tert*-butyl carbamate **2.48** was deprotected under acidic conditions to the corresponding amine TFA salt **2.49**.<sup>[48]</sup>



Scheme 2.24. Acidic deprotection of *tert*-butyl carbamate **2.48** to amine TFA salt **2.49**.

The coupling of acid **2.47** and the amine of phthalimide **2.49** afforded **CRBN-O13** with a yield of 81% after initial purification by column chromatography (Scheme 2.25). Following additional HPLC purification for cellular testing, the yield dropped to 39% with a mass yield of 25 mg (28  $\mu$ mol) which was again ample material for biological testing.



Scheme 2.25. Coupling of acid **2.47** and amine **2.49** to form PROTAC **CRBN-O13**.

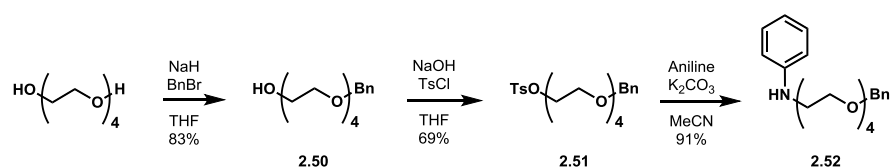
Having successfully synthesised two additional short linker PROTACs, efforts were aimed at generating two PROTACs of a medium length. The addition of an indole protecting group appeared to significantly improve the synthesis, thus this tactic was also employed for the synthesis of the next medium length linker PROTACs.

### 2.2.9 Synthesis of medium length PROTACs

For the synthesis of medium length PROTACs, the base linker was four ethylene glycol units in length. To achieve this, it was necessary to follow the initial strategy, whereby

the aniline of the **PF74** moiety was incorporated into the molecule as part of the linker. For this reason, the 4-PEG linker synthesis was analogous to the synthesis of the original 6-PEG linker (Scheme 2.3, page 102).

The 4-PEG linker synthesis began with the mono benzyl protection of tetraethylene glycol using sodium hydride and benzyl bromide which afforded benzyl ether **2.50** with an 83% yield (Scheme 2.26).<sup>[41]</sup> The remaining free alcohol of **2.50** was then activated with tosyl chloride in the presence of sodium hydroxide to the corresponding tosylate **2.51** in a 69% yield.<sup>[117]</sup> Subsequent displacement of the tosylate with aniline in the presence of potassium carbonate generated secondary aniline **2.52** in a 91% yield, and completed the 4-PEG linker synthesis.

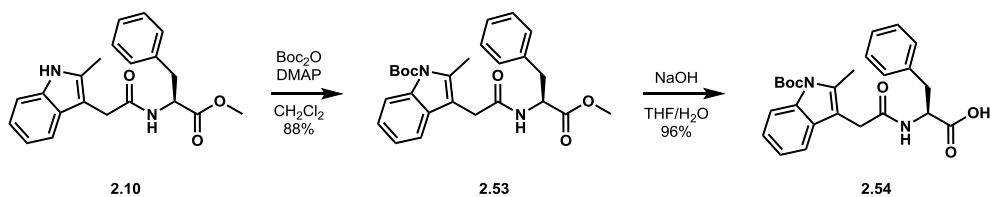


Scheme 2.26. Benzyl protection of tetraethylene glycol to form benzyl ether **2.50** followed by the activation to tosylate **2.51** and the subsequent displacement to aniline **2.52**.

As the aniline of the **PF74** moiety was to be incorporated into the molecule with the linker, the decision was taken to introduce the indole protecting group at an earlier stage for this synthesis. For the short PROTAC syntheses, the *tert*-butyl carbamate group was installed after the tertiary amide coupling (Scheme 2.21, page 121). In this synthesis, it was decided to install the protecting group before the tertiary amide coupling, thus increasing the convergence of the route. Additionally, it was noted previously that the tertiary amide coupling was perhaps hindered by the presence of the indole (Model Fragment Synthesis, page 115). It was therefore rationalised that protection of the indole moiety may improve the yield of the coupling.

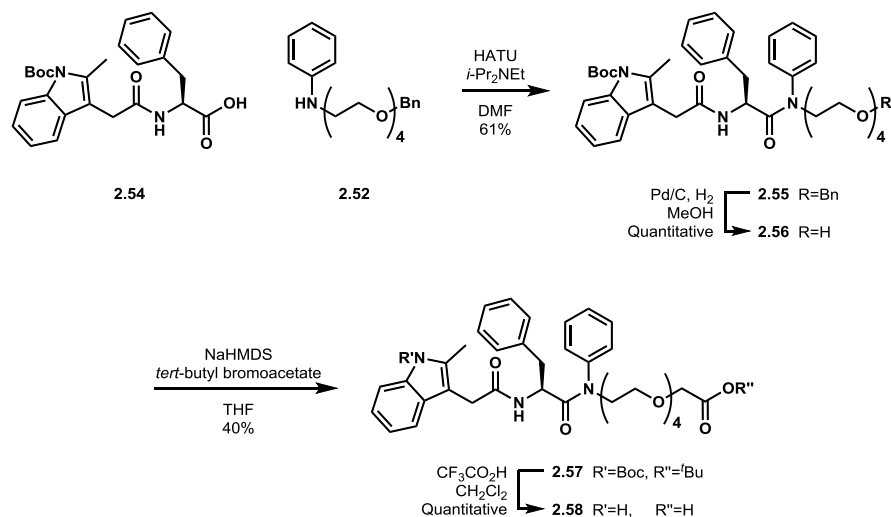
In order to generate the *tert*-butyl carbamate protected coupling partner for the 4-PEG linker **2.52**, the previously synthesised indole **2.10** (Table 2.1, page 103) was treated with di-*tert*-butyl dicarbonate and catalytic 4-dimethylaminopyridine affording *tert*-butyl carbamate **2.53** with an 88% yield (Scheme 2.27).<sup>[48]</sup> Subsequent saponification of the methyl ester of carbamate **2.53** generated acid **2.54** with a yield of 96%.<sup>[111]</sup> Interestingly, the typical acid/base extraction which is useful in the purification of organic acids could not be used for the purification of acid **2.54** due to the formation of a thick emulsion. The extraction worked as expected for the non *tert*-butyl carbamate protected analogue acid **2.11**, implying that the addition of this

protecting group was responsible for the change of behaviour. This was most likely due to an increase in lipophilicity, making the compound amphiphilic enough to form an emulsion.



Scheme 2.27. Protection of indole **2.10** to *tert*-butyl carbamate **2.53** followed by the saponification to acid **2.54**.

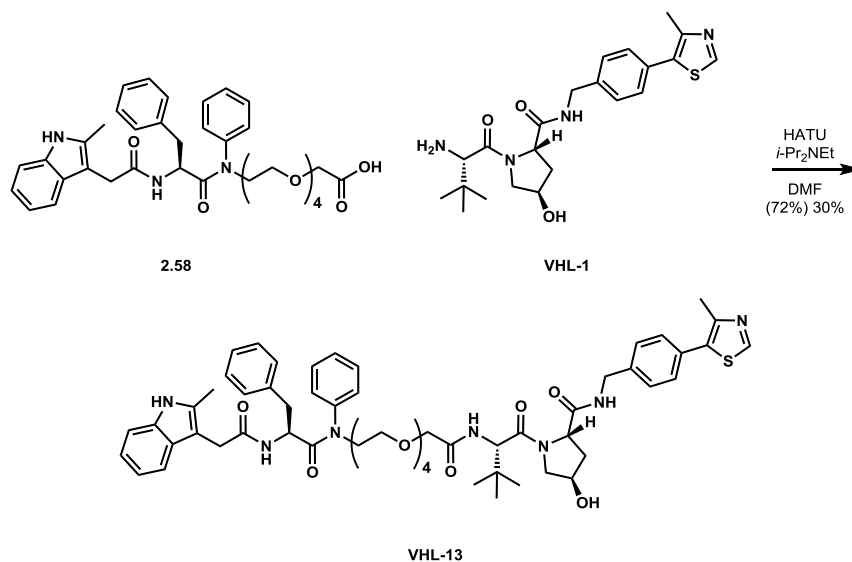
With both coupling partners synthesised, a HATU mediated coupling of acid **2.54** and secondary aniline **2.52** was conducted generating tertiary amide **2.55** with a 61% yield (Scheme 2.28). Subsequent reductive deprotection of the benzyl ether of **2.55** afforded alcohol **2.56** with a quantitative yield.<sup>[41]</sup> As was observed in the previous deprotection of benzyl ether **2.32** to alcohol **2.45** (Scheme 2.21, page 121), if the deprotection of benzyl ether **2.55** to alcohol **2.56** was left for longer than five hours (full conversion), an unidentified side product formed to the detriment of alcohol **2.56**. As both benzyl ethers **2.32** and **2.55** contain *tert*-butyl carbamate protecting groups, and the analogous benzyl ether **2.12** (Table 2.2, page 104) (with which the phenomenon was not observed) did not contain the *tert*-butyl carbamate protecting group, it seemed likely that the *tert*-butyl carbamate protecting group was integral to the undesired reaction. Following the benzyl deprotection, alcohol **2.56** was alkylated with *tert*-butyl bromoacetate using sodium bis(trimethylsilyl)amide as the base (Scheme 2.28).<sup>[41]</sup> The alkylation generated the desired *tert*-butyl ester **2.57** with a 40% yield. Subsequent double deprotection of the *tert*-butyl carbamate and the *tert*-butyl ester of **2.57** under acidic conditions, generated the corresponding free-indole containing acid **2.58**.<sup>[48]</sup>



Scheme 2.28. Coupling of acid **2.54** and aniline **2.52** to form tertiary amide **2.55** followed by benzyl deprotection to alcohol **2.56** and the subsequent alkylation to ester **2.57** followed by acidic double deprotection to acid **2.58**.

### Completion of Medium Length VHL-Based PROTAC

With **PF74** fragment **2.58** in hand, the next step was to generate the VHL and CRBN targeting PROTACs. To begin with, the VHL analogue was targeted. HATU mediated coupling of acid **2.58** with the amine of **VHL-1** was conducted, generating PROTAC **VHL-13** with a yield of 72% after initial purification by column chromatography (Scheme 2.29). After subsequent HPLC purification, the yield decreased to 30% with a mass yield of 15 mg (14  $\mu$ mol). This provided ample material for cellular testing.

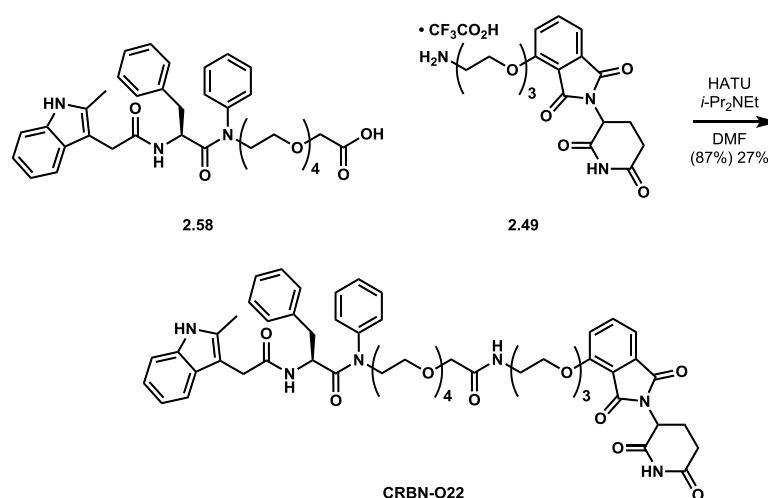


Scheme 2.29. Coupling of acid **2.58** and amine **VHL-1** to form PROTAC **VHL-13**.

### Completion of Medium Length CRBN-Based PROTAC

Following the synthesis of **VHL-13**, the preparation of the CRBN targeting analogue was addressed. To achieve this, HATU mediated coupling of acid **2.58** with the previously synthesised amine TFA salt **2.49** (Scheme 2.24, page 123) was performed,

generating **CRBN-O22** with a yield of 87% after initial purification by column chromatography (Scheme 2.30). Subsequent HPLC purification lowered the yield to 27% with a mass yield of 15 mg (15  $\mu$ mol), providing plenty of material for biological assays.



Scheme 2.30. Coupling of acid **2.58** and amine **2.49** to form PROTAC **CRBN-O22**.

### 2.2.10 PROTAC Synthesis Summary

To summarise, five molecules comprise the first generation of compounds for testing; **VHL-4**, **VHL-13**, **CRBN-O13**, **CRBN-O22** and **CRBN-N33** (Figure 2.22). All of them feature a PEG linker of varying lengths (the non-hydrogen atom (NHA) count indicated by the number in each name) and two different E3 ligases are targeted, VHL and CRBN. Furthermore, two different versions of the CRBN targeting phthalimide ligand are incorporated. PROTACs **CRBN-O13** and **CRBN-O22** contain the non-fluorescent phenolic phthalimide moiety, which features the linker attached *via* *O*-alkylation (indicated by an O in the name). Whereas PROTAC **CRBN-N33** contains the fluorescent anilinic phthalimide moiety, which features the linker attached *via* *N*-alkylation (indicated by an N in the name).

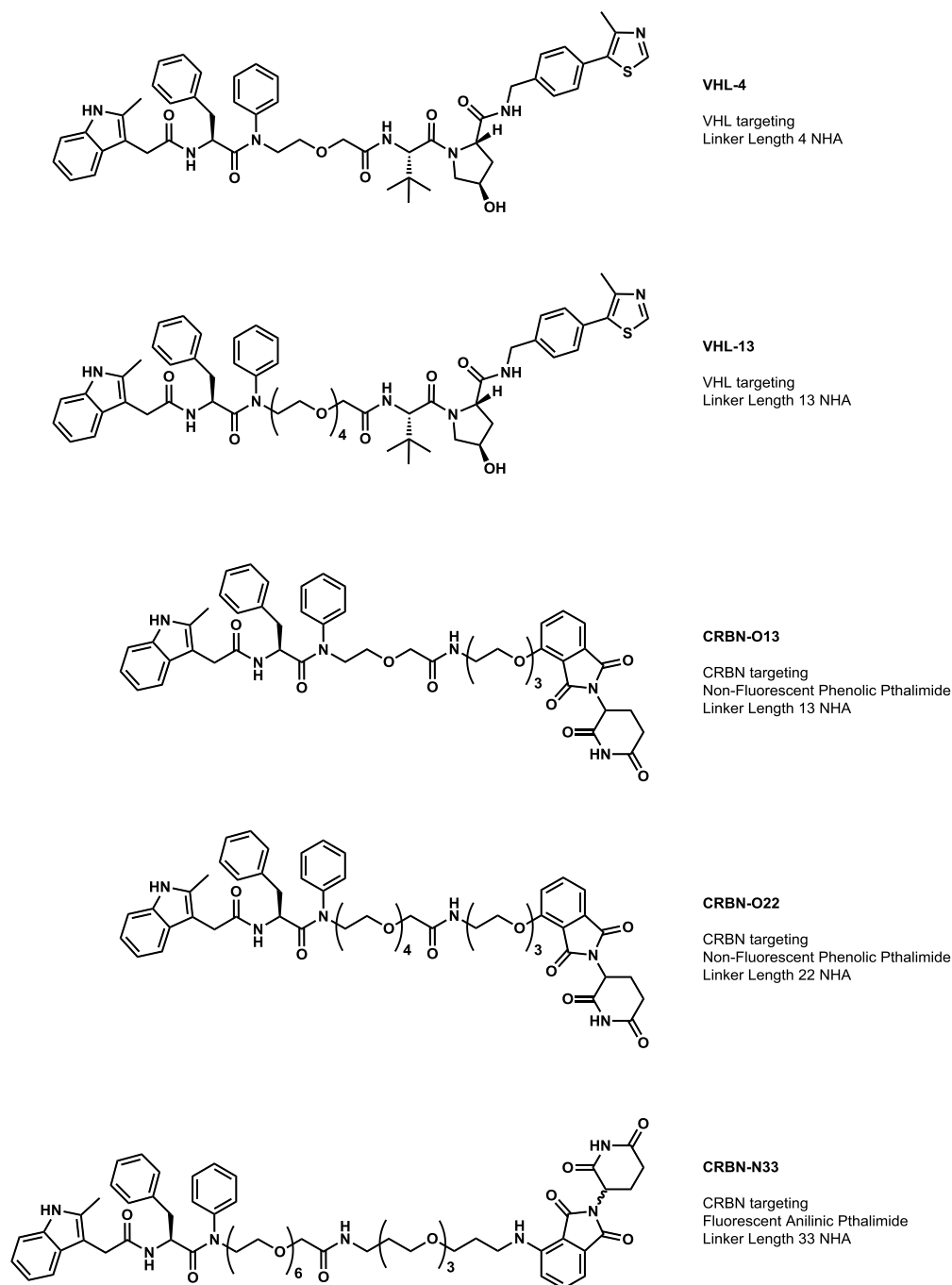


Figure 2.22. Summary of synthesised PROTACs **VHL-4**, **VHL-13**, **CRBN-O13**, **CRBN-O22** and **CRBN-N33**.

With these successful syntheses completed, the question regarding the stereochemical integrity of the phenylalanine alpha position was addressed. Ultimately, it was not deemed to be problematic for the project if epimerisation had occurred, but it was necessary to know if it was likely given the reaction conditions. This knowledge would then allow the issue to be addressed, if required, in future generations of PROTACs.

### 2.2.11 PF74 synthesis and epimerisation study

It was decided to synthesise **PF74**, both as a positive control for biological testing, but also to probe the question of stereochemical integrity of the phenylalanine alpha

position (Figure 2.23). The primary cause for concern of epimerisation was due to the reaction conditions for the secondary aniline coupling used to generate the **PF74** moiety, for example in the synthesis of tertiary amide **2.55** (Scheme 2.28, page 126). The original synthesis of **PF74** has not been published, and no information was available as to the integrity of its stereocentre. Furthermore, neither of the two published syntheses of **PF74** provided chiral HPLC retention times or  $[\alpha]_D$  values.<sup>[104][111]</sup> As the procedure carried out to synthesise the PROTACs was a modified version of that used in one of the reported **PF74** syntheses, it stood to reason that if epimerisation had occurred in the PROTAC synthesis, it would also have manifested itself in the synthesis of **PF74** described by the literature.<sup>[111]</sup>

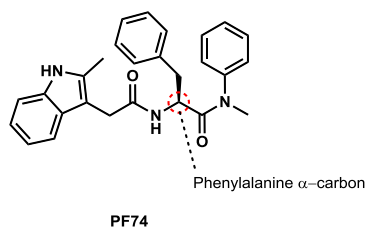
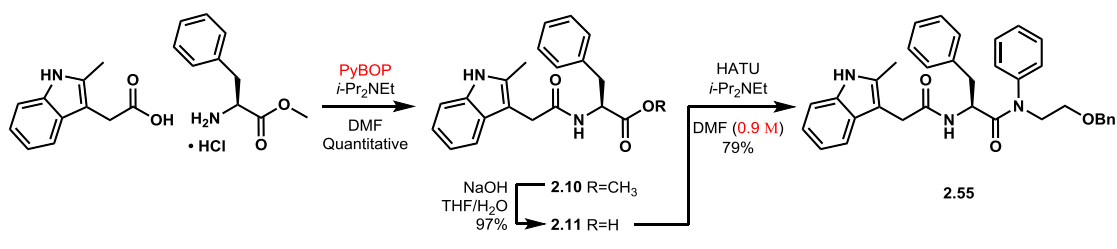


Figure 2.23. Structure of **PF74**.

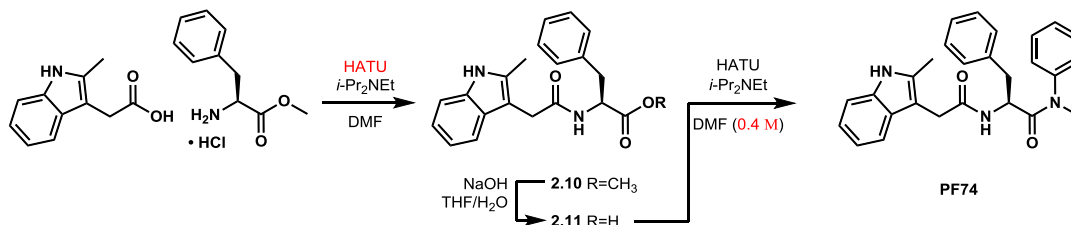
### Natural **PF74** Synthesis and Analysis

As mentioned above, the optimised procedure used for generating the **PF74** moiety of our PROTACs differed slightly from the literature procedure for the synthesis of **PF74**.<sup>[111]</sup> As result of the previously conducted<sup>[111]</sup> optimisation (Entries 3-6, Table 2.1, page 103), the initial coupling of 2-methylindole-3-acetic acid with L-phenylalanine methyl ester hydrochloride to generate methyl ester **2.10**, was conducted using PyBOP as the coupling agent (Scheme 2.31). Whereas the literature reported synthesis of **PF74** used a HATU-mediated coupling.<sup>[111]</sup> An additional deviation from the literature procedure was with regard to the secondary aniline coupling which was used throughout to install the linker, for example in the synthesis of amide **2.55** (Scheme 2.31). As a result of optimisation (Entries 3-6, Table 2.2, page 104), the coupling was performed at a concentration of 0.9 M while the literature procedure used for the synthesis of **PF74** was conducted at a concentration of 0.4 M.<sup>[111]</sup>

#### Optimised synthesis for PROTAC synthesis



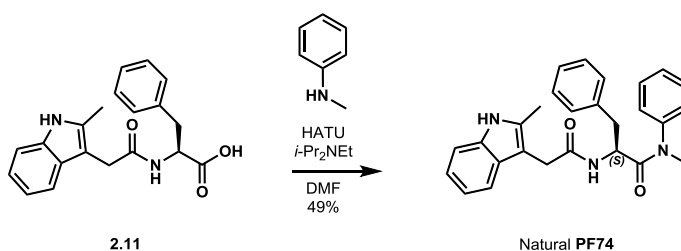
#### Literature synthesis for PF74 synthesis



Scheme 2.31. Comparison of abovementioned optimised conditions used in PROTAC syntheses with literature conditions used in **PF74** synthesis.<sup>[111]</sup>

While following the literature procedure exactly to synthesise **PF74** would have given more relevant results regarding the stereochemical integrity of commercially available **PF74**, the point of this investigation was to gain information regarding the stereochemical integrity of the synthesised PROTACs. So ultimately, the synthesis of **PF74** needed to mimic that of the PROTACs and not that of the literature synthesis of **PF74**.

Having previously prepared a stock of acid **2.11** (Table 2.1, page 103), this was utilised for the synthesis of **PF74**. Acid **2.11** was coupled with *N*-methylaniline generating **PF74** with a 49% yield (Scheme 2.32). As the synthesis of **PF74** incorporated the natural L-phenylalanine, it will be referred to as natural **PF74**.



Scheme 2.32. Coupling of acid **2.11** with *N*-methylaniline to form natural **PF74**.

The optical rotation was measured and the  $[\alpha]_D$  was calculated to be +1.40, however no literature value was reported for this value to be compared to. For this reason, a commercial sample of **PF74** was purchased and  $[\alpha]_D$  was calculated. However, only 5 mg of commercial **PF74** was purchased, which unfortunately resulted in a sample concentration too low to be able to collect consistent measurements. Despite this, the

investigation continued as planned by using chiral HPLC analysis to generate quantitative data regarding the amount of each enantiomer present. A sample of the synthesised natural **PF74** was resolved and determined to consist of 55.6% of the natural (S) enantiomer (retention time 39.0 minutes) and 44.4% of the unnatural (R) enantiomer (retention time 49.7 minutes), which was consistent with a significant degree of epimerisation (Figure 2.24).

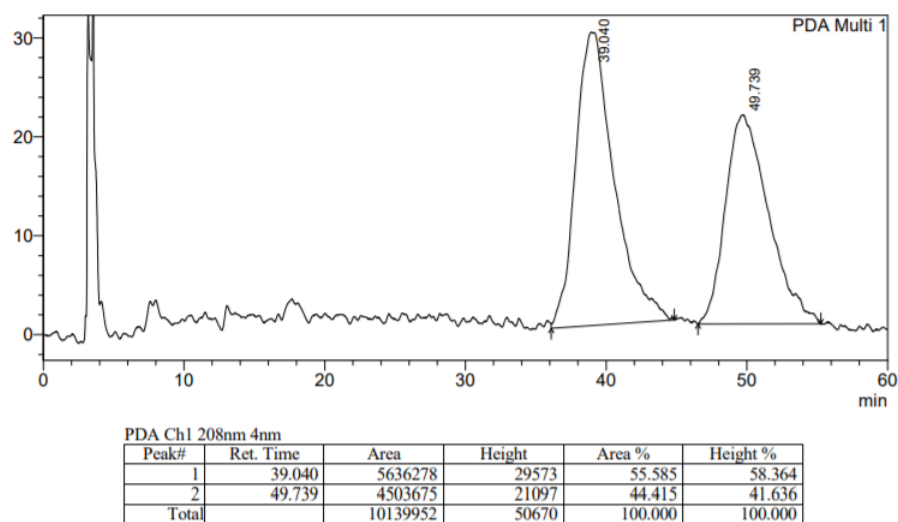


Figure 2.24. Chiral HPLC trace of synthetic natural **PF74**.

Using the same method, a sample of the commercial **PF74** was then analysed to compare with the results of the synthetic natural **PF74**. The commercial sample was determined to consist of 51.3% of the natural (S) enantiomer (retention time 39.2 minutes) and 48.7% of the unnatural (R) enantiomer (retention time 50.1 minutes), again indicating a significant degree of epimerisation to the point of being almost racemic (Figure 2.25). At this point, it should be reiterated that epimerisation is not problematic for the aims of the project; however, it was useful to know that the PROTACs being tested were likely to also have a large degree of epimerisation at the phenylalanine alpha position.

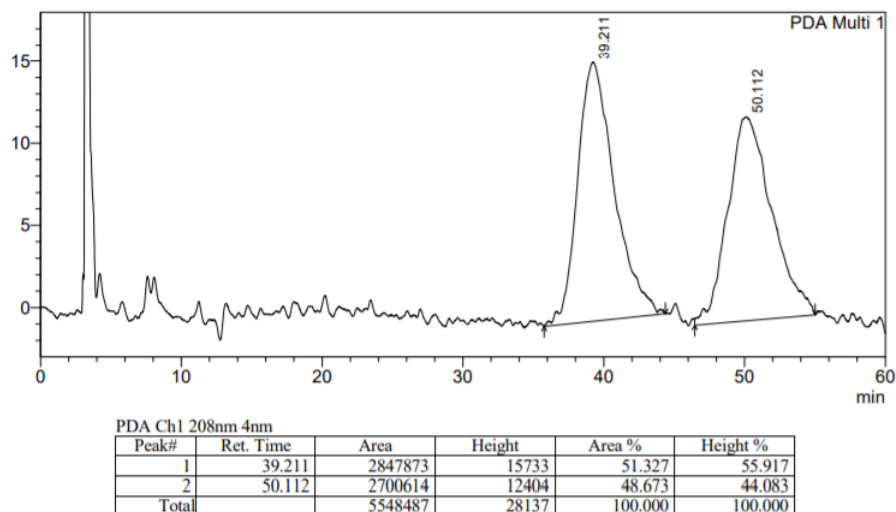
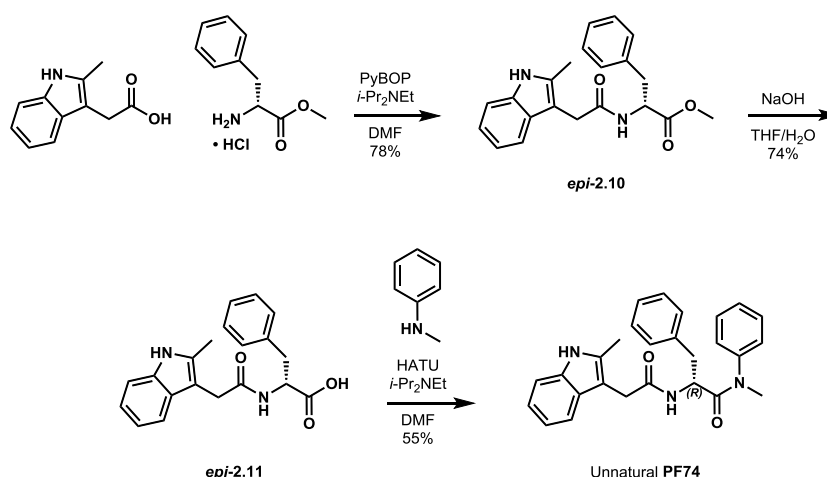


Figure 2.25. Chiral HPLC trace of commercial **PF74**.

### Unnatural **PF74** Synthesis and Analysis

To corroborate the above findings, the synthesis was conducted while incorporating the unnatural D-phenylalanine to give access to unnatural **PF74**. The synthesis was analogous to that of natural **PF74** to be able to confidently compare the results. The initial coupling of 2-methylindole-3-acetic acid with D-phenylalanine methyl ester hydrochloride generated methyl ester *epi*-**2.10** with a 78% yield (Scheme 2.33). Following the successful coupling, the saponification of methyl ester *epi*-**2.10**, afforded acid *epi*-**2.11** with a 74% yield. To complete the synthesis, acid *epi*-**2.11** was coupled with *N*-methylaniline generating unnatural **PF74** with a 55% yield.



Scheme 2.33. Synthesis of methyl ester *epi*-**2.10**, followed by saponification to *epi*-**2.11** and subsequent coupling to generate unnatural **PF74**.

For comparison to the synthetic natural **PF74**, the optical rotation was measured and the  $[\alpha]_D$  was calculated to be  $-5.57$ . More importantly however, the sample was resolved by analytical chiral HPLC using the same method as was used for natural **PF74** and the commercial **PF74**. This resolution determined the sample of unnatural

**PF74** to consist of 34.6% of the natural (*S*) enantiomer (retention time 39.0 minutes) and 65.4% of the unnatural (*R*) enantiomer (retention time 49.3 minutes) (Figure 2.26). Again this represented a significant degree of epimerisation; however, interestingly not as much as that observed in the natural **PF74** synthesis.

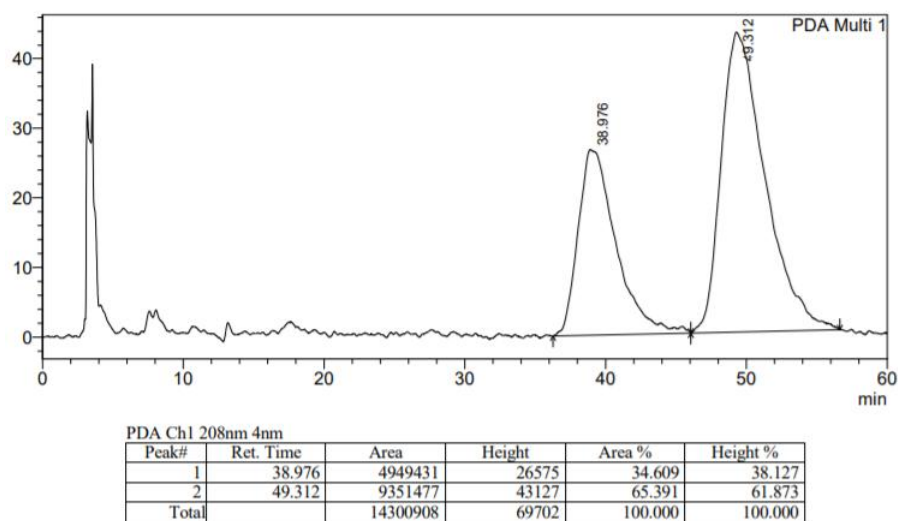
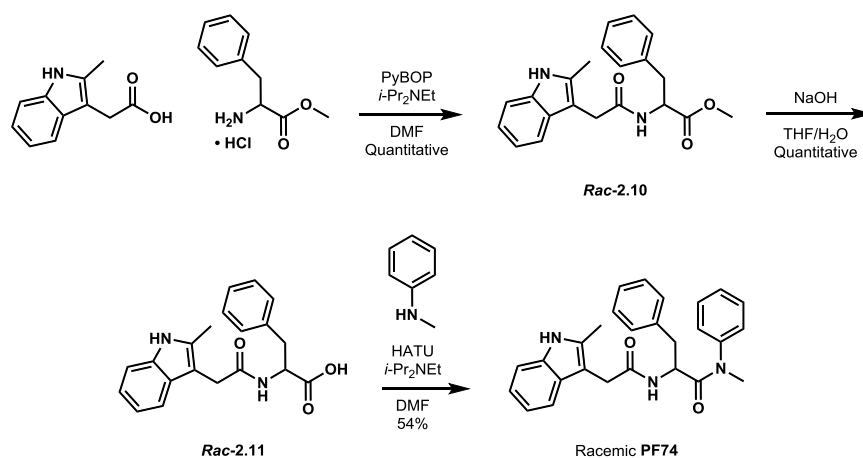


Figure 2.26. Chiral HPLC trace of synthetic unnatural **PF74**.

### Racemic **PF74** Synthesis and Analysis

Finally, for comparison and curiosity, the synthesis was repeated with incorporation of racemic DL-phenylalanine to generate racemic **PF74**. The initial coupling of 2-methylindole-3-acetic acid with DL-phenylalanine methyl ester hydrochloride generated racemic methyl ester *rac*-**2.10** with a quantitative yield (Scheme 2.34). The following saponification of ester *rac*-**2.10** to acid *rac*-**2.11** also proceeded with a quantitative yield. To complete the synthesis, acid *rac*-**2.11** was coupled with *N*-methylaniline generating racemic **PF74** with a 54% yield.



Scheme 2.34. Synthesis of methyl ester *rac*-**2.10**, followed by saponification to *rac*-**2.11** and subsequent coupling to generate racemic **PF74**.

The optical rotation was measured and the  $[\alpha]_D$  was calculated to be +0.85. This was somewhat peculiar given that racemic starting materials were utilised and should therefore have a value of zero. However, more importantly, resolution by analytical chiral HPLC determined the sample of racemic **PF74** to comprise 52.8% of the natural (*S*) enantiomer (retention time 39.1 minutes), and 47.2% of the unnatural (*R*) enantiomer (retention time 49.7 minutes) (Figure 2.27). Again, this result was somewhat unanticipated as a racemate was expected due to the racemic starting material. It is possible that the slight deviation from a pure racemate is due to error in the HPLC measurement; however, it would be interesting to probe this anomaly further by performing chiral HPLC resolution of the DL-phenylalanine methyl ester hydrochloride starting material. Regardless, the data collected from each of the **PF74** syntheses was sufficient to declare that almost complete epimerisation was present in both the commercially acquired **PF74** and the synthesised batch of natural **PF74**. With this in mind, it was therefore highly likely that the phenylalanine alpha position in each of the synthesised PROTACs had a similar level of epimerisation. However, as previously mentioned, this was not deemed to be problematic to the outcomes of the project.

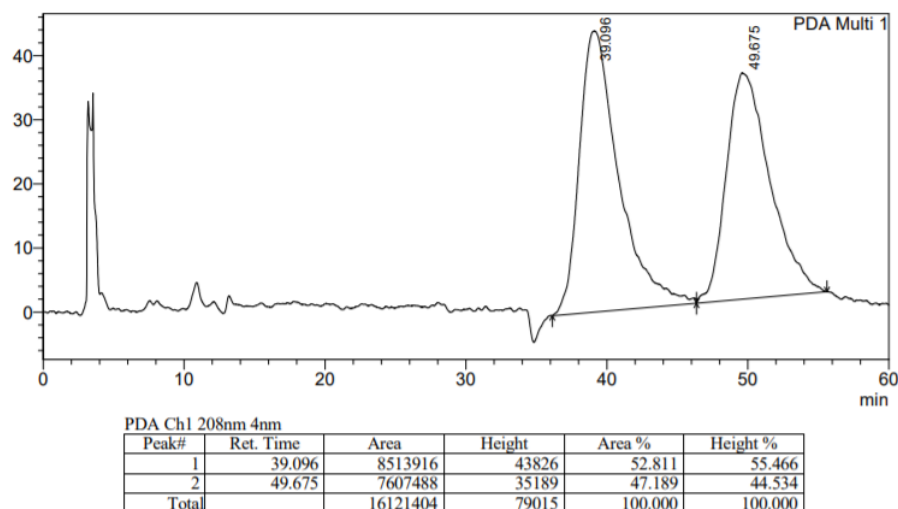


Figure 2.27. Chiral HPLC trace of synthetic racemic **PF74**.

### Collection of Enantiomerically Pure **PF74**

Having established that a high degree of epimerisation of the phenylalanine alpha position was present in **PF74**, it was therefore also likely to have occurred in the syntheses of each the PROTACs. In an effort to determine how much of an effect this epimerisation would have in cellular assays, some time was invested in attaining enantiomerically enriched samples of each of the **PF74** enantiomers. Due to the adequate separation of peaks observed in the analytical chiral HPLC traces, preparative

resolution was achieved through the collection of each enantiomer from successive runs. Each sample was then analysed by chiral HPLC to assess their enantiomeric purity. The natural (*S*)-(+)-**PF74** sample was determined to contain 99.2% of the natural (*S*) enantiomer (retention time 32.8 minutes) and 0.8% of the unnatural (*R*) enantiomer (retention time 42.0 minutes) (Figure 2.28). Due to the high enantiomeric enrichment, the HPLC resolved natural material will be referred to as (*S*)-**PF74**.

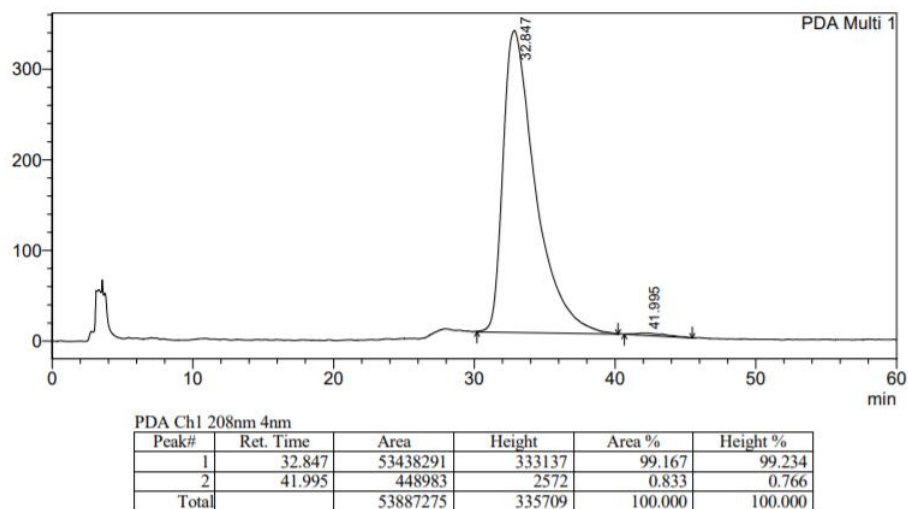


Figure 2.28. Chiral HPLC trace of enantiomerically enriched natural (*S*)-**PF74**.

The sample of unnatural (*R*)-(-)-**PF74** was determined to comprise 1.6% of the natural (*S*) enantiomer (retention time 33.5 minutes) and 98.4% of the unnatural (*R*) enantiomer (retention time 39.6 minutes) (Figure 2.29). Due to the high enantiomeric enrichment, the HPLC resolved unnatural material will be referred to as (*R*)-**PF74**. The two traces confirmed the preparative resolution was successful, achieving greater than 98% enantiomeric enrichment in each sample.

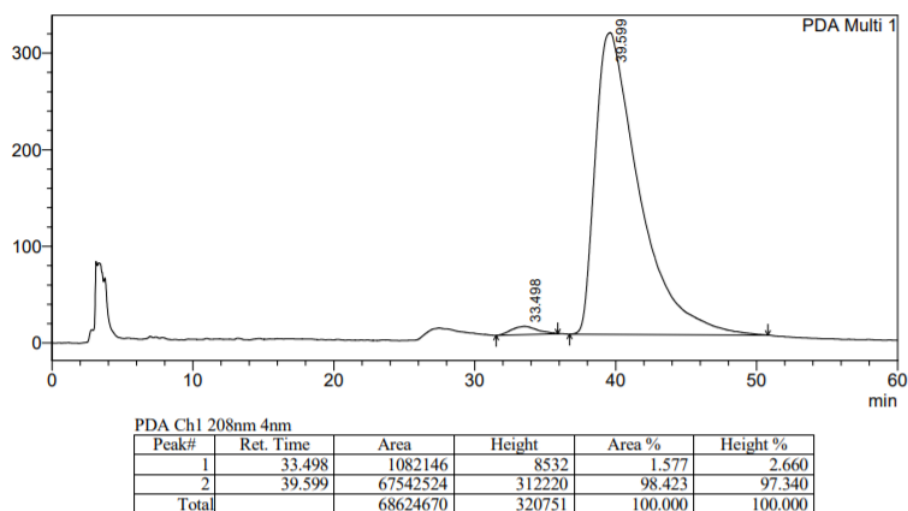


Figure 2.29. Chiral HPLC trace of enantiomerically enriched unnatural (*R*)-**PF74**.

With the two enantiomers of **PF74** successfully resolved, they could then be tested to establish which, if either, enantiomer is more active. This information could then be used to establish whether it would be worth the time investment to generate enantiomerically enriched PROTACs in subsequent generations. Furthermore, if one of the enantiomers were to be inactive, then future PROTAC design could take advantage of this inactivity for the design of negative control compounds with the same physical chemical properties.

## 2.3 Biological Assays

### 2.3.1 Materials and Methods

#### Cell Lines and Culture

All cell culture work was carried out at biosafety level 2, in category 2 biosafety cabinets and under sterile conditions. All assays used HEK 293T (human embryonic kidney) cells as the viral host. HEK 293T suspension cell line was cultured in DMEM (Dulbecco's modified Eagle's medium) (high glucose (4.5 g/L)) with sodium pyruvate (110 mg/mL), 10% FCS (fetal calf serum) and gentamicin (20 mg/L) added.<sup>[118]</sup> Suspension HEK 293T cultures were maintained in 75 cm<sup>2</sup> flasks at 37 °C with 5% CO<sub>2</sub>. Cell cultures were split every 3–4 days whereby the suspension was agitated with a pipette to generate a homogeneous single cell suspension. 5 mL aliquots were taken and centrifuged at 1200 rpm for 3 minutes. The supernatant was discarded and the cells resuspended in 30 mL of fresh media and maintained at 37 °C with 5% CO<sub>2</sub>.<sup>[119]</sup>

#### Viral Vector Preparation

HIV single cycle GFP-based vector CSGW stocks used for this project were all pseudotyped with VSV-G (vesicular stomatis virus envelope glycoprotein). CSGW-VSV-G and CSGW packing derivatives (Gag-Pol, tat and rev) p8.91Ex-VSV-G and p8.91N74D-VSV-G were generated by Dr Elena Sugrue or other members of the Dr Sam Wilson lab, situated at the Centre for Virus Research (CVR), University of Glasgow. Plasmids p8.91Ex and p8.91N74D were generously provided by Prof. Greg Towers at University College London. MLV (murine leukaemia virus) single cycle GFP-based vector CNCG stocks were generated by Dr Elena Sugrue or other members of the Dr Sam Wilson lab, situated at the Centre for Virus Research (CVR), University of Glasgow. The GFP-based vectors caused GFP (green fluorescent protein) expression in infected cells, which was measured by flow cytometry as the metric of infection.

#### Cell Counting

For cell counting, HEK 293T suspension cells were agitated by pipette to generate a homogeneous single cell suspension. A 10 mL aliquot of this suspension was taken and centrifuged at 1200 rpm for 3 minutes, the supernatant was discarded and the cell pellet was resuspended in 10 mL of fresh media to regenerate a homogenous single cell suspension. A 1 mL aliquot was taken and homogenised, before 10 µL were removed and added to 10 µL of 4% trypan blue solution. The cells were agitated, then the 20 µL stained suspension was added to a haemocytometer slide and counted.

### Cell preparation for flow cytometry

Cells were treated with 50 µL of 0.5% trypsin solution (containing 0.05% EDTA), agitated and incubated at 37 °C for 5-10 minutes. The suspension was agitated again and observed under a light microscope to confirm a homogeneous single cell suspension had formed. 100 µL of cell suspension was then transferred into round bottomed 96-well plates containing 100 µL of 4% formaldehyde solution. These plates were stored at 4 °C until analysed by flow cytometry. Flow cytometry was carried out using a Guava EasyCyte flow cytometer which collected 10 000 events and measured the percentage of GFP-positive infected cells.

### Viral Vector Titration

Viral vector stocks stored at –80 °C were thawed and 180 µL added to the first column of a 96-well plate. To the remaining 11 columns per row, 120 µL of fresh media was added. The stock was then titrated across the lane (60 µL:120 µL) excluding the final column which was used as a negative control. 50 µL of titrated viral vector was then added to 100 µL of HEK 293T cell suspension (500 000 cells/mL) in fresh media. The cells were then incubated at 37 °C and 5% CO<sub>2</sub> for 48 hours before being fixed and analysed by flow cytometry.

From the above titration, the titre (infective units/mL) of CSGW-VSV-G stock was calculated to be  $5.39 \times 10^6$ . Using this titre, the concentration of viral vector stock required to produce infection of between 15–20% of cells was calculated to be 9.25 µL of viral vector stock per 1 mL of fresh media. This dilution was then used as the viral vector dose in fixed viral vector titre assays.

### Compound Fixed Dose (Viral Vector Titration) Assay

For fixed compound dose assays, a viral vector titration was performed followed by the addition of 50 µL of a 4% DMSO solution of compound (at 4x desired final concentration) in media. The plates were then incubated at 37 °C and 5% CO<sub>2</sub> for 48 hours before being fixed and analysed by flow cytometry.

### Compound Dose Response (Fixed Viral Vector Titre) Assay

For compound dose response assays, each compound was titrated across a 96 well plate to give a maximum concentration of 25 µM to a minimum concentration of 95 pM (x4 dilution series). In addition to the compound, each well contained 100 µL of a suspension of HEK 293T cells (500 000 cells/mL) in fresh media and 50 µL of viral vector solution (9.25 µL/mL) in fresh media with a final concentration of 1% DMSO per well. The final column of each plate contained only HEK 293T cell suspension as a

negative control. The plates were then incubated at 37 °C and 5% CO<sub>2</sub> for 48 hours before being fixed and analysed by flow cytometry.

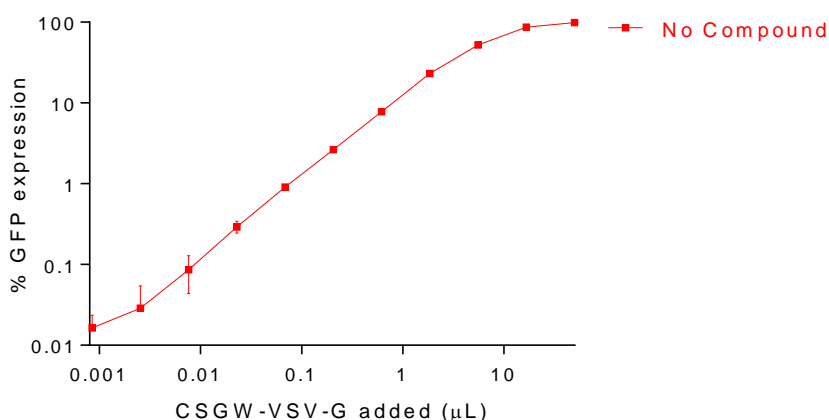
### E3 Ligase Ligand Titration (Fixed Compound Dose, Fixed Viral Vector Titre) Competition Assay

For E3 ligase ligand competition assays, each E3 ligase ligand was titrated across a 96 well plate to give a maximum concentration of 267 µM to a minimum concentration of 255 pM (x4 dilution series). In addition to the compound, each well contained 100 µL of a suspension of HEK 293T cells (500 000 cells/mL) in fresh media, 50 µL of viral vector solution (9.25 µL/mL) in fresh media and 50 µL of a 4% DMSO solution of compound (at 4x desired final concentration) in media to give a final concentration of 1% DMSO per well. The final column of each plate contained only HEK 293T cell suspension as a negative control. The plates were then incubated at 37 °C and 5% CO<sub>2</sub> for 48 hours before being fixed and analysed by flow cytometry.

#### 2.3.2 PF74 Study

##### Establishing Control Experiments

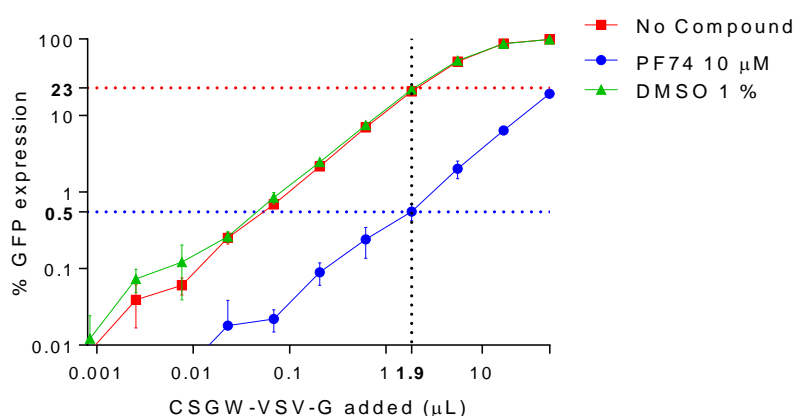
To begin testing, the viral vector CSGW-VSV-G was titrated against the HEK 393T cell line to establish the baseline infectivity with which the effects of the added compounds could be compared. The titration was performed in triplicate and the error bars displayed (Graph 2.1).



Graph 2.1. CSGW-VSV-G infection of HEK 293T cells.

Having established the baseline infectivity of CSGW-VSV-G in HEK 293T cells, the ability of the synthetic natural **PF74** to inhibit this infectivity was assessed. For this assay, CSGW-VSV-G was titrated and incubated with the cells with a fixed dose of **PF74** (10 µM) added. As the stock solution of **PF74** was in DMSO, it was necessary to establish whether DMSO had an effect on the growth and health of the cells or on the

infectivity of CSGW-VSV-G. As the final concentration of DMSO in the assay was 1% of the well volume, a 1% DMSO negative control was carried out (Graph 2.2). Upon inspection of the cells by DIC and fluorescence microscopy, they were determined to have healthy morphology and a cell count that was comparable to the non-DMSO treated cells. Furthermore, the infectivity of CSGW-VSV-G in the presence of 1% DMSO was indistinguishable from the infectivity in the absence of DMSO, thus establishing that 1% DMSO had no detrimental effect. In the presence of the synthetic natural **PF74** (10  $\mu$ M) however, the infectivity of CSGW-VSV-G was greatly reduced. For example, a dose of 1.9  $\mu$ L of CSGW-VSV-G in the absence of **PF74** produced 23% GFP expression (and thus infection) but in the presence of 10  $\mu$ M **PF74** the same dose of CSGW-VSV-G only produced 0.5% GFP expression (Graph 2.2).



Graph 2.2. Titration of CSGW-VSV-G against **PF74**, 1% DMSO vehicle control and a no compound reference.

### Synthetic and Commercial **PF74** Comparison

Having established the efficacy of the synthetic natural **PF74**, the efficacy of the synthetic unnatural **PF74**, and the commercially sourced **PF74** were tested for comparison. To avoid confusion, these compounds will be referred to as natural **PF74** (as the synthesis incorporated natural L-phenylalanine), unnatural **PF74** (as the synthesis incorporated unnatural D-phenylalanine), and commercial **PF74** (as this sample was commercially sourced) respectively and their structures are outlined below with their chiral HPLC determined enantiomeric ratios (Figure 2.13).

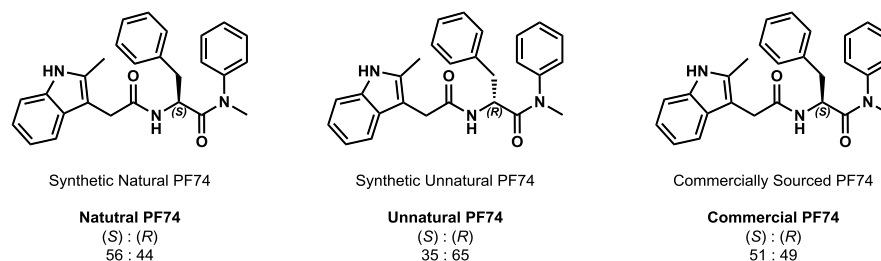
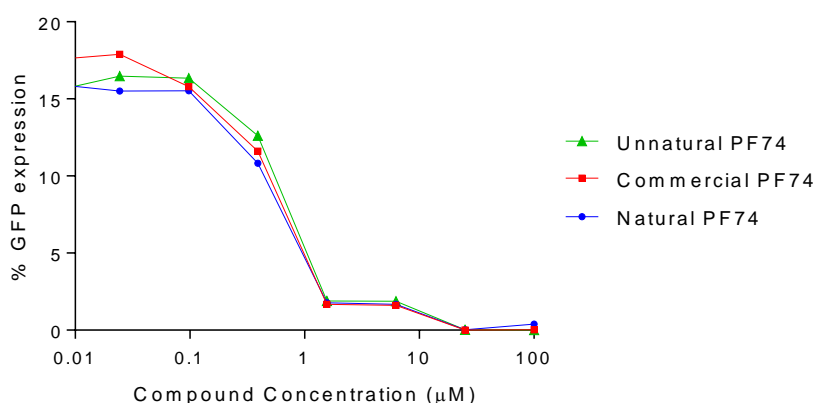


Figure 2.30. Structures of the synthetic natural, synthetic unnatural and commercially sourced **PF74** with their enantiomeric ratios.

For this dose response assay, the various **PF74** samples were titrated against the previously calculated optimal fixed titre of CSGW-VSV-G (Viral Vector Preparation, page 137). The results of this assay showed no significant difference between the different samples, however this was to be expected (Graph 2.3). From the HPLC analysis of each sample, it was determined that all three had a significant amount of epimerisation thus producing almost racemic samples (2.2.11 **PF74** synthesis and epimerisation study, page 128). As no significant difference was detected between the different **PF74** samples, only the natural **PF74** was utilised as the positive control for further testing.



Graph 2.3. Dose response of synthetic natural **PF74**, synthetic unnatural **PF74** and commercial **PF74** against a fixed titre of CSGW-VSV-G.

### Enantiomerically Enriched (S)-PF74 and (R)-PF74 Comparison

To continue the investigation, the HPLC-resolved enantiomerically pure samples were tested. To avoid confusion, the HPLC-resolved compounds will be referred to as (S)-**PF74** and (R)-**PF74** and their structures are outlined below with their chiral HPLC determined enantiomeric ratios (Figure 2.31).

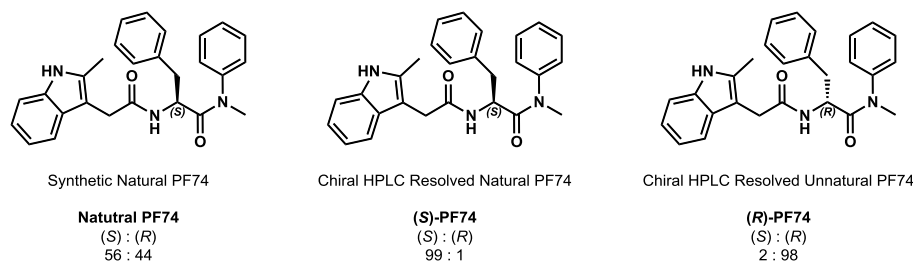
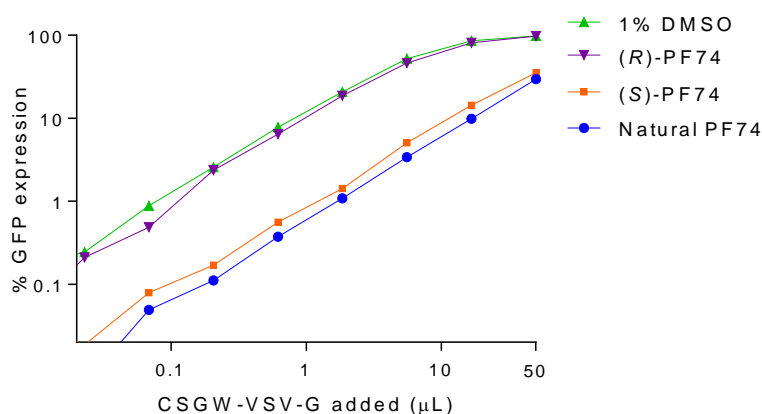


Figure 2.31. Structures of natural **PF74**, HPLC resolved **(S)-PF74** and HPLC resolved **(R)-PF74** with their enantiomeric ratios.

The dose response assay involved the titration of CSGW-VSV-G against a fixed dose (10  $\mu$ M) of each of the HPLC resolved enantiomers. The batch of almost racemic synthetic natural **PF74** served as the positive control and 1% DMSO served as the negative control. The results of the assay indicated that **(S)-PF74** had activity comparable to the synthetic natural **PF74**, and was therefore significantly more active than **(R)-PF74**, which had little activity above that of the DMSO negative control (Graph 2.4). This was a somewhat peculiar result as the natural **PF74** was determined to be almost racemic, and should therefore be half as active as the enantioenriched **(S)-PF74**.

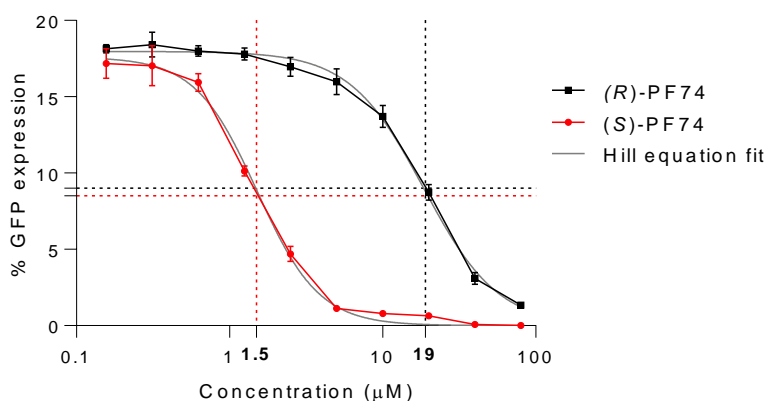


Graph 2.4. Titration of CSGW-VSV-G against enantiomerically pure natural (S) and unnatural (R) **PF74**.

### **(S)-PF74** and **(R)-PF74** $IC_{50}$ Determination

A possible explanation for the comparable efficacy of the nearly racemic natural **PF74** batch and the enantioenriched **(S)-PF74** was that only 1 mg of each the enantioenriched samples was isolated, and thus a high degree of error was inherent with the mass measurement. Consequently, the accuracy of the concentration of stock solutions from these enantioenriched samples would have been adversely affected. While this could also be used to argue that the qualitative difference in activity between the two enantiomers is invalid, the difference in activity was more than 10-fold and thus is not

likely to be a result of mass inaccuracy. With this in mind, the qualitative observation that (*S*)-PF74 was more active than (*R*)-PF74 is likely genuine. In order to better quantify the difference in efficacy of the two enantiomers, the dose response was repeated in triplicate for the purpose of IC<sub>50</sub> determination by collaborator Dr Elena Sugrue. The IC<sub>50</sub> of (*S*)-PF74 was determined to be 1.5 μM, and (*R*)-PF74 to be 19-μM, and the results are plotted against the Hill equation fit line (Graph 2.5).



Graph 2.5. IC<sub>50</sub> determination of (*S*)-PF74 and (*R*)-PF74.

### (S)-PF74 and (R)-PF74 Docking Study

In an attempt to rationalise the difference in efficacy between the two enantiomers, docking studies were carried out using Autodock (by collaborator Elena Sugrue). (*S*)-PF74 was shown to have seven potential favourable interactions at the binding site, and three locations of solvent exposure (unfavourable), indicated by the grey spheres (Figure 2.32). The favourable interactions included three  $\pi$ -cation interactions, between the two rings of the indole moiety, and the phenylalanine ring with the charged lysine 70 residue. In addition to these interactions, there were four potential hydrogen bonding interactions present between the indole *N*-H and glutamine 63, the primary amide carbonyl and a water molecule, the primary amide *N*-H and asparagine 57 and the tertiary amide carbonyl with asparagine 57. These findings closely match the literature reported binding interactions of the PF74-capsid crystal structure, which show an additional interaction between the indole moiety and arginine 173.<sup>[108]</sup> Furthermore, the binding energy was calculated using a MMBGSA function and determined to have a  $\Delta G$  of -73.8 kcal/mol.

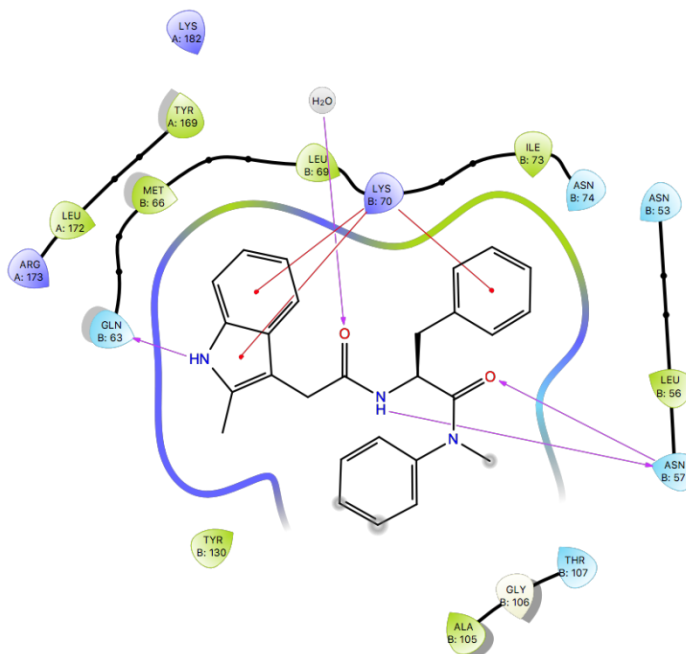


Figure 2.32. Autodock docking of (*S*)-PF74 in the hexameric CA binding site with key interactions highlighted.

Autodock docking of (*R*)-PF74 was also performed, which indicated the adoption of an alternative binding conformation (Figure 2.33). This alternate conformation was determined to have only four potential favourable interactions and three sites of unfavourable solvent exposure. The favourable interactions were the same three  $\pi$ -cation interactions between the two rings of the indole moiety, and the phenylalanine ring with the charged lysine 70 residue, and an H-bonding interaction between the carbonyl of the tertiary amide with a water molecule. The binding energy was again calculated using a MMBGSA function, and this enantiomer was determined to have a  $\Delta G$  of -55.8 kcal/mol. This is significantly higher than that of (*S*)-PF74 and thus predicts a less favourable binding conformation. This calculation coupled with the fewer favourable interactions observed from the docking study, constitute reasonable evidence as to why the efficacy of (*R*)-PF74 is almost 20-fold lower than that (*S*)-PF74.

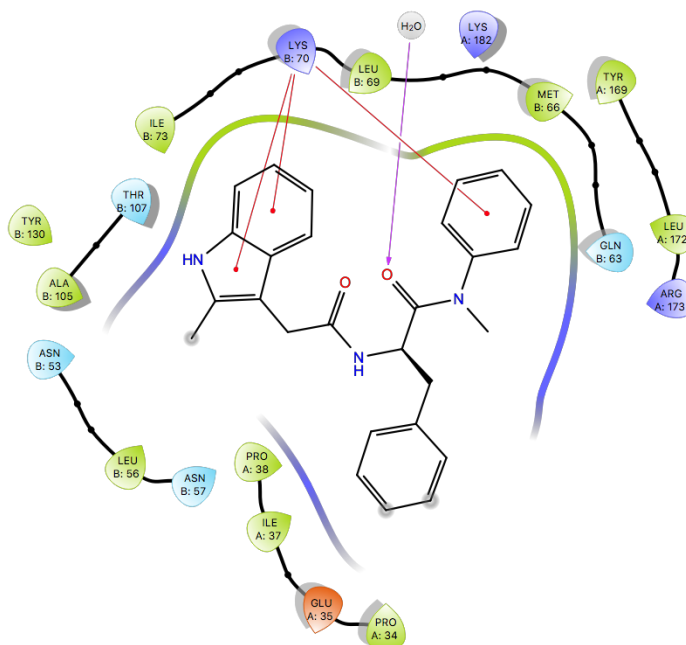


Figure 2.33. Autodock docking of **(R)-PF74** in the hexameric CA binding site with key interactions highlighted.

Interestingly, the sites of solvent exposure in **(S)-PF74** include the tertiary amide *N*-methyl group whereas this position is not included in the solvent exposed sites of **(R)-PF74**. As this position is the site of linker attachment in the PROTACs, it is possible that the diminished activity of the unnatural enantiomer could be exacerbated in the PROTACs as its most favourable binding conformation cannot be adopted. Of course this is purely speculative, and further docking studies and assays with enantiomerically pure PROTACs would need to be performed.

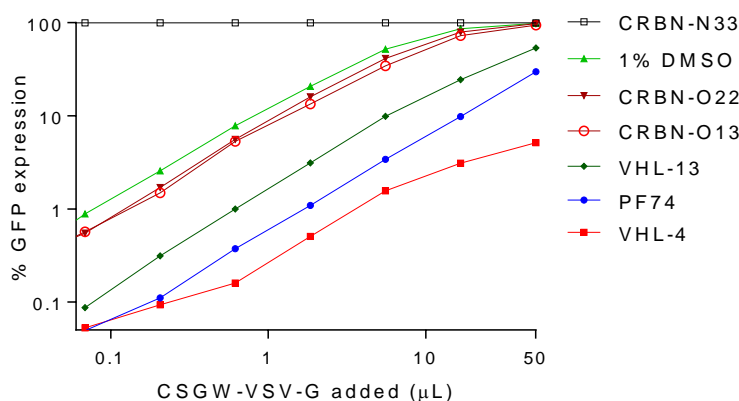
### 2.3.3 PROTAC Testing

With the **PF74** study complete, the next step was to assay the synthesised PROTACs. As these PROTACs were not resolved by preparative chiral HPLC, the decision was taken to use the synthetic natural **PF74** as the positive control and to carry out no further testing with the enantioenriched **(S)-PF74** and **(R)-PF74**. For ease of reading, the synthetic natural **PF74** will be simply referred to as **PF74**. The use of **PF74** as a positive control was complicated by the fact that it hinders HIV infection through an inhibition mechanism and not a degradation mechanism. However, as no alternative was available, the use of **PF74** would at least provide an indication of reduced HIV infection.

### Establishing PROTAC Efficacy

With that in mind, CSGW-VSV-G was titrated against a fixed concentration (10  $\mu$ M) of **CRBN-N33**, **CRBN-O22**, **CRBN-O13**, **VHL-13**, **VHL-4**, **PF74** (positive control)

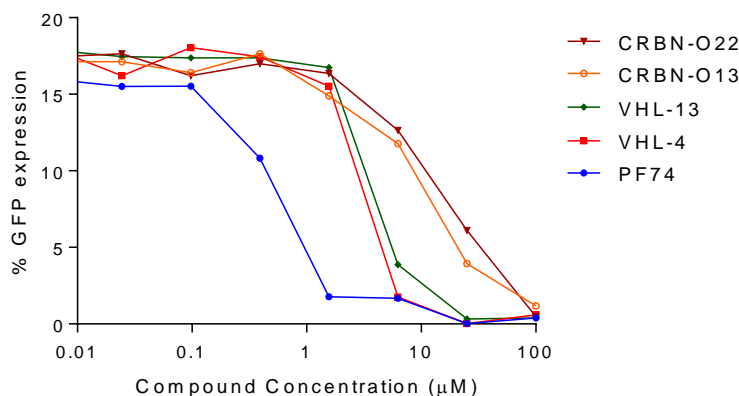
and 1% DMSO (negative control) (Graph 2.6). Promisingly, every compound produced some inhibition of HIV infection compared to the DMSO negative control. Unfortunately, as expected, the fluorescence of the anilinic phthalimide based **CRBN-N33** interfered with the measurement of GFP expression producing a false reading of 100% at every data point. For this reason, **CRBN-N33** was omitted from all future testing. The CRBN based PROTACs **CRBN-O22** and **CRBN-O13** performed poorly, only producing inhibition slightly above the baseline DMSO with the longer linker **CRBN-O22** (22 non hydrogen atoms) being marginally worse than the shorter linker (13 non hydrogen atoms) **CRBN-O13**. More interestingly, the VHL based PROTACs **VHL-13** and **VHL-4** had better inhibition of CSGW-VSV-G infection than the CRBN based PROTACs. The longer linker **VHL-13** (13 non hydrogen atoms) performed marginally worse than **PF74** but intriguingly the shorter linker **VHL-4** (4 non hydrogen atoms) appeared to be more efficacious than **PF74**.



Graph 2.6. Titration of CSGW-VSV-G against a fixed dose (10 μM) of **PF74**, **VHL-4**, **VHL-13**, **CRBN-O13**, **CRBN-O22**, **CRBN-N33** and 1% **DMSO**.

The experiment was then repeated, this time with a fixed titre of CSGW-VSV-G and a titration of the compounds in order to assess if each of the compounds displays dose-dependent activity (Graph 2.7). Dose-dependence was observed for each of the PROTACs and **PF74** and the same trend of activity was observed between the PROTACs whereby VHL-targeting PROTACs were more efficacious than CRBN-targeting PROTACs and PROTACs containing shorter linkers performed better than those with longer linkers. Interestingly, in this assay **PF74** appeared to decrease the infectivity of CSGW-VSV-G to a greater extent than **VHL-4**. This is the opposite result to that observed in the fixed compound dose-CSGW-VSV-G titration assay above (and all subsequent testing). It remains unclear why **PF74** decreased the infectivity of CSGW-VSV-G to a greater extent than **VHL-4** in the fixed titre assay, but **VHL-4** was

superior in CSGW-VSV-G titration assays. Regardless, the purpose of this assay was to assess each PROTAC for dose-dependent activity, which was successfully established.



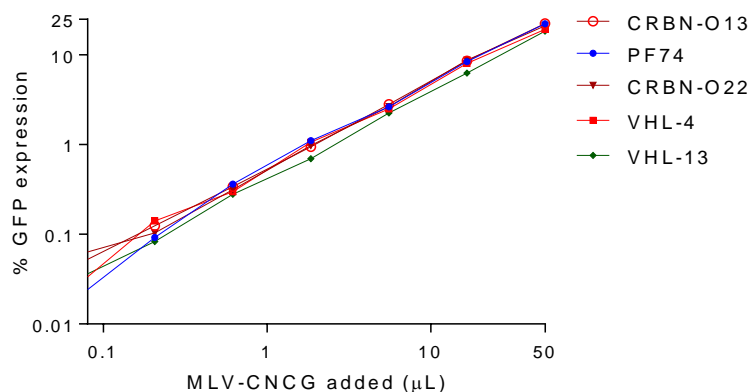
Graph 2.7. Compound dose-response assay of **PF74**, **VHL-4**, **VHL-13**, **CRBN-O13** and **CRBN-O22** against a fixed CSGW-VSV-G titre.

The results of these assays suggested that VHL-based PROTACs were more effective than CRBN-based PROTACs and that PROTACs with shorter linkers were more efficacious than longer linkers at decreasing CSGW-VSV-G infection. This observation was noteworthy, as the planning suggested a linker long enough to span the 30 Å cleft to the **PF74** binding site would be required to achieve degradation (2.1.10 First generation probe design, page 97). This therefore raised questions as to whether PROTAC-induced degradation or traditional protein inhibition was responsible for the decrease in infectivity of CSGW-VSV-G. The possibility also exists that these trends could be a result of cellular permeability and solubility of the compounds. While the results of the assay imply that all the PROTACs were at least somewhat cell permeable and soluble in the assay media, further investigation is required to quantify these parameters for each compound as this information could be beneficial to the design of future PROTAC generations. In any case, several control experiments were conducted in an attempt to probe the mechanism of the observed inhibition of CSGW-VSV-G infection.

### Confirming HIV-Specific Binding

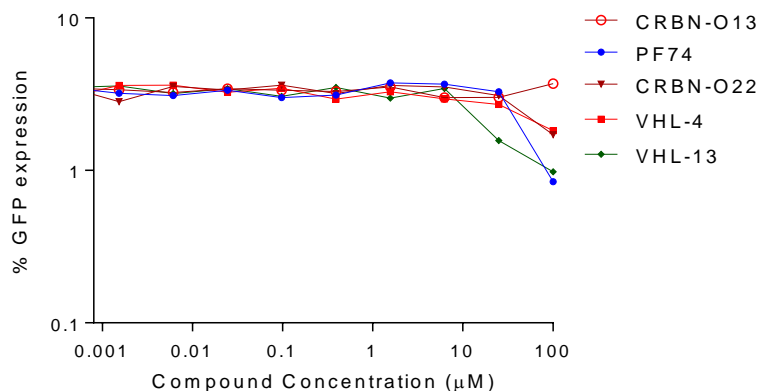
To verify that the PROTACs were engaging an HIV-specific target, a negative control assay was conducted in which the viral vector MLV-CNCG was titrated against each of the compounds. As this is a different retrovirus than HIV and does not contain the binding site of **PF74**, it was used to establish if the observed decrease in infection of CSGW-VSV-G was due to non-specific binding or HIV-specific binding. The negative control CNCG was titrated against a fixed dose (10 µM) of each PROTAC and as

expected, none of the PROTACs, or **PF74** had an effect on the infectivity of the virus (Graph 2.8). This result was consistent with HIV-specific binding.



Graph 2.8. Titration of MLV-CNCG against **PF74**, **VHL-4**, **VHL-13**, **CRBN-O13** and **CRBN-O22**.

The experiment was repeated, with a fixed titre of MLV-CNCG (50 µL/mL), and this time a dose response of each PROTAC and **PF74** was conducted (Graph 2.9). Again, no significant decrease in infectivity was observed, which was again consistent with HIV-specific binding.



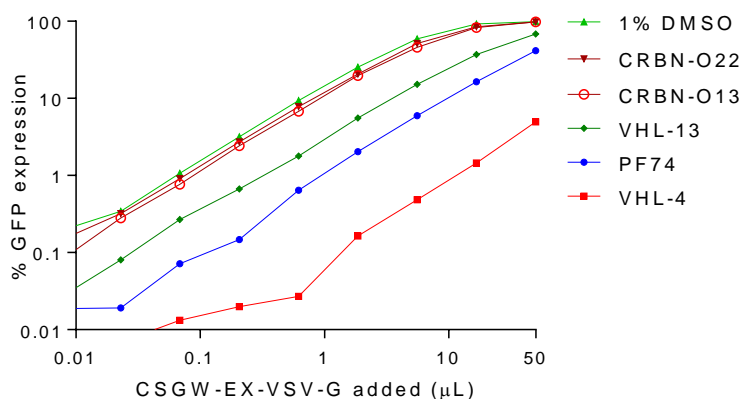
Graph 2.9. Dose response of **PF74**, **VHL-4**, **VHL-13**, **CRBN-O13** and **CRBN-O22** against a fixed titre of MLV-CNCG.

### Confirming Correct Target Engagement

While the MLV assay is a useful negative control, it can only indicate if binding is HIV-specific or not. The ideal method to probe if the PROTACs are engaging the same binding site as **PF74** would be to conduct a competition assay with **PF74**. In this, **PF74** would be titrated across cells with a fixed titre of virus and a fixed concentration of PROTAC (10 µM). If the PROTACs are binding at the same site, then an increasing dose of **PF74** would displace the PROTACs from the binding site thus diminishing their effect. However, as the positive readout in this particular assay is the same for a

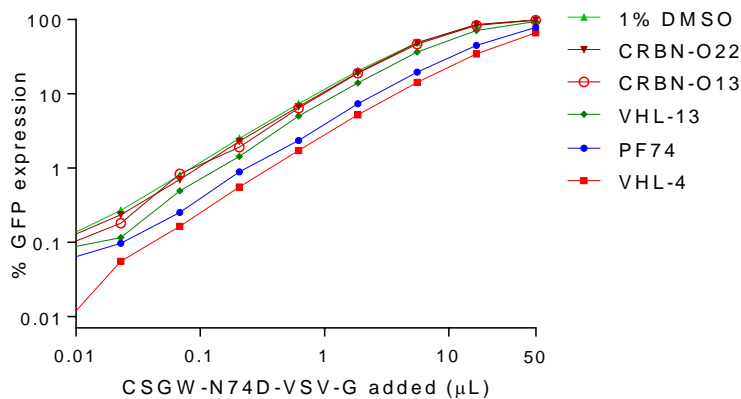
protein degradation mechanism and a protein inhibition mechanism, no distinction can be made between PROTAC efficacy and **PF74** efficacy. For this reason, the competition assay cannot be conducted.

Therefore, in order to achieve a more rigorous indication of specificity to the **PF74** binding site, the assay was repeated using the CSGW-N74D-VSV-G vector. This is a **PF74**-resistant capsid mutant of CSGW and thus an HIV relevant negative control vector.<sup>[105]</sup> Instead of using CSGW-VSV-G as the positive control vector, CSGW-EX-VSV-G was chosen as a closer match to the negative control. To establish the baseline infectivity, CSGW-EX-VSV-G was titrated against a fixed concentration (10  $\mu$ M) of each PROTAC, **PF74** and 1% DMSO (Graph 2.10). As expected from the positive control vector, the infectivity was reduced with the same trend as that observed in CSGW-VSV-G (Graph 2.6, page 146). The CRBN based PROTACs **CRBN-O22** and **CRBN-O13** caused minimal inhibition above that of the baseline DMSO. **VHL-13** caused a moderate decrease in infectivity followed by **PF74**, and finally **VHL-4** was shown to decrease the infectivity beyond that of **PF74**.



Graph 2.10. Titration of CSGW-EX-VSV-G against **PF74**, **VHL-4**, **VHL-13**, **CRBN-O13**, **CRBN-O22** and DMSO.

For the CSGW-N74D-VSV-G negative control comparison, the virus was again titrated against a fixed compound concentration (10  $\mu$ M) (Graph 2.11). These results showed each of the PROTACs and **PF74** to have a decreased effect on the infectivity of CSGW-N74D when compared to the baseline CSGW-EX-VSV-G control. This was the expected result from the **PF74** resistant CSGW-N74D-VSV-G negative control. When combined with the CSGW-EX-VSV-G positive control assay, further evidence consistent with PROTAC engagement of the **PF74** binding site is gained.



Graph 2.11. Titration of CSGW-N74D-VSV-G against **PF74**, **VHL-4**, **VHL-13**, **CRBN-O13**, **CRBN-O22** and DMSO.

### Investigating Proteasome Dependence

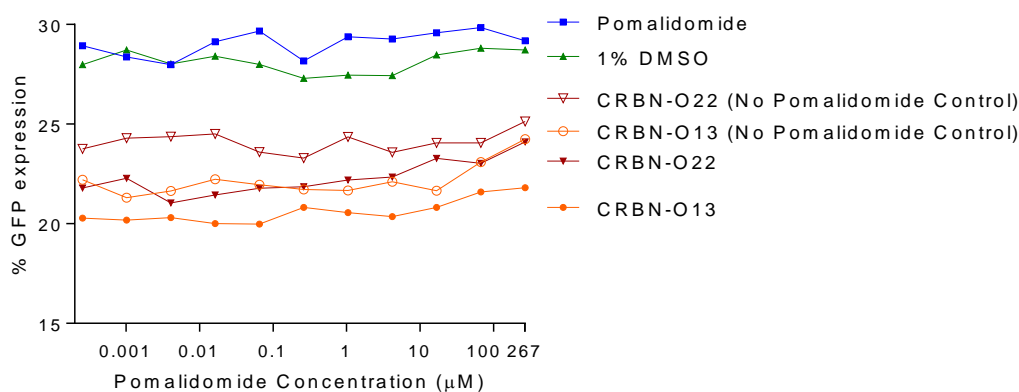
Having generated evidence that the PROTACs occupy the same binding pocket as **PF74**, the next step was to assess whether they were engaging the E3 ligase target by probing if the reduced infectivity was due to a proteasome-dependant degradation mechanism. The first assay designed for this, was to co-administer each PROTAC with the proteasome inhibitor Bortezomib. With this assay, if the observed PROTAC induced decrease of CSGW-VSV-G infectivity was mitigated upon addition of Bortezomib, then the decrease in infectivity would have likely been *via* a proteasome dependent degradation mechanism (the intended PROTAC mechanism). In order for this assay to give reliable results, the proteasome inhibitor could not hinder the growth and health of the cells or interfere with CSGW-VSV-G infectivity. Unfortunately, the dose selected for the proteasome inhibitor (based on similar assays conducted by collaborators) caused irregular cell morphology, greatly diminished cell growth and resulted in a lack of CSGW-VSV-G infection. The results of this assay were therefore nullified. The proteasome inhibitor assay should be repeated; however, it would be wise to first conduct a titration of the proteasome inhibitor to find the maximum dose tolerated by the cells and virus. Following this, an assay should be conducted to assess the efficacy of the proteasome inhibitor at this highest tolerated concentration to ensure it still inhibits degradation. Then, with this information collected, the attempted co-administration assay should be repeated at the highest tolerated dose of proteasome inhibitor.

### Investigating E3 Ligase Recruitment

The second assay devised to probe E3 ligase engagement, and subsequently the mechanism of decreased CSGW-VSV-G infection, was an E3 ligase ligand competition assay. In this assay, the E3 ligase ligand that each PROTAC was based on,

**Pomalidomide** (Figure 2.9, page 94) for CRBN based PROTACs and **VHL-1** (Figure 2.8, page 93) for VHL-based PROTACs, was titrated against a fixed titre of CSGW-VSV-G and a fixed concentration of the respective PROTACs (10  $\mu$ M). With this assay, if the PROTACs were engaging their respective E3 ligase, and the observed decrease in CSGW-VSV-G infectivity was due to a degradation mechanism, then an increasing dose of E3 ligase ligand would render the PROTACs ineffective and restore CSGW-VSV-G infectivity. Similarly to the proteasome inhibitor assay above, for this assay to be conclusive the respective E3 ligase ligands would need to have no effect on the viral infectivity, or the growth and health of the cells.

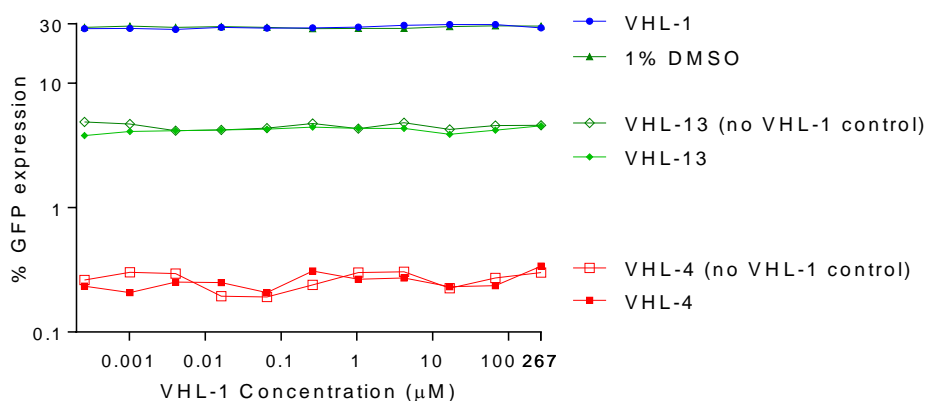
Looking at the CRBN based PROTACs first, the **Pomalidomide** control showed healthy cell morphology with a normal cell count and importantly showed CSGW-VSV-G infectivity comparable to that of DMSO (Graph 2.12). These positive results allow reliable conclusions to be drawn from the assay. However, across the concentration range of the **Pomalidomide** titration (0.255 nM–267  $\mu$ M) no deviation of CSGW-VSV-G infectivity was observed with either **CRBN-O13** or **CRBN-O22** when compared to the fixed dose control of **CRBN-O13** and **CRBN-O22** in the absence of **Pomalidomide**. This result implies that the inhibition of viral infectivity is likely independent of E3 ligase recruitment and thus not occurring *via* a degradation mechanism (at least not degradation mediated by the intended E3 ligase).



Graph 2.12. Titration of **Pomalidomide** against a fixed titre of CSGW-VSV-G and a fixed dose of **CRBN-O13**, **CRBN-O22** and DMSO.

Following these results, the analogous **VHL-1** competition assay was conducted and similarly to the **Pomalidomide** assay, treatment with **VHL-1** did not diminish the health or growth of the cells, and did not have an effect on CSGW-VSV-G infectivity compared with that of DMSO (Graph 2.13). However, over the concentration range of the **VHL-1** titration (0.255 nM–267  $\mu$ M) no variation to CSGW-VSV-G infectivity was observed with either **VHL-4** or **VHL-13** when compared to the fixed dose of **VHL-4**

and **VHL-13** in the absence of **VHL-1**. These data are again consistent with an inhibition mechanism and implies that the PROTACs tested are efficacious independent of E3 ligase recruitment.



Graph 2.13. Titration of **VHL-1** against a fixed titre of CSGW-VSV-G and a fixed dose of **VHL-4**, **VHL-13**, and DMSO.

#### 2.3.4 Summary of Biological Assaying

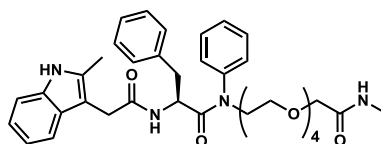
With these preliminary assays, some useful conclusions had been established. The successful results of the **PF74** enantiomer study determined (*S*)-**PF74** to be around 20-fold more efficacious than (*R*)-**PF74**. Using Autodock software, a possible explanation for this difference in potency was established in which (*R*)-**PF74** is forced to adopt an alternative binding conformation, which was calculated to have a  $\Delta G$  of binding  $18 \text{ kJmol}^{-1}$  higher in energy than the conformation adopted by (*S*)-**PF74**.

Assaying of the synthesised PROTACs established likely cellular uptake and at least partial solubility in the assay media. Furthermore, evidence for the engagement of the **PF74** binding site by the PROTACs was established. However, no engagement of the intended E3 ligase was observed, which is consistent with the hypothesis that the PROTAC-induced inhibition of CSGW-VSV-G infection is independent of an E3 ligase-mediated degradation mechanism. The serendipitous silver lining to this negative result was that **VHL-4** appeared to be a more potent inhibitor of HIV infection than **PF74**.

## 2.4 Future Work

With the successful synthesis of five PROTAC molecules and the generation of enantiomerically enriched (*S*)-**PF74** (98% ee) and (*R*)-**PF74** (97% ee), cellular assays were conducted which answered important fundamental questions and discovered that the PROTAC **VHL-4** was more efficacious at reducing CSGW-VSV-G infection than **PF74**. During this process however, some questions remained unanswered, further questions were raised and limitations with the chosen methods were identified. With this in mind, future work on the project should be directed towards answering these outstanding questions and improving upon the current limitations.

During the testing, it was suggested that the compounds might be reducing the infectivity of CSGW-VSV-G independently of an E3 ligase mediated degradation pathway. As this is the core purpose of PROTAC technology, it is of paramount importance to determine whether or not the compounds were operating *via* a degradation mechanism. Additional controls should be utilised to probe the recruitment of the relevant E3 ligase target, such as the use of a mono functionalised version of the PROTACs. For example, amide **2.59** which lacks an E3 ligase recruiting ligand could be synthesised and tested to compare with the results of the PROTACs (Figure 2.34). If amide **2.59** produced no reduction of CSGW-VSV-G infectivity, it would imply that the mechanism is reliant on E3 ligase recruitment. However, if amide **2.59** produced reduction of CSGW-VSV-G infection that was similar to the PROTACs or **PF74**, then it would be consistent with a mechanism independent of E3 ligase recruitment.



either case, a suggested course of action would be to optimise the linker length and composition.

As an E3 ligase mediated degradation mechanism appeared unlikely, an occupancy based inhibition mechanism seemed a more probable pathway of reduced CSGW-VSV-G infection. However, other possibilities exist, such as the compounds interacting with CSGW-VSV-G extracellularly to reduce the infectivity of the viral vector. One possible assay that could be developed to probe this possibility would be to pre-incubate the PROTACs with CSGW-VSV-G, followed by centrifugation and removal of the PROTAC containing supernatant. The infectivity of the pre-incubated CSGW-VSV-G could then be compared with the infectivity of the standard CSGW-VSV-G. With adequate negative controls, this assay could potentially generate useful data to probe the possibility of extracellular PROTAC:CSGW-VSV-G interaction and so to confirm or deny it as a likely mechanism of action.

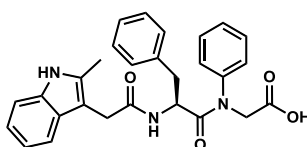
While the assays described above were useful for answering some fundamental questions of the project, they utilised **PF74** as a positive control. As **PF74** acts *via* an inhibition mechanism, its utility as a positive control for a degradation pathway was inherently somewhat limited. A useful future goal for the project would therefore be to develop a more relevant positive control, and to establish a way to quantify any degradation that may be occurring, such as western blot.

During the assaying of the synthesised PROTACs, two trends were identified. VHL targeting PROTACs were more effective at reducing CSGW-VSV-G infection than CRBN targeting PROTACs, and PROTACs with shorter linkers were more efficacious than their longer linker analogues. As an E3 ligase mediated degradation mechanism was tentatively ruled out, something else must be responsible for these phenomenon.

One plausible explanation for the differences in efficacy could be due to the structure and length of the linker. As mentioned above (2.1.7 Linker, page 94), evidence suggests that the structure and length of the linker is critical to allowing secondary stabilising interactions to form in between the target protein, PROTAC and the E3 ligase during ternary complex formation.<sup>[93]</sup> It is possible that the linkers utilised herein, are more suited for generating these stabilising secondary interactions in the VHL system compared to the CRBN system. However, the use of computational modelling and crystal structure analysis could potentially be used to guide the redesign of linker towards the aim of developing specific VHL- and CRBN-targeting linkers.

An additional plausible explanation for the differences in efficacy would be differences in the aqueous solubility and cellular permeability of the compounds. It is possible that the more efficacious VHL-targeting PROTACs are simply more soluble or cell penetrating than the CRBN-targeting analogues. As the linker can be modified to affect the PROTACs physical chemical properties such as solubility and permeability, different linkers could be developed to be used with either E3 ligase ligand.<sup>[83][93][94][95]</sup> Therefore quantitative data on solubility and permeability for each of the PROTACs should be generated which could be used to guide the design of the next generation of PROTACs.

Finally, it is clear that much optimisation of future PROTAC design is required, which inevitably involves a high degree of empirical trial and error. To this end, additional time should be invested in generating the aforementioned complete-**PF74** fragment (Figure 2.35). A stock of this material would greatly facilitate the rapid generation of PROTACs with structurally diverse linkers.



2.24

Figure 2.35. Structure of the elusive complete-**PF74** fragment.

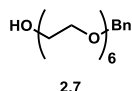
## 2.5 Experimental

### 2.5.1 General Methods

All reagents were purchased from commercial suppliers and used without further purification unless otherwise stated. Reactions involving air-sensitive agents and dry solvents were performed in glassware that had been dried in an oven (150 °C) or flame-dried *in vacuo* and allowed to cool *in vacuo* before being flushed with argon. These reactions were carried out with the exclusion of air using an argon atmosphere. Reactions were monitored by thin layer chromatography (TLC) on Merck silica gel 60 covered aluminium sheets. TLC plates were developed under UV-light and/or with an acidic ethanolic anisaldehyde solution or a KMnO<sub>4</sub>-solution. NMR spectra were recorded on a Bruker DPX-400 spectrometer (<sup>1</sup>H NMR at 400 MHz, <sup>13</sup>C NMR at 100 MHz, <sup>19</sup>F NMR at 377 MHz and <sup>11</sup>B NMR at 128 MHz) or a Bruker DPX-500 spectrometer (<sup>1</sup>H NMR at 500 MHz and <sup>13</sup>C NMR at 125 MHz). Chemical shifts are reported in ppm. <sup>1</sup>H NMR spectra were recorded with CDCl<sub>3</sub> or CD<sub>3</sub>OD as the solvent using residual CHCl<sub>3</sub> (δ = 7.26) or CHD<sub>2</sub>OD (δ = 3.31) as internal standard, and for <sup>13</sup>C NMR spectra the chemical shifts are reported relative to the central resonance of CDCl<sub>3</sub> (δ = 77.16) or CD<sub>3</sub>OD (δ = 49.00). Signals in NMR spectra are described as singlet (s), doublet (d), triplet (t), quartet (q), multiplet (m), broad (br) or a combination of these, which refers to the spin-spin coupling pattern observed. Spin-spin coupling constants are reported in Hertz (Hz) and are uncorrected. Two-dimensional NMR spectroscopy (COSY, HSQC, HMBC, NOESY) and <sup>13</sup>C DEPT NMR spectroscopy were used where appropriate to assist the assignment of signals in the <sup>1</sup>H and <sup>13</sup>C NMR spectra. IR spectra were obtained employing a Shimadzu FTIR-8400 instrument with a Golden Gate™ attachment that uses a type IIa diamond as a single reflection element so that the IR spectrum of the compound (solid or liquid) could be detected directly (thin layer). Melting point ranges were collected using a Barnstead Electrothermal 9100 melting point apparatus. High resolution mass spectra were recorded under ESI or EI conditions by the analytical services at the University of Glasgow. Liquid chromatography-mass spectrometry was conducted using a Thermo Scientific Dionex UltiMate 3000 LC system coupled with a Thermo Scientific LCQ Fleet ion trap mass spectrometer. A Dr Maisch GmbH Reprosil Gold 120 C18 3µm 150x4 mm column was used with UV absorption detected at 214 nm. A linear gradient of 5%–95% HPLC grade acetonitrile in ultra pure water with 0.1% trifluoroacetic acid over 10 or 40 minutes was utilised with a flow rate of 1 mLmin<sup>-1</sup>. Optical rotations were determined using a Rudolph Research Analytical Autopol polarimeter by irradiation with the sodium D line (λ = 589 nm). [α]<sub>D</sub> values are given in units 10<sup>-1</sup>degcm<sup>2</sup>g<sup>-1</sup>. Preparative

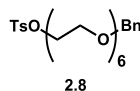
HPLC was conducted using a Dionex HPLC system using Dionex P680 pumps and a Phenomenex Gemini C18 5 $\mu$ m 250x21.2 mm column. UV absorption was detected at 214 nm and 280 nm using a Dionex UVD170U UV-vis detector. Non-linear gradients between 5%–100% HPLC grade acetonitrile in ultra pure water with 0.1% trifluoroacetic acid were utilised. Collected fractions were then lyophilised using a Christ Alpha 2–4 LO plus lyophiliser. Chiral HPLC analysis was conducted using a Shimadzu LC-20AD prominence liquid chromatograph with a CBM-20A prominence communications bus module, a DGU-20A<sub>5</sub> prominence degasser and a SPD-M20A prominence diode array detector. A Shimadzu CTO-20AC prominence column oven was utilised in combination with Diacel Chemical Industries chiralcel OD-H 5  $\mu$ m 4.6x250 mm reverse phase analytical column with an isocratic mobile phase of HPLC grade isopropyl alcohol in HPLC grade hexane.

## 2.5.2 Preparation of Compounds



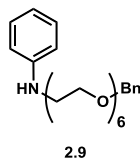
**2.7.** Prepared according to a modified literature procedure.<sup>[110]</sup> To oven dried glassware cooled under vacuum and flushed with argon was added sodium hydride (60% suspension in mineral oil) (440 mg, 11.0 mmol, 1.1 equiv.) and tetrahydrofuran (9.0 mL, 1.1 M) and the resulting suspension was cooled to 0 °C. To the suspension was added hexaethylene glycol (10 mL, 40 mmol, 4 equiv.) and the mixture was stirred at 0 °C for 20 minutes. To this suspension was slowly added benzyl bromide (1.2 mL, 10 mmol, 1 equiv.) and the resulting suspension was stirred and allowed to warm to room temperature for 18 hours. To the reaction mixture was added water (50 mL) and ethyl acetate (100 mL) and the aqueous phase was extracted with ethyl acetate (3 x 100 mL). The combined organic phases were washed with brine (70 mL), dried with magnesium sulphate, filtered and concentrated *in vacuo* generating a crude mass of 3.32 g. Purification by column chromatography on silica gel using an eluent of 50% to 100% ethyl acetate in dichloromethane yielded the title compound **2.7** (2.62 g, 7.04 mmol, 70%). Analytical data observed were in accordance with literature values.<sup>[110]</sup>

<sup>1</sup>H NMR (400 MHz, CDCl<sub>3</sub>) δ 7.36–7.22 (5H, m, 5 x Ar-CH), 4.55 (2H, s, -OCH<sub>2</sub>), 3.74–3.56 (24H, m, 12 x -OCH<sub>2</sub>), 2.60 (1H, s, -OH). <sup>13</sup>C NMR (101 MHz, CDCl<sub>3</sub>) δ 138.4 (Ar-C), 128.4 (2 x Ar-CH), 127.8 (2 x Ar-CH), 127.7 (Ar-CH), 73.3 (-OCH<sub>2</sub>), 72.6 (-OCH<sub>2</sub>), 70.7 (8 x -OCH<sub>2</sub>), 70.5 (-OCH<sub>2</sub>), 69.6 (-OCH<sub>2</sub>), 61.8 (-OCH<sub>2</sub>). HRMS (ESI) exact mass calculated for C<sub>19</sub>H<sub>32</sub>O<sub>7</sub>Na [M+Na]<sup>+</sup> m/z 395.2040, found m/z 395.2040. IR (thin film) 2866, 1456, 1095.



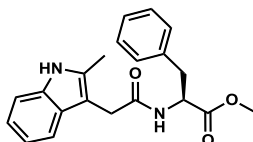
**2.8.** Prepared according to a modified literature procedure.<sup>[110]</sup> To a stirred solution of alcohol **2.7** (1.90 g, 5.10 mmol, 1 equiv.) in tetrahydrofuran (10.2 mL, 0.5 M) was added a 4.5 M aqueous solution of sodium hydroxide (245 mg in 1.30 mL, 6.12 mmol, 1.2 equiv.) and the resulting solution was cooled to 0 °C and stirred rapidly for 20 minutes. To this mixture was added 4-toluenesulfonyl chloride (1.07 g, 5.60 mmol, 1.1 equiv.) and the resulting mixture was allowed to warm to room temperature under rapid stirring for 18 hours. To the reaction mixture was added water (30 mL) and dichloromethane (50 mL) and the aqueous phase was extracted with dichloromethane (3 x 50 mL). The combined organic phases were washed with brine (40 mL), dried over magnesium sulphate, filtered and concentrated *in vacuo* yielding a crude mass of 2.68 g. Purification by column chromatography on silica gel using an eluent of 0% to 100% ethyl acetate in dichloromethane yielded the title compound **2.8** (2.09 g, 3.97 mmol, 78%). Analytical data observed were in accordance with literature values.<sup>[123]</sup>

<sup>1</sup>H NMR (400 MHz, CDCl<sub>3</sub>) δ 7.78 (2H, d, *J* = 8.2, 2 x Ar-CH), 7.37–7.21 (7H, m, 7 x Ar-CH), 4.55 (2H, s, -OCH<sub>2</sub>), 4.14 (2H, t, *J* = 4.9, -OCH<sub>2</sub>), 3.70–3.52 (22H, m, 11 x -OCH<sub>2</sub>), 2.43 (3H, s, -CH<sub>3</sub>). <sup>13</sup>C NMR (101 MHz, CDCl<sub>3</sub>) δ 144.8 (Ar-C), 138.4 (Ar-C), 133.2 (Ar-C), 129.9 (2 x Ar-CH), 128.4 (2 x Ar-CH), 128.0 (2 x Ar-CH), 127.8 (2 x Ar-CH), 127.6 (Ar-CH), 73.3 (-OCH<sub>2</sub>), 70.8 (-OCH<sub>2</sub>), 70.7 (6 x -OCH<sub>2</sub>), 70.6 (-OCH<sub>2</sub>), 70.5 (-OCH<sub>2</sub>), 69.6 (-OCH<sub>2</sub>), 69.3 (-OCH<sub>2</sub>), 68.8 (-OCH<sub>2</sub>), 21.7 (-CH<sub>3</sub>). HRMS (ESI) exact mass calculated for C<sub>26</sub>H<sub>38</sub>O<sub>9</sub>SNa [M+Na]<sup>+</sup> *m/z* 549.2129, found *m/z* 549.2107. IR (thin film) 2868, 1452, 1096.



**2.9.** Prepared according to a modified literature procedure.<sup>[124]</sup> To a stirred solution of tosylate **2.8** (2.09 g, 3.97 mmol, 1 equiv.) in acetonitrile (13 mL, 0.3 M) was added potassium carbonate (1.76 g, 12.7 mmol, 3.2 equiv.) and aniline (3.30 mL, 35.7 mmol, 9 equiv.) and the resulting solution was heated to 80 °C and stirred for 18 hours. The reaction mixture was then concentrated *in vacuo* and the resulting solid was dissolved in water (50 mL) and diethyl ether (50 mL). The aqueous phase was extracted with diethyl ether (3 x 80 mL) and the combined organic phases were washed with brine (80 mL), dried over magnesium sulphate, filtered and concentrated *in vacuo* yielding a crude mass of 4.45 g. Purification by column chromatography on silica gel using an eluent of 0% to 100% ethyl acetate in dichloromethane yielded the title compound **2.9** (1.36 g, 3.05 mmol, 77%).

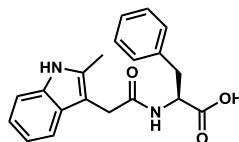
<sup>1</sup>H NMR (400 MHz, CDCl<sub>3</sub>) δ 7.36–7.32 (4H, m, 4 x Ar-CH), 7.30–7.26 (1H, m, Ar-CH), 7.20–7.13 (2H, m, 2 x Ar-CH), 6.70 (1H, tt, *J* = 7.3, 1.1, Ar-CH), 6.63 (2H, m, 2 x Ar-CH), 4.56 (2H, s, -OCH<sub>2</sub>), 4.28–3.93 (1H, m, -NH), 3.72–3.59 (22H, m, 11 x -OCH<sub>2</sub>), 3.29 (2H, t, *J* = 5.3, -NCH<sub>2</sub>). <sup>13</sup>C NMR (101 MHz, CDCl<sub>3</sub>) δ 148.3 (Ar-C), 138.3 (Ar-C), 129.2 (2 x Ar-CH), 128.4 (2 x Ar-CH), 127.8 (2 x Ar-CH), 127.7 (Ar-CH), 117.5 (Ar-CH), 113.2 (2 x Ar-CH), 73.3 (-OCH<sub>2</sub>), 70.7 (-OCH<sub>2</sub>), 70.6 (7 x -OCH<sub>2</sub>), 70.3 (-OCH<sub>2</sub>), 69.6 (-OCH<sub>2</sub>), 69.5 (-OCH<sub>2</sub>), 43.6 (-NCH<sub>2</sub>). HRMS (ESI) exact mass calculated for C<sub>25</sub>H<sub>37</sub>NO<sub>6</sub>Na [M+Na]<sup>+</sup> *m/z* 470.2513, found *m/z* 470.2513. IR (thin film) 2866, 1724, 1601.



2.10

**2.10.** Prepared according to a modified literature procedure.<sup>[111]</sup> To a stirred solution of 2-methyl-3-indoleacetic acid (5.68 g, 30.0 mmol, 1 equiv.) in *N,N*-dimethylformamide (75 mL, 0.4 M) was added L-phenylalanine methyl ester hydrochloride (6.79 g, 31.5 mmol, 1.05 equiv.), PyBOP (15.6 g, 30.0 mmol, 1 equiv.) and *N,N*-diisopropylethylamine (15.7 mL, 90.0 mmol, 3 equiv.) and the resulting solution was stirred at room temperature for 18 hours. To the crude mixture was added water (60 mL) and the resultant layers were separated. The aqueous phase was extracted with ethyl acetate (3 x 40 mL) and the combined organic phases were washed with 5% aqueous lithium chloride solution (3 x 40 mL). The combined organic phases were dried with magnesium sulphate, filtered and concentrated *in vacuo* affording a crude mass of 19.1 g. Purification by column chromatography on silica gel using an eluent of 5% ethyl acetate in dichloromethane afforded the title compound **2.10** as a viscous oil (12.2 g, 30.0 mmol, quantitative)

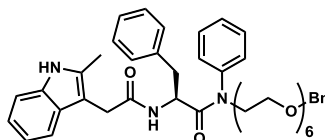
<sup>1</sup>H NMR (400 MHz, CDCl<sub>3</sub>) δ 7.88 (1H, s, Ar-NH), 7.42 (1H, d, *J* = 7.8, Ar-H), 7.31 (1H, d, *J* = 7.9, Ar-H), 7.18 (1H, t, *J* = 7.5, Ar-H), 7.13 (1H, d, *J* = 7.8, Ar-H), 7.09 (1H, d, *J* = 7.9, Ar-H), 7.00 (2H, t, *J* = 7.5, 2 x Ar-H), 6.71 (2H, d, *J* = 7.5, 2 x Ar-H), 5.99 (1H, d, *J* = 7.8, -CONH), 4.84 (1H, dt, *J* = 6.6, 6.6, -CH), 3.64 (2H, s, -COCH<sub>2</sub>), 3.64 (3H, s, -CH<sub>3</sub>), 2.97 (1H, dd, *J* = 13.9, 5.4, -CH<sub>2</sub>), 2.91 (1H, dd, *J* = 13.8, 5.5, -CH<sub>2</sub>), 2.29 (3H, s, -CH<sub>3</sub>). <sup>13</sup>C NMR (101 MHz, CDCl<sub>3</sub>) δ 171.9 (-CONH), 171.1 (-COOR), 135.6 (Ar-C), 135.5 (Ar-C), 133.4 (Ar-C), 129.2 (2 x Ar-CH), 128.5 (2 x Ar-CH), 128.4 (Ar-C), 127.0 (Ar-CH), 121.9 (Ar-CH), 120.2 (Ar-CH), 118.0 (Ar-CH), 110.5 (Ar-CH), 104.7 (Ar-C), 52.8 (-CH), 52.3 (-OCH<sub>3</sub>), 37.7 (-CH<sub>2</sub>), 32.2 (-CH<sub>2</sub>), 11.6 (-CH<sub>3</sub>). HRMS (ESI) exact mass calculated for C<sub>21</sub>H<sub>22</sub>N<sub>2</sub>O<sub>3</sub>Na [M+Na]<sup>+</sup> *m/z* 373.1523, found *m/z* 373.1514. IR (thin film) 2952, 1741, 1651. Melting point 126–130 °C.



2.11

**2.11.** Prepared according to a modified literature procedure.<sup>[111]</sup> To a stirred solution of methyl ester **2.10** (1.06 g, 3.03 mmol, 1 equiv.) in tetrahydrofuran (13 mL, 0.2 M) and water (8.8 mL) was added a solution of sodium hydroxide (182 mg, 4.55 mmol, 1.5 equiv.) in methanol (4.5 mL, 1 M) and the resulting solution was stirred vigorously at room temperature for 18 hours. To the reaction mixture was added water (20 mL) and the crude biphasic mixture was washed with dichloromethane (2 x 10 mL) to remove organic impurities. The aqueous phase was then acidified with 2 M aqueous hydrochloric acid (10 mL) forming a thick white precipitate. The aqueous phase was extracted with dichloromethane (3 x 20 mL) and the combined organic phases were dried with magnesium sulphate, filtered and concentrated *in vacuo* yielding the title compound **2.11** (989 mg, 2.94 mmol, 97%). The compound was used without further purification.

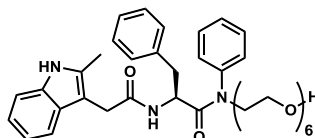
<sup>1</sup>H NMR (400 MHz, CDCl<sub>3</sub>) δ 8.14 (1H, s, Ar-NH), 7.34 (1H, d, *J* = 7.8, Ar-CH), 7.26 (1H, d, *J* = 7.0, Ar-CH), 7.16 (1H, t, *J* = 7.1, Ar-CH), 7.09 (1H, t, *J* = 7.7, Ar-CH), 7.09 (1H, t, *J* = 7.7, Ar-CH), 6.99 (2H, t, *J* = 7.6, 2 x Ar-CH), 6.74 (2H, d, *J* = 7.1, 2 x Ar-CH), 6.15 (1H, d, *J* = 7.9, -CONH), 4.76 (1H, dt, *J* = 6.7, 6.7, -CH), 3.61 (2H, s, -CH<sub>2</sub>), 3.00 (1H, dd, *J* = 13.9, 5.2, -CH<sub>2</sub>), 2.89 (1H, dd, *J* = 13.9, 6.7, -CH<sub>2</sub>), 2.13 (3H, s, -CH<sub>3</sub>). <sup>13</sup>C NMR (101 MHz, CDCl<sub>3</sub>) δ = 174.0 (-COOH), 172.9 (-CONH), 135.5 (Ar-C), 135.4 (Ar-C), 133.8 (Ar-C), 129.2 (2 x Ar-CH), 128.6 (2 x Ar-CH), 128.2 (Ar-C), 127.0 (Ar-CH), 121.8 (Ar-CH), 120.1 (Ar-CH), 117.8 (Ar-CH), 110.7 (Ar-CH), 103.7 (Ar-C), 53.2 (-CH), 37.0 (-CH<sub>2</sub>), 31.8 (-CH<sub>2</sub>), 11.4 (-CH<sub>3</sub>). HRMS (ESI) exact mass calculated for C<sub>20</sub>H<sub>20</sub>N<sub>2</sub>O<sub>3</sub>Na [M+Na]<sup>+</sup> *m/z* 359.1366, found *m/z* 359.1355. IR (thin film) 2916, 1724, 1618. Melting point 140–143 °C.



2.12

**2.12.** Prepared according to a modified literature procedure.<sup>[111]</sup> To a stirred solution of acid **2.11** (540 mg, 1.62 mmol, 1 equiv.) in *N,N*-dimethylformamide (1.8 mL, 0.9 M) was added aniline **2.9** (1.10 g, 2.40 mmol, 1.5 equiv.), HATU (912 mg, 2.40 mmol, 1.5 equiv.) and *N,N*-diisopropylethylamine (0.58 mL, 3.2 mmol, 2 equiv.) and the resulting solution was heated to 65 °C and stirred for 48 hours. To the crude mixture was added dichloromethane (20 mL) and half saturated aqueous sodium hydrogen carbonate solution (20 mL) and the aqueous phase was extracted with dichloromethane (3 x 30 mL). The combined organic phases were washed with 5% aqueous lithium chloride solution (3 x 30 mL), dried over magnesium sulphate, filtered and concentrated *in vacuo* affording a crude mass of 2.20 g. Purification by column chromatography on silica gel using an eluent of 50% to 100% ethyl acetate in dichloromethane to recover unreacted aniline followed by 4% ethanol in dichloromethane afforded the title compound **2.12** (704 mg, 0.920 mmol, 57%).

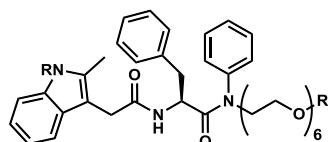
<sup>1</sup>H NMR (400 MHz, CDCl<sub>3</sub>) δ 8.15 (1H, s, Ar-NH), 7.42–7.27 (12H, m, 12 x Ar-CH), 7.18–6.92 (5H, m, 5 x Ar-CH), 6.66 (2H, d, *J* = 7.3, 2 x Ar-CH), 6.17 (1H, d, *J* = 8.3, -CONH), 4.70 (1H, dt, *J* = 7.2, 7.1, -CH), 4.55 (2H, s, -OCH<sub>2</sub>), 3.86–3.41 (26H, m, -COCH<sub>2</sub>, 11 x -OCH<sub>2</sub>, -NCH<sub>2</sub>), 2.74 (1H, dd, *J* = 13.4, 6.6, -CH<sub>2</sub>), 2.51 (1H, dd, *J* = 13.4, 6.9, -CH<sub>2</sub>), 2.31 (3H, s, -CH<sub>3</sub>). <sup>13</sup>C NMR (101 MHz, CDCl<sub>3</sub>) δ 171.3 (-CONR<sub>2</sub>), 170.9 (-CONH), 141.2 (Ar-C), 138.2 (Ar-C), 136.0 (Ar-C), 135.5 (Ar-C), 133.5 (Ar-C), 129.7 (Ar-C), 129.6 (2 x Ar-CH), 129.3 (2 x Ar-CH), 128.5 (2 x Ar-CH), 128.3 (2 x Ar-CH), 128.3 (Ar-CH), 128.2 (2 x Ar-CH), 127.7 (2 x Ar-CH), 127.6 (Ar-CH), 126.6 (Ar-CH), 121.2 (Ar-CH), 119.5 (Ar-CH), 117.6 (Ar-CH), 110.6 (Ar-CH), 104.0 (Ar-C), 73.2 (-OCH<sub>2</sub>), 70.6 (2 x -OCH<sub>2</sub>), 70.5 (5 x -OCH<sub>2</sub>), 70.4 (-OCH<sub>2</sub>), 70.0 (-OCH<sub>2</sub>), 69.4 (-OCH<sub>2</sub>), 67.6 (-OCH<sub>2</sub>), 51.3 (-CH), 49.1 (-NCH<sub>2</sub>), 38.5 (-CH<sub>2</sub>), 32.1 (-COCH<sub>2</sub>), 11.4 (-CH<sub>3</sub>). HRMS (ESI) exact mass calculated for C<sub>45</sub>H<sub>55</sub>N<sub>3</sub>O<sub>8</sub>Na [M+Na]<sup>+</sup> *m/z* 788.3881, found *m/z* 788.3850. IR (thin film) 2866, 1643, 1593.



2.13

**2.13.** Prepared according to a modified literature procedure.<sup>[41]</sup> To a stirred suspension of 10% palladium on carbon (42 mg, 0.039 mmol, 5.0 mol%) in methanol (39 mL, 0.02 M) under argon atmosphere was added benzyl ether **2.12** (600 mg, 0.780 mmol, 1 equiv.) at room temperature. The flask was then evacuated and the suspension sparged with hydrogen gas for 5 minutes and then stirred at room temperature under a hydrogen atmosphere for 18 hours. The hydrogen was then removed under reduced pressure and the suspension sparged with argon three times. The suspension was then filtered through a suspension of celite (200 g) in dichloromethane (200 mL) and the celite washed with dichloromethane (400 mL). The organic phase was then concentrated *in vacuo* generating the title compound **2.13** (530 mg, 0.780 mmol, quantitative).

<sup>1</sup>H NMR (400 MHz, CDCl<sub>3</sub>) δ 8.14 (1H, s, Ar-NH), 7.46–7.26 (6H, m, 6 x Ar-CH), 7.20–6.95 (6H, m, 6 x Ar-CH), 6.66 (2H, d, *J* = 7.4, 2 x Ar-CH), 6.17 (1H, d, *J* = 8.3, -CONH), 4.70 (1H, dt, *J* = 7.1, 7.1, -CH), 3.85–3.42 (26H, m, -COCH<sub>2</sub>, 11 x -OCH<sub>2</sub>, -NCH<sub>2</sub>), 2.74 (1H, dd, *J* = 13.4, 6.6, -CH<sub>2</sub>), 2.56 (1H, br s, -OH), 2.51 (1H, dd, *J* = 13.4, 7.0, -CH<sub>2</sub>), 2.32 (3H, s, -CH<sub>3</sub>). <sup>13</sup>C NMR (101 MHz, CDCl<sub>3</sub>) δ 171.1 (-CONR<sub>2</sub>), 171.0 (-CONH), 140.9 (Ar-C), 135.8 (Ar-C), 135.3 (Ar-C), 133.5 (Ar-C), 129.4 (2 x Ar-CH), 129.0 (2 x Ar-CH), 128.2 (2 x Ar-CH), 128.1 (Ar-CH), 128.0 (2 x Ar-CH), 127.9 (Ar-C), 126.4 (Ar-CH), 120.7 (Ar-CH), 119.0 (Ar-CH), 117.3 (Ar-CH), 110.5 (Ar-CH), 103.4 (Ar-C), 72.3 (-OCH<sub>2</sub>), 70.2 (5 x -OCH<sub>2</sub>), 70.1 (-OCH<sub>2</sub>), 69.9 (-OCH<sub>2</sub>), 69.8 (-OCH<sub>2</sub>), 67.3 (-OCH<sub>2</sub>), 61.2 (-OCH<sub>2</sub>), 51.2 (-CH), 48.9 (-NCH<sub>2</sub>), 38.2 (-CH<sub>2</sub>), 31.8 (-COCH<sub>2</sub>), 11.1 (-CH<sub>3</sub>). HRMS (ESI) exact mass calculated for C<sub>38</sub>H<sub>49</sub>N<sub>3</sub>O<sub>8</sub>Na [M+Na]<sup>+</sup> *m/z* 698.3412, found *m/z* 698.3404. IR (thin film) 2868, 1639, 1593.



- 2.1** R=H R'=CH<sub>2</sub>COO<sup>t</sup>Bu  
**2.14** R=CH<sub>2</sub>COO<sup>t</sup>Bu R'=H  
**2.15** R=CH<sub>2</sub>COO<sup>t</sup>Bu R'=CH<sub>2</sub>COO<sup>t</sup>Bu

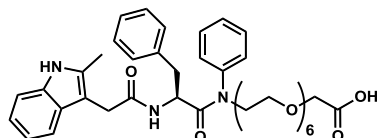
**2.1.** Prepared according to a modified literature procedure.<sup>[41]</sup> To oven dried glassware cooled under vacuum and flushed with argon was added sodium *tert*-butoxide (53 mg, 0.47 mmol, 1.1 equiv.), *tert*-butanol (1.5 mL, 0.3 M) and alcohol **2.13** (300 mg, 0.450 mmol, 1 equiv.) and the mixture was stirred at room temperature for 20 minutes. To this solution was slowly added *tert*-butyl bromoacetate (0.066 mL, 0.45 mmol, 1 equiv.) and the resulting solution was stirred at room temperature for 18 hours. To the reaction mixture was added water (10 mL) and dichloromethane (20 mL) and the aqueous phase was extracted with dichloromethane (3 x 20 mL). The combined organic phases were washed with brine (20 mL), dried with magnesium sulphate, filtered and concentrated *in vacuo* generating a crude mass of 246 mg. Purification by column chromatography on silica gel using an eluent of 4% to 20% ethanol in dichloromethane yielded the title compound **2.1** (41 mg, 0.052 mmol, 12%), the *N*-alkylated product **2.14** (8 mg, 0.01 mmol, 2%) and the dialkylated material **2.15**. (71 mg, 0.079 mmol, 18%).

**2.1.** R<sub>f</sub> = 0.42 (5% methanol in dichloromethane). <sup>1</sup>H NMR (400 MHz, CDCl<sub>3</sub>) δ 8.15 (1H, s, Ar-NH), 7.41–7.29 (5H, m, 5 x Ar-CH), 7.19–6.94 (7H, m, 7 x Ar-CH), 6.66 (2H, d, *J* = 7.3, 2 x Ar-CH), 6.16 (1H, d, *J* = 8.2, -CONH), 4.70 (1H, dt, *J* = 7.1, 7.1 -CH), 4.01 (2H, s, -COCH<sub>2</sub>), 3.85–3.41 (26H, m, -COCH<sub>2</sub>, 11 x -OCH<sub>2</sub>, -NCH<sub>2</sub>), 2.74 (1H, dd, *J* = 13.4, 6.6, -CH<sub>2</sub>), 2.51 (1H, dd, *J* = 13.4, 6.9, -CH<sub>2</sub>), 2.33 (3H, s, -CH<sub>3</sub>), 1.47 (9H, s, -C(CH<sub>3</sub>)<sub>3</sub>). <sup>13</sup>C NMR (101 MHz, CDCl<sub>3</sub>) δ 171.3 (-CONR<sub>2</sub>), 170.8 (-CONH), 169.8 (-COOR), 141.3 (Ar-C), 136.2 (Ar-C), 135.5 (Ar-C), 133.5 (Ar-C), 129.7 (2 x Ar-CH), 129.4 (2 x Ar-CH), 128.6 (2 x Ar-CH), 128.5 (Ar-CH), 128.4 (2 x Ar-CH), 128.3 (Ar-CH), 126.7 (Ar-CH), 121.5 (Ar-CH), 119.7 (Ar-CH), 117.9 (Ar-CH), 110.6 (Ar-CH), 104.5 (Ar-C), 81.7 (-OCR<sub>3</sub>), 70.8 (-OCH<sub>2</sub>), 70.7 (3 x -OCH<sub>2</sub>), 70.6 (5 x -OCH<sub>2</sub>), 70.1 (-OCH<sub>2</sub>), 69.1 (-COCH<sub>2</sub>), 67.7 (-OCH<sub>2</sub>), 51.4 (-CH), 49.1 (-NCH<sub>2</sub>), 38.5 (-CH<sub>2</sub>), 32.2 (-COCH<sub>2</sub>), 28.2 (3C, -C(CH<sub>3</sub>)<sub>3</sub>), 11.7 (-CH<sub>3</sub>). HRMS (ESI) exact mass calculated for C<sub>44</sub>H<sub>59</sub>N<sub>3</sub>O<sub>10</sub>Na [M+Na]<sup>+</sup> m/z 812.4093, found m/z 812.4069. IR (thin film) 2872, 1745, 1645, 1593.

**2.14.** R<sub>f</sub> = 0.36 (5% methanol in dichloromethane). <sup>1</sup>H NMR (400 MHz, CDCl<sub>3</sub>) δ 7.42–7.29 (5H, m, 5 x Ar-CH), 7.26–6.89 (7H, m, 7 x Ar-CH), 6.60 (2H, d, *J* = 7.3, 2 x

Ar-CH), 6.15 (1H, d,  $J = 8.1$ , -CONH), 4.70 (2H, s, -COCH<sub>2</sub>), 4.65 (1H, dt,  $J = 7.3$ , 7.3, -CH), 3.88–3.44 (26H, m, -COCH<sub>2</sub>, -NCH<sub>2</sub>, -CH<sub>2</sub>OH, 10 x -OCH<sub>2</sub>), 2.73 (1H, dd,  $J = 13.4$ , 6.1, -CH<sub>2</sub>), 2.48 (1H, dd,  $J = 13.5$ , 7.6, -CH<sub>2</sub>), 2.26 (3H, s, -CH<sub>3</sub>), 1.44 (9H, s, -C(CH<sub>3</sub>)<sub>3</sub>). <sup>13</sup>C NMR (101 MHz, CDCl<sub>3</sub>)  $\delta$  171.3 (-CONR<sub>2</sub>), 170.7 (-CONH), 167.7 (-COOR), 141.4 (Ar-C), 136.7 (Ar-C), 136.2 (Ar-C), 134.8 (Ar-C), 129.6 (2 x Ar-CH), 129.2 (2 x Ar-CH), 128.6 (2 x Ar-CH), 128.2 (3 x Ar-CH), 127.8 (Ar-C), 126.5 (Ar-CH), 121.6 (Ar-CH), 120.0 (Ar-CH), 118.1 (Ar-CH), 108.4 (Ar-CH), 105.0 (Ar-C), 82.6 (-OCR<sub>3</sub>), 72.6 (-OCH<sub>2</sub>), 70.6 (3 x -OCH<sub>2</sub>), 70.5 (3 x -OCH<sub>2</sub>), 70.3 (-OCH<sub>2</sub>), 70.2 (-OCH<sub>2</sub>), 67.8 (-OCH<sub>2</sub>), 61.8 (-CH<sub>2</sub>OH), 51.4 (-CH), 49.2 (-NCH<sub>2</sub>), 45.8 (-COCH<sub>2</sub>), 38.3 (-CH<sub>2</sub>), 32.4 (-COCH<sub>2</sub>), 28.0 (3C, -C(CH<sub>3</sub>)<sub>3</sub>), 10.1 (-CH<sub>3</sub>). HRMS (ESI) exact mass calculated for C<sub>44</sub>H<sub>59</sub>N<sub>3</sub>O<sub>10</sub>Na [M+Na]<sup>+</sup>  $m/z$  812.4093, found  $m/z$  812.4075. IR (thin film) 2870, 1744, 1647, 1595.

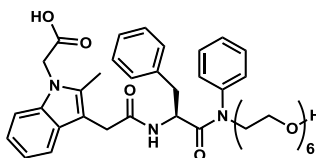
**2.15.**  $R_f = 0.45$  (5% methanol in dichloromethane). <sup>1</sup>H NMR (400 MHz, CDCl<sub>3</sub>)  $\delta$  7.42–7.29 (5H, m, 5 x Ar-CH), 7.23–6.96 (7H, m, 7 x Ar-CH), 6.60 (2H, dd,  $J = 7.1$ , 1.1, 2 x Ar-CH), 6.11 (1H, d,  $J = 8.1$ , -CONH), 4.70 (2H, s, -COCH<sub>2</sub>), 4.65 (1H, td,  $J = 7.7$ , 6.3, -CH), 4.01 (2H, s, -COCH<sub>2</sub>), 3.84 (1H, dt,  $J = 13.6$ , 5.9, -NCH<sub>2</sub>), 3.79–3.45 (25H, m, -NCH<sub>2</sub>, -COCH<sub>2</sub>, 11 x -OCH<sub>2</sub>), 2.73 (1H, dd,  $J = 13.5$ , 6.2, -CH<sub>2</sub>), 2.47 (1H, dd,  $J = 13.5$ , 7.6, -CH<sub>2</sub>), 2.26 (3H, s, -CH<sub>3</sub>), 1.47 (9H, s, -C(CH<sub>3</sub>)<sub>3</sub>), 1.44 (9H, s, -C(CH<sub>3</sub>)<sub>3</sub>). <sup>13</sup>C NMR (101 MHz, CDCl<sub>3</sub>)  $\delta$  171.3 (-CONR<sub>2</sub>), 170.7 (-CONH), 169.7 (-COOR), 167.8 (-COOR), 141.5 (Ar-C), 136.8 (Ar-C), 136.2 (Ar-C), 134.9 (Ar-C), 129.7 (2 x Ar-CH), 129.3 (2 x Ar-CH), 128.7 (2 x Ar-CH), 128.3 (Ar-CH), 128.2 (2 x Ar-CH), 127.9 (Ar-CH), 126.6 (Ar-CH), 121.7 (Ar-CH), 120.1 (Ar-CH), 118.2 (Ar-CH), 108.5 (Ar-CH), 105.1 (Ar-C), 82.6 (-OCR<sub>3</sub>), 81.6 (-OCR<sub>3</sub>), 70.8 (-OCH<sub>2</sub>), 70.7 (4 x -OCH<sub>2</sub>), 70.6 (4 x -OCH<sub>2</sub>), 70.2 (-OCH<sub>2</sub>), 69.1 (-COCH<sub>2</sub>), 67.9 (-OCH<sub>2</sub>), 51.5 (-CH), 49.2 (-NCH<sub>2</sub>), 45.8 (-COCH<sub>2</sub>), 38.3(-CH<sub>2</sub>), 32.5 (-COCH<sub>2</sub>), 28.2 (3C, -C(CH<sub>3</sub>)<sub>3</sub>), 28.1 (3C, -C(CH<sub>3</sub>)<sub>3</sub>), 10.2 (-CH<sub>3</sub>). HRMS (ESI) exact mass calculated for C<sub>50</sub>H<sub>69</sub>N<sub>3</sub>O<sub>12</sub>Na [M+Na]<sup>+</sup>  $m/z$  926.4773, found  $m/z$  926.4894. IR (thin film) 2870, 1744, 1651, 1597.



2.16

**2.16.** Prepared according to a modified literature procedure.<sup>[41]</sup> To a stirred solution of ester **2.1** (16 mg, 0.020 mmol, 1 equiv.) in dichloromethane (0.34 mL, 0.1 M) was added trifluoroacetic acid (0.34 mL) and the resulting solution was stirred at room temperature for 1 hour. Volatiles were removed *in vacuo* and dichloromethane (2 mL) was added, followed by *in vacuo* concentration (three times) generating the title compound **2.16** (22 mg). The crude material was used without further purification.

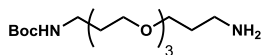
HRMS (ESI) exact mass calculated for C<sub>40</sub>H<sub>51</sub>N<sub>3</sub>O<sub>10</sub>Na [M+Na]<sup>+</sup> m/z 756.3467, found m/z 756.3442.



2.17

**2.17.** Prepared according to a modified literature procedure.<sup>[41]</sup> To a stirred solution of ester **2.14** (34 mg, 0.043 mmol, 1 equiv.) in dichloromethane (0.5 mL, 0.1 M) was added trifluoroacetic acid (0.5 mL) and the resulting solution was stirred at room temperature for 1 hour. Volatiles were removed *in vacuo* and dichloromethane (2 mL) was added, followed by *in vacuo* concentration (three times) generating the title compound **2.17** (45 mg). The crude material was used without further purification.

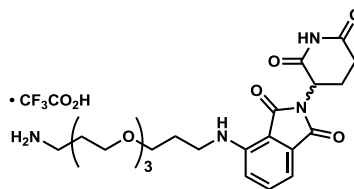
HRMS (ESI) exact mass calculated for C<sub>40</sub>H<sub>51</sub>N<sub>3</sub>O<sub>10</sub>Na [M+Na]<sup>+</sup> m/z 756.3467, found m/z 756.3452.



2.19

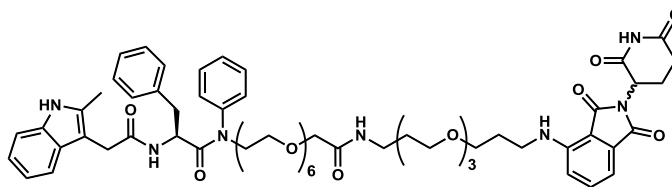
**2.19.** Prepared according to a modified literature procedure.<sup>[48]</sup> To a stirred solution of diamine **2.18** (10.0 mL, 44.0 mmol, 2 equiv.) in dichloromethane (440 mL, 0.1 M) was added di-*tert*-butyl dicarbonate (5.30 g, 24.0 mmol, 1 equiv.) and the resulting solution was stirred at room temperature for 18 hours. To the reaction mixture was added dichloromethane (200 mL) and 1 M aqueous sodium carbonate (200 mL) and the phases were separated. The aqueous phase was extracted with dichloromethane (3 x 200 mL) and the combined organic phases were washed with 1 M aqueous sodium carbonate (3 x 200 mL), dried over magnesium sulphate, filtered and concentrated *in vacuo* yielding a crude mass of 7.00 g. Purification by chromatography on silica gel using an eluent of 8% methanol and 1% saturated aqueous ammonium hydroxide in dichloromethane afforded the title compound **2.19** (6.02 g, 18.8 mmol, 78%). Analytical data observed were in accordance with literature values.<sup>[48]</sup>

<sup>1</sup>H NMR (400 MHz, CDCl<sub>3</sub>) δ 5.08 (1H, s, -CONH), 3.67–3.50 (12H, m, 6 x -OCH<sub>2</sub>), 3.22 (2H, dt, *J* = 6.3, 6.3, -NHCH<sub>2</sub>), 2.81 (2H, t, *J* = 6.6, -CH<sub>2</sub>NH<sub>2</sub>), 1.82–1.66 (4H, m, 2 x -CH<sub>2</sub>), 1.43 (9H, s, -C(CH<sub>3</sub>)<sub>3</sub>), 1.24 (2H, t, *J* = 7.0, -NH<sub>2</sub>). <sup>13</sup>C NMR (101 MHz, CDCl<sub>3</sub>) δ 156.1 (-NCOOR), 78.8 (-OCR<sub>3</sub>), 70.6 (2 x -OCH<sub>2</sub>), 70.2 (-OCH<sub>2</sub>), 70.1 (-OCH<sub>2</sub>), 69.5 (-OCH<sub>2</sub>), 53.5 (-OCH<sub>2</sub>), 39.6 (-CH<sub>2</sub>NH<sub>2</sub>), 38.5 (-NHCH<sub>2</sub>), 32.9 (-CH<sub>2</sub>), 29.7 (-CH<sub>2</sub>), 28.4 (3C, -C(CH<sub>3</sub>)<sub>3</sub>). HRMS (ESI) exact mass calculated for C<sub>15</sub>H<sub>33</sub>N<sub>2</sub>O<sub>5</sub> [M+H]<sup>+</sup> *m/z* 321.2384, found *m/z* 321.2369. IR (thin film) 2865, 1705, 1698, 1518.



2.21

**2.21.** Prepared according to a modified literature procedure.<sup>[48]</sup> To a stirred solution of *tert*-butyl carbamate **2.2** (28 mg, 0.049 mmol, 1 equiv.) in dichloromethane (0.80 mL, 0.1 M) was added trifluoroacetic acid (0.80 mL) and the resulting solution was stirred at room temperature for 1 hour. Volatiles were removed *in vacuo* and dichloromethane (5 mL) was added, followed by *in vacuo* concentration (three times) generating the title compound **2.21** (41 mg). The crude material was used without further purification.

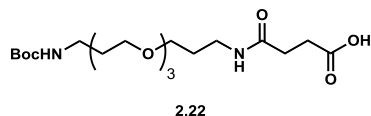


CRBN-N33

**CRBN-N33.** Prepared according to a modified literature procedure.<sup>[109]</sup> To a stirred solution of acid **2.16** (21 mg, 0.029 mmol, 1 equiv.) in *N,N*-dimethylformamide (0.29 mL, 0.1 M) was added amine TFA salt **2.21** (17 mg, 0.029 mmol, 1 equiv.), HATU (11 mg, 0.029 mmol, 1 equiv.) and *N,N*-diisopropylethylamine (25  $\mu$ L, 0.15 mmol, 5 equiv.) and the resulting solution was stirred at room temperature for 48 hours. To the reaction mixture was added dichloromethane (3 mL) and half saturated aqueous sodium hydrogen carbonate solution (3 mL) and the resultant phases were separated. The aqueous phase was extracted with dichloromethane (3 x 5 mL) and the combined organic phases washed with 5% aqueous lithium chloride solution (3 x 5 mL). The combined organic phases were dried with magnesium sulphate, filtered and concentrated *in vacuo* affording a crude mass of 33 mg. Purification by column chromatography on silica gel using an eluent of 3% to 20% ethanol in dichloromethane afforded the title compound **CRBN-N33** (12 mg, 0.010 mmol, 35%). Further purification by reverse phase preparative HPLC using a gradient of 5% to 95% acetonitrile in water over 50 minutes eluted the title compound with a retention time of 35 minutes. The product fraction was lyophilised generating the title compound **CRBN-N33** as a yellow powder (3 mg, 0.003 mmol, 7%).

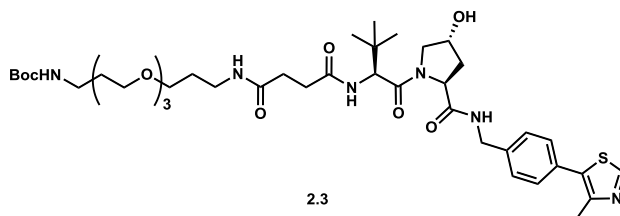
<sup>1</sup>H NMR (400 MHz, CDCl<sub>3</sub>)  $\delta$  8.58 (0.5H, s, -CONHCO), 8.51 (0.5H, s, -CONHCO), 8.33 (1H, s, Ar-NH), 7.49 (0.5H, dd, *J* = 8.6, 7.0, Ar-CH), 7.48 (0.5H, dd, *J* = 8.6, 7.1, Ar-CH), 7.43–7.24 (6H, m, 6 x Ar-CH), 7.19–6.97 (7H, m, 7 x Ar-CH), 6.92 (1H, d, *J* = 8.7, Ar-CH), 6.65 (1H, d, *J* = 6.8, 2 x Ar-CH), 6.65 (1H, s, -CONH), 6.64 (1H, d, *J* = 7.0, 2 x Ar-CH), 6.42 (0.5H, d, *J* = 8.2, -CONH), 6.37 (0.5H, d, *J* = 8.1, -CONH), 4.90 (0.5H, dd, *J* = 5.2, 3.6, -CH), 4.87 (0.5H, dd, *J* = 5.3, 3.5, -CH), 4.67 (1H, ddd, *J* = 7.3, 7.3, 7.3, -CH), 4.00 (2H, s, -COCH<sub>2</sub>), 3.90–3.78 (1H, m, -NCH<sub>2</sub>), 3.73 (1H, ddd, *J* = 12.6, 6.0, 5.9, -OCH<sub>2</sub>), 3.70–3.44 (36H, m, -NCH<sub>2</sub>, -OCH<sub>2</sub>, -COCH<sub>2</sub>, 16 x -OCH<sub>2</sub>), 3.44–3.32 (4H, m, 2 x -NCH<sub>2</sub>), 2.89–2.65 (5H, m, -NH, -COCH<sub>2</sub>, -CH<sub>2</sub>, -CH<sub>2</sub>, ), 2.52 (0.5H, dd, *J* = 13.4, 7.4, -CH<sub>2</sub>), 2.52 (0.5H, dd, *J* = 13.4, 7.4, -CH<sub>2</sub>), 2.30 (1.5H, s, -CH<sub>3</sub>), 2.28 (1.5H, s, -CH<sub>3</sub>), 2.15–2.05 (1H, m, -CH<sub>2</sub>), 1.91 (2H, tt, *J* = 6.1, 6.0, -CH<sub>2</sub>), 1.78 (2H, tt, *J* = 6.5, 6.4, -CH<sub>2</sub>). <sup>13</sup>C NMR (101 MHz, CDCl<sub>3</sub>)  $\delta$  171.5 (2 x -CONR<sub>2</sub>), 171.3 (2 x -CONH), 170.9 (2 x -CONH), 170.1 (-CONH), 169.5 (2 x -CONH), 168.6 (-CONR<sub>2</sub>), 167.9 (-CONR<sub>2</sub>), 167.8 (-CONR<sub>2</sub>), 147.1 (Ar-C), 141.4 (Ar-C), 136.3 (2 x

Ar-C), 136.2 (Ar-CH), 135.5 (2 x Ar-C), 133.5 (Ar-C), 133.4 (Ar-C), 132.7 (Ar-C), 129.7 (2 x Ar-CH), 129.4 (2 x Ar-CH), 128.7 (Ar-CH), 128.5 (2 x Ar-C), 128.4 (2 x Ar-CH), 128.3 (4 x Ar-CH), 126.7 (2 x Ar-CH), 121.5 (Ar-CH), 119.8 (Ar-CH), 118.0 (Ar-CH), 116.8 (Ar-CH), 111.5 (Ar-CH), 110.6 (Ar-CH), 110.0 (Ar-C), 104.7 (Ar-C), 71.1 (-OCH<sub>2</sub>), 70.7 (8 x -OCH<sub>2</sub>), 70.6 (-COCH<sub>2</sub>, 2 x -OCH<sub>2</sub>), 70.4 (2 x -OCH<sub>2</sub>), 70.2 (-OCH<sub>2</sub>), 69.4 (-OCH<sub>2</sub>), 69.1 (-OCH<sub>2</sub>), 67.8 (-OCH<sub>2</sub>), 51.4 (-CH), 49.2 (-NCH<sub>2</sub>), 49.0 (-CH), 40.4 (-NCH<sub>2</sub>), 38.5 (2 x -CH<sub>2</sub>), 36.7 (-NCH<sub>2</sub>), 32.2 (-COCH<sub>2</sub>), 31.6 (-COCH<sub>2</sub>), 29.7 (-CH<sub>2</sub>), 29.4 (-CH<sub>2</sub>), 22.9 (-CH<sub>2</sub>), 11.8 (-CH<sub>3</sub>). HRMS (ESI) exact mass calculated for C<sub>63</sub>H<sub>81</sub>N<sub>7</sub>O<sub>16</sub>Na [M+Na]<sup>+</sup> m/z 1214.5632, found m/z 1214.5615.



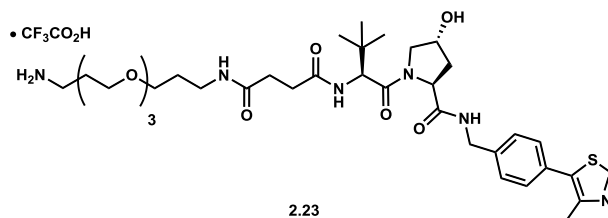
**2.22.** Prepared according to a modified literature procedure.<sup>[114]</sup> To a stirred solution amine **2.19** (100 mg, 0.313 mmol, 1 equiv.) in dichloromethane (1 mL, 0.3 M) was added succinic anhydride (313 mg, 0.313 mmol, 1 equiv.) and 4-dimethylaminopyridine (4 mg, 0.03 mmol, 0.1 equiv.) and the resulting solution was stirred at room temperature for 18 hours. To this solution was added dichloromethane (5 mL) and 1 M aqueous hydrochloric acid. The organic phase was then washed with 1 M aqueous hydrochloric acid (3 x 5 mL), dried over magnesium sulphate, filtered and concentrated *in vacuo* yielding the title compound **2.22** (126 mg, 0.300 mmol, 96%). No further purification was required. Analytical data observed were in accordance with literature data.<sup>[114]</sup>

<sup>1</sup>H NMR (400 MHz, CDCl<sub>3</sub>) δ 6.95 (1H, dt, *J* = 17.7, 5.6, -CONH), 5.18–4.99 (1H, m, -OCONH), 3.74–3.42 (12H, m, 6 x -OCH<sub>2</sub>), 3.30 (2H, dt, *J* = 5.8, 5.8, -NHCH<sub>2</sub>), 3.14 (2H, dt, *J* = 5.8, 5.8, -NHCH<sub>2</sub>), 2.61 (2H, t, *J* = 6.7, -CH<sub>2</sub>COOH), 2.45 (2H, t, *J* = 6.8, -COCH<sub>2</sub>), 1.83–1.61 (4H, m, 2 x -CH<sub>2</sub>), 1.38 (9H, s, -C(CH<sub>3</sub>)<sub>3</sub>). <sup>13</sup>C NMR (101 MHz, CDCl<sub>3</sub>) δ 175.1 (-COOH), 172.5 (-CONH), 156.2 (-NCOOR), 79.1 (-OCR<sub>3</sub>), 70.5 (-OCH<sub>2</sub>), 70.4 (-OCH<sub>2</sub>), 70.1 (2 x -OCH<sub>2</sub>), 69.9 (-OCH<sub>2</sub>), 69.4 (-OCH<sub>2</sub>), 38.4 (-NCH<sub>2</sub>), 38.0 (-NCH<sub>2</sub>), 30.9 (-COCH<sub>2</sub>), 30.0 (-COCH<sub>2</sub>), 29.7 (-CH<sub>2</sub>), 28.7 (-CH<sub>2</sub>), 28.5 (3C, -C(CH<sub>3</sub>)<sub>3</sub>). HRMS (ESI) exact mass calculated for C<sub>19</sub>H<sub>36</sub>N<sub>2</sub>O<sub>8</sub>Na [M+Na]<sup>+</sup> *m/z* 443.2364, found *m/z* 443.2347. IR (thin film) 2865, 1707, 1693, 1518.

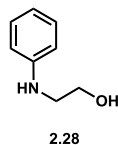


**2.3.** Prepared according to a modified literature procedure.<sup>[109]</sup> To a stirred solution of acid **2.22** (126 mg, 0.300 mmol, 1 equiv.) in *N,N*-dimethylformamide (1.0 mL, 0.3 M) was added amine **VHL-1** (129 mg, 0.300 mmol, 1 equiv.), HATU (114 mg, 0.300 mmol, 1 equiv.) and *N,N*-diisopropylethylamine (0.16 mL, 0.90 mmol, 3 equiv.) and the resulting solution was stirred at room temperature for 48 hours. To the crude mixture was added ethyl acetate (10 mL) and half saturated aqueous sodium hydrogen carbonate solution (10 mL) and the aqueous phase was extracted with ethyl acetate (3 x 10 mL). The combined organic phases were washed with 5% aqueous lithium chloride solution (3 x 10 mL), dried over magnesium sulphate, filtered and concentrated *in vacuo* affording a crude mass of 139 mg. Purification by column chromatography on silica gel using an eluent of 10% to 30% ethanol in dichloromethane afforded the title compound **2.3** (125 mg, 0.150 mmol, 50%).

<sup>1</sup>H NMR (400 MHz, CDCl<sub>3</sub>) δ 8.65 (1H, s, -SCHN), 7.77 (1H, s, -CONH), 7.47–7.27 (4H, m, 4 x Ar-CH), 6.80 (1H, s, -CONH), 5.10 (1H, s, -OCONH), 4.68 (1H, t, *J* = 8.1, -CH), 4.57–4.39 (3H, m, -CH, -CHOH, -NCH<sub>2</sub>), 4.30 (1H, dd, *J* = 15.1, 5.5, -NCH<sub>2</sub>), 3.90 (1H, d, *J* = 11.2, -CH<sub>2</sub>), 3.67–3.39 (13H, m, -CH<sub>2</sub>, 6 x -OCH<sub>2</sub>), 3.23 (2H, q, *J* = 6.6, -NCH<sub>2</sub>), 3.20–3.03 (2H, m, -NCH<sub>2</sub>), 2.64–2.36 (6H, m, -CH<sub>3</sub>, -COCH<sub>2</sub>, -COCH<sub>2</sub>), 2.37–2.36 (2H, m, -COCH<sub>2</sub>, -CH<sub>2</sub>), 2.12 (1H, dd, *J* = 13.4, 8.0, -CH<sub>2</sub>), 1.76–1.62 (4H, m, 2 x -CH<sub>2</sub>), 1.38 (9H, s, -C(CH<sub>3</sub>)<sub>3</sub>), 0.92 (9H, s, -C(CH<sub>3</sub>)<sub>3</sub>). <sup>13</sup>C NMR (101 MHz, CDCl<sub>3</sub>) δ 172.6 (-CONH), 172.3 (-CONH), 171.5 (2 x -CONH), 156.1 (-NCOOR), 150.3 (-SCHN), 148.4 (Ar-C), 138.5 (Ar-C), 131.8 (Ar-C), 130.7 (Ar-C), 129.4 (2 x Ar-CH), 128.0 (2 x Ar-CH), 79.0 (-OCH<sub>2</sub>), 70.5 (3 x -OCH<sub>2</sub>), 70.2 (-CHOH), 70.0 (-OCH<sub>2</sub>), 69.8 (-OCH<sub>2</sub>), 69.5 (-OCH<sub>2</sub>), 58.7 (-CH), 57.7 (-CH), 56.9 (-CH<sub>2</sub>), 43.1 (-NCH<sub>2</sub>), 38.4 (-NCH<sub>2</sub>), 37.9 (-NCH<sub>2</sub>), 36.8 (-CH<sub>2</sub>), 35.5 (-CR<sub>3</sub>), 31.4 (-COCH<sub>2</sub>), 31.3 (-COCH<sub>2</sub>), 29.7 (-CH<sub>2</sub>), 28.8 (-CH<sub>2</sub>), 28.5 (3C, -C(CH<sub>3</sub>)<sub>3</sub>), 26.5 (3C, -C(CH<sub>3</sub>)<sub>3</sub>), 16.1 (-CH<sub>3</sub>). HRMS (ESI) exact mass calculated for C<sub>41</sub>H<sub>64</sub>N<sub>6</sub>O<sub>10</sub>SNa [M+Na]<sup>+</sup> *m/z* 855.4297, found *m/z* 855.4271. IR (thin film) 2870, 1684, 1525.

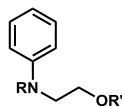


**2.23.** Prepared according to a modified literature procedure.<sup>[48]</sup> To a stirred solution of *tert*-butyl carbamate **2.3** (43 mg, 0.052 mmol, 1 equiv.) in dichloromethane (0.85 mL, 0.1 M) was added trifluoroacetic acid (0.85 mL) and the resulting solution was stirred at room temperature for 1 hour. Volatiles were removed *in vacuo* and dichloromethane (5 mL) was added, followed by *in vacuo* concentration (three times) generating the title compound **2.23** (53 mg). The crude material was used without further purification.



**2.28.** Prepared according to a modified literature procedure.<sup>[116]</sup> To a stirred solution of copper (I) chloride (360 mg, 3.60 mmol, 10 mol%) and potassium hydroxide (4.0 g, 72 mmol, 2 equiv.) in 2-aminoethanol (6.5 mL, 110 mmol, 3 equiv.) at 0 °C was added iodobenzene (7.3 g, 36 mmol, 1 equiv.) and the resulting solution was stirred at 0 °C to room temperature for 18 hours. Water (100 mL) was added and the aqueous phase was extracted with ethyl acetate (3 x 100 mL). The combined organic phases were dried with magnesium sulphate, filtered and concentrated *in vacuo* yielding a crude mass of 5.20 g. Purification by column chromatography on silica gel using an eluent of 33% ethyl acetate in petroleum ether yielded the title compound **2.28** (4.90 g, 36.0 mmol, quantitative). Analytical data observed were in accordance with literature values.<sup>[116]</sup>

<sup>1</sup>H NMR (400 MHz, CDCl<sub>3</sub>) δ 7.22 (2H, ddd, *J* = 8.4, 7.4, 1.0, 2 x Ar-CH), 6.78 (1H, dddd, *J* = 7.3, 7.3, 1.2, 1.2, Ar-CH), 6.70–6.62 (2H, m, 2 x Ar-CH), 3.78 (2H, t, *J* = 5.1, -CH<sub>2</sub>OH), 3.26 (2H, t, *J* = 5.2 -NCH<sub>2</sub>). <sup>13</sup>C NMR (101 MHz, CDCl<sub>3</sub>) δ 148.1 (Ar-C), 129.3 (2 x Ar-CH), 117.9 (Ar-CH), 113.3 (2 x Ar-CH), 61.1 (-CH<sub>2</sub>OH), 46.1 (-NCH<sub>2</sub>). HRMS (ESI) exact mass calculated for C<sub>8</sub>H<sub>12</sub>NO [M+H]<sup>+</sup> *m/z* 138.0913, found *m/z* 138.0915. IR (thin film) 2850, 1601.



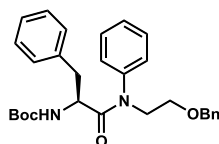
2.29 R=H, R'=Bn  
 2.30 R=Bn R'=H  
 2.31 R=Bn R'=Bn

**2.29, 2.30** and **2.31**. Prepared according to a modified literature procedure.<sup>[41]</sup> To oven dried glassware cooled under vacuum and flushed with argon was added sodium hydride (60% suspension in mineral oil) (878 mg, 22.1 mmol, 1.2 equiv.) and tetrahydrofuran (120 mL, 0.15 M) and the resulting suspension was cooled to 0 °C. To the suspension was added alcohol **2.28** (2.50 g, 18.4 mmol, 1 equiv.) and the mixture was stirred at 0 °C for 20 minutes. To this was slowly added benzyl bromide (1.75 mL, 14.7 mmol, 0.8 equiv.) and the resulting stirred suspension was allowed to warm to room temperature for 18 hours. To the reaction mixture was added water (70 mL) and the aqueous phase was extracted with dichloromethane (3 x 90 mL). The combined organic phases were washed with brine (70 mL), dried with magnesium sulphate, filtered and concentrated *in vacuo* generating a crude mass of 4.30 g. Purification by column chromatography on silica gel using an eluent of 5% ethyl acetate in petroleum ether yielded the title compound **2.29** (2.03 g, 8.94 mmol, 61%), the N alkylated **2.30** (82 mg, 0.368 mmol, 2%) and the dialkylated **2.31** (720 mg, 2.27 mmol, 15%). Analytical data observed were in accordance with literature values.<sup>[125]</sup>

**2.29**. R<sub>f</sub> 0.75 in 33% ethyl acetate in petroleum ether. <sup>1</sup>H NMR (400 MHz, CDCl<sub>3</sub>) δ 7.41–7.28 (5H, m, 5 x Ar-CH), 7.19 (2H, ddd, *J* = 8.2, 7.6, 1.0, 2 x Ar-CH), 6.73 (1H, ddd, *J* = 7.4, 7.4, 1.1, Ar-CH), 6.65 (2H, br d, *J* = 8.4, 2 x Ar-CH), 4.57 (2H, s, -OCH<sub>2</sub>), 4.06 (1H, s, -NH), 3.72 (2H, t, *J* = 5.3, -OCH<sub>2</sub>), 3.34 (2H, t, *J* = 5.3, -NCH<sub>2</sub>). <sup>13</sup>C NMR (101 MHz, CDCl<sub>3</sub>) δ 148.2 (Ar-C), 138.2 (Ar-C), 129.4 (2 x Ar-CH), 128.6 (2 x Ar-CH), 127.9 (3 x Ar-CH), 117.9 (Ar-CH), 113.4 (2 x Ar-CH), 73.3 (-OCH<sub>2</sub>), 68.8 (-OCH<sub>2</sub>), 43.9 (-NCH<sub>2</sub>). HRMS (ESI) exact mass calculated for C<sub>15</sub>H<sub>17</sub>NONa [M+Na]<sup>+</sup> m/z 250.1202, found m/z 250.1196. IR (thin film) 2855, 1601, 1504.

**2.30**. R<sub>f</sub> 0.47 in 33% ethyl acetate in petroleum ether. <sup>1</sup>H NMR (400 MHz, CDCl<sub>3</sub>) δ 7.34–7.29 (2H, m, 2 x Ar-CH), 7.25–7.17 (5H, m, 5 x Ar-CH), 6.82–6.77 (2H, m, 2 x Ar-CH), 6.73 (1H, tt, *J* = 7.3, 0.9, Ar-CH), 4.63 (2H, s, -NCH<sub>2</sub>), 3.84 (2H, t, *J* = 5.8, -CH<sub>2</sub>OH), 3.62 (2H, t, *J* = 5.8, -NCH<sub>2</sub>), 1.66 (1H, br s, -OH). <sup>13</sup>C NMR (101 MHz, CDCl<sub>3</sub>) δ 149.0 (Ar-C), 138.8 (Ar-C), 129.4 (2 x Ar-CH), 128.8 (2 x Ar-CH), 127.1 (Ar-CH), 126.8 (2 x Ar-CH), 117.3 (Ar-CH), 113.1 (2 x Ar-CH), 60.5 (-CH<sub>2</sub>OH), 55.3 (-NCH<sub>2</sub>), 53.5 (-NCH<sub>2</sub>). HRMS (ESI) exact mass calculated for C<sub>15</sub>H<sub>17</sub>NONa [M+Na]<sup>+</sup> m/z 250.1202, found m/z 250.1198.

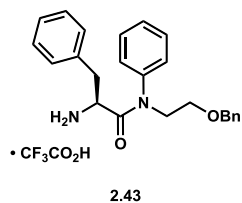
**2.31.**  $R_f$  0.86 in 33% ethyl acetate in petroleum ether.  $^1\text{H}$  NMR (400 MHz,  $\text{CDCl}_3$ )  $\delta$  7.40–7.15 (7H, m, 7 x Ar-CH), 7.26–7.16 (5H, m, 5 x Ar-CH), 6.80–6.65 (3H, m, 3 x Ar-CH), 4.65 (2H, s, -NCH<sub>2</sub>), 4.54 (2H, s, -OCH<sub>2</sub>), 3.73 (2H, d,  $J = 4.5$ , -OCH<sub>2</sub>), 3.71 (2H, d,  $J = 4.5$ , -NCH<sub>2</sub>).  $^{13}\text{C}$  NMR (101 MHz,  $\text{CDCl}_3$ )  $\delta$  148.6 (Ar-C), 139.1 (Ar-C), 138.4 (Ar-C), 129.3 (2 x Ar-CH), 128.7 (2 x Ar-CH), 128.5 (2 x Ar-CH), 127.7 (4 x Ar-CH), 126.9 (Ar-CH), 126.7 (Ar-CH), 116.5 (Ar-CH), 112.4 (2 x Ar-CH), 73.5 (-OCH<sub>2</sub>), 68.1 (-OCH<sub>2</sub>), 55.1 (-NCH<sub>2</sub>), 51.0 (-OCH<sub>2</sub>). HRMS (ESI) exact mass calculated for  $\text{C}_{22}\text{H}_{23}\text{NONa}$   $[\text{M}+\text{Na}]^+$   $m/z$  340.1671, found  $m/z$  340.1658. IR (thin film) 2853, 1597, 1504.



2.34

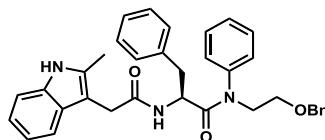
**2.34.** Prepared according to a modified literature procedure.<sup>[111]</sup> To a stirred solution of Boc-L-phenylalanine (3.91 g, 14.7 mmol, 1.0 equiv.) in *N,N*-dimethylformamide (25 mL, 0.9 M) was added aniline **2.29** (5.02 g, 22.1 mmol, 1.5 equiv.), HATU (8.40 g, 22.1 mmol, 1.5 equiv.) and *N,N*-diisopropylethylamine (5.15 mL, 29.5 mmol, 2 equiv.) and the resulting solution was stirred at 60 °C for 48 hours. To the crude mixture was added ethyl acetate (40 mL) and half saturated aqueous sodium hydrogen carbonate solution (40 mL) and the resultant phases were separated. The aqueous phase was extracted with ethyl acetate (3 x 40 mL) and the combined organic phases washed with 5% aqueous lithium chloride solution (3 x 40 mL). The combined organic phases were dried with magnesium sulphate, filtered and concentrated *in vacuo* affording a crude mass of 11.6 g. Purification by column chromatography on silica gel using an eluent of 20% ethyl acetate in petroleum ether afforded the title compound **2.34** as a viscous oil (6.59 g, 13.9 mmol, 95%).

<sup>1</sup>H NMR (400 MHz, CDCl<sub>3</sub>) δ 7.37–7.22 (9H, m, 9 x Ar-CH), 7.20–7.15 (3H, m, 3 x Ar-CH), 6.96–6.85 (3H, m, 3 x Ar-CH), 5.17 (1H, d, *J* = 9.1, -CONH), 4.50–4.43 (1H, m, -CH), 4.46 (2H, s, -OCH<sub>2</sub>), 3.92 (1H, dt, *J* = 13.8, 6.0, -NCH<sub>2</sub>), 3.88–3.78 (1H, m, -NCH<sub>2</sub>), 3.59 (2H, m, -OCH<sub>2</sub>), 2.89 (1H, dd, *J* = 13.3, 6.9, -CH<sub>2</sub>), 2.66 (1H, dd, *J* = 13.7, 6.8, -CH<sub>2</sub>), 1.37 (9H, s, -C(CH<sub>3</sub>)<sub>3</sub>). <sup>13</sup>C NMR (101 MHz, CDCl<sub>3</sub>) δ 171.9 (-CONR<sub>2</sub>), 154.7 (-OCONH), 141.3 (Ar-C), 138.0 (Ar-C), 136.6 (Ar-C), 129.5 (2 x Ar-CH), 129.4 (2 x Ar-CH), 128.4 (2 x Ar-CH), 128.3 (2 x Ar-CH), 128.2 (2 x Ar-CH), 128.1 (Ar-CH), 127.6 (3 x Ar-CH), 126.6 (Ar-CH), 79.3 (-OCR<sub>3</sub>), 72.8 (-OCH<sub>2</sub>), 67.0 (-OCH<sub>2</sub>), 52.5 (-CH), 49.2 (-NCH<sub>2</sub>), 39.5 (-CH<sub>2</sub>), 28.3 (3C, -C(CH<sub>3</sub>)<sub>3</sub>). HRMS (ESI) exact mass calculated for C<sub>29</sub>H<sub>34</sub>N<sub>2</sub>O<sub>4</sub>Na [M+Na]<sup>+</sup> *m/z* 497.2411, found *m/z* 497.2397. IR (thin film) 2924, 1710, 1651.



**2.43.** Prepared according to a modified literature procedure.<sup>[48]</sup> To a stirred solution of *tert*-butyl carbamate **2.34** (1.40 g, 2.97 mmol, 1 equiv.) in dichloromethane (30 mL, 0.1 M) was added trifluoroacetic acid (30 mL) and the resulting solution was stirred at room temperature for 1 hour. Volatiles were removed *in vacuo* and dichloromethane (30 mL) was added, followed by *in vacuo* concentration three times generating the title compound **2.43** (2.26 g). The crude material was used without further purification.

HRMS (ESI) exact mass calculated for C<sub>24</sub>H<sub>26</sub>N<sub>2</sub>O<sub>2</sub>Na [M+Na]<sup>+</sup> m/z 397.1886, found m/z 397.1869. IR (thin film) 2930, 1728, 1639, 1595.



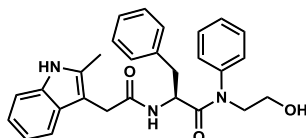
2.32

**2.32 Method A.** Prepared according to a modified literature procedure.<sup>[111]</sup> To a stirred solution of acid **2.11** (188 mg, 0.560 mmol, 1 equiv.) in *N,N*-dimethylformamide (0.62 mL, 0.9 M) was added aniline **2.9** (223 mg, 0.840 mmol, 1.5 equiv.), HATU (320 mg, 0.840 mmol, 1.5 equiv.) and *N,N*-diisopropylethylamine (0.20 mL, 1.1 mmol, 2 equiv.) and the resulting solution was stirred at room temperature for 18 hours. To the crude mixture was added ethyl acetate (10 mL) and half saturated aqueous sodium hydrogen carbonate solution (5 mL) and the resultant layers were separated. The aqueous phase was extracted with ethyl acetate (3 x 10 mL) and the combined organic phases washed with 5% aqueous lithium chloride solution (3 x 10 mL). The combined organic phases were dried with magnesium sulphate, filtered and concentrated *in vacuo* affording a crude mass of 19.1 g. Purification by column chromatography on silica gel using an eluent of 40% ethyl acetate in petroleum ether afforded the title compound **2.32** as a viscous oil (241 mg, 0.442 mmol, 79%)

**2.32 Method B.** To a stirred solution of 2-methyl-3-indoleacetic acid (540 mg, 2.70 mmol, 1 equiv.) in *N,N*-dimethylformamide (6.75 mL, 0.4 M) was added amine TFA salt **2.43** (1.46 g, 3.00 mmol, 1.1 equiv.), HATU (1.03 g, 2.70 mmol, 1 equiv.) and *N,N*-diisopropylethylamine (1.9 mL, 11 mmol, 4 equiv.) and the resulting solution was stirred at room temperature for 48 hours. To the crude mixture was added ethyl acetate (20 mL) and half saturated aqueous sodium hydrogen carbonate solution (20 mL) and the resultant phases were separated. The aqueous phase was extracted with ethyl acetate (3 x 20 mL) and the combined organic phases washed with 5% aqueous lithium chloride solution (3 x 20 mL). The combined organic phases were dried with magnesium sulphate, filtered and concentrated *in vacuo* affording a crude mass of 1.71 g. Purification by column chromatography on silica gel using an eluent of 50% to 60% ethyl acetate in petroleum ether afforded the title compound **2.32** as a viscous oil (1.48 g, 2.70 mmol, quantitative).

<sup>1</sup>H NMR (400 MHz, CDCl<sub>3</sub>) δ 7.91 (1H, s, Ar-NH), 7.42–7.21 (11H, m, 11 x Ar-CH), 7.17–7.12 (1H, m, Ar-CH), 7.12–7.05 (2H, m, 2 x Ar-CH), 7.02 (3H, t, *J* = 7.5, 3 x Ar-CH), 6.64 (2H, d, *J* = 7.1, 2 x Ar-CH), 6.15 (1H, d, *J* = 8.3, -CONH), 4.71 (1H, dt, *J* = 7.2, 7.2, -CH), 4.43 (2H, s, -OCH<sub>2</sub>), 3.89–3.74 (2H, m, -NCH<sub>2</sub>), 3.64–3.45 (4H, m, -COCH<sub>2</sub>, -OCH<sub>2</sub>), 2.73 (1H, dd, *J* = 13.4, 6.6, -CH<sub>2</sub>), 2.49 (1H, dd, *J* = 13.4, 7.0,

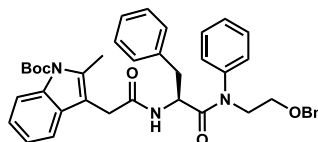
-CH<sub>2</sub>), 2.29 (3H, s, -CH<sub>3</sub>). <sup>13</sup>C NMR (101 MHz, CDCl<sub>3</sub>) δ 171.5 (-CONR<sub>2</sub>), 171.0 (-CONH), 141.2 (Ar-C), 138.1 (Ar-C), 136.1 (Ar-C), 135.5 (Ar-CH), 133.6 (Ar-C), 129.7 (Ar-CH), 129.3 (2 x Ar-CH), 128.6 (Ar-CH), 128.4 (4 x Ar-CH, Ar-C), 128.3 (2 x Ar-CH), 127.7 (4 x Ar-CH), 126.8 (Ar-CH), 121.4 (Ar-CH), 119.7 (Ar-CH), 117.8 (Ar-C), 110.6 (Ar-CH), 104.3 (Ar-C), 72.9 (-OCH<sub>2</sub>), 67.0 (-OCH<sub>2</sub>), 51.4 (-CH), 49.4 (-NCH<sub>2</sub>), 38.6 (-CH<sub>2</sub>), 32.2 (-CH<sub>2</sub>), 11.5 (-CH<sub>3</sub>). HRMS (ESI) exact mass calculated for C<sub>35</sub>H<sub>35</sub>N<sub>3</sub>O<sub>3</sub>Na [M+Na]<sup>+</sup> m/z 568.2571, found m/z 568.2546. IR (thin film) 2855, 1715, 1640, 1594.



2.27

**2.27.** Prepared according to a modified literature procedure.<sup>[41]</sup> To a stirred suspension of 10% palladium on carbon (24 mg, 0.024 mmol, 5.0 mol%) in methanol (22 mL, 0.02 M) under argon atmosphere was added benzyl ether **2.32** (241 mg, 0.440 mmol, 1 equiv.) at room temperature. The flask was then evacuated and the suspension sparged with hydrogen gas for 5 minutes and then stirred at room temperature under a hydrogen atmosphere for 5 hours. The hydrogen was then removed under reduced pressure and the suspension sparged with argon three times. The suspension was then filtered through a pad of celite (200 g) in dichloromethane (200 mL) and the celite washed with dichloromethane (400 mL). The organic phase was then concentrated *in vacuo* generating the title compound **2.27** (200 mg, 0.440 mmol, quantitative).

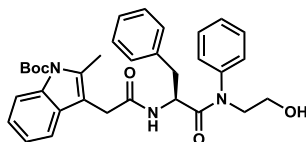
<sup>1</sup>H NMR (400 MHz, CDCl<sub>3</sub>) δ 8.26 (1H, s, Ar-NH), 7.39–7.32 (4H, m, 4 x Ar-CH), 7.27 (1H, d, *J* = 8.0, Ar-CH), 7.18–7.12 (2H, m, 2 x Ar-CH), 7.11–7.05 (3H, m, 3 x Ar-CH), 6.96 (2H, m, 2 x Ar-CH), 6.68 (2H, d, *J* = 7.3, 2 x Ar-CH), 6.18 (1H, d, *J* = 7.9, -CONH), 4.67 (1H, dt, *J* = 7.3, 7.3, -CH), 3.92–3.83 (1H, m, -NCH<sub>2</sub>), 3.72–3.60 (3H, m, -NCH<sub>2</sub>, -OCH<sub>2</sub>), 3.59 (1H, s, -COCH<sub>2</sub>), 3.58 (1H, s, -COCH<sub>2</sub>), 2.75 (1H, dd, *J* = 13.3, 7.0, -CH<sub>2</sub>), 2.55 (1H, dd, *J* = 13.4, 7.1, -CH<sub>2</sub>), 2.26 (3H, s, -CH<sub>3</sub>), 1.81 (1H, s, -OH). <sup>13</sup>C NMR (101 MHz, CDCl<sub>3</sub>) δ 173.1 (-CONR<sub>2</sub>), 171.1 (-CONH<sub>2</sub>), 141.5 (Ar-C), 136.0 (Ar-C), 135.5 (Ar-C), 133.5 (Ar-C), 130.0 (2 x Ar-CH), 129.3 (2 x Ar-CH), 128.6 (Ar-C), 128.5 (2 x Ar-CH), 128.4 (Ar-CH), 128.3 (2 x Ar-CH), 127.0 (Ar-CH), 121.7 (Ar-CH), 119.9 (Ar-CH), 117.9 (Ar-CH), 110.6 (Ar-CH), 104.5 (Ar-C), 60.9 (-CH<sub>2</sub>OH), 53.4 (-NCH<sub>2</sub>), 51.7 (-CH), 38.7 (-CH<sub>2</sub>), 32.2 (-COCH<sub>2</sub>), 11.7 (-CH<sub>3</sub>). HRMS (ESI) exact mass calculated for C<sub>28</sub>H<sub>29</sub>N<sub>3</sub>O<sub>3</sub>Na [M+Na]<sup>+</sup> *m/z* 478.2101, found *m/z* 478.2092. IR (thin film) 2853, 1639, 1594.



2.44

**2.44.** Prepared according to a modified literature procedure.<sup>[48]</sup> To a stirred solution of indole **2.32** (404 mg, 0.740 mmol, 1 equiv.) in dichloromethane (3.7 mL, 0.20 M) was added di-*tert*-butyl dicarbonate (205  $\mu$ L, 0.890 mmol, 1.2 equiv.) and 4-dimethylaminopyridine (0.5 mg, 0.07 mmol, 10 mol%) and the resulting solution was stirred at room temperature for 6 hours. To the crude mixture was added ethyl acetate (10 mL) and half-saturated aqueous sodium hydrogen carbonate (10 mL) and the phases were separated. The aqueous phase was extracted with ethyl acetate (3 x 10 mL) and the combined organic phases were washed with brine (30 mL), dried over magnesium sulphate, filtered and concentrated *in vacuo* yielding a crude mass of 423 mg. Purification by chromatography on silica gel using an eluent of 30% to 70% ethyl acetate in petroleum ether afforded the title compound **2.44** (397 mg, 0.615 mmol, 83%).

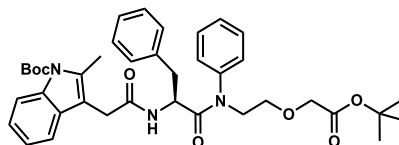
<sup>1</sup>H NMR (400 MHz, CDCl<sub>3</sub>)  $\delta$  8.11 (1H, d,  $J = 8.2$ , Ar-CH), 7.39–7.25 (10H, m, 10 x Ar-CH), 7.27–6.97 (6H, m, 6 x Ar-CH), 6.63 (2H, d,  $J = 7.1$ , 2 x Ar-CH), 6.06 (1H, d,  $J = 8.2$ , -CONH), 4.72 (1H, dt,  $J = 7.5, 7.4$ , -CH), 4.44 (2H, s, -OCH<sub>2</sub>), 3.89 (1H, dt,  $J = 13.9, 5.7$ , -NCH<sub>2</sub>), 3.79 (1H, dt,  $J = 13.8, 5.9$ , -NCH<sub>2</sub>), 3.63–3.45 (4H, m, -COCH<sub>2</sub>, -OCH<sub>2</sub>), 2.74 (1H, dd,  $J = 13.5, 6.4$ , -CH<sub>2</sub>), 2.51 (1H, dd,  $J = 13.5, 7.3$ , -CH<sub>2</sub>), 2.46 (3H, s, -CH<sub>3</sub>), 1.70 (9H, s, -C(CH<sub>3</sub>)<sub>3</sub>). <sup>13</sup>C NMR (101 MHz, CDCl<sub>3</sub>)  $\delta$  171.4 (-CONR<sub>2</sub>), 169.6 (-CONH), 150.7 (-NCOOR), 141.4 (Ar-C), 138.2 (Ar-C), 136.1 (Ar-C), 135.9 (Ar-C), 135.7 (Ar-C), 129.8 (2 x Ar-CH), 129.4 (Ar-C), 129.3 (2 x Ar-CH), 128.6 (2 x Ar-CH), 128.5 (2 x Ar-CH), 128.4 (3 x Ar-CH), 127.8 (3 x Ar-CH), 126.8 (Ar-CH), 124.0 (Ar-CH), 123.0 (Ar-CH), 117.9 (Ar-CH), 115.7 (Ar-CH), 111.6 (Ar-C), 84.0 (-OCR<sub>3</sub>), 73.0 (-OCH<sub>2</sub>), 67.1 (-OCH<sub>2</sub>), 51.3 (-CH), 49.4 (-NCH<sub>2</sub>), 38.6 (-CH<sub>2</sub>), 32.3 (-COCH<sub>2</sub>), 28.5 (3C, -C(CH<sub>3</sub>)<sub>3</sub>), 14.1 (-CH<sub>3</sub>). HRMS (ESI) exact mass calculated for C<sub>40</sub>H<sub>43</sub>N<sub>3</sub>O<sub>5</sub>Na [M+Na]<sup>+</sup>  $m/z$  668.3095, found  $m/z$  668.3063. IR (thin film) 2920, 1721, 1642, 1594.



2.45

**2.45.** Prepared according to a modified literature procedure.<sup>[41]</sup> To a stirred suspension of 10% palladium on carbon (80 mg, 0.047 mmol, 5.0 mol%) in methanol (63 mL, 0.02 M) under argon atmosphere was added benzyl ether **2.44** (800 mg, 0.930 mmol, 1 equiv.) at room temperature. The flask was then evacuated and the suspension sparged with hydrogen gas for 5 minutes and then stirred at room temperature under a hydrogen atmosphere for 5 hours. The hydrogen was then removed under reduced pressure and the suspension sparged with argon three times. The suspension was then filtered through a pad of celite (300 g) in dichloromethane (200 mL) and the celite washed with dichloromethane (500 mL). The organic phase was then concentrated *in vacuo* generating the title compound **2.45** (777 mg, 0.930 mmol, quantitative).

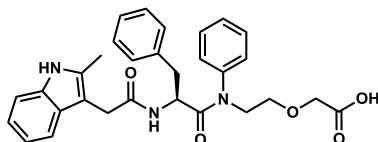
<sup>1</sup>H NMR (400 MHz, CDCl<sub>3</sub>) δ 8.13 (1H, dt, *J* = 8.3, 0.9, Ar-CH), 7.42–7.24 (7H, m, 7 x Ar-CH), 7.22–7.05 (4H, m, 4 x Ar-CH), 6.66 (2H, d, *J* = 7.1, 2 x Ar-CH), 6.07 (1H, d, *J* = 7.8, -CONH), 4.65 (1H, t, *J* = 7.3, -CH), 3.93–3.82 (1H, m, -NCH<sub>2</sub>), 3.76–3.63 (3H, m, -NCH<sub>2</sub>, -OCH<sub>2</sub>), 3.58 (1H, d, *J* = 17.1, -COCH<sub>2</sub>), 3.51 (1H, d, *J* = 17.0, -COCH<sub>2</sub>), 2.87 (1H, br s, -OH), 2.77 (1H, dd, *J* = 13.4, 6.9, -CH<sub>2</sub>), 2.56 (1H, dd, *J* = 13.4, 7.4, -CH<sub>2</sub>), 2.46 (3H, s, -CH<sub>3</sub>), 1.70 (9H, s, -C(CH<sub>3</sub>)<sub>3</sub>). <sup>13</sup>C NMR (101 MHz, CDCl<sub>3</sub>) δ 173.0 (-CONR<sub>2</sub>), 169.9 (-CONH), 150.6 (-NCOOR), 141.4 (Ar-C), 135.9 (2 x Ar-C), 135.7 (Ar-C), 130.0 (2 x Ar-CH), 129.3 (Ar-C), 129.2 (2 x Ar-CH), 128.6 (Ar-CH), 128.5 (2 x Ar-CH), 128.2 (2 x Ar-CH), 127.0 (Ar-CH), 124.0 (Ar-CH), 123.0 (Ar-CH), 117.8 (Ar-CH), 115.7 (Ar-CH), 111.4 (Ar-C), 84.0 (-OCR<sub>3</sub>), 60.9 (-OCH<sub>2</sub>), 53.4 (-NCH<sub>2</sub>), 51.6 (-CH), 38.5 (-CH<sub>2</sub>), 32.1 (-COCH<sub>2</sub>), 28.4 (3C, -C(CH<sub>3</sub>)<sub>3</sub>), 14.1 (-CH<sub>3</sub>). HRMS (ESI) exact mass calculated for C<sub>33</sub>H<sub>37</sub>N<sub>3</sub>O<sub>5</sub>Na [M+Na]<sup>+</sup> *m/z* 578.2625, found *m/z* 578.2610. IR (thin film) 2920, 1725, 1639, 1594.



2.46

**2.46.** Prepared according to a modified literature procedure.<sup>[41]</sup> To oven dried glassware cooled under vacuum and flushed with argon was added a solution of alcohol **2.45** (300 mg, 0.540 mmol, 1 equiv.) in tetrahydrofuran (1.8 mL, 0.30 M) and the solution was cooled to  $-78$  °C. To this was added a 2 M solution of sodium bis(trimethylsilyl)amide in tetrahydrofuran (100  $\mu$ L, 1.08 mmol, 2 equiv.) and the resulting mixture was stirred at  $-78$  °C for 15 minutes. To this was added *tert*-butyl bromoacetate (80  $\mu$ L, 0.540 mmol, 1 equiv.) and the resulting reaction mixture was allowed to warm, to room temperature and stirred for an additional 4 hours. To this was added water (5 mL) and dichloromethane (10 mL) and the aqueous phase was extracted with dichloromethane (3 x 10 mL). The combined organic phases were washed with brine (10 mL), dried with magnesium sulphate, filtered and concentrated *in vacuo* generating a crude mass of 458 mg. Purification by column chromatography on silica gel using an eluent of 10% ethyl acetate in dichloromethane yielded the title compound **2.46** (144 mg, 0.215 mmol, 40%).

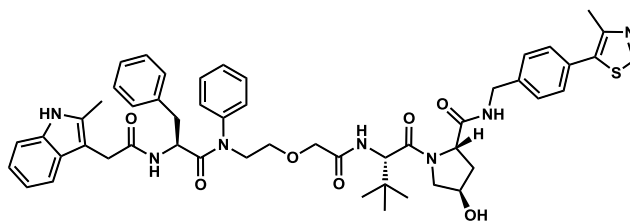
<sup>1</sup>H NMR (400 MHz, CDCl<sub>3</sub>)  $\delta$  8.12 (1H, ddd,  $J = 9.0, 8.3, 0.9$ , Ar-CH), 7.41–7.15 (8H, m, 8 x Ar-CH), 7.15–7.02 (3H, m, 3 x Ar-CH), 6.65 (2H, d,  $J = 7.0$ , 2 x Ar-CH), 6.08 (1H, d,  $J = 8.1$ , -CONH), 4.72 (1H, dt,  $J = 7.4, 7.4$ , -CH), 3.96–3.83 (1H, m, -NCH<sub>2</sub>), 3.89 (2H, d,  $J = 5.1$ , -COCH<sub>2</sub>), 3.75 (1H, dt,  $J = 13.8, 6.0$ , -NCH<sub>2</sub>), 3.69–3.60 (2H, m, -OCH<sub>2</sub>), 3.57 (1H, d,  $J = 16.8$ , -COCH<sub>2</sub>), 3.50 (1H, d,  $J = 17.0$ , -COCH<sub>2</sub>), 2.77 (1H, dd,  $J = 13.5, 6.4$ , -CH<sub>2</sub>), 2.53 (1H, dd,  $J = 13.5, 7.2$ , -CH<sub>2</sub>), 2.47 (3H, s, -CH<sub>3</sub>), 1.70 (9H, s, -C(CH<sub>3</sub>)<sub>3</sub>), 1.45 (9H, s, -C(CH<sub>3</sub>)<sub>3</sub>). <sup>13</sup>C NMR (101 MHz, CDCl<sub>3</sub>)  $\delta$  171.4 (-CONR<sub>2</sub>), 169.6 (-CONH), 169.4 (-COOR), 150.6 (-NCOOR), 141.5 (Ar-C), 136.1 (Ar-C), 135.9 (Ar-C), 135.6 (Ar-C), 129.8 (2 x Ar-CH), 129.4 (Ar-C), 129.3 (2 x Ar-CH), 128.6 (2 x Ar-CH), 128.5 (Ar-CH), 128.3 (2 x Ar-CH), 126.8 (Ar-CH), 124.0 (Ar-CH), 122.9 (Ar-CH), 117.9 (Ar-CH), 115.7 (Ar-CH), 111.6 (Ar-C), 84.0 (-OCR<sub>3</sub>), 81.7 (-OCR<sub>3</sub>), 68.8 (-COCH<sub>2</sub>), 68.2 (-OCH<sub>2</sub>), 51.3 (-CH), 49.4 (-NCH<sub>2</sub>), 38.4 (-CH<sub>2</sub>), 32.2 (-COCH<sub>2</sub>), 28.4 (3C, -C(CH<sub>3</sub>)<sub>3</sub>), 28.2 (3C, -C(CH<sub>3</sub>)<sub>3</sub>), 14.1 (-CH<sub>3</sub>). HRMS (ESI) exact mass calculated for C<sub>39</sub>H<sub>47</sub>N<sub>3</sub>O<sub>7</sub>Na [M+Na]<sup>+</sup>  $m/z$  692.3306, found  $m/z$  692.3290. IR (thin film) 2930, 1728, 1639, 1595.



2.47

**2.47.** Prepared according to a modified literature procedure.<sup>[48]</sup> To a stirred solution of *tert*-butyl carbamate **2.46** (40 mg, 0.060 mmol, 1 equiv.) in dichloromethane (0.60 mL, 0.1 M) was added trifluoroacetic acid (0.60 mL) and the resulting solution was stirred at room temperature for 1 hour. Volatiles were removed *in vacuo* and dichloromethane (2 mL) was added, followed by *in vacuo* concentration (three times) generating the title compound **2.47** (58 mg). The crude material was used without further purification.

HRMS (ESI) exact mass calculated for C<sub>30</sub>H<sub>31</sub>N<sub>3</sub>O<sub>5</sub>Na [M+Na]<sup>+</sup> m/z 536.2156, found m/z 536.2146. IR (thin film) 2926, 1732, 1622, 1593.

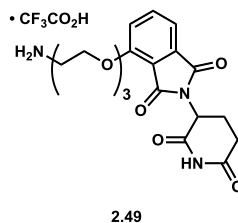


VHL-4

**VHL-4.** Prepared according to a modified literature procedure.<sup>[109]</sup> To a stirred solution of acid **2.47** (30 mg, 0.059 mmol, 1 equiv.) in *N,N*-dimethylformamide (0.15 mL, 0.4 M) was added amine **VHL-1** (26 mg, 0.059 mmol, 1 equiv.), HATU (23 mg, 0.059 mmol, 1 equiv.) and *N,N*-diisopropylethylamine (61  $\mu$ L, 0.35 mmol, 6 equiv.) and the resulting solution was stirred at room temperature for 48 hours. To the crude mixture was added dichloromethane (2 mL) and half saturated aqueous sodium hydrogen carbonate solution (2 mL) and the resultant phases were separated. The aqueous phase was extracted with dichloromethane (3 x 5 mL) and the combined organic phases washed with 5% aqueous lithium chloride solution (3 x 5 mL). The combined organic phases were dried with magnesium sulphate, filtered and concentrated *in vacuo* affording a crude mass of 82 mg. Purification by column chromatography on silica gel using an eluent of 40% to 100% acetone in dichloromethane afforded the title compound **VHL-4** (42 mg, 0.045 mmol, 77%). Further purification by reverse phase preparative HPLC using a gradient of 20% to 55% acetonitrile in water over 10 minutes followed by 55% to 80% acetonitrile over 35 minutes eluted the title compound with a retention time of 23.5–25.7 minutes. The product fraction was lyophilised generating the title compound **VHL-4** as a white powder (26 mg, 0.028 mmol, 48%).

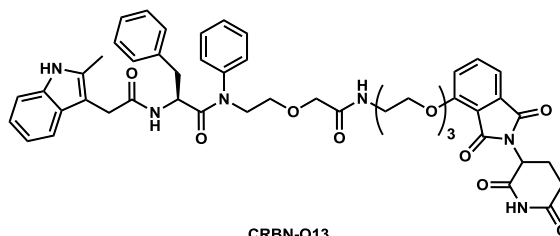
<sup>1</sup>H NMR (500 MHz, CDCl<sub>3</sub>)  $\delta$  8.85 (1H, s, -NCHS-), 8.45 (1H, s, Ar-NH), 7.38–7.28 (9H, m, 9 x Ar-CH), 7.24 (1H, s, Ar-CH), 7.17 (1H, d, *J* = 8.7, ), 7.12 (2H, ddd, *J* = 7.5, 7.3, 1.3, 2 x Ar-CH), 7.08–7.00 (3H, m, 3 x Ar-CH), 6.64 (2H, d, *J* = 7.2, 2 x Ar-CH), 6.36 (1H, d, *J* = 8.1, -CONH), 4.68–4.60 (2H, m, -CH, -CH), 4.53 (1H, d, *J* = 8.6, -CH), 4.52–4.47 (1H, dd, *J* = 15.2, 6.2, -NHCH<sub>2</sub>Ar), 4.46 (1H, br s, -OCH), 4.33 (1H, dd, *J* = 15.0, 5.5, -NHCH<sub>2</sub>), 4.02 (1H, d, *J* = 11.3, -OCH<sub>2</sub>), 3.99–3.91 (1H, m, -NCH<sub>2</sub>), 3.88 (1H, d, *J* = 15.1, -NCH<sub>2</sub>), 3.79 (1H, d, *J* = 15.1, -NCH<sub>2</sub>), 3.65–3.58 (2H, m, -OCH<sub>2</sub>, -NCH<sub>2</sub>), 3.56 (2H, d, *J* = 4.6, -COCH<sub>2</sub>), 3.54–3.45 (2H, m, -COCH<sub>2</sub>), 2.72 (1H, dd, *J* = 13.3, 6.8, -CH<sub>2</sub>), 2.51 (1H, dd, *J* = 13.5, 7.3, -CH<sub>2</sub>), 2.51 (3H, s, -CH<sub>3</sub>), 2.42 (1H, ddd, *J* = 12.9, 8.0, 4.6, -CH<sub>2</sub>), 2.24 (3H, s, -CH<sub>3</sub>), 2.07 (1H, dd, *J* = 13.5, 8.0, -CH<sub>2</sub>), 0.95 (9H, s, -C(CH<sub>3</sub>)<sub>3</sub>). <sup>13</sup>C NMR (126 MHz, CDCl<sub>3</sub>)  $\delta$  171.8 (-CONR<sub>2</sub>), 171.6 (-CONH), 171.2 (2 x -CONH), 170.1 (-CONR<sub>2</sub>), 151.4 (-SCHN), 147.0 (Ar-C), 140.8

(Ar-C), 138.9 (Ar-C), 136.1 (Ar-C), 135.5 (Ar-C), 133.7 (Ar-C), 132.8 (Ar-C), 130.0 (2 x Ar-CH), 129.9 (Ar-C), 129.6 (2 x Ar-CH), 129.3 (2 x Ar-CH), 128.7 (Ar-CH), 128.4 (4 x Ar-CH), 128.3 (Ar-C), 128.2 (2 x Ar-CH), 126.9 (Ar-CH), 121.5 (Ar-CH), 119.8 (Ar-CH), 117.9 (Ar-CH), 110.6 (Ar-CH), 104.3 (Ar-C), 70.2 (-OCH), 69.9 (-NCH<sub>2</sub>), 68.0 (-COCH<sub>2</sub>), 58.8 (-CH), 57.3 (-CH), 56.9 (-OCH<sub>2</sub>), 51.7 (-CH), 48.8 (-NCH<sub>2</sub>), 43.2 (-NHCH<sub>2</sub>), 38.5 (-CH<sub>2</sub>), 36.6 (-CH<sub>2</sub>), 35.4 (-CR<sub>3</sub>), 32.0 (-COCH<sub>2</sub>), 26.5 (3C, -C(CH<sub>3</sub>)<sub>3</sub>), 15.3 (-CH<sub>3</sub>), 11.6 (-CH<sub>3</sub>). HRMS (ESI) exact mass calculated for C<sub>52</sub>H<sub>59</sub>N<sub>7</sub>O<sub>7</sub>SNa [M+Na]<sup>+</sup> m/z 948.4089, found m/z 948.4100. IR (thin film) 2959, 1730, 1635, 1595.



**2.49.** Prepared according to a modified literature procedure.<sup>[48]</sup> To a stirred solution of racemic *tert*-butyl carbamate **2.48** (30 mg, 0.059 mmol, 1 equiv.) in dichloromethane (0.55 mL, 0.1 M) was added trifluoroacetic acid (0.55 mL) and the resulting solution was stirred at room temperature for 1 hour. Volatiles were removed *in vacuo* and dichloromethane (3 mL) was added, followed by *in vacuo* concentration (three times) generating the title compound **2.49** (49 mg). The crude material was used without further purification.

HRMS (ESI) exact mass calculated for C<sub>19</sub>H<sub>24</sub>N<sub>3</sub>O<sub>7</sub> [M+H]<sup>+</sup> m/z 406.1609, found m/z 406.1598. IR (thin film) 2922, 1771, 1703, 1614.

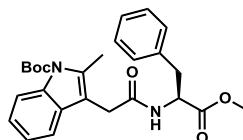


**CRBN-O13.** Prepared according to a modified literature procedure.<sup>[109]</sup> To a stirred solution of acid **2.47** (36 mg, 0.072 mmol, 1 equiv.) in *N,N*-dimethylformamide (0.18 mL, 0.4 M) was added racemic amine TFA salt **2.49** (37 mg, 0.072 mmol, 1 equiv.), HATU (27 mg, 0.072 mmol, 1 equiv.) and *N,N*-diisopropylethylamine (100  $\mu$ L, 0.58 mmol, 8 equiv.) and the resulting solution was stirred at room temperature for 48 hours. To the crude mixture was added dichloromethane (3 mL) and half saturated aqueous sodium hydrogen carbonate solution (3 mL) and the resultant phases were separated. The aqueous phase was extracted with dichloromethane (3 x 5 mL) and the combined organic phases washed with 5% aqueous lithium chloride solution (3 x 5 mL). The combined organic phases were dried with magnesium sulphate, filtered and concentrated *in vacuo* affording a crude mass of 95 mg. Purification by column chromatography on silica gel using an eluent of 20% to 40% ethyl acetate in dichloromethane afforded the title compound **CRBN-O13** (52 mg, 0.058 mmol, 81%). Further purification by reverse phase preparative HPLC using a gradient of 20% to 50% acetonitrile in water over 10 minutes followed by 50% to 100% acetonitrile over 60 minutes eluted the title compound with a retention time of 27.4–28.7 minutes. The product fraction was lyophilised generating the title compound **CRBN-O13** as a white powder (25 mg, 0.028 mmol, 39%).

Spectra were complicated by the presence of rotamers (conformational isomers). Variable temperature <sup>1</sup>H NMR at 25 °C, 35 °C and 55 °C showed the convergence of complicated peaks towards their expected multiplicities.

<sup>1</sup>H NMR (25 °C) (400 MHz, CDCl<sub>3</sub>)  $\delta$  9.18 (0.5H, s, -CONHCO), 9.04 (0.5H, s, -CONHCO), 8.57 (0.5H, s, Ar-NH) 8.56 (0.5H, s, Ar-NH), 7.61 (0.5H, dd, *J* = 7.8, 7.8, Ar-CH), 7.59 (0.5H, dd, *J* = 7.8, 7.8, Ar-CH), 7.43 (0.5H, d, *J* = 7.5, Ar-CH), 7.41 (0.5H, d, *J* = 7.5, Ar-CH), 7.39–6.80 (14H, m, 13 x Ar-CH, -CONH), 6.69–6.60 (2H, m, 2 x Ar-CH), 6.46 (0.5H, d, *J* = 8.0, -CONH), 6.39 (0.5H, d, *J* = 8.0, -CONH), 4.79–4.84 (1H, m, -CH), 4.72–4.57 (1H, m, -CH), 4.31–4.16 (2H, m, ArO-CH<sub>2</sub>), 3.97–3.33 (18H, m, -COCH<sub>2</sub>, -COCH<sub>2</sub>, 2 x -NCH<sub>2</sub>, 5 x -OCH<sub>2</sub>), 2.84–2.69 (2H, m, -COCH<sub>2</sub>), 2.73 (1H, dd, *J* = 12.9, 7.1, -CH<sub>2</sub>), 2.70–2.55 (1H, m, -COCH<sub>2</sub>), 2.53 (0.5H, dd, *J* = 13.4, 7.3, -CH<sub>2</sub>), 2.52 (0.5H, dd, *J* = 13.4, 7.3, -CH<sub>2</sub>), 2.23 (1.5H, s, -CH<sub>3</sub>), 2.20 (1.5H,

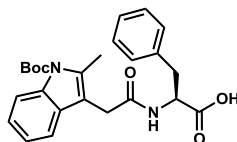
s, -CH<sub>3</sub>) 2.06 (1H, m, -COCH<sub>2</sub>). <sup>13</sup>C NMR (101 MHz, CDCl<sub>3</sub>) δ 172.0 (-CONR<sub>2</sub>), 171.9 (-CONR<sub>2</sub>), 171.5 (2 x -CONHCO), 171.4 (-CONH), 171.3 (-CONH), 169.9 (-CONH), 168.7 (-CONHCO), 168.6 (-CONHCO), 167.3 (-CONR<sub>2</sub>), 167.2 (-CONR<sub>2</sub>), 165.9 (2 x -CONR<sub>2</sub>), 156.4 (Ar-C), 141.0 (Ar-C), 140.9 (Ar-C), 136.6 (2 x Ar-CH), 136.2 (Ar-C), 136.1 (Ar-C), 135.4 (2 x Ar-C), 133.9 (Ar-C), 133.8 (Ar-C), 133.6 (2 x Ar-C), 129.9 (Ar-C, 2 x Ar-CH), 129.3 (2 x Ar-CH), 128.7 (Ar-CH), 128.6 (Ar-CH), 128.5 (2 x Ar-CH), 128.4 (4 x Ar-CH), 128.3 (2 x Ar-CH), 126.8 (2 x Ar-CH), 121.4 (2 x Ar-CH), 119.7 (Ar-CH), 119.3 (2 x Ar-CH), 117.9 (Ar-CH), 117.3 (Ar-C), 116.2 (Ar-CH), 110.6 (Ar-CH), 104.4 (Ar-C), 104.3 (Ar-C), 71.3 (-OCH<sub>2</sub>), 71.2 (-OCH<sub>2</sub>), 70.4 (-OCH<sub>2</sub>), 70.3 (-OCH<sub>2</sub>), 70.2 (-OCH<sub>2</sub>), 70.1 (-OCH<sub>2</sub>), 69.7 (-OCH<sub>2</sub>), 69.3 (2 x -COCH<sub>2</sub>), 69.2 (2 x -OCH<sub>2</sub>), 68.4 (-OCH<sub>2</sub>), 68.3 (-OCH<sub>2</sub>), 51.8 (-CH), 51.7 (-CH), 49.3 (-CH), 49.1 (-NCH<sub>2</sub>), 48.9 (-NCH<sub>2</sub>), 38.8 (-NCH<sub>2</sub>), 38.7 (-NCH<sub>2</sub>), 38.4 (-CH<sub>2</sub>), 38.3 (-CH<sub>2</sub>), 32.1 (-COCH<sub>2</sub>), 31.4 (-COCH<sub>2</sub>), 22.7 (-CH<sub>2</sub>), 11.6 (2 x -CH<sub>3</sub>). HRMS (ESI) exact mass calculated for C<sub>49</sub>H<sub>52</sub>N<sub>6</sub>O<sub>11</sub>Na [M+Na]<sup>+</sup> m/z 923.3586, found m/z 923.3547. IR (thin film) 2907, 1769, 1709, 1653, 1595.



2.53

**2.53.** Prepared according to a modified literature procedure.<sup>[48]</sup> To a stirred solution of indole **2.10** (2.44 g, 6.97 mmol, 1 equiv.) in dichloromethane (35 mL, 0.20 M) was added di-*tert*-butyl dicarbonate (1.83 g, 8.37 mmol, 1.2 equiv.) and 4-dimethylaminopyridine (8.5 mg, 0.70 mmol, 1.0 mol%) and the resulting solution was stirred at room temperature for 18 hours. To the crude mixture was added dichloromethane (30 mL) and half-saturated aqueous sodium hydrogen carbonate (30 mL) and the phases were separated. The aqueous phase was extracted with dichloromethane (3 x 30 mL) and the combined organic phases were washed with brine (30 mL), dried over magnesium sulphate, filtered and concentrated *in vacuo* yielding a crude mass of 3.16 g. Purification by chromatography on silica gel using an eluent of 3% to 6% ethyl acetate in dichloromethane afforded the title compound **2.53** (2.76 g, 6.13 mmol, 88%).

<sup>1</sup>H NMR (400 MHz, CDCl<sub>3</sub>) δ 8.14 (1H, ddd, *J* = 8.3, 1.0, 1.0, Ar-CH), 7.37 (1H, ddd, *J* = 7.6, 1.5, 0.7, Ar-CH), 7.30 (1H, ddd, *J* = 8.5, 7.3, 1.5, Ar-CH), 7.23 (1H, ddd, *J* = 7.4, 7.4, 1.1, Ar-CH), 7.15–7.09 (1H, m, Ar-CH), 7.08–7.01 (2H, m, 2 x Ar-CH), 6.74–6.67 (2H, m, 2 x Ar-CH), 5.86 (1H, d, *J* = 8.2, -CONH), 4.81 (1H, dt, *J* = 8.2, 5.8, -CH), 3.66 (3H, s, -CH<sub>3</sub>), 3.60 (2H, s, -COCH<sub>2</sub>), 2.97 (1H, dd, *J* = 13.8, 5.6, -CH<sub>2</sub>), 2.92 (1H, dd, *J* = 13.7, 5.9, -CH<sub>2</sub>), 2.44 (3H, s, -CH<sub>3</sub>), 1.71 (9H, s, -C(CH<sub>3</sub>)<sub>3</sub>). <sup>13</sup>C NMR (101 MHz, CDCl<sub>3</sub>) δ = 171.7 (-COOR), 169.9 (-CONH), 150.6 (-NCOOR), 135.9 (Ar-C), 135.7 (Ar-C), 135.5 (Ar-C), 129.2 (Ar-C), 129.0 (2 x Ar-CH), 128.5 (2 x Ar-CH), 127.1 (Ar-CH), 124.2 (Ar-CH), 123.1 (Ar-CH), 117.8 (Ar-CH), 115.7 (Ar-CH), 111.3 (Ar-C), 84.1 (-OCR<sub>3</sub>), 52.8 (-CH), 52.4 (-OCH<sub>3</sub>), 37.6 (-CH<sub>2</sub>), 32.1 (-COCH<sub>2</sub>), 28.4 (3C, -C(CH<sub>3</sub>)<sub>3</sub>), 14.0 (-CH<sub>3</sub>). HRMS (ESI) exact mass calculated for C<sub>26</sub>H<sub>30</sub>N<sub>2</sub>O<sub>5</sub>Na [M+Na]<sup>+</sup> *m/z* 473.2052, found *m/z* 473.2047. IR (thin film) 2978, 1730, 1654.

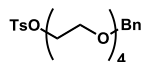


2.54

**2.54.** Prepared according to a modified literature procedure.<sup>[111]</sup> To a stirred solution of **2.53** (2.76 g, 6.13 mmol, 1 equiv.) in tetrahydrofuran (28 mL) and water (19 mL) was added a solution of sodium hydroxide (424 mg, 10.6 mmol, 1.5 equiv.) in methanol (10.6 mL, 1 M) and the resulting solution was stirred vigorously at room temperature for 18 hours. Dichloromethane was added (40 mL) and the crude mixture was acidified with hydrochloric acid (1 M, 20 mL) forming a thick white precipitate. The aqueous phase was extracted with dichloromethane (3 x 40 mL) and the combined organic phases were dried with magnesium sulphate, filtered and concentrated *in vacuo* yielding the title compound **2.54** (2.56 g, 5.86 mmol, 96%). Compound **2.54** was used without further purification.

<sup>1</sup>H NMR (400 MHz, CDCl<sub>3</sub>) δ 8.14 (1H, ddd, *J* = 8.2, 0.9, 0.9, Ar-CH), 7.36–7.26 (2H, m, 2 x Ar-CH), 7.23 (1H, ddd, *J* = 7.4, 7.4, 1.1, Ar-CH), 7.13 (1H, t, *J* = 7.3, Ar-CH), 7.05 (2H, dd, *J* = 7.5, 7.5, 2 x Ar-CH), 6.77–6.70 (2H, m, 2 x Ar-CH), 5.87 (1H, d, *J* = 7.6, -CONH), 4.74 (1H, dt, *J* = 6.4, 6.4, -CH), 3.61 (2H, s, -COCH<sub>2</sub>), 3.02 (1H, dd, *J* = 14.1, 5.5, -CH<sub>2</sub>), 2.96 (1H, dd, *J* = 14.0, 6.7, -CH<sub>2</sub>), 2.37 (3H, s, -CH<sub>3</sub>), 1.71 (9H, s, -C(CH<sub>3</sub>)<sub>3</sub>). <sup>13</sup>C NMR (101 MHz, CDCl<sub>3</sub>) δ = 173.7 (-COOH), 171.4 (-CONH), 150.6 (-NCOOR), 135.9 (2 x Ar-C), 135.2 (Ar-CH), 129.1 (Ar-C, 2 x Ar-CH), 128.7 (2 x Ar-CH), 127.2 (Ar-CH), 124.3 (Ar-CH), 123.2 (Ar-CH), 117.8 (Ar-CH), 115.7 (Ar-CH), 110.8 (Ar-C), 84.3 (-OCR<sub>3</sub>), 53.1 (-CH), 36.8 (-CH<sub>2</sub>), 31.9 (-COCH<sub>2</sub>), 28.5 (3C, -C(CH<sub>3</sub>)<sub>3</sub>), 14.0 (-CH<sub>3</sub>). HRMS (ESI) exact mass calculated for C<sub>25</sub>H<sub>28</sub>N<sub>2</sub>O<sub>5</sub>Na [M+Na]<sup>+</sup> *m/z* 459.1890, found *m/z* 459.1877. IR (thin film) 2978, 1728, 1627. [α]<sub>D</sub><sup>16.9°C</sup> +9.40 (*c* = 1.00, CHCl<sub>3</sub>).

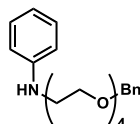




2.51

**2.51.** Prepared according to a modified literature procedure.<sup>[117]</sup> To a stirred solution of alcohol **2.50** (6.75 g, 23.8 mmol, 1 equiv.) in tetrahydrofuran (48 mL, 0.5 M) was added a 4.5 M aqueous solution of sodium hydroxide (6.30 mL, 26.1 mmol, 1.2 equiv.) and the resulting solution was cooled to 0 °C and stirred rapidly for 20 minutes. To this mixture was added 4-toluenesulfonyl chloride (4.98 g, 26.1 mmol, 1.1 equiv.) and the resulting mixture was allowed to warm to room temperature under rapid stirring for 18 hours. To the reaction mixture was added water (100 mL) and dichloromethane (200 mL) and the aqueous phase was extracted with dichloromethane (3 x 150 mL). The combined organic phases were washed with brine (100 mL), dried over magnesium sulphate, filtered and concentrated *in vacuo* yielding a crude mass of 9.29 g. Purification by column chromatography on silica gel using an eluent of 0% to 20% ethyl acetate in dichloromethane yielded the title compound **2.51** (7.17 g, 16.4 mmol, 69%). Analytical data observed were in accordance with literature values.<sup>[117]</sup>

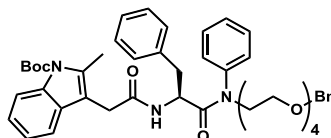
<sup>1</sup>H NMR (400 MHz, CDCl<sub>3</sub>) δ 7.79 (2H, d, *J* = 8.5, 2 x Ar-CH), 7.35–7.32 (5H, m, 5 x Ar-CH), 7.32–7.31 (1H, m, Ar-CH), 7.31–7.26 (1H, m, Ar-CH), 4.56 (2H, s, -OCH<sub>2</sub>), 4.17–4.13 (2H, m, -OCH<sub>2</sub>), 3.69–3.65 (4H, m, 2 x -OCH<sub>2</sub>), 3.65–3.61 (6H, m, 3 x -OCH<sub>2</sub>), 3.60–3.56 (4H, m, 2 x -OCH<sub>2</sub>), 2.44 (3H, s, -CH<sub>3</sub>). <sup>13</sup>C NMR (101 MHz, CDCl<sub>3</sub>) δ 144.9 (Ar-C), 138.4 (Ar-C), 133.2 (Ar-C), 129.9 (2 x Ar-CH), 128.5 (2 x Ar-CH), 128.1 (2 x Ar-CH), 127.9 (2 x Ar-CH), 127.7 (Ar-CH), 73.4 (-OCH<sub>2</sub>), 70.9 (-OCH<sub>2</sub>), 70.8 (3 x -OCH<sub>2</sub>), 70.7 (-OCH<sub>2</sub>), 69.6 (-OCH<sub>2</sub>), 69.4 (-OCH<sub>2</sub>), 68.8 (-OCH<sub>2</sub>), 21.8 (-CH<sub>3</sub>). HRMS (ESI) exact mass calculated for C<sub>22</sub>H<sub>30</sub>O<sub>7</sub>SNa [M+Na]<sup>+</sup> m/z 461.1604, found m/z 461.1587. IR (thin film) 2860, 1719, 1567, 1452.



2.52

**2.52.** Prepared according to a modified literature procedure.<sup>[124]</sup> To a stirred solution of tosylate **2.51** (5.10 g, 11.6 mmol, 1 equiv.) in acetonitrile (40 mL, 0.3 M) was added potassium carbonate (5.10 g, 37.2 mmol, 3.2 equiv.) and aniline (9.75 mL, 105 mmol, 9 equiv.) and the resulting solution was heated to 80 °C and stirred for 18 hours. The reaction mixture was then concentrated *in vacuo* and the resulting solid was dissolved in water (100 mL) and diethyl ether (100 mL). The aqueous phase was extracted with diethyl ether (3 x 150 mL) and the combined organic phases were washed with brine (100 mL), dried over magnesium sulphate, filtered and concentrated *in vacuo* yielding a crude mass of 12.7 g. Purification by column chromatography on silica gel using an eluent of 0% to 20% ethyl acetate in dichloromethane yielded the title compound **2.52** (3.82 g, 10.6 mmol, 91%).

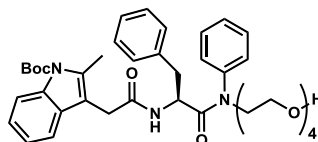
<sup>1</sup>H NMR (400 MHz, CDCl<sub>3</sub>) δ 7.39–7.32 (4H, m, 4 x Ar-CH), 7.31–7.27 (1H, m, Ar-CH), 7.18 (2H, dt, *J* = 8.4, 7.5, 2 x Ar-CH), 6.71 (1H, tt, *J* = 7.3, 1.2, Ar-CH), 6.64 (2H, dd, *J* = 8.7, 1.1, 2 x Ar-CH), 4.57 (2H, s, -OCH<sub>2</sub>), 4.01 (1H, s, -NH), 3.75–3.61 (14H, m, 7 x -OCH<sub>2</sub>), 3.29 (2H, t, *J* = 5.3, -NCH<sub>2</sub>). <sup>13</sup>C NMR (101 MHz, CDCl<sub>3</sub>) δ 148.3 (Ar-C), 138.4 (Ar-C), 129.3 (2 x Ar-CH), 128.4 (2 x Ar-CH), 127.8 (2 x Ar-CH), 127.7 (Ar-CH), 117.6 (Ar-CH), 113.2 (2 x Ar-CH), 73.3 (-OCH<sub>2</sub>), 70.8 (3 x -OCH<sub>2</sub>), 70.7 (-OCH<sub>2</sub>), 70.4 (-OCH<sub>2</sub>), 69.7 (-OCH<sub>2</sub>), 69.6 (-OCH<sub>2</sub>), 43.6 (-NCH<sub>2</sub>). HRMS (ESI) exact mass calculated for C<sub>21</sub>H<sub>29</sub>NO<sub>4</sub>Na [M+Na]<sup>+</sup> *m/z* 382.1989, found *m/z* 382.1978. IR (thin film) 2864, 1602, 1506.



2.55

**2.55.** Prepared according to a modified literature procedure.<sup>[111]</sup> To a stirred solution of acid **2.54** (900 mg, 2.07 mmol, 1 equiv.) in *N,N*-dimethylformamide (2.0 mL, 1 M) was added aniline **2.52** (1.01 g, 3.11 mmol, 1.5 equiv.), HATU (1.16 g, 3.11 mmol, 1.5 equiv.) and *N,N*-diisopropylethylamine (0.72 mL, 4.1 mmol, 2 equiv.) and the resulting solution was heated to 65 °C and stirred for 48 hours. To the crude mixture was added ethyl acetate (20 mL) and half saturated aqueous sodium hydrogen carbonate solution (20 mL) and the aqueous phase was extracted with ethyl acetate (3 x 30 mL). The combined organic phases were washed with 5% aqueous lithium chloride solution (3 x 30 mL), dried over magnesium sulphate, filtered and concentrated *in vacuo* affording a crude mass of 2.19 g. Purification by column chromatography on silica gel using an eluent of 15% to 30% ethyl acetate in dichloromethane afforded the title compound **2.55** (983 mg, 1.26 mmol, 61%).

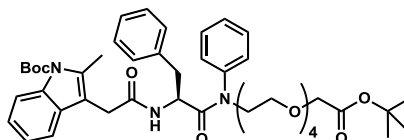
<sup>1</sup>H NMR (400 MHz, CDCl<sub>3</sub>) δ 8.12 (1H, d, *J* = 8.3, Ar-CH), 7.40–7.23 (10H, m, 10 x Ar-CH), 7.28–7.22 (1H, m, Ar-CH), 7.19 (1H, td, *J* = 7.4, 1.1, Ar-CH), 7.12 (1H, tt, *J* = 7.3, 1.0, Ar-CH), 7.09–6.97 (3H, m, 3 x Ar-CH), 6.63 (2H, dd, *J* = 7.1, 1.2, 2 x Ar-CH), 6.06 (1H, d, *J* = 8.2, -CONH), 4.71 (1H, td, *J* = 7.6, 6.3, -CH), 4.54 (2H, s, -OCH<sub>2</sub>), 3.85 (1H, dt, *J* = 13.6, 5.8, -NCH<sub>2</sub>), 3.73 (1H, dt, *J* = 13.8, 6.0, -NCH<sub>2</sub>), 3.70–3.44 (16H, m, -COCH<sub>2</sub>, 7 x -OCH<sub>2</sub>), 2.75 (1H, dd, *J* = 13.5, 6.3, -CH<sub>2</sub>), 2.51 (1H, dd, *J* = 13.5, 7.3, -CH<sub>2</sub>), 2.46 (3H, s, -CH<sub>3</sub>), 1.70 (9H, s, -C(CH<sub>3</sub>)<sub>3</sub>). <sup>13</sup>C NMR (101 MHz, CDCl<sub>3</sub>) δ 171.3 (-CONR<sub>2</sub>), 169.6 (-CONH), 150.7 (-NCOOR), 141.5 (Ar-C), 138.4 (Ar-C), 136.1 (Ar-C), 135.9 (Ar-C), 135.6 (Ar-C), 129.8 (2 x Ar-CH), 129.4 (Ar-C), 129.3 (2 x Ar-CH), 128.7 (2 x Ar-CH), 128.5 (2 x Ar-CH), 128.4 (3 x Ar-CH), 127.9 (2 x Ar-CH), 127.7 (Ar-CH), 126.8 (Ar-CH), 124.0 (Ar-CH), 123.0 (Ar-CH), 117.9 (Ar-CH), 115.7 (Ar-CH), 111.5 (Ar-C), 84.0 (-OCR<sub>3</sub>), 73.4 (-OCH<sub>2</sub>), 70.8 (3 x -OCH<sub>2</sub>), 70.7 (-OCH<sub>2</sub>), 70.3 (-OCH<sub>2</sub>), 69.5 (-OCH<sub>2</sub>), 67.9 (-OCH<sub>2</sub>), 51.3 (-CH), 49.3 (-NCH<sub>2</sub>), 38.5 (-CH<sub>2</sub>), 32.2 (-COCH<sub>2</sub>), 28.5 (3C, -C(CH<sub>3</sub>)<sub>3</sub>), 14.2 (-CH<sub>3</sub>). HRMS (ESI) exact mass calculated for C<sub>46</sub>H<sub>55</sub>N<sub>3</sub>O<sub>8</sub>Na [M+Na]<sup>+</sup> m/z 800.3881, found m/z 800.3843. IR (thin film) 2927, 1730, 1649, 1595. [α]<sub>D</sub><sup>16.9°C</sup> +14.70 (*c* = 1.00, CHCl<sub>3</sub>).



2.56

**2.56.** Prepared according to a modified literature procedure.<sup>[41]</sup> To a stirred suspension of 10% palladium on carbon (21 mg, 0.014 mmol, 5.0 mol%) in methanol (14 mL, 0.02 M) under argon atmosphere was added benzyl ether **2.55** (210 mg, 0.270 mmol, 1 equiv.) at room temperature. The flask was then evacuated and the suspension sparged with hydrogen gas for 5 minutes and then stirred at room temperature under a hydrogen atmosphere for 5 hours. The hydrogen was then removed under reduced pressure and the suspension sparged with argon three times. The suspension was then filtered through a pad of celite (100 g) in dichloromethane (100 mL) and the celite was washed with dichloromethane (300 mL). The organic phase was then concentrated *in vacuo* generating the title compound **2.56** (195 mg, 0.270 mmol, quantitative).

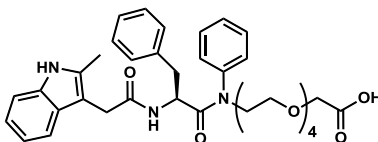
<sup>1</sup>H NMR (400 MHz, CDCl<sub>3</sub>) δ 8.11 (1H, dd, *J* = 8.1, 1.0, Ar-CH), 7.40–7.33 (3H, m, 3 x Ar-CH), 7.33–7.20 (2H, m, 2 x Ar-CH), 7.18 (1H, td, *J* = 7.4, 1.1, Ar-CH), 7.12 (1H, tt, *J* = 7.4, 1.3, Ar-CH), 7.09–7.01 (4H, m, 4 x Ar-CH), 6.63 (2H, d, *J* = 7.0, 2 x Ar-CH), 6.13 (1H, d, *J* = 8.2, -CONH), 4.70 (1H, td, *J* = 7.8, 6.3, -CH), 3.80 (2H, t, *J* = 6.0, -NCH<sub>2</sub>), 3.70–3.65 (2H, m, -OCH<sub>2</sub>), 3.63–3.49 (12H, m, 6 x -OCH<sub>2</sub>), 3.54 (1H, d, *J* = 16.5, -COCH<sub>2</sub>), 3.48 (1H, d, *J* = 16.9, -COCH<sub>2</sub>), 2.76 (1H, dd, *J* = 13.5, 6.3, -CH<sub>2</sub>), 2.52 (1H, dd, *J* = 13.5, 7.5, -CH<sub>2</sub>), 2.46 (3H, s, -CH<sub>3</sub>), 1.70 (9H, s, -C(CH<sub>3</sub>)<sub>3</sub>).  
<sup>13</sup>C NMR (101 MHz, CDCl<sub>3</sub>) δ 171.4 (-CONR<sub>2</sub>), 169.6 (-CONH), 150.6 (-NCOOR), 141.3 (Ar-C), 136.1 (Ar-C), 135.8 (Ar-C), 135.6 (Ar-C), 129.7 (2 x Ar-CH), 129.4 (Ar-C), 129.2 (2 x Ar-CH), 128.6 (2 x Ar-CH), 128.4 (Ar-CH), 128.3 (2 x Ar-CH), 126.8 (Ar-CH), 123.9 (Ar-CH), 122.9 (Ar-CH), 117.9 (Ar-CH), 115.6 (Ar-CH), 111.5 (Ar-C), 83.9 (-OCR<sub>3</sub>), 72.6 (-OCH<sub>2</sub>), 70.7 (-OCH<sub>2</sub>), 70.6 (-OCH<sub>2</sub>), 70.4 (-OCH<sub>2</sub>), 70.2 (-OCH<sub>2</sub>), 67.8 (-OCH<sub>2</sub>), 61.8 (-CH<sub>2</sub>OH), 51.3 (-CH), 49.2 (-NCH<sub>2</sub>), 38.4 (-CH<sub>2</sub>), 32.1 (-COCH<sub>2</sub>), 28.4 (3C, -C(CH<sub>3</sub>)<sub>3</sub>), 14.1 (-CH<sub>3</sub>). HRMS (ESI) exact mass calculated for C<sub>39</sub>H<sub>49</sub>N<sub>3</sub>O<sub>8</sub>Na [M+Na]<sup>+</sup> *m/z* 710.3412, found *m/z* 710.3383. IR (thin film) 2926, 1728, 1643, 1595.



2.57

**2.57.** Prepared according to a modified literature procedure.<sup>[41]</sup> To oven dried glassware cooled under vacuum and flushed with argon was added a solution of alcohol **2.56** (195 mg, 0.280 mmol, 1 equiv.) in tetrahydrofuran (0.90 mL, 0.35 M) and the solution was cooled to  $-78$  °C. To this was added a 2 M solution of sodium bis(trimethylsilyl)amide in tetrahydrofuran (51  $\mu$ L, 0.56 mmol, 2 equiv.) and the resulting mixture was stirred at  $-78$  °C for 15 minutes. To this was added *tert*-butyl bromoacetate (40  $\mu$ L, 0.28 mmol, 1 equiv.) and the resulting reaction mixture was allowed to warm, to room temperature and stirred for an additional 4 hours. To this was added water (3 mL) and dichloromethane (10 mL) and the aqueous phase was extracted with dichloromethane (3 x 10 mL). The combined organic phases were washed with brine (10 mL), dried with magnesium sulphate, filtered and concentrated *in vacuo* generating a crude mass of 248 mg. Purification by column chromatography on silica gel using an eluent of 5% to 30% acetone in dichloromethane yielded the title compound **2.56** (90 mg, 0.11 mmol, 40%).

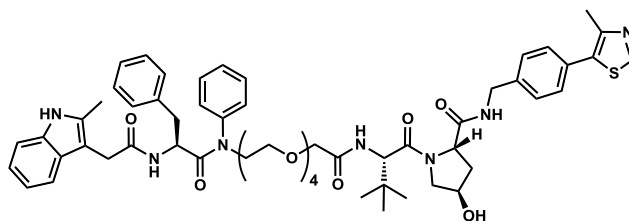
$^1\text{H}$  NMR (500 MHz,  $\text{CDCl}_3$ )  $\delta$  8.11 (1H, d,  $J = 8.3$ , Ar-CH), 7.39–7.32 (3H, m, 3 x Ar-CH), 7.30 (1H, d,  $J = 7.7$ , Ar-CH), 7.25 (1H, t,  $J = 7.4$ , Ar-CH), 7.19 (1H, t,  $J = 7.4$ , Ar-CH), 7.12 (1H, t,  $J = 7.4$ , Ar-CH), 7.09–7.00 (4H, m, 4 x Ar-CH), 6.63 (2H, d,  $J = 7.2$ , 2 x Ar-CH), 6.07 (1H, d,  $J = 8.2$ , -CONH), 4.71 (1H, td,  $J = 7.2$ , -CH), 3.99 (2H, s, -COCH<sub>2</sub>), 3.85 (1H, dt,  $J = 13.7, 5.8$ , -NCH<sub>2</sub>), 3.73 (1H, dt,  $J = 13.2, 6.0$ , -NCH<sub>2</sub>), 3.69–3.45 (16H, m, -COCH<sub>2</sub>, 7 x -OCH<sub>2</sub>), 2.75 (1H, dd,  $J = 13.5, 6.3$ , -CH<sub>2</sub>), 2.51 (1H, dd,  $J = 13.5, 7.4$ , CH<sub>2</sub>), 2.46 (3H, s, -CH<sub>3</sub>), 1.70 (9H, s, -C(CH<sub>3</sub>)<sub>3</sub>), 1.46 (9H, s, -C(CH<sub>3</sub>)<sub>3</sub>).  $^{13}\text{C}$  NMR (126 MHz,  $\text{CDCl}_3$ )  $\delta$  171.3 (-CONR<sub>2</sub>), 169.8 (-COOR), 169.5 (-CONH), 150.6 (-NCOOR), 141.4 (Ar-C), 136.1 (Ar-C), 135.9 (Ar-C), 135.6 (Ar-C), 129.7 (2 x Ar-CH), 129.4 (Ar-C), 129.2 (2 x Ar-CH), 128.6 (2 x Ar-CH), 128.4 (Ar-CH), 128.3 (2 x Ar-CH), 126.8 (Ar-CH), 123.9 (Ar-CH), 122.9 (Ar-CH), 117.9 (Ar-CH), 115.6 (Ar-CH), 111.5 (Ar-C), 84.0 (-OCR<sub>3</sub>), 81.6 (-OCR<sub>3</sub>), 70.8 (-OCH<sub>2</sub>), 70.7 (3 x -OCH<sub>2</sub>), 70.6 (-OCH<sub>2</sub>), 70.2 (-OCH<sub>2</sub>), 69.1 (-COCH<sub>2</sub>), 67.9 (-OCH<sub>2</sub>), 51.3 (-CH), 49.3 (-NCH<sub>2</sub>), 38.4 (-CH<sub>2</sub>), 32.2 (-COCH<sub>2</sub>), 28.4 (3C, -C(CH<sub>3</sub>)<sub>3</sub>), 28.2 (3C, -C(CH<sub>3</sub>)<sub>3</sub>), 14.1 (-CH<sub>3</sub>). HRMS (ESI) exact mass calculated for C<sub>45</sub>H<sub>59</sub>N<sub>3</sub>O<sub>10</sub>Na [M+Na]<sup>+</sup> m/z 824.4093, found m/z 824.4057. IR (thin film) 2922, 1728, 1643, 1595.



2.58

**2.58.** Prepared according to a modified literature procedure.<sup>[48]</sup> To a stirred solution of *tert*-butyl carbamate **2.57** (37 mg, 0.046 mmol, 1 equiv.) in dichloromethane (0.45 mL, 0.1 M) was added trifluoroacetic acid (0.45 mL) and the resulting solution was stirred at room temperature for 1 hour. Volatiles were removed *in vacuo* and dichloromethane (2 mL) was added, followed by *in vacuo* concentration (three times) generating the title compound **2.58** (39 mg). The crude material was used without further purification.

HRMS (ESI) exact mass calculated for C<sub>36</sub>H<sub>43</sub>N<sub>3</sub>O<sub>8</sub>Na [M+Na]<sup>+</sup> m/z 668.2942, found m/z 668.2917. IR (thin film) 1728, 1643, 1581.



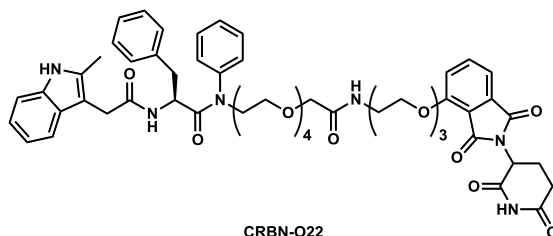
VHL-13

**VHL-13.** Prepared according to a modified literature procedure.<sup>[109]</sup> To a stirred solution of acid **2.58** (30 mg, 0.047 mmol, 1 equiv.) in *N,N*-dimethylformamide (0.1 mL, 0.4 M) was added amine **VHL-1** (21 mg, 0.047 mmol, 1 equiv.), HATU (18 mg, 0.047 mmol, 1 equiv.) and *N,N*-diisopropylethylamine (50  $\mu$ L, 0.28 mmol, 6 equiv.) and the resulting solution was stirred at room temperature for 48 hours. To the crude mixture was added dichloromethane (2 mL) and half saturated aqueous sodium hydrogen carbonate solution (2 mL) and the resultant phases were separated. The aqueous phase was extracted with dichloromethane (3 x 5 mL) and the combined organic phases washed with 5% aqueous lithium chloride solution (3 x 5 mL). The combined organic phases were dried with magnesium sulphate, filtered and concentrated *in vacuo* affording a crude mass of 76 mg. Purification by column chromatography on silica gel using an eluent of 50% to 100% acetone in dichloromethane afforded the title compound **VHL-13** (36 mg, 0.034 mmol, 72%). Further purification by reverse phase preparative HPLC using a gradient of 20% to 55% acetonitrile in water over 10 minutes followed by 55% to 80% acetonitrile over 35 minutes eluted the title compound with a retention time of 23.3–24.5 minutes. The product fraction was lyophilised generating the title compound **VHL-13** as a white powder (15 mg, 0.014 mmol, 30%).

Spectra were complicated by the presence of rotamers (conformational isomers). Variable temperature <sup>1</sup>H NMR at 25 °C, 35 °C and 55 °C showed the convergence of complicated peaks towards their expected multiplicities.

<sup>1</sup>H NMR (500 MHz, CDCl<sub>3</sub>)  $\delta$  8.87 (1H, s, -SCHN), 8.59–8.49 (1H, m, Ar-NH), 7.47–7.27 (10H, m, 10 x Ar-CH), 7.12 (1H, ddd,  $J = 7.4, 7.3, 1.4$ , Ar-CH), 7.12 (1H, t,  $J = 7.4$ , Ar-CH), 7.09–6.87 (4H, m, 4 x Ar-CH), 6.63 (1H, d,  $J = 6.9$ , 2 x Ar-CH), 6.62 (1H, d,  $J = 6.9$ , 2 x Ar-CH), 6.31 (1H, d,  $J = 8.0$ , -CONH), 4.74–4.63 (2H, m, 2 x -CH), 4.59–4.47 (2H, m, -CH, -NHC<sub>2</sub>), 4.43 (1H, br s, -OCH), 4.35 (0.5H, dd,  $J = 15.1, 6.5$ , -NCH<sub>2</sub>), 4.33 (0.5H, dd,  $J = 15.1, 6.5$ , -NCH<sub>2</sub>), 4.04 (1H, t,  $J = 10.3$ , -OCH<sub>2</sub>), 4.02 (0.5H, d,  $J = 15.7$ , -NCH<sub>2</sub>), 3.99 (0.5H, d,  $J = 15.7$ , -NCH<sub>2</sub>), 3.94 (0.5H, d,  $J = 15.7$ , -NCH<sub>2</sub>), 3.90 (0.5H, d,  $J = 15.7$ , -NCH<sub>2</sub>), 3.83–3.67 (2H, m, -NCH<sub>2</sub>), 3.64–3.43 (17H, m, 8 x -OCH<sub>2</sub>, -OCH<sub>2</sub>), 2.73 (1H, dd,  $J = 13.5, 6.4$ , -CH<sub>2</sub>), 2.71 (1H, dd,  $J = 13.6, 6.3$ ,

-CH<sub>2</sub>), 2.52 (1.5H, s, -CH<sub>3</sub>), 2.52 (1.5H, s, -CH<sub>3</sub>), 2.51–2.37 (2H, m, -CH<sub>2</sub>, -CH<sub>2</sub>), 2.26 (1.5H, s, -CH<sub>3</sub>), 2.25 (1.5H, s, -CH<sub>3</sub>), 2.12 (0.5H, dd, *J* = 13.5, 7.8, -CH<sub>2</sub>), 2.11 (0.5H, dd, *J* = 13.5, 7.8, -CH<sub>2</sub>), 0.97 (9H, s, -C(CH<sub>3</sub>)<sub>3</sub>). <sup>13</sup>C NMR (126 MHz, CDCl<sub>3</sub>) δ 171.6 (2 x -CONR<sub>2</sub>), 171.5 (-CONH), 171.4 (2 x -CONH), 171.3 (-CONH), 171.2 (-CONH), 170.8 (-CONR<sub>2</sub>), 170.7 (-CONR<sub>2</sub>), 151.5 (-SCHN), 146.9 (Ar-C), 141.1 (Ar-C), 139.0 (2 x Ar-C), 136.1 (Ar-C), 136.0 (Ar-C), 135.5 (Ar-C), 133.7 (2 x Ar-C), 132.9 (Ar-C), 129.9 (2 x Ar-C), 129.8 (2 x Ar-CH), 129.6 (2 x Ar-CH), 129.3 (4 x Ar-CH), 128.6 (2 x Ar-CH), 128.4 (5 x Ar-CH), 128.3 (Ar-C), 126.9 (Ar-CH), 121.6 (Ar-CH), 119.8 (Ar-CH), 117.9 (Ar-CH), 117.8 (Ar-CH), 110.7 (Ar-CH), 110.6 (Ar-CH), 104.2 (Ar-C), 71.2 (-OCH<sub>2</sub>), 71.1 (-OCH<sub>2</sub>), 70.7 (2 x -OCH<sub>2</sub>), 70.6 (6 x -OCH<sub>2</sub>), 70.4 (2 x -NCH<sub>2</sub>), 70.2 (2 x -OCH, 2 x -OCH<sub>2</sub>), 67.6 (-COCH<sub>2</sub>), 58.8 (-CH), 57.3 (2 x -CH), 56.9 (2 x -OCH<sub>2</sub>), 51.7 (-CH), 51.6 (-CH), 49.2 (-NCH<sub>2</sub>), 43.3 (2 x -NCH<sub>2</sub>), 38.4 (-CH<sub>2</sub>), 38.3 (-CH<sub>2</sub>), 36.4 (-CH<sub>2</sub>), 36.3 (-CH<sub>2</sub>), 35.3 (2 x -CR<sub>3</sub>), 32.0 (2 x -COCH<sub>2</sub>), 26.5 (3C, -C(CH<sub>3</sub>)<sub>3</sub>), 15.3 (-CH<sub>3</sub>), 11.6 (-CH<sub>3</sub>). HRMS (ESI) exact mass calculated for C<sub>58</sub>H<sub>71</sub>N<sub>7</sub>O<sub>10</sub>SNa [M+Na]<sup>+</sup> *m/z* 1080.4875, found *m/z* 1080.4833. IR (thin film) 2916, 1730, 1656, 1595.

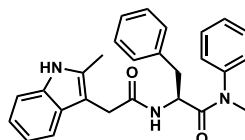


**CRBN-O22.** Prepared according to a modified literature procedure.<sup>[109]</sup> To a stirred solution of acid **2.58** (36 mg, 0.056 mmol, 1 equiv.) in *N,N*-dimethylformamide (0.13 mL, 0.4 M) was added racemic amine TFA salt **2.49** (31 mg, 0.056 mmol, 1 equiv.), HATU (22 mg, 0.056 mmol, 1 equiv.) and *N,N*-diisopropylethylamine (78  $\mu$ L, 0.45 mmol, 8 equiv.) and the resulting solution was stirred at room temperature for 48 hours. To the crude mixture was added dichloromethane (3 mL) and half saturated aqueous sodium hydrogen carbonate solution (3 mL) and the resultant phases were separated. The aqueous phase was extracted with dichloromethane (3 x 5 mL) and the combined organic phases washed with 5% aqueous lithium chloride solution (3 x 5 mL). The combined organic phases were dried with magnesium sulphate, filtered and concentrated *in vacuo* affording a crude mass of 137 mg. Purification by column chromatography on silica gel using an eluent of 30% to 100% acetone in dichloromethane afforded the title compound **CRBN-O22** (50 mg, 0.048 mmol, 87%). Further purification by reverse phase preparative HPLC using a gradient of 20% to 50% acetonitrile in water over 10 minutes followed by 50% to 100% acetonitrile over 60 minutes eluted the title compound with a retention time of 27.5–27.9 minutes. The product fraction was lyophilised generating the title compound **CRBN-O22** as a white powder (15 mg, 0.015 mmol, 27%).

Spectra were complicated by the presence of rotamers (conformational isomers). Variable temperature <sup>1</sup>H NMR at 25 °C, 35 °C and 55 °C showed the convergence of complicated peaks towards their expected multiplicities.

<sup>1</sup>H NMR (400 MHz, CDCl<sub>3</sub>)  $\delta$  9.00 (0.5H, s, -CONHCO), 8.94 (0.5H, s, -CONHCO), 8.42 (1H, s, Ar-NH), 7.66 (0.5H, dd,  $J = 8.5, 7.3$ , Ar-H), 7.65 (0.5H, dd,  $J = 8.5, 7.3$ , Ar-CH), 7.46 (0.5H, d,  $J = 7.3$ , Ar-CH), 7.45 (0.5H, d,  $J = 7.3$ , Ar-CH), 7.40–7.30 (4H, m, 4 x Ar-CH), 7.31–7.17 (3H, m, 3 x Ar-CH), 7.15–6.96 (7H, m, 5 x Ar-CH, -CONH), 6.69–6.62 (2H, m, 2 x Ar-CH), 6.41 (0.5H, d,  $J = 8.4$ , Ar-CH), 6.38 (0.5H, d,  $J = 8.4$ , Ar-CH), 4.92 (0.5H, dd,  $J = 9.5, 7.5$ , -CH), 4.91 (0.5H, dd,  $J = 9.5, 7.4$ , -CH), 4.69 (1H, ddd,  $J = 7.3, 7.3, 7.3$ , -CH), 4.34–4.24 (2H, m, Ar-OCH<sub>2</sub>), 3.96 (2H, s, -COCH<sub>2</sub>), 3.92–3.87 (2H, m, -OCH<sub>2</sub>), 3.82–3.69 (4H, m, -NCH<sub>2</sub>, -OCH<sub>2</sub>), 3.67–3.40 (20H, m, -COCH<sub>2</sub>, 9 x -OCH<sub>2</sub>), 3.49–3.44 (2H, m, -NCH<sub>2</sub>), 2.85–2.70 (3H, m, -CH<sub>2</sub>, -CH<sub>2</sub>),

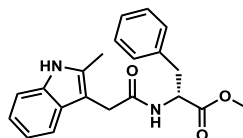
-CH<sub>2</sub>), 2.69–2.59 (1H, m, -CH<sub>2</sub>), 2.52 (0.5H, dd, *J* = 13.2, 7.6, -CH<sub>2</sub>), 2.51 (0.5H, dd, *J* = 13.2, 7.6, -CH<sub>2</sub>), 2.25 (1.5H, s, -CH<sub>3</sub>), 2.24 (1.5H, s, -CH<sub>3</sub>), 2.13–2.01 (1H, m, -CH<sub>2</sub>). <sup>13</sup>C NMR (126 MHz, CDCl<sub>3</sub>) δ 171.7 (2 x -CONR<sub>2</sub>), 171.4 (2 x -CONH), 171.2 (-CONH), 171.1 (-CONH), 170.4 (-CONH), 168.5 (-CONH), 167.2 (2 x -CONR<sub>2</sub>), 165.8 (2 x -CONR<sub>2</sub>), 156.5 (Ar-C), 141.3 (Ar-C), 136.6 (2 x Ar-CH), 136.3 (2 x Ar-C), 135.5 (Ar-C), 135.4 (Ar-C), 133.9 (Ar-C), 133.6 (2 x Ar-C), 129.8 (2 x Ar-CH), 129.4 (4 x Ar-CH), 128.6 (Ar-CH), 128.5 (2 x Ar-C, 2 x Ar-CH), 128.3 (4 x Ar-CH), 126.8 (Ar-CH), 126.7 (Ar-CH), 121.5 (2 x Ar-CH), 119.8 (Ar-CH), 119.5 (Ar-CH), 119.4 (Ar-CH), 118.0 (Ar-CH), 117.9 (Ar-CH), 117.4 (Ar-C), 116.3 (Ar-CH), 110.6 (Ar-CH), 110.5 (Ar-CH), 104.5 (2 x Ar-C), 71.3 (-OCH<sub>2</sub>), 71.0 (2 x -OCH<sub>2</sub>), 70.6 (3C, -COCH<sub>2</sub>, 2 x -OCH<sub>2</sub>), 70.5 (-OCH<sub>2</sub>), 70.3 (2 x -OCH<sub>2</sub>), 70.1 (2 x -OCH<sub>2</sub>), 69.8 (-OCH<sub>2</sub>), 69.4 (2 x -OCH<sub>2</sub>), 67.7 (-OCH<sub>2</sub>), 67.6 (-OCH<sub>2</sub>), 51.6 (-CH), 51.5 (-CH), 49.3 (-CH), 49.2 (-NCH<sub>2</sub>), 49.1 (-NCH<sub>2</sub>), 38.8 (2 x -NCH<sub>2</sub>), 38.4 (-CH<sub>2</sub>), 38.3 (-CH<sub>2</sub>), 32.1 (2 x -COCH<sub>2</sub>), 31.5 (-COCH<sub>2</sub>), 31.4 (-COCH<sub>2</sub>), 22.7 (-CH<sub>2</sub>), 11.7 (-CH<sub>3</sub>), 11.6 (-CH<sub>3</sub>). HRMS (ESI) exact mass calculated for C<sub>55</sub>H<sub>64</sub>N<sub>6</sub>O<sub>14</sub>Na [M+Na]<sup>+</sup> m/z 1055.4373, found m/z 1055.4403. IR (thin film) 2906, 1769, 1713, 1653, 1531.



Natural PF74

Natural **PF74**. Prepared according to a modified literature procedure.<sup>[111]</sup> To a stirred solution of acid **2.11** (100 mg, 0.300 mmol, 1 equiv.) in *N,N*-dimethylformamide (0.3 mL, 0.9 M) was added *N*-methylaniline (49  $\mu$ L, 0.45 mmol, 1.5 equiv.), HATU (171 mg, 0.450 mmol, 1.5 equiv.) and *N,N*-diisopropylethylamine (0.11 mL, 0.60 mmol, 2 equiv.) and the resulting solution was heated to 65 °C and stirred for 48 hours. To the reaction mixture was added dichloromethane (10 mL) and half saturated aqueous sodium hydrogen carbonate solution (10 mL) and the aqueous phase was extracted with dichloromethane (3 x 15 mL). The combined organic phases were washed with 5% aqueous lithium chloride solution (6 x 15 mL), dried over magnesium sulphate, filtered and concentrated *in vacuo* affording a crude mass of 197 mg. Purification by column chromatography on silica gel using an eluent of 1% to 5% ethanol in dichloromethane afforded the title compound natural **PF74** (63 mg, 0.15 mmol, 49%).

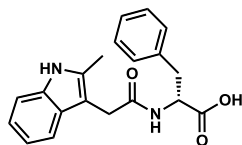
<sup>1</sup>H NMR (400 MHz, CDCl<sub>3</sub>)  $\delta$  8.26 (1H, s, Ar-NH), 7.39–7.31 (4H, m, 4 x Ar-CH), 7.26 (1H, d, *J* = 8.0, Ar-CH), 7.18–7.04 (5H, m, 5 x Ar-CH), 6.97–6.89 (2H, m, 2 x Ar-CH), 6.71–6.65 (2H, m, 2 x Ar-CH), 6.22 (1H, d, *J* = 8.3, -CONH), 4.81 (1H, ddd, *J* = 8.2, 6.9, 6.9, -CH), 3.59 (1H, s, -COCH<sub>2</sub>), 3.58 (1H, s, -COCH<sub>2</sub>), 3.17 (3H, s, -NCH<sub>3</sub>), 2.74 (1H, dd, *J* = 13.3, 6.9, -CH<sub>2</sub>), 2.54 (1H, dd, *J* = 13.3, 7.0, -CH<sub>2</sub>), 2.26 (3H, s, -CH<sub>3</sub>). <sup>13</sup>C NMR (101 MHz, CDCl<sub>3</sub>)  $\delta$  171.4 (-CONR<sub>2</sub>), 170.9 (-CONH), 142.6 (Ar-C), 136.2 (Ar-C), 135.5 (2 x Ar-C), 129.9 (2 x Ar-CH), 129.3 (2 x Ar-CH), 128.4 (Ar-C, 2 x Ar-CH), 128.2 (Ar-CH), 127.5 (2 x Ar-CH), 126.8 (Ar-CH), 121.6 (Ar-CH), 119.9 (Ar-CH), 117.9 (Ar-CH), 110.6 (Ar-CH), 104.6 (Ar-C), 51.2 (-CH), 38.9 (-CH<sub>2</sub>), 37.8 (-NCH<sub>3</sub>), 32.3 (-COCH<sub>2</sub>), 11.7 (-CH<sub>3</sub>). HRMS (ESI) exact mass calculated for C<sub>27</sub>H<sub>27</sub>N<sub>3</sub>O<sub>2</sub>Na [M+Na]<sup>+</sup> *m/z* 448.1995, found *m/z* 448.1977. IR (thin film) 2924, 1638, 1595. Chiral HPLC (OD-H, 7% *i*-PrOH in *n*-hexane, 1 mLmin<sup>-1</sup>,  $\lambda$  208 nm) *t*<sub>Rnatural</sub> = 39.040 min (55.6%), *t*<sub>Runnatural</sub> = 49.739 min (44.4%). [ $\alpha$ ]<sub>D</sub><sup>19.8</sup> +1.40 (*c* = 1.00, CHCl<sub>3</sub>). Preparative chiral HPLC purified (*S*)-**PF74** (OD-H, 7% *i*-PrOH in *n*-hexane, 1 mLmin<sup>-1</sup>,  $\lambda$  208 nm) *t*<sub>Rnatural</sub> = 32.847 min (99.2%), *t*<sub>Runnatural</sub> = 41.995 min (0.8%).



*Epi-2.10*

***Epi-2.10***. Prepared according to a modified literature procedure.<sup>[111]</sup> To a stirred solution of 2-methyl-3-indoleacetic acid (500 mg, 2.64 mmol, 1 equiv.) in *N,N*-dimethylformamide (6.6 mL, 0.4 M) was added D-phenylalanine methyl ester hydrochloride (597 mg, 2.77 mmol, 1.05 equiv.), PyBOP (1.37 g, 2.64 mmol, 1 equiv.) and *N,N*-diisopropylethylamine (1.40 mL, 7.92 mmol, 3 equiv.) and the resulting solution was stirred at room temperature for 18 hours. The crude mixture was quenched with water (20 mL) and the resultant layers were separated. The aqueous phase was extracted with ethyl acetate (3 x 30 mL) and the combined organic phases washed with 5% aqueous lithium chloride solution (5 x 20 mL). The combined organic phases were dried with magnesium sulphate, filtered and concentrated *in vacuo* affording a crude mass of 968 mg. Purification by column chromatography on silica gel using an eluent of 10% to 20% ethyl acetate in dichloromethane afforded the title compound ***epi-2.10*** (719 mg, 2.05 mmol, 78%).

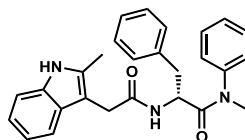
Spectroscopic data matched that of methyl ester **2.10**.



*Epi-2.11*

***Epi-2.11***. Prepared according to a modified literature procedure.<sup>[111]</sup> To a stirred solution of methyl ester ***epi-2.10*** (500 mg, 1.43 mmol, 1 equiv.) in tetrahydrofuran (6.1 mL, 0.2 M) and water (4.3 mL) was added a 1 M methanolic solution of sodium hydroxide (2.3 mL, 2.1 mmol, 1.5 equiv.) and the resulting solution was stirred vigorously at room temperature for 18 hours. To the reaction mixture was added water (20 mL) and the biphasic mixture was washed with dichloromethane (2 x 10 mL) to remove organic impurities. The aqueous phase was then acidified with 1 M aqueous hydrochloric acid (5 mL) forming a thick white precipitate. The aqueous phase was extracted with dichloromethane (3 x 20 mL) and the combined organic phases were dried with magnesium sulphate, filtered and concentrated *in vacuo* yielding the title compound ***epi-2.11*** (358 mg, 1.06 mmol, 74%). The compound was used without further purification.

Spectroscopic data matched that of acid **2.11**.

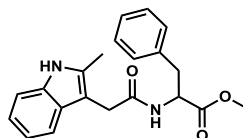


Unnatural **PF74**

Unnatural **PF74**. Prepared according to a modified literature procedure.<sup>[111]</sup> To a stirred solution of acid *epi*-**2.11** (100 mg, 0.300 mmol, 1 equiv.) in *N,N*-dimethylformamide (0.3 mL, 0.9 M) was added *N*-methylaniline (49  $\mu$ L, 0.45 mmol, 1.5 equiv.), HATU (171 mg, 0.450 mmol, 1.5 equiv.) and *N,N*-diisopropylethylamine (0.11 mL, 0.60 mmol, 2 equiv.) and the resulting solution was heated to 65 °C and stirred for 48 hours. To the reaction mixture was added dichloromethane (10 mL) and half saturated aqueous sodium hydrogen carbonate solution (10 mL) and the aqueous phase was extracted with dichloromethane (3 x 15 mL). The combined organic phases were washed with 5% aqueous lithium chloride solution (6 x 15 mL), dried over magnesium sulphate, filtered and concentrated *in vacuo* affording a crude mass of 105 mg. Purification by column chromatography on silica gel using an eluent of 1.5% to 4% ethanol in dichloromethane afforded the title compound unnatural **PF74** (70 mg, 0.17 mmol, 55%).

Spectroscopic data matched that of natural **PF74**.

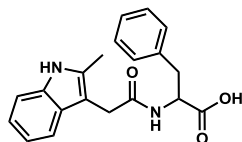
Chiral HPLC (OD-H, 7% *i*-PrOH in *n*-hexane, 1 mLmin<sup>-1</sup>,  $\lambda$  208 nm)  $t_{Rnatural} = 38.976$  min (34.6%),  $t_{Runnatural} = 49.312$  min (65.4%).  $[\alpha]_D^{20.2} -5.57$  ( $c = 1.00$ , CHCl<sub>3</sub>). Preparative chiral HPLC purified (*R*)-**PF74** (OD-H, 7% *i*-PrOH in *n*-hexane, 1 mLmin<sup>-1</sup>,  $\lambda$  208 nm)  $t_{Rnatural} = 33.498$  min (1.6%),  $t_{Runnatural} = 39.599$  min (98.4%).



**Rac-2.10**

**Rac-2.10.** Prepared according to a modified literature procedure.<sup>[111]</sup> To a stirred solution of 2-methyl-3-indoleacetic acid (500 mg, 2.64 mmol, 1 equiv.) in *N,N*-dimethylformamide (6.6 mL, 0.4 M) was added DL-phenylalanine methyl ester hydrochloride (597 mg, 2.77 mmol, 1.05 equiv.), PyBOP (1.37 g, 2.64 mmol, 1 equiv.) and *N,N*-diisopropylethylamine (1.40 mL, 7.92 mmol, 3 equiv.) and the resulting solution was stirred at room temperature for 18 hours. The crude mixture was quenched with water (20 mL) and the resultant layers were separated. The aqueous phase was extracted with ethyl acetate (3 x 30 mL) and the combined organic phases washed with 5% aqueous lithium chloride solution (5 x 20 mL). The combined organic phases were dried with magnesium sulphate, filtered and concentrated *in vacuo* affording a crude mass of 1.08 g. Purification by column chromatography on silica gel using an eluent of 10% to 100% ethyl acetate in dichloromethane afforded the title compound **rac-2.10** (925 mg, 2.64 mmol, quantitative)

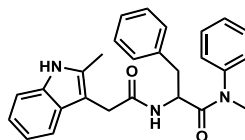
Spectroscopic data matched that of methyl ester **2.10**.



*Rac-2.11*

***Rac-2.11***. Prepared according to a modified literature procedure.<sup>[111]</sup> To a stirred solution of acid ***rac-2.10*** (500 mg, 1.43 mmol, 1 equiv.) in tetrahydrofuran (6.1 mL, 0.2 M) and water (4.3 mL) was added a 1 M methanolic solution of sodium hydroxide (2.3 mL, 2.1 mmol, 1.5 equiv.) and the resulting solution was stirred vigorously at room temperature for 18 hours. To the reaction mixture was added water (20 mL) and the biphasic mixture was washed with dichloromethane (2 x 10 mL) to remove organic impurities. The aqueous phase was then acidified with 1 M aqueous hydrochloric acid (5 mL) forming a thick white precipitate. The aqueous phase was extracted with dichloromethane (3 x 20 mL) and the combined organic phases were dried with magnesium sulphate, filtered and concentrated *in vacuo* yielding the title compound ***rac-2.11*** (491 mg, 1.46 mmol, quantitative). Compound was used without further purification.

Spectroscopic data matched that of acid **2.11**.

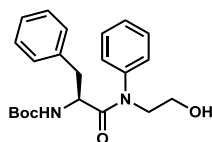


Racemic PF74

Racemic **PF74**. Prepared according to a modified literature procedure.<sup>[111]</sup> To a stirred solution of acid **rac-2.11** (100 mg, 0.300 mmol, 1 equiv.) in *N,N*-dimethylformamide (0.3 mL, 0.9 M) was added *N*-methylaniline (49  $\mu$ L, 0.45 mmol, 1.5 equiv.), HATU (171 mg, 0.45 mmol, 1.5 equiv.) and *N,N*-diisopropylethylamine (0.11 mL, 0.60 mmol, 2 equiv.) and the resulting solution was heated to 65 °C and stirred for 48 hours. To the crude mixture was added dichloromethane (10 mL) and half saturated aqueous sodium hydrogen carbonate solution (10 mL) and the aqueous phase was extracted with dichloromethane (3 x 15 mL). The combined organic phases were washed with 5% aqueous lithium chloride solution (6 x 15 mL), dried over magnesium sulphate, filtered and concentrated *in vacuo* affording a crude mass of 104 mg. Purification by column chromatography on silica gel using an eluent of 1.5% to 4% ethanol in dichloromethane afforded the title compound racemic **PF74** (69 mg, 0.16 mmol, 54%).

Spectroscopic data matched that of natural **PF74**.

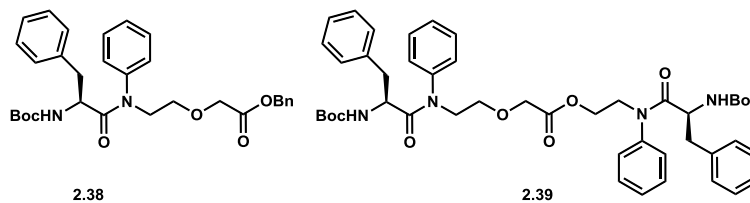
Chiral HPLC (OD-H, 7% *i*-PrOH in *n*-hexane, 1 mLmin<sup>-1</sup>,  $\lambda$  208 nm)  $t_{R\text{natural}} = 39.096$  min (52.8%),  $t_{R\text{unnatural}} = 49.675$  min (47.2%).  $[\alpha]_D^{19.2} +0.85$  ( $c = 1.00$ , CHCl<sub>3</sub>).



2.35

**2.35.** Prepared according to a modified literature procedure.<sup>[41]</sup> To a stirred suspension of 10% palladium on carbon (370 mg, 0.348 mmol, 5.0 mol%) in methanol (335 mL, 0.02 M) under argon atmosphere was added benzyl ether **2.34** (3.30 g, 6.70 mmol, 1 equiv.) at room temperature. The flask was then evacuated and the suspension sparged with hydrogen gas for 5 minutes and then stirred at room temperature under a hydrogen atmosphere for 5 hours. The hydrogen was then removed under reduced pressure and the suspension sparged with argon three times. The suspension was then filtered through a pad of celite (500 g) in dichloromethane (500 mL) and the celite washed with dichloromethane (800 mL). The organic phase was then concentrated *in vacuo* generating the title compound **2.35** (2.45 mg, 6.40 mmol, 96%).

<sup>1</sup>H NMR (400 MHz, CDCl<sub>3</sub>) δ 7.45–7.30 (4H, m, 4 x Ar-CH), 7.30–7.13 (3H, m, 3 x Ar-CH), 7.07–6.70 (3H, m, 3 x Ar-CH), 5.14 (1H, d, *J* = 6.5, -CONH), 4.42 (1H, dt, *J* = 7.3, 6.5, -CH), 4.03–3.88 (1H, m, -NCH<sub>2</sub>), 3.72 (2H, t, *J* = 4.8, -OCH<sub>2</sub>), 3.69–3.59 (1H, m, -NCH<sub>2</sub>), 2.91 (1H, dd, *J* = 13.2, 7.4, -CH<sub>2</sub>), 2.72 (1H, dd, *J* = 13.0, 6.9, -CH<sub>2</sub>), 1.38 (9H, s, -C(CH<sub>3</sub>)<sub>3</sub>). <sup>13</sup>C NMR (101 MHz, CDCl<sub>3</sub>) δ 173.8 (-CONR<sub>2</sub>), 155.0 (-NCOOR), 141.5 (Ar-C), 136.5 (Ar-C), 129.9 (2 x Ar-CH), 129.6 (2 x Ar-CH), 128.5 (3 x Ar-CH), 128.2 (2 x Ar-CH), 127.0 (Ar-CH), 79.8 (-OCR<sub>3</sub>), 61.1 (-OCH<sub>2</sub>), 53.5 (-NCH<sub>2</sub>), 52.9 (-CH), 39.6 (-CH<sub>2</sub>), 28.4 (3C, -C(CH<sub>3</sub>)<sub>3</sub>). HRMS (ESI) exact mass calculated for C<sub>22</sub>H<sub>28</sub>N<sub>2</sub>O<sub>4</sub>Na [M+Na]<sup>+</sup> *m/z* 407.1941, found *m/z* 407.1922. IR (thin film) 2923, 1711, 1650, 1595.

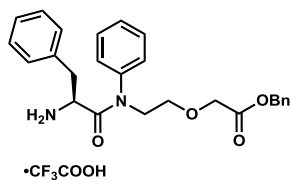


**2.38** and **2.39**. Prepared according to a modified literature procedure.<sup>[41]</sup> To oven dried glassware cooled under vacuum and flushed with argon was added sodium hydride (60% suspension in mineral oil) (14 mg, 0.34 mmol, 1.2 equiv.) and tetrahydrofuran (1.5 mL, 0.2 M) and alcohol **2.35** (106 mg, 0.280 mmol, 1 equiv.) and the mixture was stirred at 0 °C for 20 minutes. To this solution was slowly added benzyl bromoacetate (0.049 mL, 0.31 mmol, 1.1 equiv.) and the resulting solution was stirred at room temperature for 18 hours. To the reaction mixture was added water (10 mL) and ethyl acetate (20 mL) and the aqueous phase was extracted with ethyl acetate (3 x 20 mL). The combined organic phases were washed with brine (20 mL), dried with magnesium sulphate, filtered and concentrated *in vacuo* generating a crude mass of 147 mg. Purification by column chromatography on silica gel using an eluent of 33% to 100% ethyl acetate in dichloromethane yielded the title compound **2.38** (23 mg, 0.043 mmol, 15%), and the dialkylated **2.39** (19 mg, 0.023 mmol, 16%).

**2.38**.  $R_f = 0.52$  (50% ethyl acetate in petroleum ether).  $^1\text{H NMR}$  (400 MHz,  $\text{CDCl}_3$ )  $\delta$  7.40–7.27 (7H, m, 7 x Ar-CH), 7.23–7.15 (4H, m, 4 x Ar-CH), 7.07–6.80 (4H, m, 4 x Ar-CH), 5.17 (2H, s,  $-\text{OCH}_2$ ), 5.14 (1H, s,  $-\text{CONH}$ ), 4.46 (1H, dt,  $J = 8.0, 7.8$ ,  $-\text{CH}$ ), 4.08 (2H, s,  $-\text{COCH}_2$ ), 3.85 (2H, t,  $J = 5.8$ ,  $-\text{NCH}_2$ ), 3.68 (2H, t,  $J = 5.8$ ,  $-\text{OCH}_2$ ), 2.89 (1H, dd,  $J = 13.4, 6.9$ ,  $-\text{CH}_2$ ), 2.66 (1H, dd,  $J = 13.4, 7.0$ ,  $-\text{CH}_2$ ), 1.36 (9H, s,  $-\text{C}(\text{CH}_3)_3$ ).  $^{13}\text{C NMR}$  (101 MHz,  $\text{CDCl}_3$ )  $\delta$  172.1 ( $-\text{CONR}_2$ ), 170.1 ( $-\text{COOR}$ ), 154.8 ( $-\text{NCOOR}$ ), 141.4 (Ar-C), 136.7 (Ar-C), 135.5 (Ar-C), 129.7 (2 x Ar-CH), 129.6 (2 x Ar-CH), 129.5 (Ar-CH), 128.8 (2 x Ar-CH), 128.6 (3 x Ar-CH), 128.5 (2 x Ar-CH), 128.4 (2 x Ar-CH), 126.7 (Ar-CH), 79.5 ( $-\text{OCR}_3$ ), 68.5 ( $-\text{OCH}_2$ ), 68.3 ( $-\text{COCH}_2$ ), 66.7 ( $-\text{OCH}_2$ ), 52.6 ( $-\text{CH}$ ), 49.3 ( $-\text{NCH}_2$ ), 39.6 ( $-\text{CH}_2$ ), 28.4 (3C,  $-\text{C}(\text{CH}_3)_3$ ). HRMS (ESI) exact mass calculated for  $\text{C}_{31}\text{H}_{36}\text{N}_2\text{O}_6\text{Na}$   $[\text{M}+\text{Na}]^+$   $m/z$  555.2466, found  $m/z$  555.2451. IR (thin film) 2933, 1746, 1709, 1652, 1595.

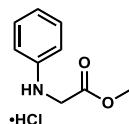
**2.39**.  $R_f = 0.23$  (50% ethyl acetate in petroleum ether).  $^1\text{H NMR}$  (400 MHz,  $\text{CDCl}_3$ )  $\delta$  7.33 (6H, s, 6 x Ar-CH), 7.24–7.12 (6H, m, 6 x Ar-CH), 7.05–6.78 (8H, m, 8 x Ar-CH), 5.26–5.15 (2H, m, 2 x  $-\text{CONH}$ ), 4.49–4.37 (2H, m, 2 x  $-\text{CH}$ ), 4.30–4.17 (2H, m,  $-\text{OCH}_2$ ), 4.06–3.94 (1H, m,  $-\text{NCH}_2$ ), 3.90 (2H, s,  $-\text{COCH}_2$ ), 3.90–3.69 (3H, m,  $-\text{NCH}_2$ ,  $-\text{NCH}_2$ ), 3.66–3.54 (2H, m,  $-\text{OCH}_2$ ), 2.94–2.83 (2H, m,  $-\text{CH}_2$ ,  $-\text{CH}_2$ ), 2.72–2.61 (2H, m,  $-\text{CH}_2$ ,  $-\text{CH}_2$ ), 1.39 (9H, s,  $-\text{C}(\text{CH}_3)_3$ ), 1.34 (9H, s,  $-\text{C}(\text{CH}_3)_3$ ).  $^{13}\text{C NMR}$

(101 MHz, CDCl<sub>3</sub>) δ 172.3 (-CONR<sub>2</sub>), 172.1 (-CONR<sub>2</sub>), 170.0 (-COOR), 154.9 (2 x -NCOOR), 141.2 (2 x Ar-C), 136.7 (2 x Ar-C), 129.9 (2 x Ar-CH), 129.8 (2 x Ar-CH), 129.6 (2 x Ar-CH), 129.5 (2 x Ar-CH), 128.6 (2 x Ar-CH), 128.5 (2 x Ar-CH), 128.4 (5 x Ar-CH), 128.3 (Ar-CH), 126.9 (Ar-CH), 126.7 (Ar-CH), 79.6 (-OCR<sub>3</sub>), 79.5 (-OCR<sub>3</sub>), 68.3 (-OCH<sub>2</sub>), 67.9 (-COCH<sub>2</sub>), 61.9 (-OCH<sub>2</sub>), 52.6 (2 x -CH), 49.1 (-NCH<sub>2</sub>), 48.5 (-NCH<sub>2</sub>), 39.7 (-CH<sub>2</sub>), 39.6 (-CH<sub>2</sub>), 28.4 (6C, 2 x -C(CH<sub>3</sub>)<sub>3</sub>). HRMS (ESI) exact mass calculated for C<sub>46</sub>H<sub>56</sub>N<sub>4</sub>O<sub>9</sub>Na [M+Na]<sup>+</sup> m/z 831.3940, found m/z 831.3958. IR (thin film) 2922, 1758, 1710, 1651, 1595.



**2.40**

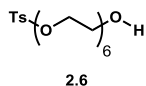
**2.40.** Prepared according to a modified literature procedure.<sup>[48]</sup> To a stirred solution of *tert*-butyl carbamate **2.38** (20 mg, 0.038 mmol, 1 equiv.) in dichloromethane (0.63 mL, 0.1 M) was added trifluoroacetic acid (0.63 mL) and the resulting solution was stirred at room temperature for 1 hour. Volatiles were removed *in vacuo* and dichloromethane (5 mL) was added, followed by *in vacuo* concentration (three times) generating the title compound **2.40** (35 mg). The crude material was used without further purification.



2.25

**2.25.** Prepared according to a modified literature procedure.<sup>[115]</sup> To a stirred suspension of *N*-phenylglycine (2.00 g, 13.2 mmol, 1 equiv.) in methanol (10 mL, 1.3 M) at 0 °C was added dropwise thionyl chloride (1.44 mL, 19.8 mmol, 1.5 equiv.) and the resulting mixture was stirred at 0°C for 15 minutes before being heated to reflux and stirred for six hours. The crude reaction mixture was then concentrated *in vacuo* and the remaining solid recrystallised from methanol and diethyl ether yielding the hydrochloride salt **2.25** (2.63g, 13.1 mmol, 99%).

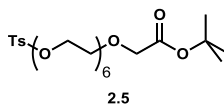
<sup>1</sup>H NMR (400 MHz, MeOD)  $\delta$  7.61–7.48 (5H, m, 5 x Ar-CH), 4.40 (2H, s, -COCH<sub>2</sub>), 3.86 (3H, s, -CH<sub>3</sub>). <sup>13</sup>C NMR (101 MHz, MeOD)  $\delta$  168.1 (-COOR), 136.8 (Ar-C), 131.4 (2 x Ar-CH), 130.7 (Ar-CH), 123.6 (2 x Ar-CH), 53.6 (-OCH<sub>3</sub>), 52.0 (-COCH<sub>2</sub>). HRMS (ESI) exact mass calculated for C<sub>9</sub>H<sub>11</sub>O<sub>2</sub>NNa [M+Na]<sup>+</sup> m/z 188.0682, found m/z 188.0685. IR (thin film) 2941, 1746, 1597. Melting point 150–154 °C.



**2.6.** Prepared according to a modified literature procedure.<sup>[110]</sup> To a stirred solution of hexaethylene glycol (5.0 mL, 20 mmol, 10 equiv.) in tetrahydrofuran (0.66 mL, 30 M) was added a solution of sodium hydroxide (120 mg, 3.00 mmol, 1.6 equiv.) in water (0.64 mL, 4.7 M) and the resulting solution was cooled to 0 °C and stirred rapidly for 20 minutes. To this mixture was added a solution of 4-toluenesulfonyl chloride (368 mg, 1.90 mmol, 1 equiv.) in tetrahydrofuran (3 mL, 0.6 M) and the resulting mixture was allowed to warm to room temperature under rapid stirring for 18 hours. To the reaction mixture was added water (50 mL) and dichloromethane (70 mL) and the aqueous phase was extracted with dichloromethane (3 x 70 mL). The combined organic phases were washed with brine (70 mL), dried over magnesium sulphate, filtered and concentrated *in vacuo* yielding a crude mass of 2.25 g. Purification by column chromatography on silica gel using an eluent of 0% to 10% methanol in dichloromethane yielded the title compound **2.6** (230 mg, 0.616 mmol, 32%). Analytical data observed were in accordance with literature values.<sup>[110]</sup>

<sup>1</sup>H NMR (400 MHz, CDCl<sub>3</sub>) δ 7.84–7.75 (2H, m, 2 x Ar-CH), 7.38–7.28 (2H, m, 2 x Ar-CH), 4.21–4.11 (2H, m, -TsOCH<sub>2</sub>), 3.81–3.52 (22H, m, 11 x -OCH<sub>2</sub>), 2.51 (1H, br s, -OH), 2.44 (3H, s, -CH<sub>3</sub>). HRMS (ESI) exact mass calculated for C<sub>19</sub>H<sub>32</sub>O<sub>9</sub>Na [M+Na]<sup>+</sup> m/z 459.1659, found m/z 459.1642. IR (thin film) 2870, 1599.





**2.5.** Prepared according to a modified literature procedure.<sup>[110]</sup> To a stirred solution of alcohol **2.4** (290 mg, 0.730 mmol, 1 equiv.) in dichloromethane (2.5 mL, 0.3 M) was added triethylamine (0.12 mL, 0.88 mmol, 1.2 equiv.) and the resulting solution was cooled to 0 °C and stirred rapidly for 20 minutes. To this mixture was added 4-toluenesulfonyl chloride (168 mg, 0.88 mmol, 1.2 equiv.) and the resulting mixture was allowed to warm to room temperature under rapid stirring for 18 hours. To the reaction mixture was added water (10 mL) and dichloromethane (20 mL) and the aqueous phase was extracted with dichloromethane (3 x 20 mL). The combined organic phases were washed with brine (20 mL), dried over magnesium sulphate, filtered and concentrated *in vacuo* yielding a crude mass of 370 mg. Purification by column chromatography on silica gel using an eluent of 50% ethyl acetate in dichloromethane yielded the title compound **2.5** (100 mg, 0.180 mmol, 25%). Analytical data observed were in accordance with literature values.<sup>[109]</sup>

<sup>1</sup>H NMR (400 MHz, CDCl<sub>3</sub>) δ 7.83–7.77 (2H, m, 2 x Ar-CH), 7.34 (2H, d, *J* = 7.9, 2 x Ar-CH), 4.18–4.13 (2H, m, -TsOCH<sub>2</sub>), 4.01 (2H, s, -COCH<sub>2</sub>), 3.75–3.60 (18H, m, 9 x -OCH<sub>2</sub>), 3.60–3.56 (4H, m, 2 x -OCH<sub>2</sub>), 2.45 (3H, s, -CH<sub>3</sub>), 1.47 (9H, s, -C(CH<sub>3</sub>)<sub>3</sub>).  
<sup>13</sup>C NMR (101 MHz, CDCl<sub>3</sub>) δ 169.7 (-COOR), 144.8 (Ar-C), 133.1 (Ar-C), 129.8 (2 x Ar-CH), 128.0 (2 x Ar-CH), 81.5 (-OCR<sub>3</sub>), 70.8 (-OCH<sub>2</sub>), 70.7 (-OCH<sub>2</sub>), 70.6 (7 x -OCH<sub>2</sub>), 70.5 (-OCH<sub>2</sub>), 69.2 (-OCH<sub>2</sub>), 69.1 (-OCH<sub>2</sub>), 68.7 (-OCH<sub>2</sub>), 28.1 (3C, -C(CH<sub>3</sub>)<sub>3</sub>), 21.6 (-CH<sub>3</sub>).

## References

- [1] Y. Seesao, M. Gay, S. Merlin, E. Viscogliosi, C. M. Aliouat-Denis, C. Audebert, *J. Microbiol. Methods* **2017**, *138*, 37–49.
- [2] M. S. Chan, *Parasitol. Today* **1997**, *13*, 438–43.
- [3] J. Horton, *Trends Parasitol.* **2003**, *19*, 527–31.
- [4] G. Stepek, D. J. Buttle, I. R. Duce, J. M. Behnke, *Int. J. Exp. Pathol.* **2006**, *87*, 325–41.
- [5] J. T. Jones, A. Haegeman, E. G. J. Danchin, H. S. Gaur, J. Helder, M. G. K. Jones, T. Kikuchi, R. Manzanilla-López, J. E. Palomares-Rius, W. M. L. Wesemael, et al., *Mol. Plant Pathol.* **2013**, *14*, 946–961.
- [6] S. Singh, B. Singh, A. P. Singh, *Procedia Environ. Sci.* **2015**, *29*, 215–216.
- [7] D. L. Coyne, L. Cortada, J. J. Dalzell, A. O. Claudius-Cole, S. Haukeland, N. Luambano, H. Talwana, *Annu. Rev. Phytopathol.* **2018**, *56*, 381–403.
- [8] J. M. Nicol, S. J. Turner, D. L. Coyne, L. den Nijs, S. Hockland, Z. T. Maafi, in *Genomics and Molecular Genetics of Plant-Nematode Interactions*, Springer Netherlands, Dordrecht, **2011**, pp. 21–43.
- [9] J. Charlier, S. M. Thamsborg, D. J. Bartley, P. J. Skuce, F. Kenyon, T. Geurden, H. Hoste, A. R. Williams, S. Sotiraki, J. Höglund, et al., *Transbound. Emerg. Dis.* **2018**, *65*, 217–234.
- [10] F. Roeber, A. R. Jex, R. B. Gasser, *Parasit. Vectors* **2013**, *6*, 153.
- [11] M. van der Voort, J. Charlier, L. Lauwers, J. Vercruyssen, G. Van Huylenbroeck, J. Van Meensel, *Prev. Vet. Med.* **2013**, *109*, 228–235.
- [12] T. Barragry, *N. Z. Vet. J.* **2011**, *32*, 161–164.
- [13] Q. A. McKellar, E. W. Scott, *J. Vet. Pharmacol. Ther.* **1990**, *13*, 223–247.
- [14] M. Abongwa, R. J. Martin, A. P. Robertson, *Acta Vet. Brno.* **2017**, *67*, 137–152.
- [15] E. Lacey, *Parasitol. Today* **1990**, *6*, 112–115.
- [16] R. Laing, V. Gillan, E. Devaney, *Trends Parasitol.* **2017**, *33*, 463–472.
- [17] World Health Organisation, *WHO Model List of Essential Medicines 19th List*,

**2015.**

- [18] D. H. Kwon, K. S. Yoon, J. M. Clark, S. H. Lee, *Insect Mol. Biol.* **2010**, *19*, 583–591.
- [19] D. M. Yates, A. J. Wolstenholme, *Int. J. Parasitol.* **2004**, *34*, 1075–1081.
- [20] R. E. Hibbs, E. Gouaux, *Nature* **2011**, *474*, 54–60.
- [21] R. J. Martin, J. R. Kusel, *Parasitology* **1992**, *104*, 549–555.
- [22] H. Mrozik, P. Eskola, M. H. Fisher, J. R. Egerton, S. Cifelli, D. A. Ostlind, *J. Med. Chem.* **1982**, *25*, 658–63.
- [23] A. J. Wolstenholme, A. T. Rogers, *Parasitology* **2005**, *131*, 85–95.
- [24] R. M. Kaplan, *Trends Parasitol.* **2004**, *20*, 477–81.
- [25] P. Köhler, *Int. J. Parasitol.* **2001**, *31*, 336–45.
- [26] M. Areskog, S. Sollenberg, A. Engström, G. von Samson-Himmelstjerna, J. Höglund, *Parasit. Vectors* **2014**, *7*, 13.
- [27] J. H. Gill, J. M. Redwin, J. A. Van Wyk, E. Lacey, *Int. J. Parasitol.* **1991**, *21*, 771–776.
- [28] A. I. Njue, J. Hayashi, L. Kinne, X. P. Feng, R. K. Prichard, *J. Neurochem.* **2004**, *89*, 1137–1147.
- [29] S. J. LeBlanc, K. D. Lissemore, D. F. Kelton, T. F. Duffield, K. E. Leslie, *J. Dairy Sci.* **2006**, *89*, 1267–1279.
- [30] P. J. Hotez, P. J. Brindley, J. M. Bethony, C. H. King, E. J. Pearce, J. Jacobson, *J. Clin. Invest.* **2008**, *118*, 1311–21.
- [31] C. Ménez, M. Alberich, D. Kansoh, A. Blanchard, A. Lespine, *Antimicrob. Agents Chemother.* **2016**, *60*, 4809–19.
- [32] D. J. France, G. Stepek, D. R. Houston, L. Williams, G. McCormack, M. D. Walkinshaw, A. P. Page, *Bioorg. Med. Chem. Lett.* **2015**, *25*, 5752–5755.
- [33] J. A. Dent, M. M. Smith, D. K. Vassilatis, L. Avery, *PNAS* **2000**, *97*, 2674–2679.
- [34] D. K. Vassilatis, J. P. Arena, R. H. Plasterk, H. A. Wilkinson, J. M. Schaeffer, D.

- F. Cully, L. H. Van der Ploeg, *J. Biol. Chem.* **1997**, 272, 33167–74.
- [35] A. P. Page, *Int. J. Parasitol.* **2018**, 48, 1035–1042.
- [36] N. S. Delany, D. L. Laughton, A. J. Wolstenholme, *Mol. Biochem. Parasitol.* **1998**, 97, 177–187.
- [37] S. Jagannathan, D. L. Laughton, C. L. Critten, T. M. Skinner, L. Horoszok, A. J. Wolstenholme, *Mol. Biochem. Parasitol.* **1999**, 103, 129–140.
- [38] W. Schafer, *Curr. Biol.* **2016**, 26, 955–959.
- [39] T. M. Werkhoven, R. van Nispen, J. Lugtenburg, *European J. Org. Chem.* **1999**, 1999, 2909–2914.
- [40] K. C. Nicolaou, M. W. Härter, J. L. Gunzner, A. Nadin, *Liebigs Ann.* **1997**, 1997, 1283–1301.
- [41] D. P. Bondeson, A. Mares, I. E. D. Smith, E. Ko, S. Campos, A. H. Miah, K. E. Mulholland, N. Routly, D. L. Buckley, J. L. Gustafson, et al., *Nat. Chem. Biol.* **2015**, 11, 611–617.
- [42] A. Loudet, K. Burgess, *Chem. Rev.* **2007**, 107, 4891–4932.
- [43] S. M. Crawford, A. Thompson, *Org. Lett.* **2010**, 12, 1424–1427.
- [44] J. Wang, M. Uttamchandani, J. Li, M. Hu, S. Q. Yao, C. M. Overall, O. Kleifeld, Y. Liu, M. P. Patricelli, B. F. Cravatt, et al., *Chem. Commun.* **2006**, 6, 3783–3785.
- [45] J. M. Schaeffer, H. Stiffey, **2000**, 295, 291–295.
- [46] M. Yu, J. K.-H. Wong, C. Tang, P. Turner, M. H. Todd, P. J. Rutledge, *Beilstein J. Org. Chem.* **2015**, 11, 37–41.
- [47] C. Gröst, T. Berg, R. Huisgen, V. V. Rostovtsev, L. G. Green, V. V. Fokin, K. B. Sharpless, C. W. Tornøe, C. Christensen, M. Meldal, et al., *Org. Biomol. Chem.* **2015**, 13, 3866–3870.
- [48] M. Braun, U. Hartnagel, E. Ravanelli, B. Schade, C. Böttcher, O. Vostrowsky, A. Hirsch, *European J. Org. Chem.* **2004**, 2004, 1983–2001.
- [49] S. Brenner, *Genetics* **1974**, 77, 71–94.

- [50] D. J. Bumbarger, S. Wijeratne, C. Carter, J. Crum, M. H. Ellisman, J. G. Baldwin, *J. Comp. Neurol.* **2009**, *512*, 271–281.
- [51] N. J. Yang, M. J. Hinner, *Methods Mol. Biol.* **2015**, *1266*, 29–53.
- [52] H. Pajouhesh, G. R. Lenz, *NeuroRX* **2005**, *2*, 541–553.
- [53] S.-H. Son, S. Daikoku, A. Ohtake, K. Suzuki, K. Kabayama, Y. Ito, O. Kanie, *Chem. Commun.* **2014**, *50*, 3010–3013.
- [54] B. Jolicoeur, W. D. Lubell, *Org. Lett.* **2006**, *8*, 6107–6110.
- [55] E. Redman, V. Grillo, G. Saunders, E. Packard, F. Jackson, M. Berriman, J. S. Gilleard, *Genetics* **2008**, *180*, 1877–87.
- [56] A. J. W. S. M. Williamson, B. Storey, S. Howell, K. M. Harper, R. M. Kaplan, *Mol. Biochem. Parasitol.* **2011**, *180*, 99–105.
- [57] S. R. Doyle, R. Laing, D. J. Bartley, C. Britton, U. Chaudhry, J. S. Gilleard, N. Holroyd, B. K. Mable, K. Maitland, A. A. Morrison, et al., *Genome Biol. Evol.* **2018**, *10*, 396–409.
- [58] C. J. O. Brien, Z. S. Nixon, A. J. Holohan, S. R. Kunkel, J. L. Tellez, B. J. Doonan, E. E. Coyle, F. Lavigne, L. J. Kang, K. C. Przeworski, *Chem. Eur. J.* **2013**, *19*, 15281–15289.
- [59] R. Bihovsky, I. Pendrak, *Bioorg. Med. Chem. Lett.* **1996**, *6*, 1541–1542.
- [60] J. M. Schaeffer, H. Stiffey, *Anal. Biochem.* **1989**, *177*, 291–295.
- [61] D. Guénard, S. Thoret, J. Dubois, M. T. Adeline, Q. Wang, F. Guéritte, *Bioorg. Med. Chem.* **2000**, *8*, 145–56.
- [62] P. Bean, *Clin. Infect. Dis.* **2005**, *41*, 96–100.
- [63] UNAIDS, *Global HIV and AIDS Statistics — 2019 Fact Sheet*, **2019**.
- [64] B. G. Brenner, M. A. Wainberg, D. Turner, *Expert Opin. Biol. Ther.* **2002**, *2*, 751–761.
- [65] S. G. Deeks, J. Overbaugh, A. Phillips, S. Buchbinder, *Nat. Rev. Dis. Prim.* **2015**, *1*, 15035.
- [66] L. Yu, V. Mohanram, O. E. Simonson, C. I. E. Smith, A.-L. Spetz, A. J.

Mohamed, *Biochem. Biophys. Res. Commun.* **2009**, 385, 100–105.

- [67] S. B. Laskey, R. F. Siliciano, *Nat. Rev. Microbiol.* **2014**, 12, 772–780.
- [68] World Health Organisation, *HIV DRUG RESISTANCE REPORT 2017*, Geneva, **2017**.
- [69] M. M. Zdanowicz, *Am. J. Pharm. Educ.* **2006**, 70, 100.
- [70] D. D. Richman, S. C. Morton, T. Wrin, N. Hellmann, S. Berry, M. F. Shapiro, S. A. Bozzette, *AIDS* **2004**, 18, 1393–1401.
- [71] H. S. Weinstock, I. Zaidi, W. Heneine, D. Bennett, J. G. Garcia-Lerma, J. M. Douglas, Jr., M. LaLota, G. Dickinson, S. Schwarcz, L. Torian, et al., *J. Infect. Dis.* **2004**, 189, 2174–2180.
- [72] P. S. Pennings, *Infect. Dis. Rep.* **2013**, 5, 5.
- [73] A. C. Lai, C. M. Crews, *Nat. Rev. Drug Discov.* **2017**, 16, 101–114.
- [74] M. K. Hellerstein, *Metab. Eng.* **2008**, 10, 1–9.
- [75] S. An, L. Fu, *EBioMedicine* **2018**, 36, 553–562.
- [76] C. M. Crews, *Chem. Biol.* **2010**, 17, 551–5.
- [77] G. M. Cooper, in *The Cell A Molecular Approach*, Sinauer Associates, Sunderland (MA), **2000**.
- [78] S. W. Lee, G. Dai, Z. Hu, X. Wang, J. Du, W. E. Mitch, *J. Am. Soc. Nephrol.* **2004**, 15, 1537–45.
- [79] B. Zhao, K. Bhuripanyo, J. Schneider, K. Zhang, H. Schindelin, D. Boone, J. Yin, *ACS Chem. Biol.* **2012**, 7, 2027–35.
- [80] G. M. Burslem, B. E. Smith, A. C. Lai, S. Jaime-Figueroa, D. C. McQuaid, D. P. Bondeson, M. Toure, H. Dong, Y. Qian, J. Wang, et al., *Cell Chem. Biol.* **2018**, 25, 67–77.
- [81] M. Zengerle, K.-H. Chan, A. Ciulli, *ACS Chem. Biol.* **2015**, 10, 1770–7.
- [82] P. M. Cromm, C. M. Crews, *Cell Chem. Biol.* **2017**, 24, 1181–1190.
- [83] B. E. Smith, S. L. Wang, S. Jaime-Figueroa, A. Harbin, J. Wang, B. D. Hamman, C. M. Crews, *Nat. Commun.* **2019**, 10, 131.

- [84] D. L. Buckley, I. V. Molle, P. C. Gareiss, H. S. Tae, J. Michel, D. J. Noblin, W. L. Jorgensen, A. Ciulli, C. M. Crews, *J. Am. Chem. Soc.* **2012**, *134*, 4465.
- [85] C. Galdeano, M. S. Gadd, P. Soares, S. Scaffidi, I. Van Molle, I. Birced, S. Hewitt, D. M. Dias, A. Ciulli, *J. Med. Chem.* **2014**, *57*, 8657.
- [86] T. Ito, H. Ando, T. Suzuki, T. Ogura, K. Hotta, Y. Imamura, Y. Yamaguchi, H. Handa, *Science (80-. )*. **2010**, *327*, 1345–1350.
- [87] A. Lopez-Girona, D. Mendy, T. Ito, K. Miller, A. K. Gandhi, J. Kang, S. Karasawa, G. Carmel, P. Jackson, M. Abbasian, et al., *Leukemia* **2012**, *26*, 2326.
- [88] E. Tokunaga, T. Yamamoto, E. Ito, N. Shibata, *Sci. Rep.* **2018**, *8*, 17131.
- [89] B. Knoche, G. Blaschke, *J. Chromatogr. A* **1994**, *666*, 235–240.
- [90] G. E. Winter, D. L. Buckley, J. Paulk, J. M. Roberts, A. Souza, S. Dhe-Paganon, J. E. Bradner, *Science* **2015**, *348*, 1376–81.
- [91] H.-T. Huang, D. Dobrovolsky, J. Paulk, G. Yang, E. L. Weisberg, Z. M. Doctor, D. L. Buckley, J.-H. Cho, E. Ko, J. Jang, et al., *Cell Chem. Biol.* **2018**, *25*, 88.
- [92] M. Schiedel, D. Herp, S. Hammelmann, S. Swyter, A. Lehotzky, D. Robaa, J. Oláh, J. Ovádi, W. Sippl, M. Jung, *J. Med. Chem.* **2018**, *61*, 482–491.
- [93] D. P. Bondeson, B. E. Smith, G. M. Burslem, A. D. Buhimschi, J. Hines, S. Jaime-Figueroa, J. Wang, B. D. Hamman, A. Ishchenko, C. M. Crews, *Cell Chem. Biol.* **2018**, *25*, 78–87.
- [94] A. C. Lai, M. Toure, D. Hellerschmied, J. Salami, S. Jaime-Figueroa, E. Ko, J. Hines, C. M. Crews, *Angew. Chemie Int. Ed.* **2016**, *55*, 807–810.
- [95] I. W. Hamley, *Biomacromolecules* **2014**, *15*, 1543–1559.
- [96] A. Zorba, C. Nguyen, Y. Xu, J. Starr, K. Borzilleri, J. Smith, H. Zhu, K. A. Farley, W. Ding, J. Schiemer, et al., *Proc. Natl. Acad. Sci. U. S. A.* **2018**, *115*, 7285–7292.
- [97] E. M. Campbell, T. J. Hope, *Nat. Rev. Microbiol.* **2015**, *13*, 471–483.
- [98] G. A. C. B. (Arbeitskreis German Advisory Committee Blood (Arbeitskreis Blut), Subgroup ‘Assessment of Pathogens Transmissible by Blood’, S. ‘Assessment of P. T. by Blood’, *Transfus. Med. Hemother.* **2016**, *43*, 203–22.

- [99] B. Chen, *Biochemistry* **2016**, *55*, 2539–2552.
- [100] R. Blumenthal, S. Durell, M. Viard, *J. Biol. Chem.* **2012**, *287*, 40841–9.
- [101] K. Montrose, G. W. Krissansen, *Biochem. Biophys. Res. Commun.* **2014**, *453*, 735–740.
- [102] M. de Wispelaere, G. Du, K. A. Donovan, T. Zhang, N. A. Eleuteri, J. C. Yuan, J. Kalabathula, R. P. Nowak, E. S. Fischer, N. S. Gray, et al., *Nat. Commun.* **2019**, *10*, 3468.
- [103] S. Rankovic, R. Ramalho, C. Aiken, I. Rousso, *J. Virol.* **2018**, *92*, 845–18.
- [104] W. S. Blair, C. Pickford, S. L. Irving, D. G. Brown, M. Anderson, R. Bazin, J. Cao, G. Ciaramella, J. Isaacson, L. Jackson, et al., *PLoS Pathog.* **2010**, *6*, e1001220.
- [105] J. Zhou, A. J. Price, U. D. Halambage, L. C. James, C. Aiken, *J. Virol.* **2015**, *89*, 9068–79.
- [106] X. Zuo, Z. Huo, D. Kang, G. Wu, Z. Zhou, X. Liu, P. Zhan, *Expert Opin. Ther. Pat.* **2018**, *28*, 299–316.
- [107] A. J. Price, D. A. Jacques, W. A. McEwan, A. J. Fletcher, S. Essig, J. W. Chin, U. D. Halambage, C. Aiken, L. C. James, *PLoS Pathog.* **2014**, *10*, e1004459.
- [108] A. Bhattacharya, S. L. Alam, T. Fricke, K. Zadrozny, J. Sedzicki, A. B. Taylor, B. Demeler, O. Pornillos, B. K. Ganser-Pornillos, F. Diaz-Griffero, et al., *Proc. Natl. Acad. Sci. U. S. A.* **2014**, *111*, 18625–30.
- [109] A. P. Crew, K. Raina, H. Dong, Y. Qian, J. Wang, D. Vigil, Y. V. Serebrenik, B. D. Hamman, A. Morgan, C. Ferraro, et al., *J. Med. Chem.* **2018**, *61*, 583–598.
- [110] S. Kachbi-Khelfallah, M. Monteil, M. Cortes-Clerget, E. Migianu-Griffoni, J.-L. Pirat, O. Gager, J. Deschamp, M. Lecouvey, *Beilstein J. Org. Chem.* **2016**, *12*, 1366–1371.
- [111] U. D. Halambage, J. P. Wong, B. J. Melancon, C. W. Lindsley, C. Aiken, *Antimicrob. Agents Chemother.* **2015**, *59*, 5190–5.
- [112] M. J. Fray, *J. Chem. Educ* **2014**, *91*, 140.
- [113] D. S. Kemp, J. Rebek, *J. Am. Chem. Soc.* **1970**, *92*, 5792–5793.

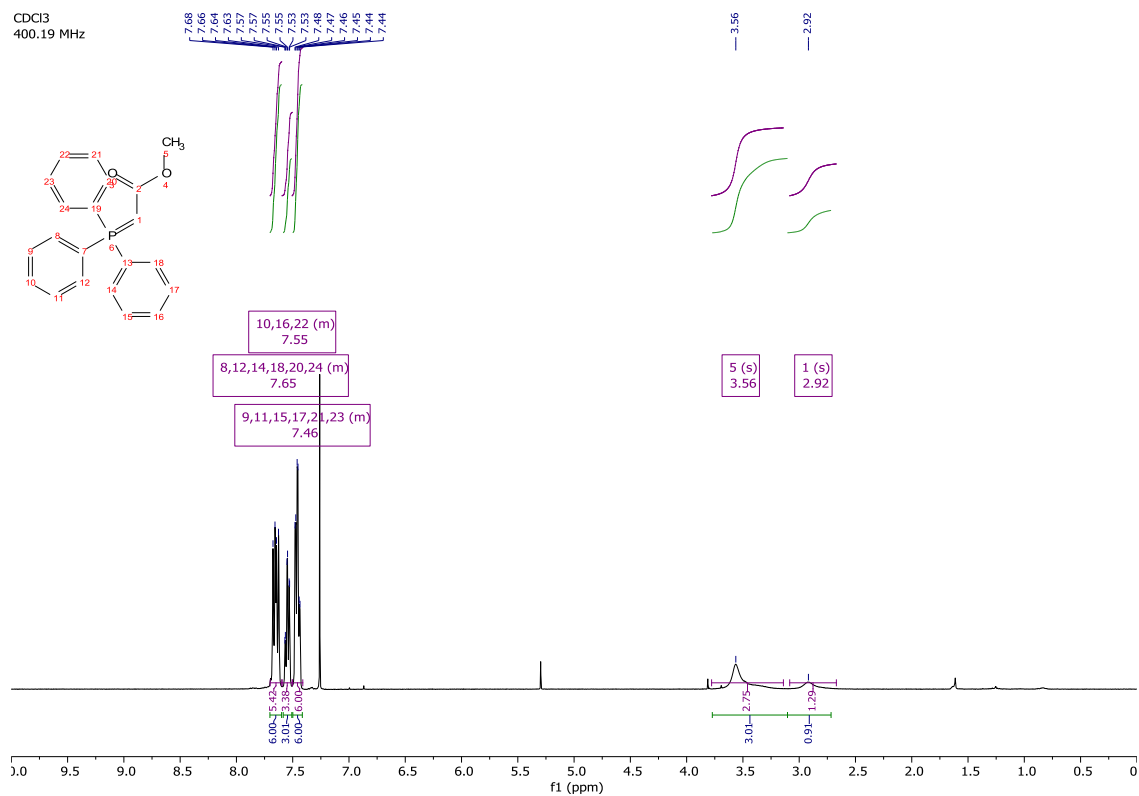
- [114] Z. P. Gates, B. Dhayalan, S. B. H. Kent, *Chem. Commun.* **2016**, 52, 13979–13982.
- [115] R. Karpoormath, Y. Sayed, T. Govender, H. G. Kruger, M. E. S. Soliman, G. E. M. Maguire, *Med. Chem. Res.* **2013**, 22, 3918–3933.
- [116] H. Yin, M. Jin, W. Chen, C. Chen, L. Zheng, P. Wei, S. Han, *Tetrahedron Lett.* **2012**, 53, 1265–1270.
- [117] K. Maranski, Y. G. Andreev, P. G. Bruce, *Angew. Chemie Int. Ed.* **2014**, 53, 6411–6413.
- [118] ATCC, “HEK 293T Culture Conditions,” can be found under [http://www.lgcstandards-atcc.org/products/all/CRL-11268.aspx?geo\\_country=de#culturemethod](http://www.lgcstandards-atcc.org/products/all/CRL-11268.aspx?geo_country=de#culturemethod), **2016**.
- [119] W. Vera Ortega, Approaching a Tat-Rev Independent HIV-1 Clone towards a Model for Research, University of Glasgow, **2018**.
- [120] A. Lopez-Girona, D. Mendy, T. Ito, K. Miller, A. K. Gandhi, J. Kang, S. Karasawa, G. Carmel, P. Jackson, M. Abbasian, et al., *Leukemia* **2012**, 26, 2326–35.
- [121] I. Boichenko, S. Deiss, K. Bär, M. D. Hartmann, B. Hernandez Alvarez, *J. Med. Chem.* **2016**, 59, 770–774.
- [122] P. Soares, X. Lucas, A. Ciulli, *Bioorg. Med. Chem.* **2018**, 26, 2992–2995.
- [123] F. A. Loiseau, M. Alison, K. K. Hii, *J. Org. Chem* **2004**, 69, 639–647.
- [124] A. M. Birch, P. A. Bradley, J. C. Gill, F. Kerrigan, P. L. Needham, *J. Med. Chem.* **1999**, 42, 3342–3355.
- [125] M.-L. Yuan, J.-H. Xie, Q.-L. Zhou, *ChemCatChem* **2016**, 8, 3036–3040.

# Appendix

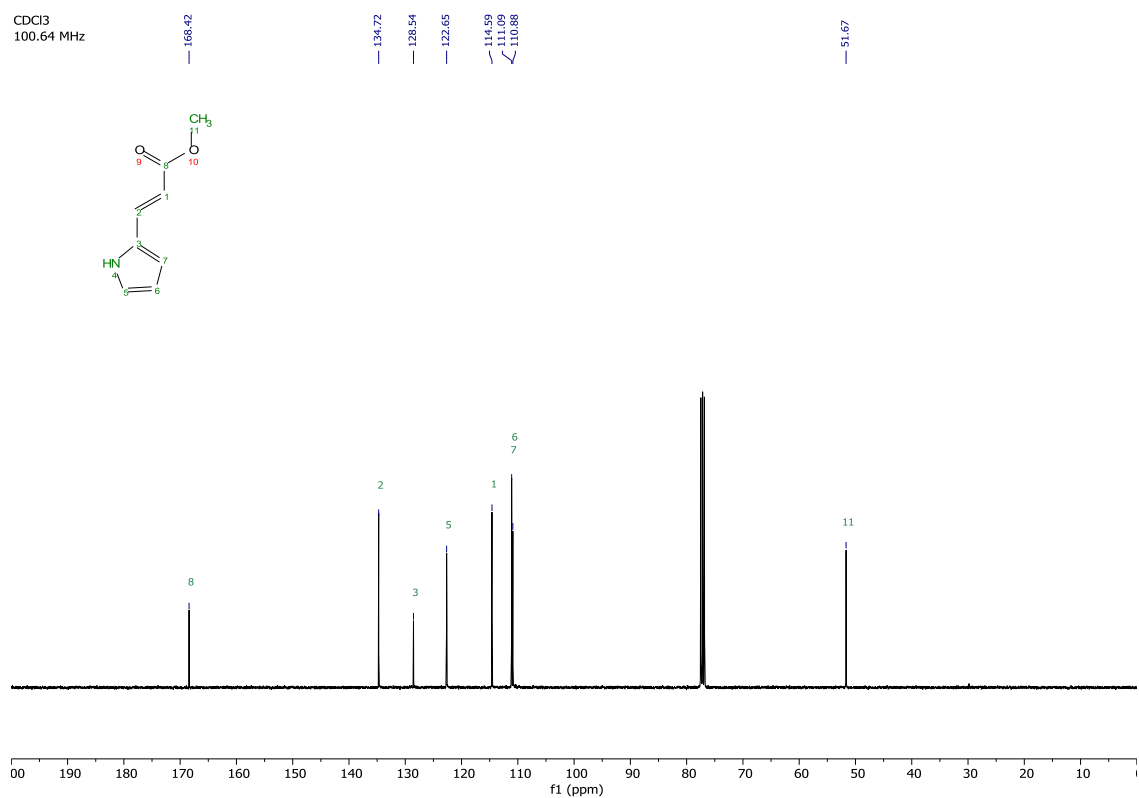
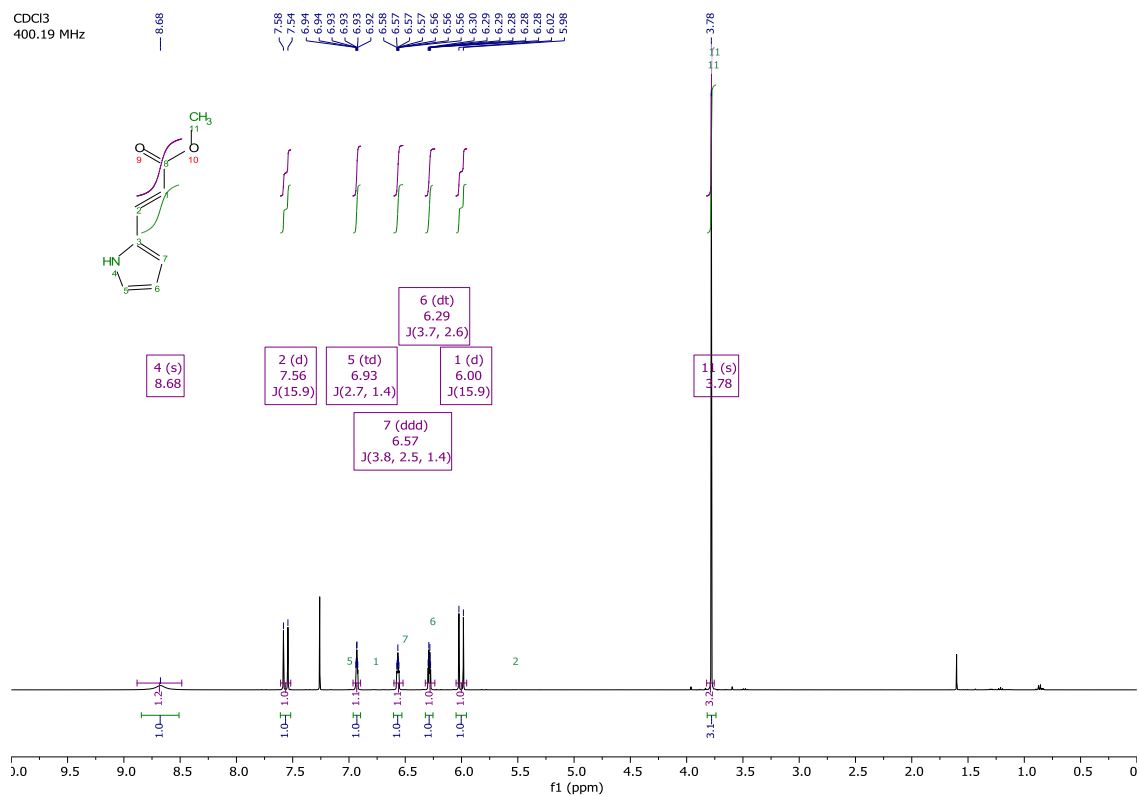
## Chapter 1 Chemistry

### Compound Characterisation Data

$^1\text{H}$  NMR spectrum of ylide **1.2**.

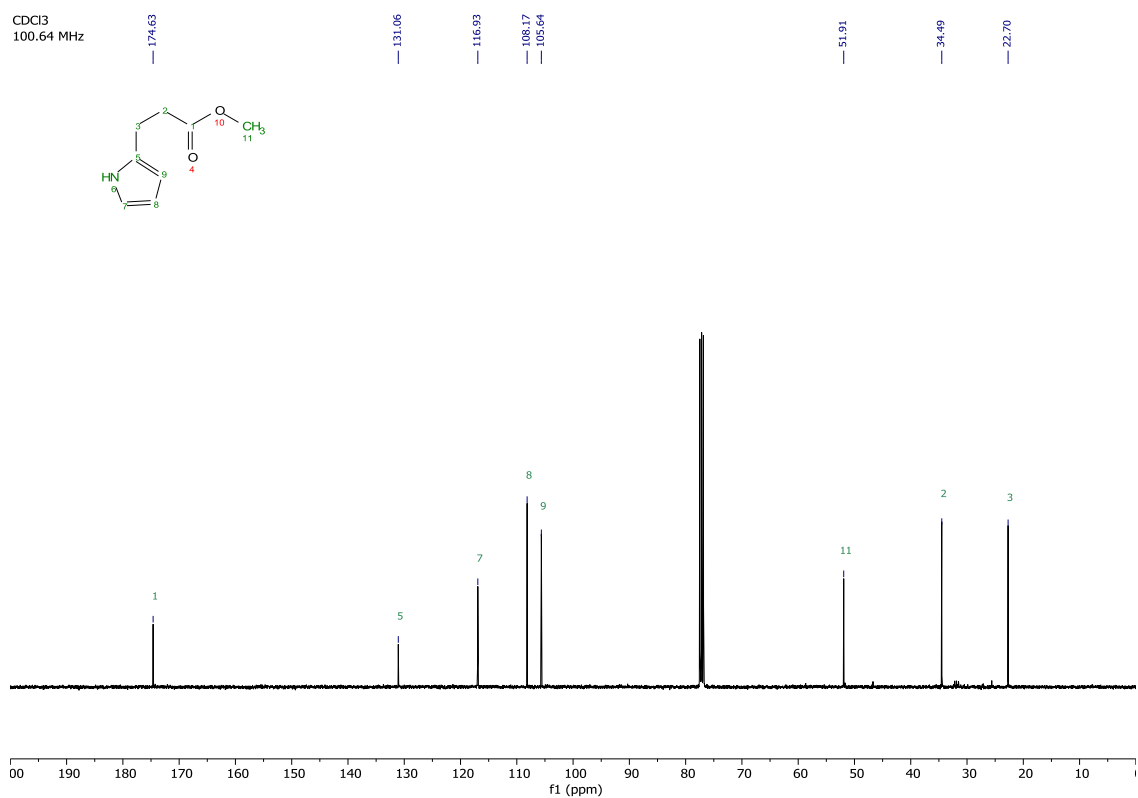
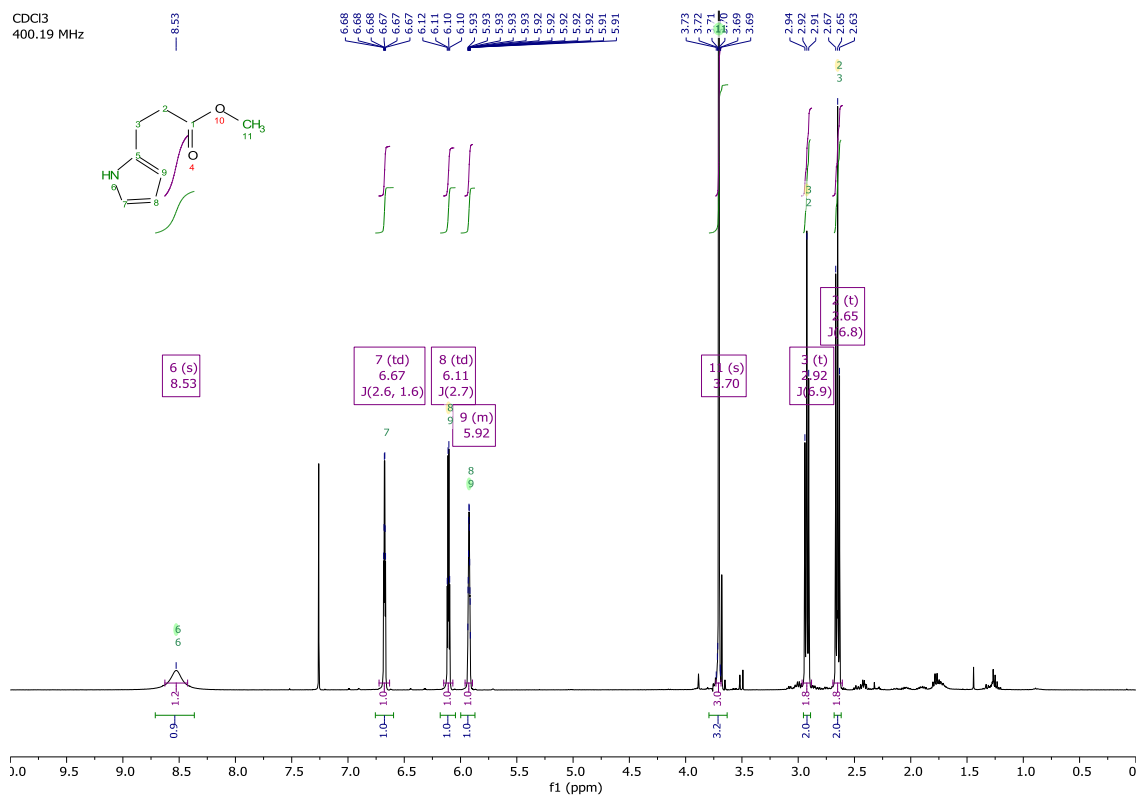


$^1\text{H}$  and  $^{13}\text{C}$  NMR spectra of alkene **1.3E**.

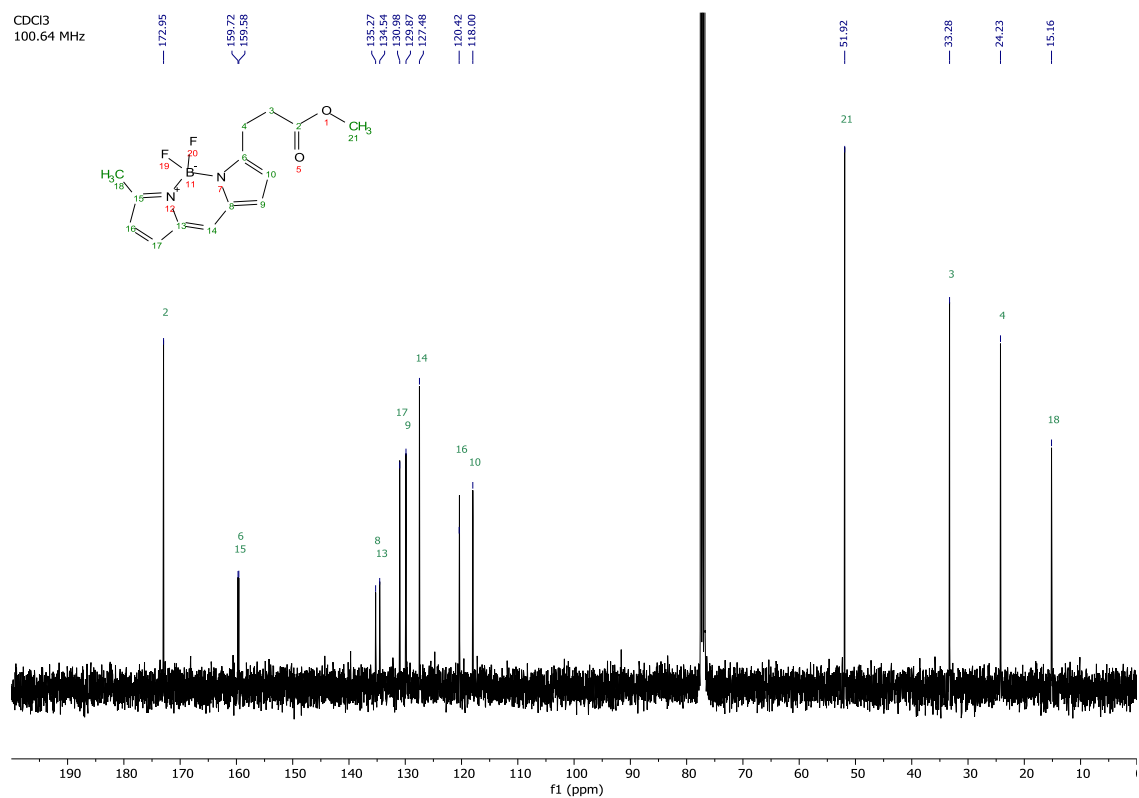
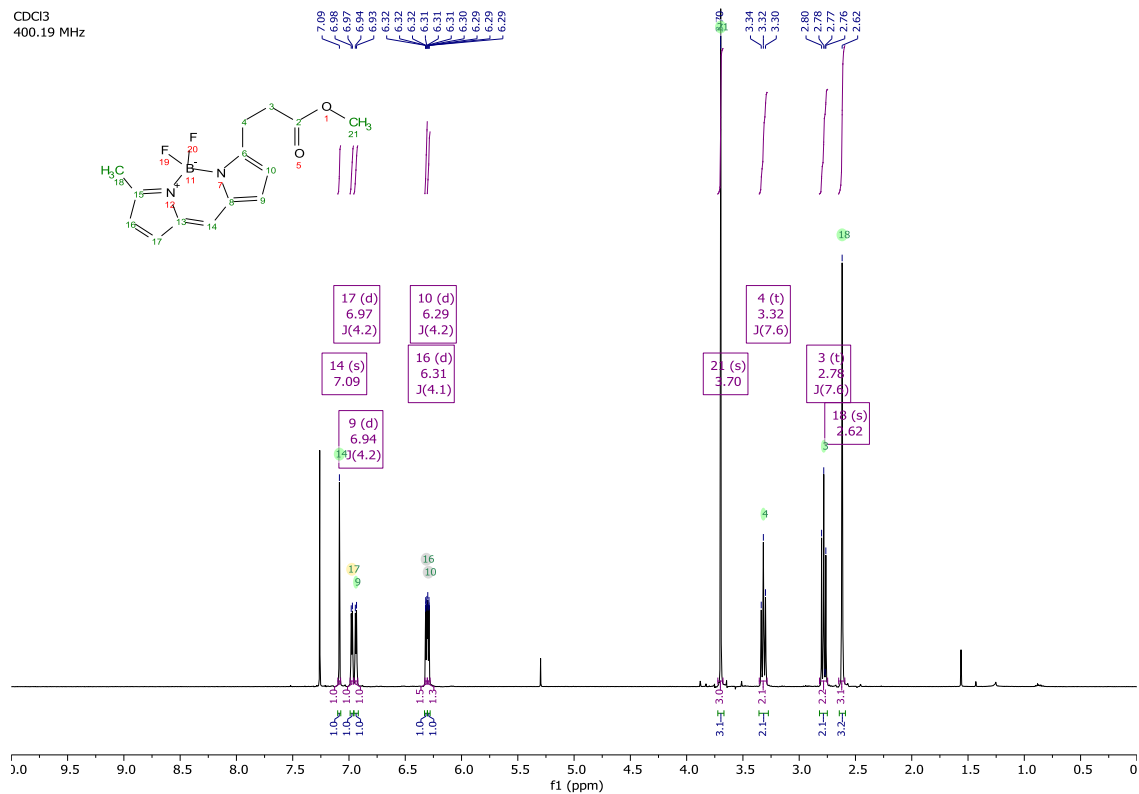




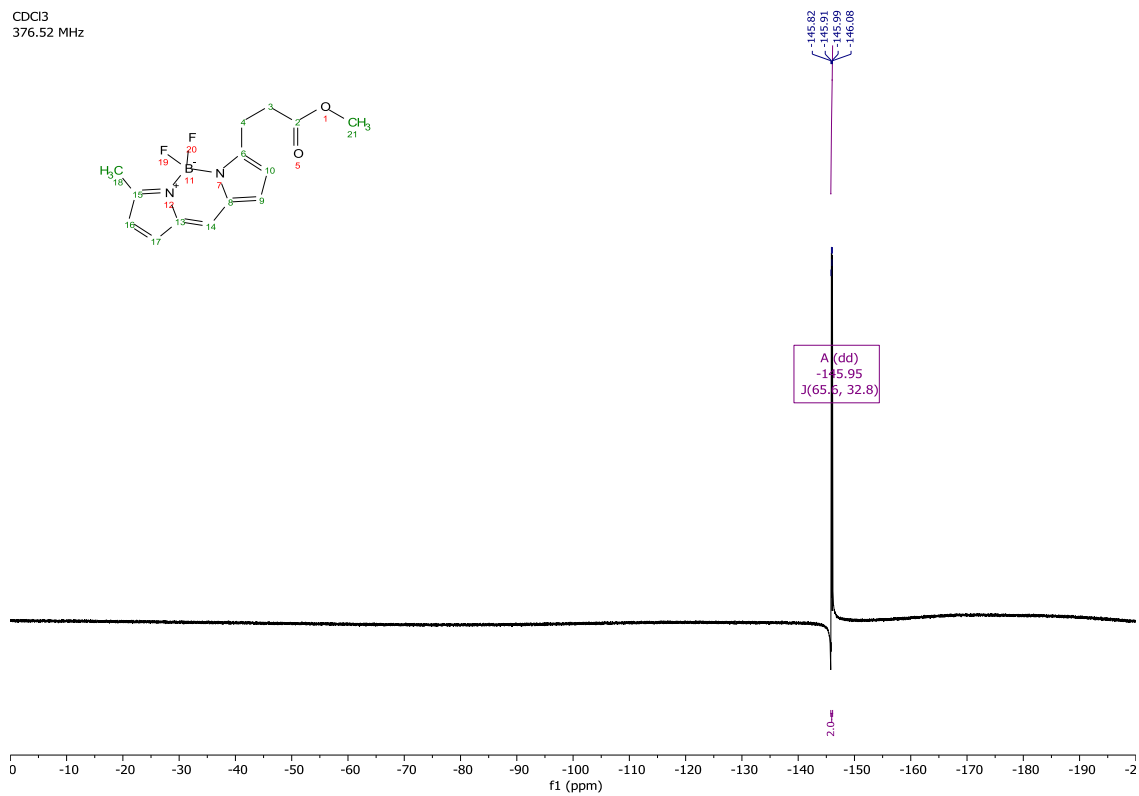
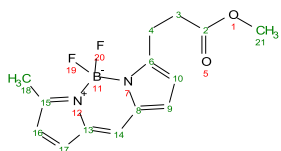
# <sup>1</sup>H and <sup>13</sup>C NMR spectra of pyrrole 1.4.



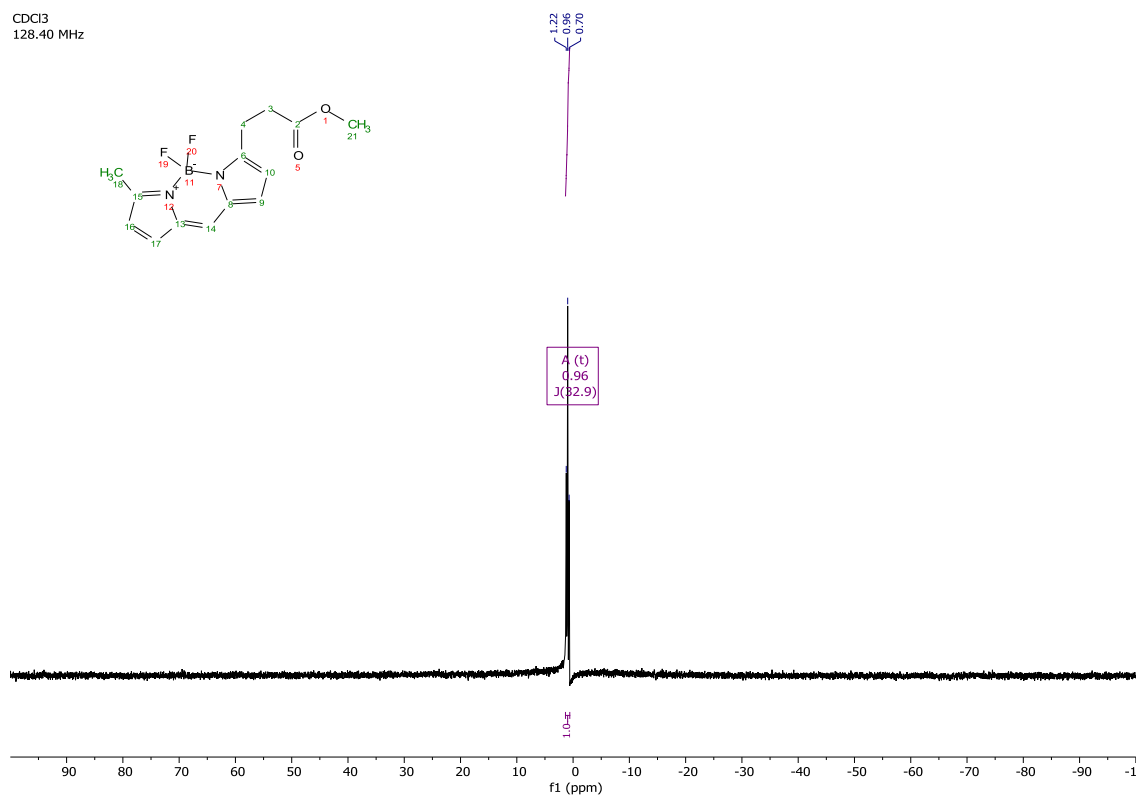
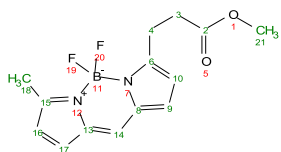
$^1\text{H}$ ,  $^{13}\text{C}$ ,  $^{19}\text{F}$ ,  $^{11}\text{B}$ , COSY and HMBC NMR spectra of bodipy **1.6**.

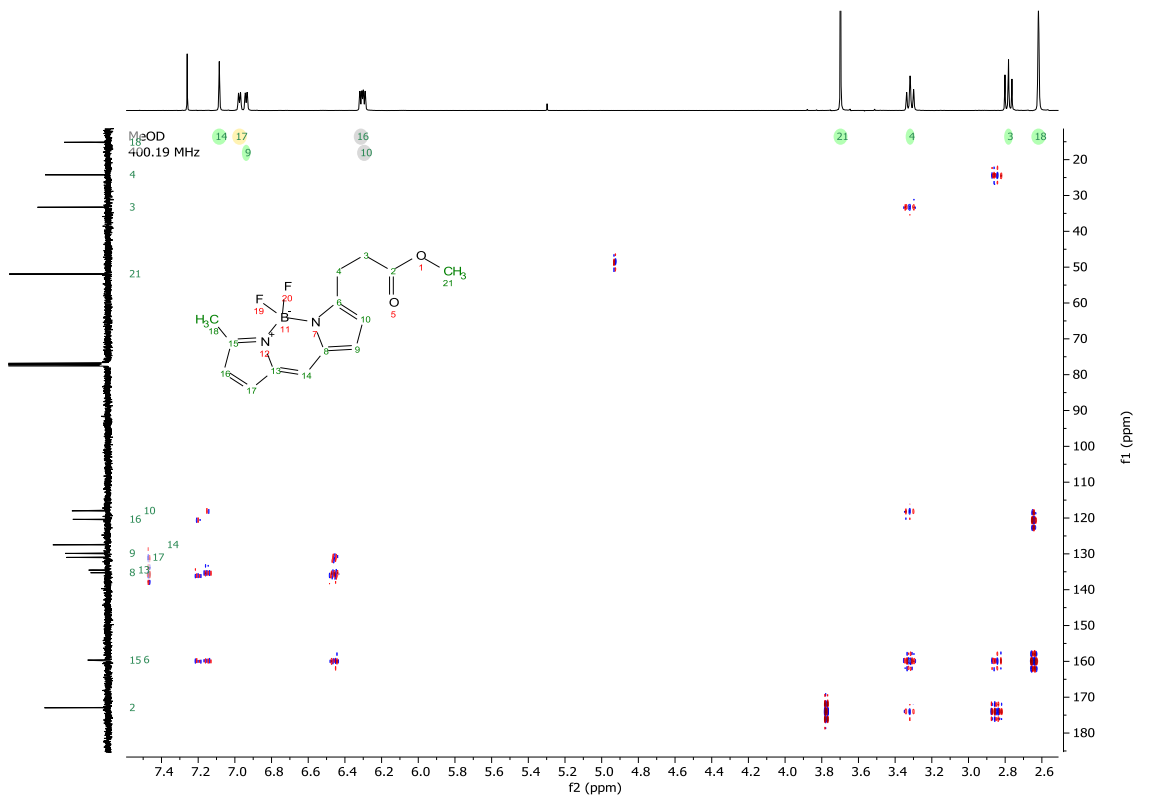
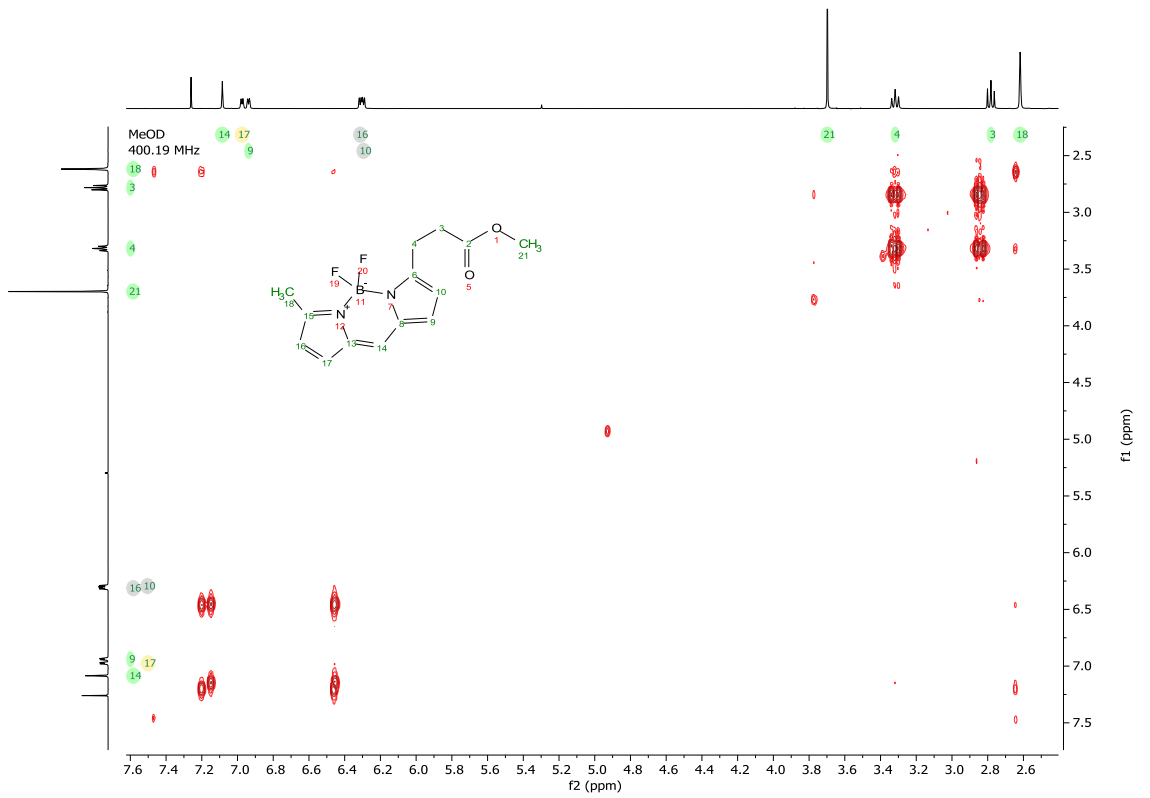


CDCl<sub>3</sub>  
376.52 MHz



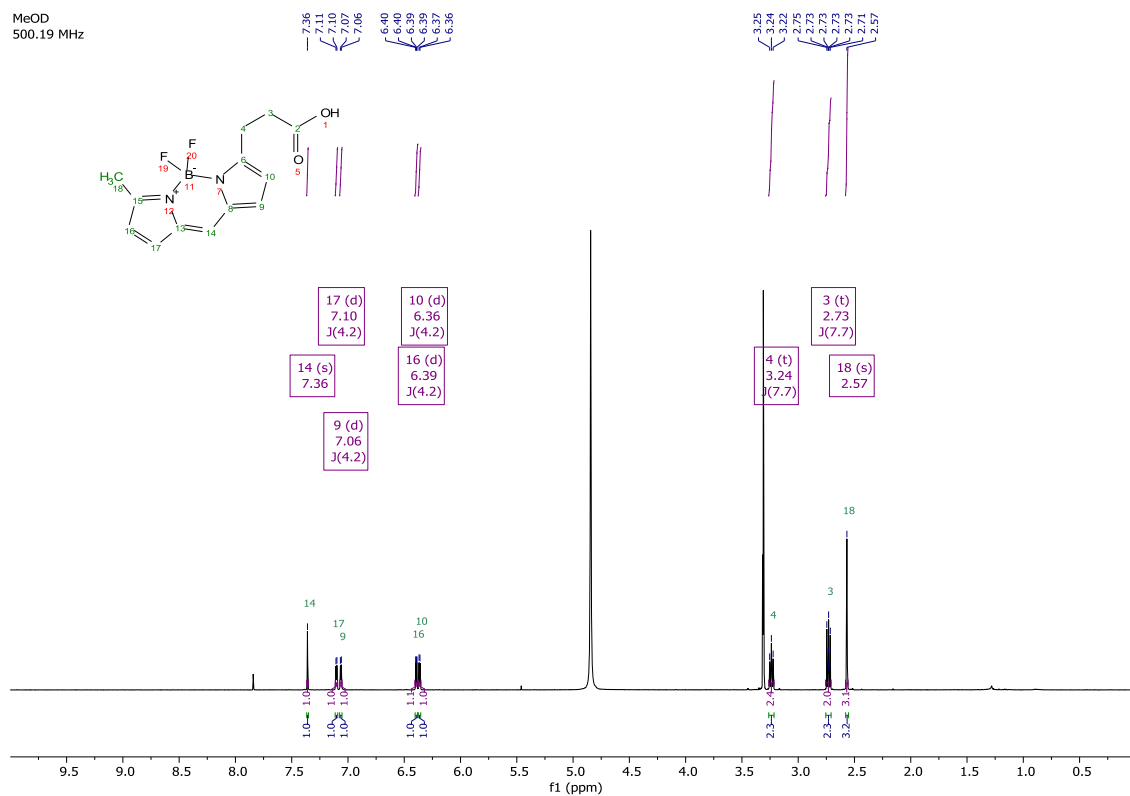
CDCl<sub>3</sub>  
128.40 MHz



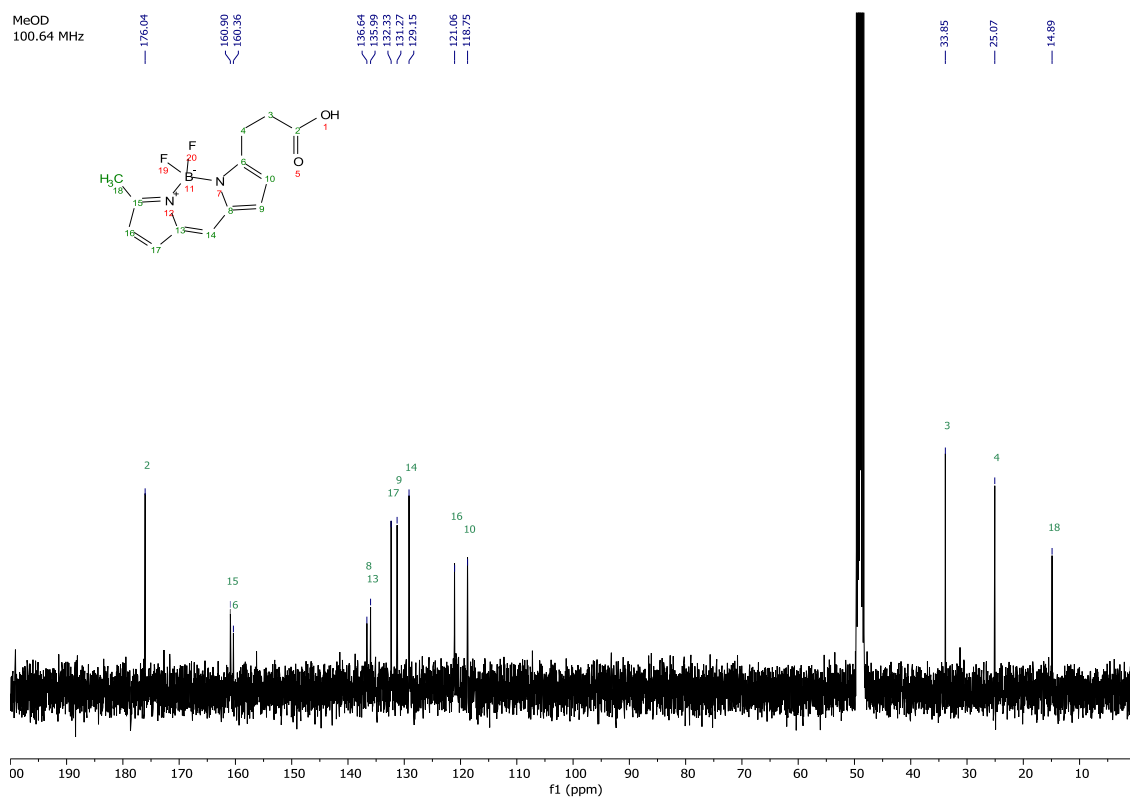


# <sup>1</sup>H and <sup>13</sup>C NMR spectra of boday 1.7.

MeOD  
500.19 MHz

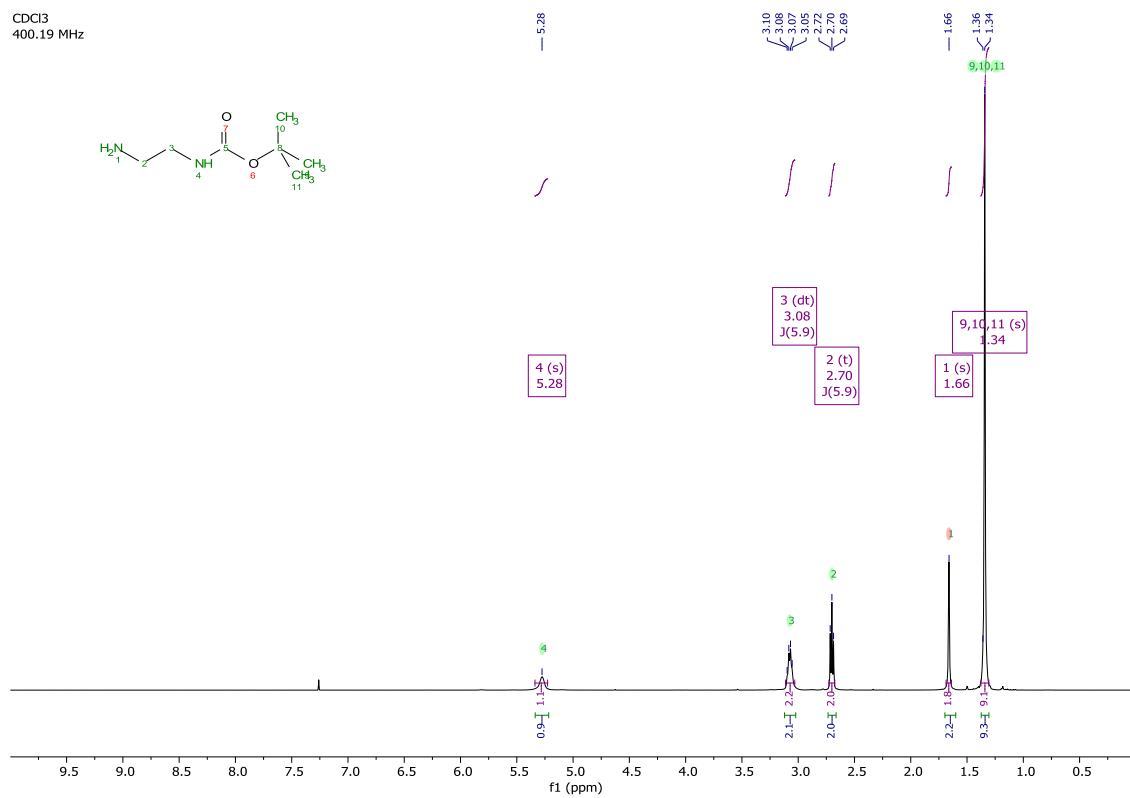


MeOD  
100.64 MHz

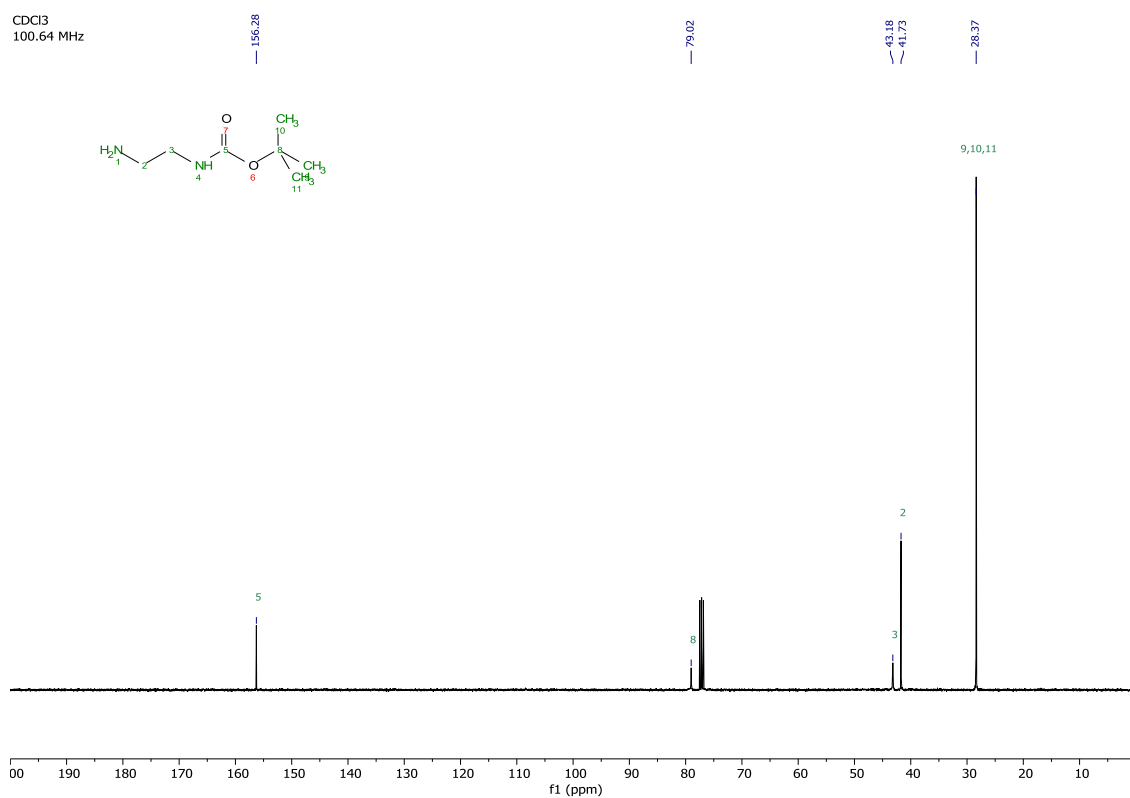


# $^1\text{H}$ and $^{13}\text{C}$ NMR spectra of *tert*-butyl carbamate **1.8**.

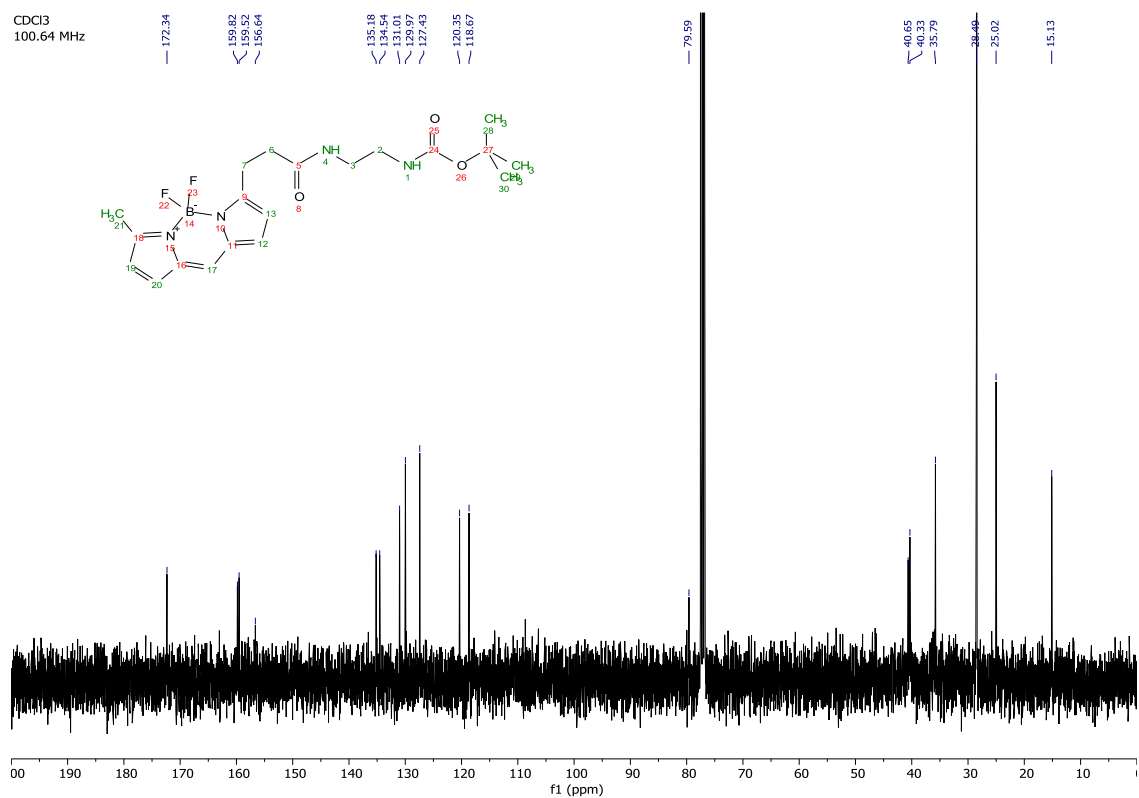
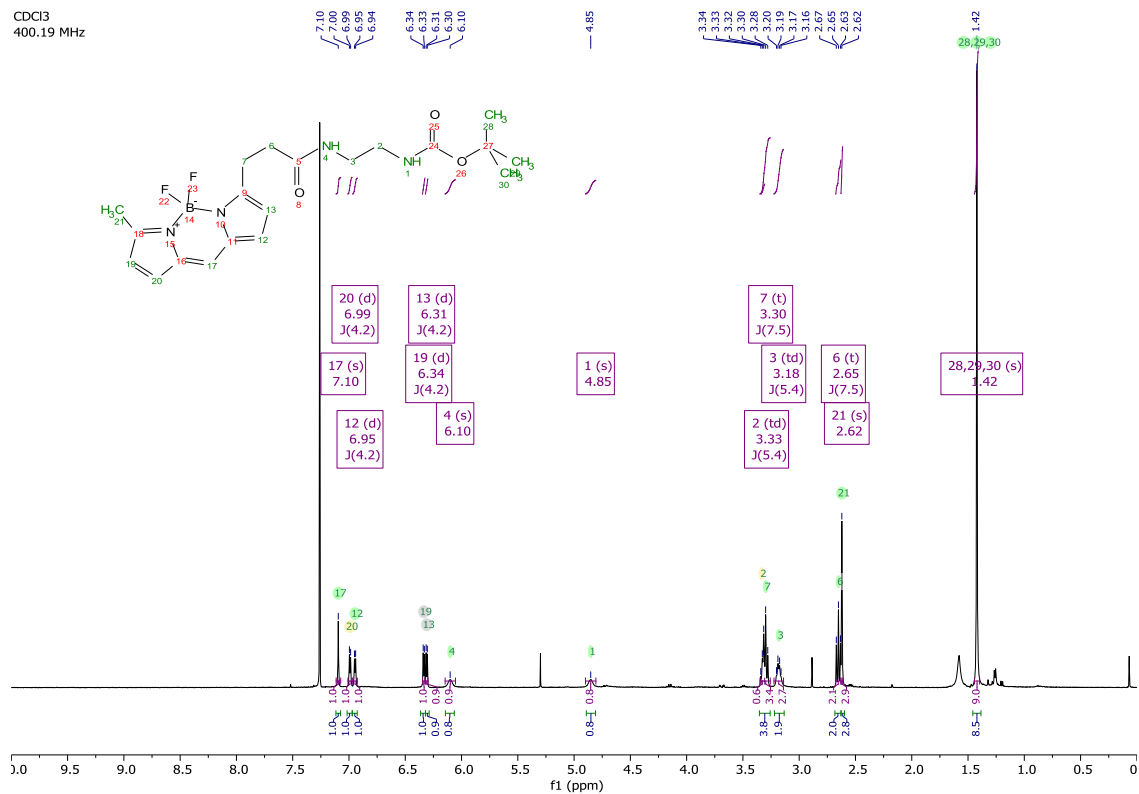
CDCl<sub>3</sub>  
400.19 MHz



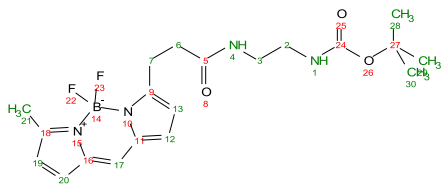
CDCl<sub>3</sub>  
100.64 MHz



$^1\text{H}$ ,  $^{13}\text{C}$ ,  $^{19}\text{F}$ ,  $^{11}\text{B}$  and COSY NMR spectra of bodipy **1.9**.



CDCl<sub>3</sub>  
376.52 MHz

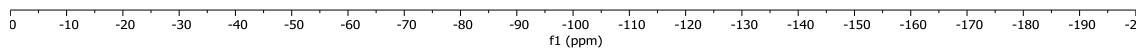


144.99  
145.08  
145.17  
145.26

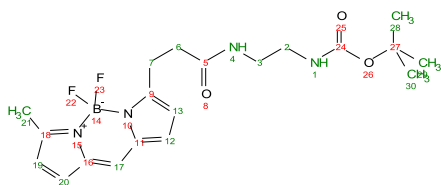
A (dd)  
-145.12  
J(66.0, 33.0)



2.0-H

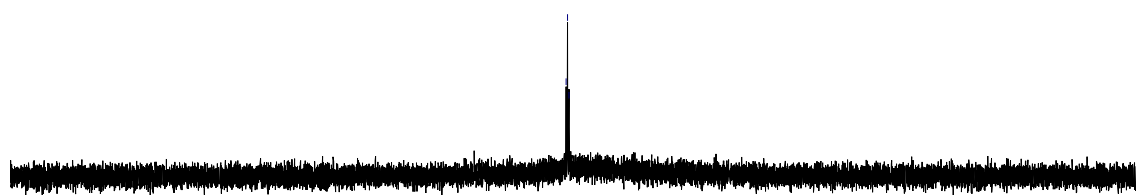


CDCl<sub>3</sub>  
128.40 MHz

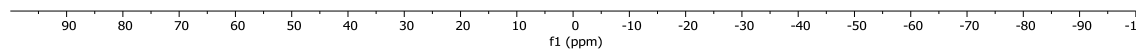


1.24  
0.99  
0.73

A (t)  
0.99  
J(32.9)

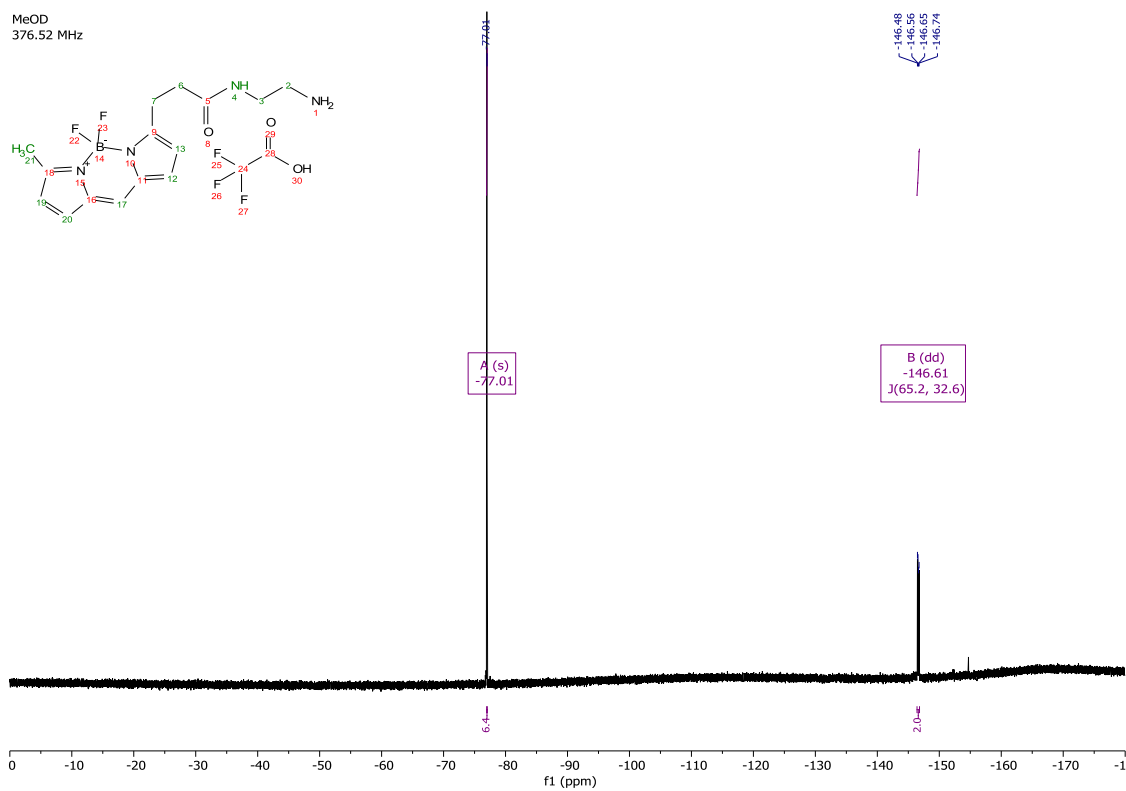
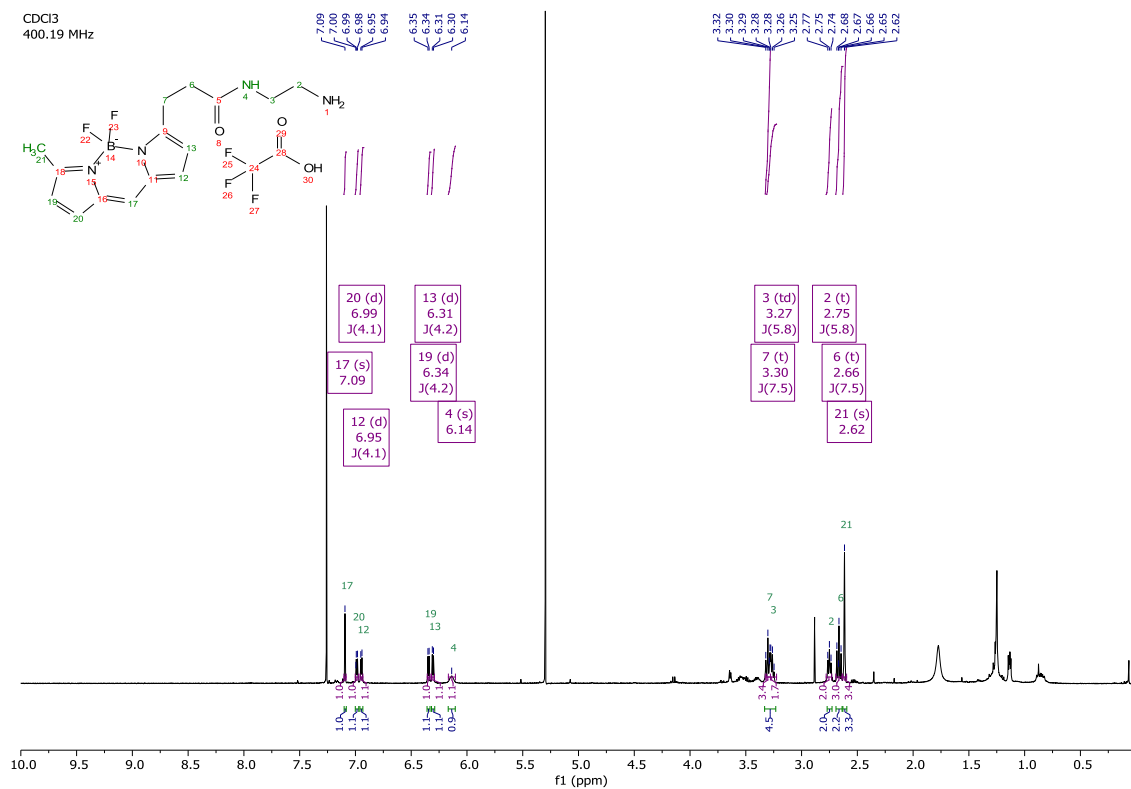


1.0-H



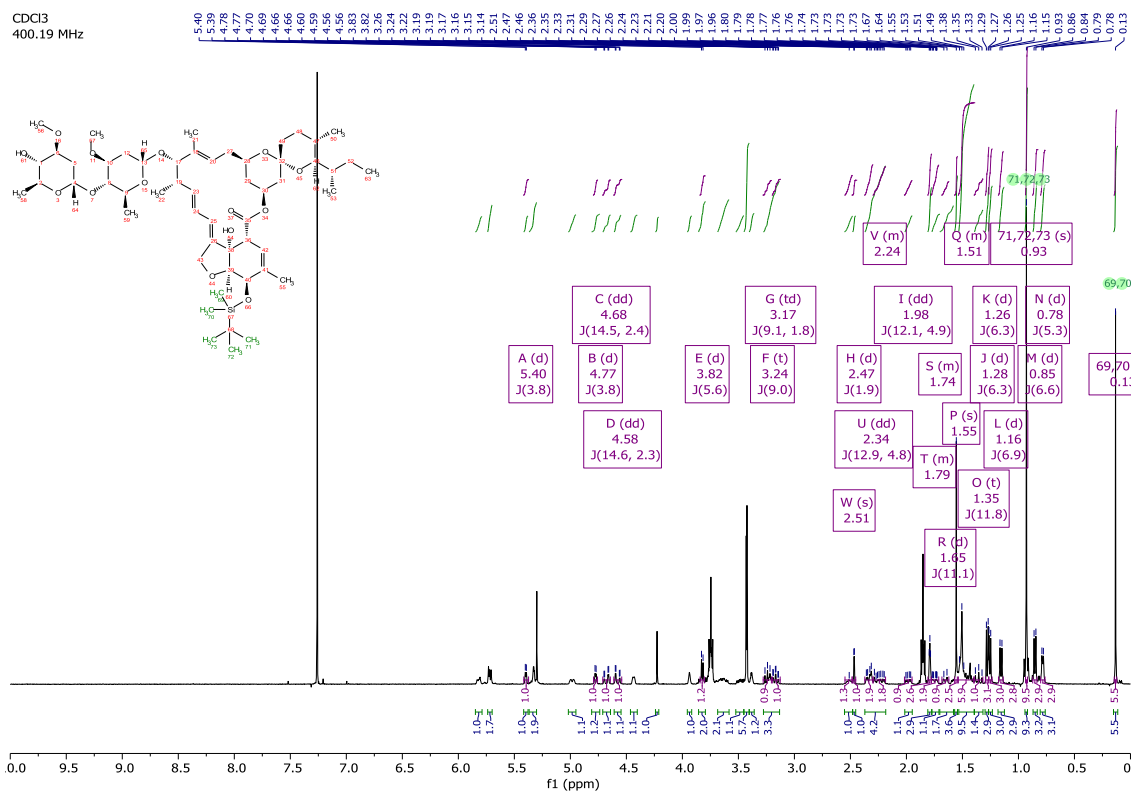


$^1\text{H}$ ,  $^{19}\text{F}$ , and  $^{11}\text{B}$  NMR spectra of amine TFA salt **1.1**.

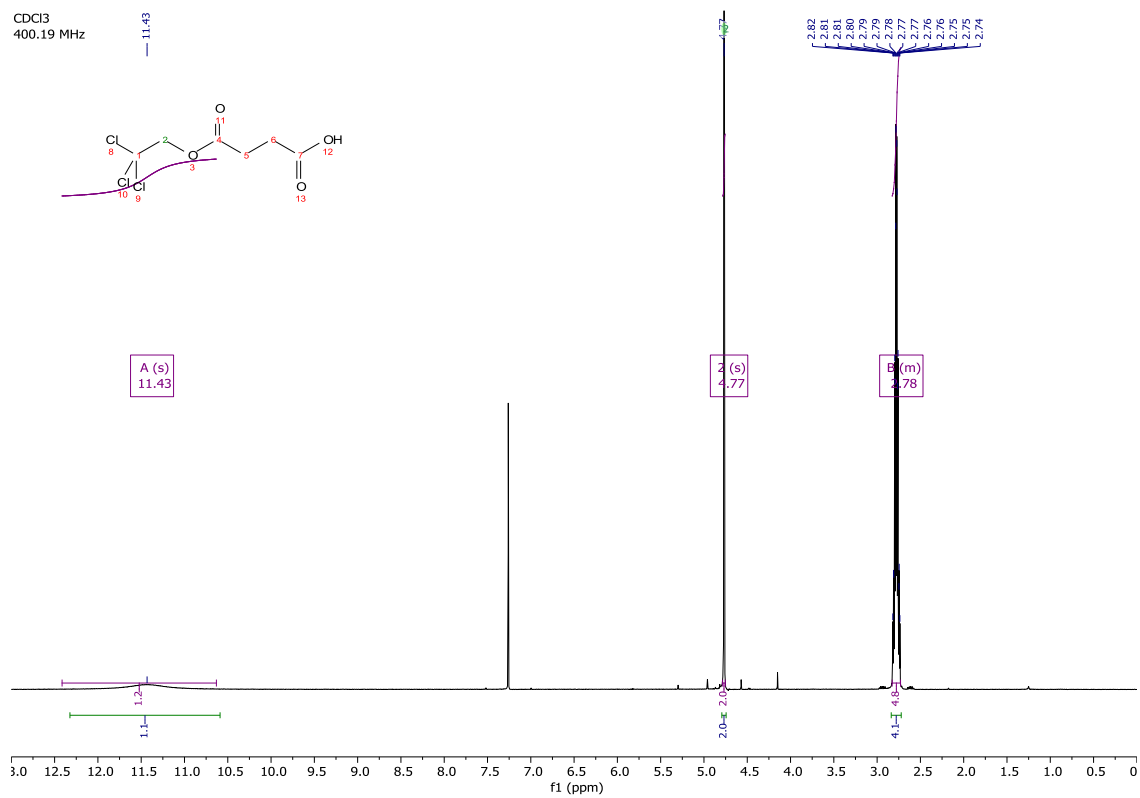




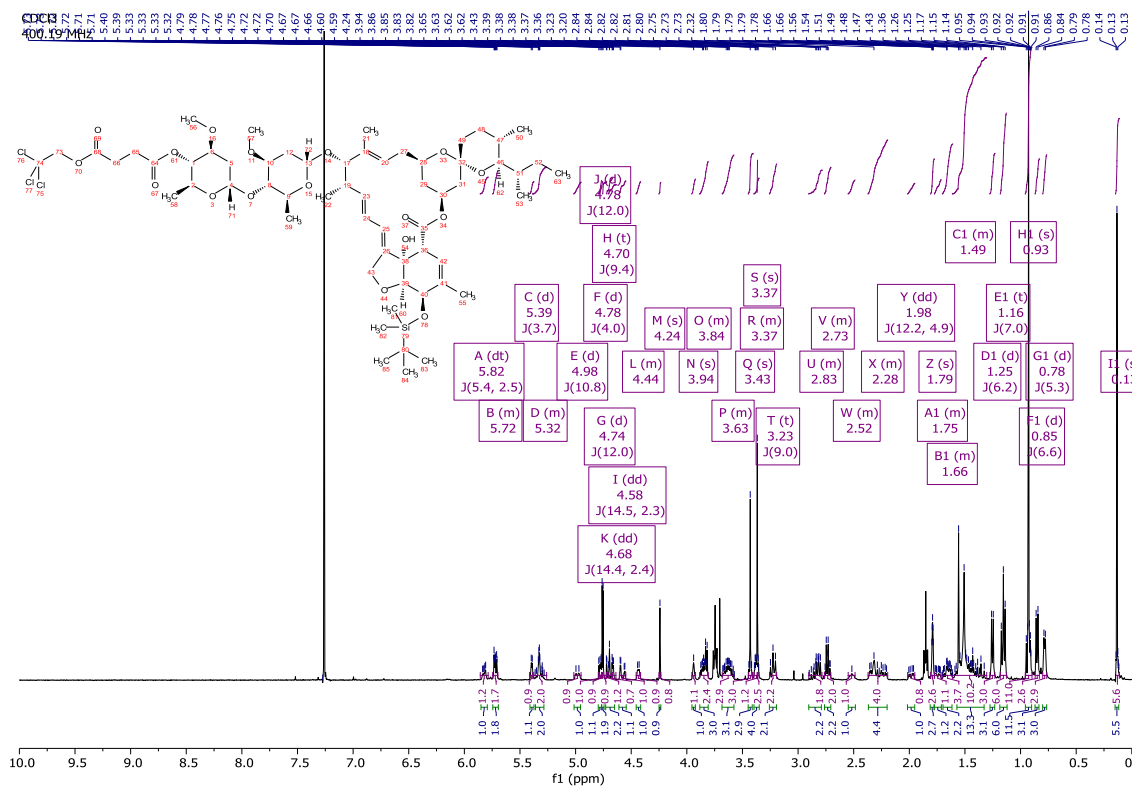
# $^1\text{H}$ and $^{13}\text{C}$ NMR spectra of silyl ether **1.12**.



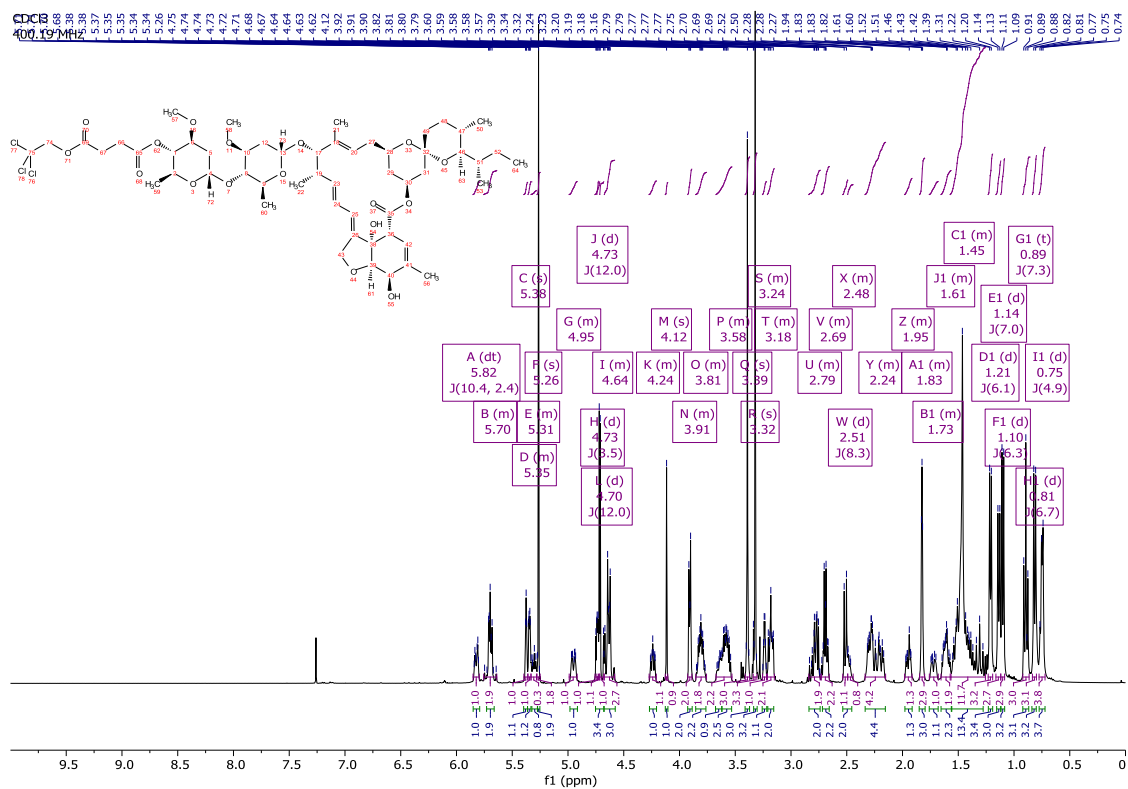
# <sup>1</sup>H NMR spectrum of acid **1.13**.



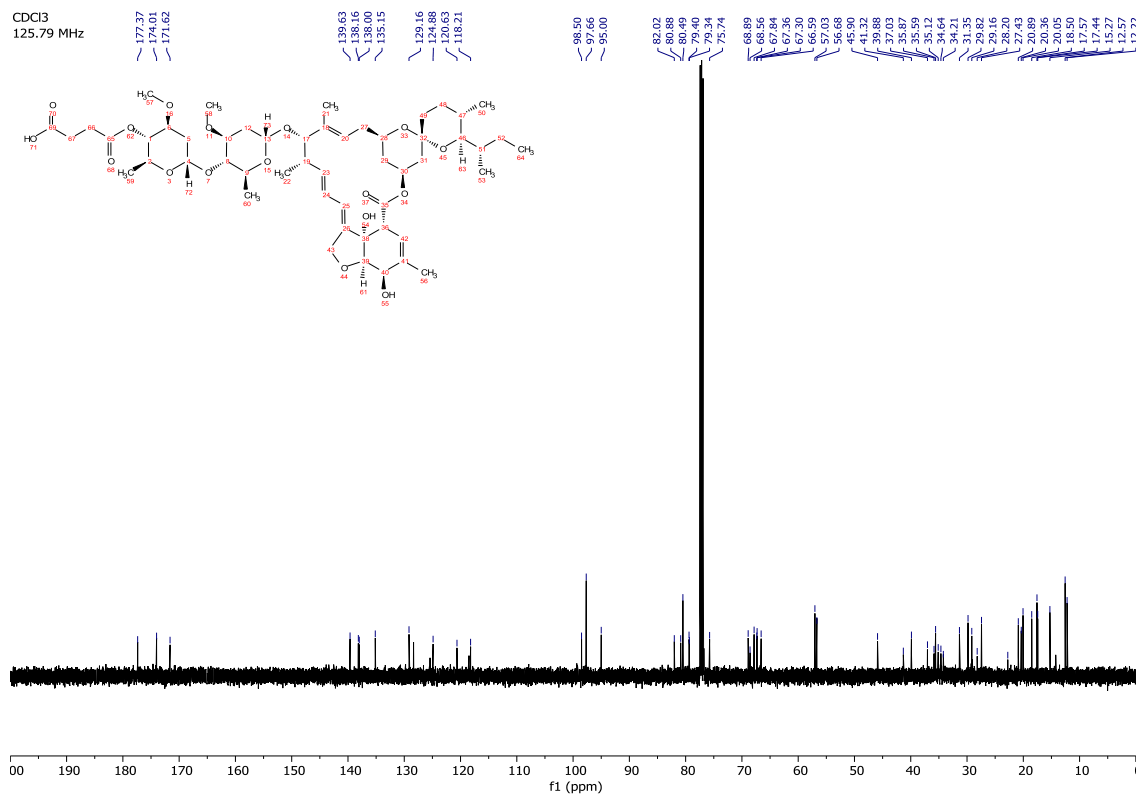
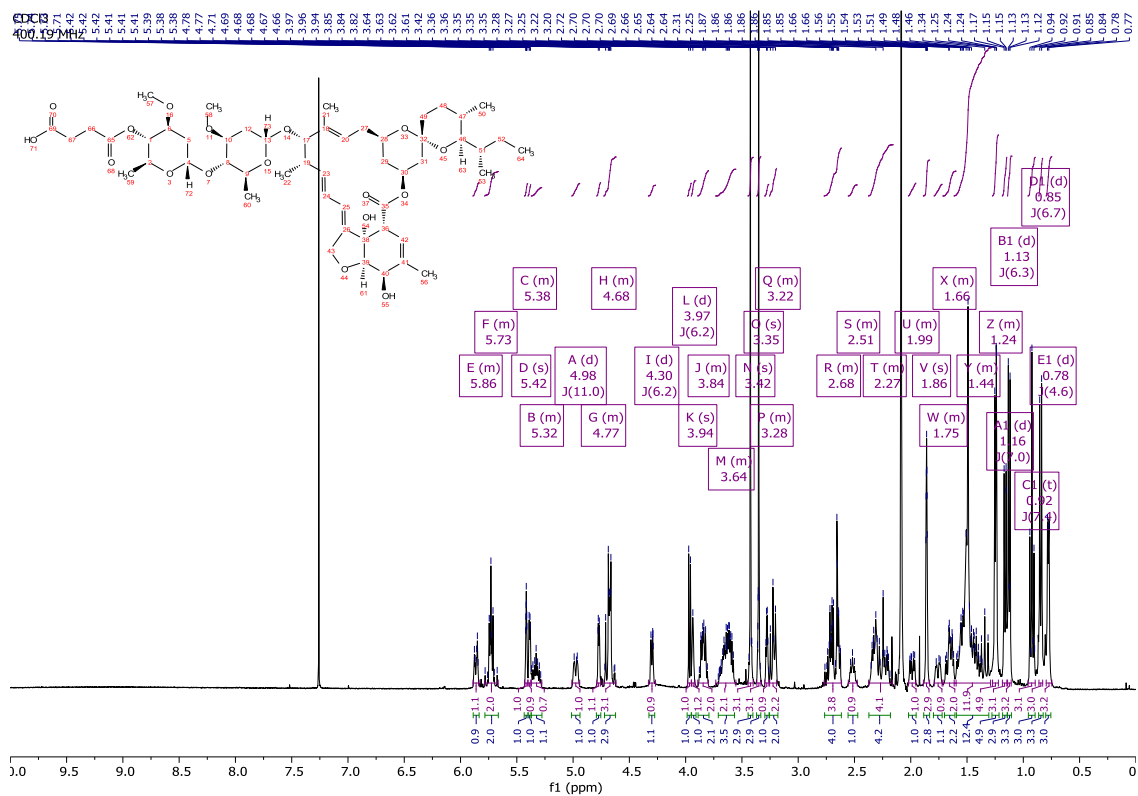
<sup>1</sup>H NMR spectrum of ester **1.15**.



<sup>1</sup>H NMR spectrum of allylic alcohol **1.16**.

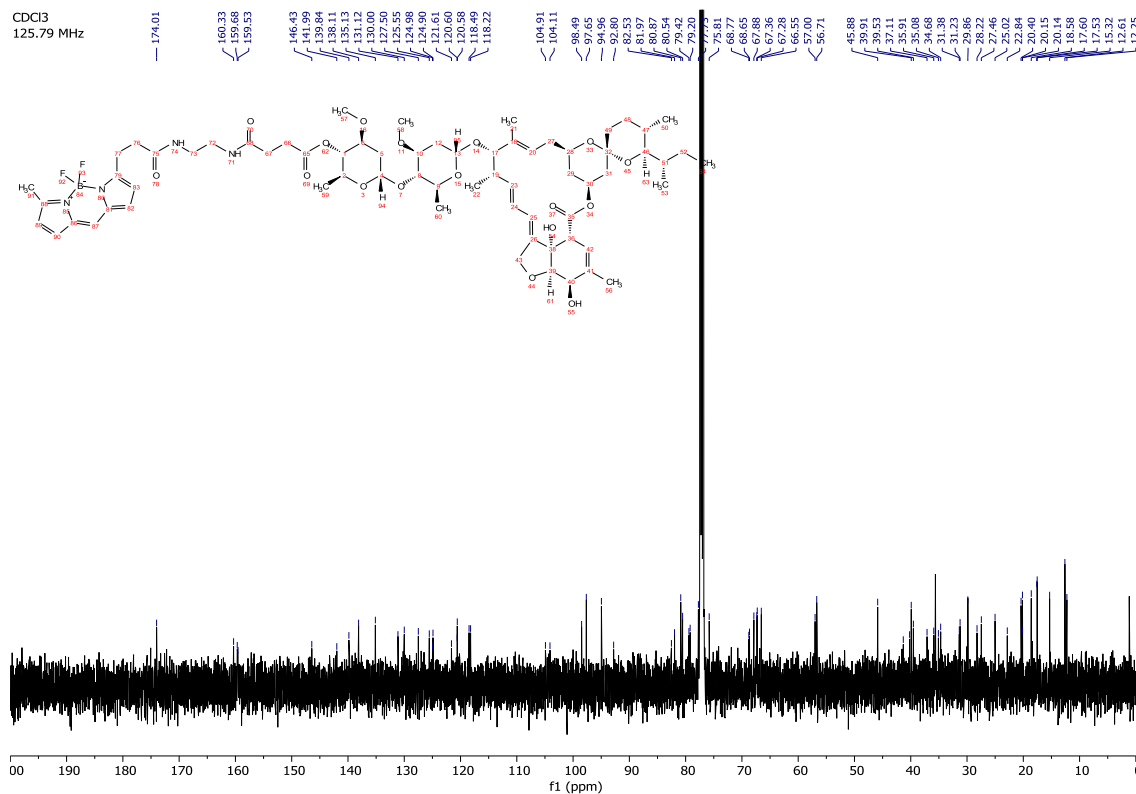
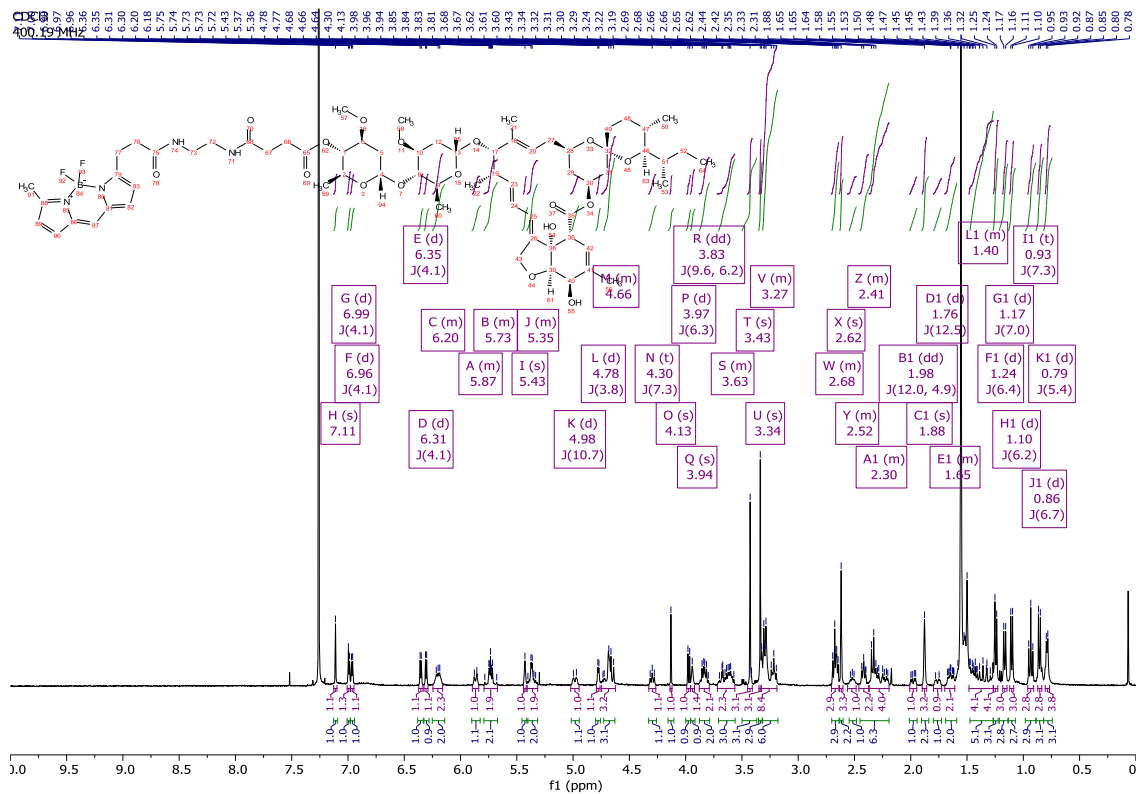


$^1\text{H}$  and  $^{13}\text{C}$  NMR spectra of acid **1.11**.

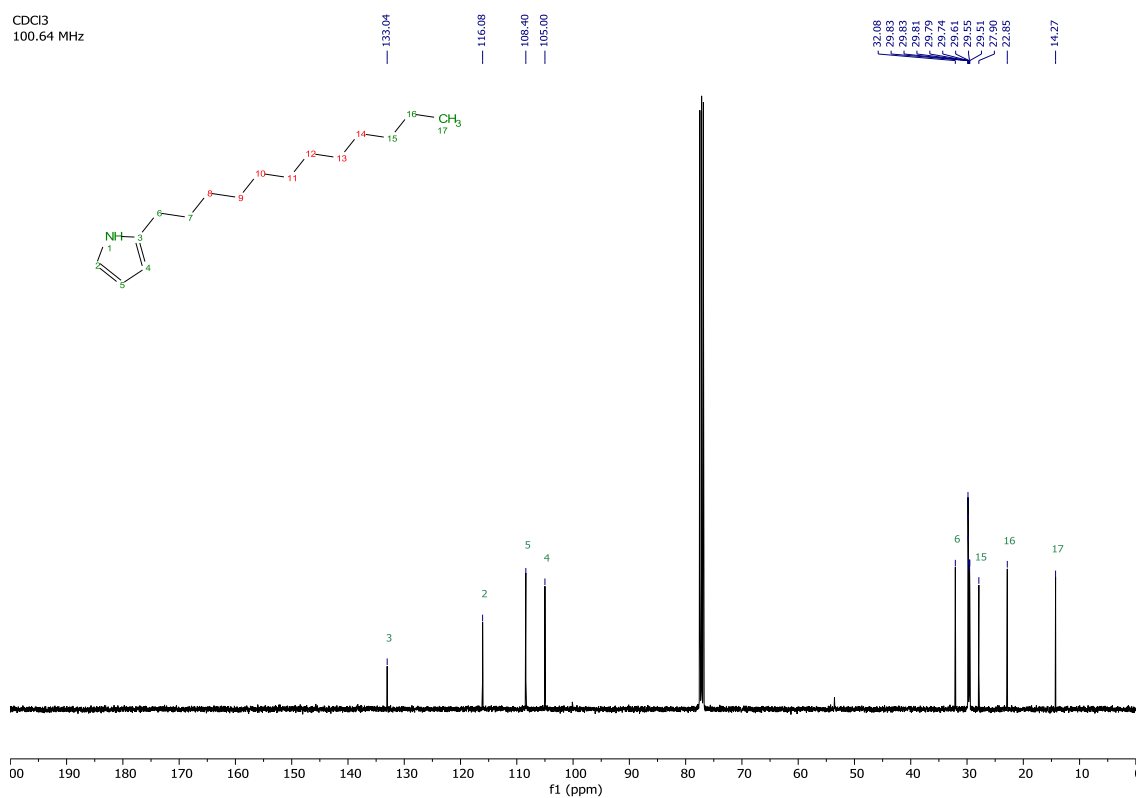
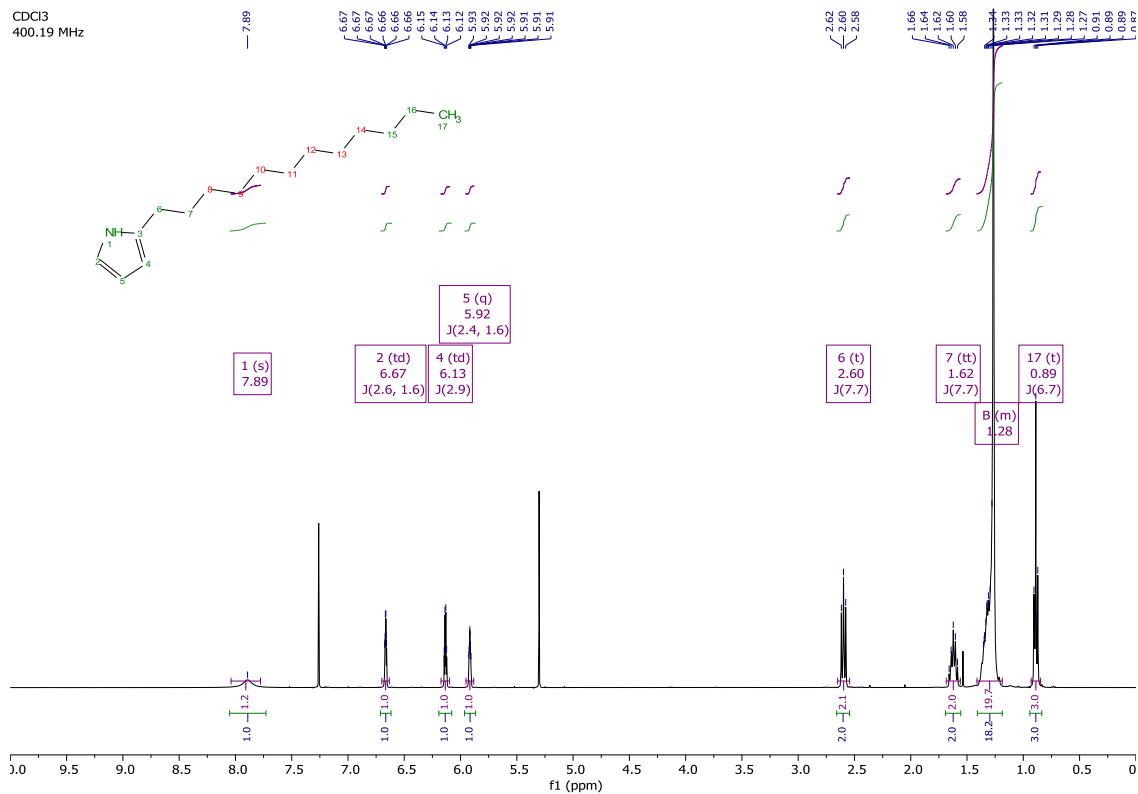




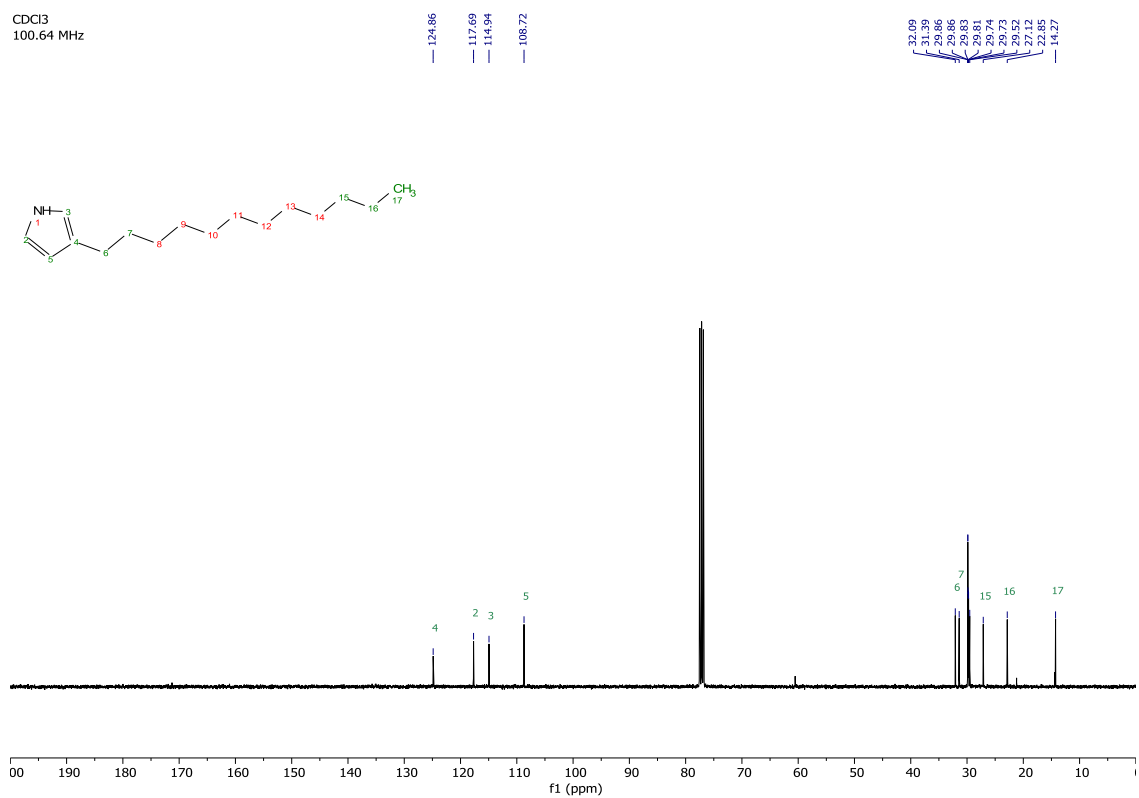
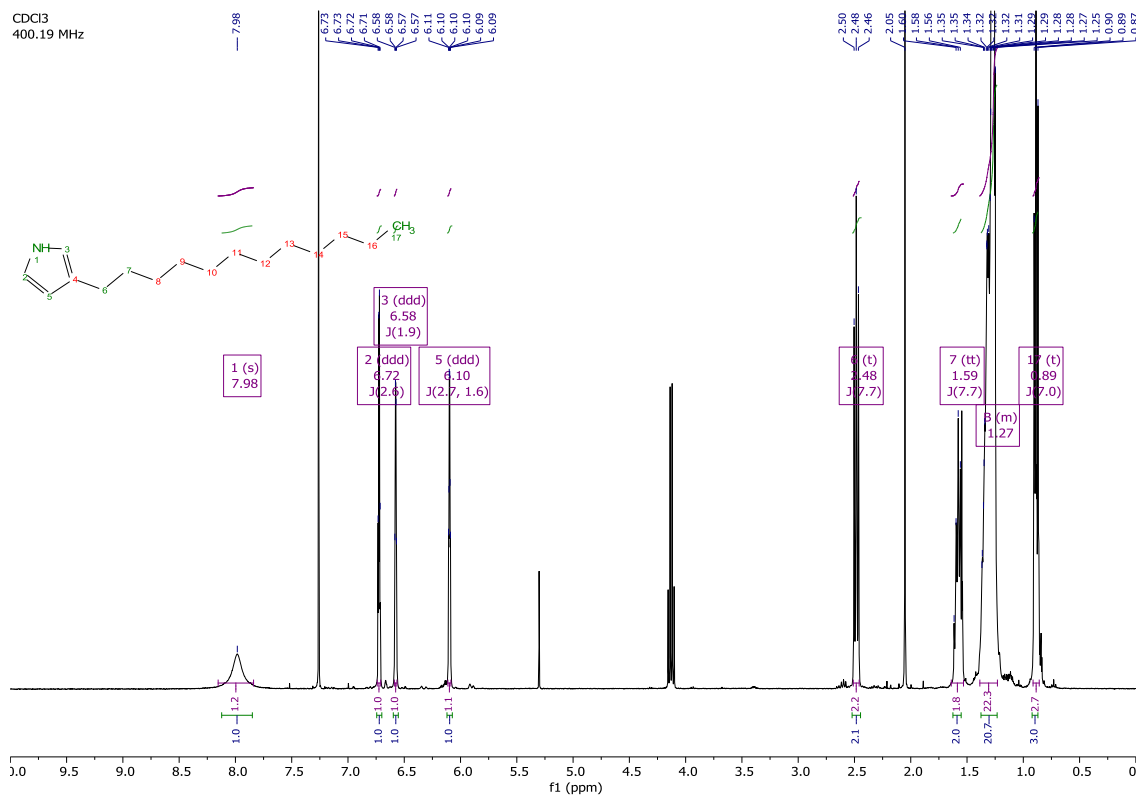
# <sup>1</sup>H and <sup>13</sup>C NMR spectra of BLI.



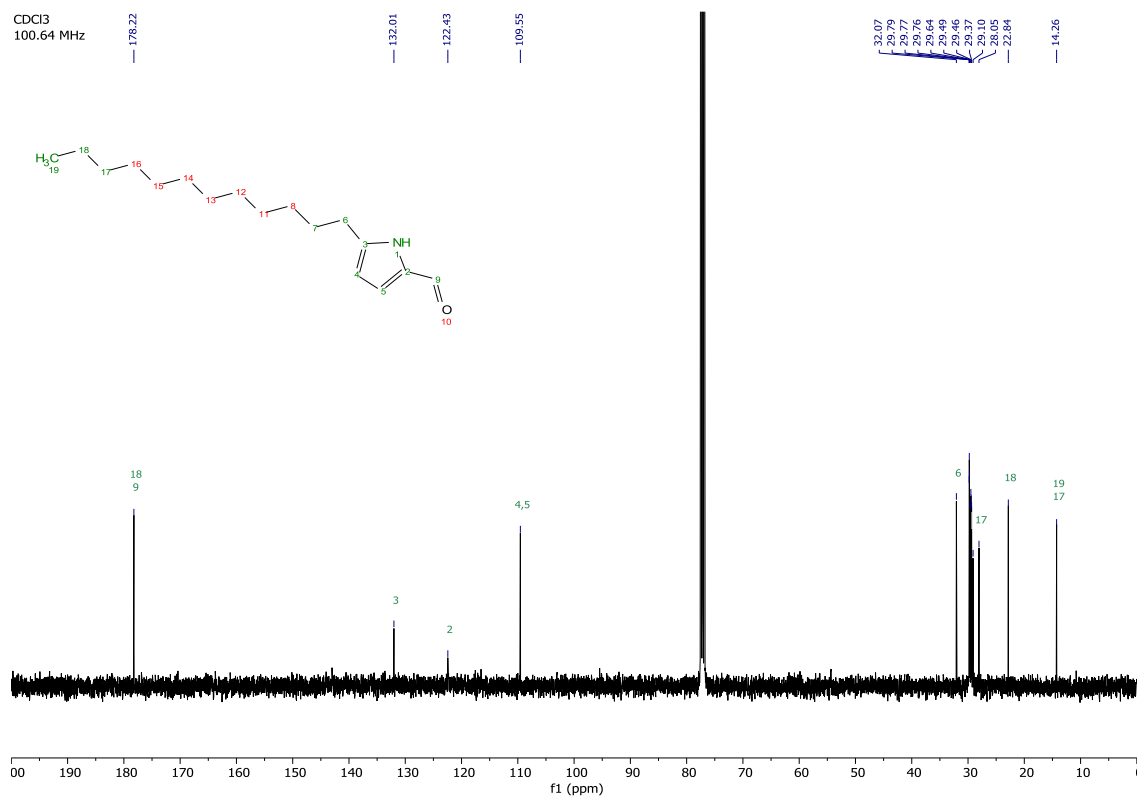
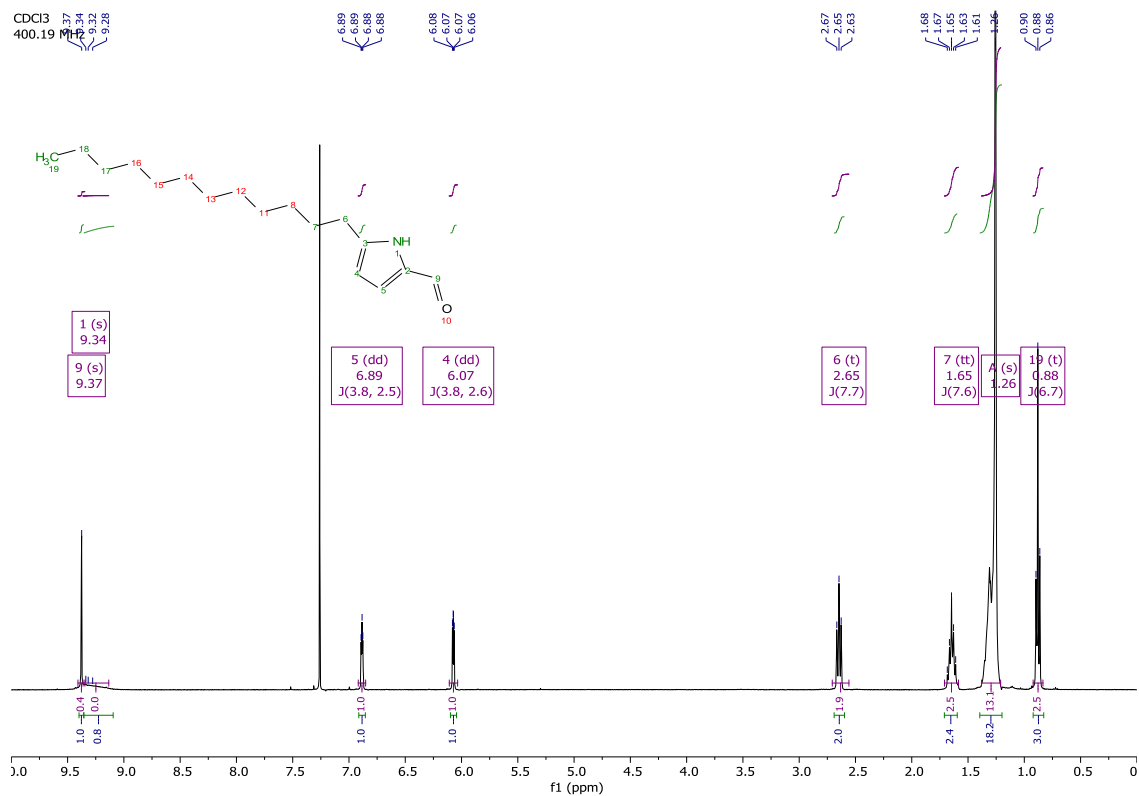
# <sup>1</sup>H and <sup>13</sup>C NMR spectra of 2-alkylated pyrrole **1.19**.



$^1\text{H}$  and  $^{13}\text{C}$  NMR spectra of 3-alkylated pyrrole **1.19b**.

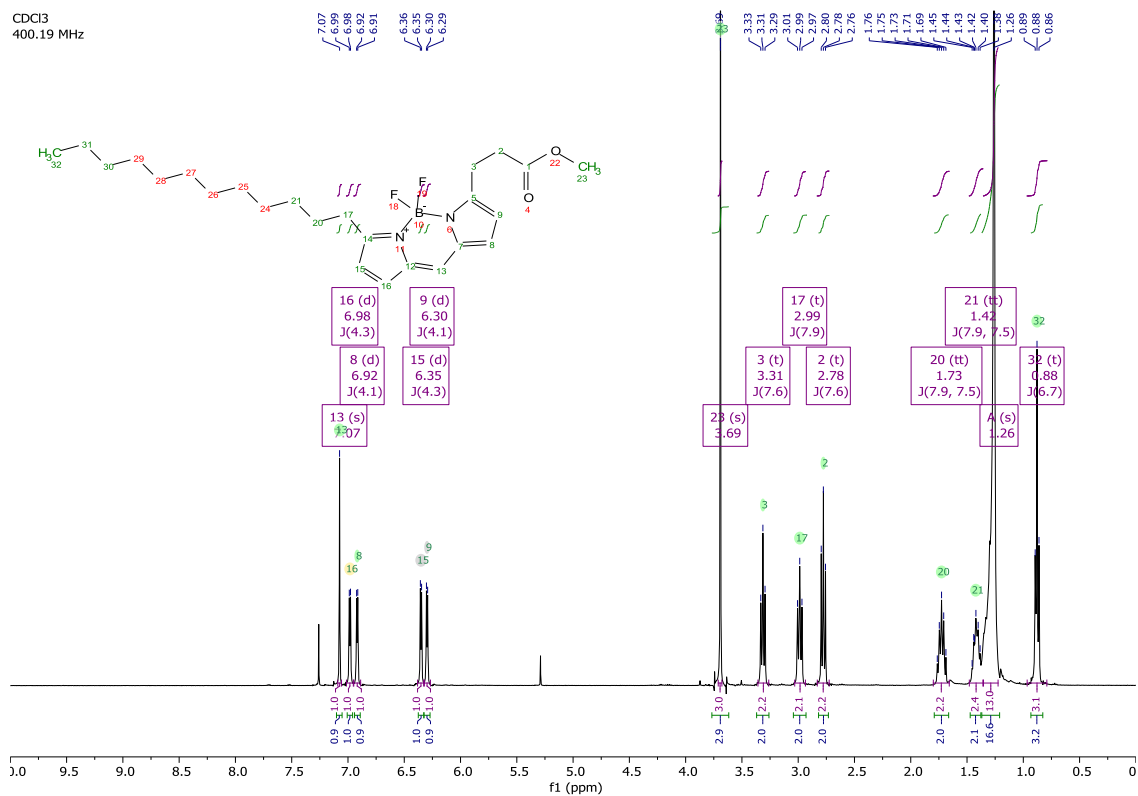


<sup>1</sup>H and <sup>13</sup>C NMR spectra of aldehyde **1.20**.

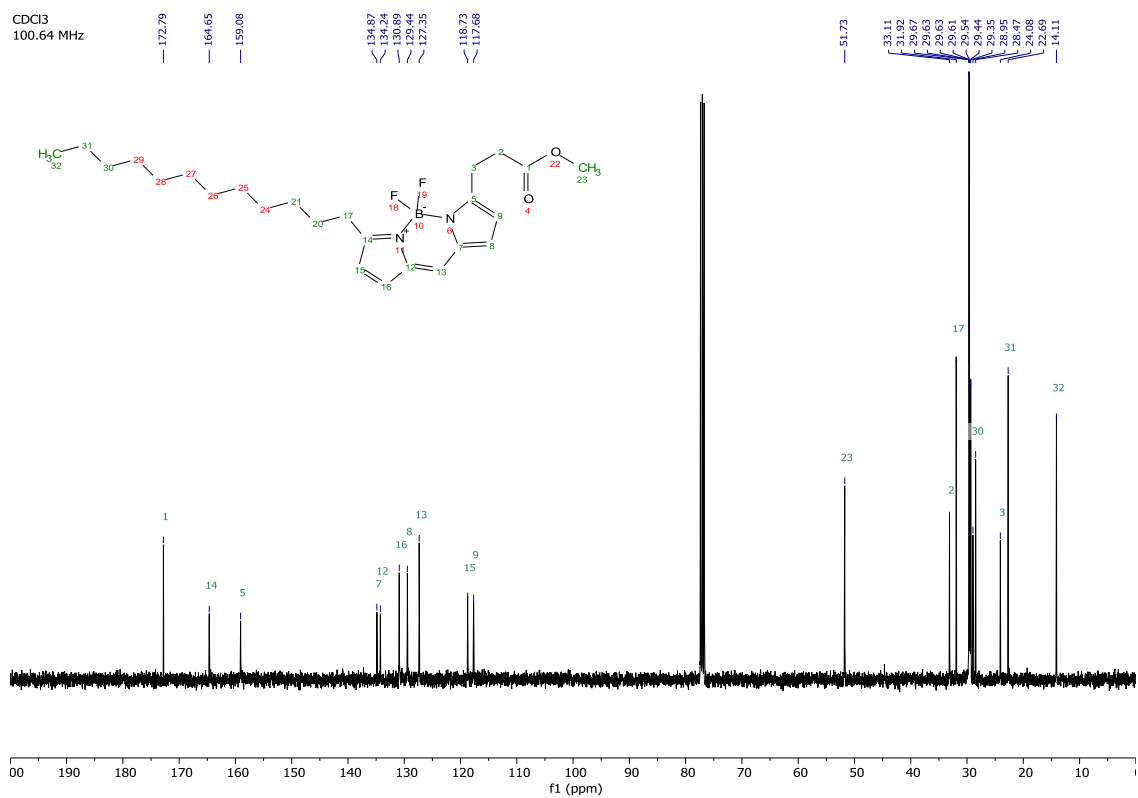


# <sup>1</sup>H and <sup>13</sup>C NMR spectra of bodypi 1.21.

CDCl<sub>3</sub>  
400.19 MHz

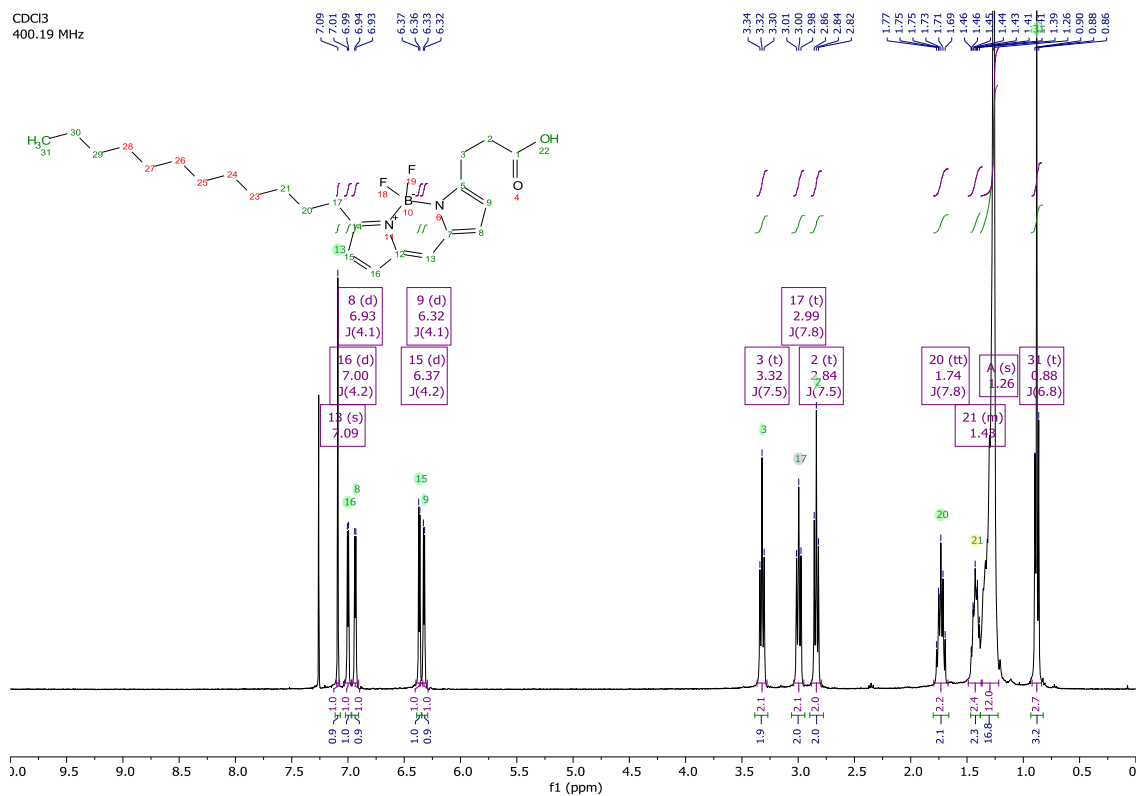


CDCl<sub>3</sub>  
100.64 MHz

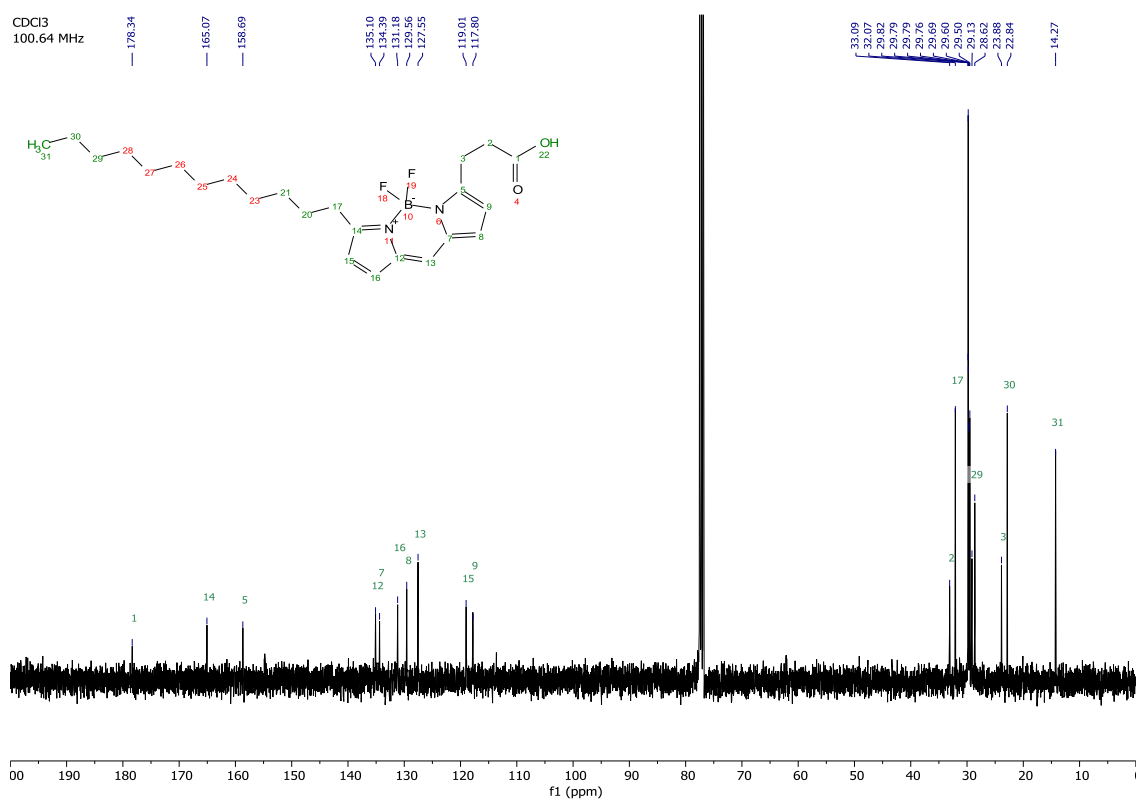


# <sup>1</sup>H and <sup>13</sup>C NMR spectra of bodypy 1.18.

CDCl<sub>3</sub>  
400.19 MHz



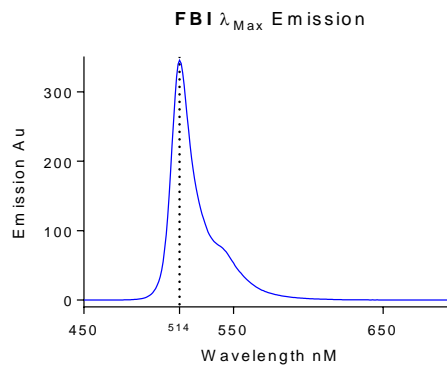
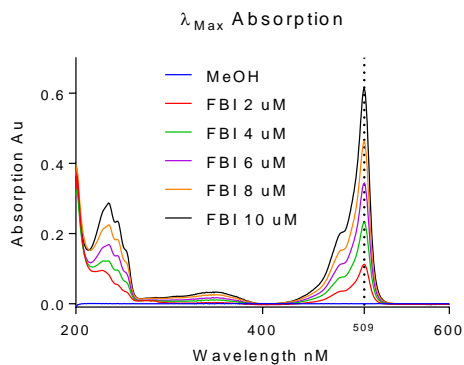
CDCl<sub>3</sub>  
100.64 MHz



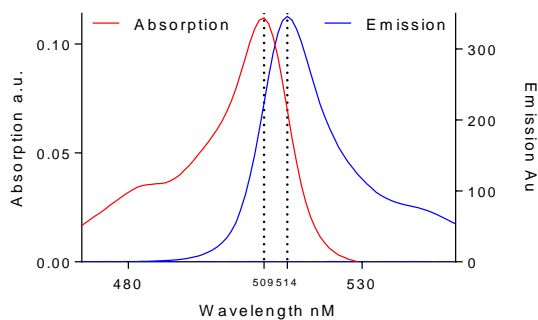




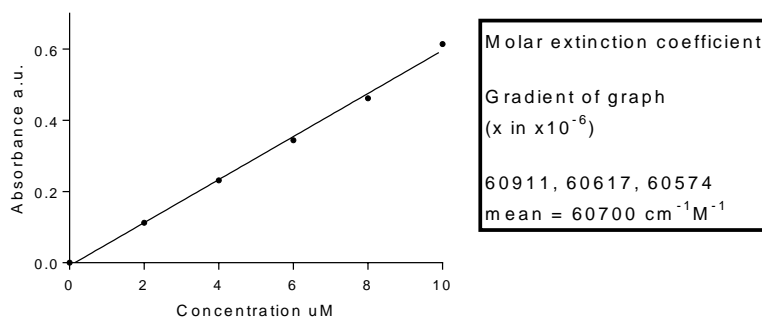
## UV/Vis and fluorimetry data for FBI.



FBI 2  $\mu\text{M}$   $\lambda_{\text{Max}}$  Combined Absorption and Emission



FBI Absorbance Vs Concentration



## Absorbance Data.

### Wavelength

nM	MeOH	FBI 2 uM	FBI 4 uM	FBI 6 uM	FBI 8 uM	FBI 10 uM
1000.	0.0001	-0.0004	0.0002	0.0004	0.0015	-0.0002
999.	0.0000	-0.0004	0.0002	0.0003	0.0014	-0.0002
998.	0.0000	-0.0005	0.0002	0.0004	0.0015	-0.0001
997.	0.0000	-0.0004	0.0003	0.0005	0.0014	-0.0002
996.	0.0001	-0.0003	0.0003	0.0005	0.0015	-0.0001
995.	0.0000	-0.0004	0.0004	0.0005	0.0015	-0.0001

994.	0.0001	-0.0004	0.0004	0.0006	0.0015	0.0000
993.	0.0001	-0.0004	0.0005	0.0006	0.0015	-0.0001
992.	0.0001	-0.0004	0.0004	0.0007	0.0014	-0.0002
991.	0.0000	-0.0003	0.0004	0.0007	0.0014	-0.0001
990.	0.0000	-0.0003	0.0005	0.0007	0.0015	0.0000
989.	0.0000	-0.0003	0.0006	0.0008	0.0015	0.0000
988.	0.0001	-0.0003	0.0006	0.0008	0.0014	0.0000
987.	0.0000	-0.0002	0.0005	0.0007	0.0014	0.0000
986.	0.0001	-0.0001	0.0006	0.0008	0.0014	0.0000
985.	0.0001	0.0000	0.0007	0.0010	0.0015	0.0002
984.	0.0001	0.0000	0.0008	0.0009	0.0015	0.0002
983.	0.0001	0.0000	0.0007	0.0010	0.0015	0.0001
982.	0.0000	-0.0001	0.0008	0.0009	0.0015	0.0000
981.	0.0000	0.0000	0.0007	0.0009	0.0015	0.0000
980.	0.0000	-0.0002	0.0005	0.0008	0.0013	0.0000
979.	0.0002	0.0000	0.0008	0.0010	0.0014	0.0001
978.	0.0001	-0.0001	0.0007	0.0011	0.0014	0.0001
977.	0.0003	0.0002	0.0009	0.0012	0.0016	0.0003
976.	0.0000	0.0000	0.0008	0.0010	0.0015	0.0000
975.	-0.0001	-0.0002	0.0006	0.0008	0.0014	-0.0001
974.	0.0002	0.0000	0.0007	0.0011	0.0014	0.0001
973.	0.0001	0.0000	0.0007	0.0010	0.0013	0.0001
972.	-0.0001	-0.0001	0.0007	0.0008	0.0012	0.0000
971.	0.0001	0.0000	0.0006	0.0009	0.0013	0.0001
970.	0.0002	-0.0001	0.0007	0.0010	0.0013	0.0000
969.	0.0002	0.0000	0.0007	0.0011	0.0014	0.0003
968.	0.0002	0.0000	0.0008	0.0009	0.0012	0.0001
967.	0.0001	-0.0002	0.0006	0.0007	0.0012	-0.0001

966.	0.0000	-0.0002	0.0006	0.0008	0.0012	0.0000
965.	0.0001	-0.0001	0.0006	0.0008	0.0012	0.0000
964.	0.0000	-0.0002	0.0005	0.0008	0.0011	-0.0001
963.	0.0001	-0.0002	0.0006	0.0009	0.0011	0.0000
962.	0.0001	-0.0001	0.0006	0.0009	0.0012	0.0000
961.	0.0001	-0.0002	0.0005	0.0007	0.0010	-0.0001
960.	0.0003	-0.0002	0.0007	0.0008	0.0011	-0.0001
959.	-0.0001	-0.0003	0.0003	0.0006	0.0009	-0.0003
958.	0.0000	-0.0005	0.0004	0.0005	0.0008	-0.0003
957.	-0.0001	-0.0005	0.0002	0.0003	0.0007	-0.0004
956.	0.0000	-0.0006	0.0001	0.0002	0.0006	-0.0005
955.	0.0000	-0.0007	-0.0001	0.0000	0.0005	-0.0005
954.	0.0001	-0.0008	-0.0003	-0.0002	0.0003	-0.0008
953.	0.0001	-0.0009	-0.0004	-0.0004	0.0003	-0.0008
952.	0.0001	-0.0009	-0.0004	-0.0005	0.0002	-0.0009
951.	0.0000	-0.0013	-0.0006	-0.0006	0.0000	-0.0011
950.	0.0002	-0.0012	-0.0006	-0.0006	0.0001	-0.0011
949.	0.0000	-0.0014	-0.0009	-0.0008	-0.0001	-0.0012
948.	0.0001	-0.0013	-0.0007	-0.0007	-0.0001	-0.0012
947.	0.0000	-0.0015	-0.0010	-0.0010	-0.0003	-0.0013
946.	0.0000	-0.0014	-0.0008	-0.0009	-0.0002	-0.0012
945.	0.0000	-0.0013	-0.0009	-0.0010	-0.0003	-0.0012
944.	0.0000	-0.0013	-0.0009	-0.0011	-0.0004	-0.0013
943.	0.0001	-0.0013	-0.0008	-0.0010	-0.0003	-0.0013
942.	0.0001	-0.0014	-0.0010	-0.0011	-0.0003	-0.0013
941.	0.0001	-0.0012	-0.0008	-0.0009	-0.0002	-0.0011
940.	0.0001	-0.0013	-0.0009	-0.0011	-0.0003	-0.0013
939.	0.0001	-0.0014	-0.0008	-0.0010	-0.0004	-0.0013

938.	0.0001	-0.0013	-0.0009	-0.0011	-0.0003	-0.0013
937.	0.0001	-0.0014	-0.0011	-0.0011	-0.0004	-0.0013
936.	0.0001	-0.0014	-0.0009	-0.0011	-0.0004	-0.0013
935.	0.0001	-0.0014	-0.0010	-0.0011	-0.0004	-0.0012
934.	-0.0001	-0.0015	-0.0012	-0.0013	-0.0005	-0.0014
933.	0.0000	-0.0014	-0.0011	-0.0012	-0.0005	-0.0014
932.	0.0000	-0.0015	-0.0012	-0.0013	-0.0006	-0.0014
931.	0.0000	-0.0015	-0.0011	-0.0013	-0.0004	-0.0015
930.	0.0000	-0.0015	-0.0012	-0.0013	-0.0005	-0.0014
929.	-0.0001	-0.0016	-0.0012	-0.0014	-0.0005	-0.0015
928.	-0.0001	-0.0015	-0.0013	-0.0014	-0.0006	-0.0014
927.	0.0001	-0.0016	-0.0012	-0.0014	-0.0005	-0.0015
926.	0.0000	-0.0016	-0.0013	-0.0014	-0.0006	-0.0015
925.	0.0000	-0.0017	-0.0014	-0.0016	-0.0008	-0.0015
924.	0.0000	-0.0017	-0.0014	-0.0015	-0.0006	-0.0015
923.	0.0001	-0.0017	-0.0013	-0.0016	-0.0006	-0.0015
922.	0.0001	-0.0015	-0.0013	-0.0013	-0.0006	-0.0012
921.	0.0000	-0.0018	-0.0015	-0.0015	-0.0007	-0.0015
920.	-0.0001	-0.0017	-0.0014	-0.0014	-0.0007	-0.0015
919.	-0.0001	-0.0017	-0.0014	-0.0015	-0.0008	-0.0016
918.	0.0001	-0.0016	-0.0013	-0.0014	-0.0006	-0.0015
917.	0.0001	-0.0016	-0.0014	-0.0015	-0.0006	-0.0015
916.	0.0002	-0.0016	-0.0013	-0.0015	-0.0006	-0.0015
915.	0.0000	-0.0017	-0.0014	-0.0015	-0.0007	-0.0016
914.	0.0000	-0.0018	-0.0015	-0.0016	-0.0009	-0.0017
913.	0.0001	-0.0017	-0.0013	-0.0016	-0.0007	-0.0016
912.	0.0001	-0.0017	-0.0015	-0.0017	-0.0009	-0.0016
911.	0.0000	-0.0018	-0.0016	-0.0018	-0.0010	-0.0018

910.	0.0001	-0.0017	-0.0015	-0.0017	-0.0009	-0.0017
909.	0.0001	-0.0017	-0.0015	-0.0016	-0.0008	-0.0016
908.	0.0000	-0.0017	-0.0014	-0.0015	-0.0008	-0.0016
907.	0.0001	-0.0017	-0.0014	-0.0014	-0.0008	-0.0016
906.	0.0000	-0.0017	-0.0014	-0.0016	-0.0009	-0.0016
905.	0.0000	-0.0018	-0.0014	-0.0016	-0.0008	-0.0017
904.	0.0000	-0.0018	-0.0015	-0.0016	-0.0009	-0.0017
903.	0.0000	-0.0018	-0.0014	-0.0015	-0.0008	-0.0017
902.	0.0001	-0.0018	-0.0014	-0.0015	-0.0008	-0.0016
901.	0.0000	-0.0017	-0.0014	-0.0014	-0.0009	-0.0017
900.	0.0000	-0.0017	-0.0013	-0.0014	-0.0008	-0.0016
899.	0.0001	-0.0016	-0.0013	-0.0013	-0.0007	-0.0015
898.	0.0000	-0.0017	-0.0014	-0.0014	-0.0008	-0.0016
897.	0.0000	-0.0017	-0.0013	-0.0014	-0.0008	-0.0015
896.	0.0000	-0.0017	-0.0013	-0.0013	-0.0008	-0.0016
895.	0.0000	-0.0017	-0.0013	-0.0014	-0.0007	-0.0015
894.	0.0000	-0.0016	-0.0013	-0.0014	-0.0008	-0.0017
893.	0.0001	-0.0017	-0.0012	-0.0012	-0.0005	-0.0013
892.	0.0001	-0.0017	-0.0011	-0.0012	-0.0005	-0.0014
891.	0.0001	-0.0017	-0.0013	-0.0012	-0.0006	-0.0015
890.	0.0000	-0.0017	-0.0012	-0.0011	-0.0005	-0.0014
889.	0.0000	-0.0017	-0.0011	-0.0012	-0.0005	-0.0014
888.	0.0000	-0.0017	-0.0012	-0.0011	-0.0005	-0.0015
887.	-0.0001	-0.0018	-0.0012	-0.0011	-0.0006	-0.0015
886.	-0.0001	-0.0018	-0.0012	-0.0012	-0.0007	-0.0015
885.	0.0000	-0.0018	-0.0012	-0.0011	-0.0005	-0.0014
884.	0.0000	-0.0017	-0.0012	-0.0012	-0.0004	-0.0014
883.	0.0000	-0.0019	-0.0012	-0.0011	-0.0005	-0.0016

882.	0.0000	-0.0018	-0.0011	-0.0011	-0.0005	-0.0014
881.	0.0001	-0.0019	-0.0012	-0.0012	-0.0004	-0.0016
880.	0.0000	-0.0017	-0.0011	-0.0011	-0.0005	-0.0013
879.	0.0001	-0.0017	-0.0012	-0.0012	-0.0004	-0.0014
878.	0.0000	-0.0017	-0.0012	-0.0013	-0.0006	-0.0014
877.	0.0000	-0.0017	-0.0012	-0.0013	-0.0006	-0.0014
876.	0.0000	-0.0017	-0.0012	-0.0012	-0.0006	-0.0014
875.	0.0002	-0.0016	-0.0011	-0.0013	-0.0006	-0.0014
874.	0.0000	-0.0017	-0.0012	-0.0013	-0.0006	-0.0014
873.	0.0000	-0.0016	-0.0012	-0.0012	-0.0006	-0.0013
872.	0.0000	-0.0017	-0.0012	-0.0013	-0.0006	-0.0016
871.	0.0000	-0.0016	-0.0011	-0.0012	-0.0006	-0.0014
870.	0.0000	-0.0017	-0.0012	-0.0013	-0.0007	-0.0014
869.	0.0000	-0.0017	-0.0012	-0.0013	-0.0007	-0.0015
868.	0.0000	-0.0016	-0.0011	-0.0013	-0.0006	-0.0014
867.	0.0001	-0.0016	-0.0012	-0.0013	-0.0006	-0.0014
866.	-0.0001	-0.0018	-0.0013	-0.0014	-0.0007	-0.0015
865.	0.0001	-0.0016	-0.0011	-0.0013	-0.0007	-0.0014
864.	0.0000	-0.0017	-0.0011	-0.0013	-0.0006	-0.0015
863.	0.0001	-0.0016	-0.0012	-0.0013	-0.0005	-0.0014
862.	0.0000	-0.0017	-0.0011	-0.0014	-0.0006	-0.0015
861.	0.0000	-0.0016	-0.0011	-0.0013	-0.0006	-0.0014
860.	0.0000	-0.0017	-0.0011	-0.0013	-0.0006	-0.0014
859.	0.0000	-0.0017	-0.0013	-0.0013	-0.0007	-0.0014
858.	0.0001	-0.0016	-0.0011	-0.0013	-0.0005	-0.0013
857.	0.0000	-0.0017	-0.0011	-0.0014	-0.0006	-0.0014
856.	0.0000	-0.0017	-0.0011	-0.0014	-0.0006	-0.0015
855.	0.0000	-0.0017	-0.0012	-0.0013	-0.0006	-0.0014

854.	0.0000	-0.0017	-0.0013	-0.0014	-0.0007	-0.0015
853.	0.0000	-0.0017	-0.0012	-0.0013	-0.0005	-0.0014
852.	0.0001	-0.0018	-0.0012	-0.0013	-0.0007	-0.0014
851.	0.0000	-0.0018	-0.0013	-0.0013	-0.0005	-0.0014
850.	0.0001	-0.0017	-0.0011	-0.0013	-0.0006	-0.0013
849.	0.0000	-0.0018	-0.0012	-0.0014	-0.0006	-0.0015
848.	0.0000	-0.0017	-0.0012	-0.0013	-0.0005	-0.0014
847.	0.0001	-0.0017	-0.0012	-0.0014	-0.0006	-0.0014
846.	0.0000	-0.0017	-0.0012	-0.0014	-0.0005	-0.0015
845.	0.0001	-0.0018	-0.0013	-0.0014	-0.0006	-0.0013
844.	0.0000	-0.0018	-0.0013	-0.0014	-0.0006	-0.0015
843.	0.0001	-0.0017	-0.0011	-0.0013	-0.0005	-0.0013
842.	0.0000	-0.0018	-0.0012	-0.0014	-0.0005	-0.0014
841.	0.0001	-0.0017	-0.0012	-0.0013	-0.0005	-0.0013
840.	-0.0001	-0.0018	-0.0012	-0.0014	-0.0006	-0.0014
839.	0.0000	-0.0018	-0.0012	-0.0015	-0.0005	-0.0014
838.	0.0000	-0.0017	-0.0012	-0.0014	-0.0005	-0.0014
837.	0.0000	-0.0019	-0.0013	-0.0014	-0.0006	-0.0015
836.	-0.0001	-0.0018	-0.0013	-0.0014	-0.0006	-0.0014
835.	0.0001	-0.0017	-0.0012	-0.0014	-0.0005	-0.0014
834.	0.0001	-0.0016	-0.0012	-0.0013	-0.0005	-0.0014
833.	0.0000	-0.0017	-0.0013	-0.0014	-0.0005	-0.0014
832.	0.0000	-0.0017	-0.0013	-0.0014	-0.0006	-0.0015
831.	0.0000	-0.0017	-0.0011	-0.0013	-0.0005	-0.0014
830.	0.0001	-0.0016	-0.0012	-0.0013	-0.0005	-0.0013
829.	0.0001	-0.0017	-0.0012	-0.0013	-0.0005	-0.0014
828.	0.0000	-0.0018	-0.0012	-0.0013	-0.0005	-0.0014
827.	0.0001	-0.0017	-0.0011	-0.0014	-0.0004	-0.0014

826.	0.0001	-0.0017	-0.0012	-0.0014	-0.0005	-0.0013
825.	0.0000	-0.0017	-0.0012	-0.0014	-0.0004	-0.0014
824.	0.0000	-0.0018	-0.0012	-0.0015	-0.0006	-0.0015
823.	0.0000	-0.0017	-0.0012	-0.0014	-0.0005	-0.0014
822.	0.0001	-0.0016	-0.0012	-0.0014	-0.0005	-0.0014
821.	0.0000	-0.0018	-0.0012	-0.0014	-0.0005	-0.0015
820.	0.0000	-0.0018	-0.0012	-0.0014	-0.0005	-0.0015
819.	0.0000	-0.0018	-0.0012	-0.0014	-0.0004	-0.0014
818.	0.0001	-0.0016	-0.0012	-0.0014	-0.0004	-0.0013
817.	0.0001	-0.0017	-0.0011	-0.0014	-0.0004	-0.0014
816.	0.0000	-0.0017	-0.0012	-0.0015	-0.0004	-0.0014
815.	0.0000	-0.0018	-0.0013	-0.0015	-0.0005	-0.0014
814.	0.0000	-0.0017	-0.0012	-0.0014	-0.0005	-0.0015
813.	0.0000	-0.0017	-0.0012	-0.0015	-0.0006	-0.0015
812.	0.0000	-0.0018	-0.0012	-0.0015	-0.0004	-0.0014
811.	-0.0001	-0.0016	-0.0012	-0.0014	-0.0005	-0.0013
810.	0.0000	-0.0017	-0.0012	-0.0014	-0.0004	-0.0014
809.	-0.0001	-0.0018	-0.0013	-0.0016	-0.0005	-0.0015
808.	0.0000	-0.0018	-0.0012	-0.0015	-0.0006	-0.0014
807.	0.0000	-0.0017	-0.0013	-0.0014	-0.0006	-0.0015
806.	0.0000	-0.0018	-0.0012	-0.0015	-0.0006	-0.0015
805.	0.0000	-0.0016	-0.0012	-0.0014	-0.0006	-0.0015
804.	0.0000	-0.0017	-0.0012	-0.0015	-0.0006	-0.0015
803.	0.0000	-0.0018	-0.0012	-0.0014	-0.0005	-0.0014
802.	0.0000	-0.0018	-0.0013	-0.0015	-0.0005	-0.0015
801.	-0.0001	-0.0018	-0.0013	-0.0014	-0.0006	-0.0014
800.	-0.0001	-0.0018	-0.0013	-0.0016	-0.0005	-0.0015
799.	0.0000	-0.0018	-0.0012	-0.0015	-0.0006	-0.0014

798.	-0.0001	-0.0017	-0.0012	-0.0015	-0.0005	-0.0014
797.	0.0001	-0.0018	-0.0011	-0.0014	-0.0006	-0.0015
796.	-0.0001	-0.0017	-0.0012	-0.0015	-0.0006	-0.0015
795.	0.0000	-0.0018	-0.0012	-0.0014	-0.0005	-0.0015
794.	0.0000	-0.0017	-0.0012	-0.0015	-0.0006	-0.0015
793.	0.0000	-0.0017	-0.0012	-0.0014	-0.0005	-0.0015
792.	-0.0001	-0.0018	-0.0012	-0.0015	-0.0006	-0.0015
791.	0.0000	-0.0018	-0.0013	-0.0015	-0.0005	-0.0015
790.	0.0000	-0.0018	-0.0012	-0.0015	-0.0006	-0.0016
789.	-0.0001	-0.0018	-0.0012	-0.0016	-0.0006	-0.0016
788.	0.0000	-0.0018	-0.0012	-0.0015	-0.0007	-0.0016
787.	-0.0001	-0.0017	-0.0013	-0.0017	-0.0007	-0.0017
786.	-0.0001	-0.0020	-0.0014	-0.0018	-0.0008	-0.0017
785.	0.0000	-0.0019	-0.0013	-0.0017	-0.0006	-0.0016
784.	0.0000	-0.0018	-0.0013	-0.0017	-0.0007	-0.0016
783.	0.0001	-0.0018	-0.0013	-0.0016	-0.0006	-0.0015
782.	0.0001	-0.0018	-0.0013	-0.0017	-0.0008	-0.0016
781.	0.0000	-0.0018	-0.0013	-0.0017	-0.0007	-0.0016
780.	0.0000	-0.0018	-0.0013	-0.0016	-0.0007	-0.0016
779.	0.0000	-0.0019	-0.0013	-0.0017	-0.0007	-0.0016
778.	-0.0001	-0.0019	-0.0014	-0.0017	-0.0007	-0.0017
777.	0.0000	-0.0019	-0.0013	-0.0016	-0.0007	-0.0016
776.	0.0001	-0.0017	-0.0013	-0.0016	-0.0007	-0.0016
775.	0.0000	-0.0019	-0.0013	-0.0016	-0.0005	-0.0014
774.	0.0000	-0.0018	-0.0013	-0.0014	-0.0005	-0.0015
773.	0.0000	-0.0018	-0.0010	-0.0014	-0.0005	-0.0014
772.	0.0000	-0.0017	-0.0012	-0.0014	-0.0005	-0.0015
771.	-0.0001	-0.0018	-0.0012	-0.0015	-0.0007	-0.0016

770.	-0.0001	-0.0018	-0.0012	-0.0015	-0.0007	-0.0017
769.	-0.0001	-0.0017	-0.0012	-0.0014	-0.0007	-0.0016
768.	0.0000	-0.0019	-0.0013	-0.0016	-0.0008	-0.0017
767.	-0.0001	-0.0017	-0.0012	-0.0016	-0.0007	-0.0016
766.	0.0000	-0.0019	-0.0012	-0.0015	-0.0006	-0.0016
765.	0.0000	-0.0018	-0.0012	-0.0016	-0.0007	-0.0017
764.	-0.0001	-0.0019	-0.0013	-0.0016	-0.0008	-0.0017
763.	-0.0002	-0.0019	-0.0014	-0.0016	-0.0009	-0.0018
762.	-0.0001	-0.0018	-0.0012	-0.0016	-0.0007	-0.0017
761.	-0.0001	-0.0020	-0.0014	-0.0016	-0.0008	-0.0017
760.	-0.0001	-0.0019	-0.0013	-0.0016	-0.0008	-0.0017
759.	-0.0001	-0.0019	-0.0013	-0.0016	-0.0008	-0.0017
758.	-0.0001	-0.0019	-0.0014	-0.0016	-0.0008	-0.0017
757.	0.0000	-0.0018	-0.0013	-0.0015	-0.0008	-0.0017
756.	-0.0001	-0.0020	-0.0013	-0.0017	-0.0008	-0.0018
755.	0.0000	-0.0019	-0.0013	-0.0016	-0.0008	-0.0018
754.	-0.0001	-0.0019	-0.0013	-0.0016	-0.0008	-0.0018
753.	-0.0001	-0.0020	-0.0014	-0.0017	-0.0009	-0.0018
752.	-0.0001	-0.0020	-0.0013	-0.0017	-0.0009	-0.0018
751.	0.0000	-0.0019	-0.0013	-0.0016	-0.0008	-0.0018
750.	0.0000	-0.0019	-0.0013	-0.0016	-0.0008	-0.0018
749.	-0.0001	-0.0019	-0.0014	-0.0016	-0.0009	-0.0019
748.	0.0000	-0.0020	-0.0014	-0.0017	-0.0009	-0.0019
747.	0.0000	-0.0020	-0.0013	-0.0017	-0.0008	-0.0017
746.	-0.0001	-0.0020	-0.0014	-0.0018	-0.0009	-0.0019
745.	-0.0001	-0.0019	-0.0014	-0.0016	-0.0009	-0.0018
744.	0.0000	-0.0019	-0.0013	-0.0017	-0.0009	-0.0018
743.	-0.0002	-0.0020	-0.0014	-0.0018	-0.0010	-0.0020

742.	-0.0001	-0.0019	-0.0013	-0.0016	-0.0009	-0.0018
741.	-0.0001	-0.0020	-0.0013	-0.0017	-0.0009	-0.0019
740.	-0.0001	-0.0019	-0.0013	-0.0017	-0.0009	-0.0019
739.	-0.0002	-0.0019	-0.0013	-0.0017	-0.0009	-0.0019
738.	-0.0001	-0.0020	-0.0015	-0.0018	-0.0010	-0.0019
737.	-0.0002	-0.0021	-0.0015	-0.0018	-0.0010	-0.0020
736.	0.0000	-0.0020	-0.0013	-0.0017	-0.0009	-0.0019
735.	-0.0002	-0.0020	-0.0014	-0.0018	-0.0010	-0.0020
734.	-0.0001	-0.0020	-0.0014	-0.0018	-0.0009	-0.0019
733.	-0.0001	-0.0020	-0.0015	-0.0018	-0.0011	-0.0020
732.	-0.0002	-0.0021	-0.0014	-0.0019	-0.0010	-0.0020
731.	-0.0001	-0.0020	-0.0015	-0.0018	-0.0010	-0.0020
730.	-0.0002	-0.0021	-0.0016	-0.0019	-0.0011	-0.0020
729.	-0.0001	-0.0020	-0.0015	-0.0018	-0.0010	-0.0020
728.	-0.0001	-0.0020	-0.0014	-0.0019	-0.0011	-0.0020
727.	-0.0001	-0.0021	-0.0016	-0.0019	-0.0011	-0.0020
726.	-0.0002	-0.0021	-0.0015	-0.0019	-0.0011	-0.0020
725.	0.0000	-0.0020	-0.0015	-0.0018	-0.0011	-0.0020
724.	-0.0002	-0.0020	-0.0015	-0.0019	-0.0011	-0.0020
723.	-0.0002	-0.0021	-0.0016	-0.0019	-0.0012	-0.0020
722.	0.0000	-0.0020	-0.0014	-0.0018	-0.0010	-0.0019
721.	0.0000	-0.0020	-0.0015	-0.0019	-0.0011	-0.0020
720.	-0.0001	-0.0021	-0.0015	-0.0020	-0.0012	-0.0020
719.	-0.0001	-0.0021	-0.0014	-0.0019	-0.0010	-0.0020
718.	-0.0001	-0.0020	-0.0015	-0.0019	-0.0010	-0.0019
717.	0.0000	-0.0021	-0.0015	-0.0019	-0.0010	-0.0020
716.	-0.0001	-0.0020	-0.0015	-0.0019	-0.0011	-0.0021
715.	0.0000	-0.0020	-0.0014	-0.0019	-0.0010	-0.0020

714.	-0.0001	-0.0021	-0.0015	-0.0019	-0.0011	-0.0020
713.	-0.0001	-0.0021	-0.0015	-0.0019	-0.0011	-0.0021
712.	-0.0001	-0.0021	-0.0015	-0.0018	-0.0011	-0.0020
711.	-0.0001	-0.0021	-0.0015	-0.0020	-0.0010	-0.0020
710.	-0.0002	-0.0021	-0.0016	-0.0020	-0.0011	-0.0021
709.	0.0000	-0.0021	-0.0015	-0.0019	-0.0011	-0.0020
708.	-0.0002	-0.0021	-0.0015	-0.0020	-0.0012	-0.0022
707.	0.0000	-0.0019	-0.0015	-0.0018	-0.0010	-0.0020
706.	-0.0001	-0.0021	-0.0016	-0.0020	-0.0012	-0.0021
705.	-0.0002	-0.0020	-0.0017	-0.0019	-0.0011	-0.0021
704.	-0.0001	-0.0021	-0.0016	-0.0020	-0.0012	-0.0021
703.	-0.0001	-0.0020	-0.0016	-0.0020	-0.0011	-0.0021
702.	-0.0001	-0.0021	-0.0016	-0.0020	-0.0011	-0.0020
701.	-0.0001	-0.0020	-0.0016	-0.0020	-0.0011	-0.0021
700.	-0.0001	-0.0020	-0.0016	-0.0020	-0.0012	-0.0021
699.	-0.0001	-0.0020	-0.0015	-0.0020	-0.0011	-0.0020
698.	-0.0001	-0.0021	-0.0016	-0.0020	-0.0011	-0.0021
697.	-0.0002	-0.0021	-0.0017	-0.0020	-0.0011	-0.0021
696.	-0.0001	-0.0021	-0.0016	-0.0020	-0.0013	-0.0022
695.	-0.0001	-0.0021	-0.0016	-0.0020	-0.0012	-0.0021
694.	-0.0001	-0.0021	-0.0017	-0.0021	-0.0012	-0.0021
693.	-0.0001	-0.0021	-0.0016	-0.0020	-0.0012	-0.0021
692.	-0.0002	-0.0021	-0.0017	-0.0021	-0.0012	-0.0022
691.	0.0000	-0.0020	-0.0016	-0.0020	-0.0011	-0.0020
690.	-0.0001	-0.0020	-0.0017	-0.0021	-0.0012	-0.0021
689.	-0.0001	-0.0020	-0.0017	-0.0020	-0.0011	-0.0022
688.	0.0000	-0.0022	-0.0017	-0.0020	-0.0012	-0.0021
687.	-0.0001	-0.0020	-0.0018	-0.0020	-0.0012	-0.0021

686.	-0.0001	-0.0021	-0.0017	-0.0020	-0.0012	-0.0021
685.	-0.0001	-0.0021	-0.0017	-0.0020	-0.0011	-0.0022
684.	0.0000	-0.0021	-0.0017	-0.0020	-0.0011	-0.0021
683.	-0.0001	-0.0021	-0.0017	-0.0021	-0.0012	-0.0022
682.	-0.0001	-0.0021	-0.0017	-0.0021	-0.0011	-0.0022
681.	-0.0001	-0.0022	-0.0018	-0.0021	-0.0012	-0.0022
680.	0.0000	-0.0021	-0.0016	-0.0020	-0.0011	-0.0021
679.	-0.0001	-0.0021	-0.0018	-0.0021	-0.0012	-0.0022
678.	0.0000	-0.0020	-0.0016	-0.0020	-0.0011	-0.0021
677.	-0.0001	-0.0022	-0.0018	-0.0021	-0.0012	-0.0022
676.	-0.0001	-0.0021	-0.0017	-0.0021	-0.0012	-0.0023
675.	-0.0001	-0.0022	-0.0018	-0.0021	-0.0012	-0.0022
674.	-0.0001	-0.0021	-0.0016	-0.0021	-0.0012	-0.0021
673.	-0.0002	-0.0022	-0.0018	-0.0021	-0.0012	-0.0023
672.	-0.0001	-0.0021	-0.0018	-0.0021	-0.0013	-0.0023
671.	-0.0001	-0.0022	-0.0018	-0.0020	-0.0013	-0.0023
670.	0.0000	-0.0020	-0.0017	-0.0021	-0.0011	-0.0021
669.	-0.0001	-0.0021	-0.0017	-0.0020	-0.0011	-0.0022
668.	-0.0001	-0.0022	-0.0018	-0.0021	-0.0013	-0.0023
667.	-0.0002	-0.0022	-0.0017	-0.0024	-0.0014	-0.0024
666.	-0.0001	-0.0022	-0.0019	-0.0024	-0.0015	-0.0023
665.	0.0000	-0.0021	-0.0018	-0.0023	-0.0013	-0.0022
664.	-0.0001	-0.0021	-0.0018	-0.0023	-0.0013	-0.0023
663.	0.0000	-0.0020	-0.0017	-0.0022	-0.0013	-0.0022
662.	0.0000	-0.0022	-0.0019	-0.0023	-0.0014	-0.0022
661.	0.0000	-0.0021	-0.0018	-0.0022	-0.0013	-0.0022
660.	0.0000	-0.0021	-0.0018	-0.0022	-0.0013	-0.0023
659.	0.0000	-0.0020	-0.0018	-0.0021	-0.0011	-0.0020

658.	0.0001	-0.0021	-0.0017	-0.0019	-0.0011	-0.0022
657.	0.0001	-0.0020	-0.0015	-0.0019	-0.0011	-0.0021
656.	-0.0001	-0.0021	-0.0018	-0.0021	-0.0012	-0.0023
655.	0.0000	-0.0021	-0.0018	-0.0021	-0.0013	-0.0023
654.	-0.0001	-0.0021	-0.0017	-0.0021	-0.0013	-0.0023
653.	-0.0001	-0.0021	-0.0018	-0.0021	-0.0013	-0.0023
652.	0.0000	-0.0021	-0.0017	-0.0021	-0.0011	-0.0022
651.	0.0000	-0.0022	-0.0018	-0.0021	-0.0013	-0.0023
650.	-0.0001	-0.0022	-0.0018	-0.0021	-0.0013	-0.0023
649.	-0.0001	-0.0022	-0.0018	-0.0021	-0.0013	-0.0023
648.	0.0000	-0.0021	-0.0018	-0.0021	-0.0012	-0.0022
647.	-0.0001	-0.0022	-0.0019	-0.0022	-0.0013	-0.0024
646.	-0.0001	-0.0021	-0.0017	-0.0021	-0.0013	-0.0022
645.	-0.0002	-0.0022	-0.0018	-0.0021	-0.0013	-0.0022
644.	0.0000	-0.0021	-0.0017	-0.0020	-0.0013	-0.0023
643.	-0.0002	-0.0021	-0.0018	-0.0022	-0.0014	-0.0024
642.	0.0000	-0.0021	-0.0017	-0.0020	-0.0012	-0.0023
641.	-0.0001	-0.0021	-0.0018	-0.0021	-0.0013	-0.0024
640.	-0.0001	-0.0022	-0.0018	-0.0021	-0.0013	-0.0023
639.	0.0000	-0.0021	-0.0018	-0.0021	-0.0014	-0.0023
638.	0.0000	-0.0021	-0.0018	-0.0021	-0.0013	-0.0023
637.	-0.0001	-0.0021	-0.0018	-0.0021	-0.0013	-0.0024
636.	0.0000	-0.0021	-0.0018	-0.0021	-0.0013	-0.0023
635.	-0.0001	-0.0021	-0.0018	-0.0021	-0.0013	-0.0023
634.	-0.0001	-0.0022	-0.0019	-0.0022	-0.0014	-0.0024
633.	-0.0001	-0.0022	-0.0018	-0.0023	-0.0014	-0.0024
632.	-0.0001	-0.0022	-0.0019	-0.0022	-0.0015	-0.0025
631.	-0.0001	-0.0021	-0.0017	-0.0022	-0.0013	-0.0023

630.	0.0000	-0.0021	-0.0018	-0.0022	-0.0014	-0.0024
629.	-0.0001	-0.0022	-0.0019	-0.0022	-0.0013	-0.0023
628.	0.0000	-0.0021	-0.0018	-0.0022	-0.0013	-0.0023
627.	-0.0001	-0.0021	-0.0018	-0.0022	-0.0013	-0.0023
626.	-0.0001	-0.0021	-0.0018	-0.0023	-0.0013	-0.0024
625.	-0.0001	-0.0021	-0.0019	-0.0022	-0.0013	-0.0024
624.	-0.0001	-0.0022	-0.0018	-0.0023	-0.0013	-0.0024
623.	-0.0001	-0.0021	-0.0018	-0.0023	-0.0014	-0.0024
622.	0.0000	-0.0021	-0.0018	-0.0022	-0.0013	-0.0023
621.	-0.0001	-0.0020	-0.0019	-0.0022	-0.0012	-0.0023
620.	-0.0001	-0.0021	-0.0019	-0.0023	-0.0013	-0.0023
619.	-0.0001	-0.0022	-0.0019	-0.0022	-0.0013	-0.0023
618.	-0.0001	-0.0021	-0.0018	-0.0021	-0.0012	-0.0023
617.	-0.0001	-0.0020	-0.0018	-0.0021	-0.0013	-0.0023
616.	-0.0001	-0.0022	-0.0018	-0.0022	-0.0013	-0.0023
615.	-0.0001	-0.0021	-0.0018	-0.0022	-0.0013	-0.0023
614.	-0.0001	-0.0021	-0.0018	-0.0022	-0.0013	-0.0022
613.	0.0000	-0.0021	-0.0018	-0.0022	-0.0012	-0.0023
612.	-0.0001	-0.0021	-0.0019	-0.0022	-0.0013	-0.0022
611.	0.0000	-0.0020	-0.0017	-0.0021	-0.0012	-0.0023
610.	0.0000	-0.0021	-0.0018	-0.0021	-0.0012	-0.0022
609.	-0.0001	-0.0021	-0.0018	-0.0022	-0.0013	-0.0023
608.	-0.0001	-0.0021	-0.0019	-0.0021	-0.0013	-0.0023
607.	-0.0001	-0.0020	-0.0018	-0.0022	-0.0012	-0.0022
606.	-0.0001	-0.0021	-0.0019	-0.0023	-0.0014	-0.0023
605.	-0.0002	-0.0021	-0.0019	-0.0022	-0.0013	-0.0023
604.	-0.0001	-0.0021	-0.0019	-0.0022	-0.0013	-0.0023
603.	-0.0001	-0.0021	-0.0018	-0.0021	-0.0012	-0.0022

602.	-0.0001	-0.0021	-0.0019	-0.0022	-0.0013	-0.0023
601.	-0.0001	-0.0021	-0.0020	-0.0022	-0.0013	-0.0023
600.	-0.0001	-0.0021	-0.0019	-0.0022	-0.0013	-0.0024
599.	-0.0002	-0.0021	-0.0019	-0.0022	-0.0013	-0.0023
598.	-0.0001	-0.0021	-0.0019	-0.0022	-0.0013	-0.0023
597.	-0.0002	-0.0021	-0.0020	-0.0022	-0.0013	-0.0023
596.	-0.0001	-0.0021	-0.0019	-0.0022	-0.0013	-0.0023
595.	-0.0001	-0.0021	-0.0018	-0.0021	-0.0012	-0.0022
594.	-0.0001	-0.0021	-0.0019	-0.0022	-0.0012	-0.0023
593.	-0.0001	-0.0020	-0.0018	-0.0023	-0.0012	-0.0023
592.	-0.0001	-0.0020	-0.0018	-0.0021	-0.0012	-0.0022
591.	-0.0002	-0.0021	-0.0019	-0.0023	-0.0012	-0.0023
590.	-0.0001	-0.0021	-0.0019	-0.0022	-0.0013	-0.0023
589.	-0.0001	-0.0020	-0.0018	-0.0021	-0.0012	-0.0022
588.	-0.0001	-0.0021	-0.0019	-0.0022	-0.0012	-0.0023
587.	-0.0001	-0.0020	-0.0018	-0.0022	-0.0012	-0.0023
586.	-0.0001	-0.0021	-0.0018	-0.0022	-0.0012	-0.0022
585.	-0.0001	-0.0022	-0.0019	-0.0023	-0.0012	-0.0024
584.	-0.0001	-0.0020	-0.0018	-0.0022	-0.0011	-0.0023
583.	0.0000	-0.0021	-0.0018	-0.0022	-0.0012	-0.0022
582.	0.0000	-0.0020	-0.0019	-0.0023	-0.0012	-0.0023
581.	-0.0001	-0.0022	-0.0020	-0.0025	-0.0014	-0.0024
580.	-0.0001	-0.0021	-0.0019	-0.0023	-0.0013	-0.0024
579.	-0.0001	-0.0020	-0.0019	-0.0022	-0.0012	-0.0024
578.	-0.0001	-0.0021	-0.0019	-0.0022	-0.0012	-0.0023
577.	-0.0001	-0.0022	-0.0019	-0.0023	-0.0013	-0.0024
576.	-0.0001	-0.0021	-0.0019	-0.0023	-0.0013	-0.0024
575.	0.0000	-0.0021	-0.0019	-0.0022	-0.0013	-0.0023

574.	-0.0001	-0.0021	-0.0020	-0.0023	-0.0013	-0.0023
573.	0.0000	-0.0020	-0.0019	-0.0022	-0.0012	-0.0023
572.	0.0000	-0.0020	-0.0019	-0.0022	-0.0012	-0.0023
571.	-0.0001	-0.0021	-0.0020	-0.0022	-0.0012	-0.0023
570.	-0.0001	-0.0021	-0.0019	-0.0022	-0.0013	-0.0022
569.	0.0000	-0.0021	-0.0019	-0.0022	-0.0011	-0.0023
568.	-0.0001	-0.0020	-0.0019	-0.0023	-0.0012	-0.0022
567.	-0.0001	-0.0020	-0.0019	-0.0022	-0.0012	-0.0022
566.	0.0000	-0.0020	-0.0018	-0.0021	-0.0012	-0.0022
565.	-0.0002	-0.0021	-0.0020	-0.0023	-0.0013	-0.0023
564.	-0.0002	-0.0021	-0.0020	-0.0023	-0.0012	-0.0022
563.	-0.0001	-0.0021	-0.0019	-0.0022	-0.0012	-0.0022
562.	-0.0001	-0.0020	-0.0019	-0.0021	-0.0012	-0.0021
561.	-0.0001	-0.0021	-0.0020	-0.0023	-0.0012	-0.0022
560.	-0.0001	-0.0020	-0.0020	-0.0022	-0.0011	-0.0021
559.	-0.0002	-0.0021	-0.0019	-0.0022	-0.0011	-0.0020
558.	-0.0001	-0.0021	-0.0018	-0.0021	-0.0010	-0.0019
557.	-0.0001	-0.0020	-0.0018	-0.0022	-0.0010	-0.0020
556.	-0.0001	-0.0021	-0.0018	-0.0020	-0.0011	-0.0019
555.	-0.0001	-0.0020	-0.0018	-0.0023	-0.0011	-0.0019
554.	0.0000	-0.0020	-0.0019	-0.0023	-0.0009	-0.0017
553.	-0.0002	-0.0022	-0.0020	-0.0022	-0.0010	-0.0018
552.	-0.0002	-0.0022	-0.0019	-0.0022	-0.0009	-0.0016
551.	-0.0001	-0.0020	-0.0019	-0.0022	-0.0008	-0.0016
550.	0.0000	-0.0020	-0.0016	-0.0020	-0.0007	-0.0014
549.	-0.0001	-0.0020	-0.0018	-0.0020	-0.0007	-0.0014
548.	0.0000	-0.0020	-0.0016	-0.0020	-0.0006	-0.0011
547.	0.0000	-0.0020	-0.0016	-0.0017	-0.0002	-0.0011

546.	0.0000	-0.0021	-0.0015	-0.0016	-0.0003	-0.0010
545.	-0.0001	-0.0020	-0.0013	-0.0015	-0.0002	-0.0009
544.	0.0000	-0.0017	-0.0013	-0.0013	0.0000	-0.0005
543.	0.0000	-0.0018	-0.0013	-0.0013	0.0001	-0.0004
542.	0.0000	-0.0016	-0.0012	-0.0012	0.0002	-0.0004
541.	0.0000	-0.0016	-0.0010	-0.0010	0.0003	0.0000
540.	0.0001	-0.0016	-0.0010	-0.0009	0.0006	0.0001
539.	0.0000	-0.0016	-0.0008	-0.0008	0.0007	0.0004
538.	0.0000	-0.0016	-0.0007	-0.0005	0.0009	0.0007
537.	0.0000	-0.0015	-0.0006	-0.0004	0.0014	0.0011
536.	0.0000	-0.0014	-0.0003	0.0000	0.0018	0.0017
535.	0.0000	-0.0013	-0.0002	0.0002	0.0022	0.0022
534.	0.0000	-0.0011	-0.0001	0.0007	0.0027	0.0030
533.	0.0000	-0.0010	0.0003	0.0013	0.0033	0.0039
532.	-0.0001	-0.0009	0.0007	0.0018	0.0041	0.0050
531.	0.0000	-0.0006	0.0013	0.0025	0.0053	0.0064
530.	0.0000	-0.0001	0.0020	0.0035	0.0067	0.0081
529.	0.0000	0.0000	0.0027	0.0046	0.0081	0.0102
528.	-0.0001	0.0007	0.0038	0.0062	0.0102	0.0131
527.	0.0000	0.0013	0.0051	0.0083	0.0128	0.0165
526.	0.0001	0.0022	0.0069	0.0108	0.0162	0.0211
525.	0.0000	0.0031	0.0090	0.0140	0.0204	0.0268
524.	0.0001	0.0046	0.0118	0.0185	0.0261	0.0343
523.	0.0001	0.0063	0.0155	0.0238	0.0330	0.0436
522.	0.0000	0.0087	0.0201	0.0308	0.0423	0.0558
521.	-0.0001	0.0116	0.0262	0.0399	0.0544	0.0717
520.	0.0000	0.0155	0.0344	0.0517	0.0704	0.0927
519.	0.0000	0.0206	0.0450	0.0672	0.0913	0.1201

518.	-0.0001	0.0270	0.0584	0.0870	0.1179	0.1557
517.	-0.0001	0.0354	0.0754	0.1122	0.1514	0.2005
516.	0.0000	0.0455	0.0958	0.1426	0.1915	0.2547
515.	-0.0001	0.0570	0.1190	0.1776	0.2376	0.3172
514.	-0.0001	0.0697	0.1443	0.2159	0.2881	0.3848
513.	0.0000	0.0824	0.1701	0.2541	0.3396	0.4528
512.	-0.0001	0.0939	0.1939	0.2890	0.3872	0.5150
511.	-0.0001	0.1031	0.2132	0.3171	0.4257	0.5655
510.	-0.0001	0.1093	0.2259	0.3358	0.4512	0.5996
509.	-0.0001	0.1120	0.2313	0.3438	0.4616	0.6140
508.	-0.0001	0.1109	0.2290	0.3409	0.4573	0.6086
507.	-0.0001	0.1069	0.2208	0.3289	0.4410	0.5868
506.	0.0001	0.1008	0.2085	0.3104	0.4166	0.5536
505.	-0.0001	0.0935	0.1941	0.2888	0.3878	0.5152
504.	0.0000	0.0864	0.1796	0.2670	0.3588	0.4765
503.	0.0000	0.0796	0.1659	0.2467	0.3315	0.4405
502.	0.0000	0.0737	0.1537	0.2290	0.3073	0.4090
501.	0.0000	0.0688	0.1434	0.2139	0.2869	0.3822
500.	-0.0001	0.0645	0.1346	0.2011	0.2697	0.3591
499.	-0.0001	0.0609	0.1271	0.1902	0.2549	0.3394
498.	-0.0001	0.0577	0.1205	0.1803	0.2419	0.3219
497.	0.0000	0.0548	0.1147	0.1715	0.2302	0.3061
496.	0.0000	0.0520	0.1091	0.1630	0.2190	0.2910
495.	0.0001	0.0494	0.1037	0.1548	0.2084	0.2767
494.	0.0000	0.0467	0.0984	0.1468	0.1978	0.2627
493.	-0.0001	0.0442	0.0933	0.1393	0.1878	0.2496
492.	0.0000	0.0421	0.0887	0.1326	0.1786	0.2374
491.	-0.0001	0.0399	0.0845	0.1266	0.1705	0.2267

490.	0.0000	0.0384	0.0812	0.1217	0.1638	0.2178
489.	0.0001	0.0372	0.0788	0.1180	0.1590	0.2112
488.	-0.0001	0.0363	0.0772	0.1155	0.1557	0.2070
487.	0.0000	0.0360	0.0763	0.1143	0.1542	0.2048
486.	0.0001	0.0359	0.0760	0.1138	0.1535	0.2040
485.	-0.0001	0.0356	0.0757	0.1134	0.1530	0.2033
484.	0.0000	0.0354	0.0753	0.1127	0.1522	0.2022
483.	-0.0001	0.0350	0.0743	0.1113	0.1504	0.1998
482.	0.0000	0.0343	0.0729	0.1091	0.1474	0.1958
481.	0.0000	0.0332	0.0706	0.1059	0.1430	0.1901
480.	0.0000	0.0319	0.0682	0.1020	0.1379	0.1831
479.	0.0000	0.0305	0.0649	0.0975	0.1318	0.1752
478.	-0.0001	0.0289	0.0618	0.0928	0.1258	0.1669
477.	0.0000	0.0274	0.0588	0.0882	0.1196	0.1587
476.	0.0001	0.0259	0.0558	0.0838	0.1137	0.1507
475.	-0.0002	0.0242	0.0527	0.0789	0.1073	0.1423
474.	-0.0001	0.0226	0.0495	0.0744	0.1012	0.1342
473.	0.0000	0.0212	0.0463	0.0697	0.0948	0.1259
472.	0.0000	0.0197	0.0431	0.0651	0.0886	0.1177
471.	0.0001	0.0182	0.0402	0.0606	0.0825	0.1095
470.	0.0000	0.0167	0.0371	0.0562	0.0766	0.1017
469.	-0.0001	0.0153	0.0344	0.0519	0.0710	0.0941
468.	0.0001	0.0141	0.0319	0.0482	0.0662	0.0875
467.	-0.0001	0.0129	0.0296	0.0447	0.0616	0.0815
466.	0.0000	0.0119	0.0275	0.0417	0.0575	0.0760
465.	-0.0001	0.0109	0.0256	0.0389	0.0539	0.0712
464.	-0.0001	0.0100	0.0240	0.0365	0.0505	0.0668
463.	0.0001	0.0093	0.0226	0.0343	0.0476	0.0630

462.	-0.0001	0.0087	0.0212	0.0323	0.0449	0.0594
461.	0.0000	0.0081	0.0199	0.0306	0.0426	0.0562
460.	0.0000	0.0076	0.0189	0.0290	0.0404	0.0533
459.	0.0000	0.0069	0.0179	0.0274	0.0385	0.0507
458.	0.0000	0.0065	0.0169	0.0260	0.0365	0.0483
457.	-0.0001	0.0059	0.0159	0.0245	0.0346	0.0457
456.	0.0000	0.0055	0.0151	0.0233	0.0329	0.0434
455.	-0.0001	0.0052	0.0142	0.0220	0.0313	0.0412
454.	-0.0001	0.0046	0.0133	0.0207	0.0296	0.0389
453.	0.0000	0.0043	0.0126	0.0196	0.0281	0.0370
452.	-0.0001	0.0039	0.0118	0.0185	0.0266	0.0350
451.	0.0000	0.0037	0.0111	0.0173	0.0250	0.0329
450.	-0.0001	0.0032	0.0103	0.0161	0.0236	0.0309
449.	-0.0001	0.0029	0.0097	0.0151	0.0223	0.0291
448.	-0.0001	0.0025	0.0089	0.0141	0.0208	0.0272
447.	-0.0001	0.0022	0.0083	0.0132	0.0197	0.0257
446.	0.0000	0.0019	0.0077	0.0123	0.0185	0.0241
445.	-0.0001	0.0016	0.0072	0.0115	0.0176	0.0227
444.	-0.0001	0.0013	0.0068	0.0108	0.0164	0.0214
443.	-0.0001	0.0012	0.0062	0.0101	0.0155	0.0202
442.	-0.0001	0.0009	0.0057	0.0093	0.0144	0.0187
441.	0.0000	0.0006	0.0051	0.0084	0.0133	0.0173
440.	-0.0002	0.0003	0.0045	0.0076	0.0123	0.0159
439.	-0.0001	0.0000	0.0039	0.0069	0.0113	0.0144
438.	-0.0001	-0.0002	0.0035	0.0061	0.0104	0.0133
437.	0.0000	-0.0002	0.0031	0.0056	0.0095	0.0122
436.	-0.0001	-0.0007	0.0028	0.0050	0.0088	0.0111
435.	0.0000	-0.0007	0.0024	0.0044	0.0080	0.0102

434.	0.0000	-0.0008	0.0021	0.0039	0.0073	0.0093
433.	0.0000	-0.0010	0.0017	0.0035	0.0067	0.0085
432.	0.0000	-0.0012	0.0016	0.0030	0.0062	0.0077
431.	0.0001	-0.0013	0.0012	0.0027	0.0058	0.0070
430.	0.0001	-0.0015	0.0011	0.0022	0.0052	0.0064
429.	0.0000	-0.0016	0.0007	0.0018	0.0048	0.0057
428.	-0.0002	-0.0019	0.0004	0.0016	0.0042	0.0051
427.	0.0000	-0.0019	0.0003	0.0013	0.0039	0.0045
426.	0.0000	-0.0018	0.0002	0.0010	0.0037	0.0042
425.	0.0000	-0.0020	-0.0001	0.0008	0.0032	0.0036
424.	-0.0001	-0.0021	-0.0002	0.0005	0.0028	0.0032
423.	-0.0001	-0.0021	-0.0004	0.0003	0.0027	0.0029
422.	0.0001	-0.0022	-0.0005	0.0001	0.0024	0.0024
421.	0.0001	-0.0021	-0.0006	-0.0001	0.0021	0.0020
420.	0.0000	-0.0025	-0.0007	-0.0003	0.0018	0.0018
419.	0.0000	-0.0024	-0.0009	-0.0004	0.0016	0.0015
418.	0.0000	-0.0025	-0.0010	-0.0006	0.0013	0.0012
417.	0.0000	-0.0025	-0.0011	-0.0009	0.0011	0.0009
416.	0.0000	-0.0027	-0.0012	-0.0010	0.0008	0.0006
415.	-0.0001	-0.0028	-0.0014	-0.0011	0.0007	0.0003
414.	0.0000	-0.0026	-0.0013	-0.0012	0.0006	0.0002
413.	0.0000	-0.0028	-0.0015	-0.0015	0.0004	0.0000
412.	0.0000	-0.0027	-0.0015	-0.0014	0.0003	-0.0003
411.	0.0000	-0.0028	-0.0017	-0.0016	0.0002	-0.0004
410.	0.0001	-0.0028	-0.0018	-0.0017	0.0000	-0.0005
409.	0.0000	-0.0029	-0.0017	-0.0017	-0.0001	-0.0007
408.	0.0001	-0.0029	-0.0018	-0.0017	-0.0001	-0.0008
407.	0.0000	-0.0029	-0.0018	-0.0017	-0.0001	-0.0007

406.	-0.0001	-0.0030	-0.0019	-0.0019	-0.0002	-0.0010
405.	0.0001	-0.0030	-0.0019	-0.0019	-0.0003	-0.0010
404.	0.0000	-0.0029	-0.0019	-0.0018	-0.0003	-0.0009
403.	0.0000	-0.0031	-0.0019	-0.0020	-0.0002	-0.0009
402.	0.0001	-0.0029	-0.0019	-0.0018	-0.0003	-0.0009
401.	0.0000	-0.0029	-0.0018	-0.0019	-0.0002	-0.0009
400.	0.0002	-0.0027	-0.0017	-0.0017	-0.0001	-0.0008
399.	-0.0001	-0.0030	-0.0018	-0.0018	-0.0001	-0.0008
398.	0.0001	-0.0028	-0.0016	-0.0016	0.0002	-0.0006
397.	-0.0001	-0.0028	-0.0017	-0.0016	0.0001	-0.0005
396.	-0.0001	-0.0030	-0.0016	-0.0016	0.0004	-0.0002
395.	0.0001	-0.0027	-0.0013	-0.0011	0.0007	0.0004
394.	-0.0001	-0.0028	-0.0013	-0.0009	0.0009	0.0005
393.	0.0001	-0.0026	-0.0010	-0.0006	0.0013	0.0008
392.	-0.0001	-0.0025	-0.0009	-0.0004	0.0015	0.0013
391.	-0.0002	-0.0025	-0.0008	-0.0002	0.0019	0.0018
390.	-0.0001	-0.0023	-0.0005	0.0001	0.0024	0.0025
389.	-0.0001	-0.0022	-0.0003	0.0005	0.0029	0.0033
388.	0.0000	-0.0019	0.0002	0.0011	0.0037	0.0042
387.	-0.0001	-0.0018	0.0005	0.0015	0.0042	0.0050
386.	-0.0001	-0.0016	0.0009	0.0021	0.0051	0.0060
385.	0.0000	-0.0014	0.0012	0.0027	0.0058	0.0071
384.	0.0000	-0.0012	0.0018	0.0035	0.0068	0.0083
383.	-0.0001	-0.0013	0.0010	0.0021	0.0068	0.0069
382.	0.0007	-0.0020	0.0018	0.0032	0.0070	0.0093
381.	-0.0011	-0.0016	0.0016	0.0030	0.0076	0.0095
380.	0.0006	-0.0012	0.0025	0.0046	0.0090	0.0119
379.	-0.0003	-0.0007	0.0033	0.0052	0.0096	0.0122

378.	0.0004	-0.0004	0.0033	0.0064	0.0106	0.0136
377.	-0.0004	-0.0008	0.0039	0.0061	0.0112	0.0145
376.	0.0008	0.0003	0.0047	0.0080	0.0130	0.0159
375.	-0.0006	-0.0003	0.0034	0.0052	0.0116	0.0150
374.	0.0005	0.0005	0.0047	0.0089	0.0142	0.0178
373.	-0.0005	0.0006	0.0050	0.0085	0.0142	0.0184
372.	0.0006	0.0012	0.0061	0.0092	0.0157	0.0203
371.	-0.0005	0.0003	0.0052	0.0096	0.0153	0.0196
370.	0.0002	0.0008	0.0058	0.0101	0.0161	0.0209
369.	0.0001	0.0006	0.0060	0.0104	0.0166	0.0214
368.	0.0001	0.0013	0.0064	0.0109	0.0172	0.0224
367.	0.0000	0.0012	0.0068	0.0112	0.0177	0.0234
366.	-0.0002	0.0014	0.0066	0.0114	0.0183	0.0239
365.	0.0003	0.0017	0.0071	0.0125	0.0189	0.0245
364.	-0.0002	0.0019	0.0078	0.0130	0.0196	0.0257
363.	-0.0001	0.0010	0.0076	0.0125	0.0196	0.0258
362.	0.0003	0.0022	0.0083	0.0136	0.0210	0.0272
361.	0.0003	0.0022	0.0087	0.0134	0.0213	0.0279
360.	-0.0002	0.0022	0.0089	0.0144	0.0220	0.0285
359.	-0.0006	0.0021	0.0090	0.0143	0.0223	0.0290
358.	0.0011	0.0029	0.0102	0.0157	0.0236	0.0308
357.	0.0000	0.0025	0.0091	0.0152	0.0237	0.0303
356.	0.0002	0.0029	0.0099	0.0160	0.0239	0.0316
355.	-0.0001	0.0025	0.0097	0.0157	0.0239	0.0319
354.	0.0001	0.0028	0.0102	0.0160	0.0247	0.0319
353.	0.0002	0.0030	0.0101	0.0162	0.0244	0.0324
352.	0.0003	0.0032	0.0104	0.0167	0.0251	0.0326
351.	0.0004	0.0029	0.0109	0.0168	0.0250	0.0330

350.	-0.0001	0.0032	0.0104	0.0168	0.0253	0.0327
349.	-0.0001	0.0031	0.0099	0.0164	0.0245	0.0328
348.	-0.0008	0.0023	0.0098	0.0159	0.0243	0.0309
347.	0.0006	0.0034	0.0108	0.0173	0.0258	0.0335
346.	-0.0001	0.0024	0.0103	0.0172	0.0252	0.0322
345.	0.0000	0.0029	0.0103	0.0159	0.0235	0.0311
344.	0.0002	0.0027	0.0104	0.0160	0.0250	0.0324
343.	-0.0011	0.0027	0.0106	0.0160	0.0246	0.0320
342.	-0.0003	0.0032	0.0095	0.0160	0.0244	0.0318
341.	-0.0005	0.0020	0.0097	0.0157	0.0236	0.0318
340.	0.0007	0.0035	0.0103	0.0162	0.0247	0.0324
339.	0.0006	0.0027	0.0106	0.0158	0.0238	0.0317
338.	0.0001	0.0026	0.0100	0.0154	0.0236	0.0308
337.	-0.0007	0.0022	0.0086	0.0152	0.0234	0.0304
336.	-0.0002	0.0028	0.0101	0.0153	0.0238	0.0309
335.	0.0001	0.0026	0.0102	0.0151	0.0230	0.0306
334.	-0.0005	0.0014	0.0077	0.0144	0.0217	0.0292
333.	0.0002	0.0025	0.0097	0.0151	0.0223	0.0294
332.	-0.0001	0.0022	0.0090	0.0143	0.0221	0.0289
331.	0.0002	0.0019	0.0089	0.0135	0.0208	0.0289
330.	0.0005	0.0025	0.0086	0.0140	0.0219	0.0282
329.	-0.0009	0.0011	0.0071	0.0129	0.0196	0.0262
328.	0.0004	0.0003	0.0077	0.0132	0.0199	0.0268
327.	-0.0008	0.0014	0.0076	0.0122	0.0201	0.0255
326.	0.0000	0.0020	0.0085	0.0134	0.0201	0.0258
325.	-0.0003	0.0015	0.0077	0.0125	0.0193	0.0247
324.	-0.0001	0.0017	0.0078	0.0126	0.0191	0.0248
323.	-0.0001	0.0015	0.0077	0.0122	0.0189	0.0240

322.	-0.0002	0.0014	0.0075	0.0120	0.0185	0.0237
321.	-0.0001	0.0015	0.0074	0.0117	0.0184	0.0231
320.	-0.0003	0.0014	0.0071	0.0115	0.0179	0.0228
319.	0.0000	0.0014	0.0072	0.0115	0.0179	0.0224
318.	-0.0003	0.0013	0.0069	0.0110	0.0174	0.0219
317.	0.0000	0.0014	0.0069	0.0111	0.0173	0.0218
316.	0.0000	0.0015	0.0069	0.0109	0.0170	0.0214
315.	-0.0001	0.0013	0.0068	0.0108	0.0169	0.0211
314.	-0.0002	0.0013	0.0066	0.0105	0.0168	0.0209
313.	-0.0002	0.0014	0.0066	0.0105	0.0166	0.0208
312.	-0.0001	0.0012	0.0068	0.0106	0.0165	0.0208
311.	-0.0002	0.0014	0.0067	0.0107	0.0166	0.0206
310.	0.0000	0.0016	0.0070	0.0108	0.0169	0.0208
309.	0.0000	0.0016	0.0068	0.0106	0.0167	0.0208
308.	0.0001	0.0018	0.0071	0.0108	0.0170	0.0209
307.	-0.0002	0.0017	0.0070	0.0109	0.0167	0.0207
306.	-0.0001	0.0019	0.0070	0.0107	0.0167	0.0205
305.	-0.0001	0.0019	0.0069	0.0107	0.0168	0.0204
304.	0.0000	0.0020	0.0071	0.0107	0.0164	0.0202
303.	-0.0001	0.0020	0.0070	0.0104	0.0163	0.0198
302.	0.0001	0.0023	0.0071	0.0105	0.0162	0.0195
301.	-0.0001	0.0024	0.0068	0.0101	0.0157	0.0190
300.	-0.0001	0.0023	0.0070	0.0101	0.0157	0.0186
299.	-0.0003	0.0024	0.0069	0.0101	0.0155	0.0182
298.	0.0000	0.0025	0.0068	0.0098	0.0152	0.0180
297.	-0.0001	0.0027	0.0069	0.0098	0.0151	0.0176
296.	0.0000	0.0027	0.0070	0.0098	0.0151	0.0175
295.	-0.0002	0.0028	0.0070	0.0098	0.0150	0.0174

294.	0.0000	0.0033	0.0071	0.0099	0.0150	0.0172
293.	-0.0001	0.0035	0.0073	0.0097	0.0148	0.0172
292.	-0.0002	0.0037	0.0072	0.0098	0.0150	0.0170
291.	0.0000	0.0038	0.0075	0.0099	0.0148	0.0168
290.	-0.0002	0.0040	0.0073	0.0097	0.0146	0.0166
289.	-0.0003	0.0045	0.0074	0.0099	0.0147	0.0166
288.	0.0000	0.0053	0.0078	0.0101	0.0148	0.0167
287.	0.0000	0.0059	0.0083	0.0103	0.0152	0.0171
286.	-0.0002	0.0069	0.0086	0.0104	0.0153	0.0175
285.	-0.0001	0.0075	0.0088	0.0105	0.0154	0.0176
284.	-0.0002	0.0076	0.0087	0.0105	0.0153	0.0172
283.	0.0000	0.0078	0.0089	0.0105	0.0152	0.0172
282.	-0.0001	0.0080	0.0090	0.0105	0.0152	0.0169
281.	-0.0003	0.0077	0.0089	0.0102	0.0150	0.0163
280.	-0.0001	0.0082	0.0089	0.0104	0.0149	0.0162
279.	-0.0002	0.0082	0.0090	0.0102	0.0145	0.0159
278.	-0.0004	0.0085	0.0087	0.0099	0.0144	0.0157
277.	-0.0001	0.0088	0.0091	0.0102	0.0147	0.0158
276.	0.0000	0.0088	0.0091	0.0101	0.0145	0.0157
275.	0.0000	0.0087	0.0089	0.0100	0.0142	0.0155
274.	-0.0003	0.0085	0.0088	0.0098	0.0142	0.0150
273.	-0.0001	0.0087	0.0091	0.0099	0.0143	0.0150
272.	0.0000	0.0083	0.0088	0.0097	0.0140	0.0146
271.	-0.0003	0.0079	0.0085	0.0092	0.0135	0.0139
270.	-0.0001	0.0079	0.0083	0.0092	0.0134	0.0138
269.	-0.0001	0.0078	0.0084	0.0092	0.0137	0.0140
268.	-0.0002	0.0077	0.0085	0.0096	0.0138	0.0142
267.	-0.0002	0.0075	0.0087	0.0097	0.0143	0.0148

266.	-0.0001	0.0076	0.0091	0.0104	0.0151	0.0159
265.	-0.0001	0.0079	0.0098	0.0114	0.0164	0.0177
264.	-0.0002	0.0083	0.0107	0.0130	0.0186	0.0205
263.	-0.0001	0.0089	0.0123	0.0153	0.0217	0.0245
262.	-0.0002	0.0101	0.0148	0.0190	0.0266	0.0306
261.	0.0001	0.0119	0.0186	0.0244	0.0340	0.0401
260.	-0.0001	0.0143	0.0234	0.0317	0.0436	0.0532
259.	-0.0001	0.0179	0.0303	0.0417	0.0567	0.0707
258.	-0.0001	0.0218	0.0382	0.0536	0.0722	0.0916
257.	-0.0001	0.0258	0.0463	0.0657	0.0883	0.1129
256.	-0.0001	0.0293	0.0534	0.0760	0.1024	0.1312
255.	-0.0003	0.0320	0.0584	0.0833	0.1120	0.1439
254.	-0.0001	0.0335	0.0613	0.0874	0.1175	0.1506
253.	0.0000	0.0346	0.0628	0.0895	0.1200	0.1536
252.	0.0001	0.0354	0.0643	0.0912	0.1222	0.1561
251.	0.0000	0.0368	0.0663	0.0942	0.1263	0.1613
250.	0.0000	0.0390	0.0702	0.0998	0.1337	0.1709
249.	0.0000	0.0420	0.0756	0.1077	0.1441	0.1849
248.	0.0000	0.0452	0.0818	0.1170	0.1565	0.2012
247.	-0.0001	0.0485	0.0878	0.1260	0.1687	0.2170
246.	0.0000	0.0514	0.0926	0.1328	0.1780	0.2287
245.	0.0001	0.0534	0.0953	0.1366	0.1828	0.2344
244.	0.0001	0.0545	0.0960	0.1370	0.1834	0.2349
243.	-0.0001	0.0552	0.0956	0.1361	0.1822	0.2326
242.	0.0000	0.0562	0.0958	0.1358	0.1818	0.2315
241.	0.0001	0.0582	0.0973	0.1377	0.1842	0.2342
240.	0.0000	0.0612	0.1006	0.1420	0.1899	0.2415
239.	0.0000	0.0649	0.1052	0.1484	0.1985	0.2528

238.	0.0000	0.0697	0.1109	0.1559	0.2082	0.2655
237.	0.0001	0.0748	0.1162	0.1630	0.2174	0.2775
236.	0.0001	0.0794	0.1199	0.1674	0.2232	0.2850
235.	0.0000	0.0831	0.1215	0.1685	0.2247	0.2865
234.	0.0000	0.0857	0.1214	0.1673	0.2224	0.2835
233.	0.0002	0.0880	0.1212	0.1656	0.2202	0.2796
232.	0.0002	0.0901	0.1212	0.1643	0.2181	0.2759
231.	0.0000	0.0916	0.1213	0.1632	0.2163	0.2722
230.	0.0001	0.0930	0.1214	0.1618	0.2145	0.2684
229.	0.0001	0.0943	0.1217	0.1603	0.2121	0.2637
228.	0.0000	0.0949	0.1205	0.1576	0.2083	0.2569
227.	0.0001	0.0947	0.1189	0.1538	0.2028	0.2481
226.	0.0003	0.0941	0.1166	0.1494	0.1969	0.2386
225.	0.0001	0.0932	0.1142	0.1448	0.1904	0.2284
224.	0.0002	0.0928	0.1124	0.1405	0.1846	0.2187
223.	0.0001	0.0919	0.1101	0.1359	0.1785	0.2084
222.	0.0002	0.0915	0.1084	0.1320	0.1731	0.1990
221.	0.0003	0.0913	0.1071	0.1282	0.1681	0.1903
220.	0.0002	0.0912	0.1059	0.1250	0.1634	0.1818
219.	0.0002	0.0912	0.1047	0.1217	0.1594	0.1740
218.	0.0003	0.0919	0.1044	0.1193	0.1560	0.1673
217.	0.0002	0.0926	0.1042	0.1174	0.1533	0.1614
216.	0.0003	0.0942	0.1050	0.1166	0.1520	0.1572
215.	0.0004	0.0968	0.1065	0.1170	0.1521	0.1543
214.	0.0006	0.1002	0.1090	0.1183	0.1534	0.1530
213.	0.0003	0.1049	0.1126	0.1207	0.1557	0.1526
212.	0.0003	0.1112	0.1170	0.1245	0.1597	0.1538
211.	0.0000	0.1186	0.1225	0.1293	0.1651	0.1564

210.	0.0005	0.1294	0.1306	0.1373	0.1729	0.1616
209.	0.0002	0.1422	0.1400	0.1468	0.1830	0.1690
208.	-0.0002	0.1586	0.1523	0.1597	0.1962	0.1791
207.	0.0000	0.1794	0.1679	0.1765	0.2141	0.1931
206.	-0.0004	0.2052	0.1884	0.1977	0.2357	0.2109
205.	-0.0012	0.2355	0.2120	0.2231	0.2617	0.2337
204.	-0.0015	0.2717	0.2413	0.2548	0.2945	0.2611
203.	-0.0027	0.3146	0.2767	0.2952	0.3318	0.2963
202.	-0.0028	0.3493	0.3076	0.3341	0.3673	0.3296
201.	-0.0069	0.3656	0.3245	0.3574	0.3867	0.3530
200.	-0.0101	0.3238	0.3091	0.3311	0.3648	0.3501

#### Emission Data of 2 $\mu$ M FBI.

Emission		Emission		Emission		Emission		Emission		Emission	
$\lambda$ nM	Au	$\lambda$ nM	Au	$\lambda$ nM	Au	$\lambda$ nM	Au	$\lambda$ nM	Au	$\lambda$ nM	Au
450.0	0.047	496.0	10.639	542.0	76.274	588.0	4.246	634.0	0.204	680.0	0.105
451.0	0.024	497.0	13.425	543.0	74.347	589.0	4.022	635.0	0.278	681.0	0.042
452.0	0.105	498.0	16.698	544.0	72.165	590.0	3.747	636.0	0.229	682.0	0.055
453.0	0.014	499.0	21.040	545.0	69.560	591.0	3.578	637.0	0.257	683.0	0.040
454.0	0.090	500.0	26.728	546.0	66.703	592.0	3.287	638.0	0.268	684.0	0.065
455.0	0.103	501.0	33.643	547.0	63.465	593.0	3.132	639.0	0.224	685.0	0.090
456.0	0.066	502.0	43.043	548.0	60.148	594.0	2.966	640.0	0.262	686.0	-0.004
457.0	0.012	503.0	55.222	549.0	56.662	595.0	2.807	641.0	0.162	687.0	0.090
458.0	0.070	504.0	72.987	550.0	53.511	596.0	2.628	642.0	0.162	688.0	0.042
459.0	0.087	505.0	94.263	551.0	49.647	597.0	2.460	643.0	0.210	689.0	0.066
460.0	0.056	506.0	120.209	552.0	46.673	598.0	2.374	644.0	0.199	690.0	0.083
461.0	0.064	507.0	151.077	553.0	43.901	599.0	2.174	645.0	0.143	691.0	0.035
462.0	0.116	508.0	185.809	554.0	41.244	600.0	2.126	646.0	0.203	692.0	0.022
463.0	0.095	509.0	223.630	555.0	38.662	601.0	1.993	647.0	0.181	693.0	0.042
464.0	0.075	510.0	260.906	556.0	36.047	602.0	1.885	648.0	0.147	694.0	0.051

465.0	0.081	511.0	294.499	557.0	33.794	603.0	1.739	649.0	0.136	695.0	0.049
466.0	0.026	512.0	322.365	558.0	31.627	604.0	1.658	650.0	0.101	696.0	0.053
467.0	0.097	513.0	339.916	559.0	29.551	605.0	1.592	651.0	0.144	697.0	0.040
468.0	0.057	514.0	345.631	560.0	27.309	606.0	1.449	652.0	0.152	698.0	0.052
469.0	0.089	515.0	340.847	561.0	25.679	607.0	1.467	653.0	0.104	699.0	0.016
470.0	0.087	516.0	327.794	562.0	23.831	608.0	1.304	654.0	0.126	700.0	0.077
471.0	0.093	517.0	310.247	563.0	22.253	609.0	1.169	655.0	0.157		
472.0	0.149	518.0	288.229	564.0	20.638	610.0	1.196	656.0	0.089		
473.0	0.113	519.0	266.275	565.0	19.019	611.0	1.119	657.0	0.085		
474.0	0.081	520.0	244.032	566.0	17.753	612.0	1.121	658.0	0.119		
475.0	0.100	521.0	222.576	567.0	16.573	613.0	1.004	659.0	0.098		
476.0	0.138	522.0	204.488	568.0	15.402	614.0	0.901	660.0	0.111		
477.0	0.204	523.0	189.140	569.0	14.290	615.0	0.855	661.0	0.119		
478.0	0.268	524.0	174.918	570.0	13.412	616.0	0.837	662.0	0.122		
479.0	0.360	525.0	161.293	571.0	12.458	617.0	0.762	663.0	0.061		
480.0	0.425	526.0	150.526	572.0	11.694	618.0	0.681	664.0	0.084		
481.0	0.487	527.0	140.846	573.0	10.937	619.0	0.614	665.0	0.084		
482.0	0.578	528.0	132.137	574.0	10.179	620.0	0.520	666.0	0.084		
483.0	0.726	529.0	123.932	575.0	9.546	621.0	0.562	667.0	0.022		
484.0	0.840	530.0	116.746	576.0	8.965	622.0	0.518	668.0	0.047		
485.0	1.072	531.0	110.139	577.0	8.456	623.0	0.490	669.0	0.019		
486.0	1.249	532.0	104.222	578.0	7.869	624.0	0.466	670.0	0.061		
487.0	1.517	533.0	98.264	579.0	7.431	625.0	0.460	671.0	-0.005		
488.0	1.818	534.0	93.912	580.0	7.028	626.0	0.422	672.0	0.033		
489.0	2.239	535.0	90.160	581.0	6.559	627.0	0.412	673.0	0.052		
490.0	2.772	536.0	87.100	582.0	6.162	628.0	0.360	674.0	0.059		
491.0	3.451	537.0	84.487	583.0	5.745	629.0	0.327	675.0	0.029		
492.0	4.349	538.0	82.499	584.0	5.448	630.0	0.371	676.0	0.015		

493.0 5.369 539.0 80.715 585.0 5.152 631.0 0.341 677.0 0.086  
 494.0 6.764 540.0 79.098 586.0 4.822 632.0 0.314 678.0 0.028  
 495.0 8.453 541.0 77.806 587.0 4.512 633.0 0.345 679.0 0.063

## Chapter 1 Biology

### BLI Assay Data

2 mL NGM plates, 50  $\mu$ L OP50-1 liquid culture, 5 adult N2 *C. elegans* and 20  $\mu$ L compound solution (MeOH).

	5 Hours	24 Hours	48 Hours
No compound	Alive/Active	Alive/Active	Alive/Active
1% MeOH	Alive/Active	Alive/Active	Alive/Active
Bodipy <b>1.7</b>	Alive/Active	Alive/Active	Alive/Active
<b>Ivermectin</b> 10 nM	Dead	Dead	Dead
<b>Ivermectin</b> 100 nM	Dead	Dead	Dead
<b>BLI</b> 10 nM	Alive/Active	Alive/Active	Alive/Active
<b>BLI</b> 100 nM	Alive/Active	Alive/Active	Alive/Active
<b>BLI</b> 1 $\mu$ M	Alive/Slow	Alive/Very Slow	Alive/Very Slow
<b>BLI</b> 10 $\mu$ M	Alive/Very Slow	Dead	Dead

### FBI Assay Data

500  $\mu$ L NGM wells (24 well plate), 20  $\mu$ L OP50-1 liquid culture, 10 L4 N2 *C. elegans* and 5  $\mu$ L compound solution (MeOH).

	24 Hours	48 Hours	96 Hours
No compound	Alive/Active	Alive/Active	Alive/Active
1% MeOH	Alive/Active	Alive/Active	Alive/Active
<b>Ivermectin</b> 10 nM	Alive/Very Slow	Dead	Dead
<b>Ivermectin</b> 100 nM	Dead	Dead	Dead
<b>Ivermectin</b> 1000 nM	Dead	Dead	Dead
<b>FBI</b> 10 nM	Alive/Slow	Alive/Very Slow	Alive/Very Slow
<b>FBI</b> 100 nM	Alive/Very Slow	Dead	Dead
<b>FBI</b> 1 $\mu$ M	Dead	Dead	Dead
<b>FBI</b> 10 $\mu$ M	Dead	Dead	Dead

4 mL NGM plates, 100  $\mu$ L OP50-1 liquid culture, 10 L4 N2 *C. elegans* and 40  $\mu$ L compound solution (MeOH).

	48 Hours

<b>Ivermectin</b> 10 nM	Dead
<b>Ivermectin</b> 50 nM	Dead
<b>FBI</b> 10 nM	Alive/Very Slow
<b>FBI</b> 50 nM	Dead
<b>FBI</b> 100 nM	Dead
<b>FBI</b> 200 nM	Dead
<b>FBI</b> 400 nM	Dead
<b>FBI</b> 600 nM	Dead

4 mL NGM plates, 100  $\mu$ L OP50-1 liquid culture, 10 L4 *C. elegans* and 40  $\mu$ L compound solution (MeOH).

		48 Hours	7 Days
N2	Bodipy <b>1.21</b> 10 nM	Alive/Active	Alive/Active
	Bodipy <b>1.21</b> 10 nM	Alive/Active	Alive/Active
	<b>Ivermectin/1.21</b> 10 nM	Dead	Dead
	<b>Ivermectin/1.21</b> 50 nM	Dead	Dead
<i>TP-238</i>	<b>FBI</b> 25 nM	Alive/Active	Alive/Active
	<b>FBI</b> 50 nM	Alive/Active	Alive/Active
	<b>FBI</b> 100 nM	Alive/Active	Alive/Active
<i>Dyf-7</i>	<b>FBI</b> 25 nM	Alive/Active	Alive/Active
	<b>FBI</b> 50 nM	Alive/Active	Alive/Active
	<b>FBI</b> 100 nM	Alive/Active	Alive/Active

4 mL NGM plates, 50  $\mu$ L OP50-1 liquid culture, 10 L4 *C. elegans* and 40  $\mu$ L compound solution (MeOH).

		96 Hours
N2	<b>Ivermectin</b> 10 nM	Dead
	<b>Ivermectin</b> 50 nM	Dead
	<b>FBI</b> 10 nM	Alive/Very Slow
	<b>FBI</b> 50 nM	Dead
	Bodipy <b>1.21</b> 10 nM	Alive/Active
	Bodipy <b>1.21</b> 50 nM	Alive/Active
<i>TP-238</i>	<b>Ivermectin</b> 10 nM	Alive/Active
	<b>Ivermectin</b> 50 nM	Dead
	<b>FBI</b> 10 nM	Alive/Active
	<b>FBI</b> 50 nM	Alive/Active
	Bodipy <b>1.21</b> 10 nM	Alive/Active
	Bodipy <b>1.21</b> 50 nM	Alive/Active

4 mL NGM plates, 50  $\mu$ L OP50-1 liquid culture, 10 L4 *C. elegans* and 40  $\mu$ L compound solution (MeOH).

		24 Hours		96 Hours	
N2	<b>Ivermectin</b> 0.5 nM	Alive/Active		Alive/Active	
	<b>Ivermectin</b> 1 nM	Alive/Active		Alive/Active	
	<b>Ivermectin</b> 5 nM	Alive/Very Slow		Alive/Very Slow	
	<b>Ivermectin</b> 10 nM	Dead		Dead	
	<b>Ivermectin</b> 50 nM	Dead		Dead	
	<b>FBI</b> 0.5 nM	Alive/Active		Alive/Active	
	<b>FBI</b> 1 nM	Alive/Active		Alive/Active	
	<b>FBI</b> 5 nM	Alive/Active		Alive/Active	
	<b>FBI</b> 10 nM	Alive/Active		Alive/Active	
	<b>FBI</b> 50 nM	Alive/Very Slow		Dead	
<i>Dyf-7</i>	<b>Ivermectin</b> 0.5 nM	Alive/Active		Alive/Active	
	<b>Ivermectin</b> 1 nM	Alive/Active		Alive/Active	
	<b>Ivermectin</b> 5 nM	Alive/Active		Alive/Active	
	<b>Ivermectin</b> 10 nM	Alive/Active		Alive/Slow	
	<b>Ivermectin</b> 50 nM	Dead		Dead	
	<b>FBI</b> 0.5 nM	Alive/Active		Alive/Active	
	<b>FBI</b> 1 nM	Alive/Active		Alive/Active	
	<b>FBI</b> 5 nM	Alive/Active		Alive/Active	
	<b>FBI</b> 10 nM	Alive/Active		Alive/Active	
	<b>FBI</b> 50 nM	Alive/Active		Alive/Slow	

4 mL NGM plates, 50  $\mu$ L OP50-1 liquid culture, ~50 L1 *H. contortus* and 40  $\mu$ L compound solution (MeOH).

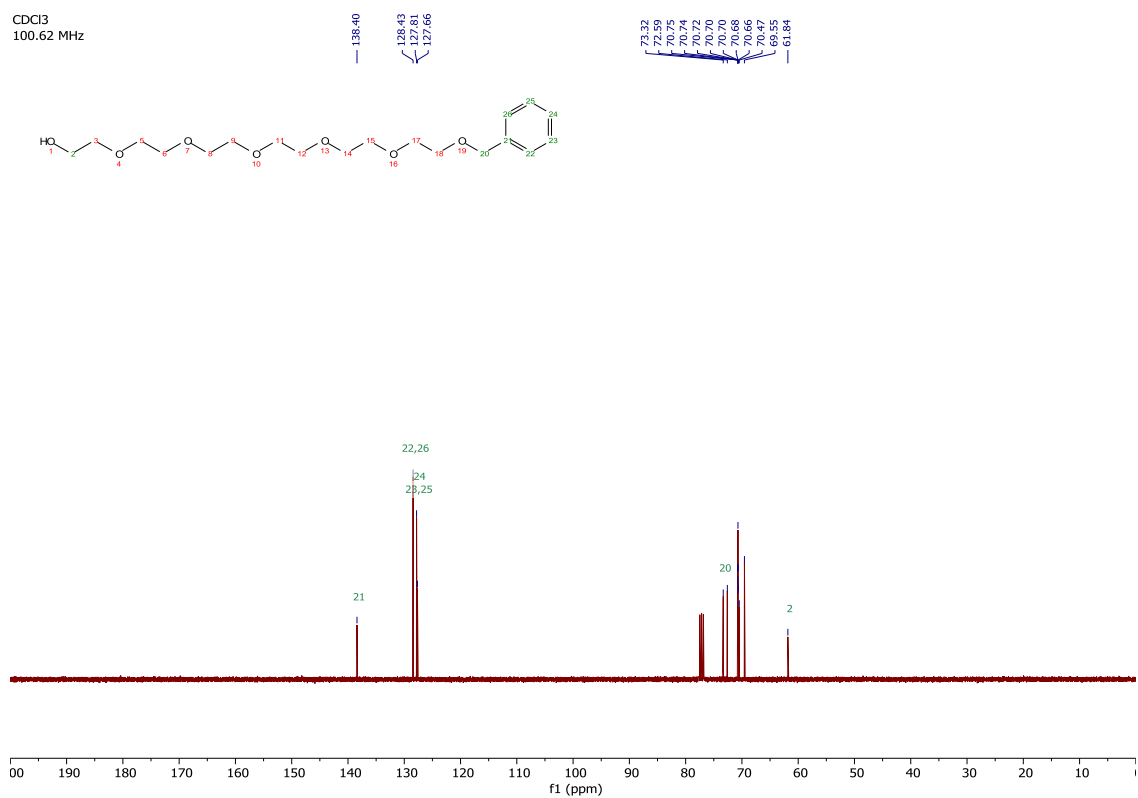
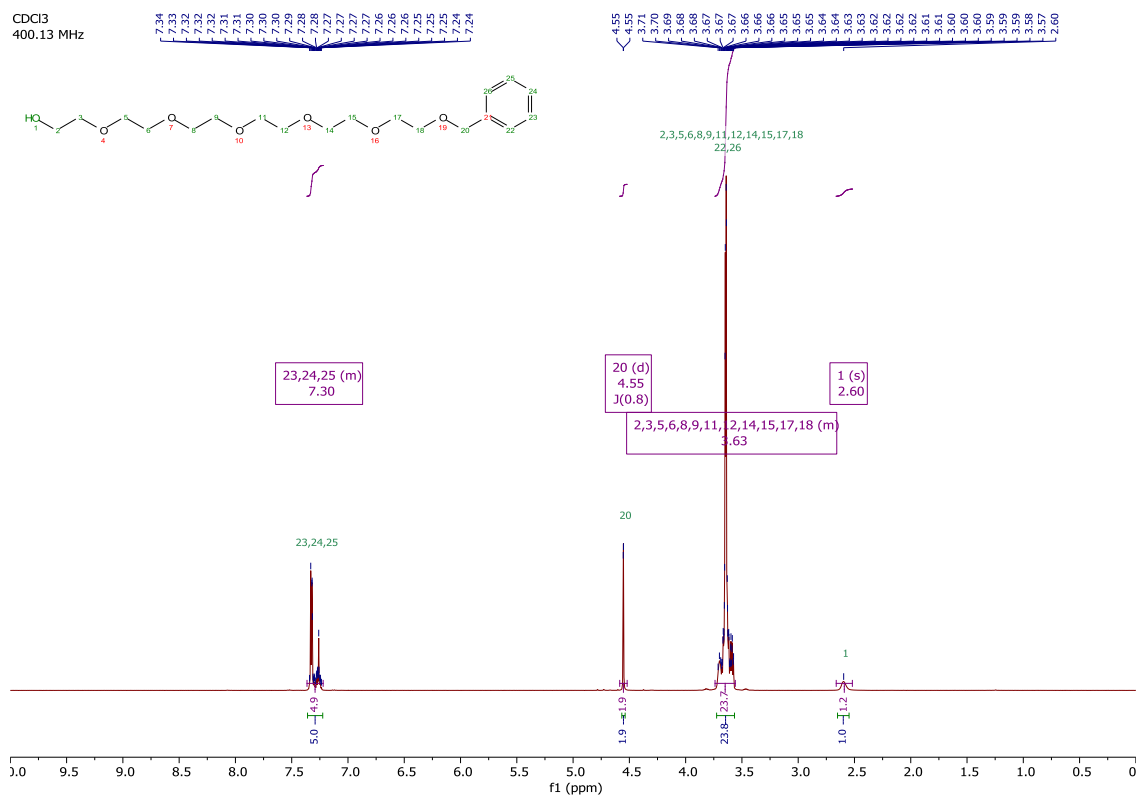
		24 Hours		96 Hours	
		L1	L2/L3	L1	L2/L3
<i>MHco3</i>	No Compound	0	/	0	/
	1% MeOH	0	/	0	/
	1% DMSO	0	/	0	/
	<b>Ivermectin</b> 0.5 nM	12	142	1	123
	<b>Ivermectin</b> 1 nM	32	51	15	25
	<b>Ivermectin</b> 5 nM	116	0	95	0
	<b>Ivermectin</b> 10 nM	79	0	67	0
	<b>Ivermectin</b> 50 nM	30	0	25	0
	<b>FBI</b> 0.5 nM	3	123	0	110
	<b>FBI</b> 1 nM	4	81	0	75

	<b>FBI 5 nM</b>	4	75	0	76
	<b>FBI 10 nM</b>	24	53	0	63
	<b>FBI 50 nM</b>	54	1	22	15
<i>MHco18</i>	No Compound	0	/	0	/
	1% MeOH	0	87	0	75
	1% DMSO	0	75	0	78
	<b>Ivermectin 0.5 nM</b>	0	87	0	83
	<b>Ivermectin 1 nM</b>	44	30	33	0
	<b>Ivermectin 5 nM</b>	52	0	45	0
	<b>Ivermectin 10 nM</b>	61	0	56	0
	<b>Ivermectin 50 nM</b>	38	0	40	0
	<b>FBI 0.5 nM</b>	0	92	0	68
	<b>FBI 1 nM</b>	0	91	0	85
	<b>FBI 5 nM</b>	2	107	0	109
	<b>FBI 10 nM</b>	3	91	0	83
	<b>FBI 50 nM</b>	7	73	0	65

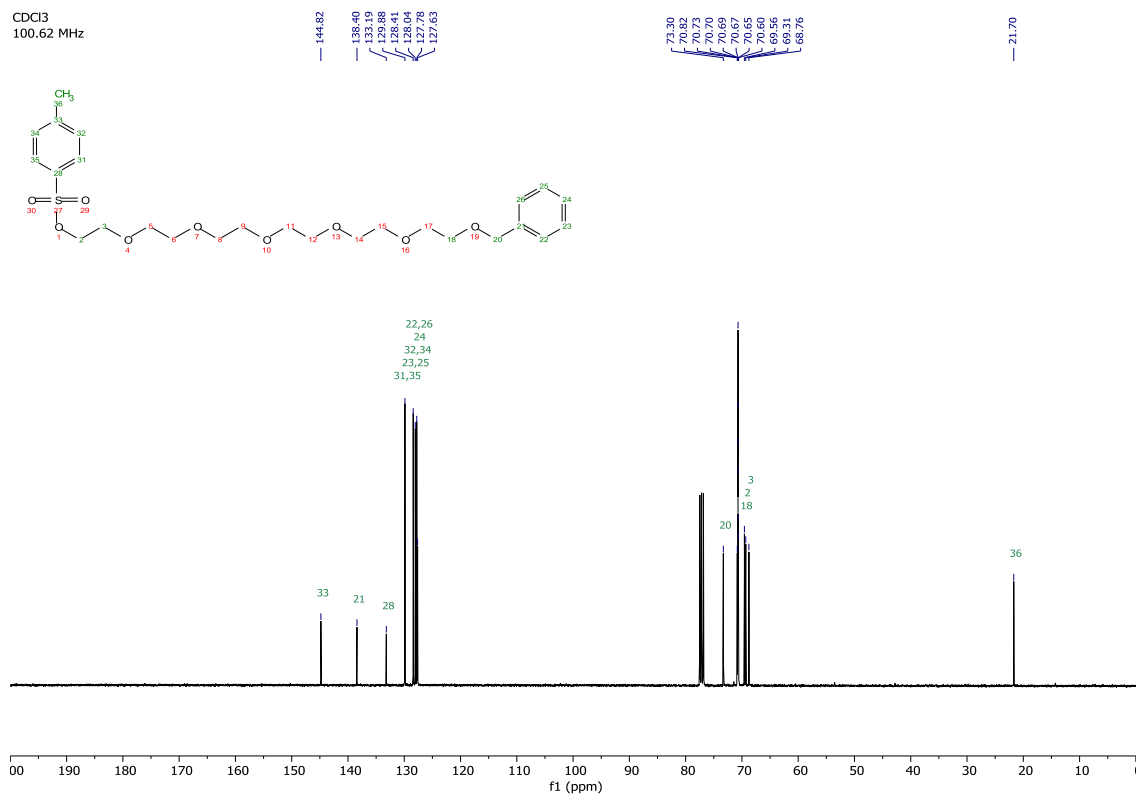
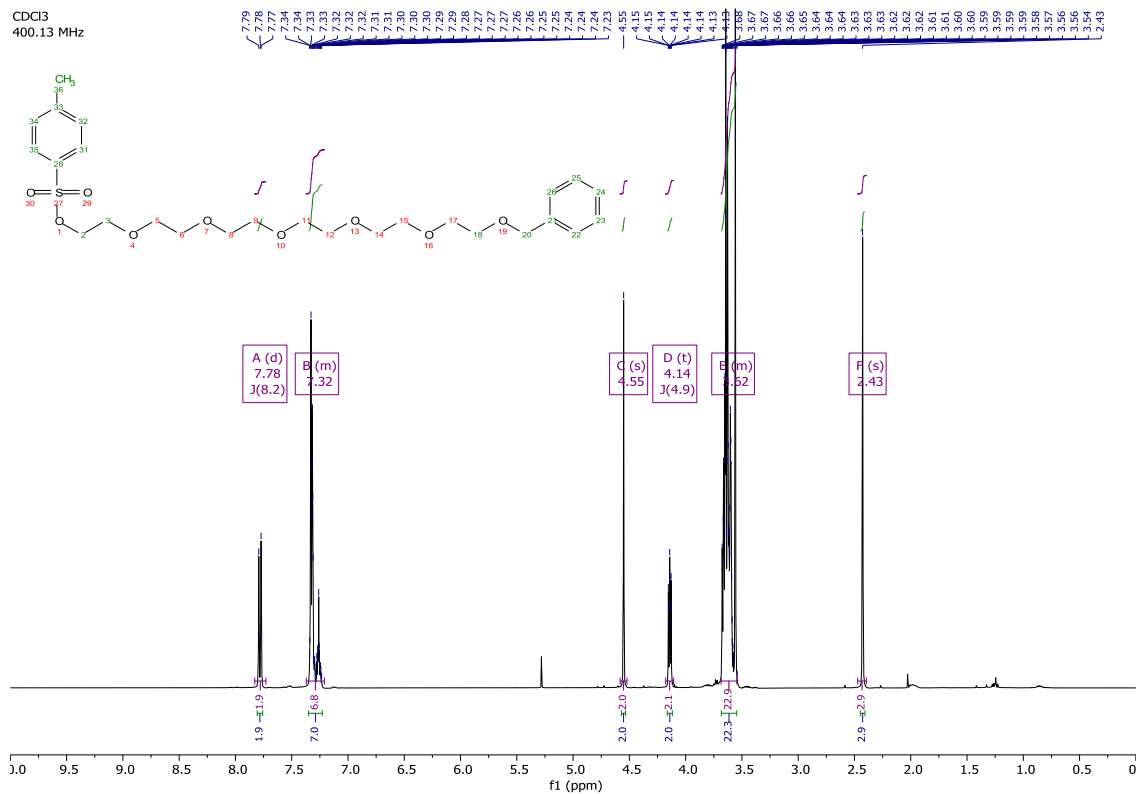
# Chapter 2 Chemistry

## Compound Characterisation Data

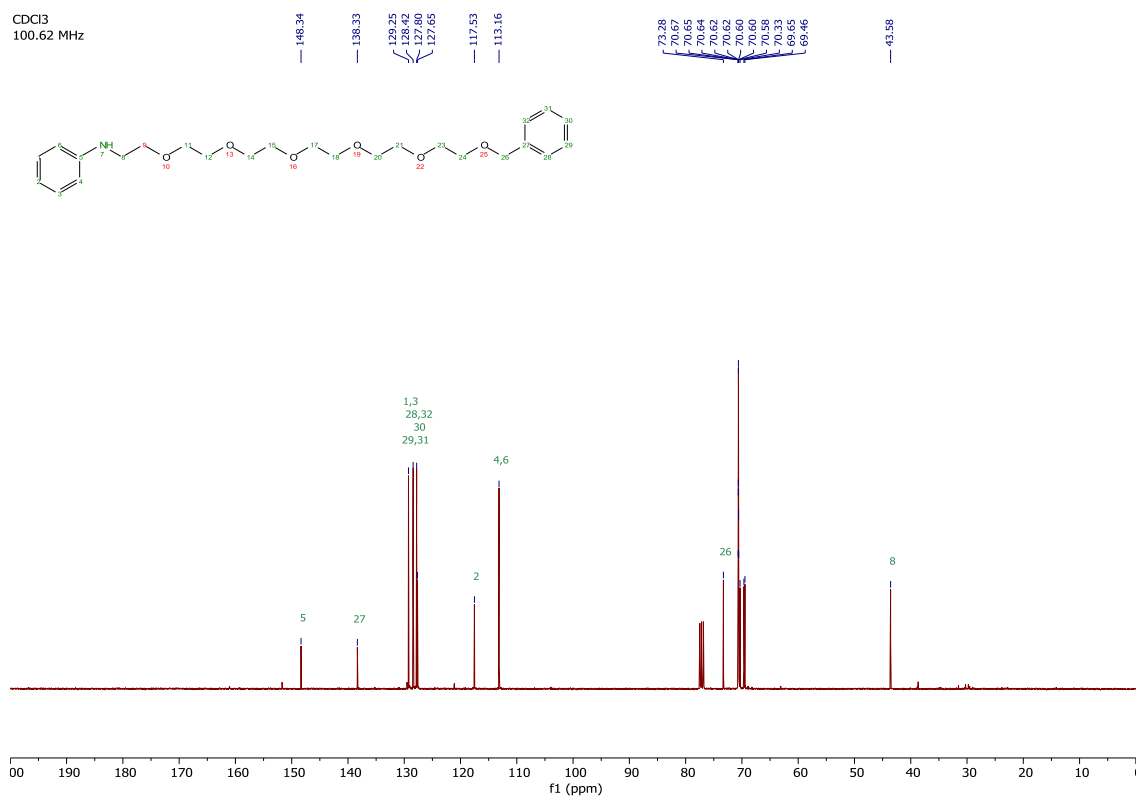
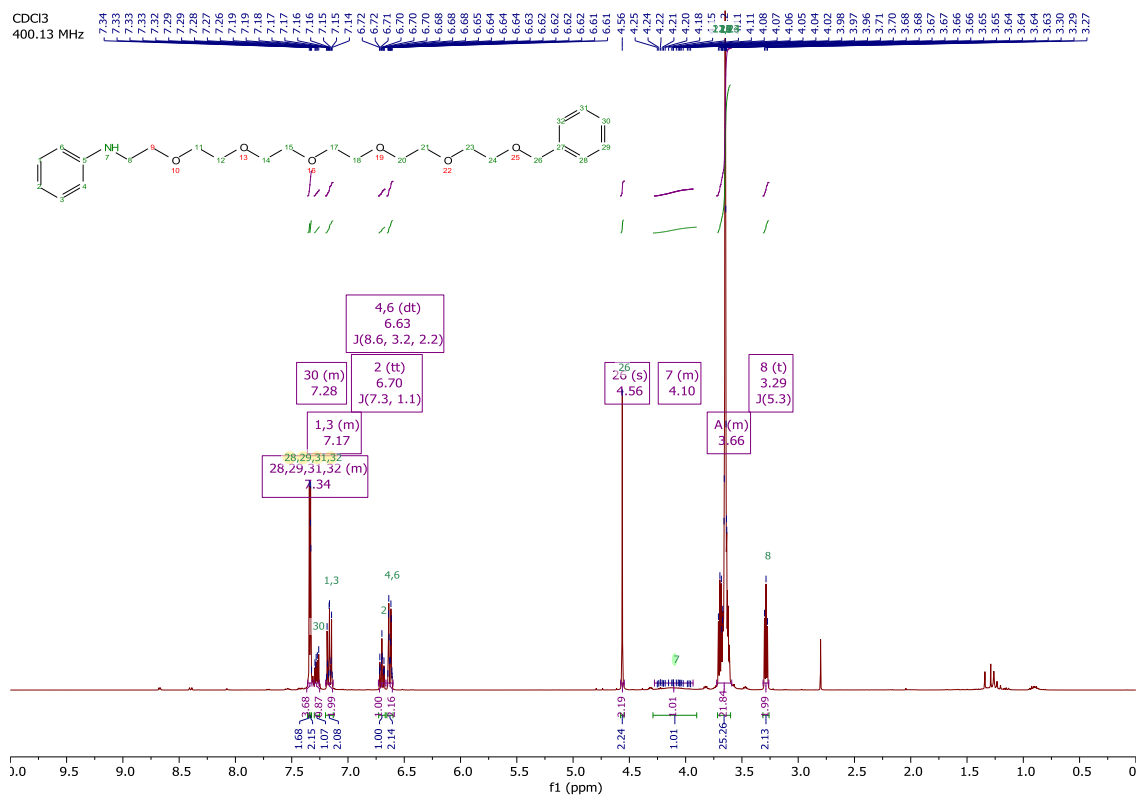
$^1\text{H}$  and  $^{13}\text{C}$  NMR spectra of benzyl ether **2.7**.

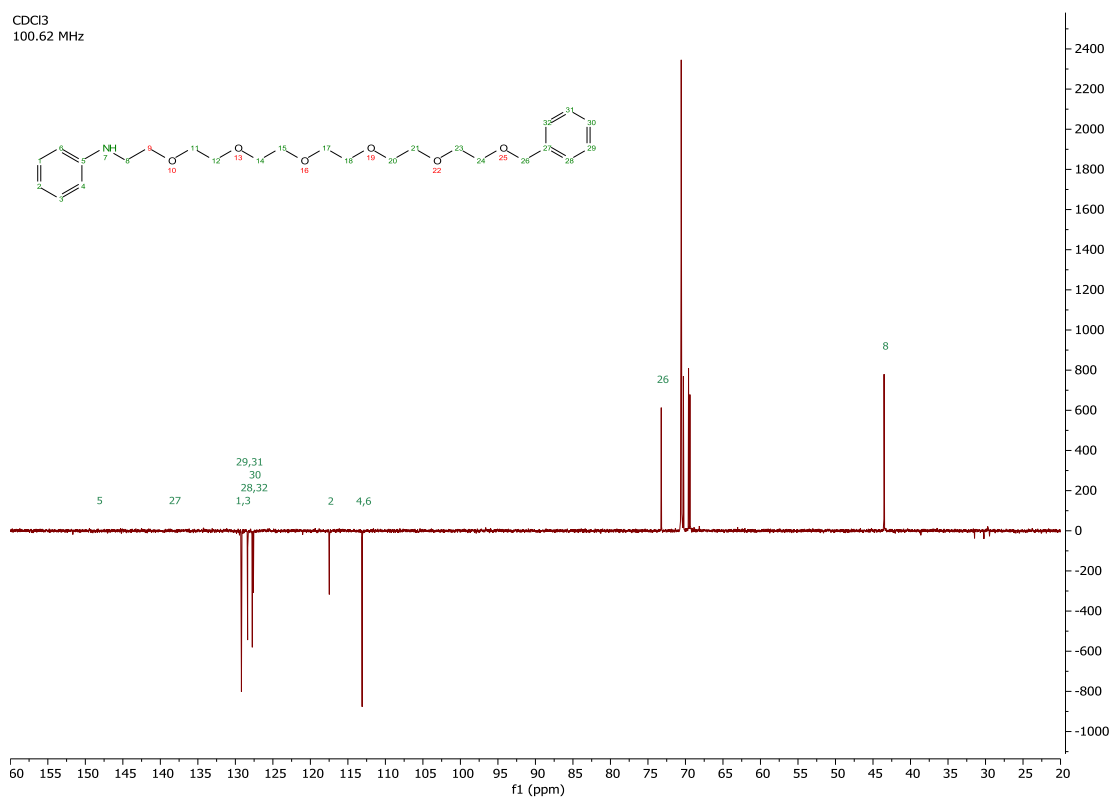
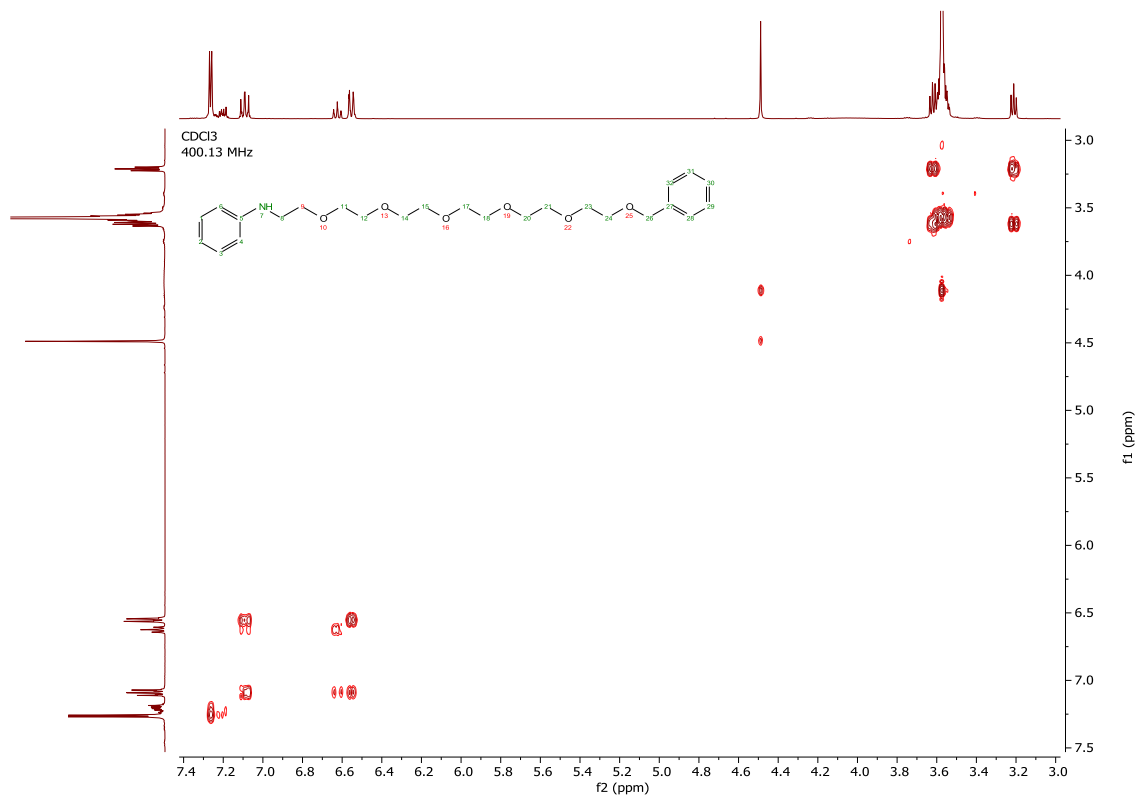


# $^1\text{H}$ and $^{13}\text{C}$ NMR spectra of tosylate **2.8**.



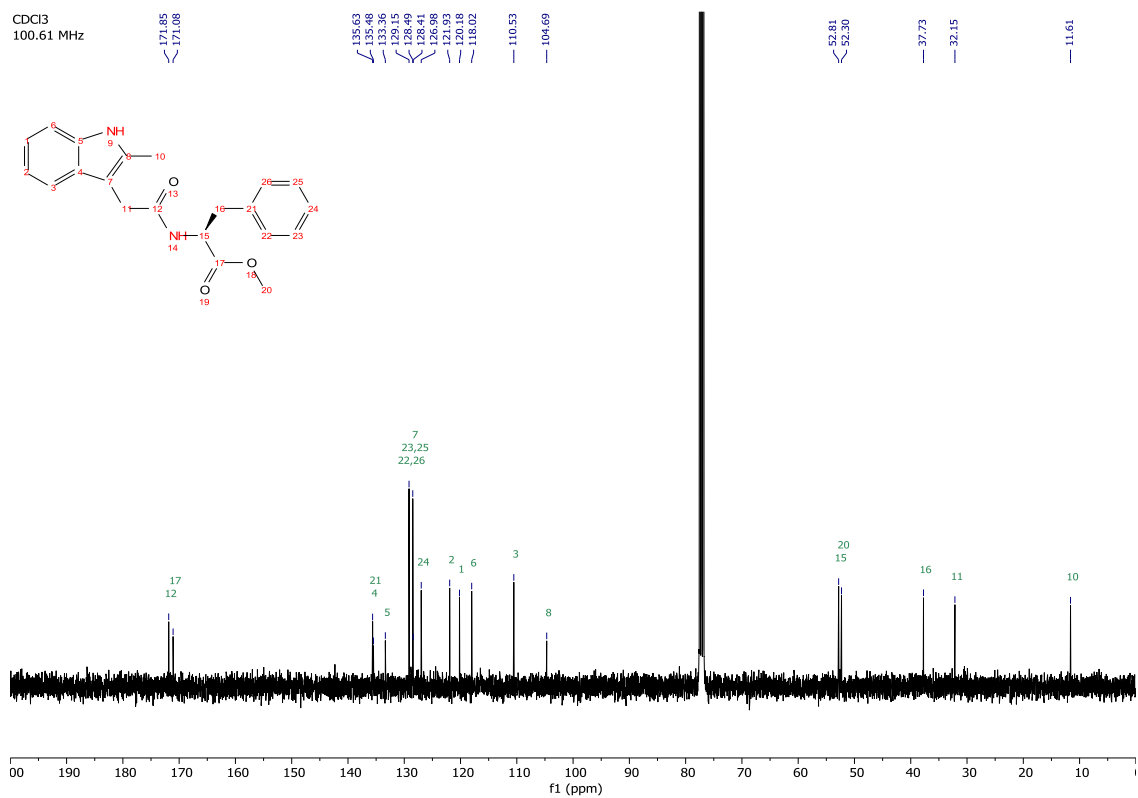
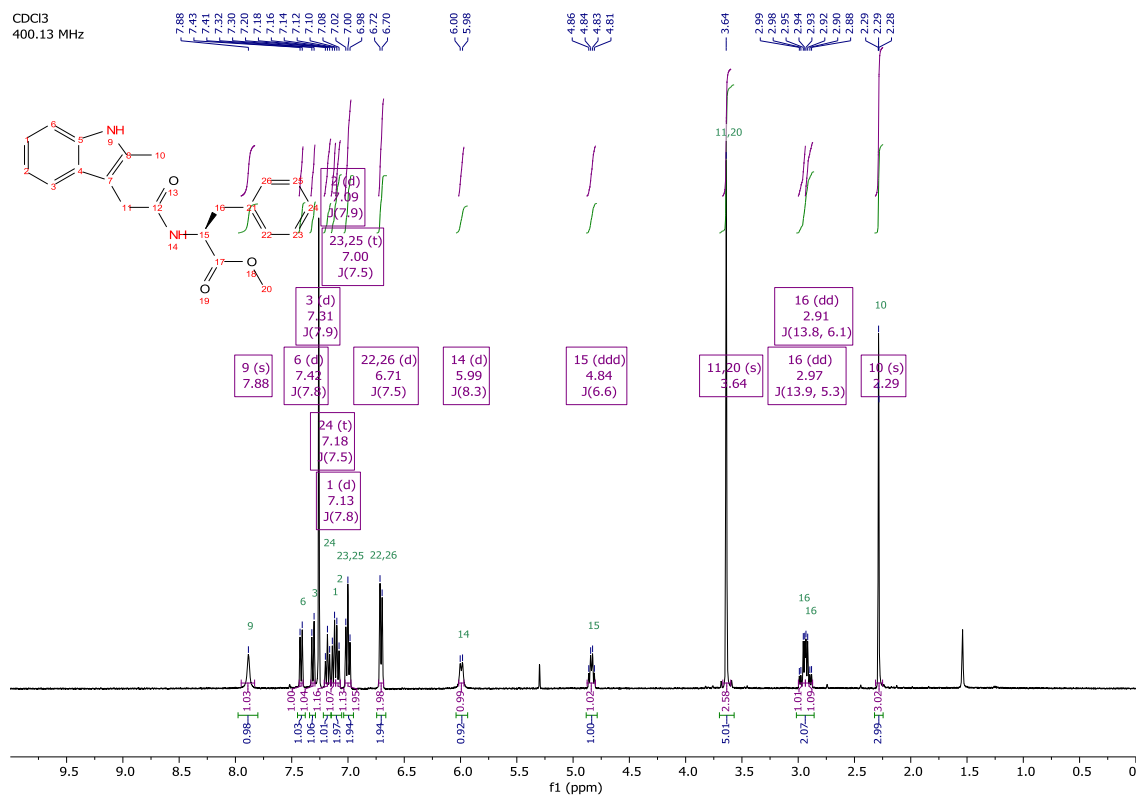
$^1\text{H}$ ,  $^{13}\text{C}$ , COSY, DEPT-135, HSQC and HMBC NMR spectra of aniline **2.9**.



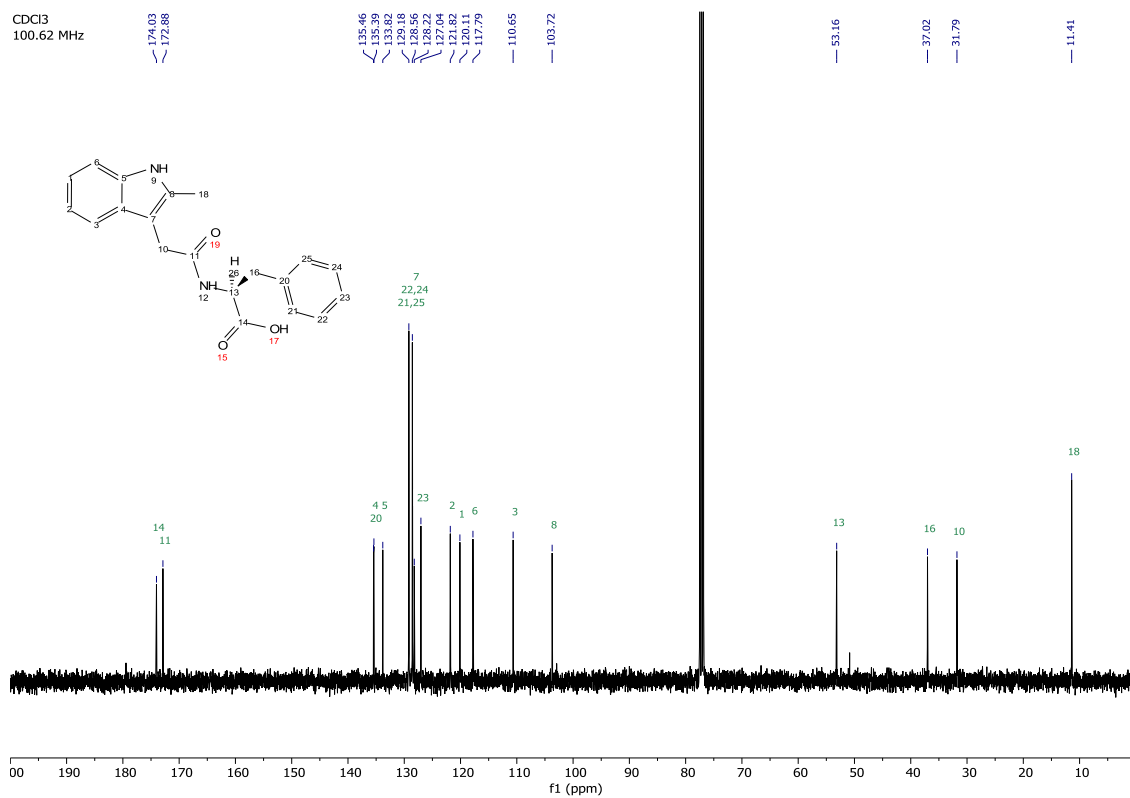
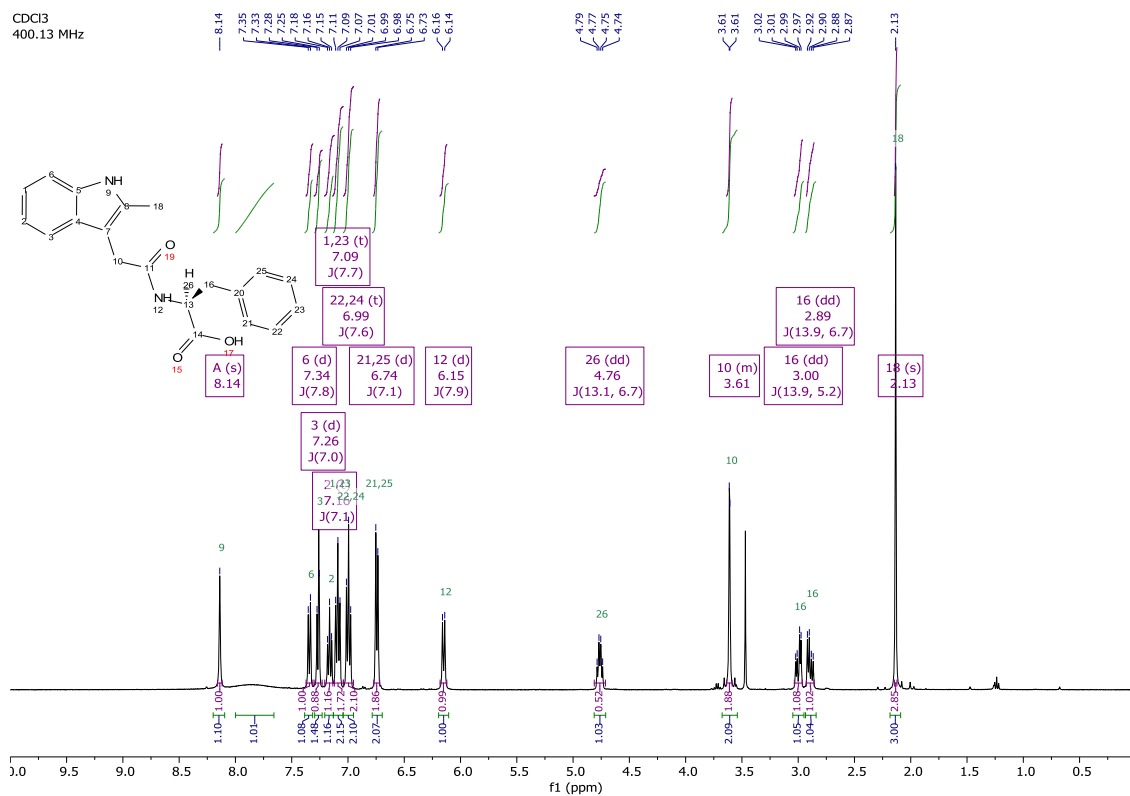


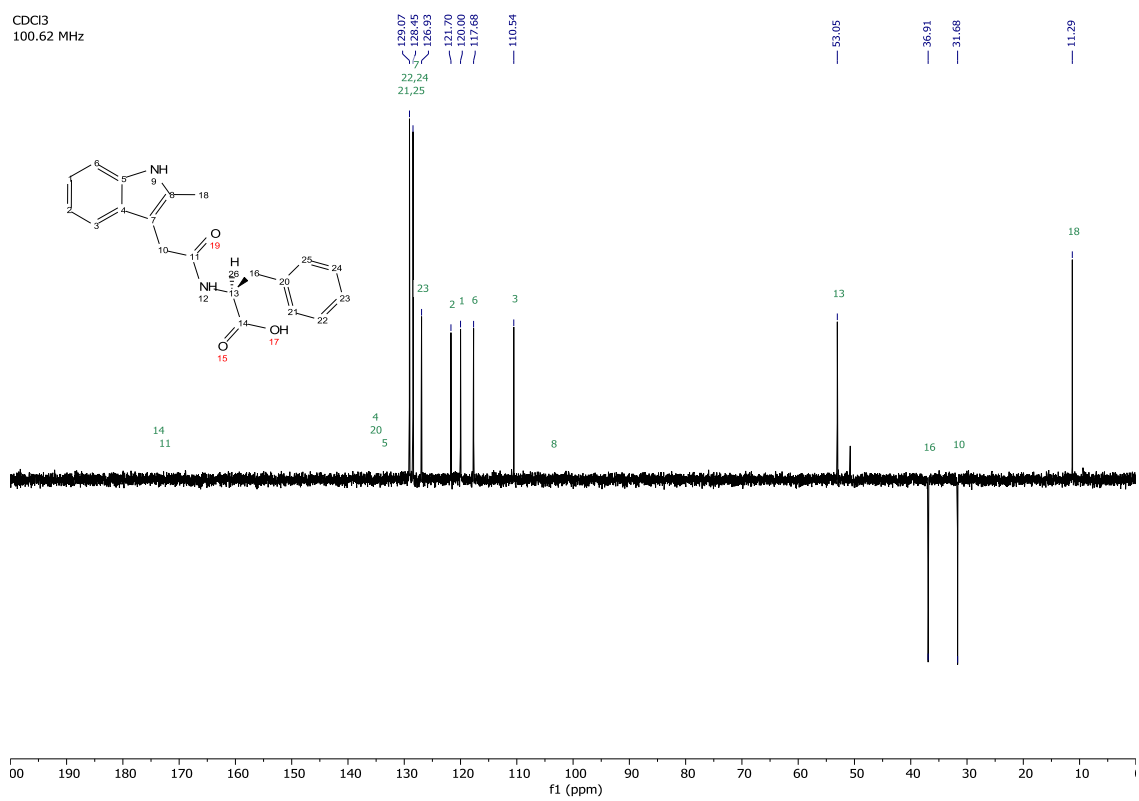
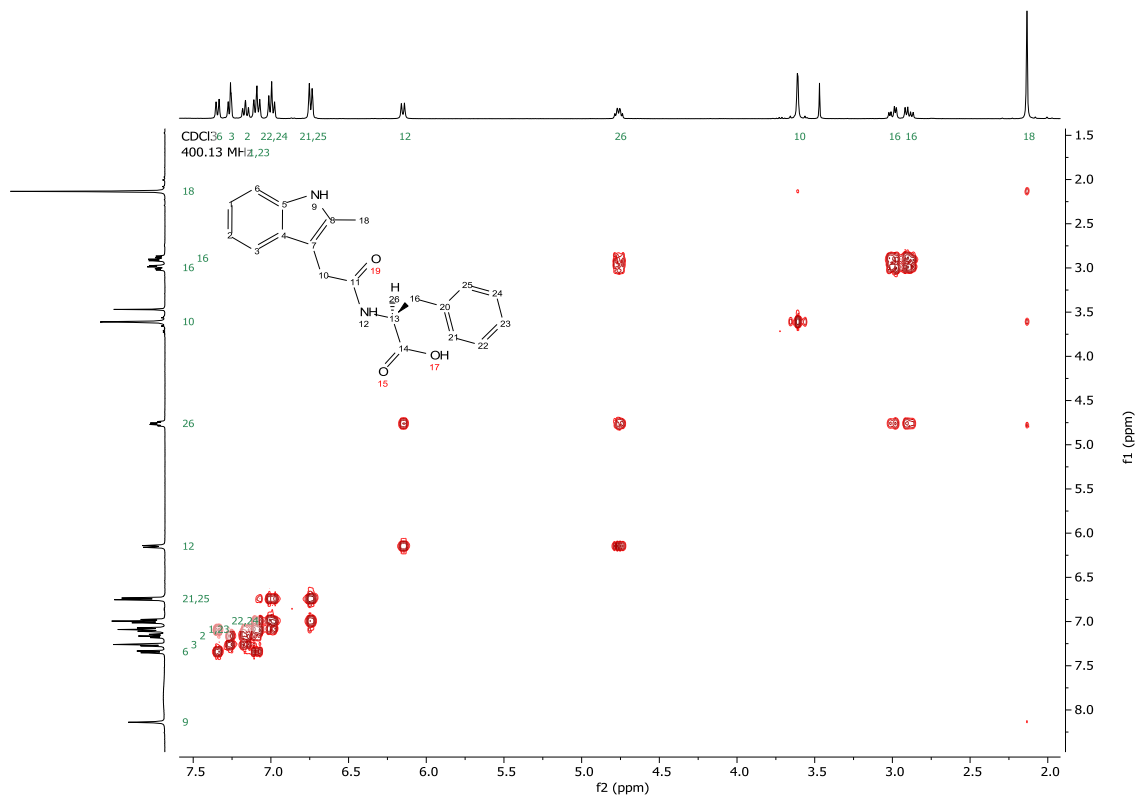


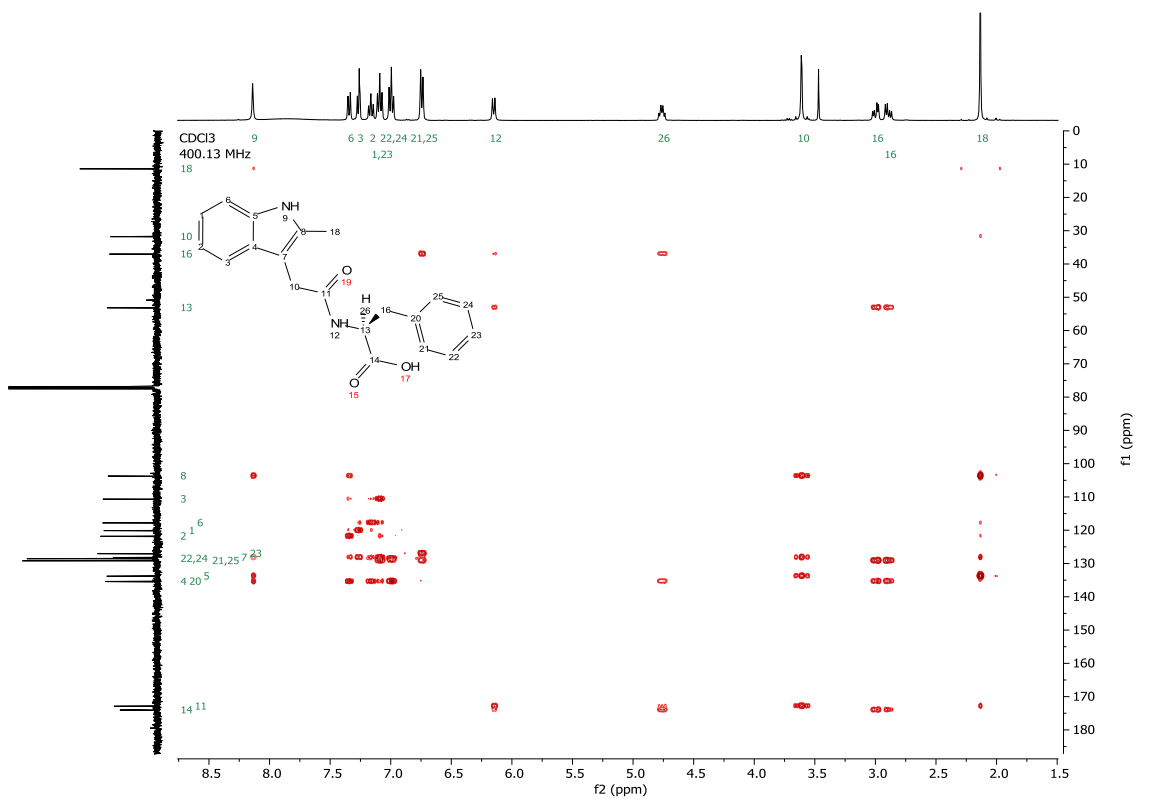
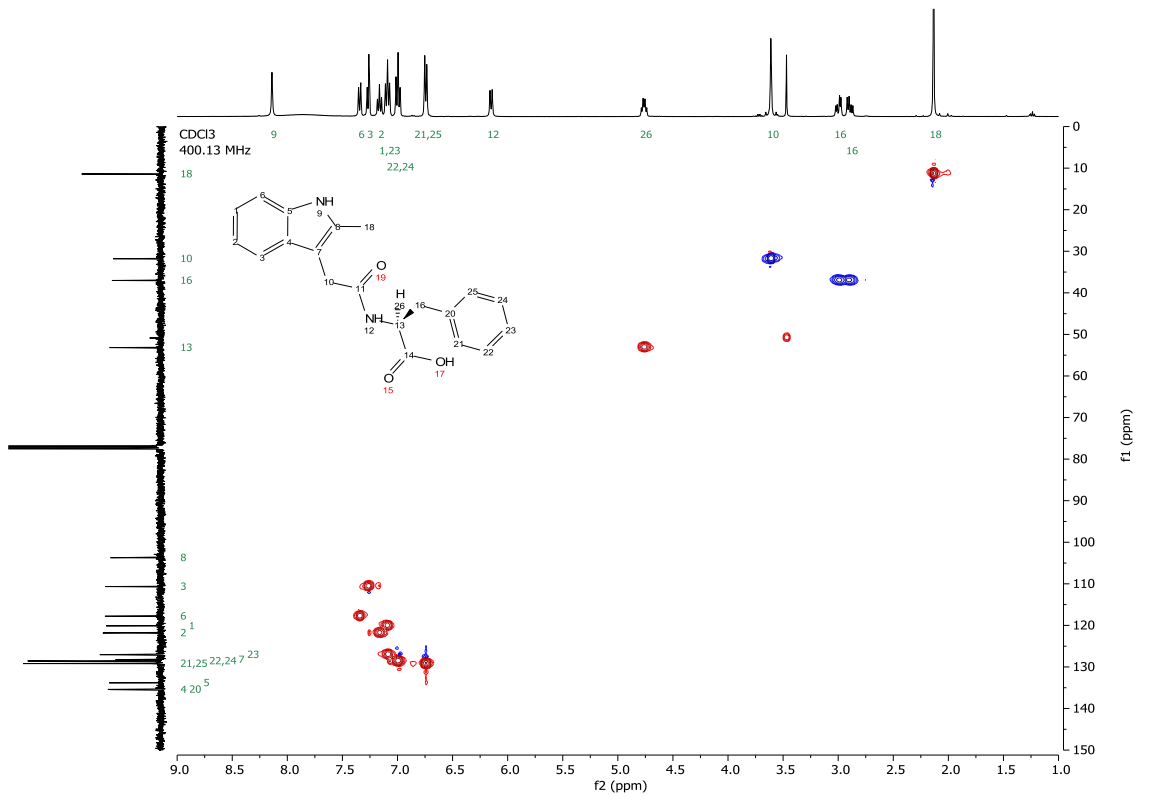
<sup>1</sup>H, and <sup>13</sup>C NMR spectra of methyl ester **2.10**.



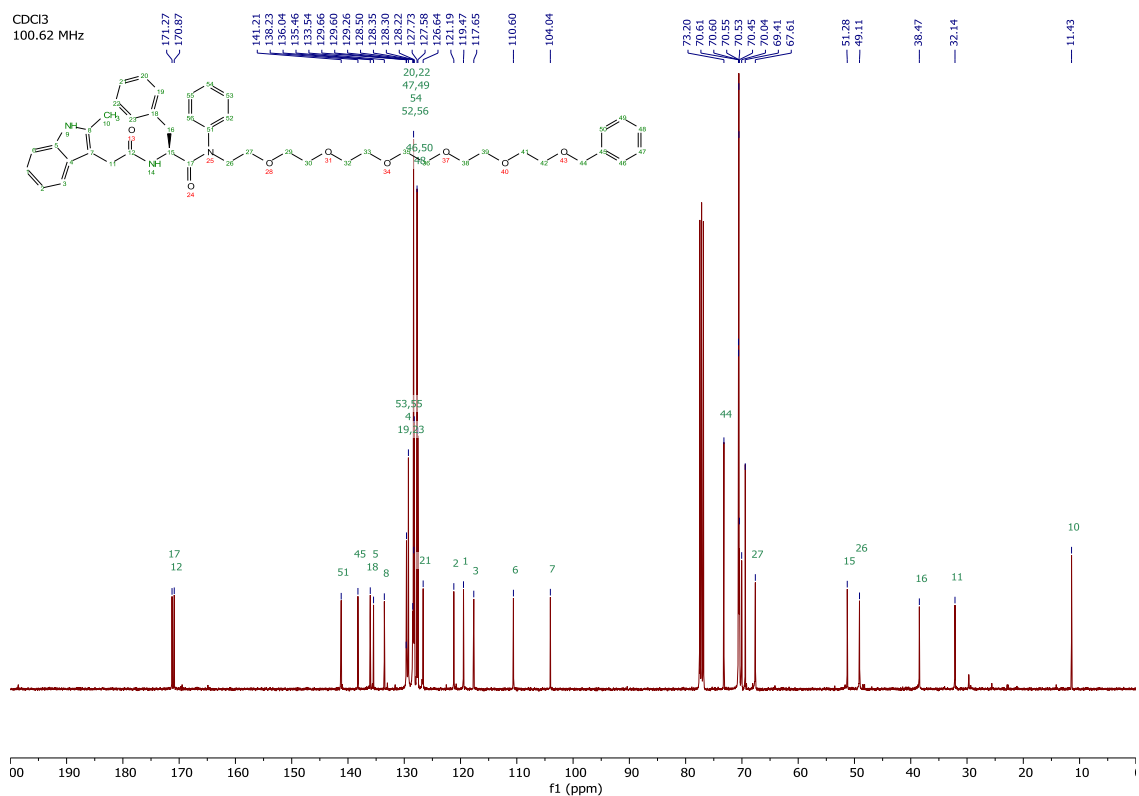
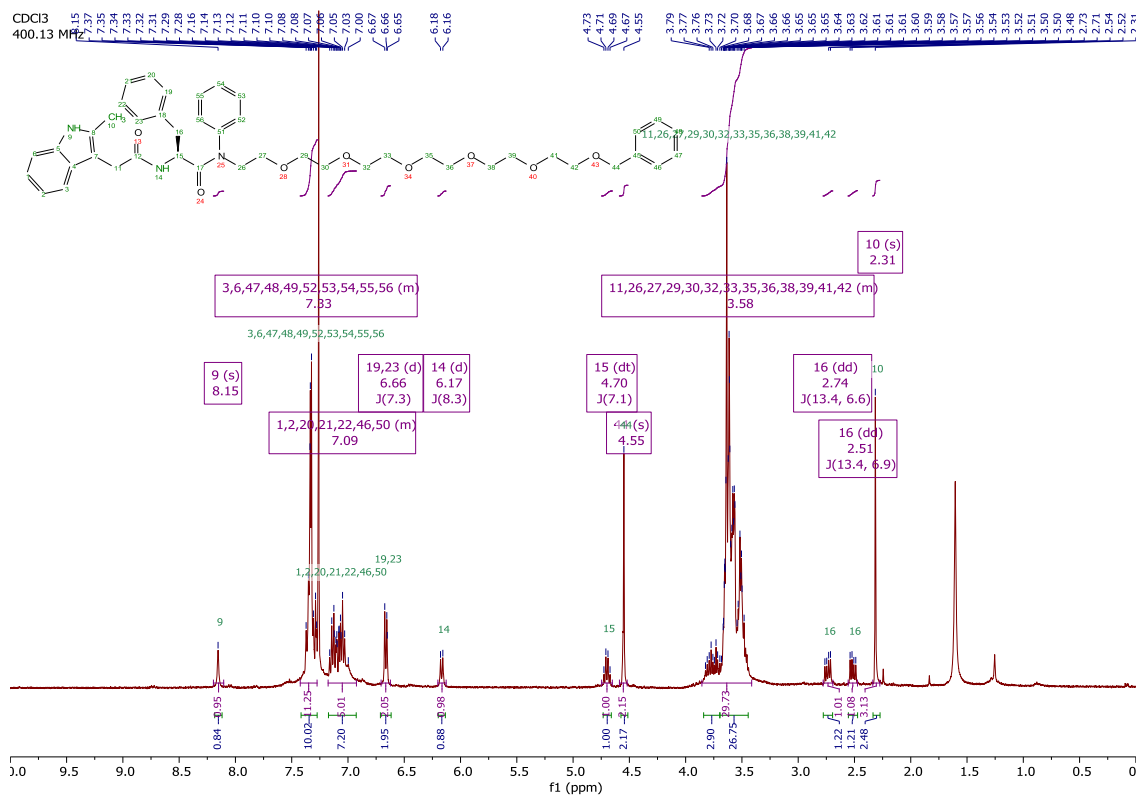
$^1\text{H}$ ,  $^{13}\text{C}$ , COSY, DEPT-135, HSQC and HMBC NMR spectra of acid **2.11**.

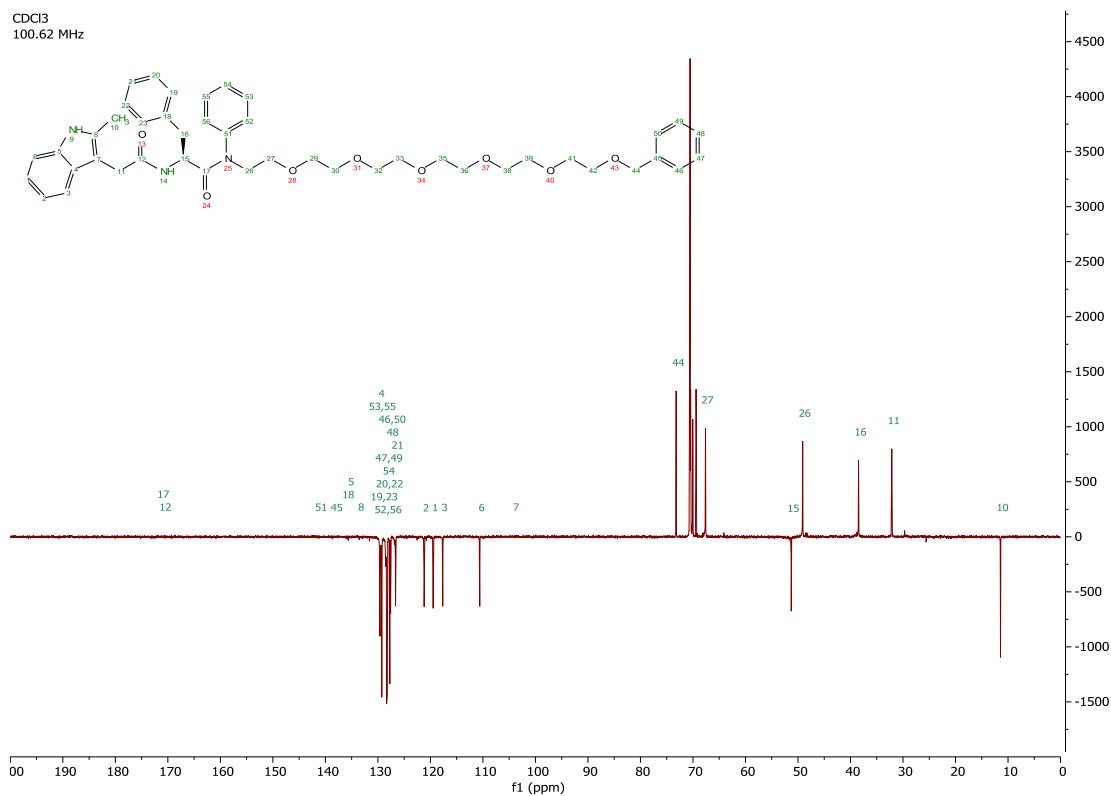
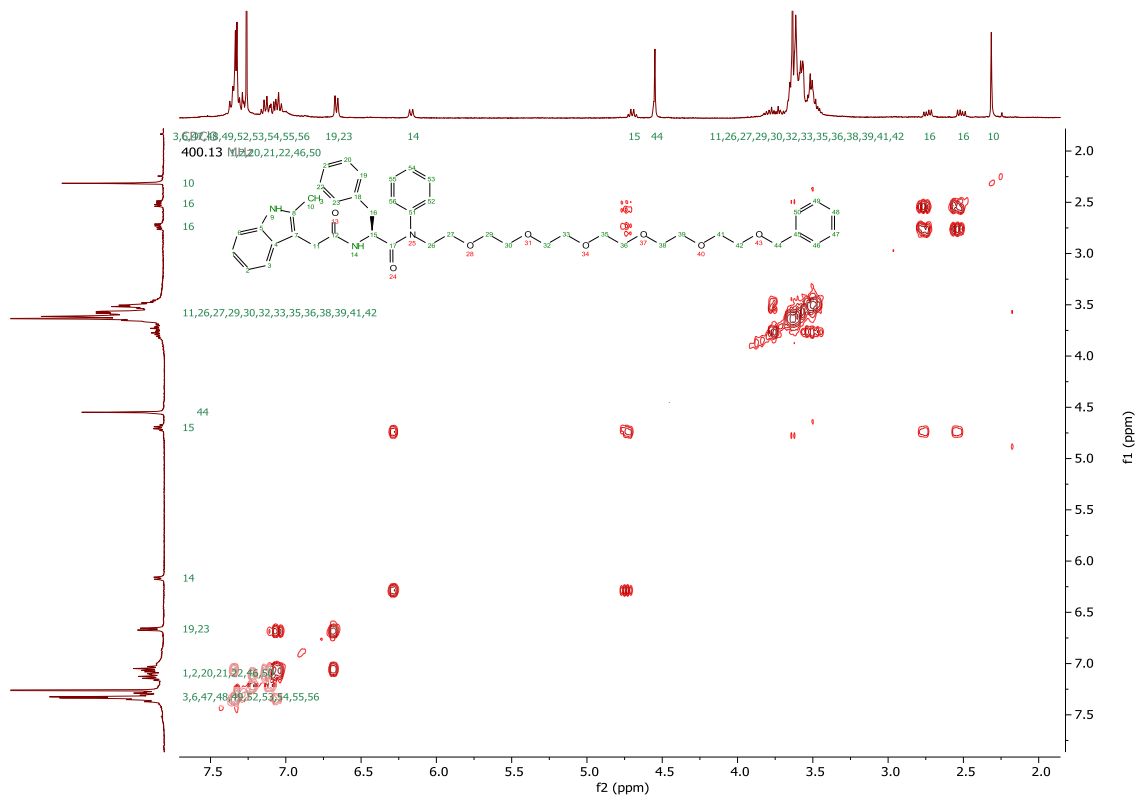


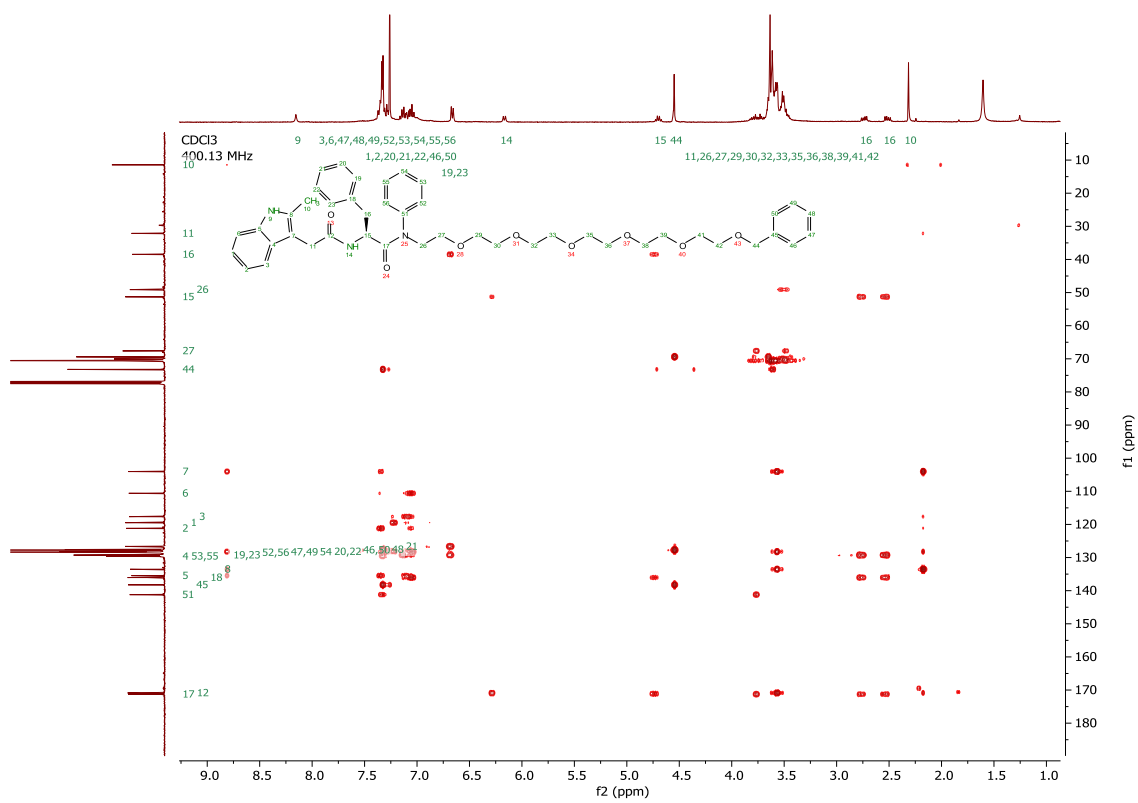
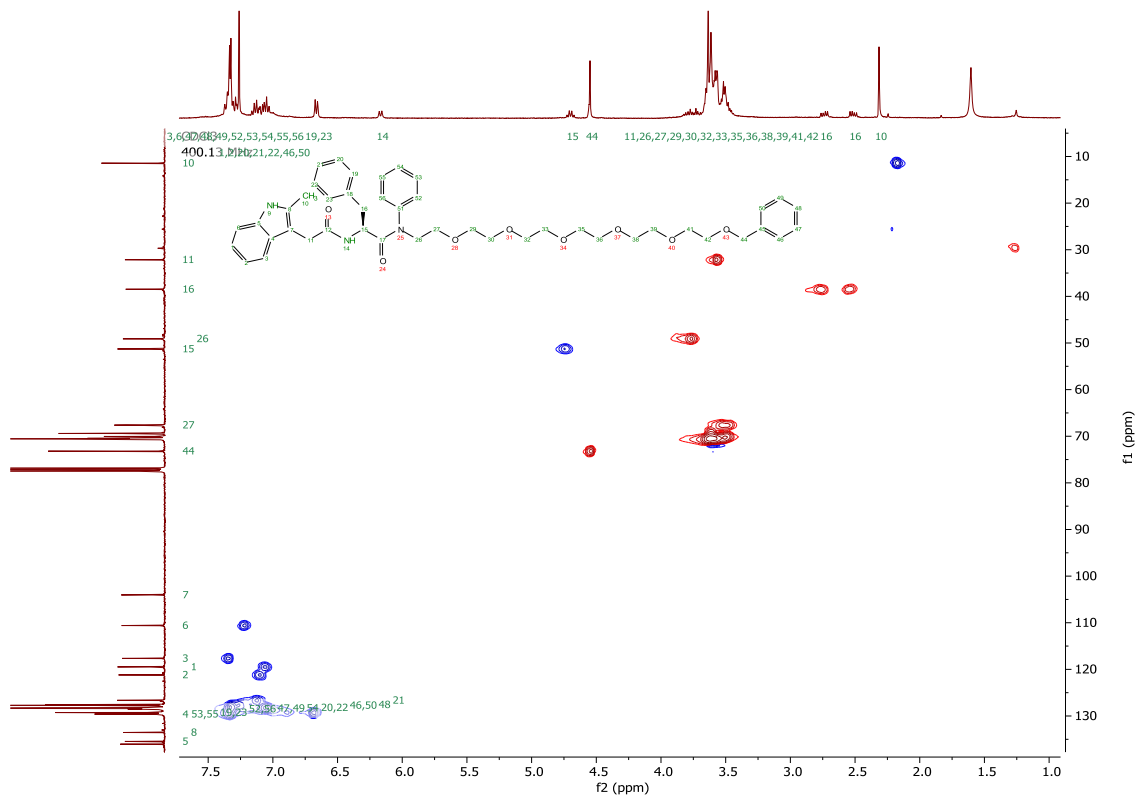




$^1\text{H}$ ,  $^{13}\text{C}$ , COSY, DEPT-135, HSQC and HMBC NMR spectra of benzyl ether **2.12**.

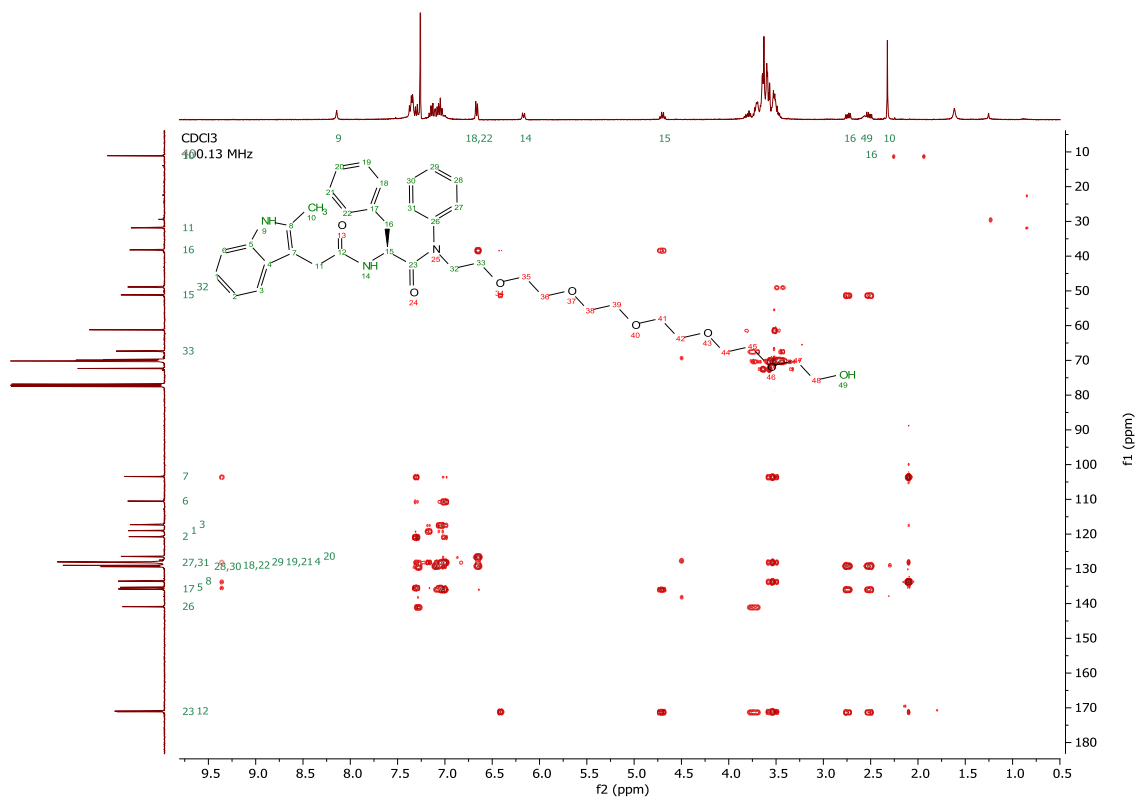
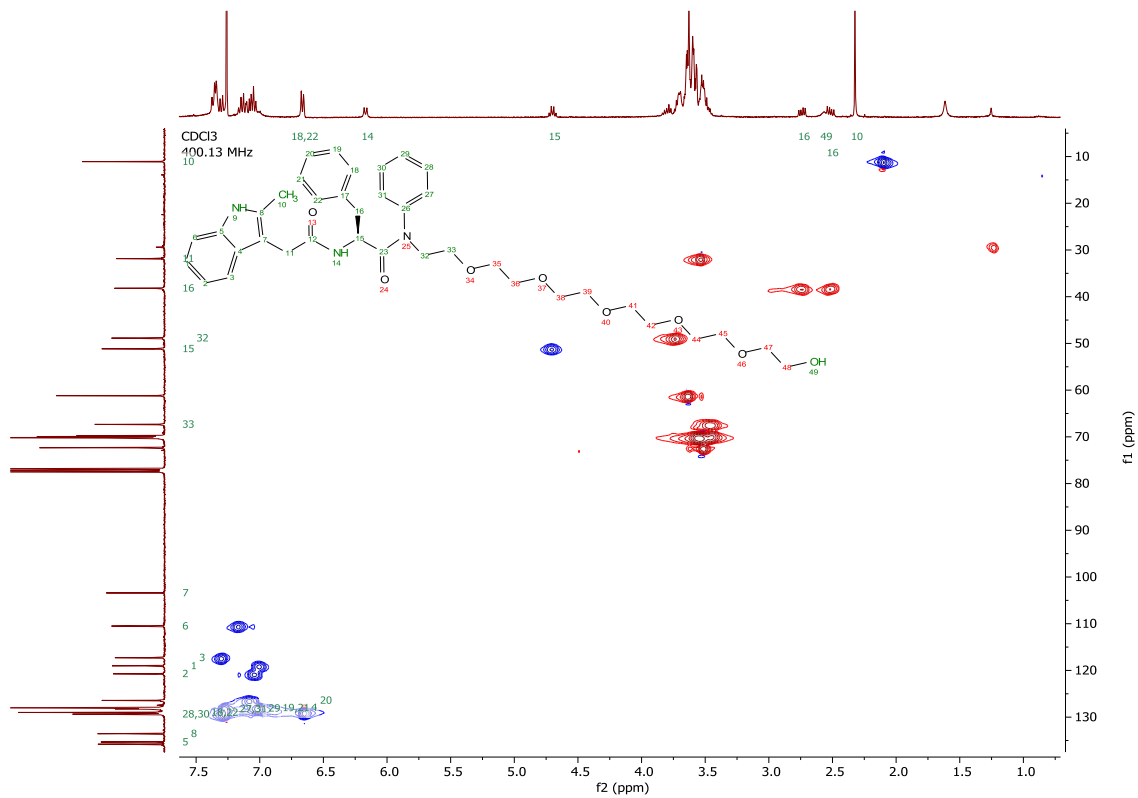




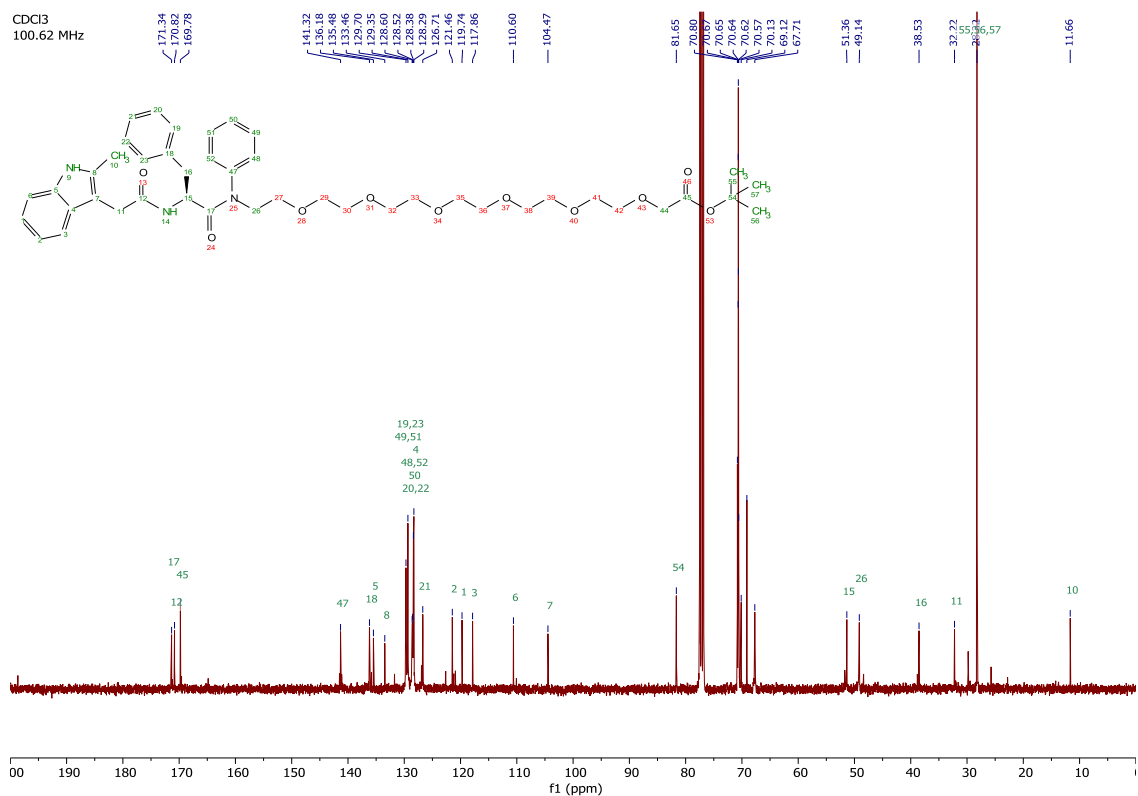
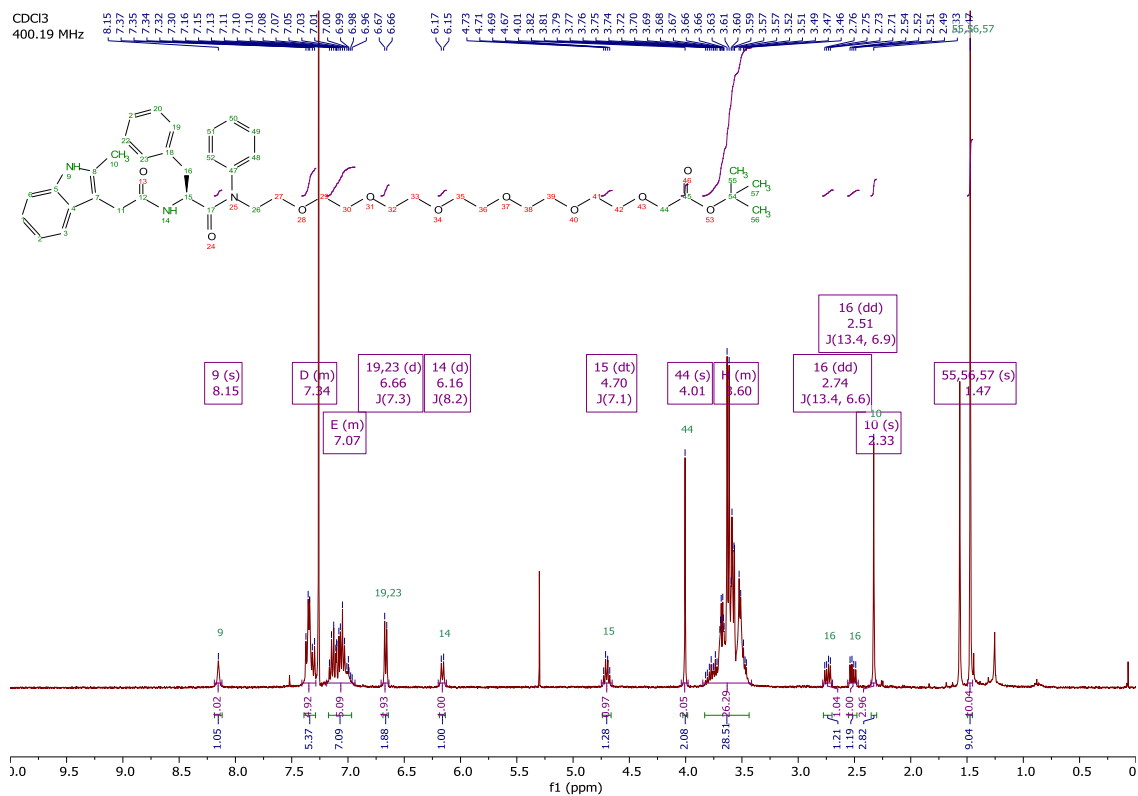


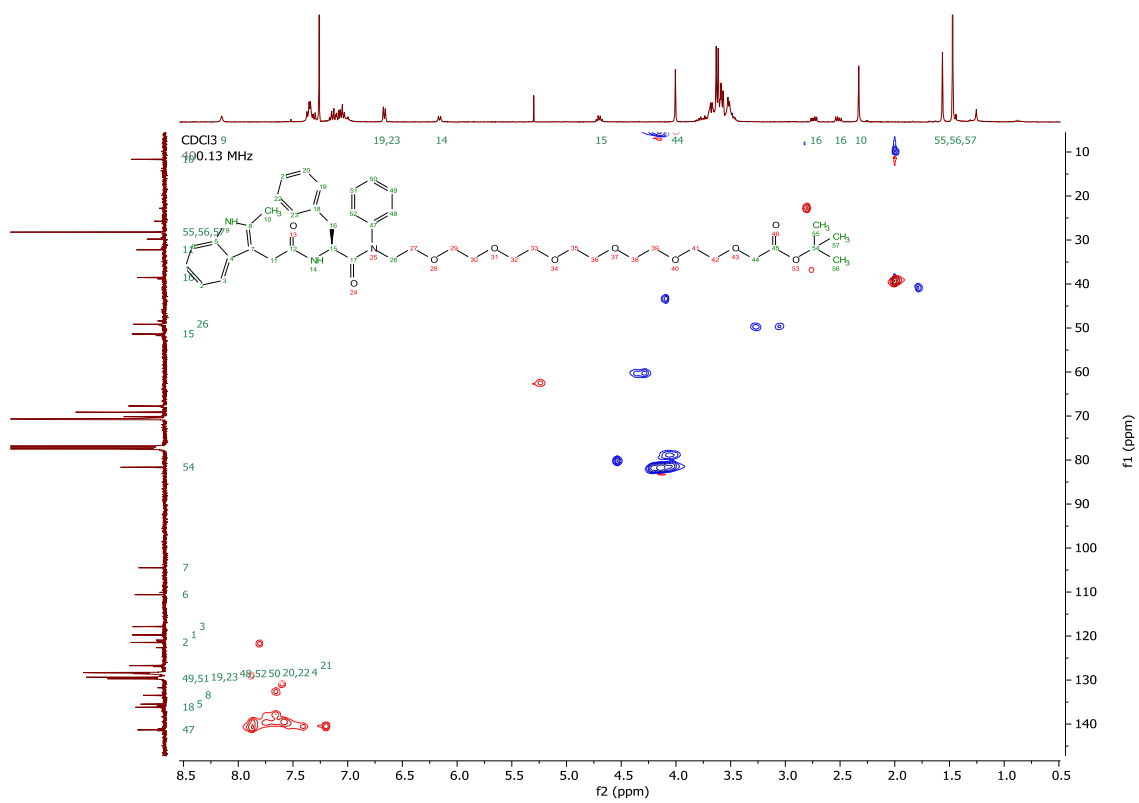
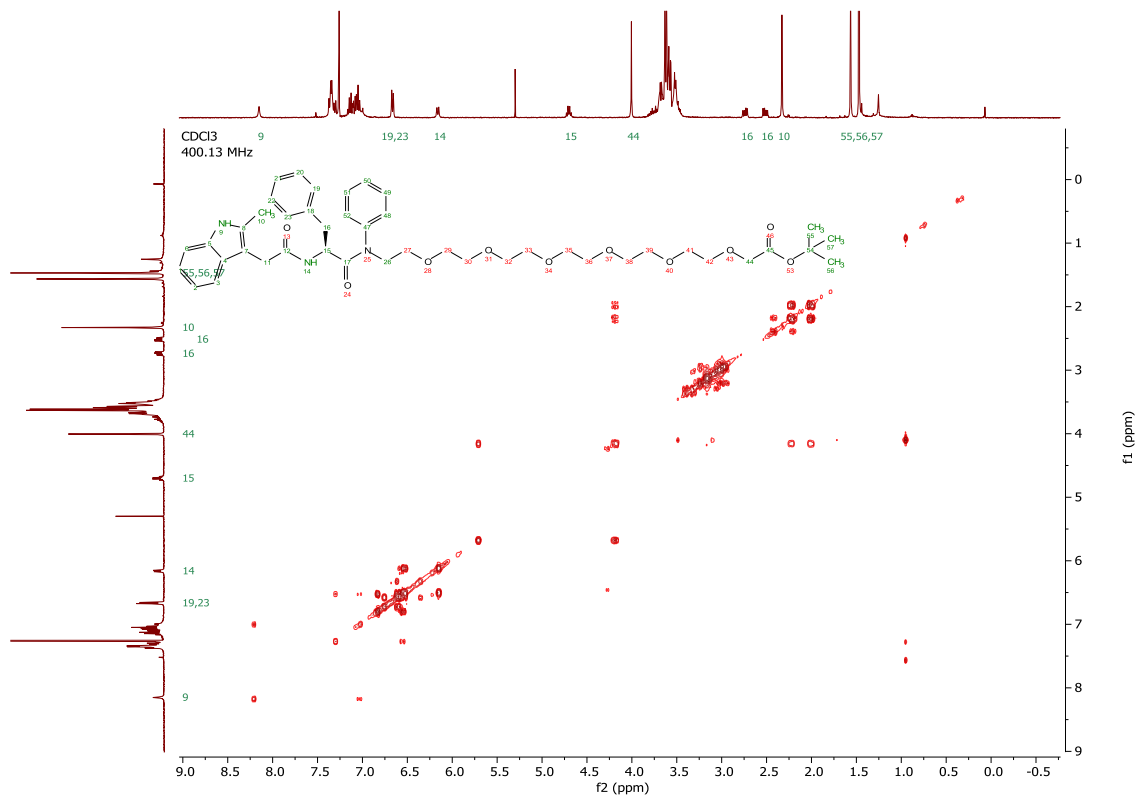




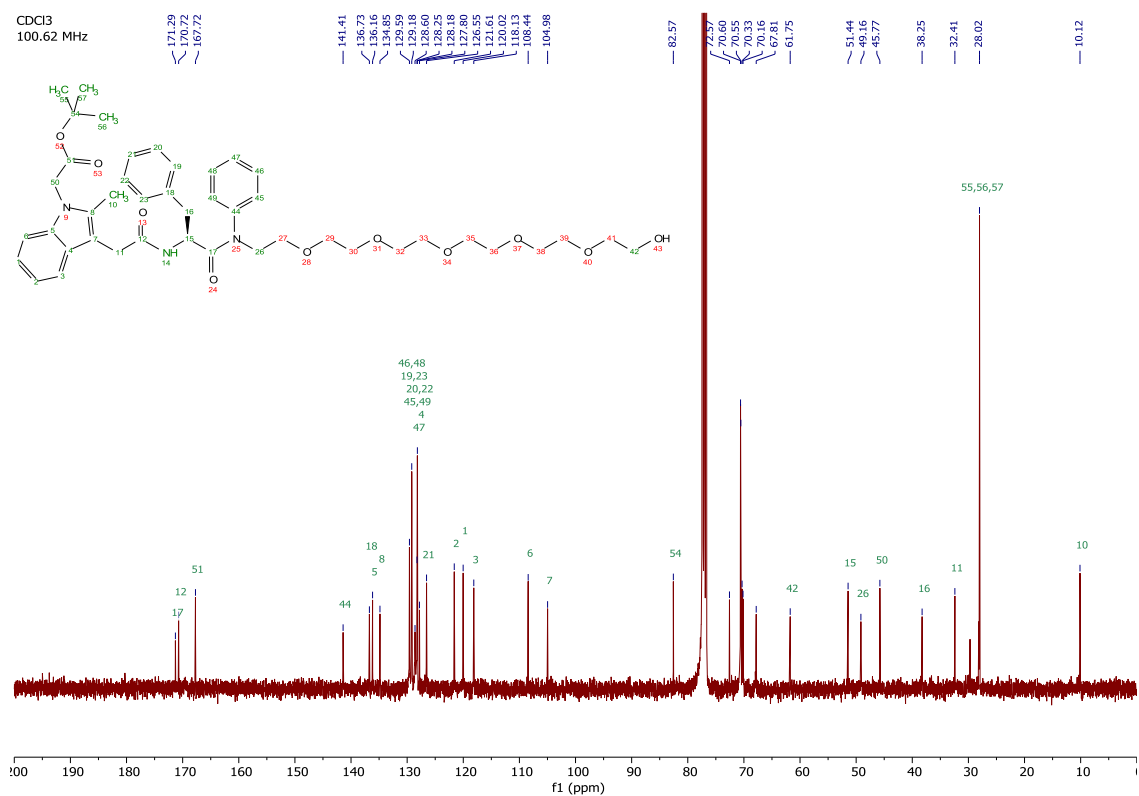
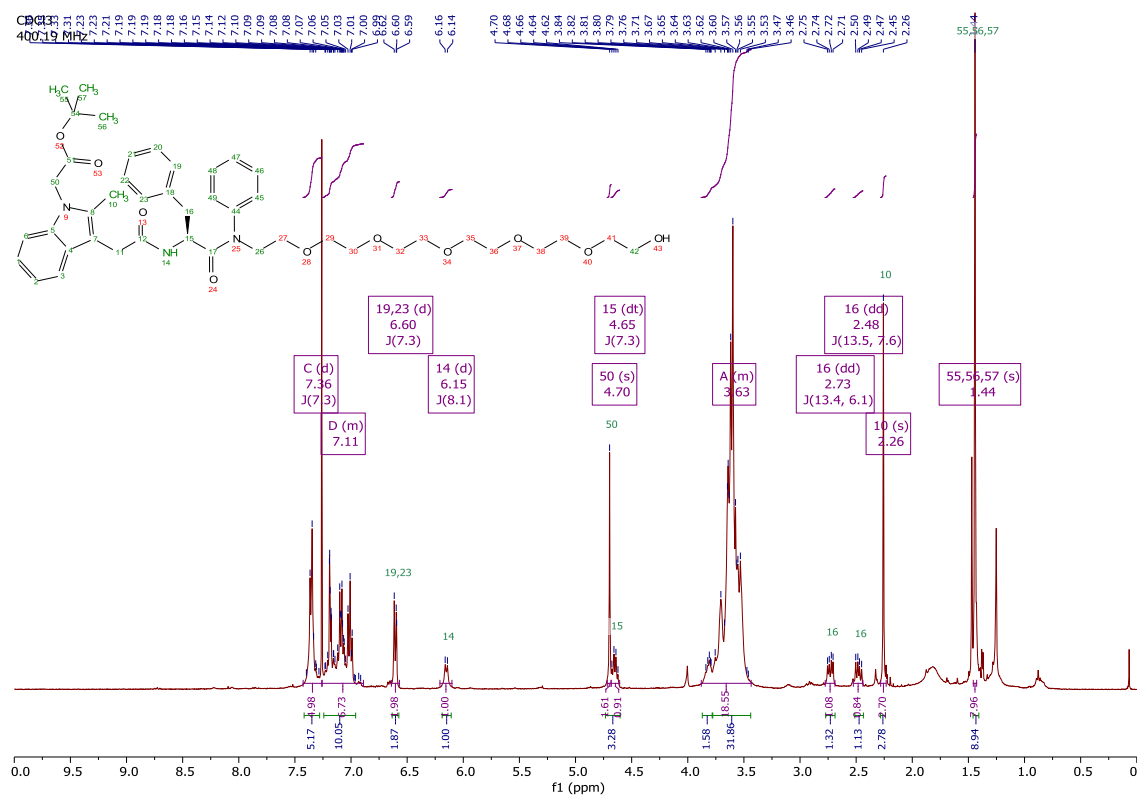


$^1\text{H}$ ,  $^{13}\text{C}$ , COSY and HSQC NMR spectra of *tert*-butyl ester **2.1**.

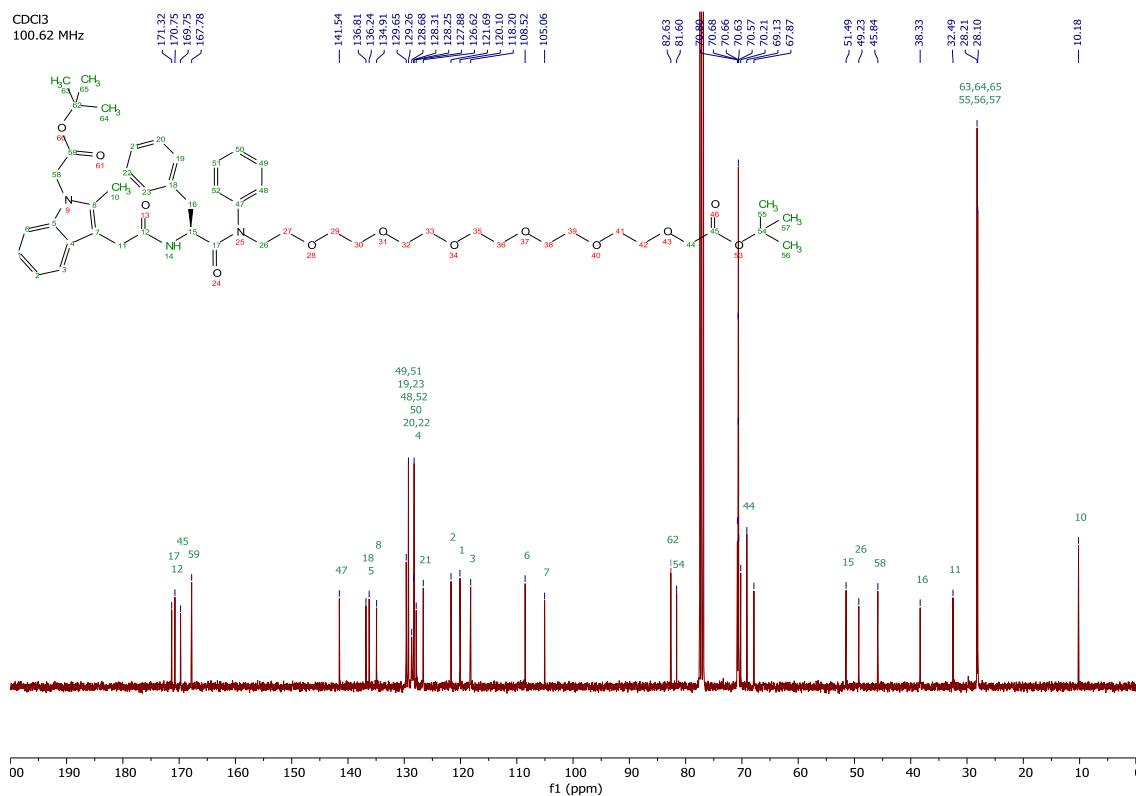
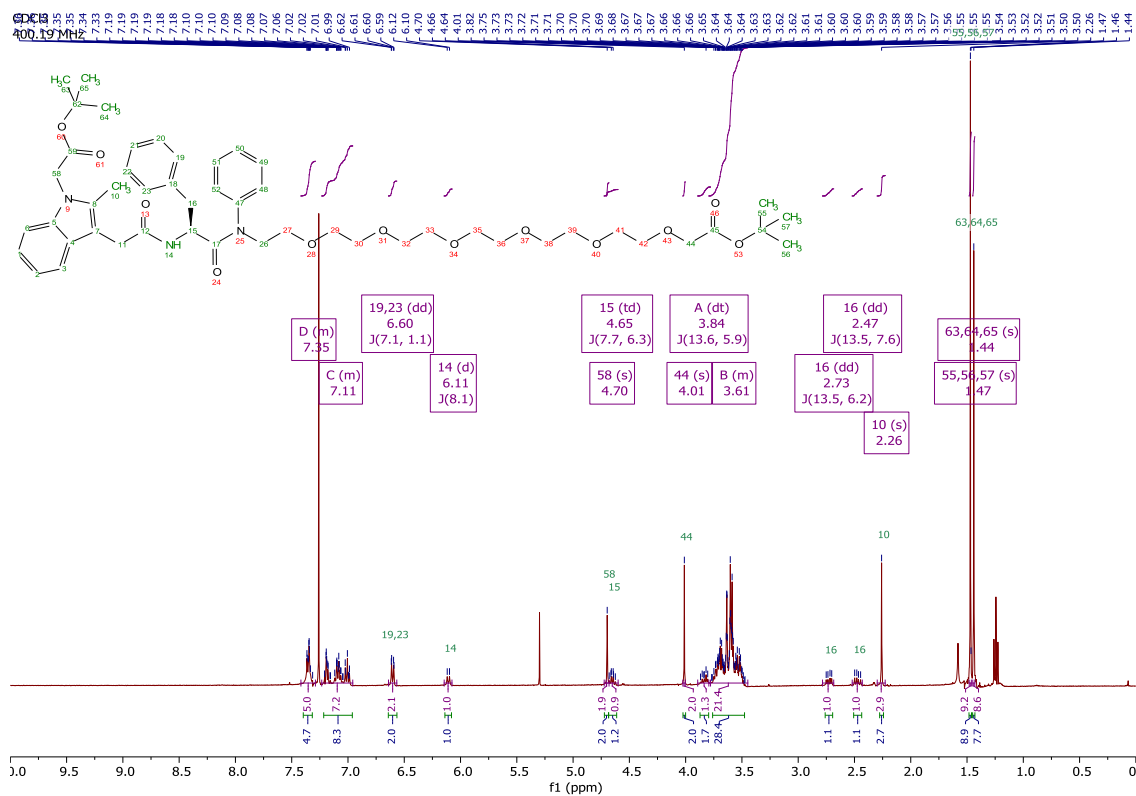




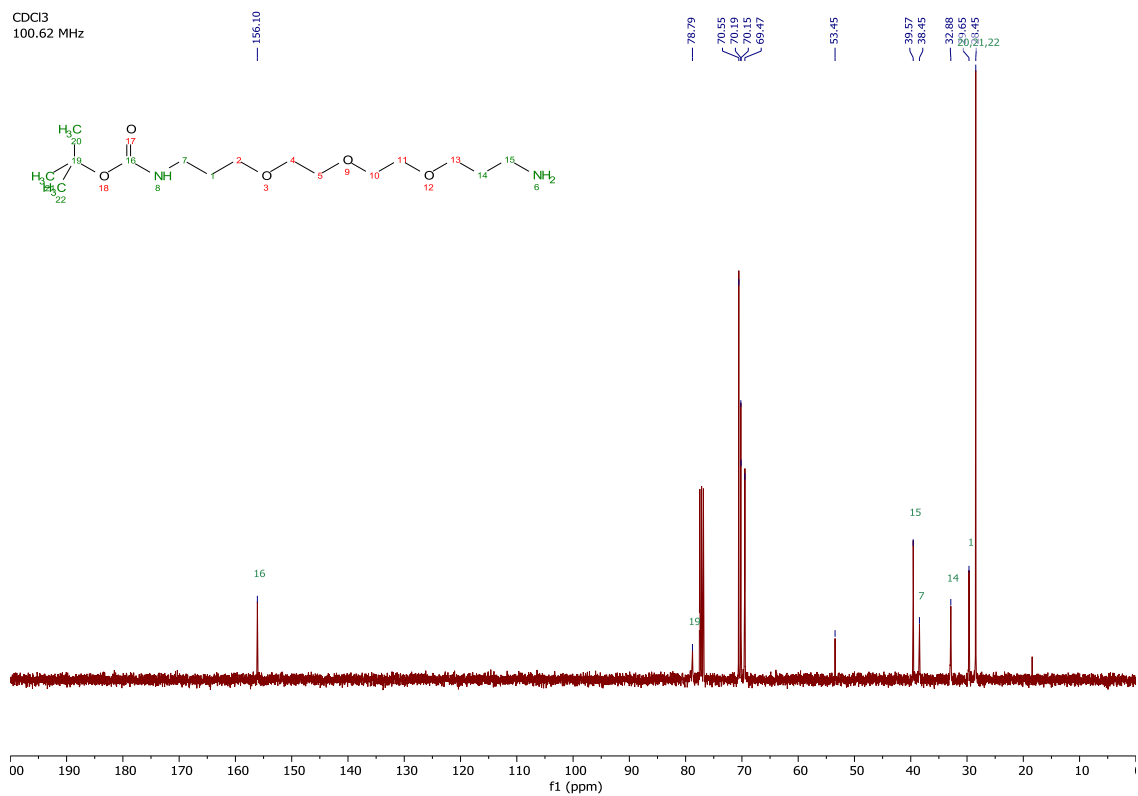
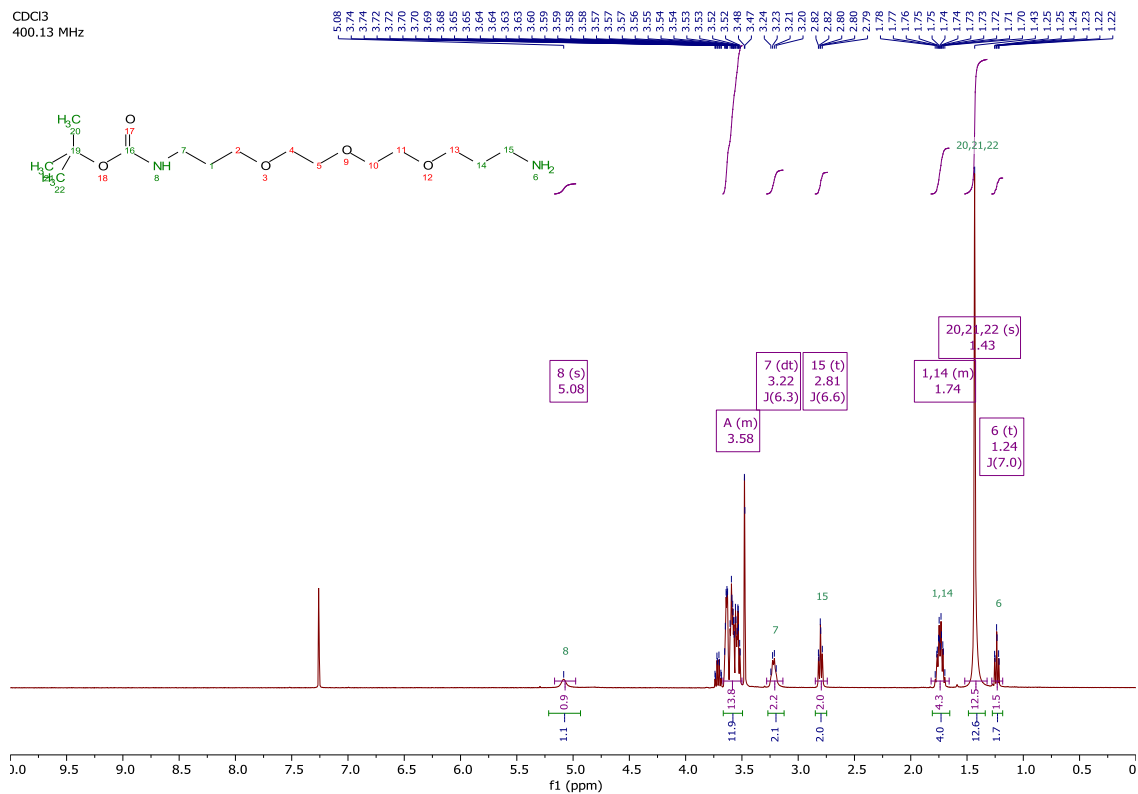
$^1\text{H}$ , and  $^{13}\text{C}$  NMR spectra of *tert*-butyl ester **2.14**.



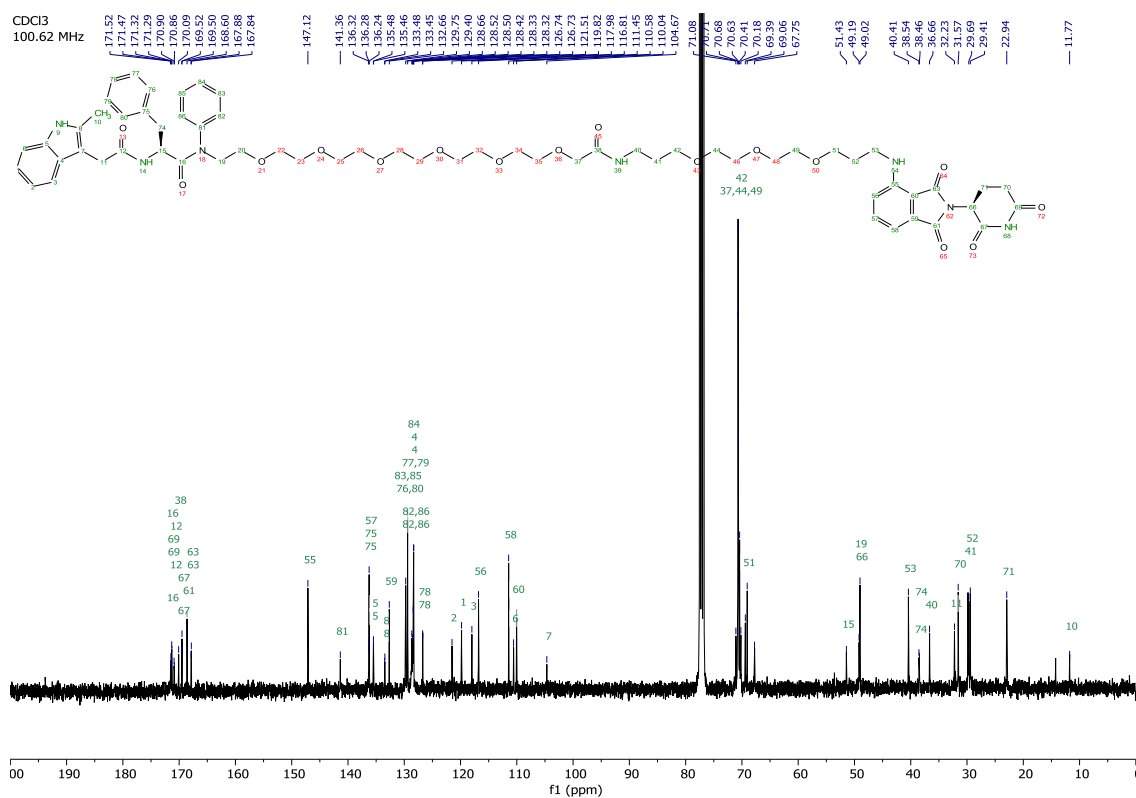
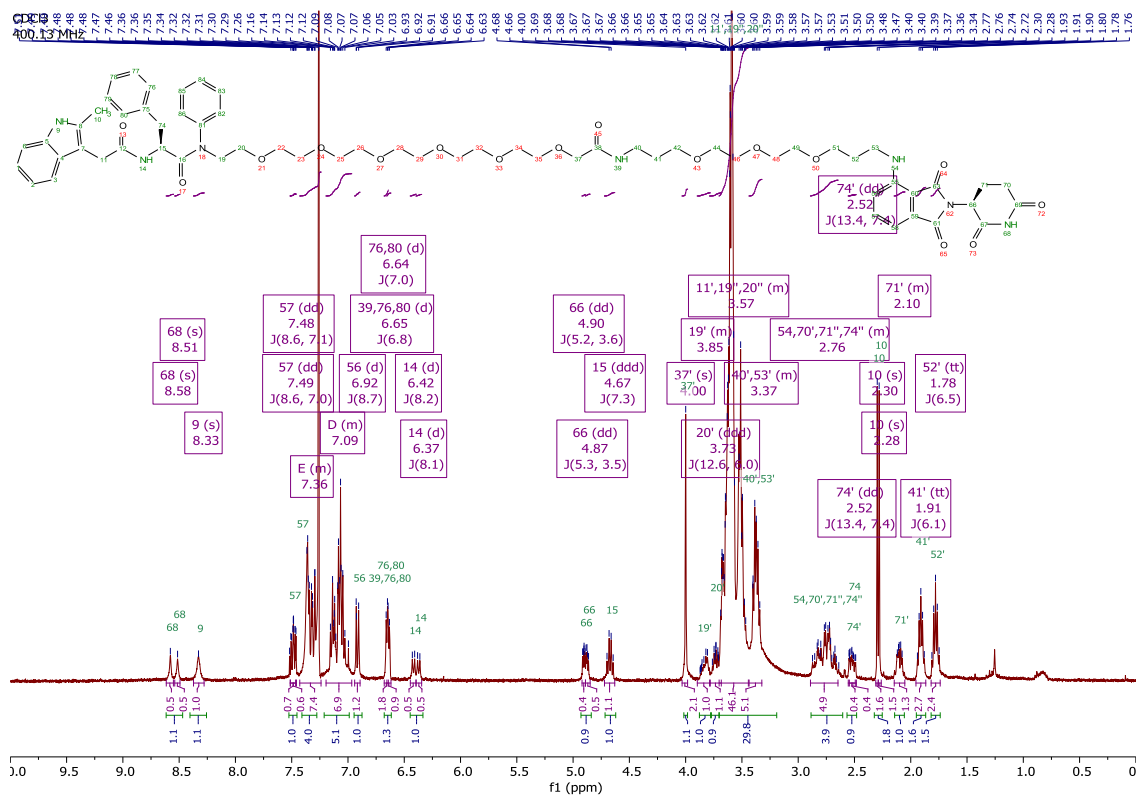
<sup>1</sup>H, and <sup>13</sup>C NMR spectra of *tert*-butyl ester **2.15**.

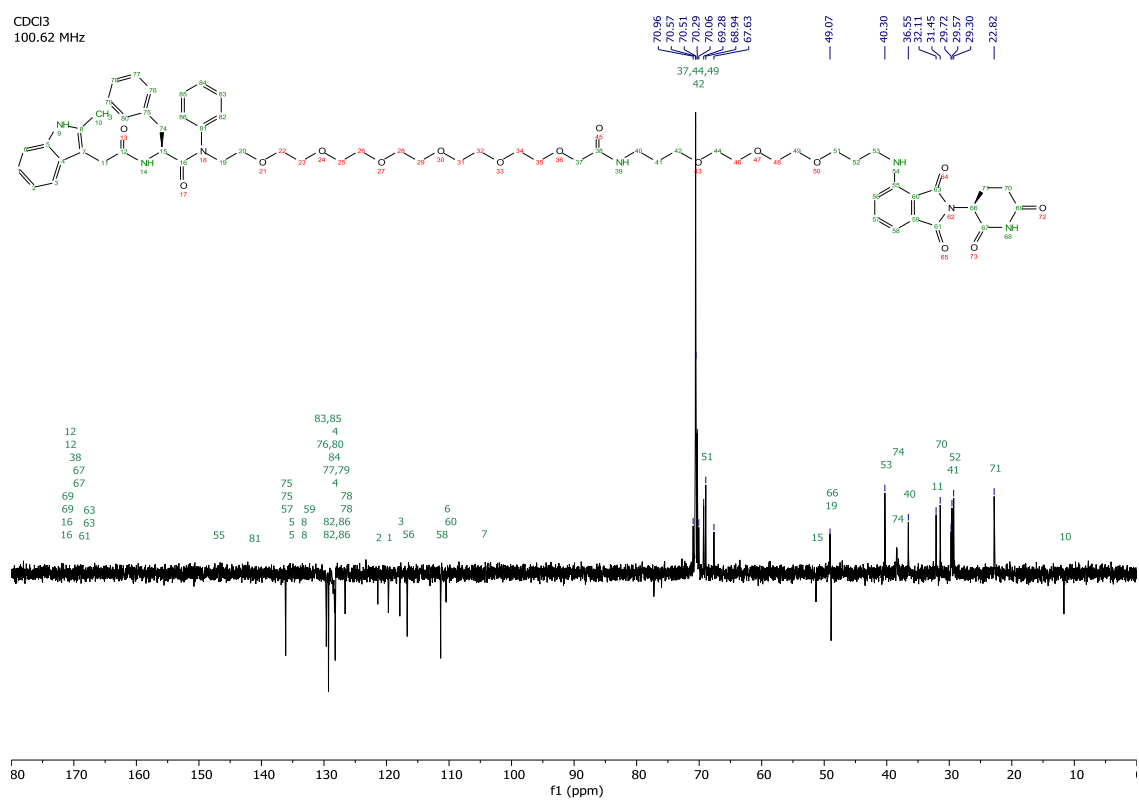
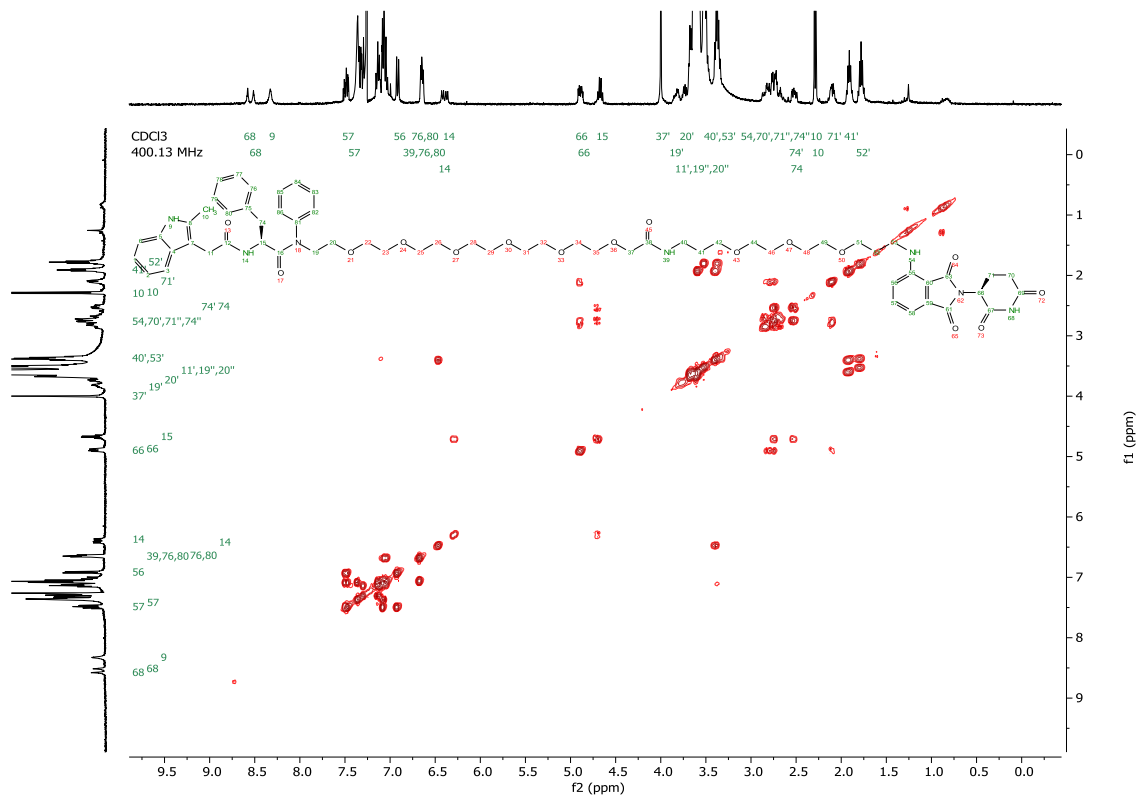


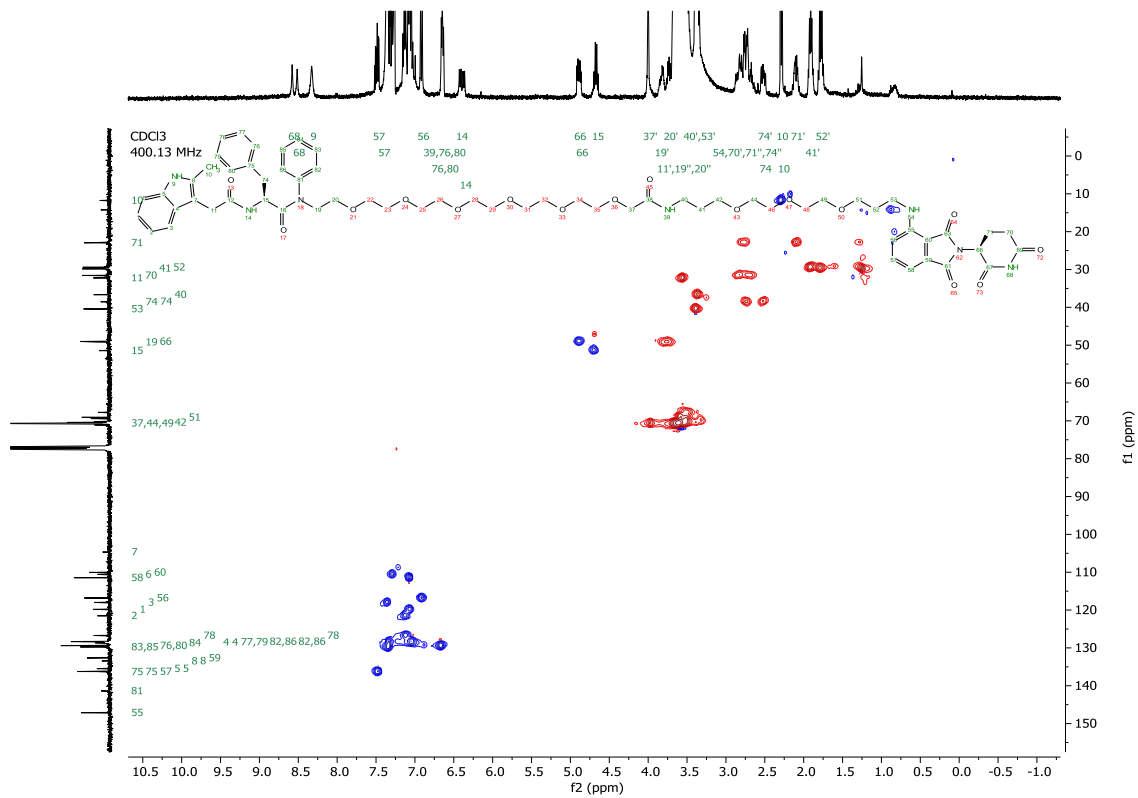
$^1\text{H}$ , and  $^{13}\text{C}$  NMR spectra of *tert*-butyl carbamate **2.19**.



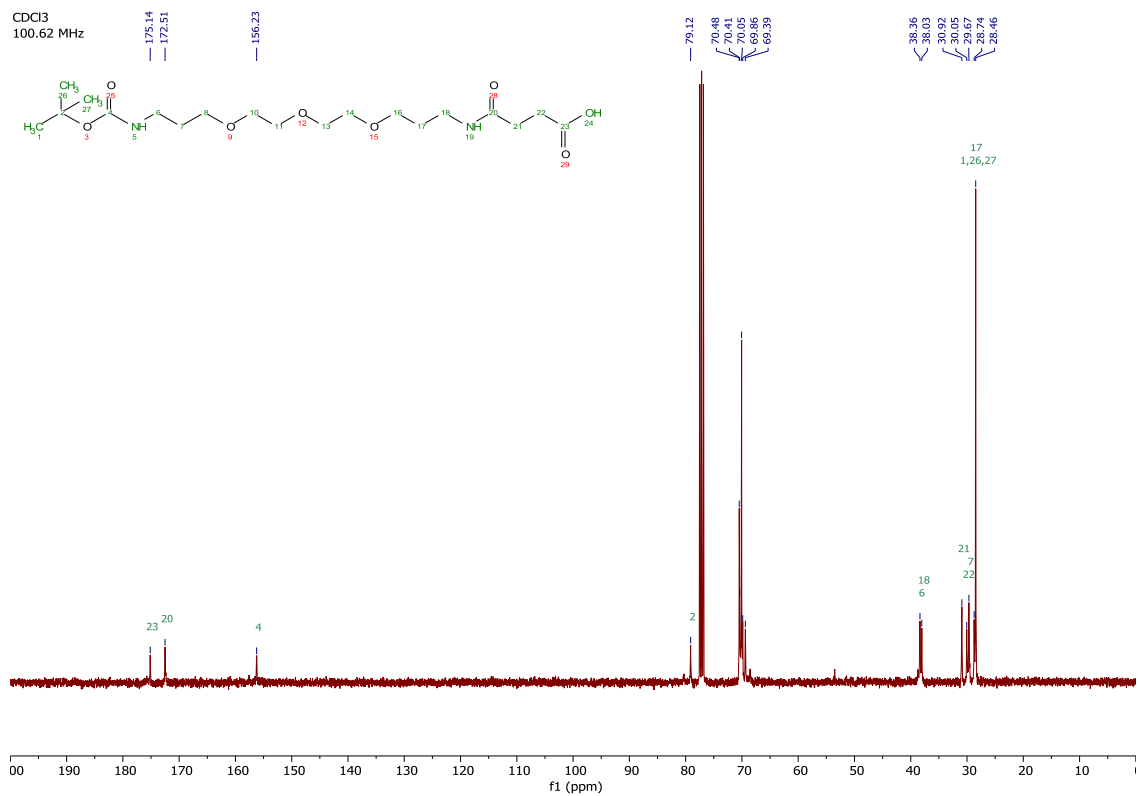
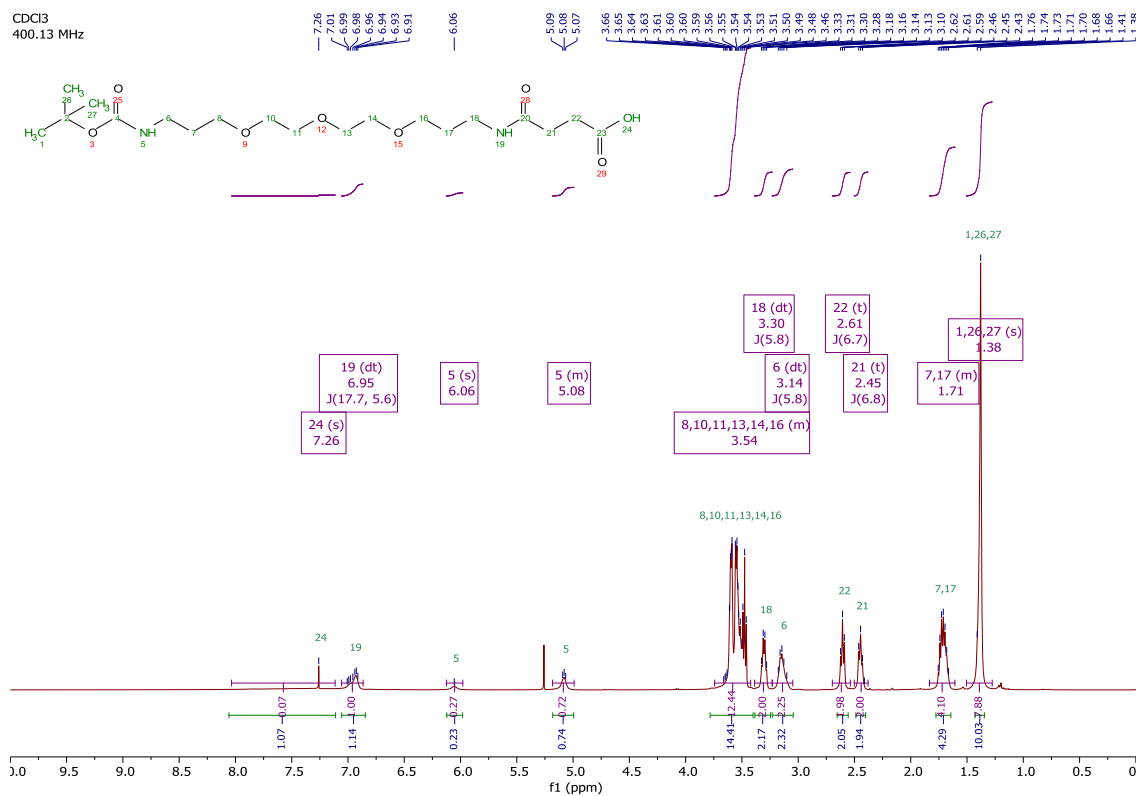
<sup>1</sup>H, <sup>13</sup>C, COSY, DEPT-135 and HSQC NMR spectra of PROTAC CRBN-N33.





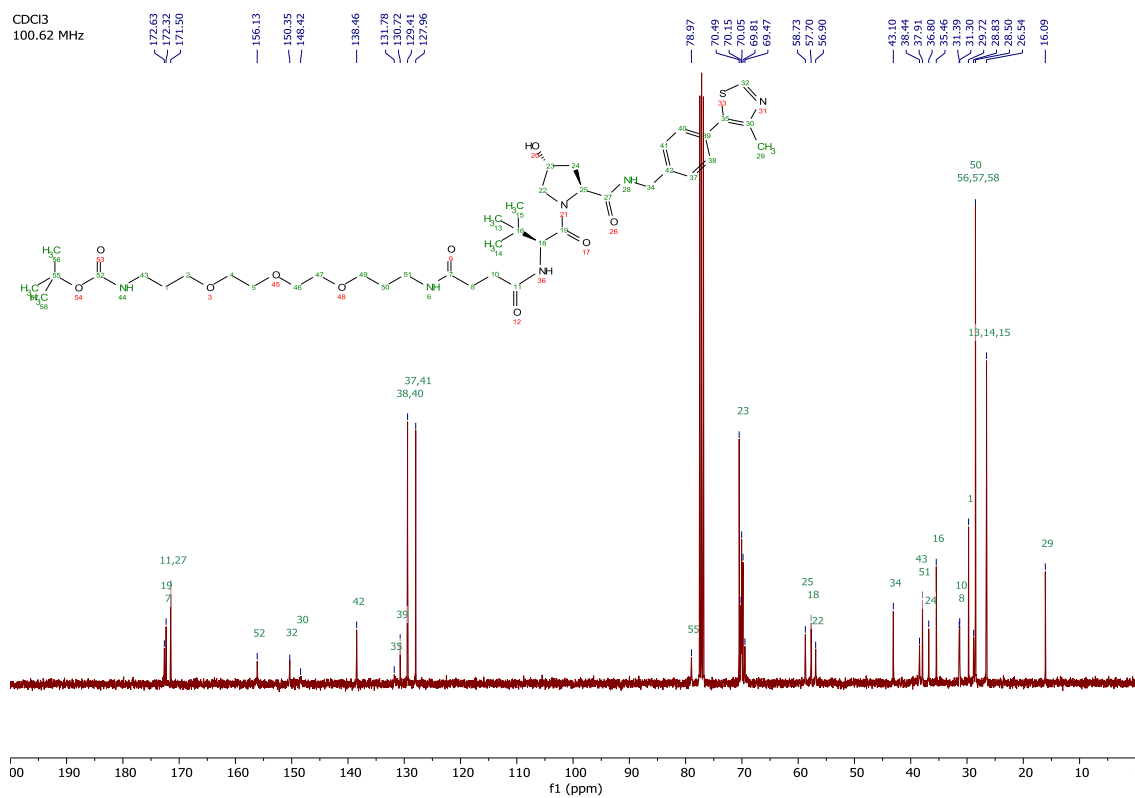
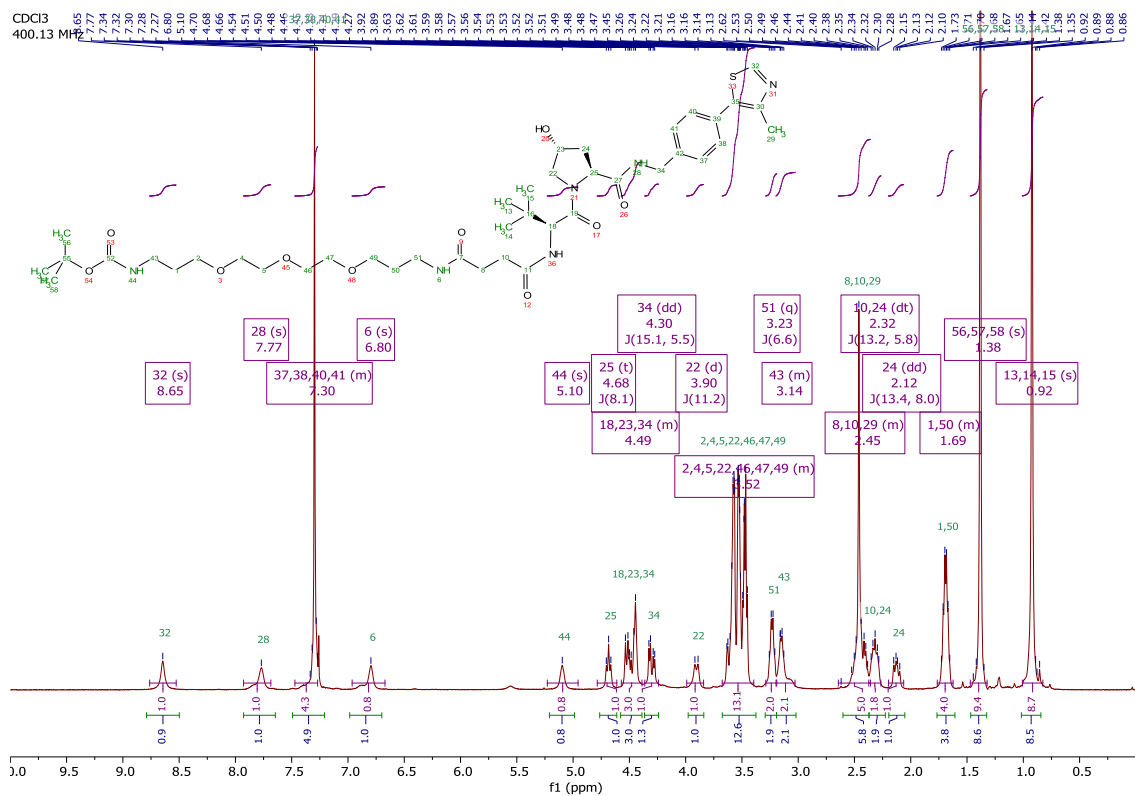


$^1\text{H}$ ,  $^{13}\text{C}$  and HSQC NMR spectra of acid **2.22**.

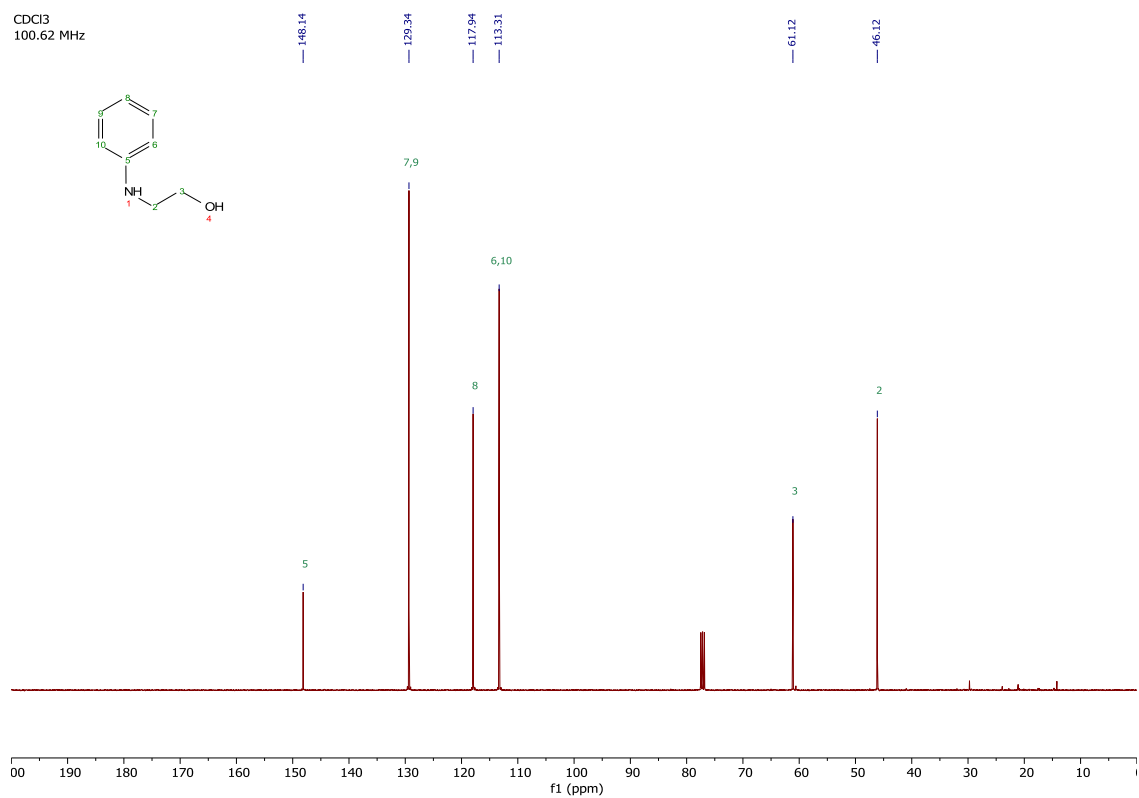
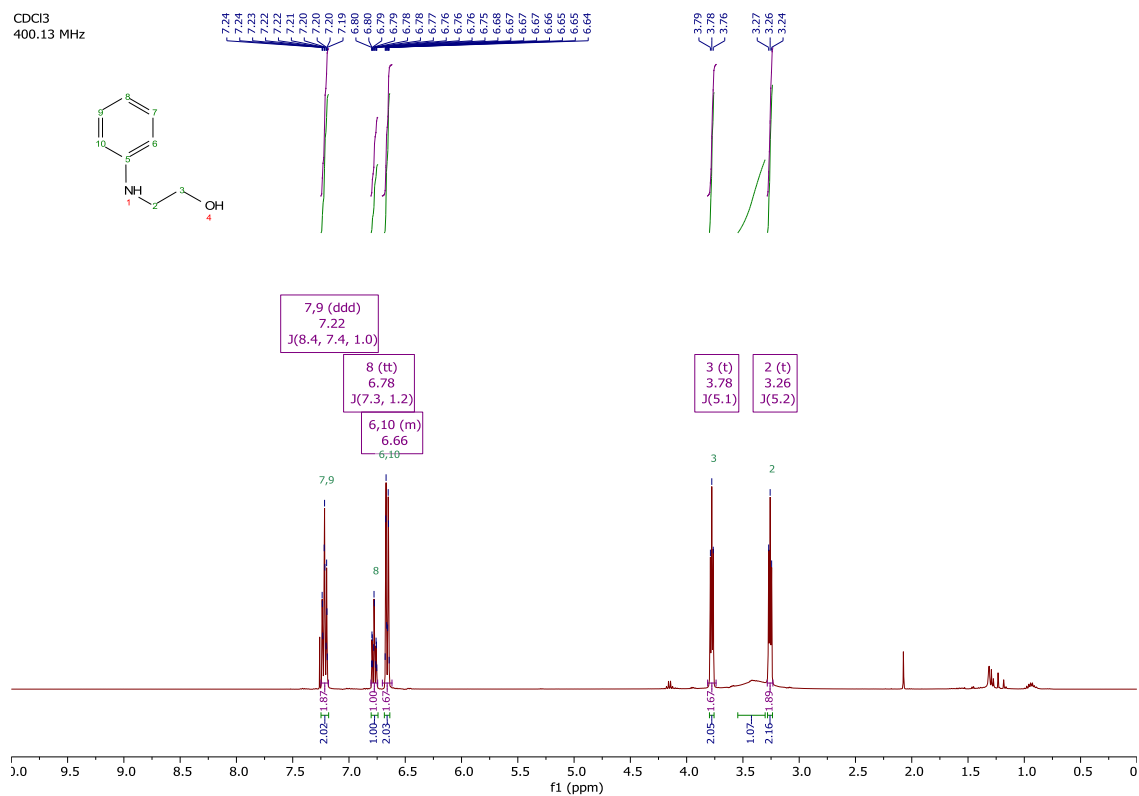


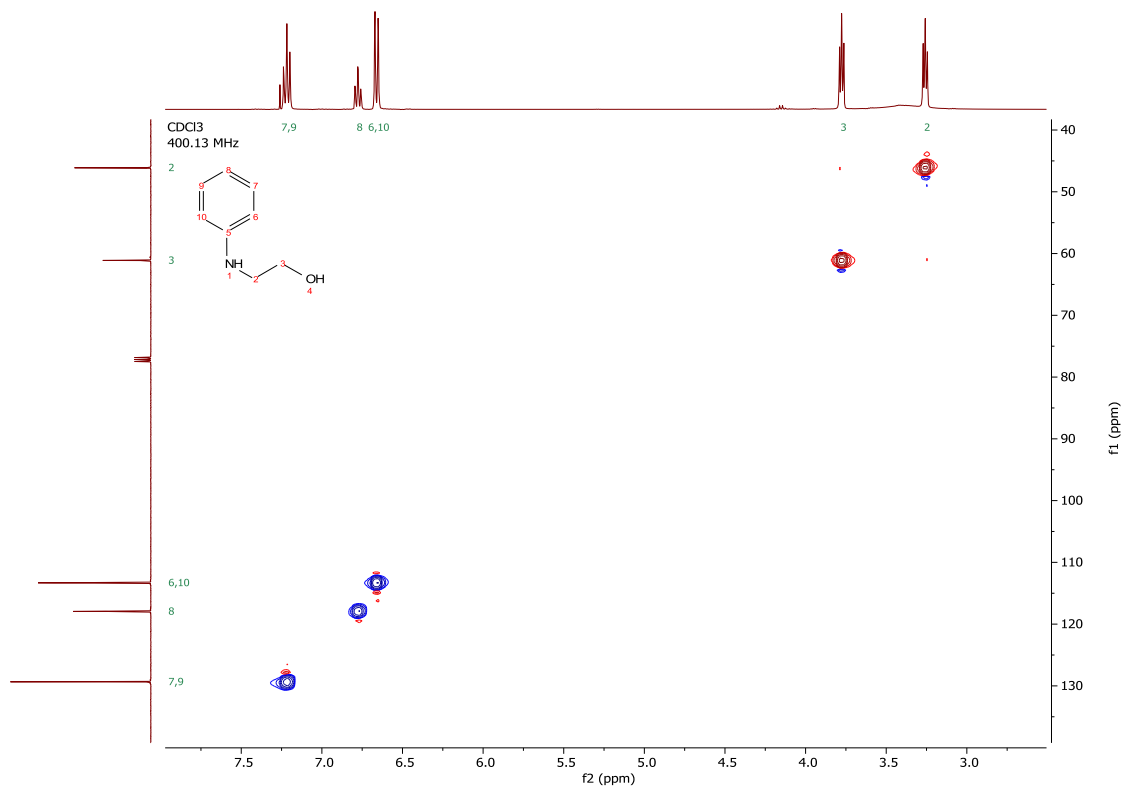
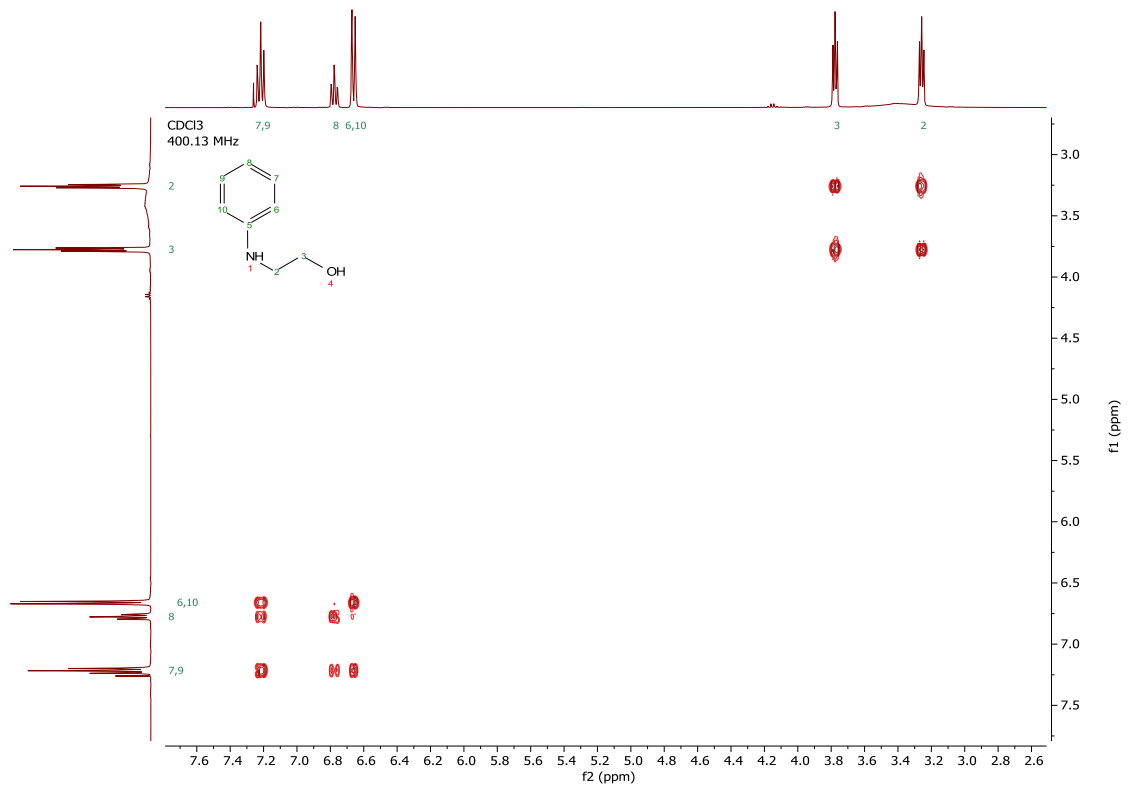


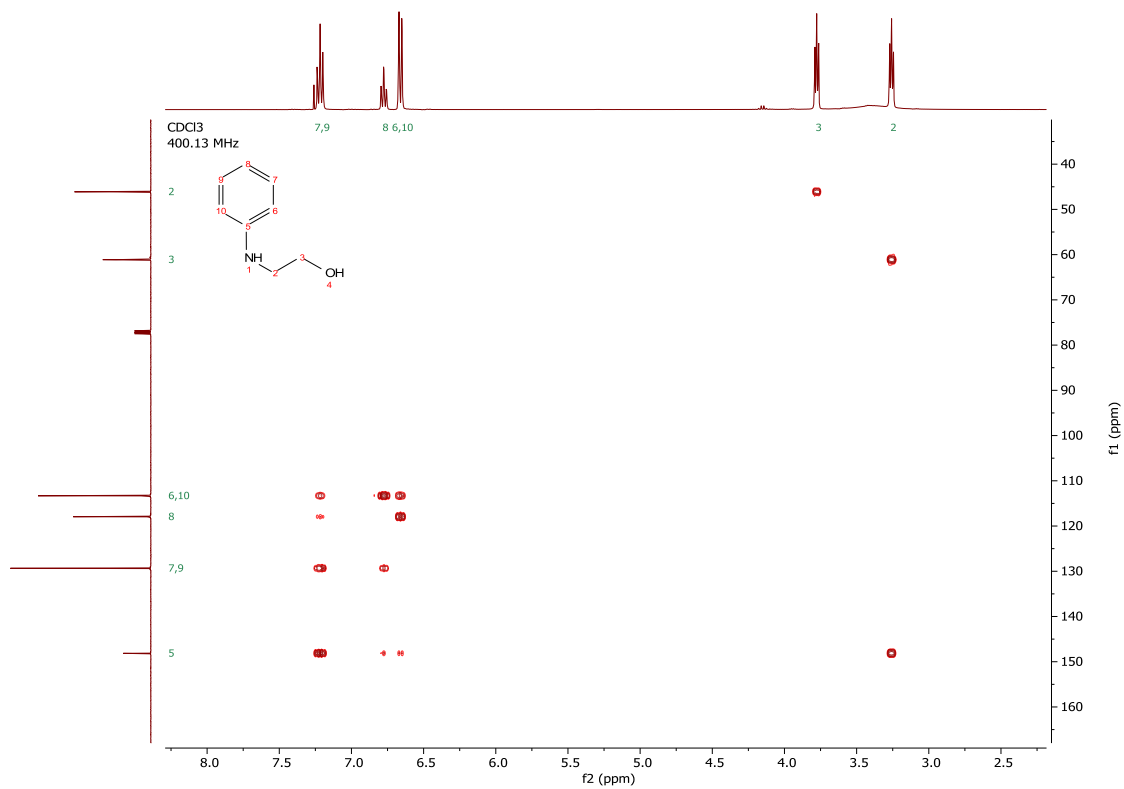
# <sup>1</sup>H and <sup>13</sup>C NMR spectra of *tert*-butyl carbamate **2.3**.



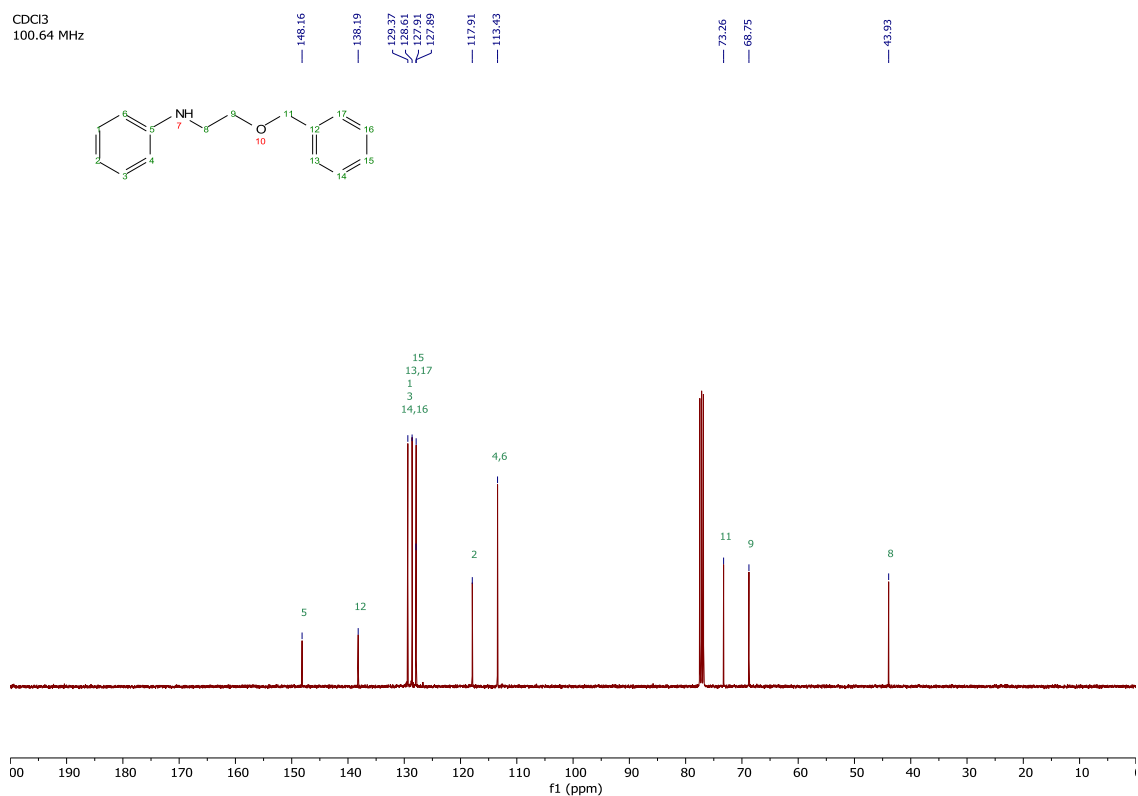
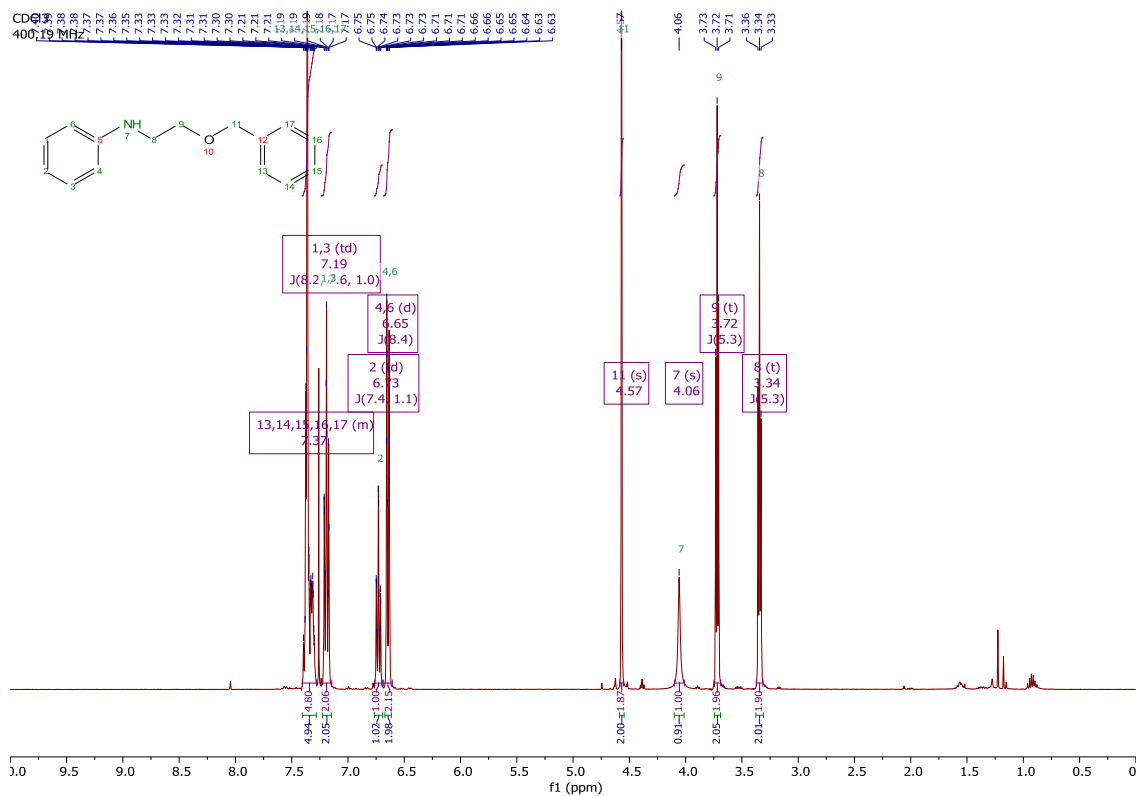
$^1\text{H}$ ,  $^{13}\text{C}$  COSY, HSQC and HMBC NMR spectra of alcohol **2.28**.

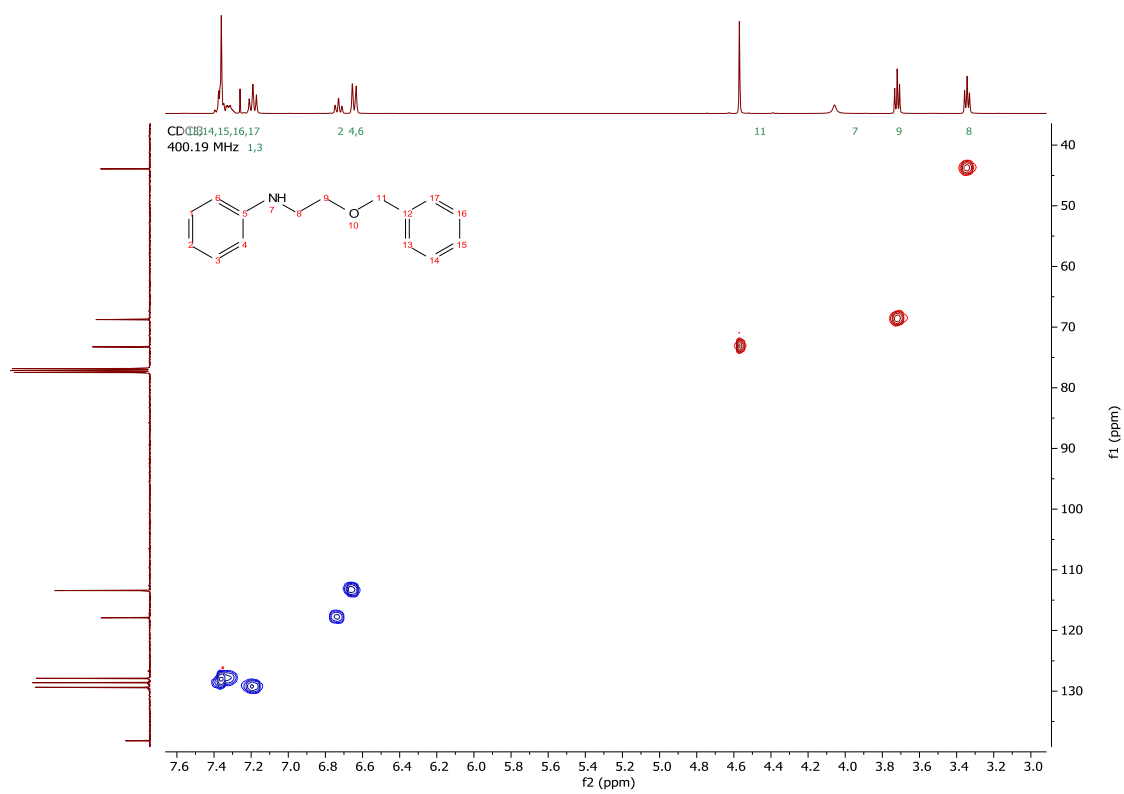
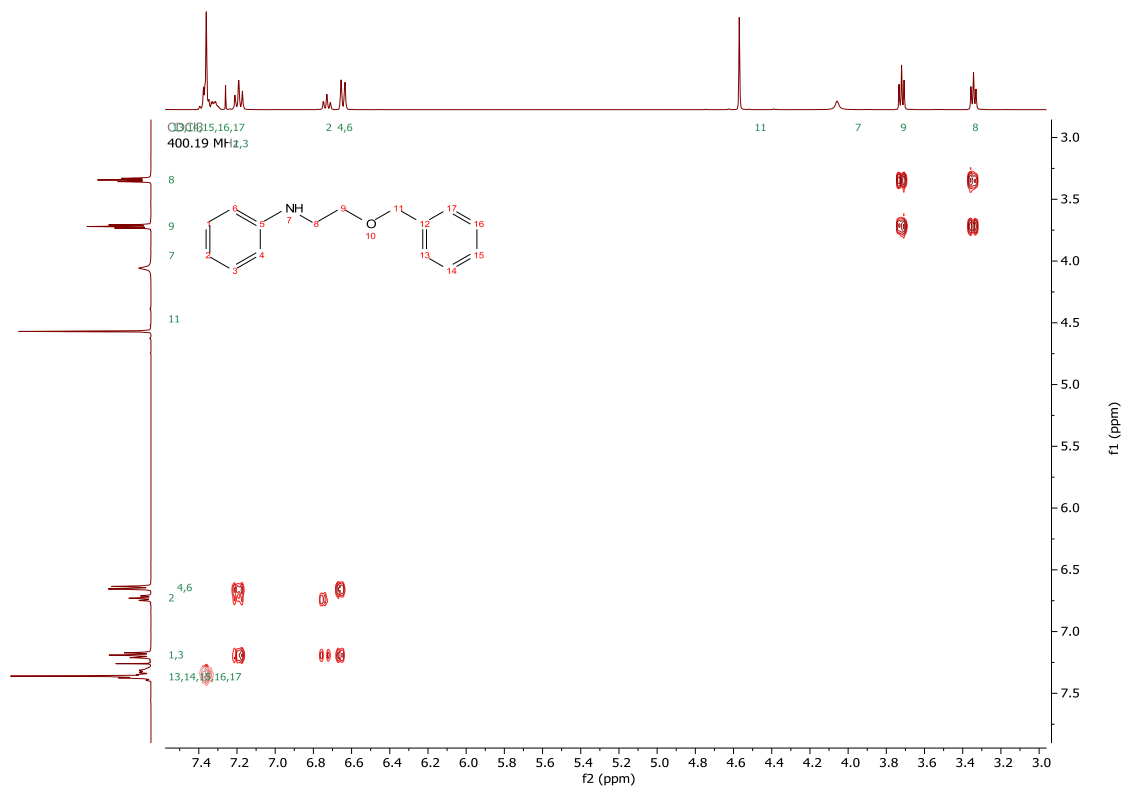






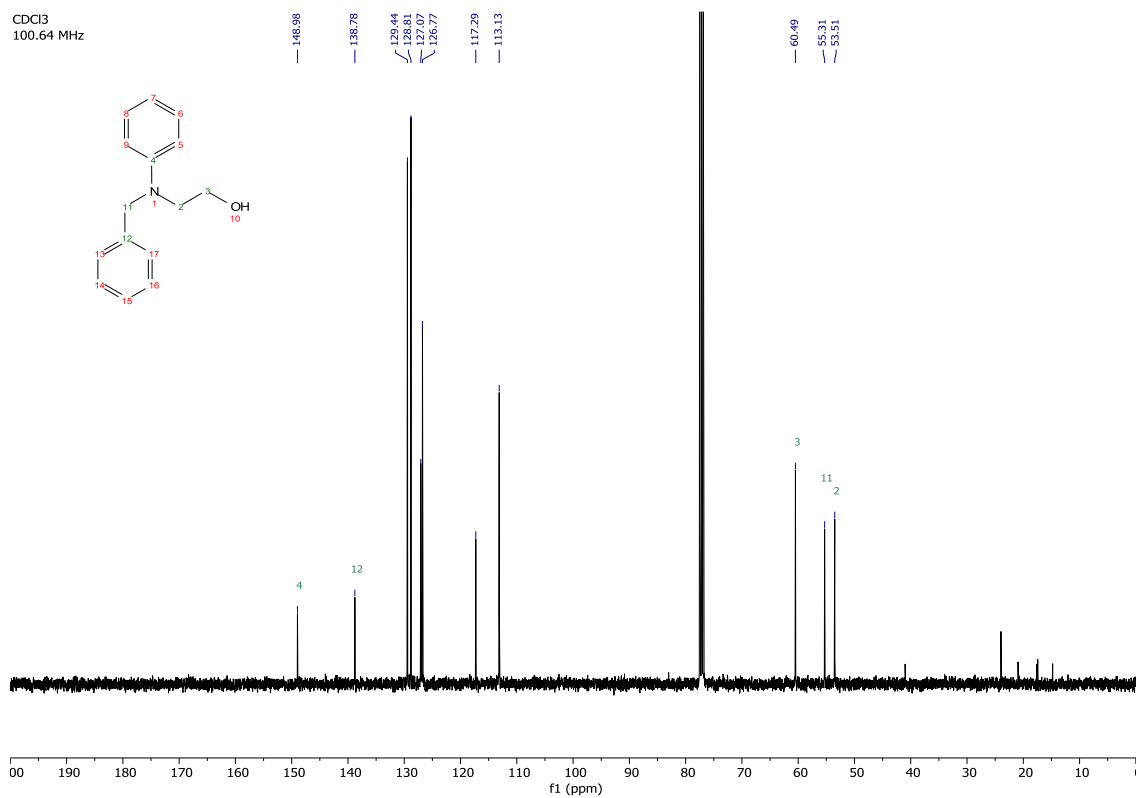
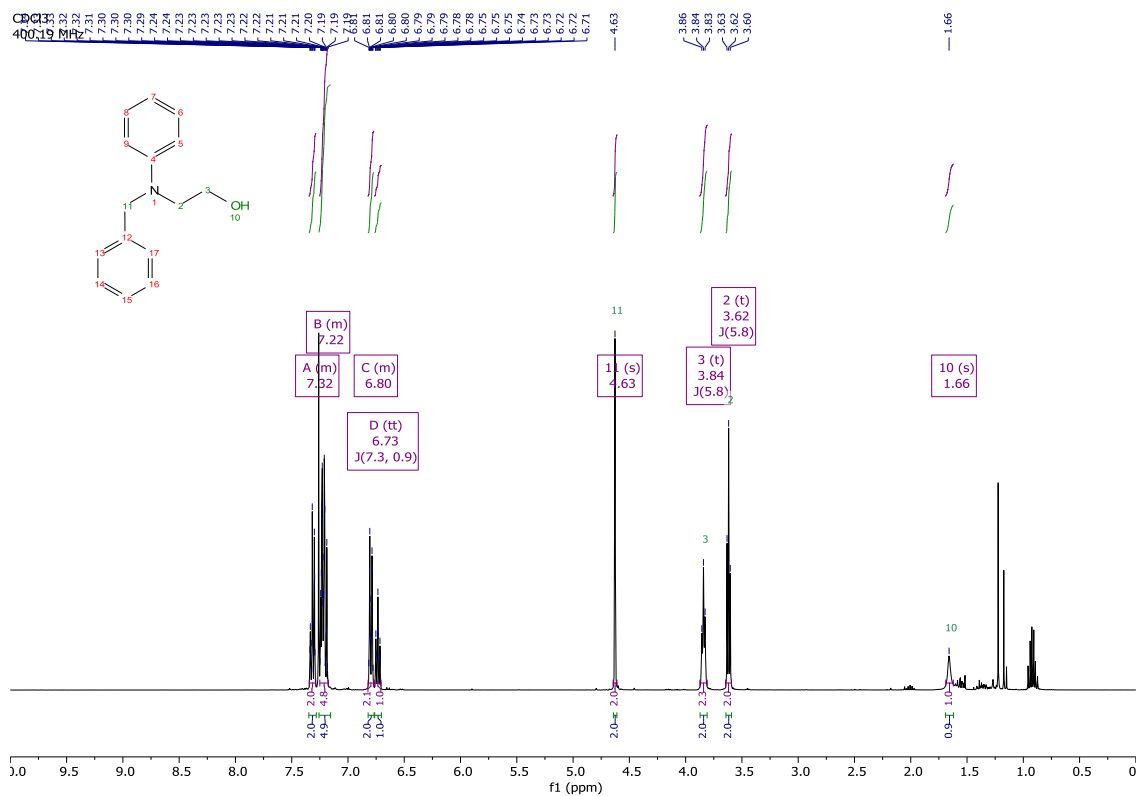
$^1\text{H}$ ,  $^{13}\text{C}$  COSY, HSQC and HMBC NMR spectra of benzyl ether **2.29**.

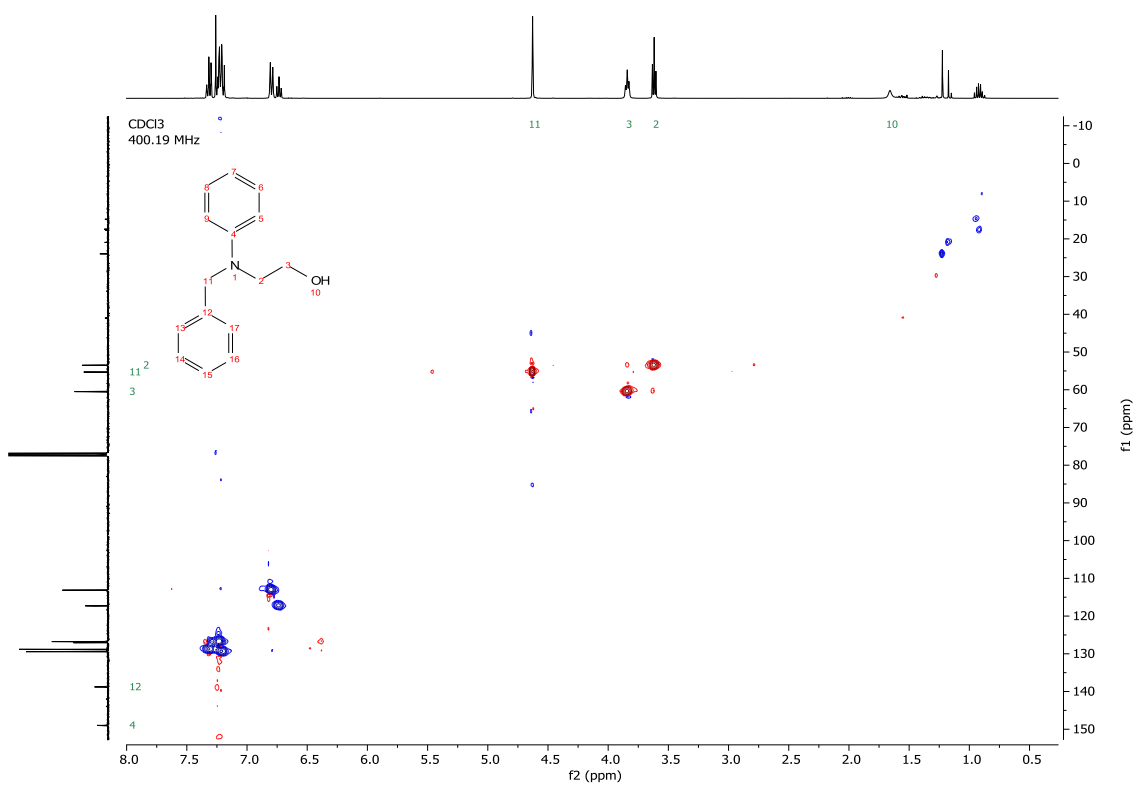
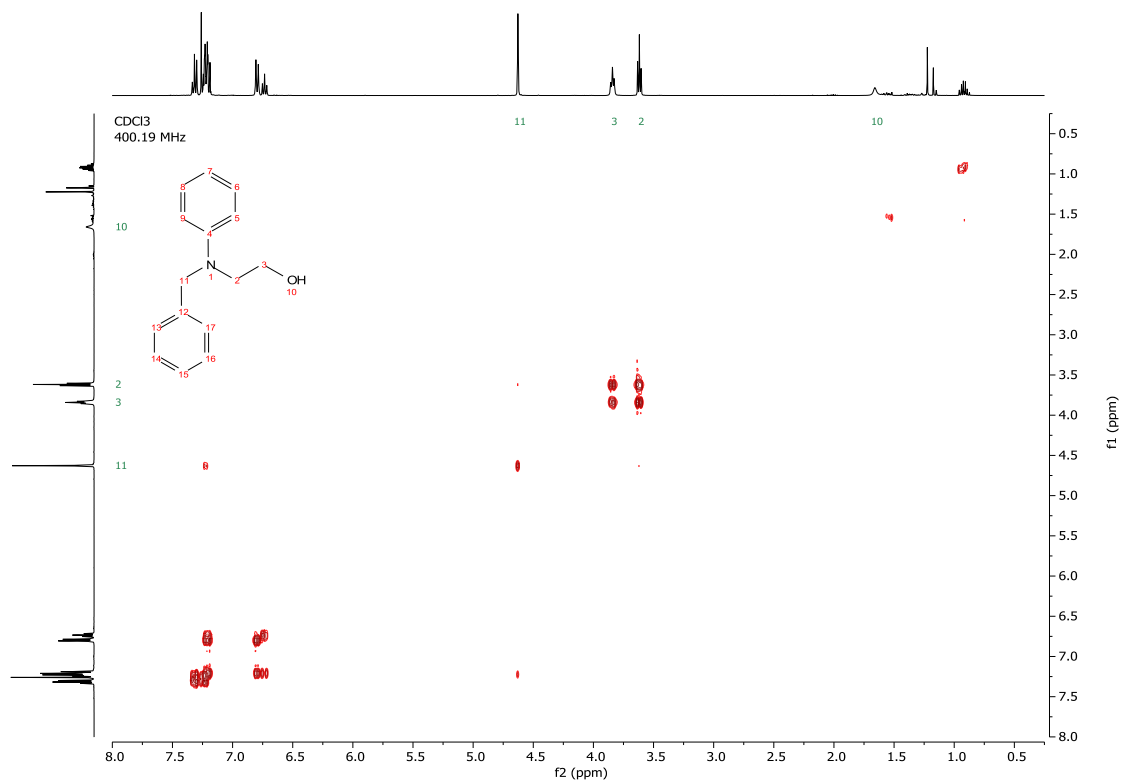


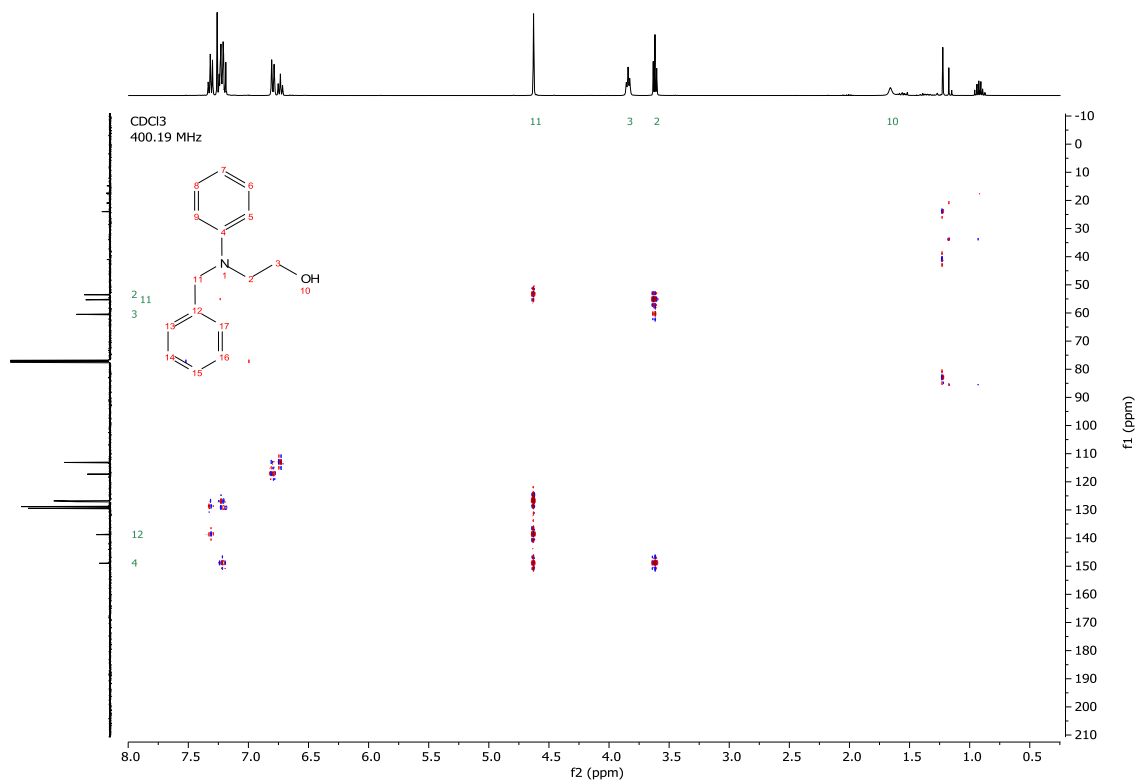




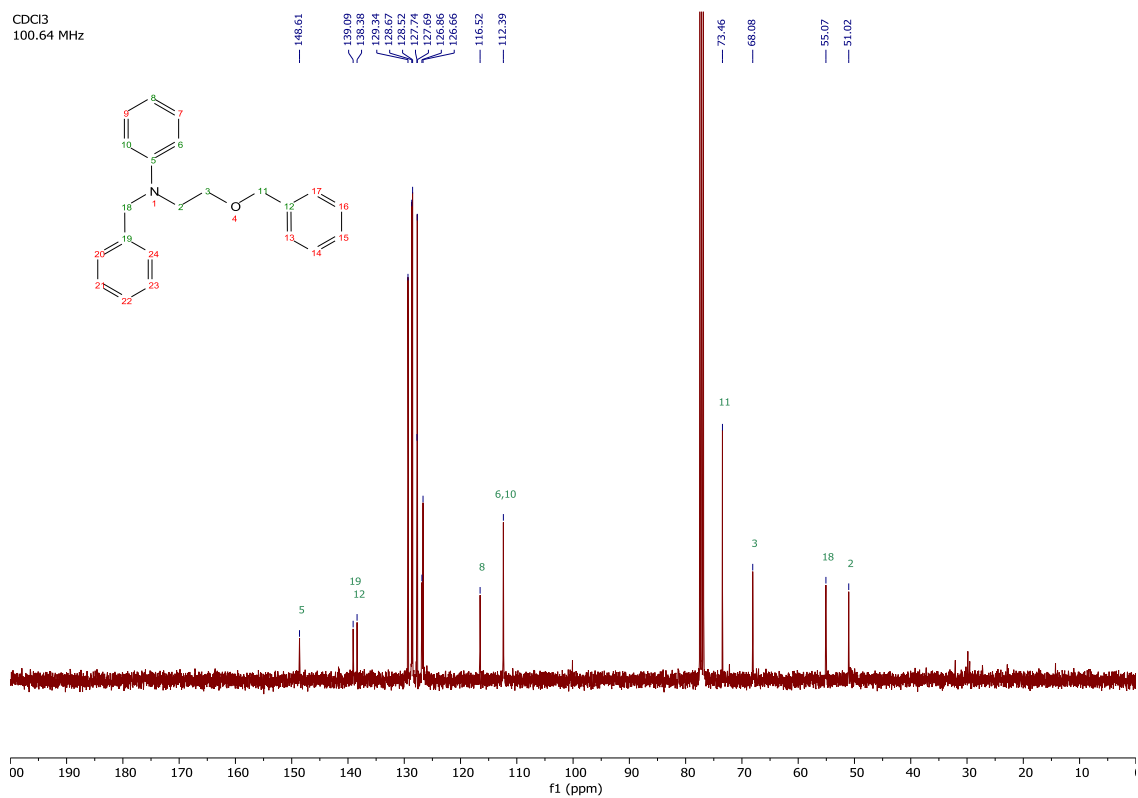
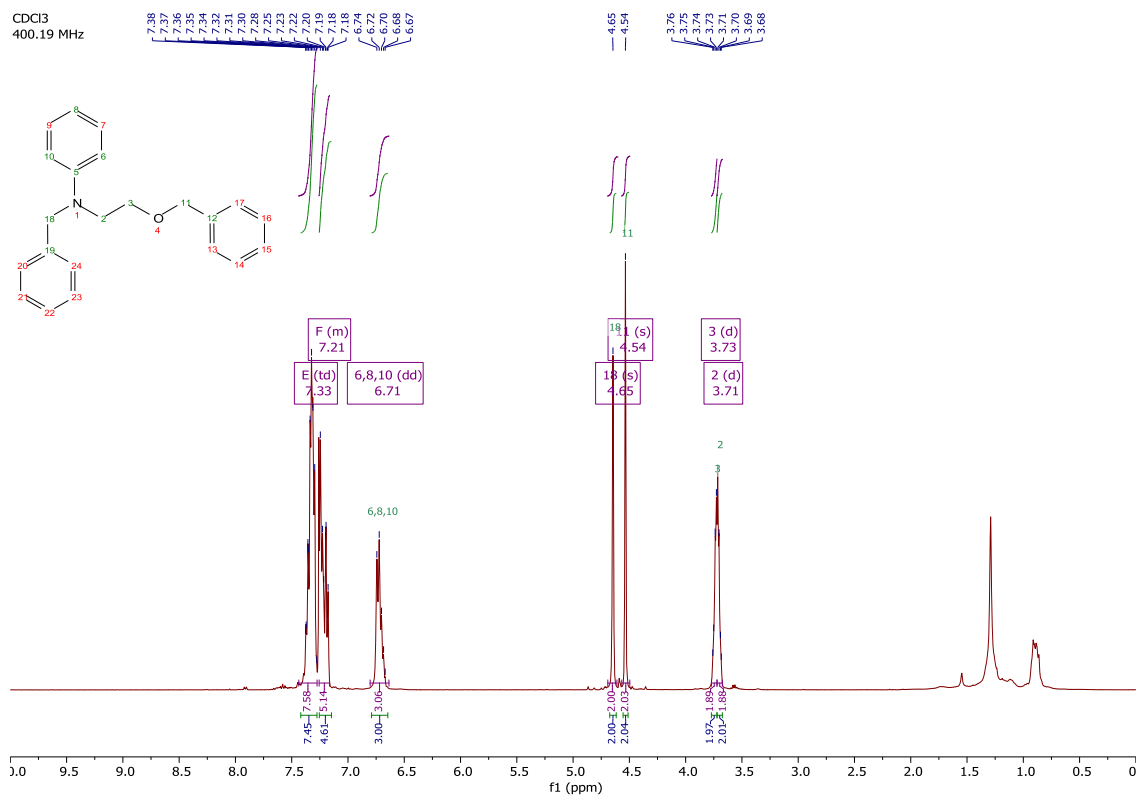
$^1\text{H}$ ,  $^{13}\text{C}$  COSY, HSQC and HMBC NMR spectra of benzyl ether **2.30**.

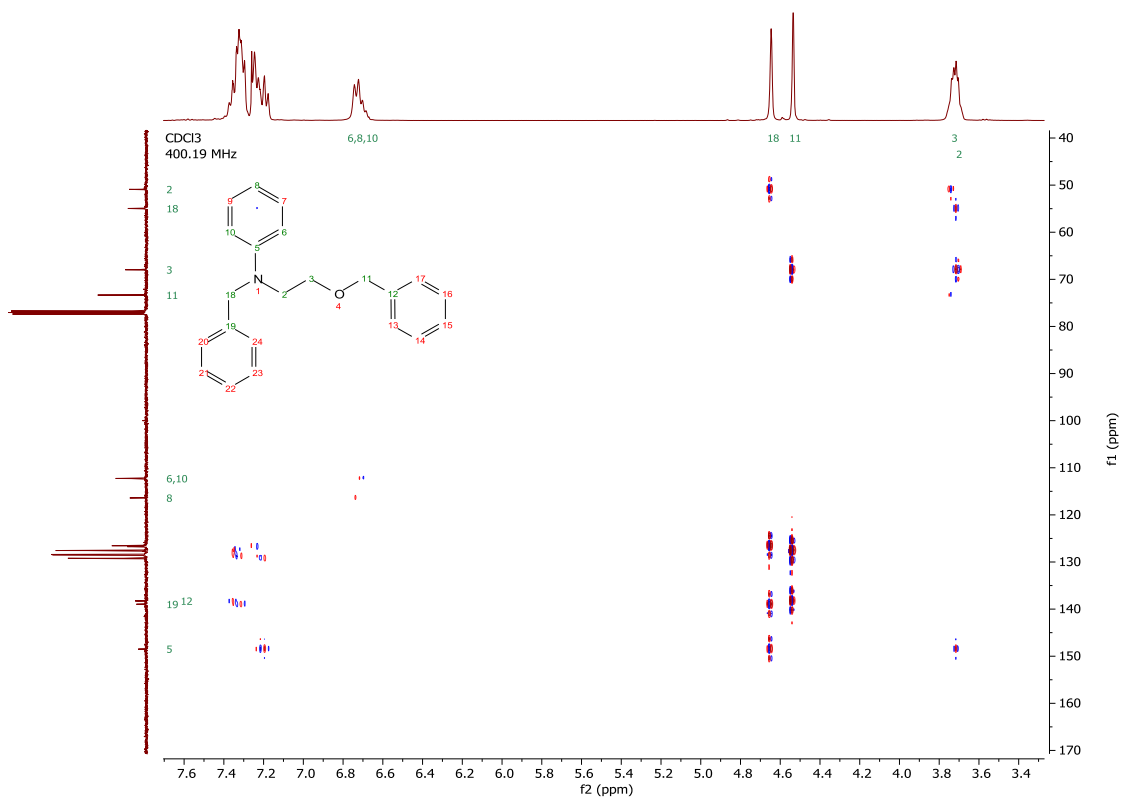
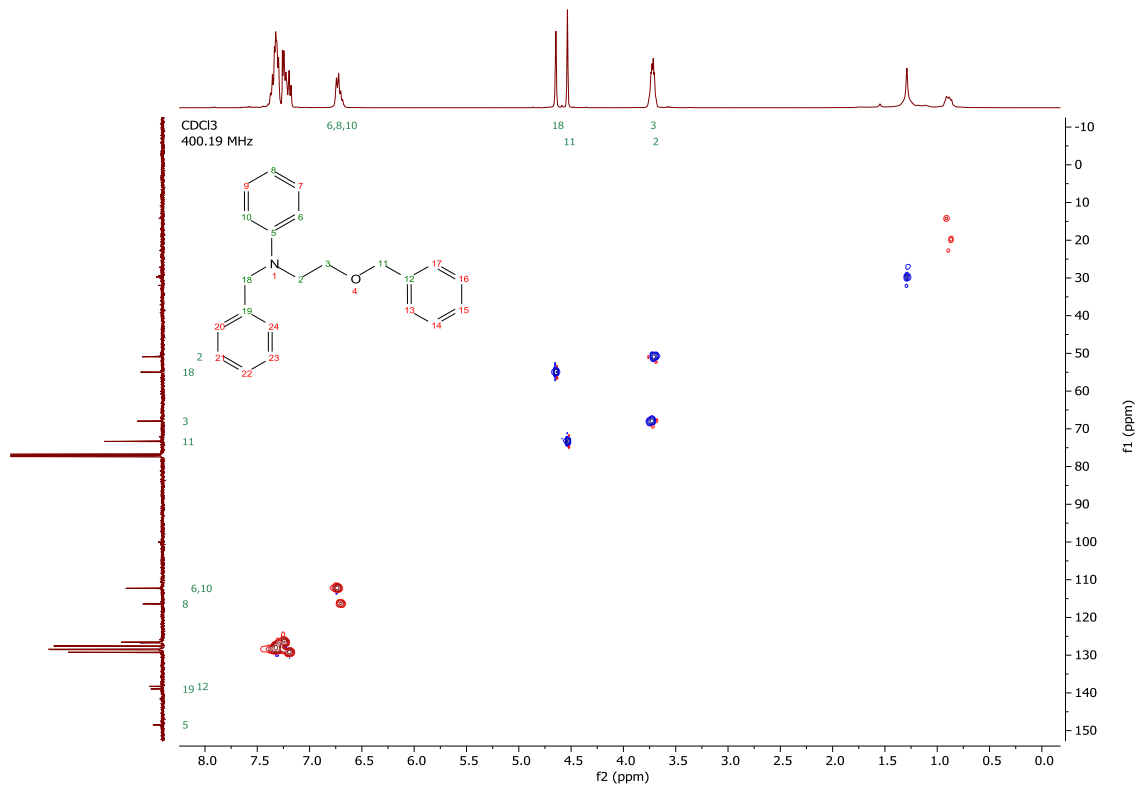




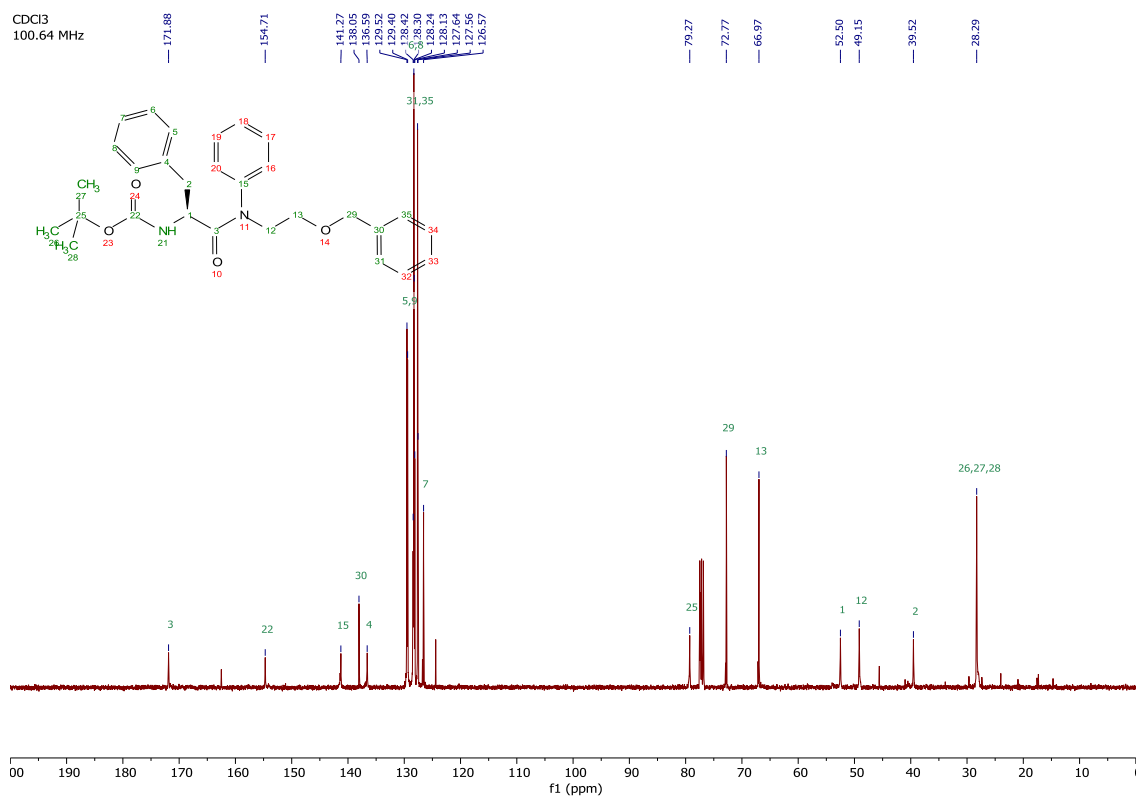
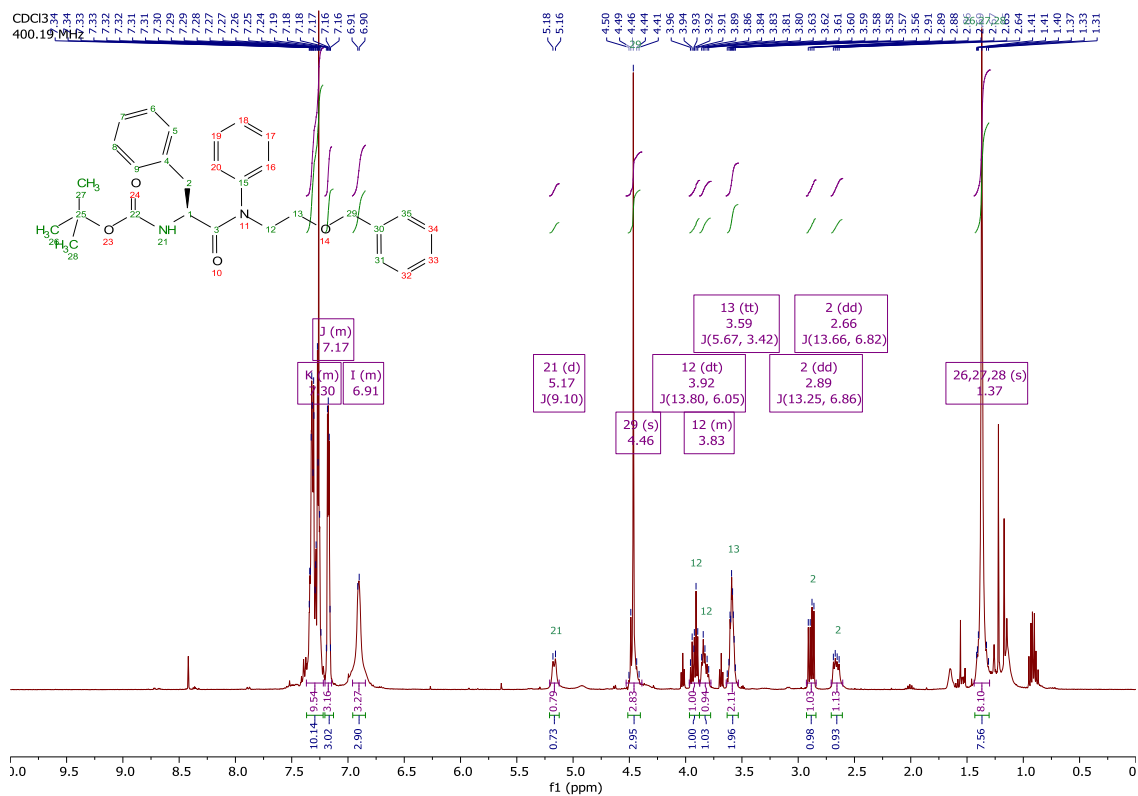


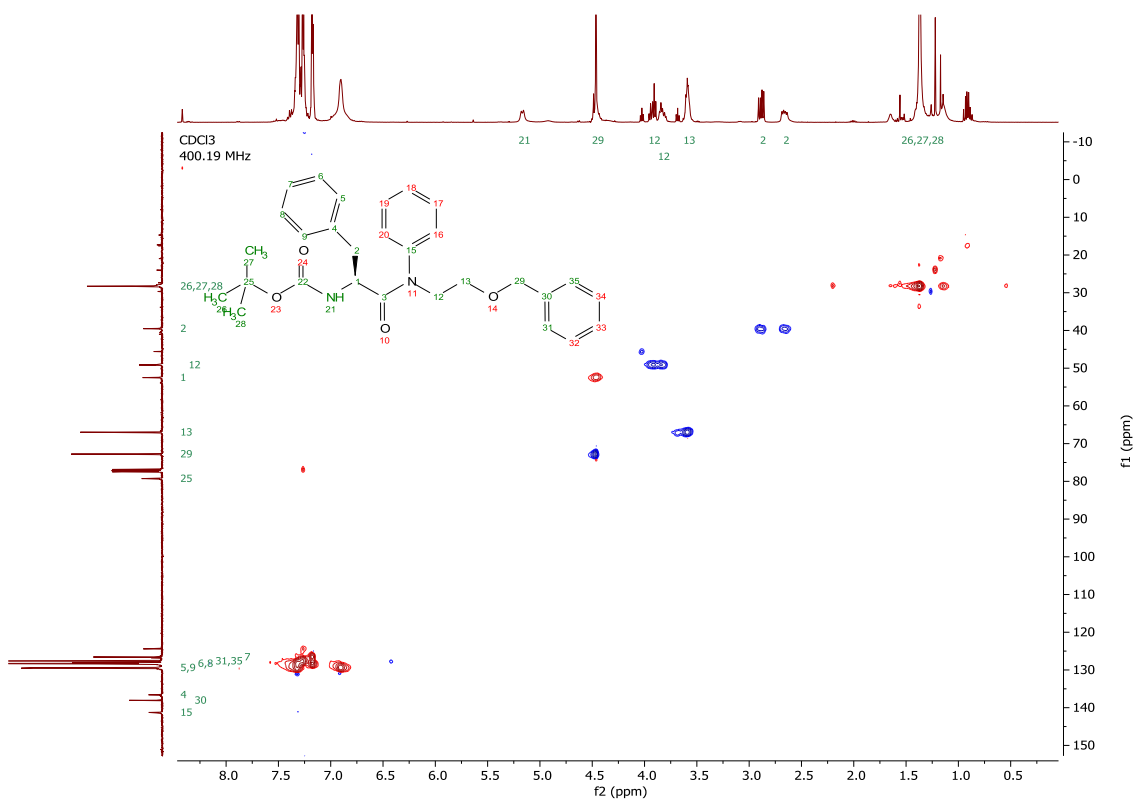
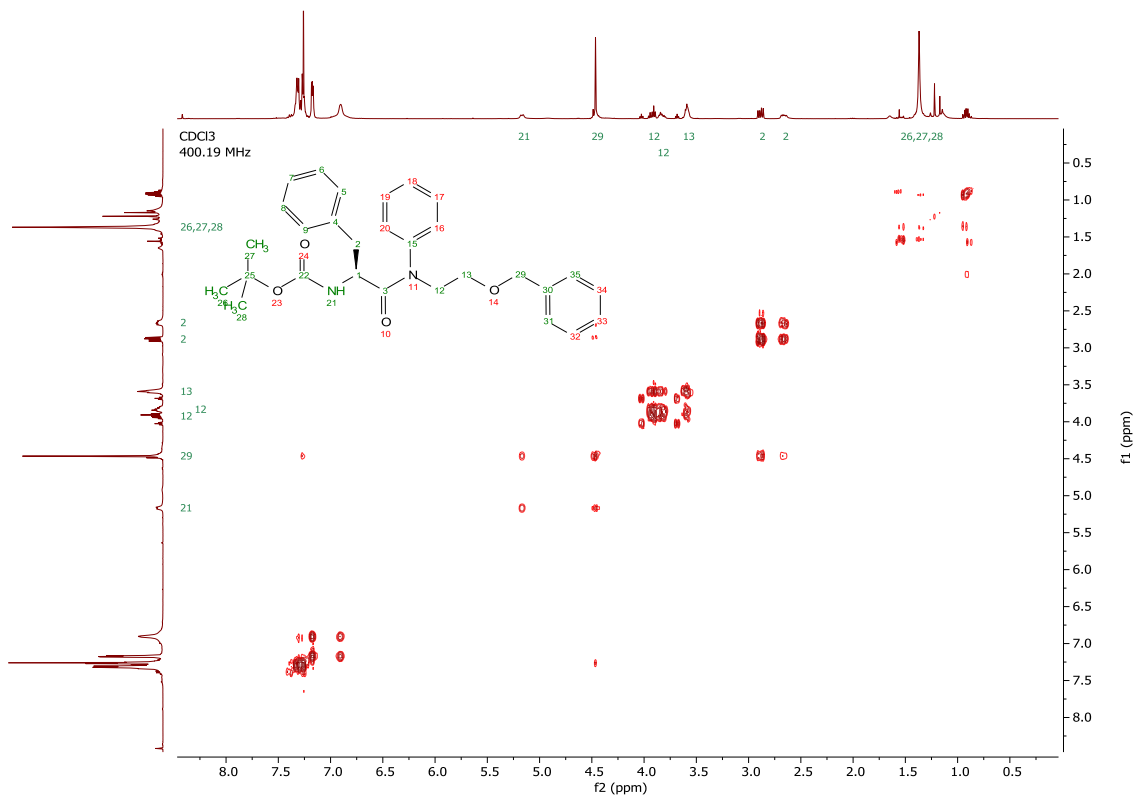
$^1\text{H}$ ,  $^{13}\text{C}$ , HSQC and HMBC NMR spectra of benzyl ether **2.31**.

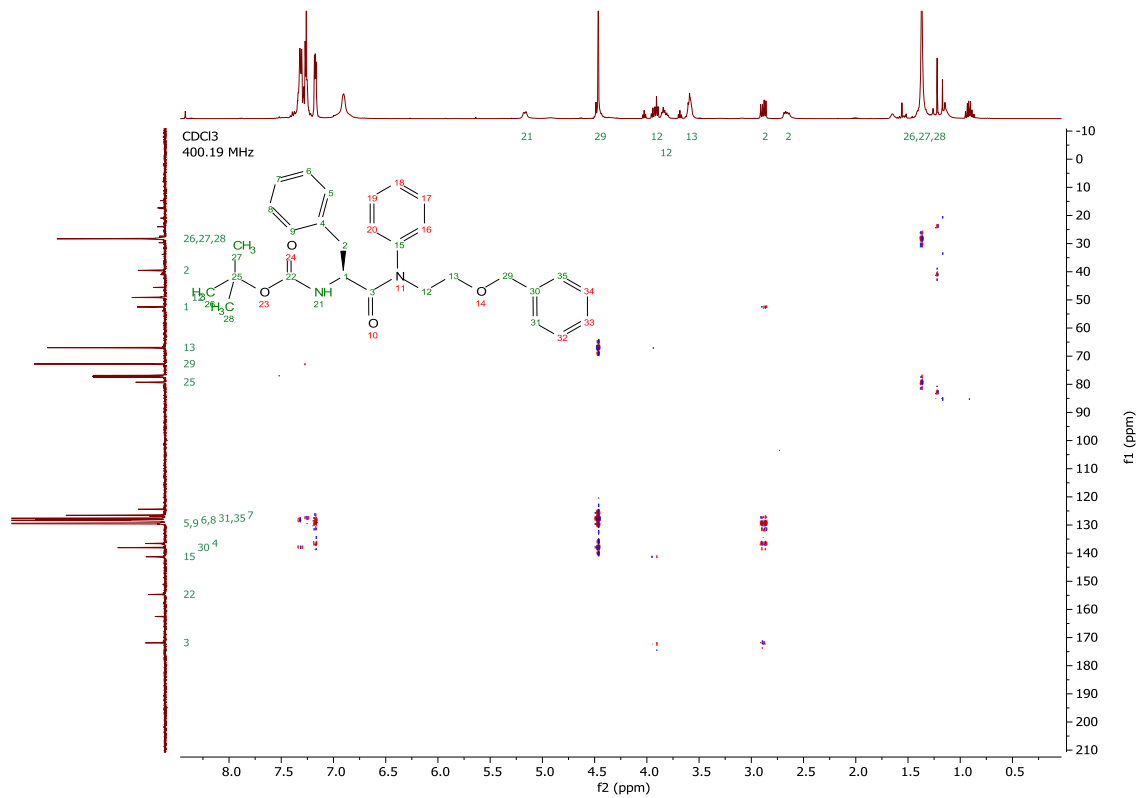




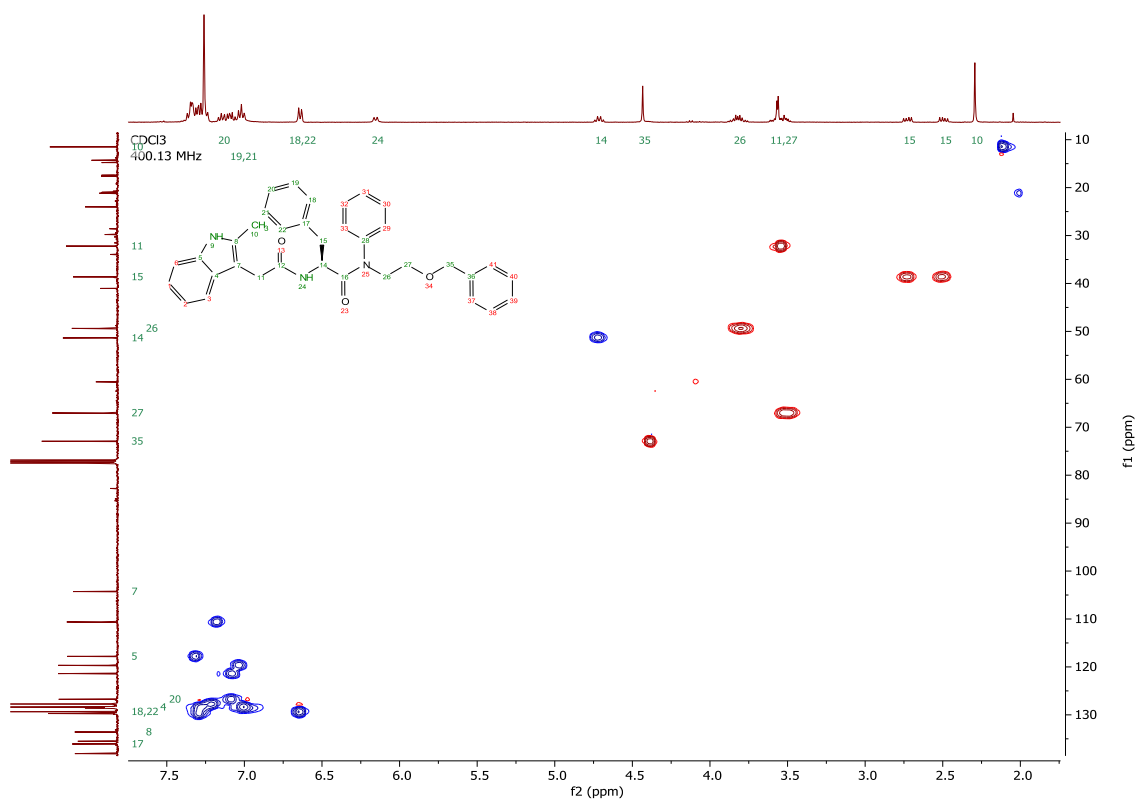
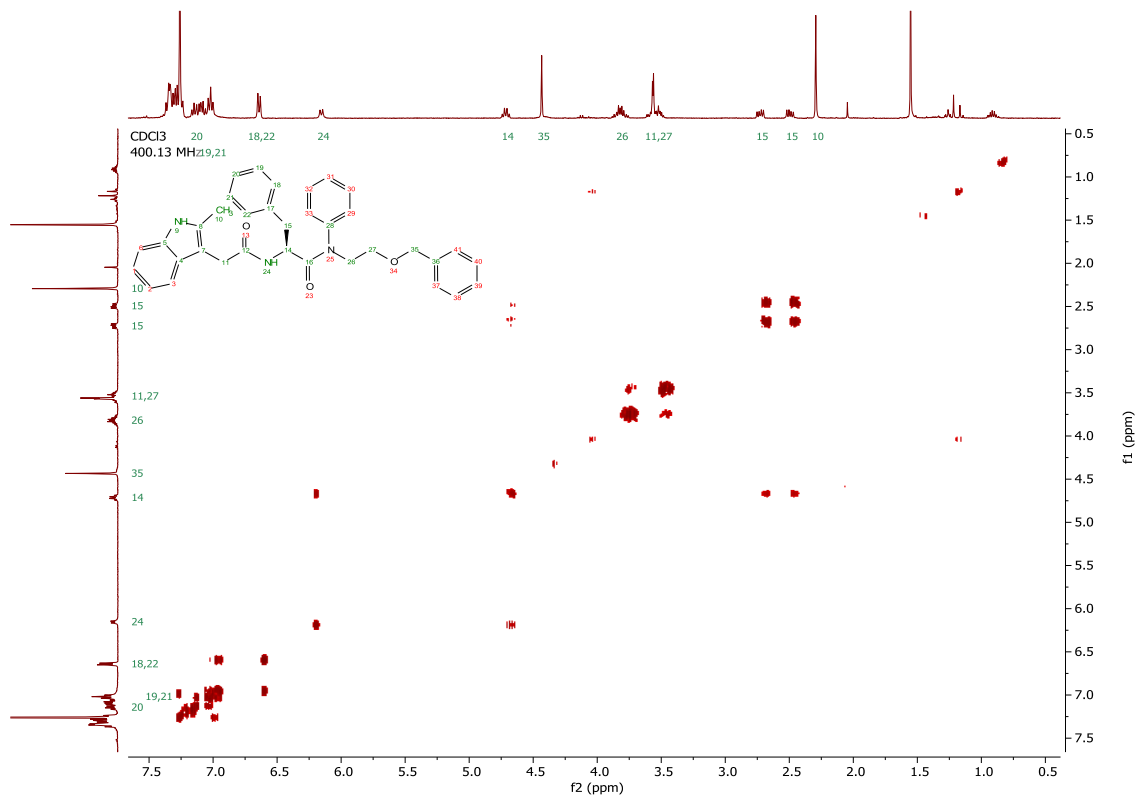
$^1\text{H}$ ,  $^{13}\text{C}$ , COSY, HSQC and HMBC NMR spectra of benzyl ether **2.34**.

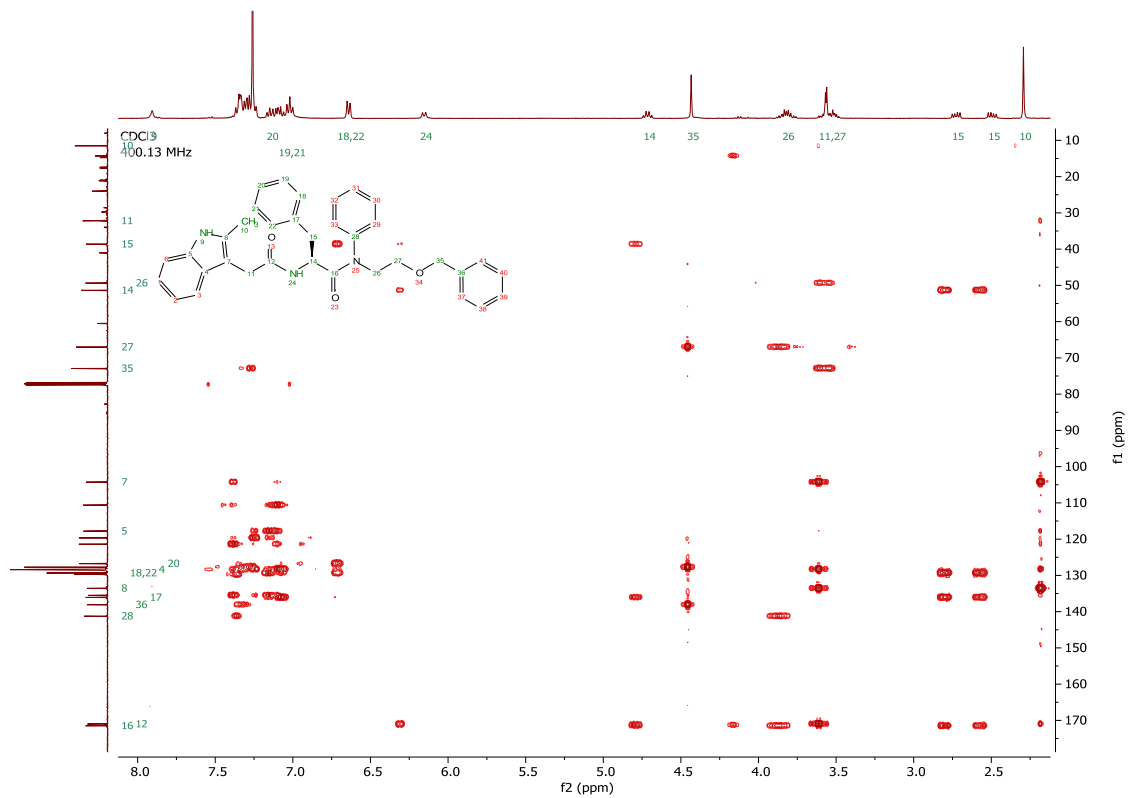




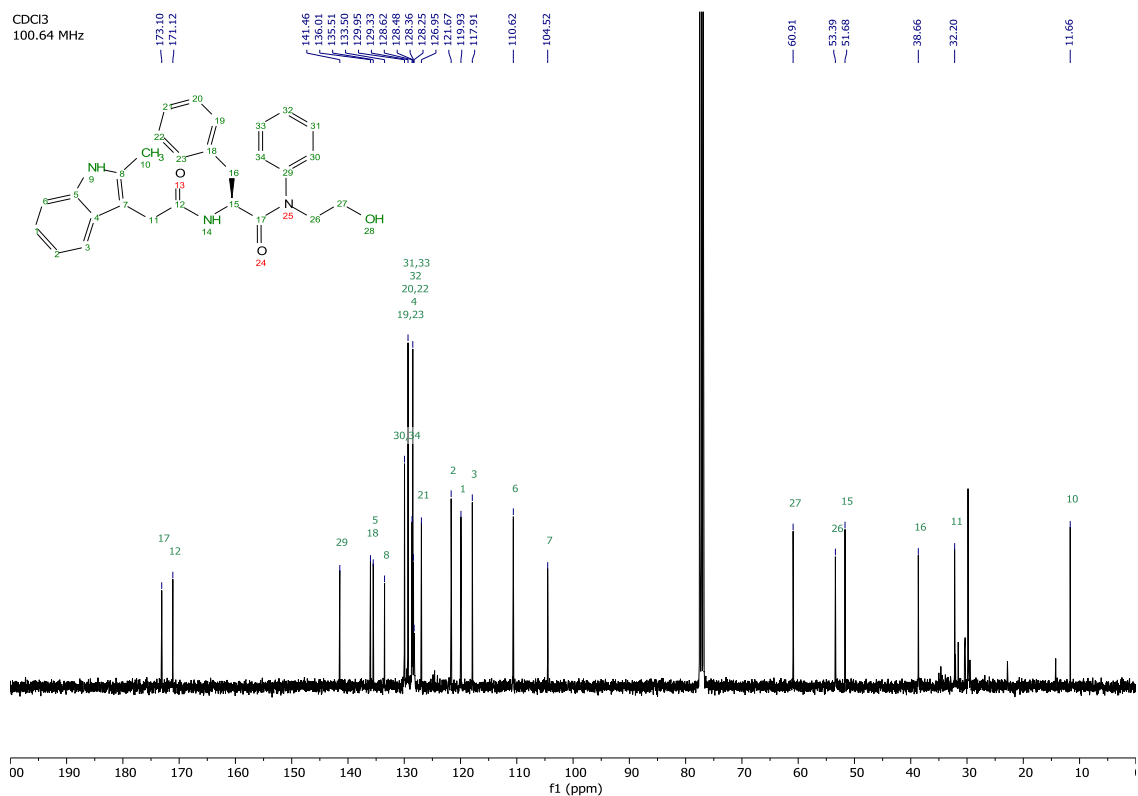
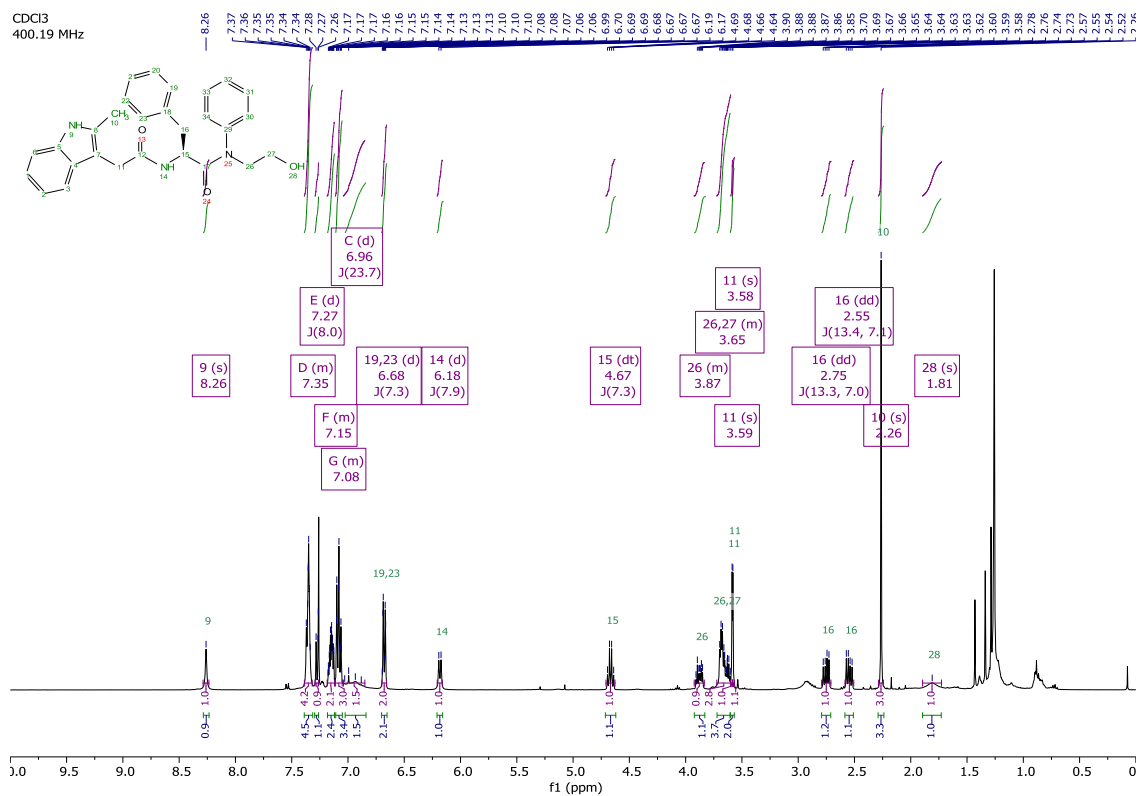


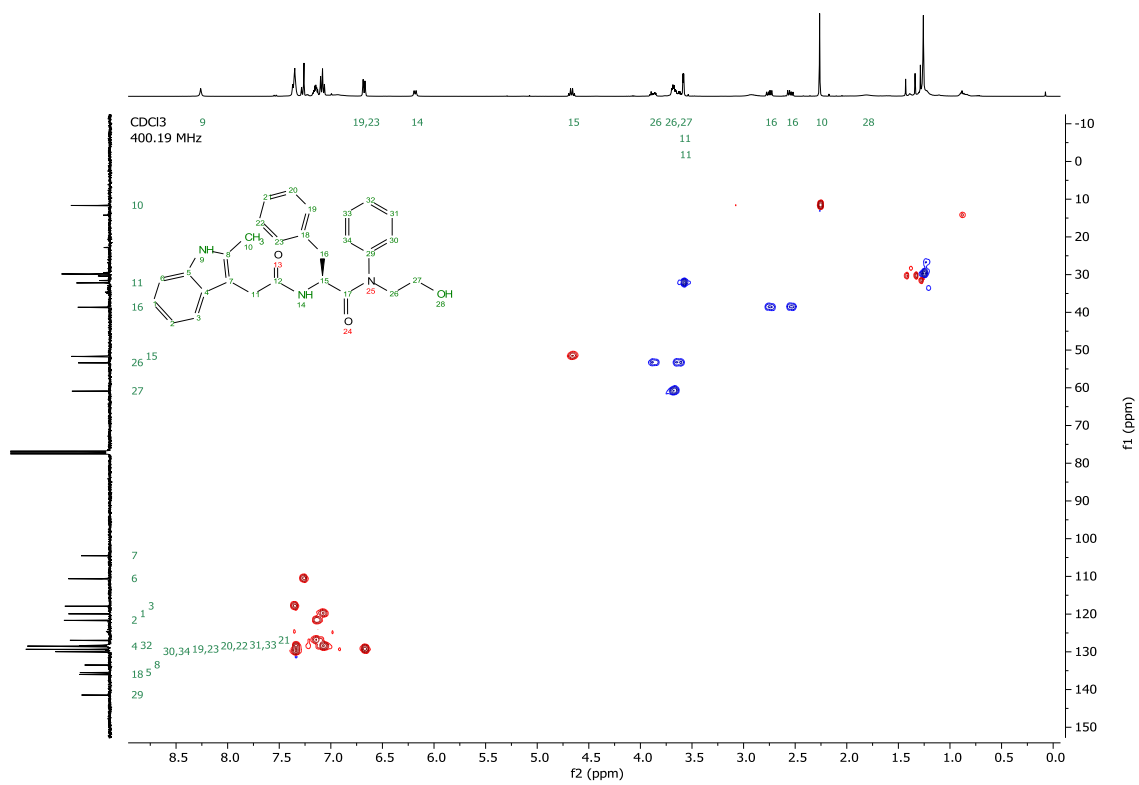
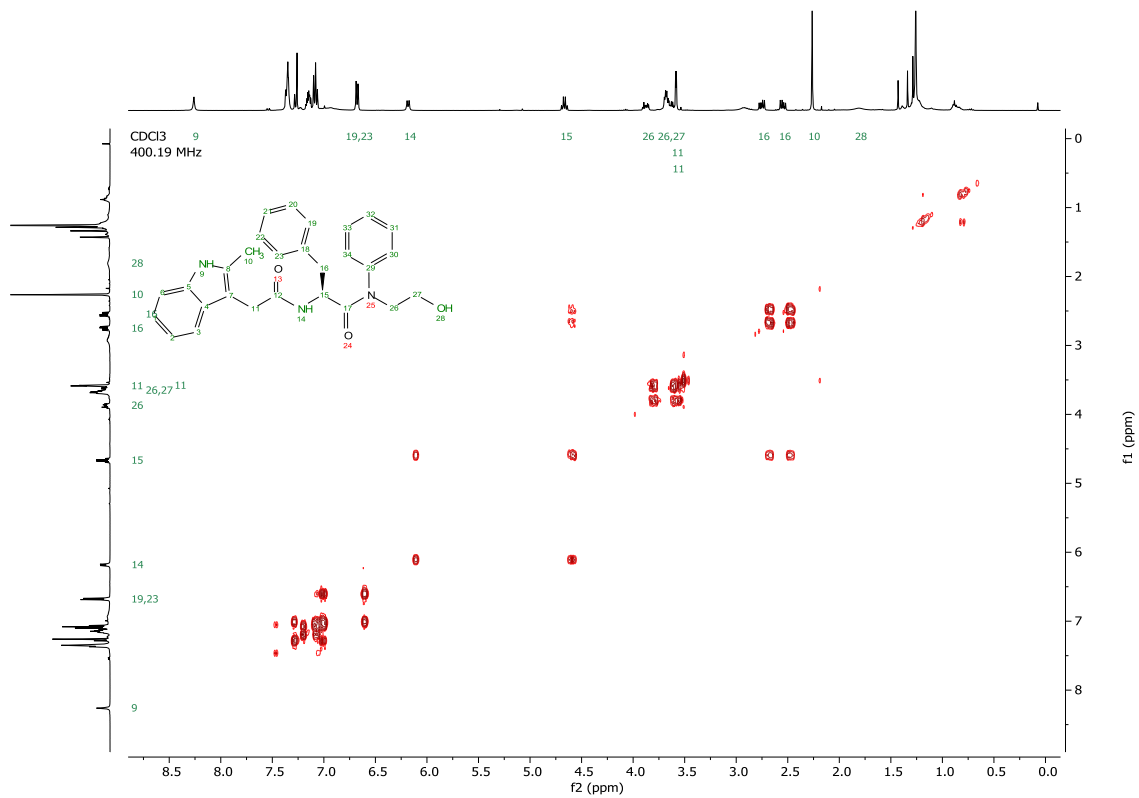


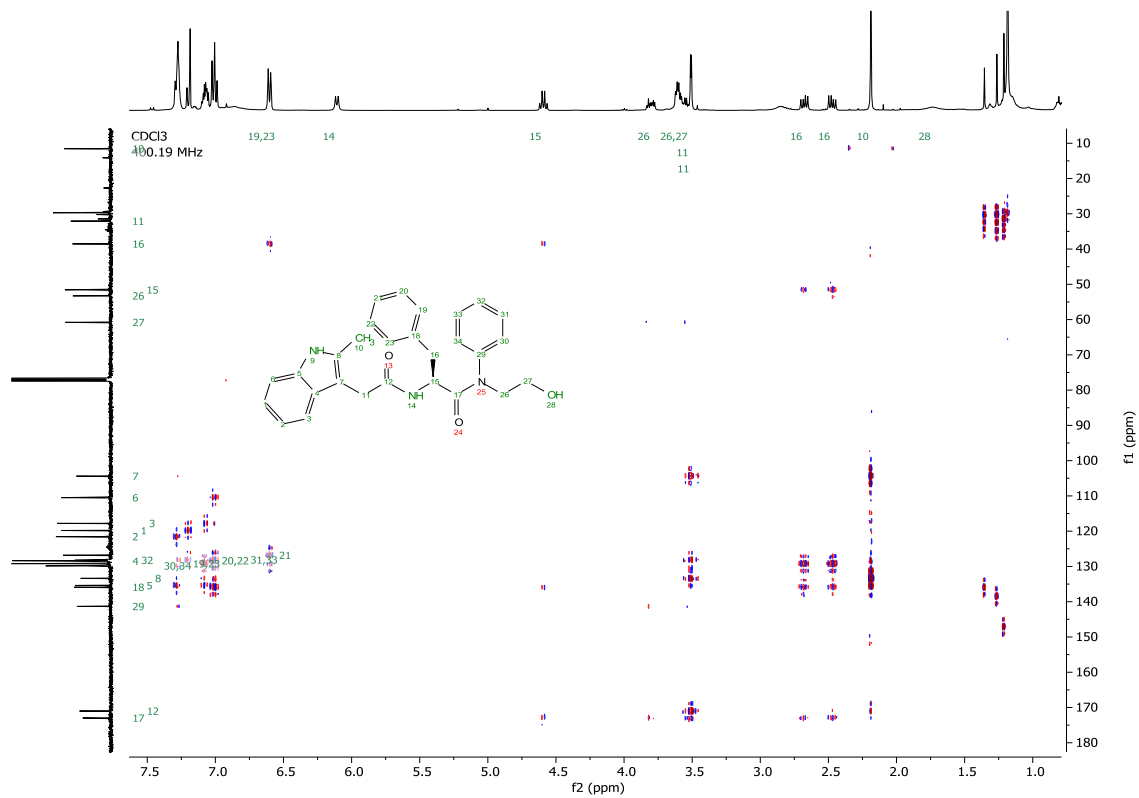




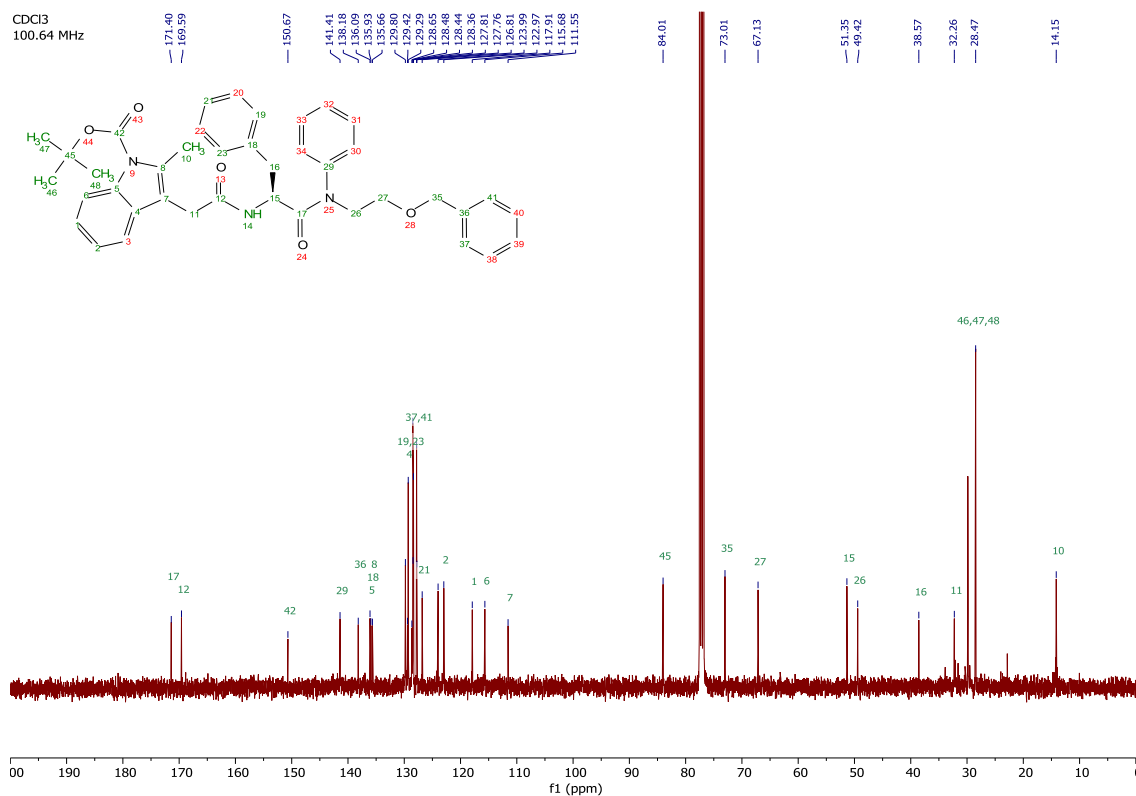
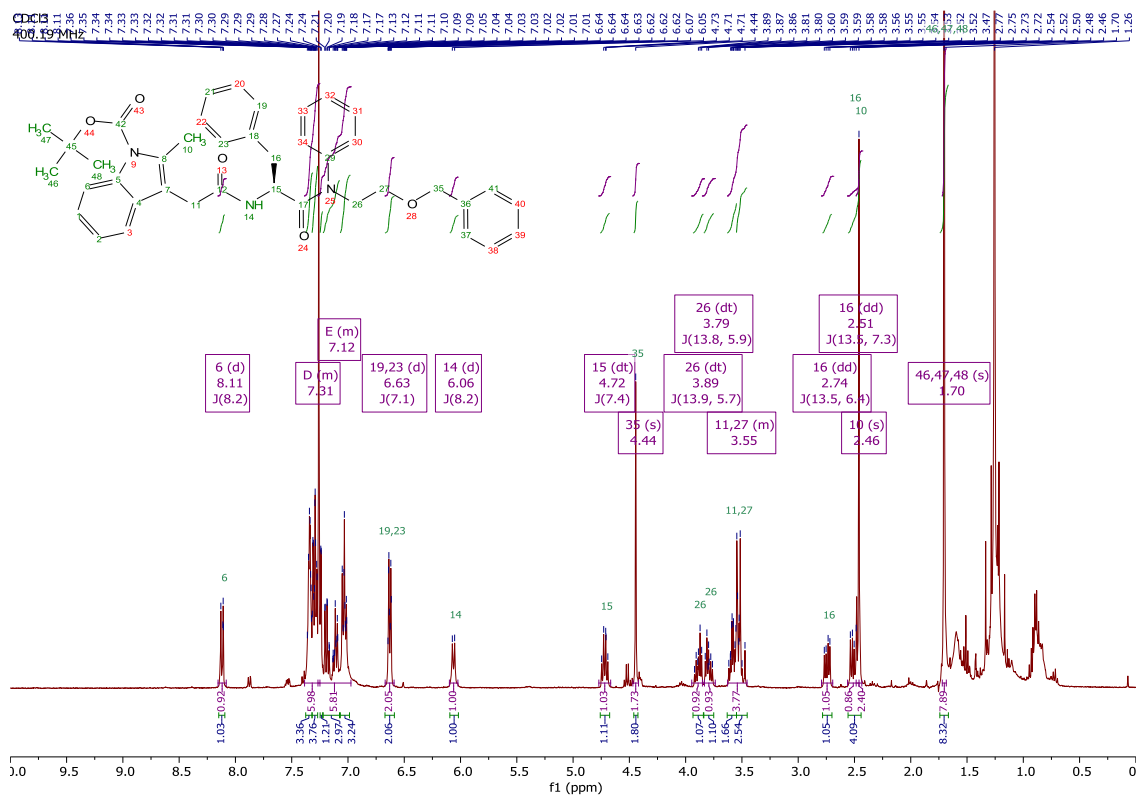
$^1\text{H}$ ,  $^{13}\text{C}$ , COSY, HSQC and HMBC NMR spectra of alcohol **2.27**.

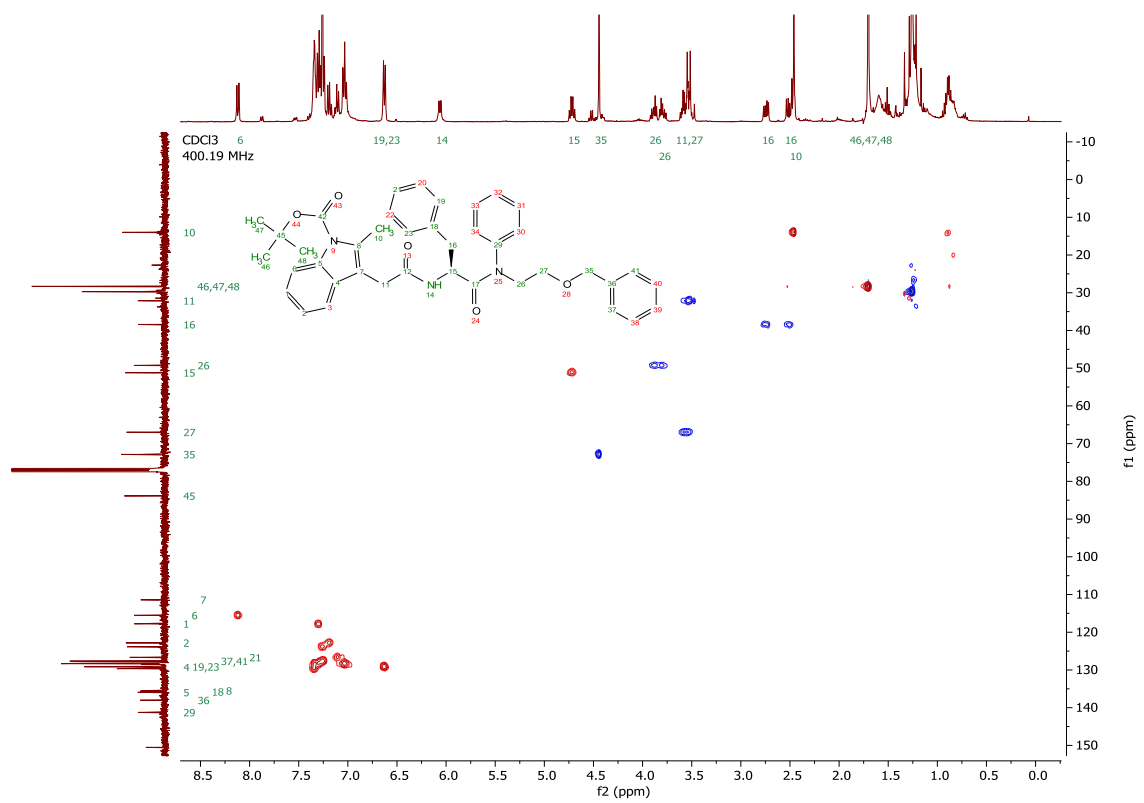
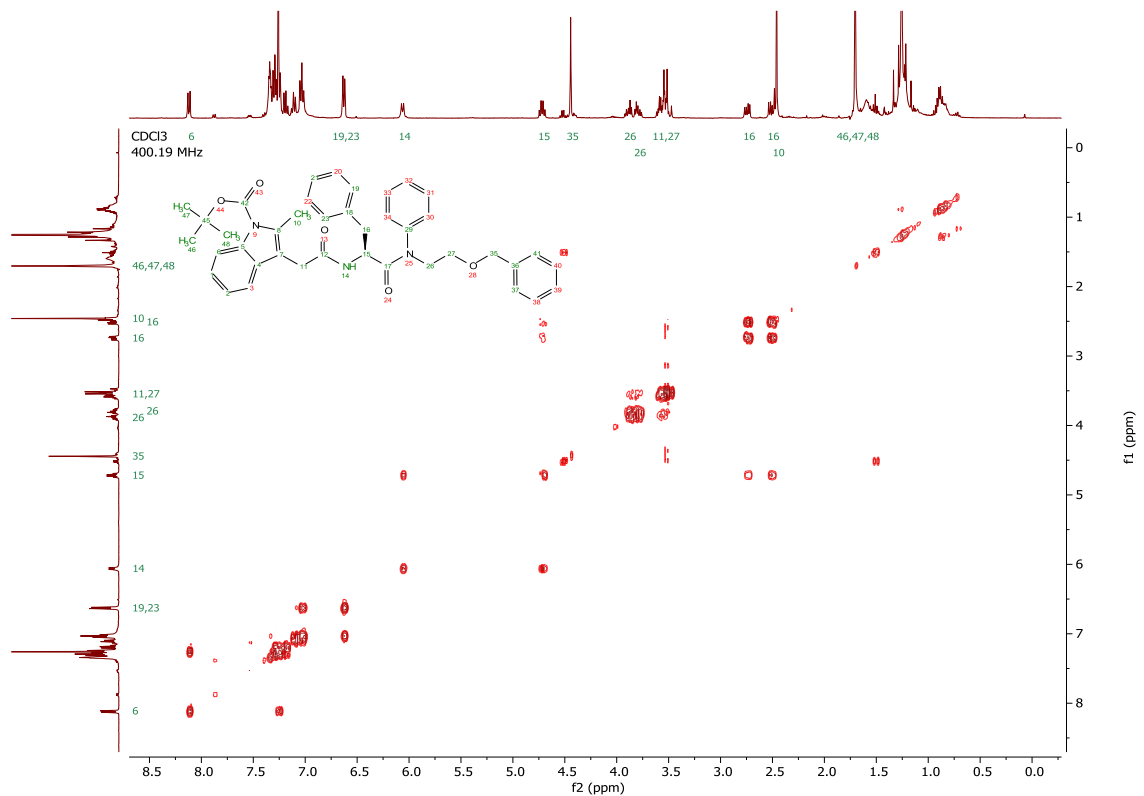


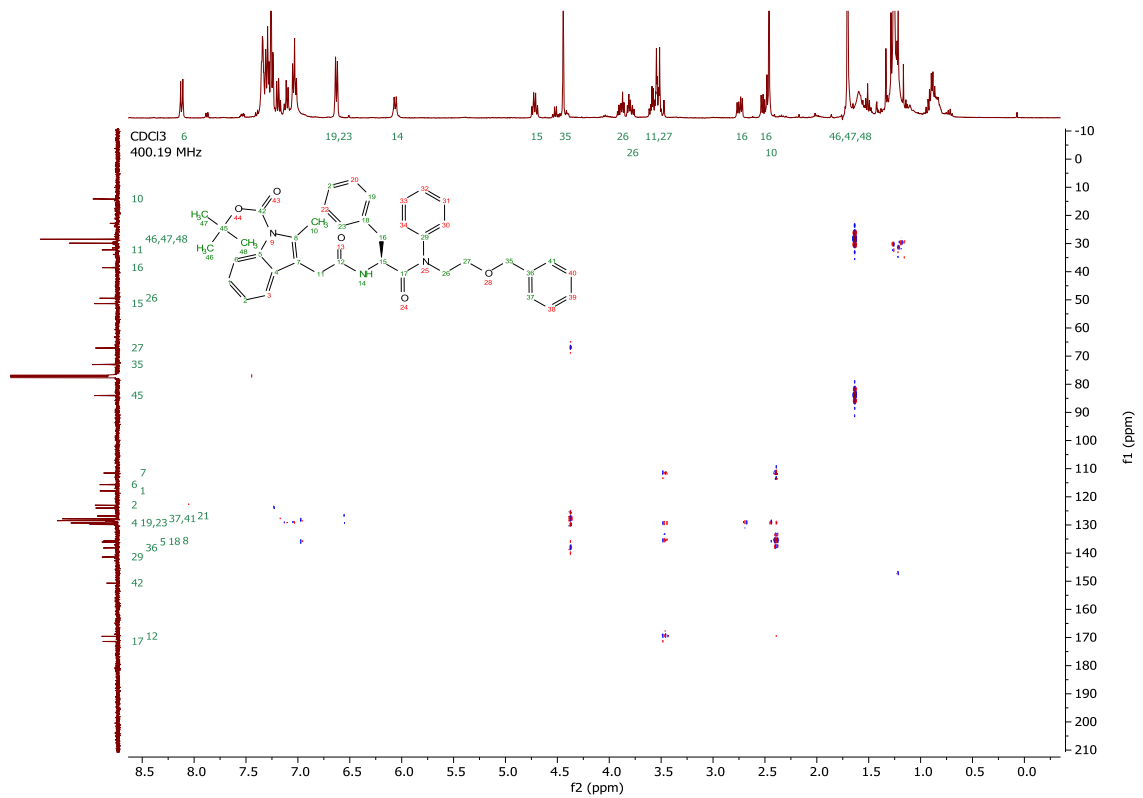




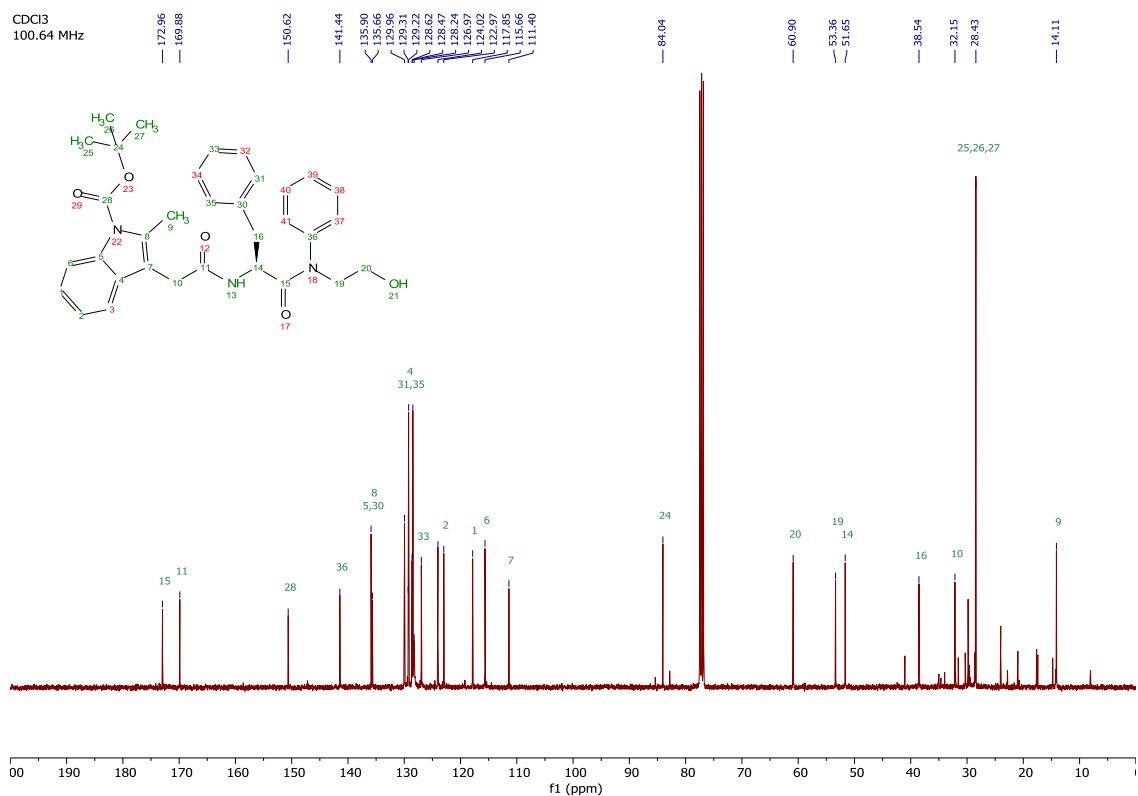
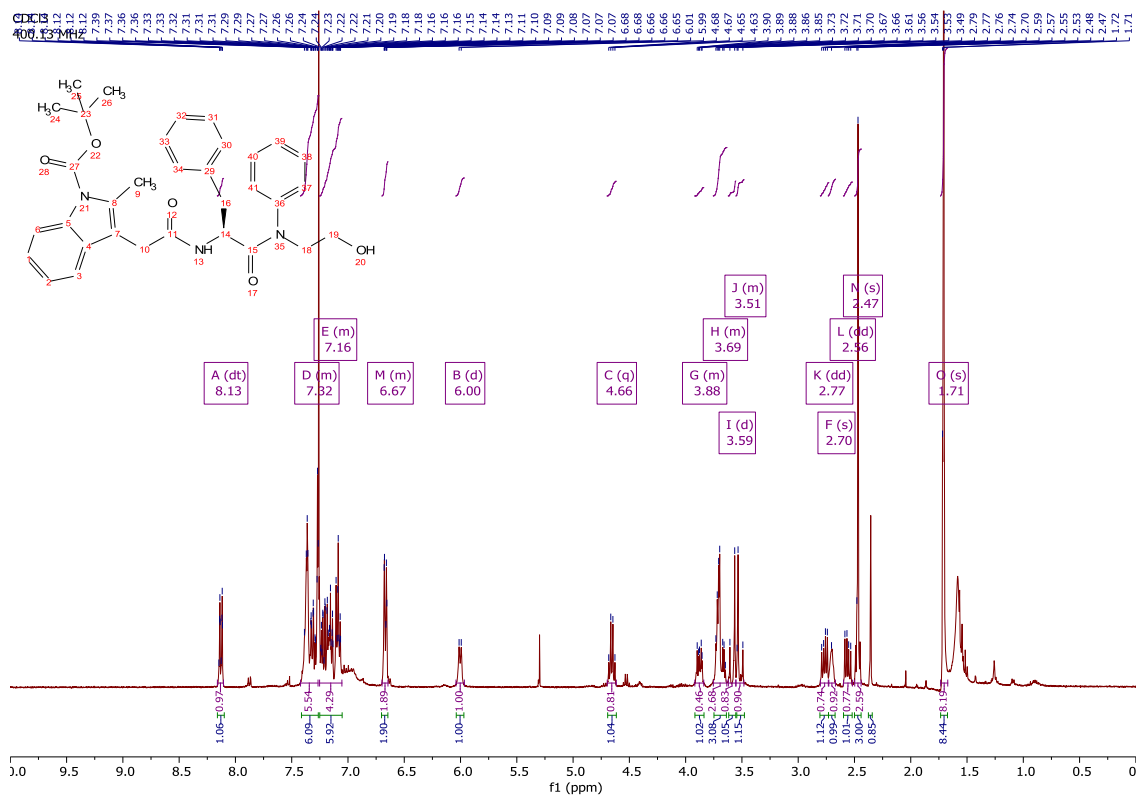
$^1\text{H}$ ,  $^{13}\text{C}$ , COSY, HSQC and HMBC NMR spectra of benzyl ether **2.44**.

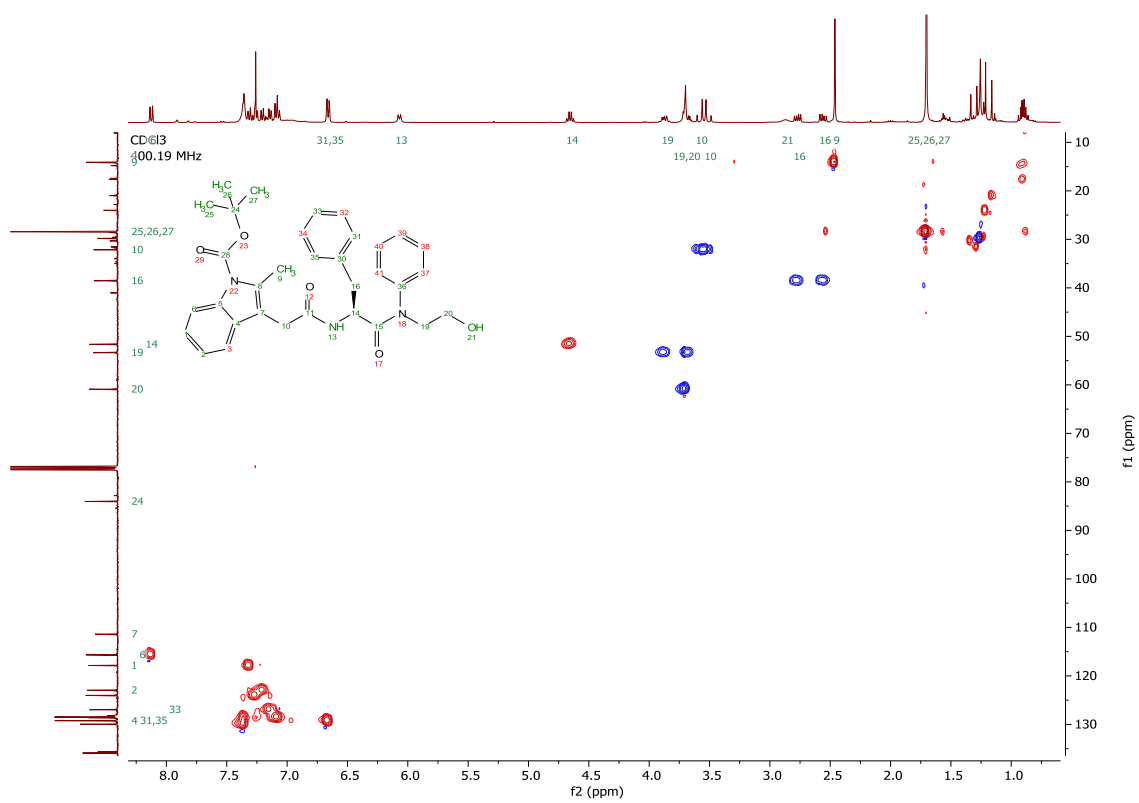
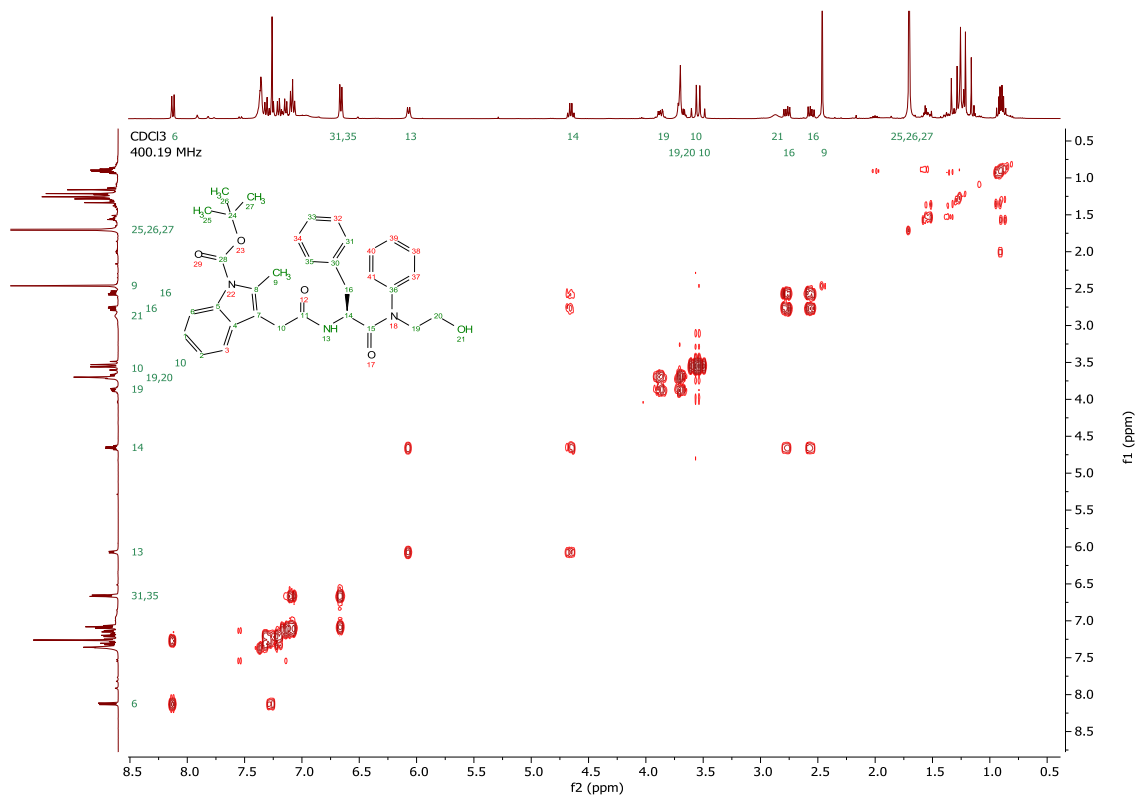


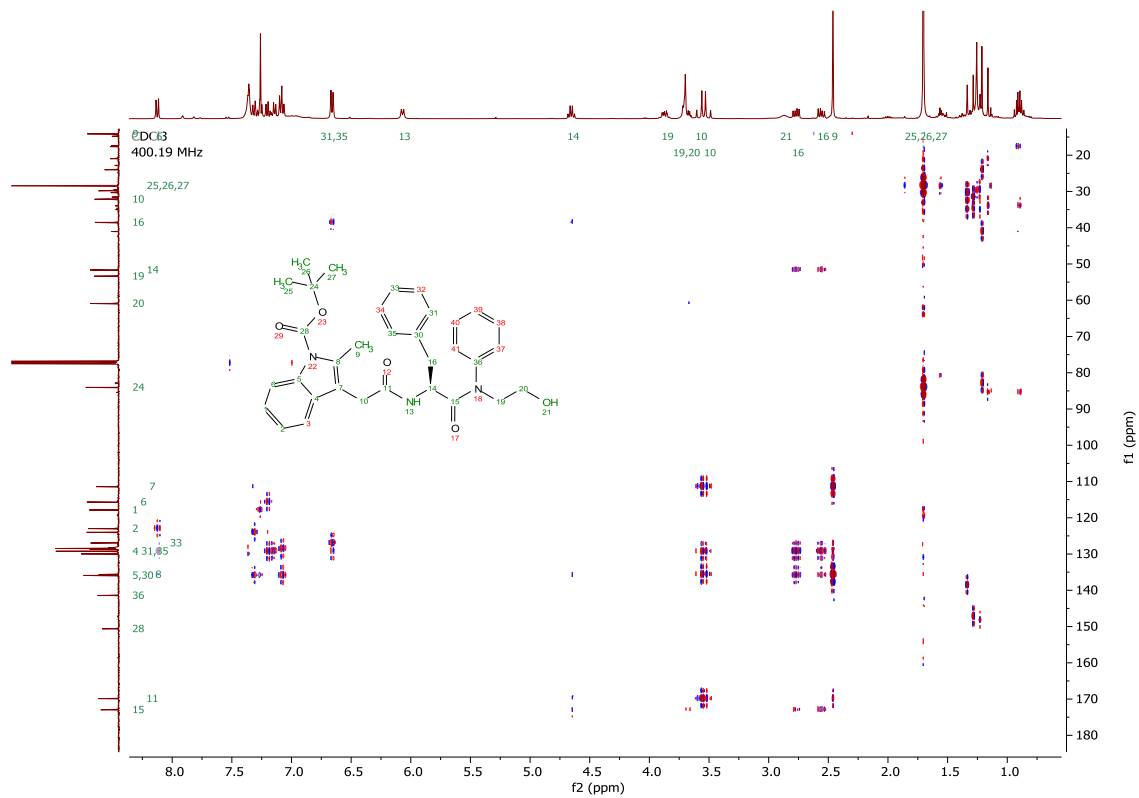




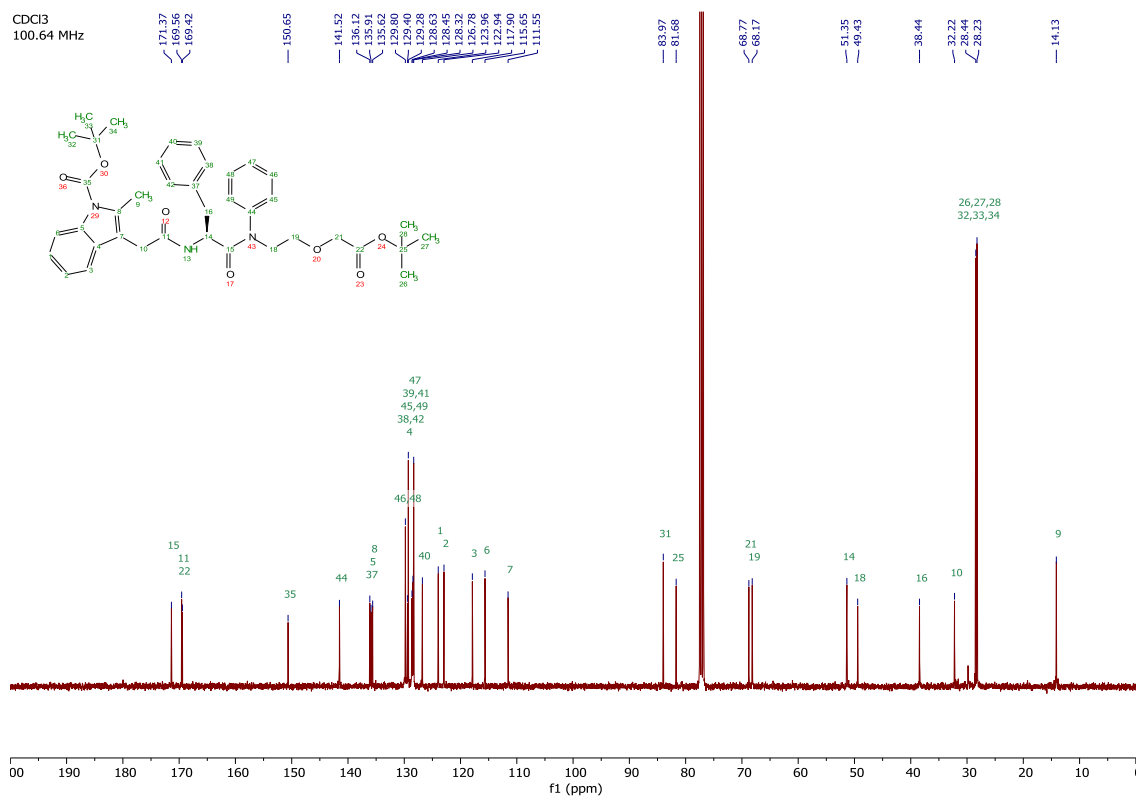
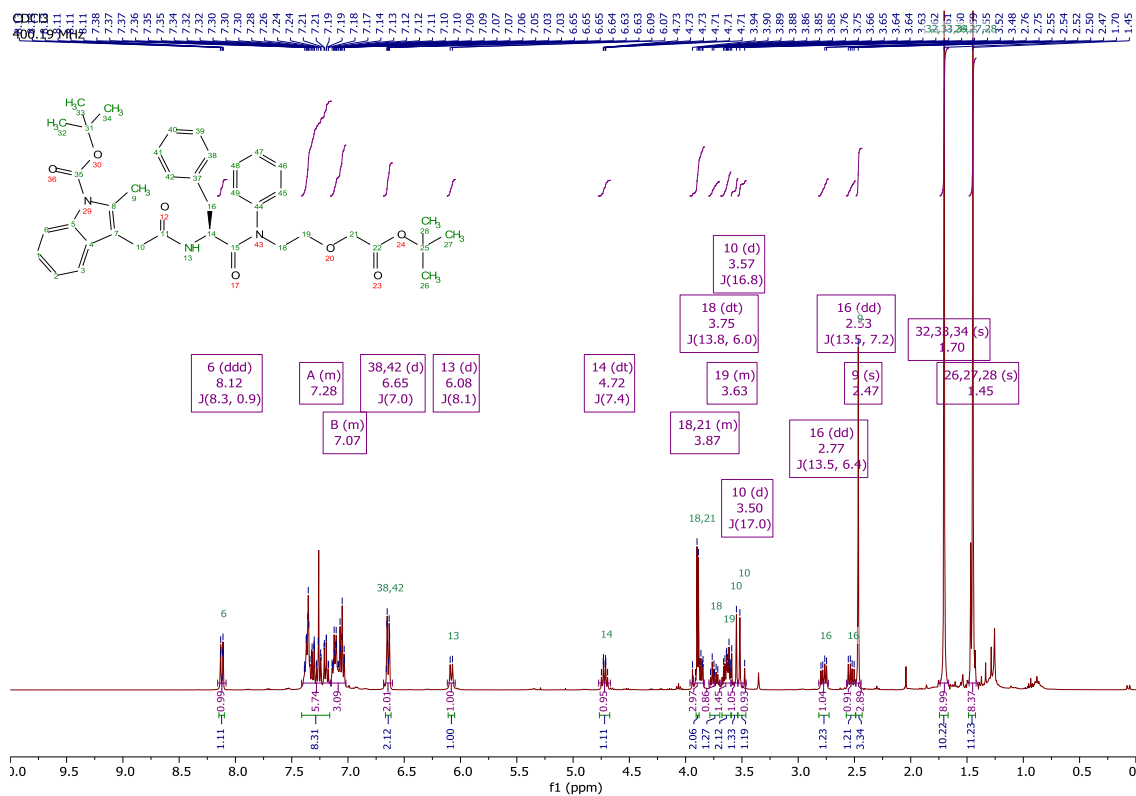
$^1\text{H}$ ,  $^{13}\text{C}$ , COSY, HSQC and HMBC NMR spectra of alcohol **2.45**.

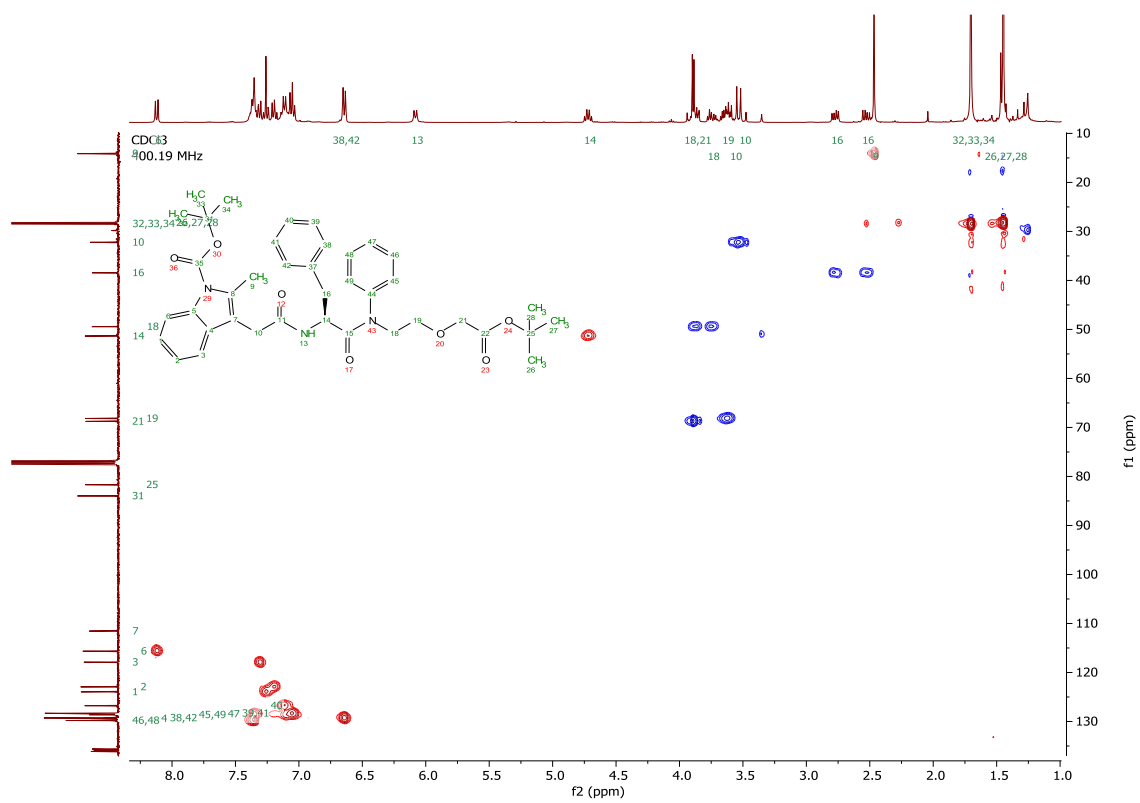
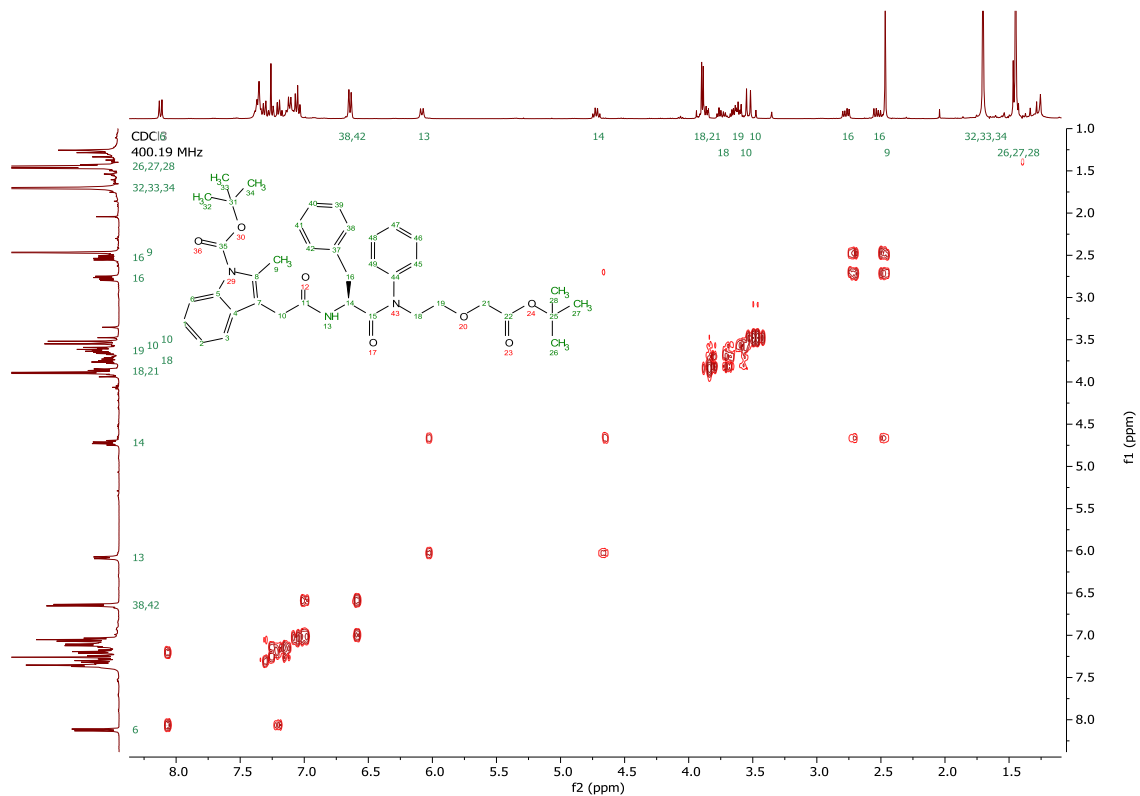


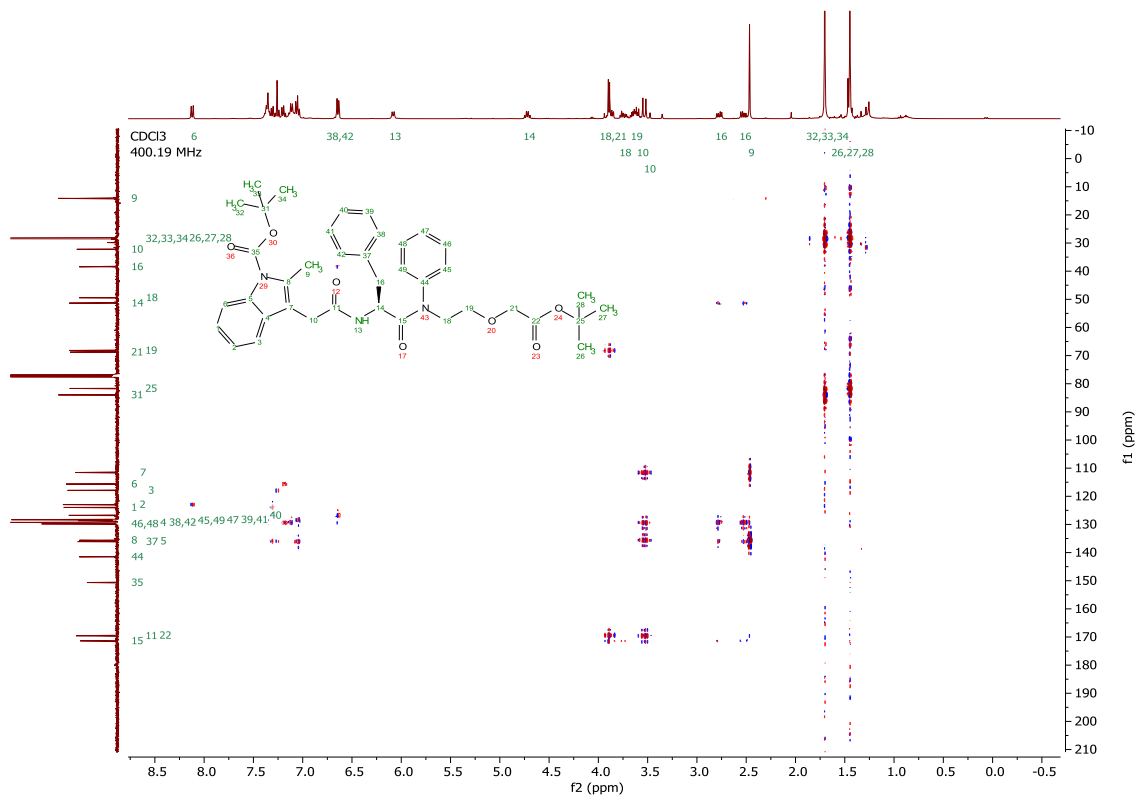




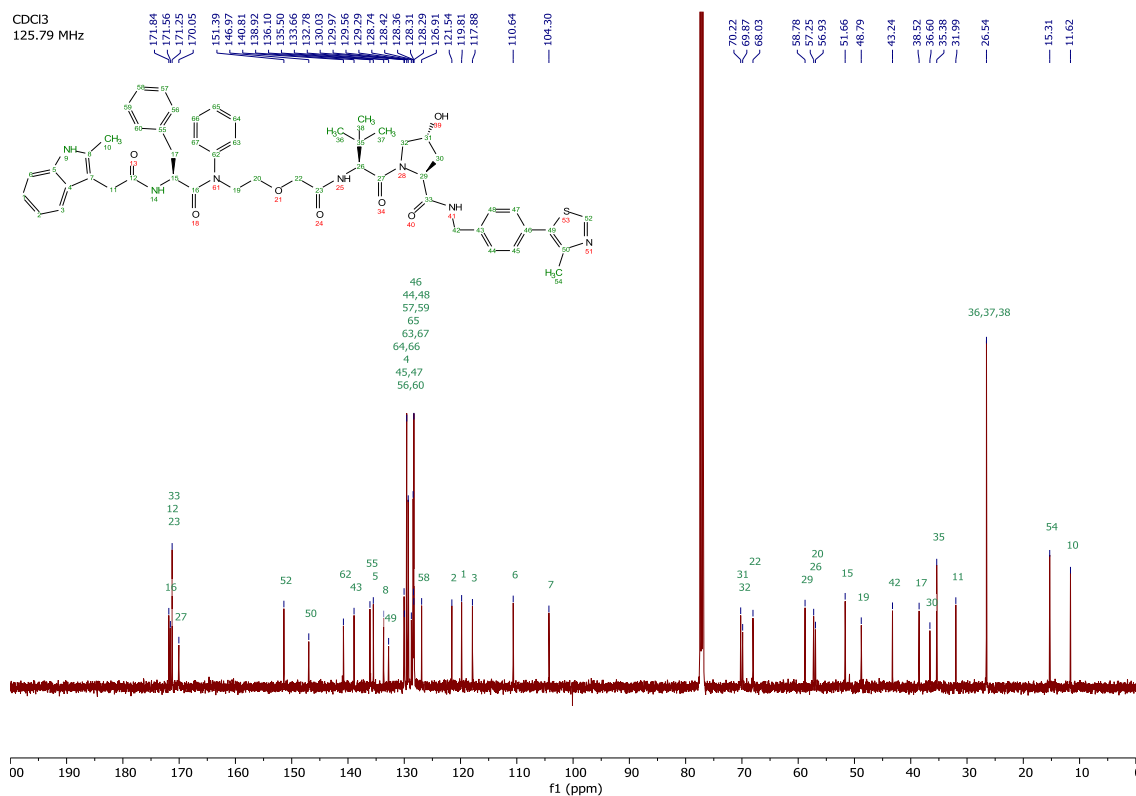
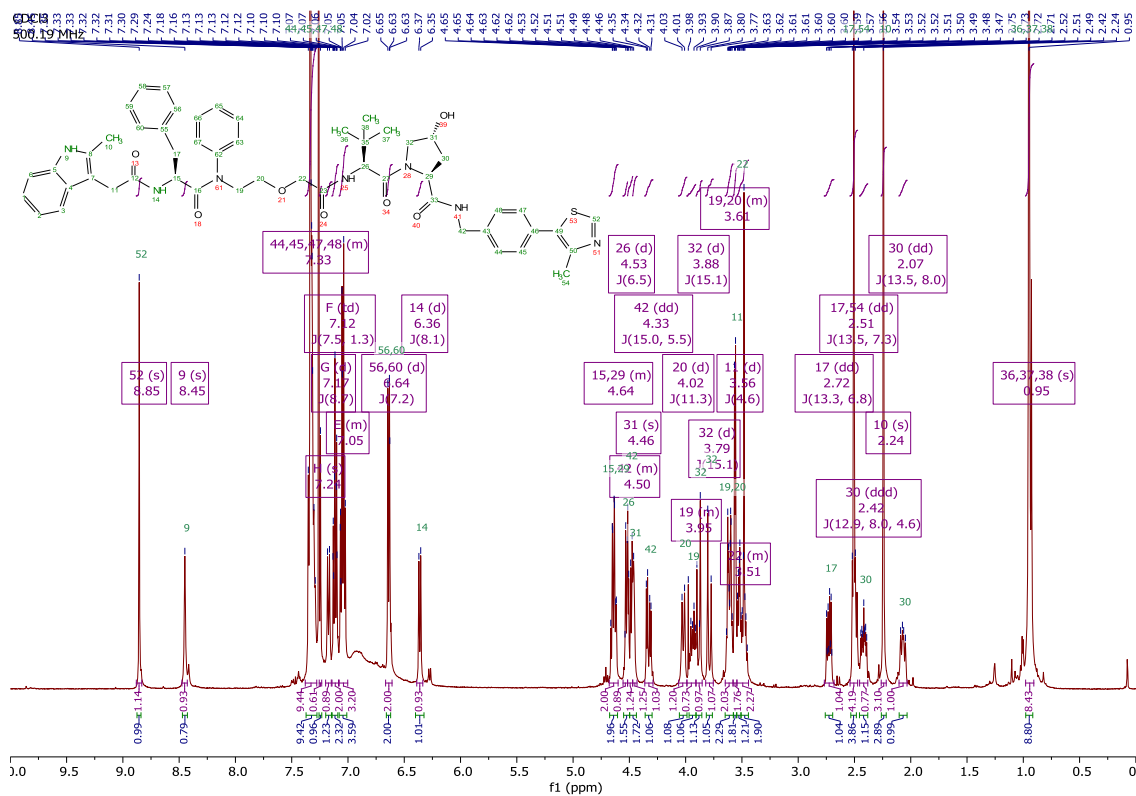
$^1\text{H}$ ,  $^{13}\text{C}$ , COSY, HSQC and HMBC NMR spectra of *tert*-butyl ester **2.46**.

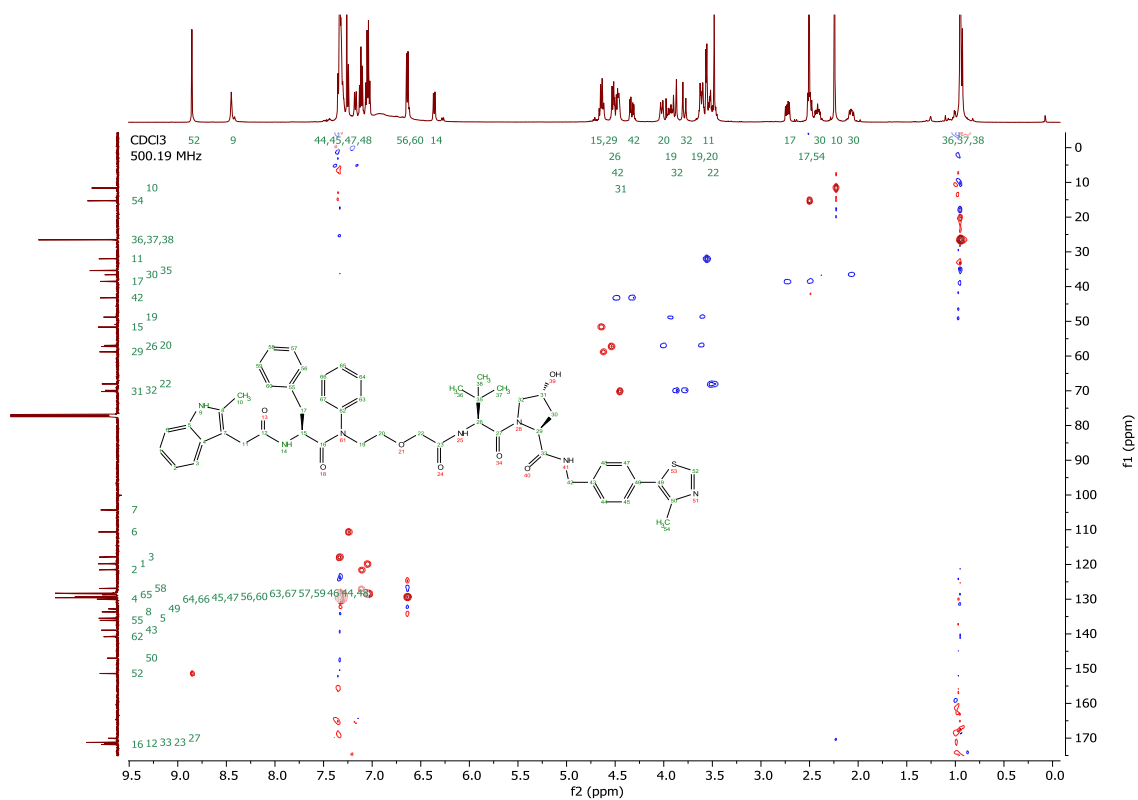
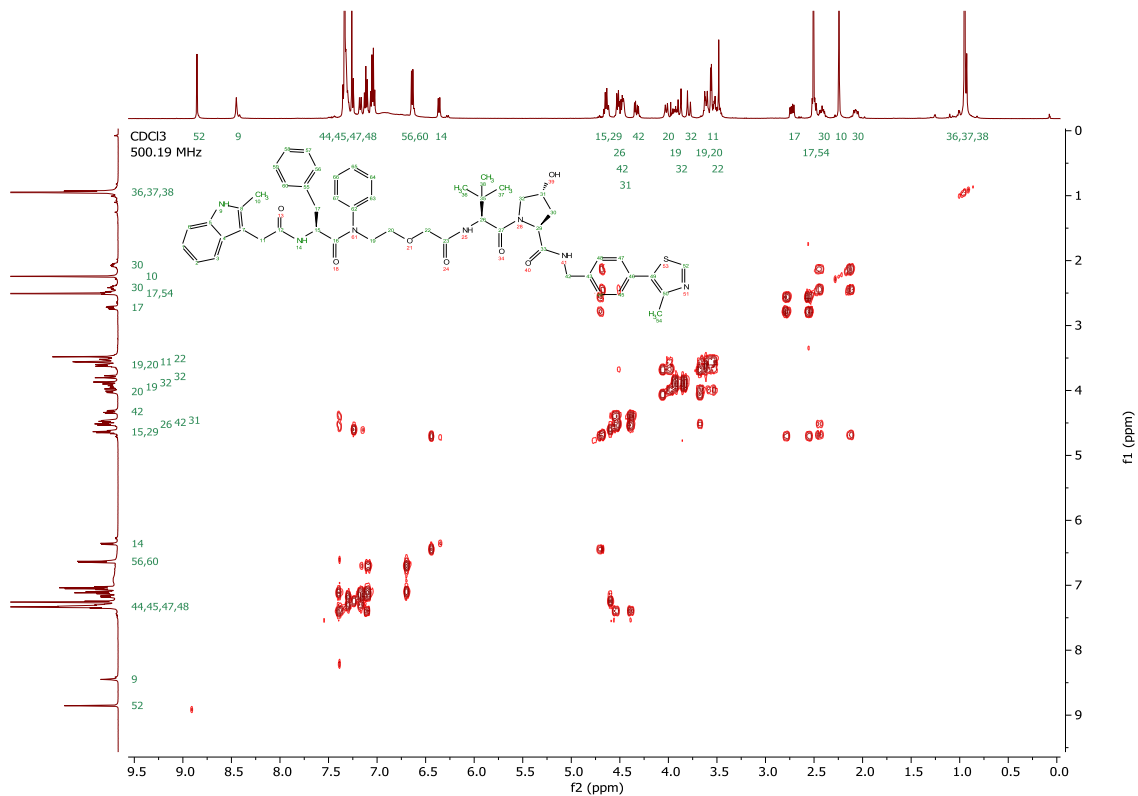


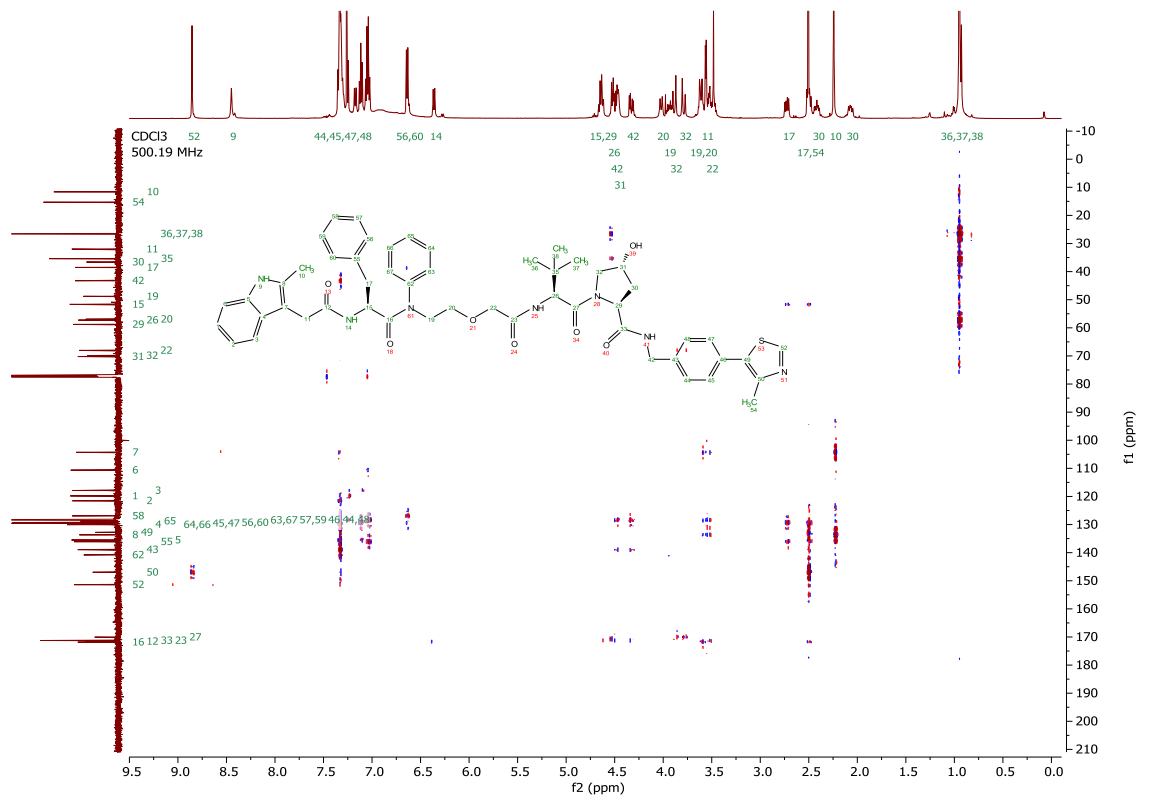




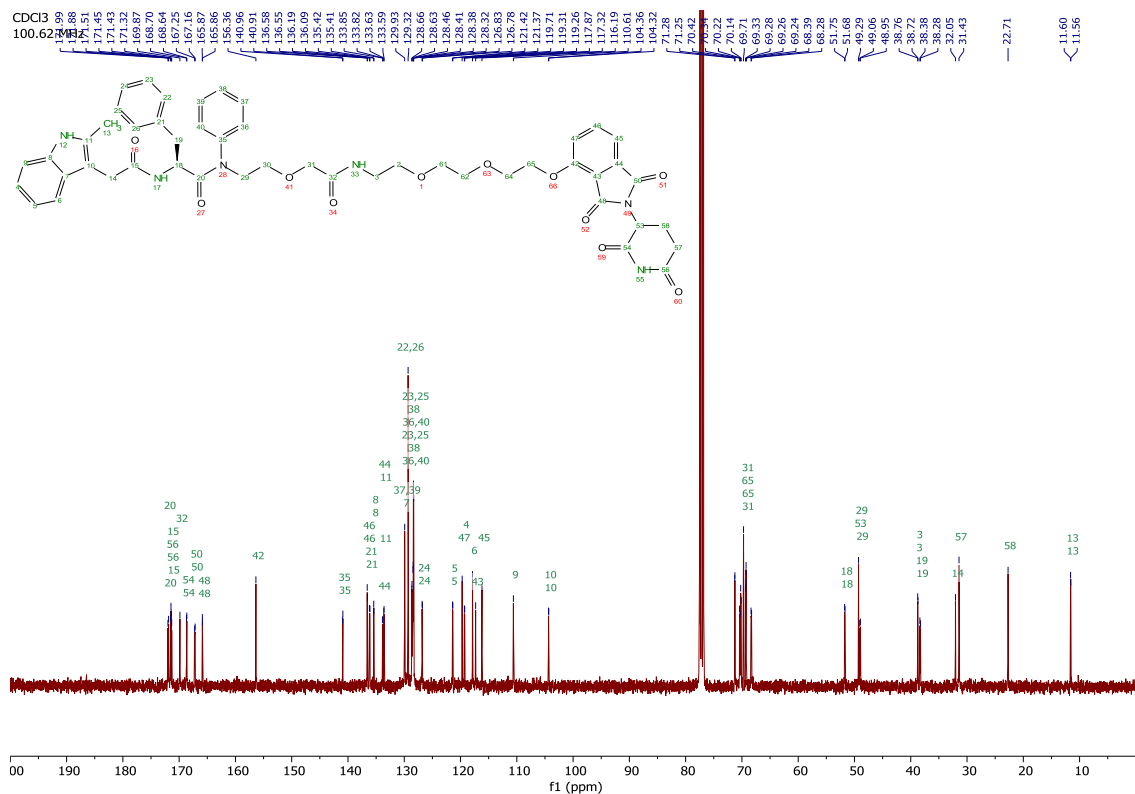
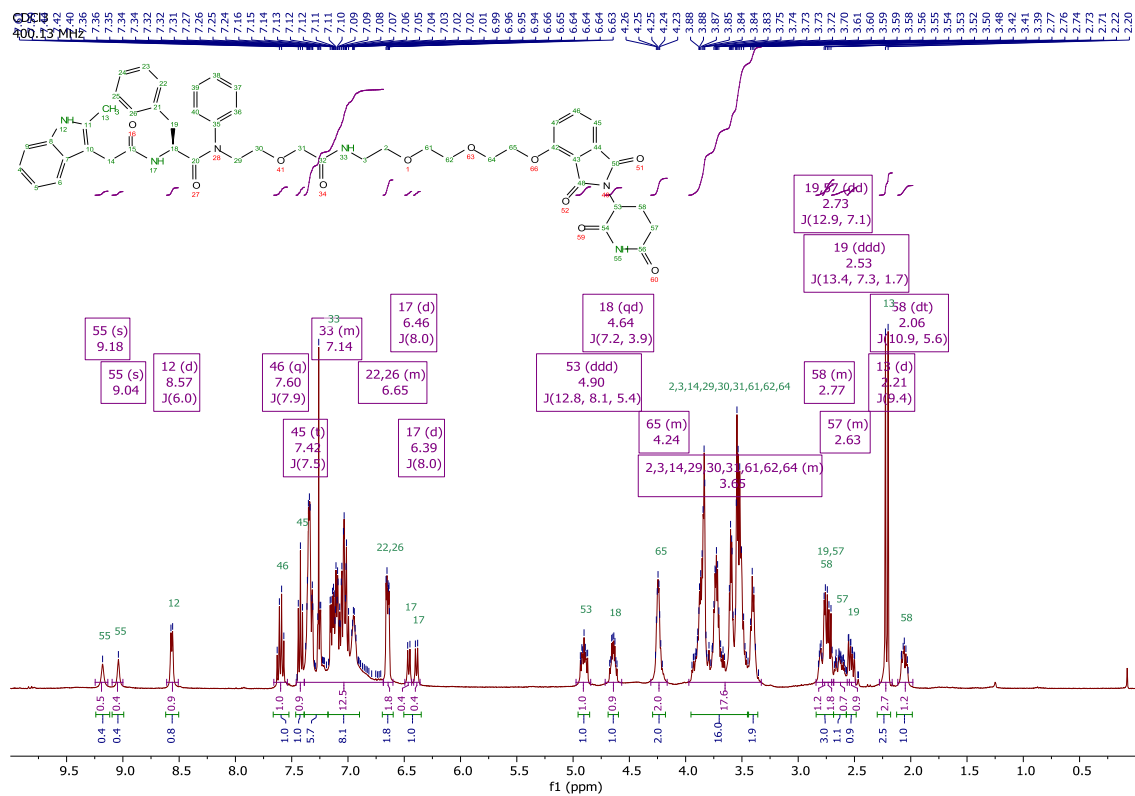
$^1\text{H}$ ,  $^{13}\text{C}$ , COSY, HSQC and HMBC NMR spectra of PROTAC VHL-4.

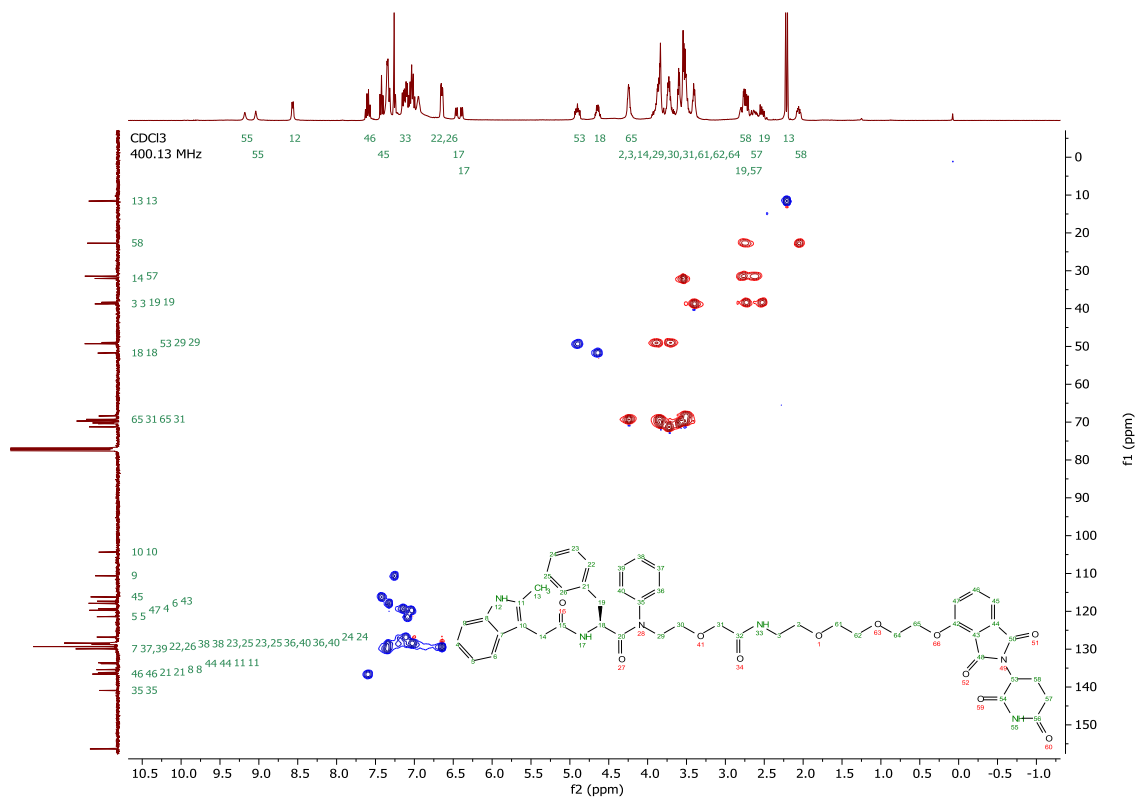
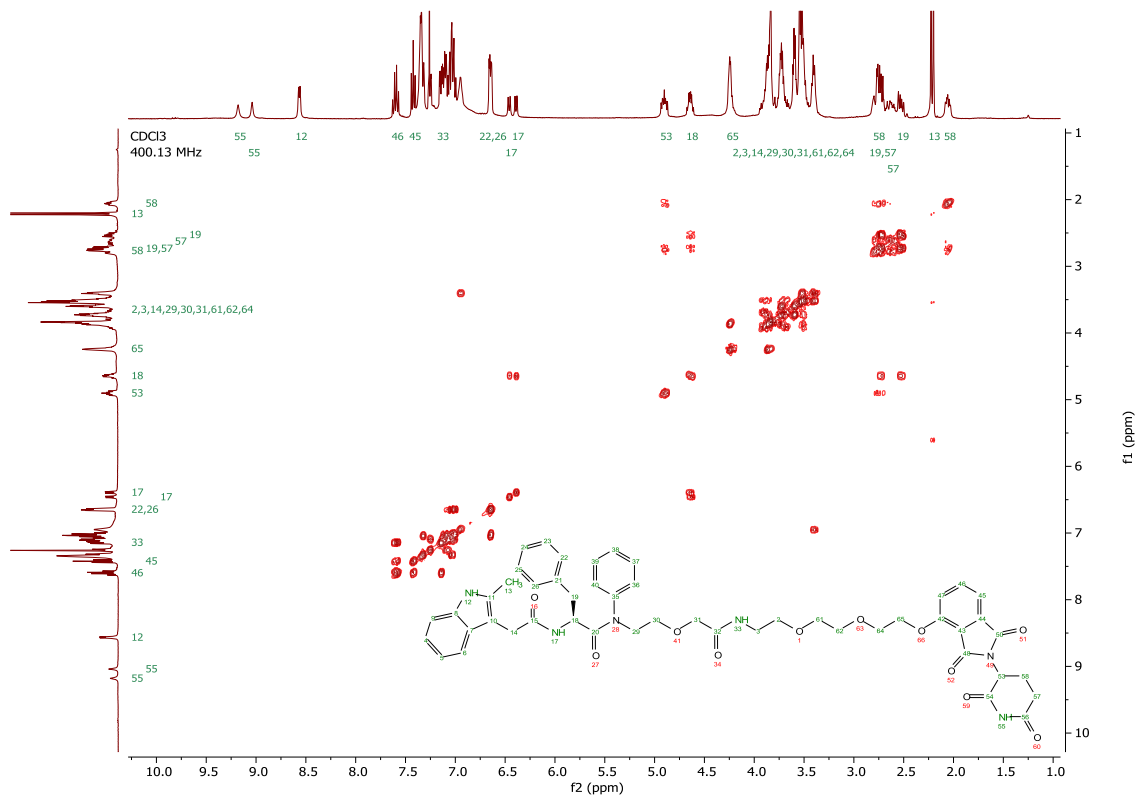


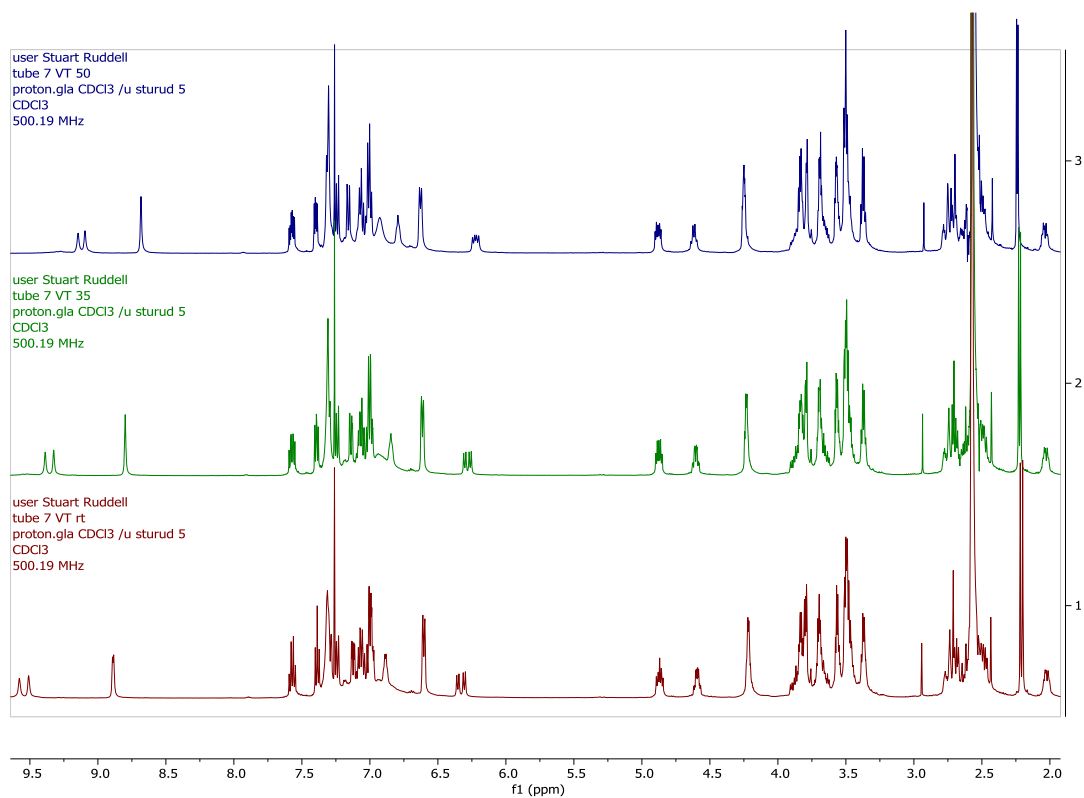
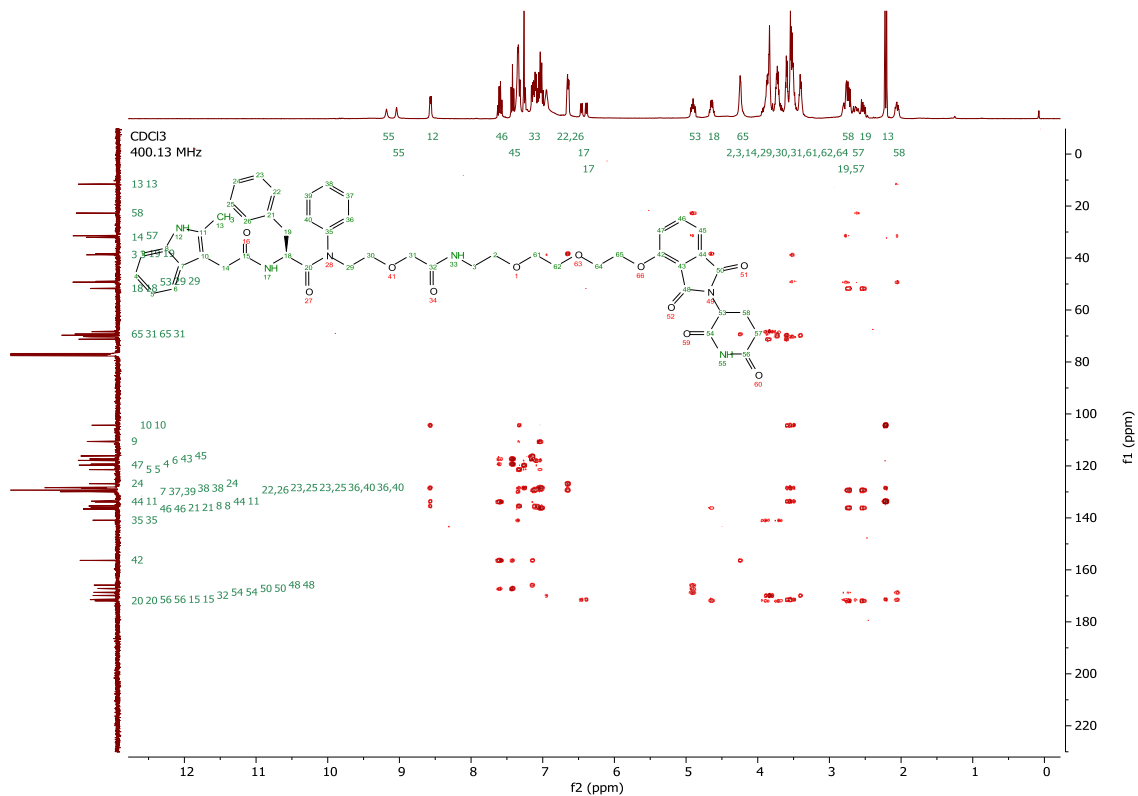




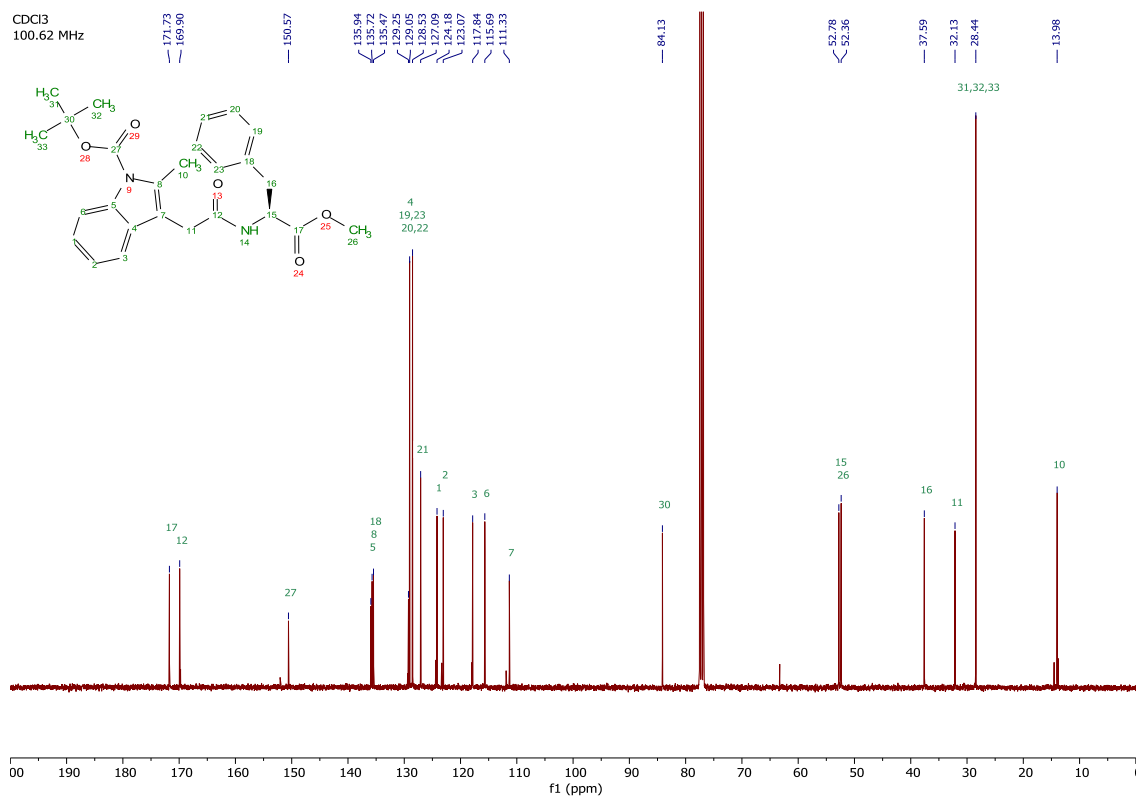
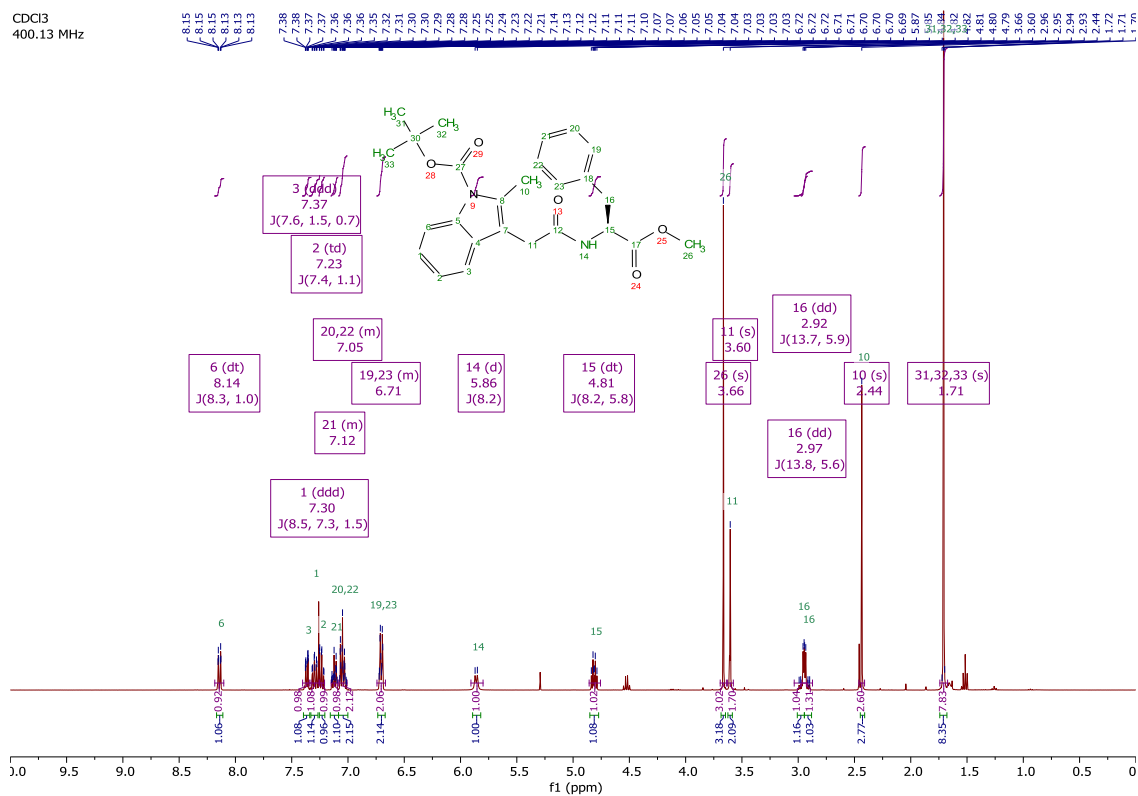
<sup>1</sup>H, <sup>13</sup>C, COSY, HSQC, HMBC and VT (rt, 35 °C, 50 °C) NMR spectra of PROTAC CRBN-O13.

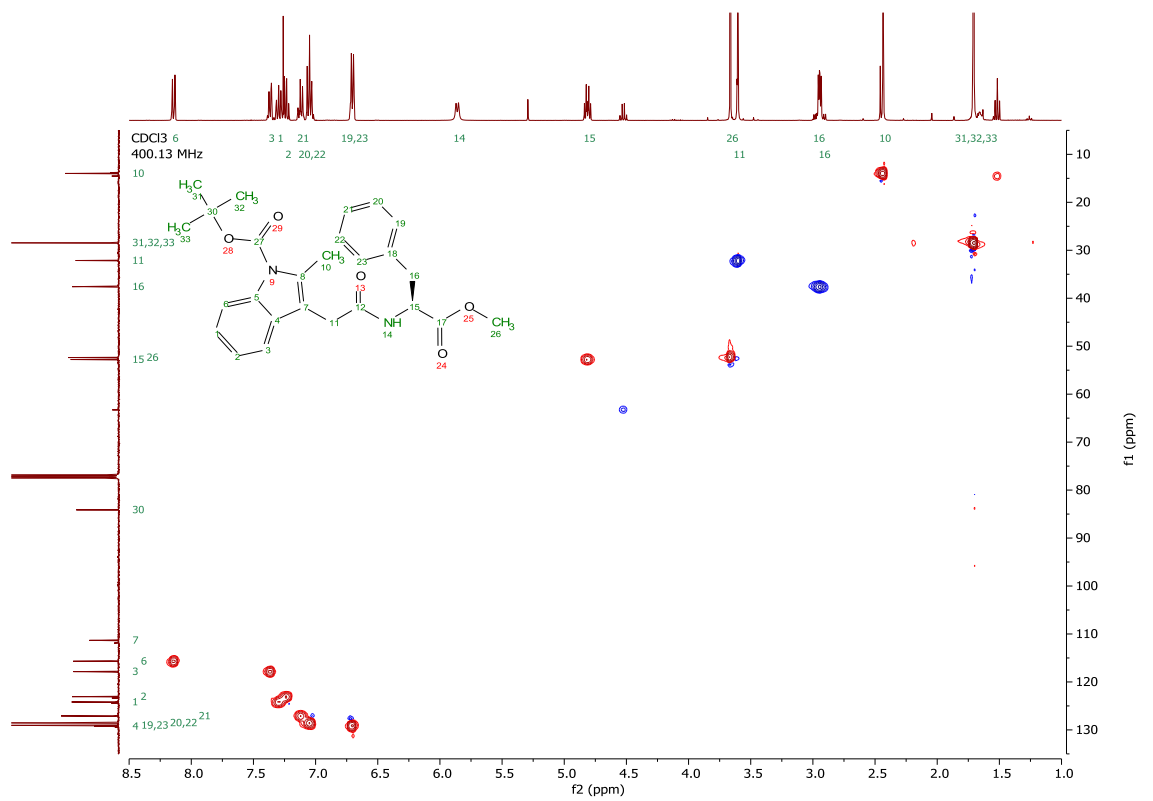
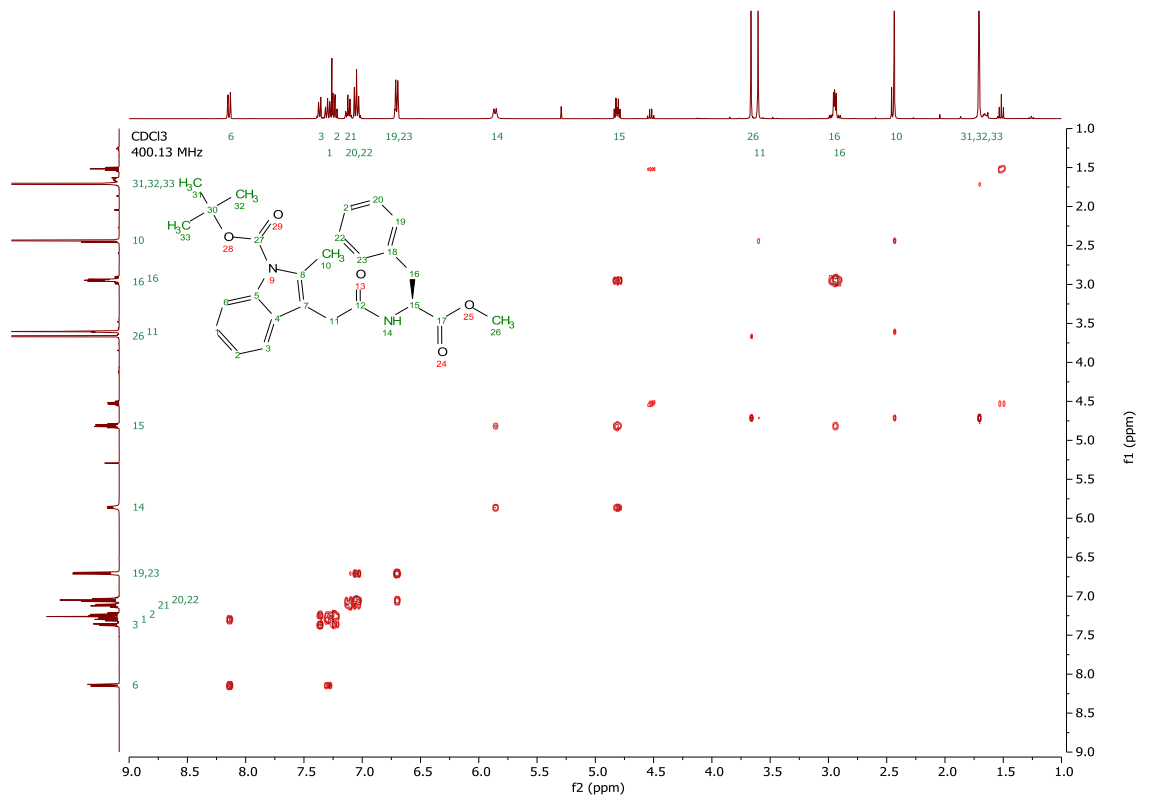


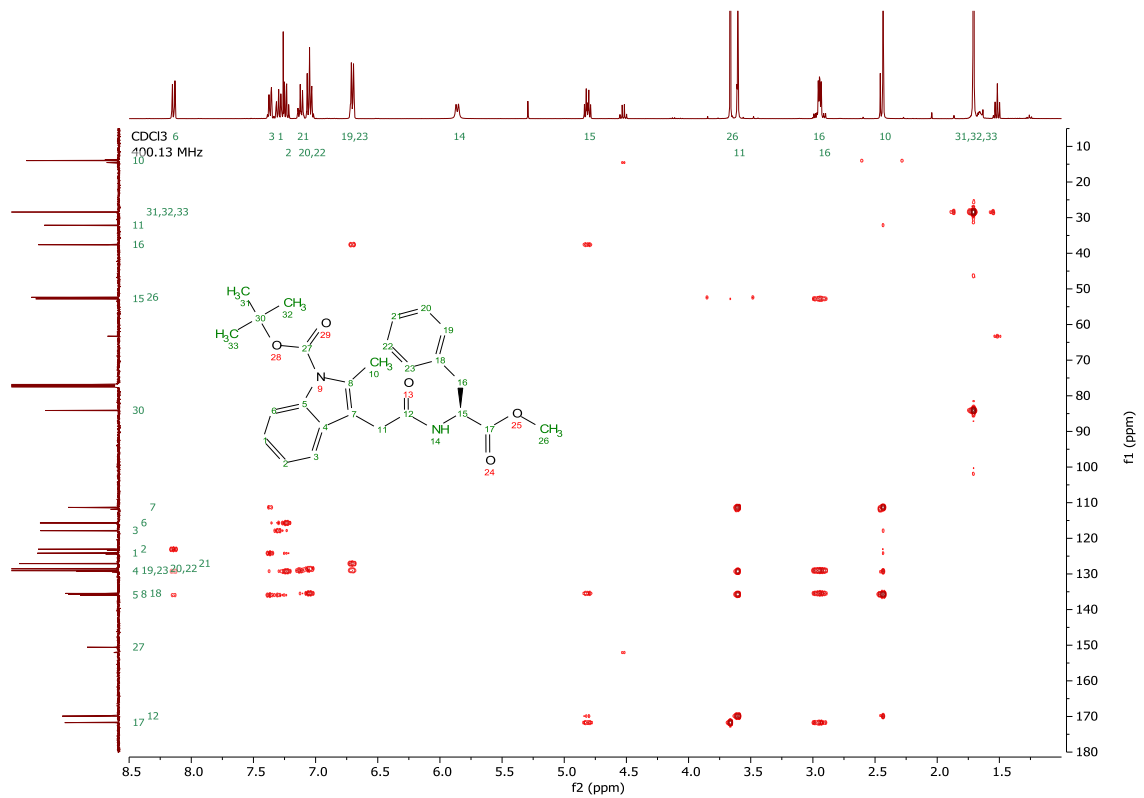




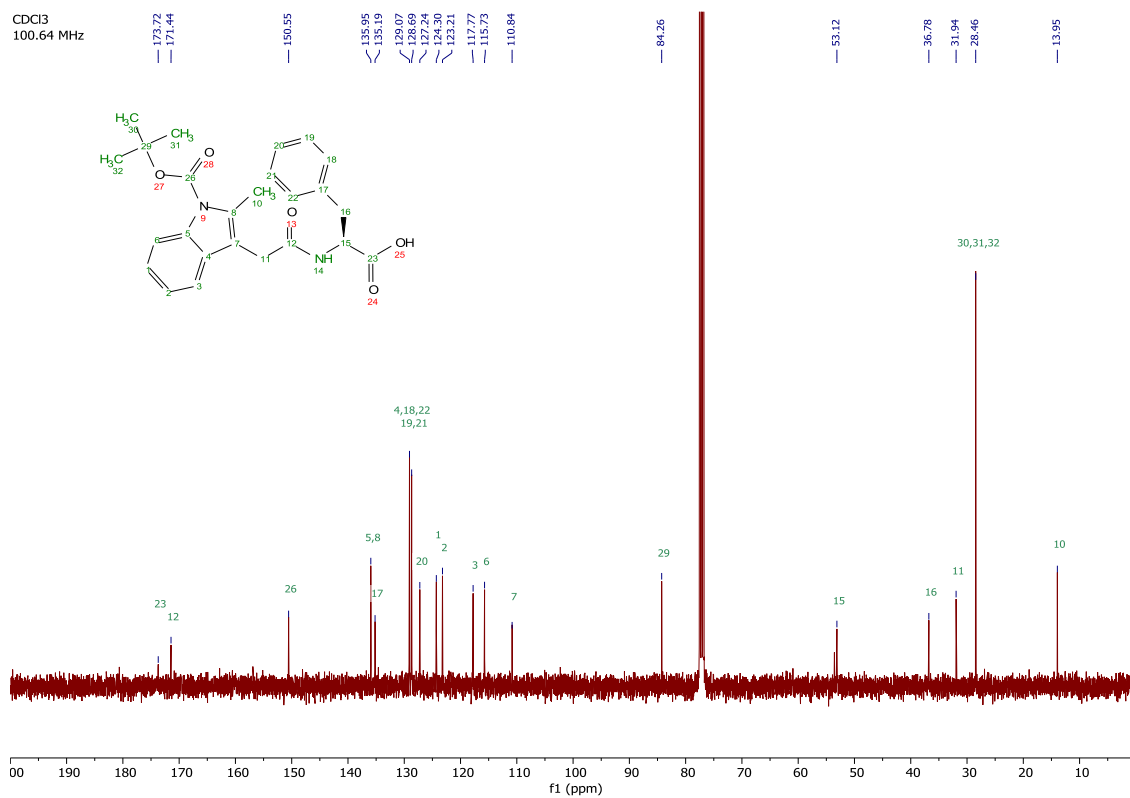
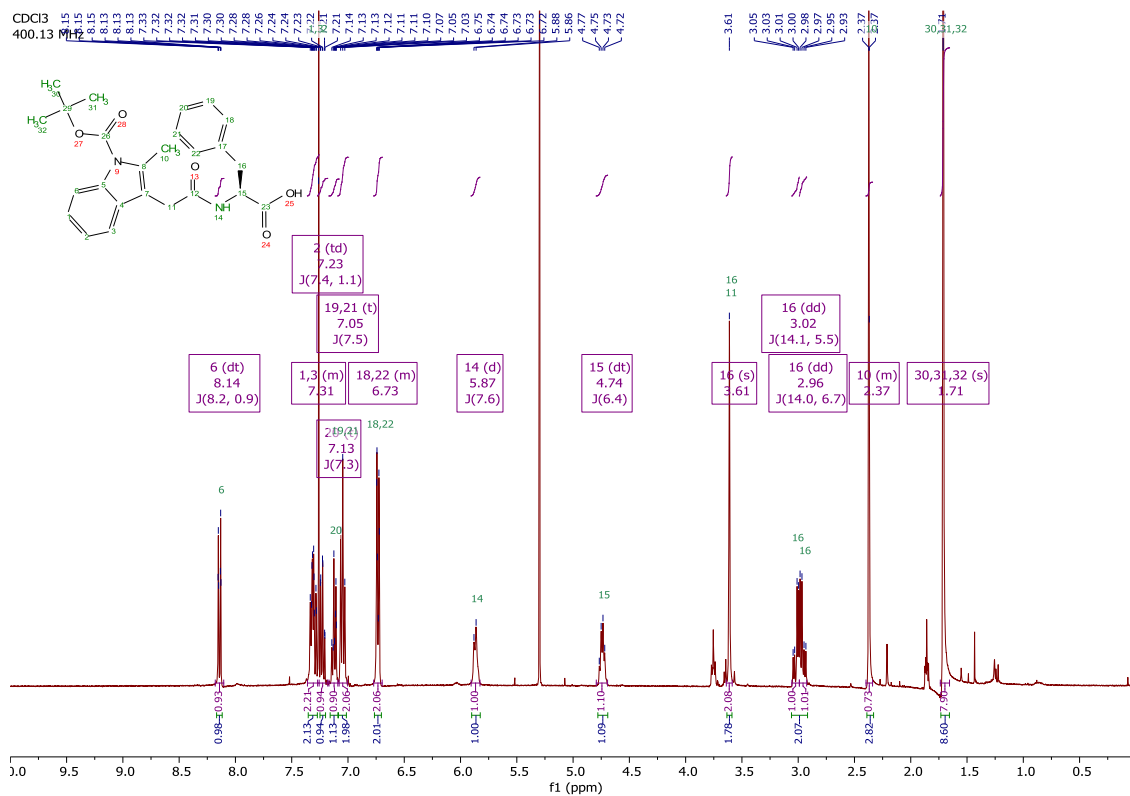
$^1\text{H}$ ,  $^{13}\text{C}$ , COSY, HSQC and HMBC NMR spectra of *tert*-butyl carbamate **2.53**.

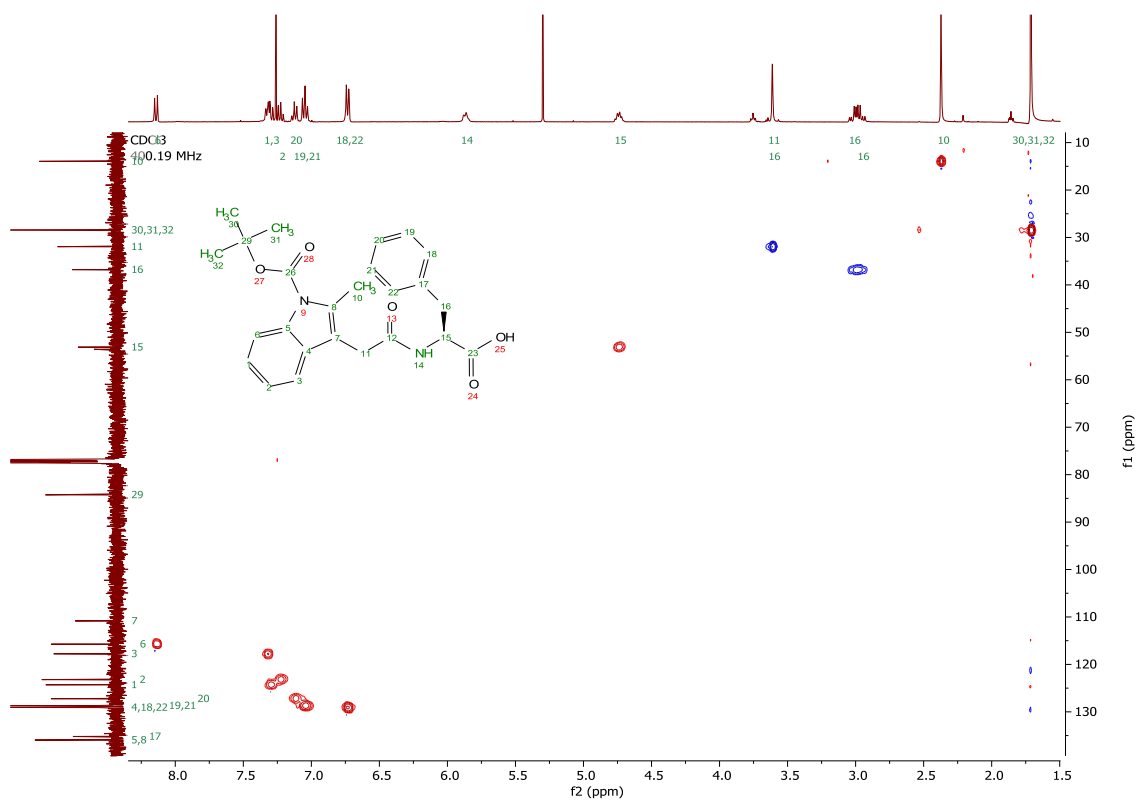
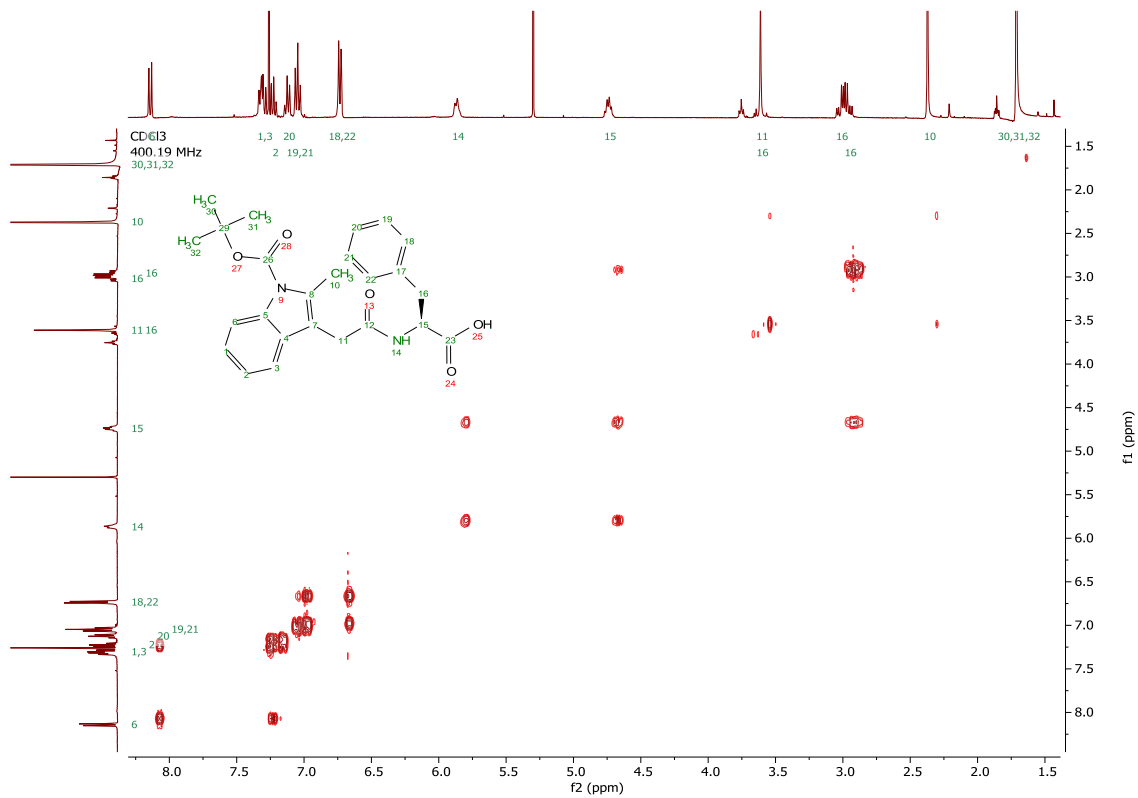


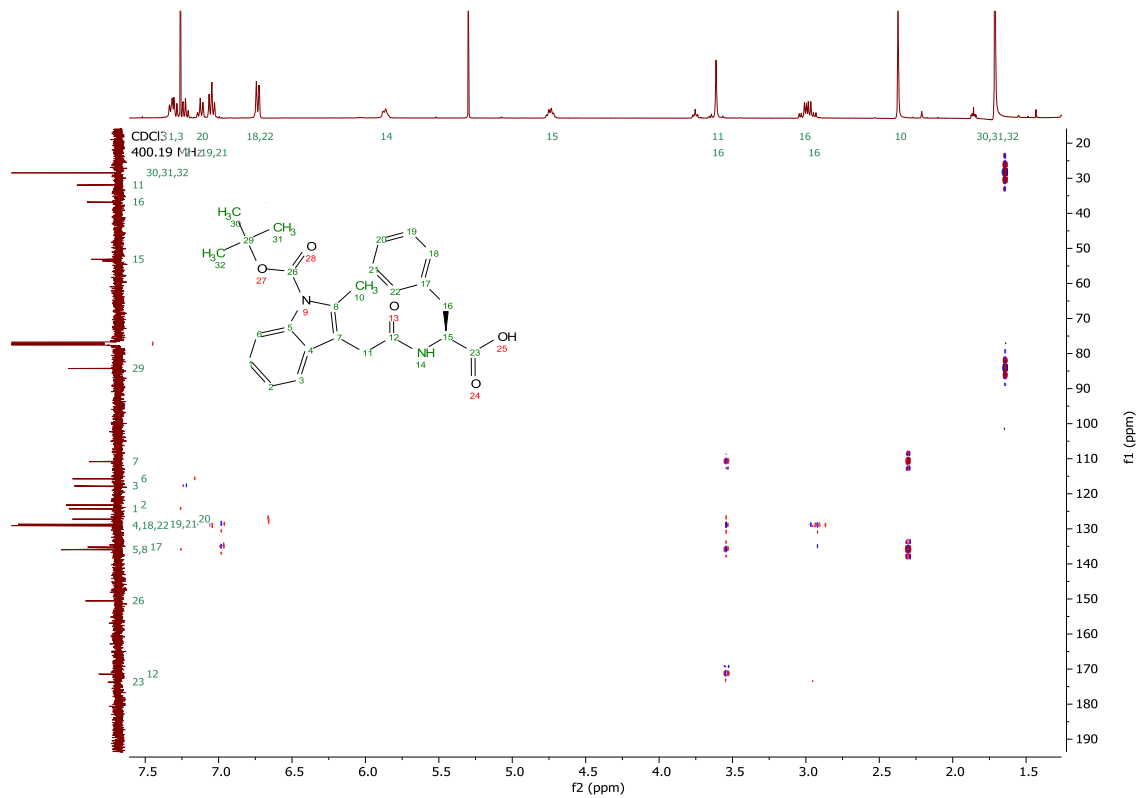




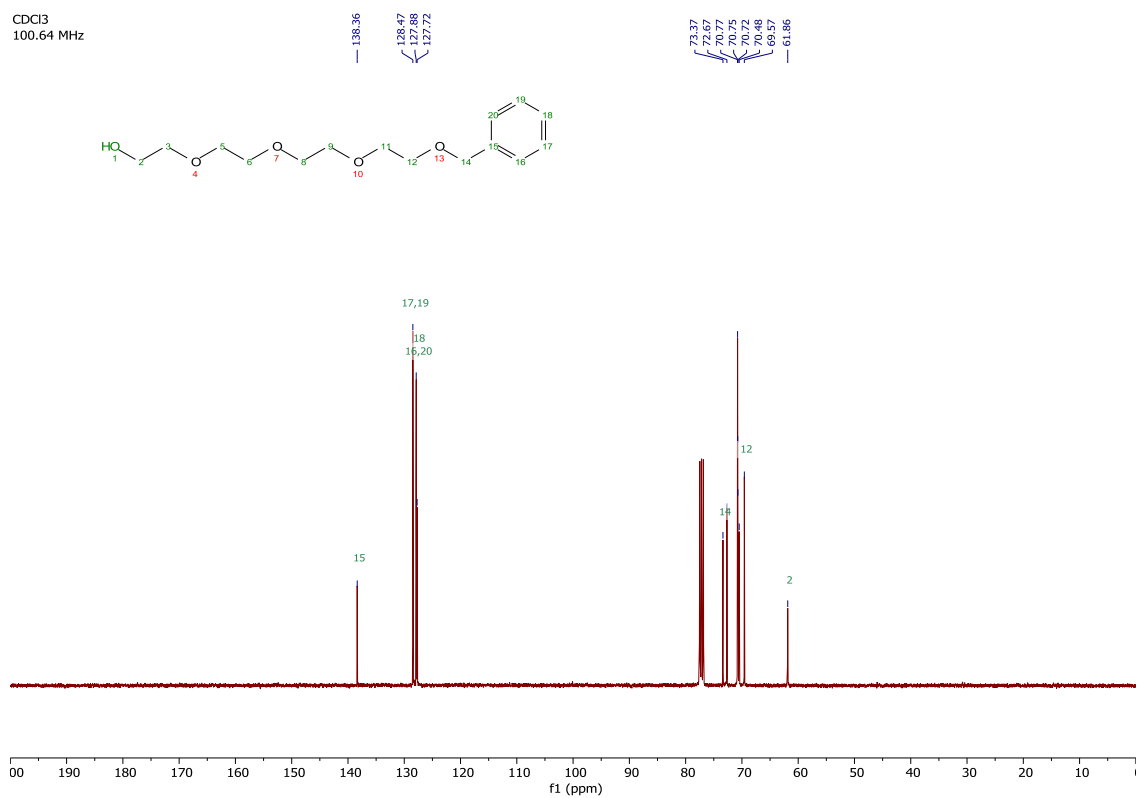
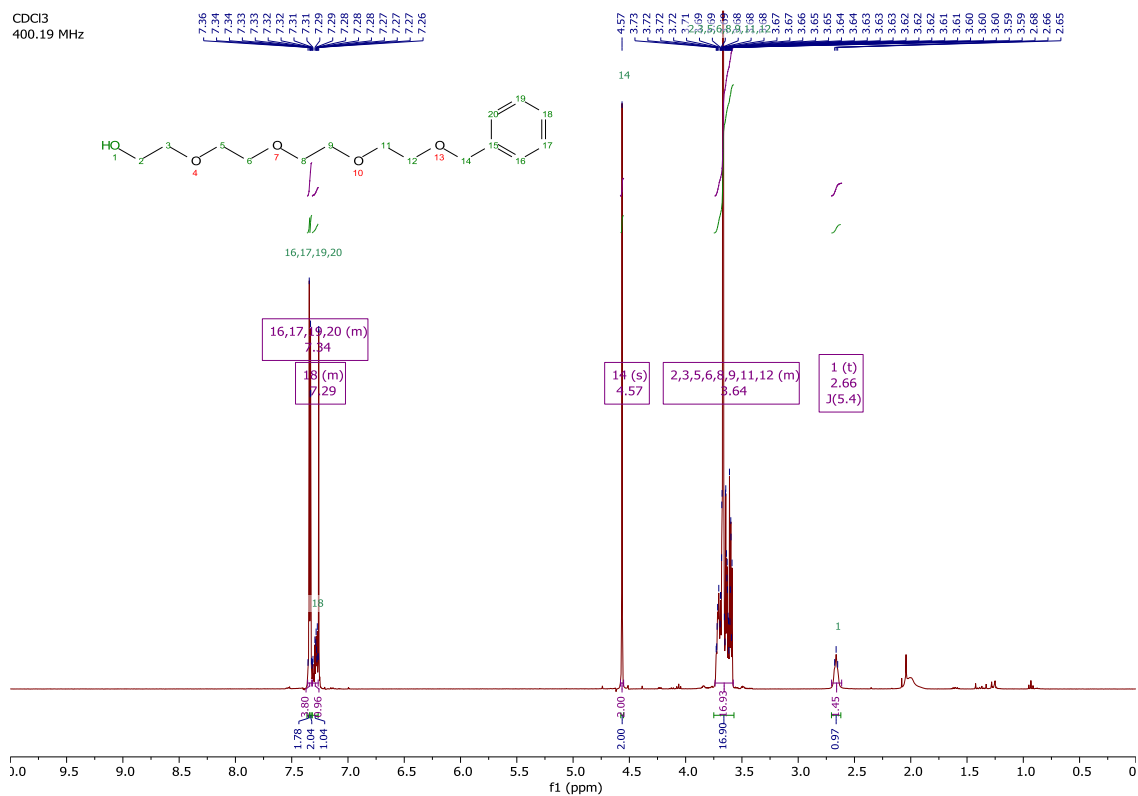
$^1\text{H}$ ,  $^{13}\text{C}$ , COSY, HSQC and HMBC NMR spectra of acid **2.54**.

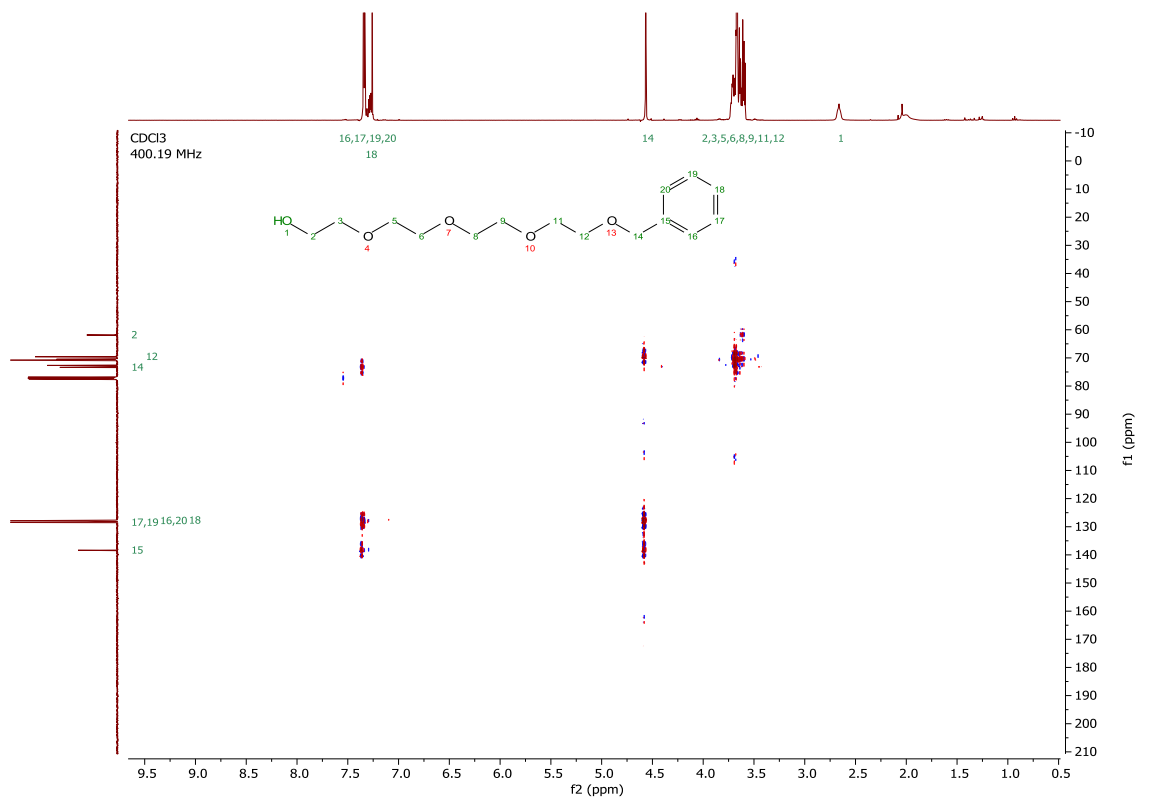
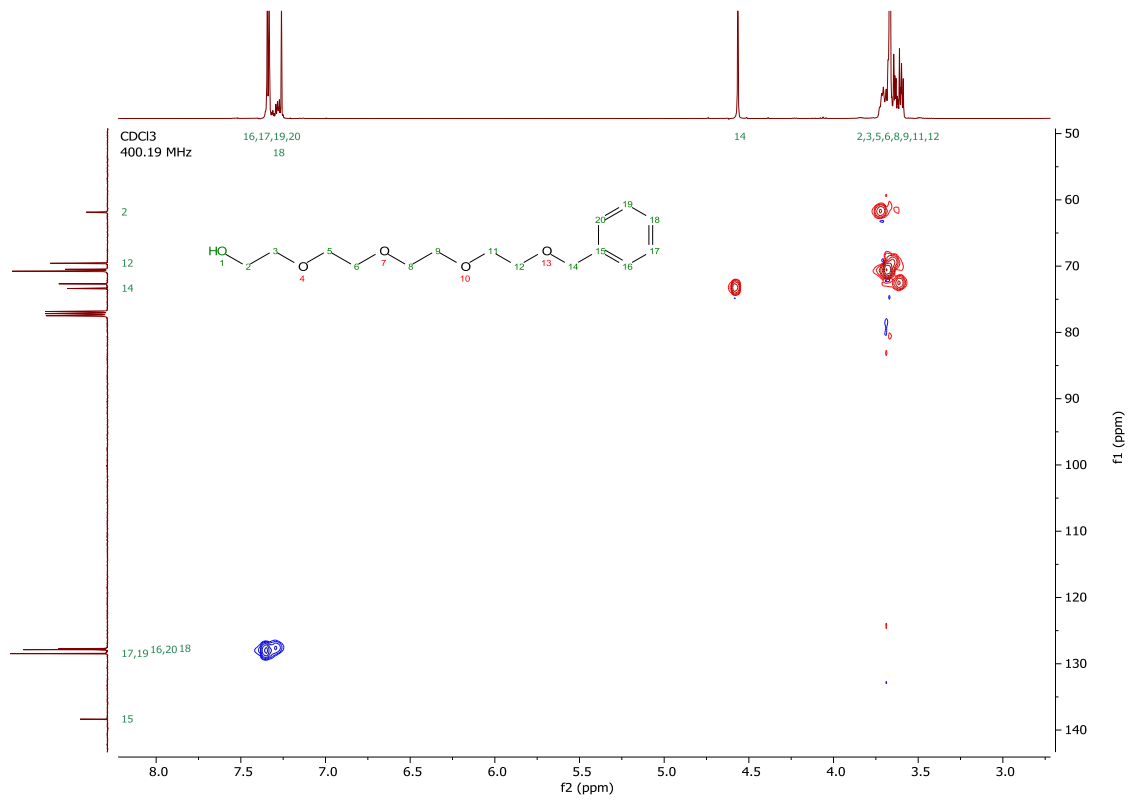




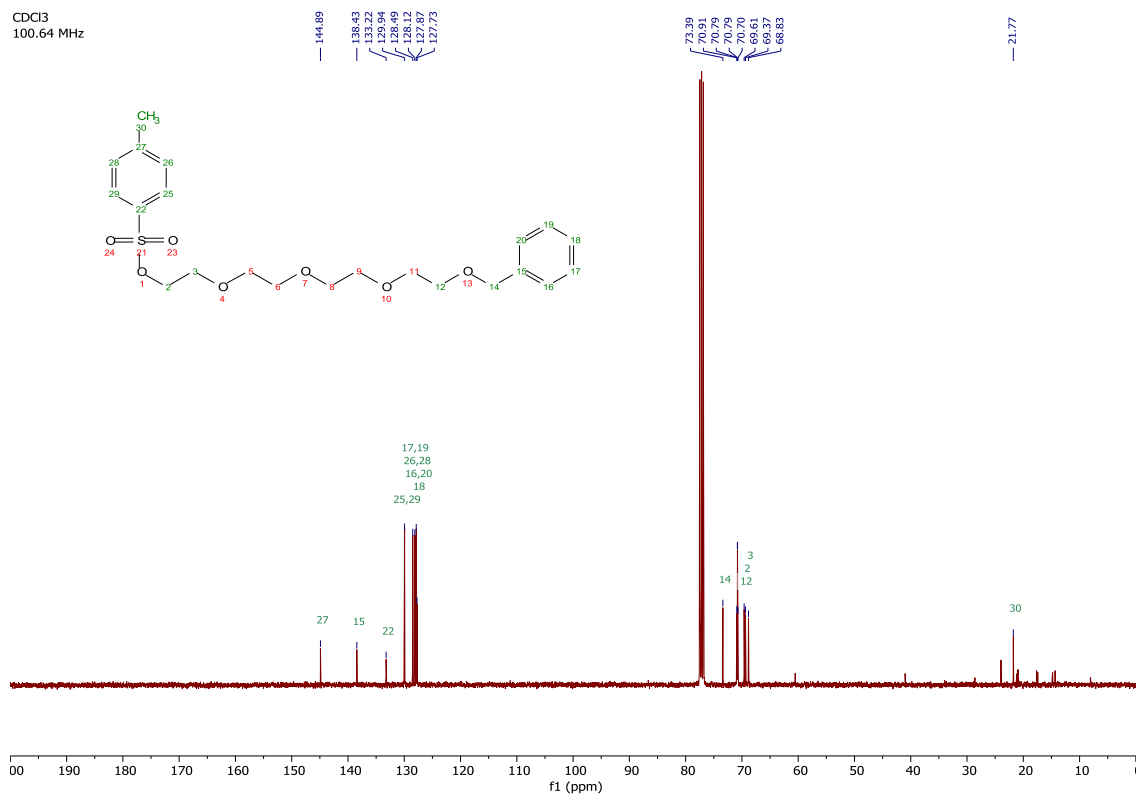
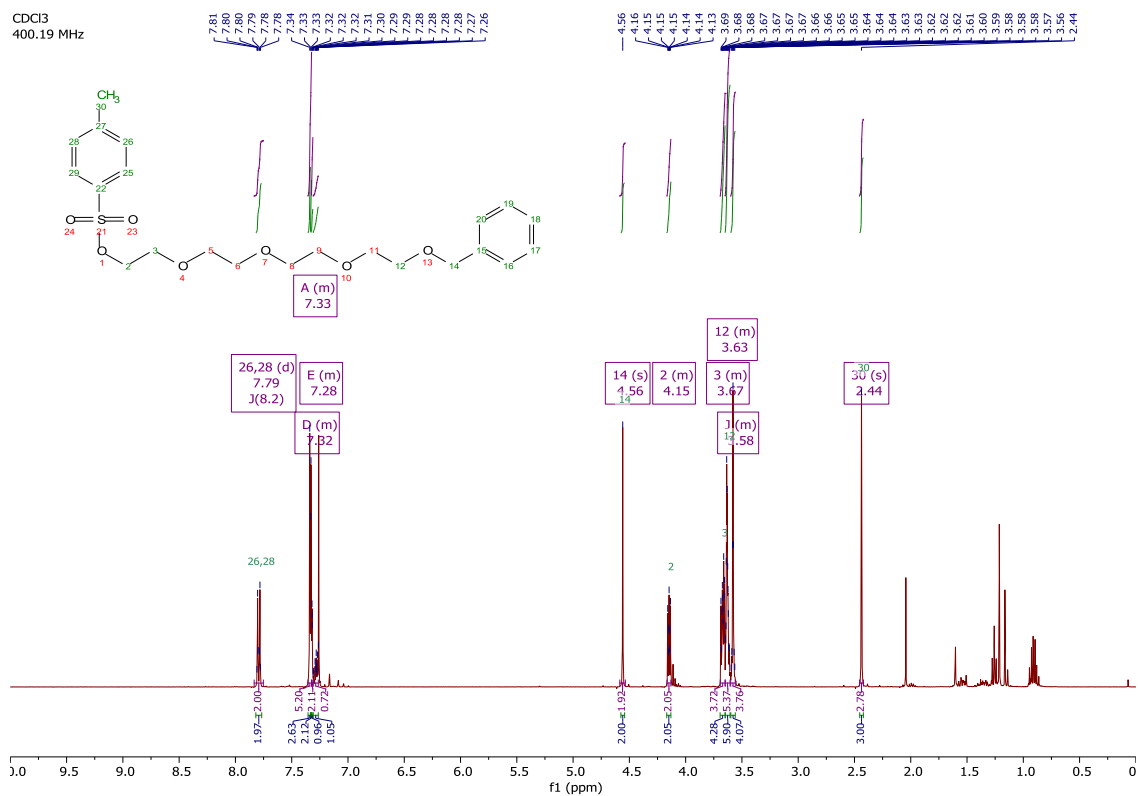


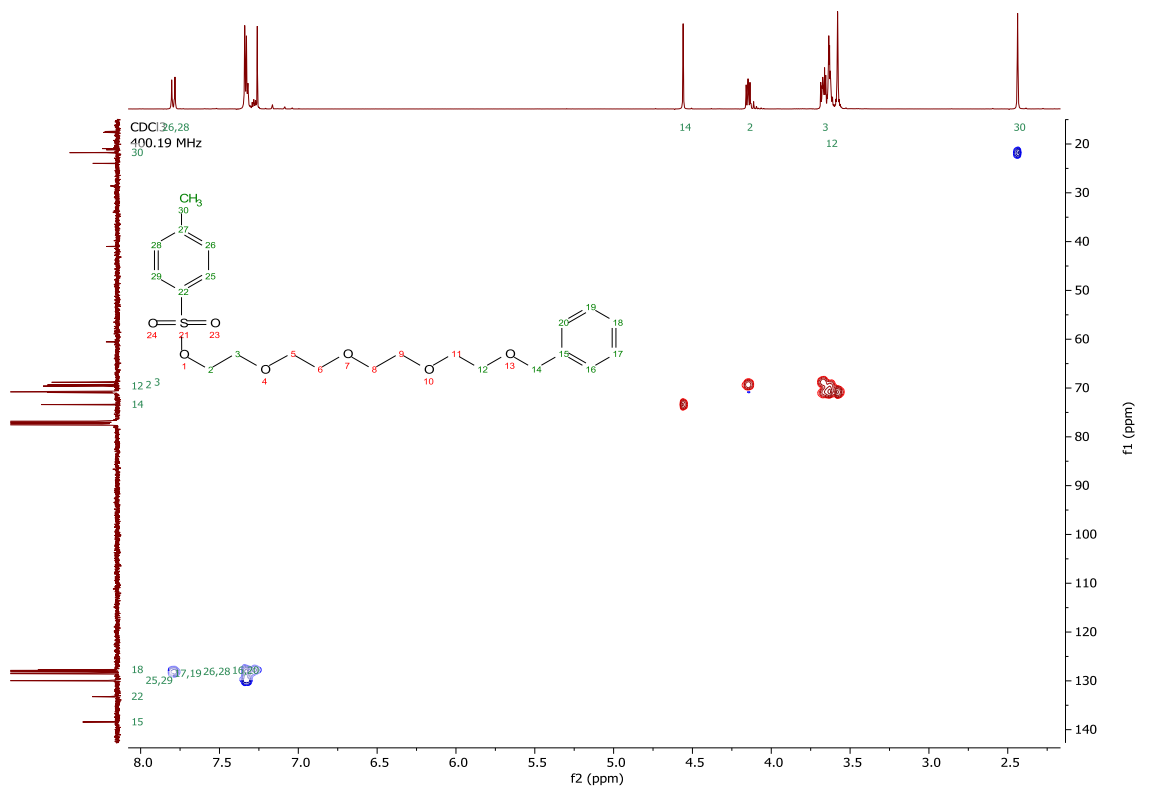
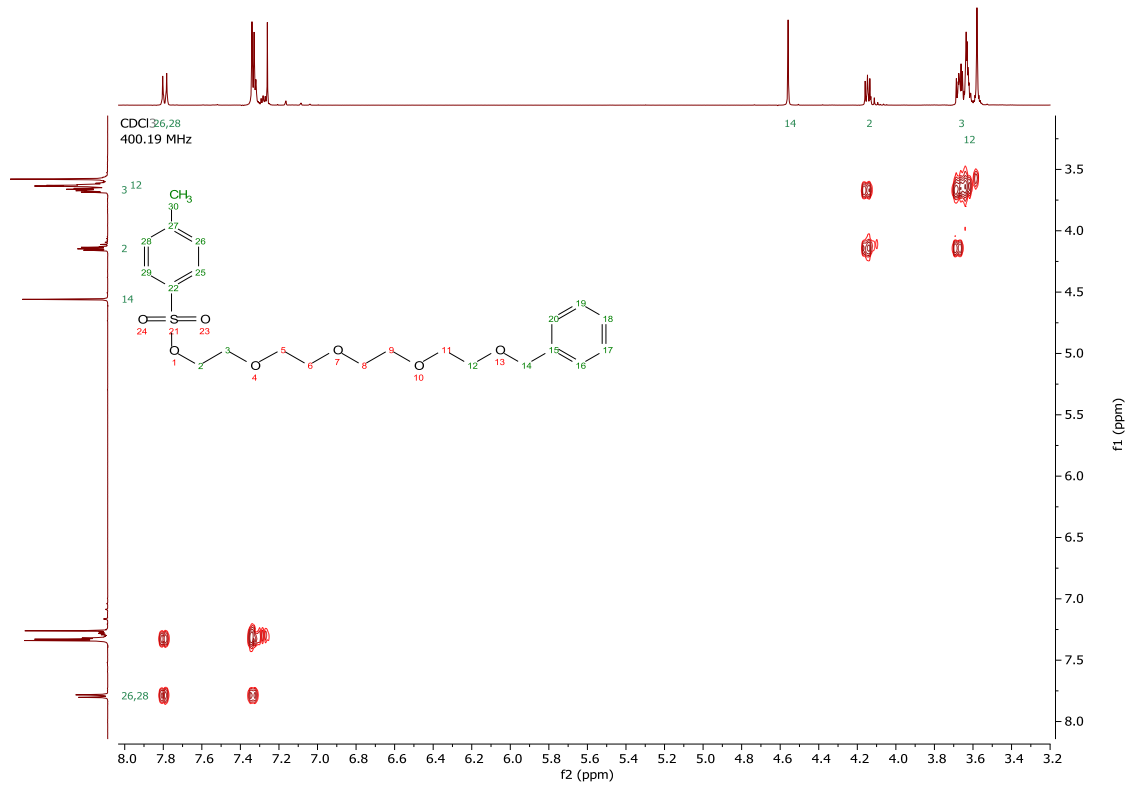
$^1\text{H}$ ,  $^{13}\text{C}$ , HSQC and HMBC NMR spectra of benzyl ether **2.50**.

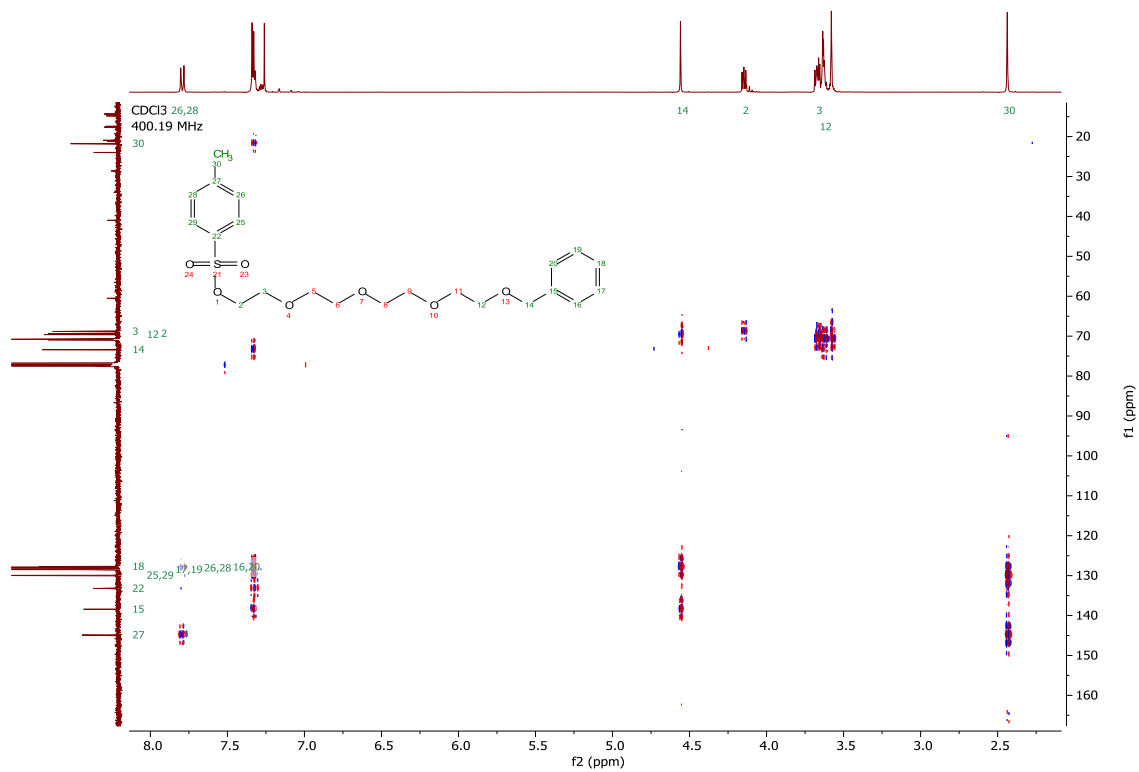




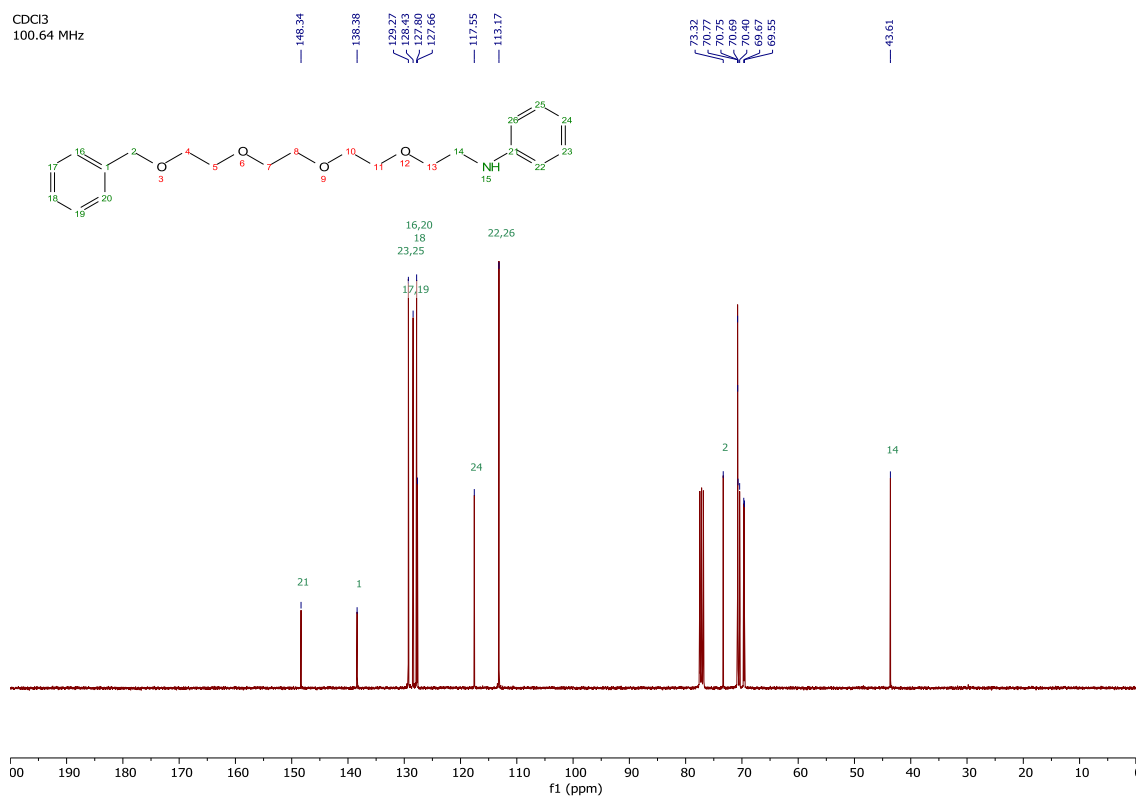
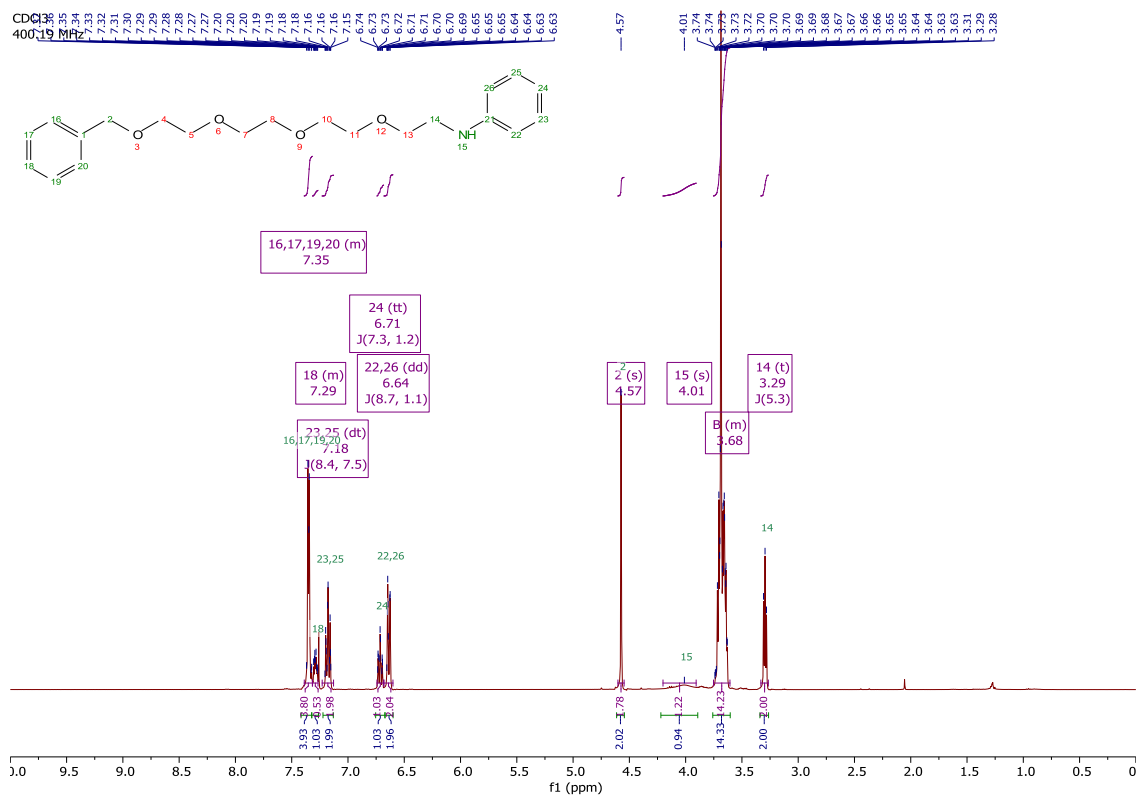
$^1\text{H}$ ,  $^{13}\text{C}$ , COSY, HSQC and HMBC NMR spectra of tosylate **2.51**.

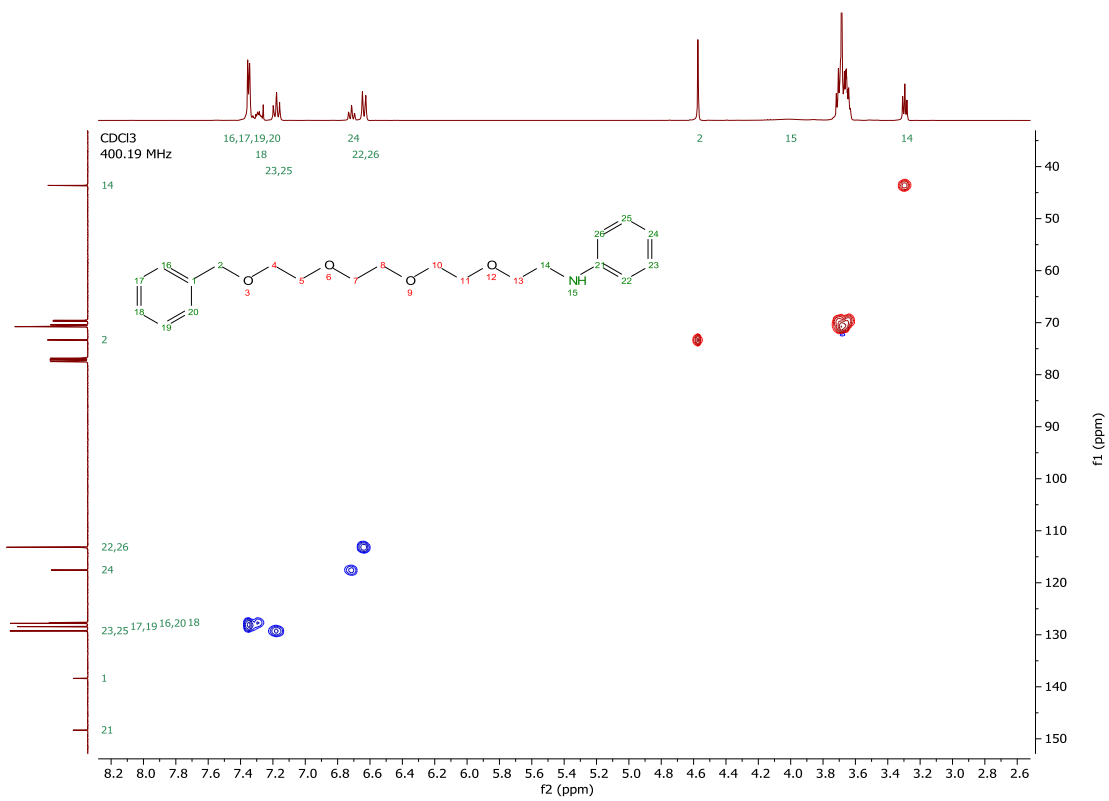
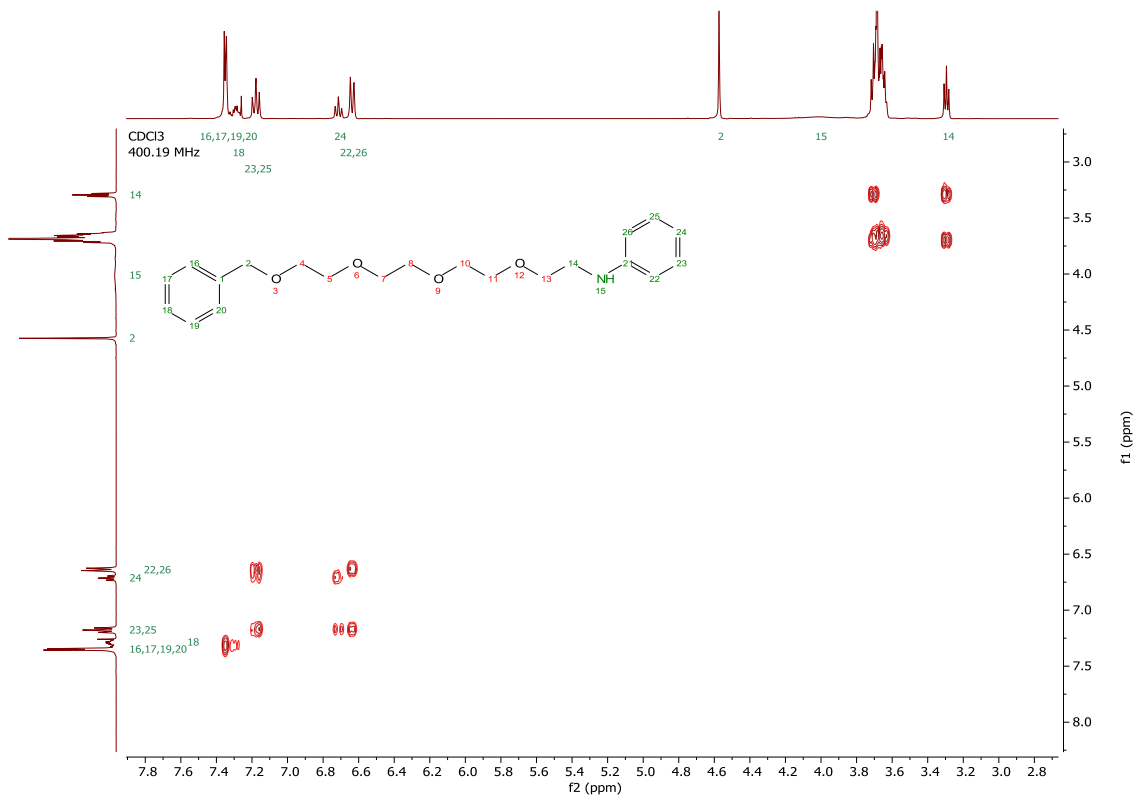


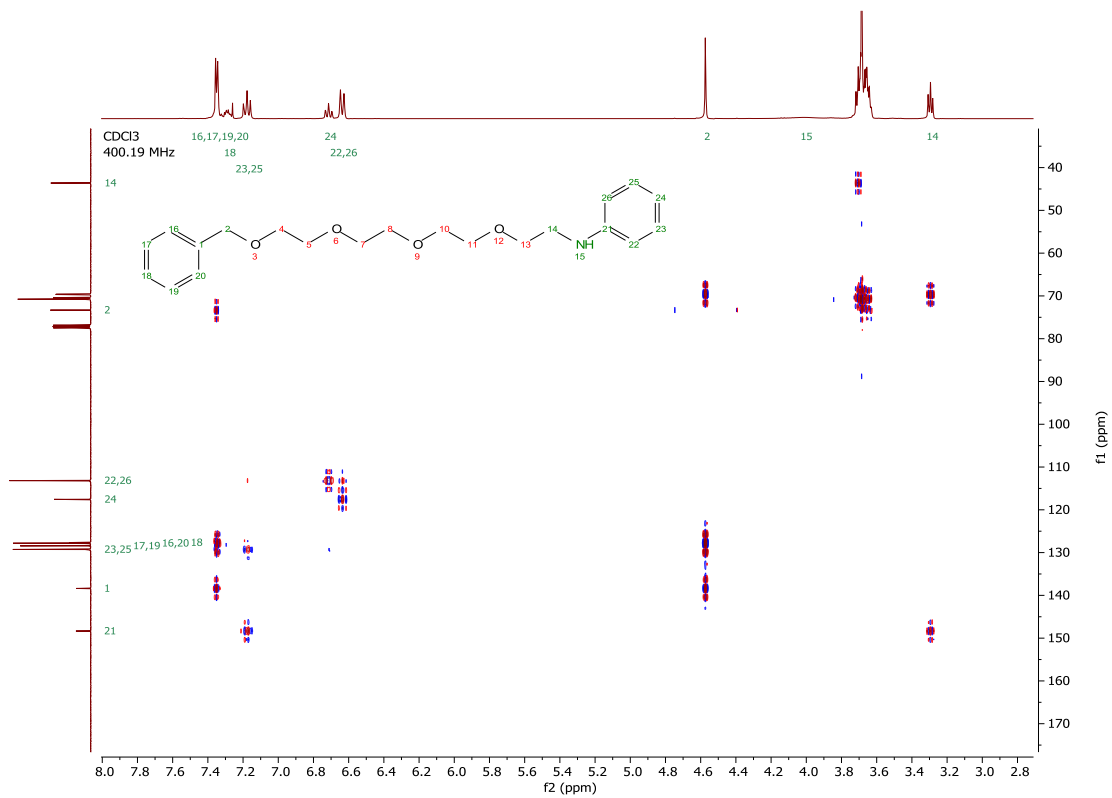




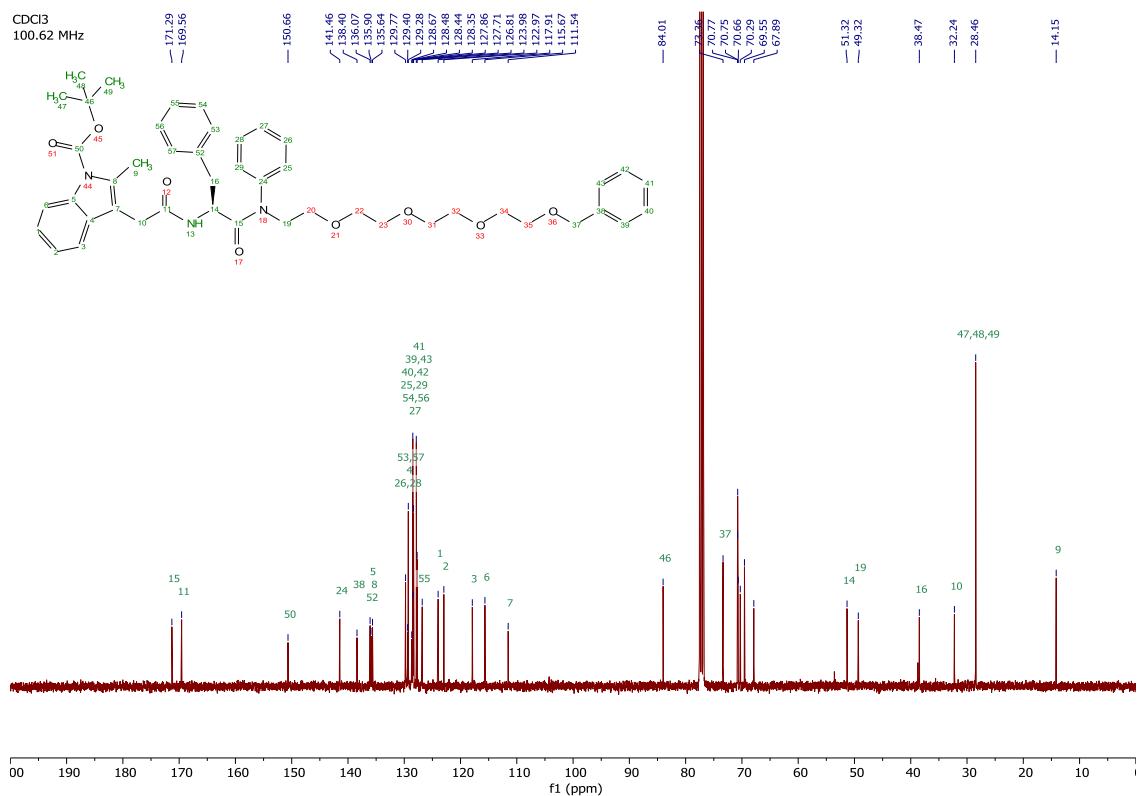
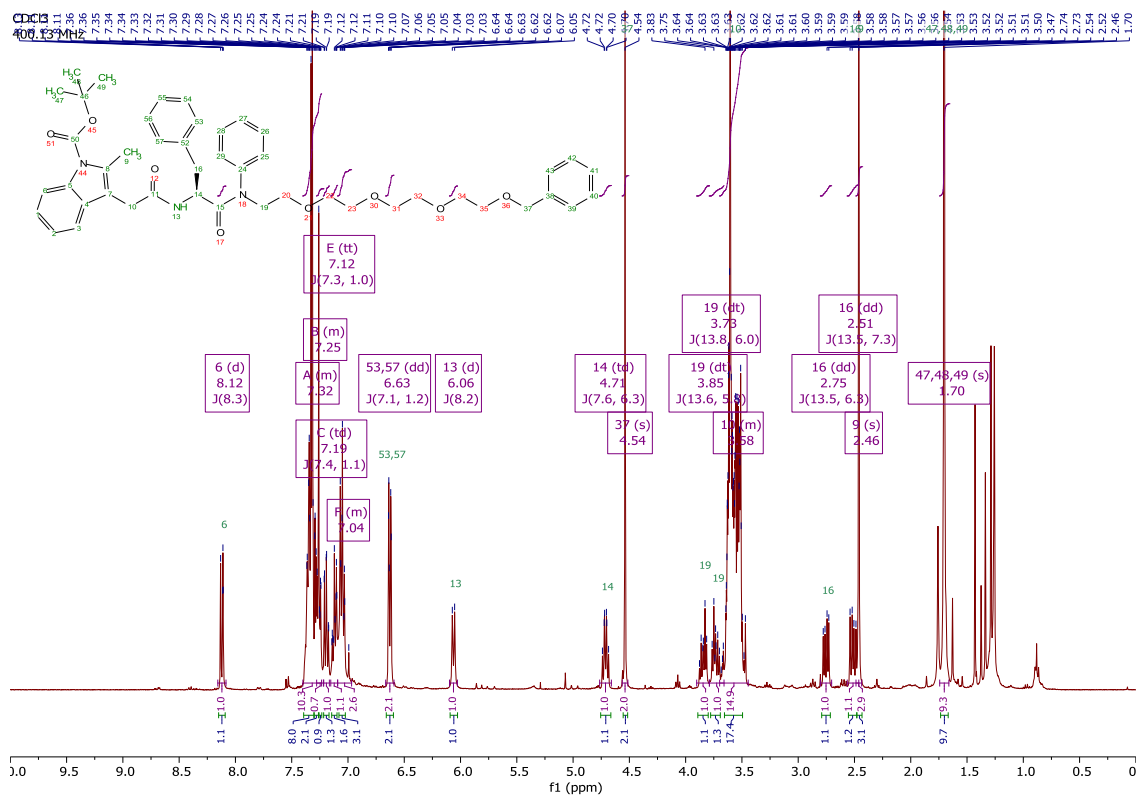
$^1\text{H}$ ,  $^{13}\text{C}$ , COSY HSQC and HMBC NMR spectra of aniline **2.52**.

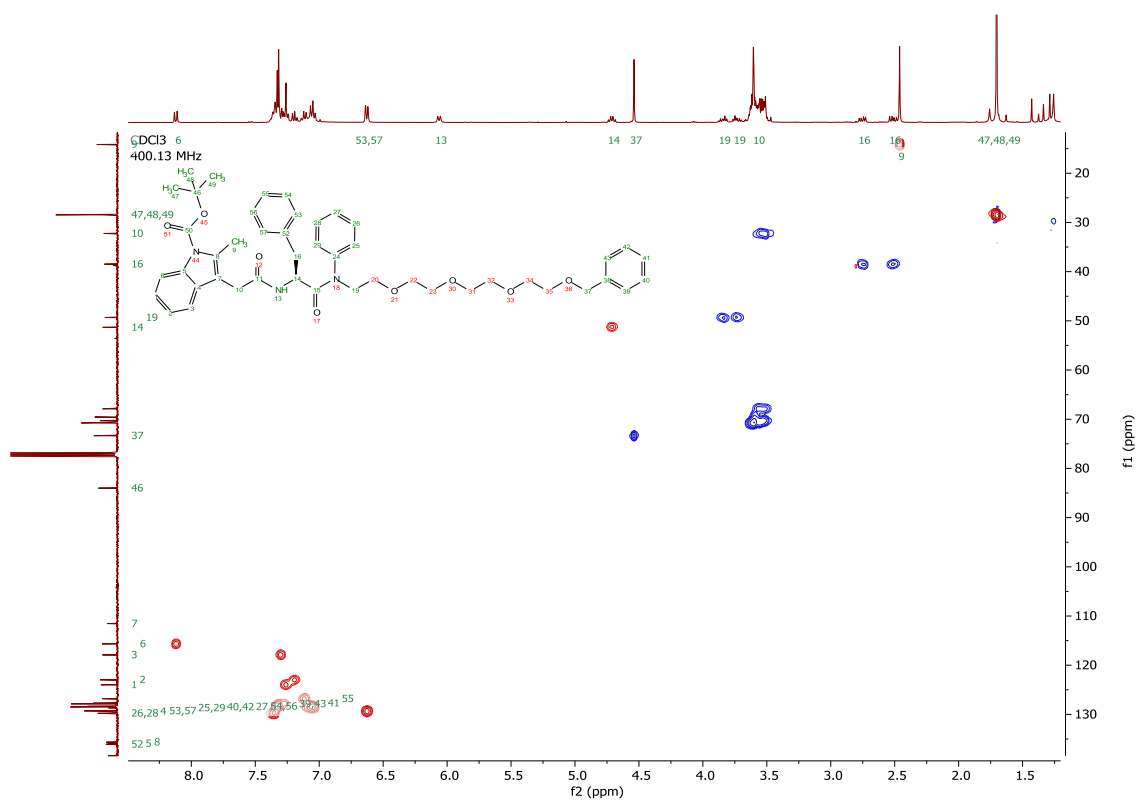
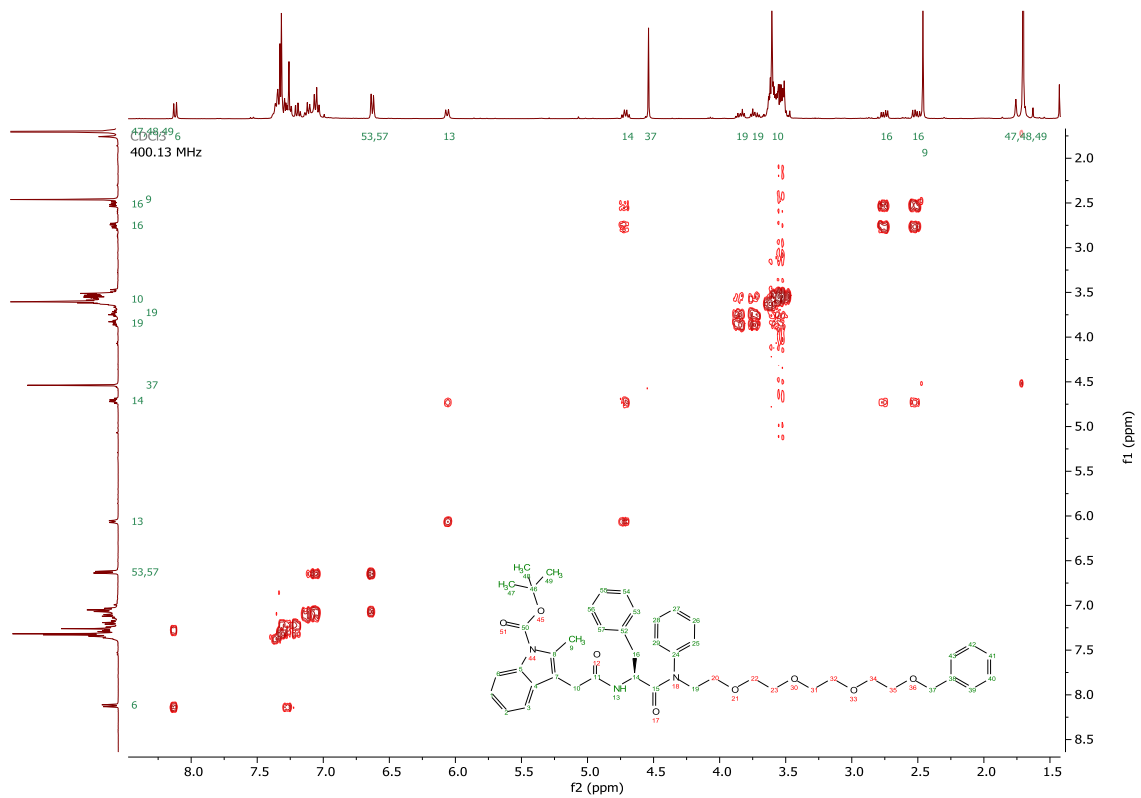


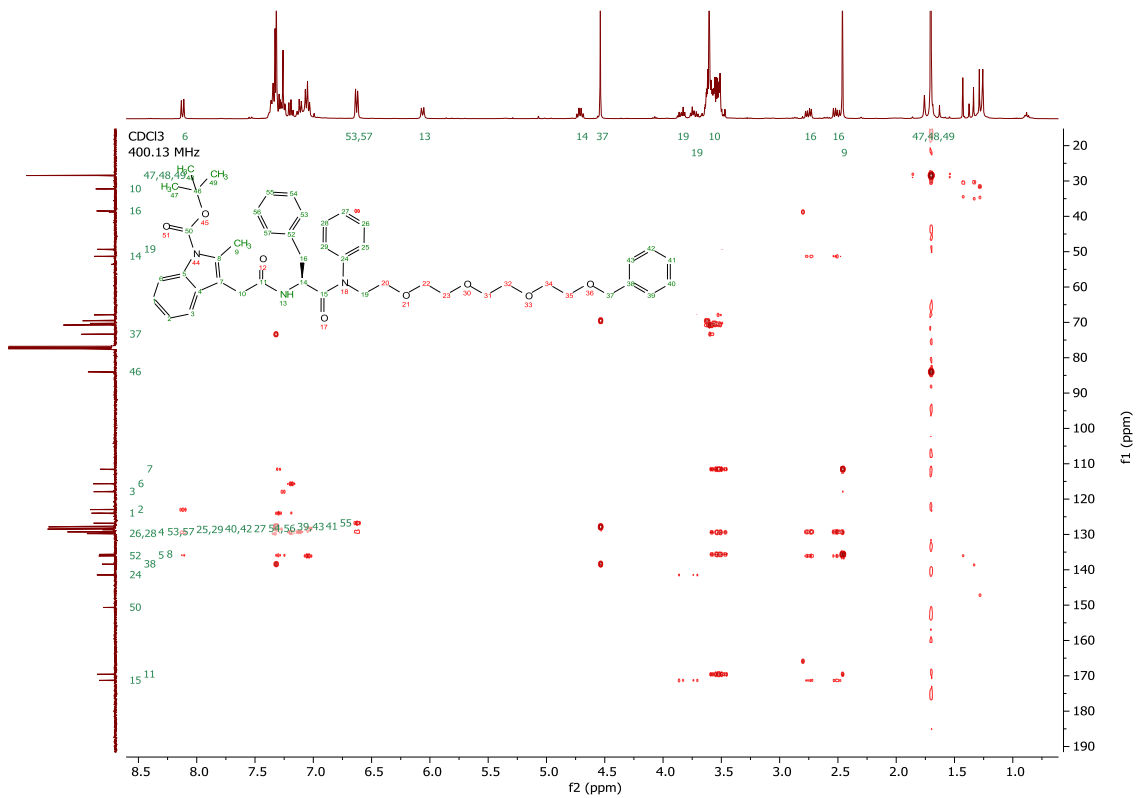




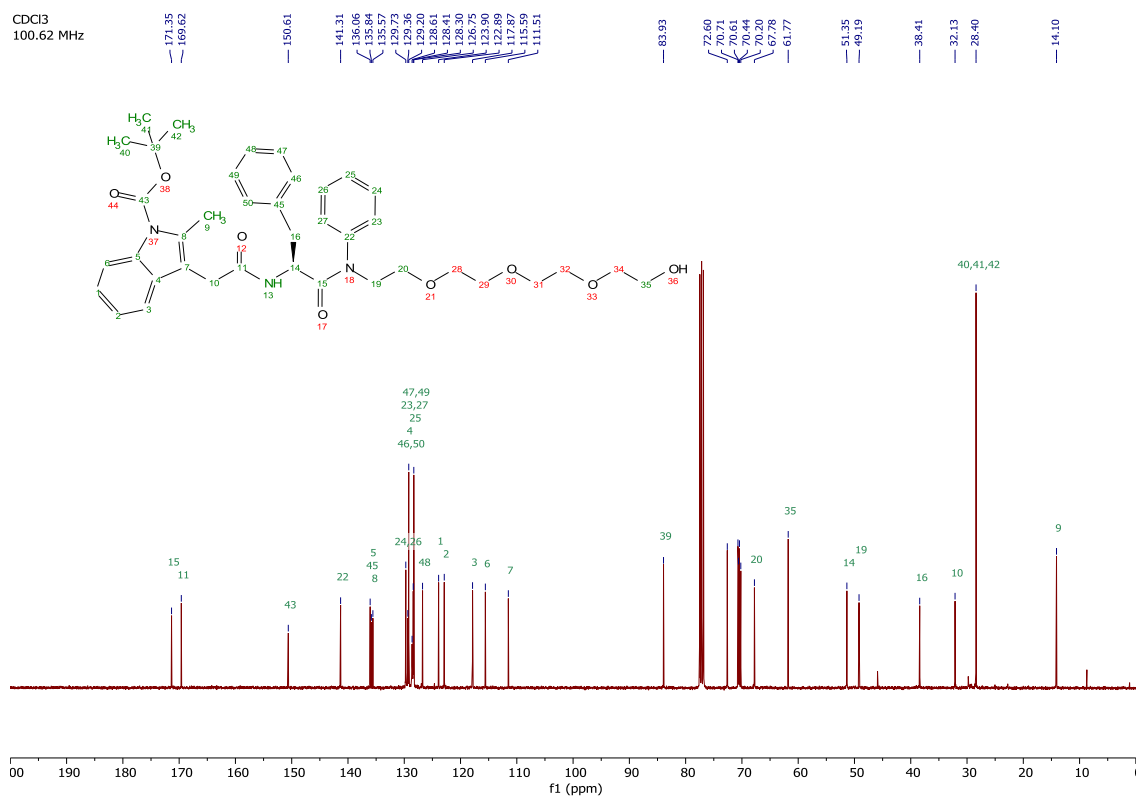
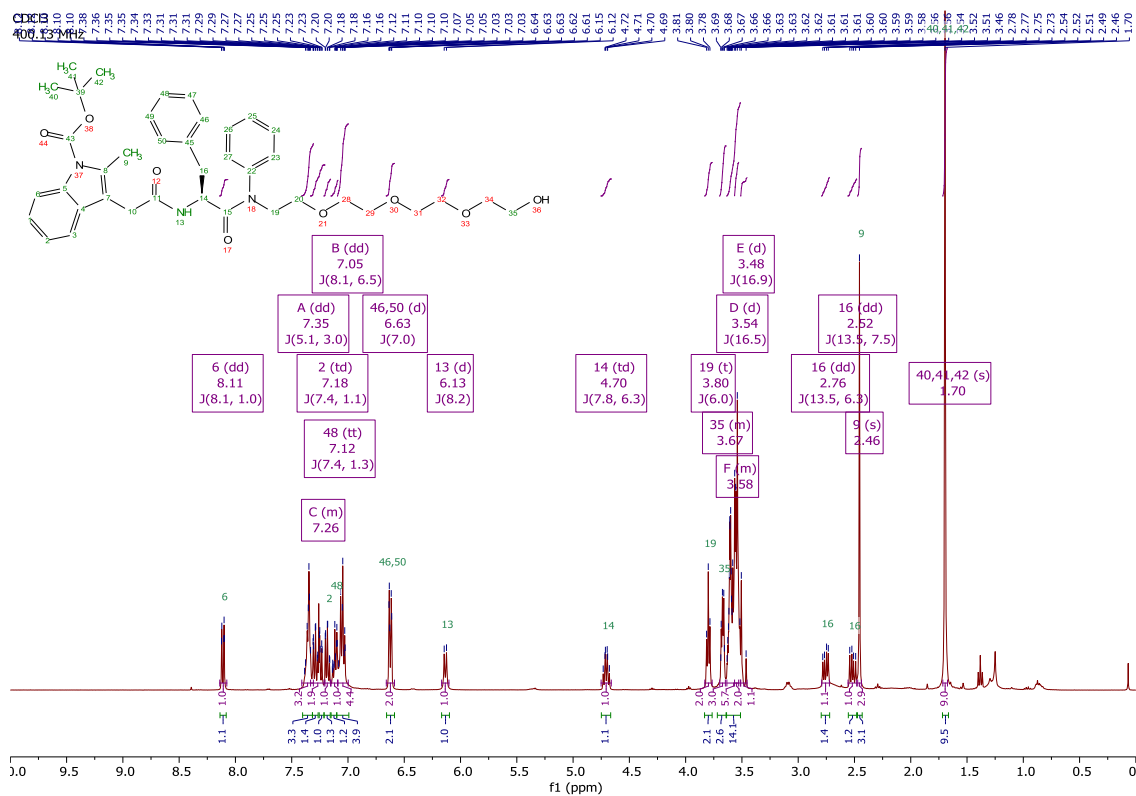
$^1\text{H}$ ,  $^{13}\text{C}$ , COSY HSQC and HMBC NMR spectra of benzyl ether **2.55**.

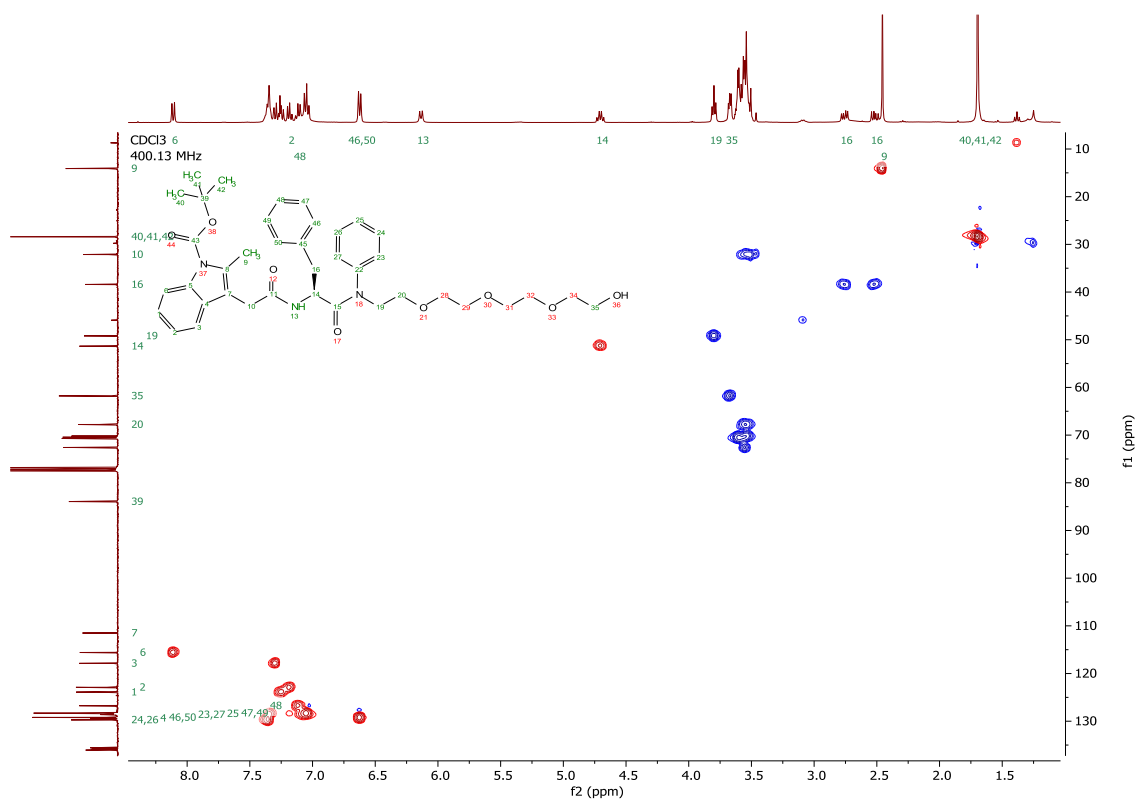
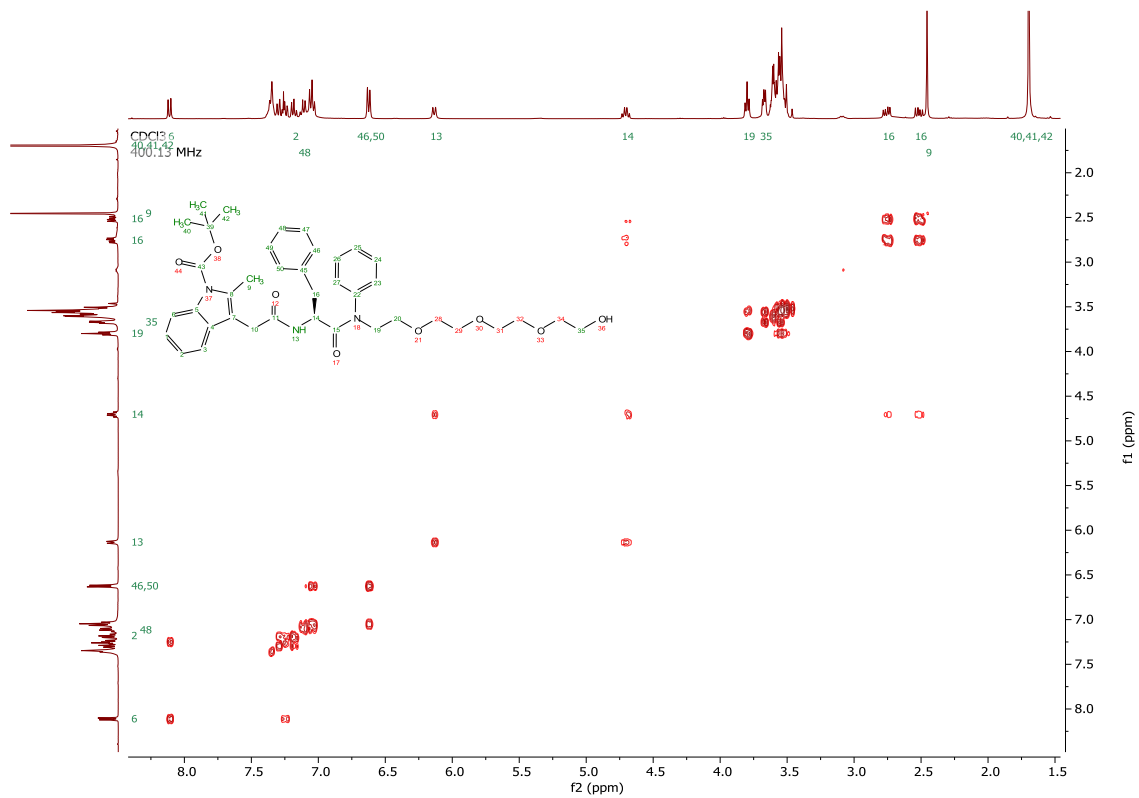


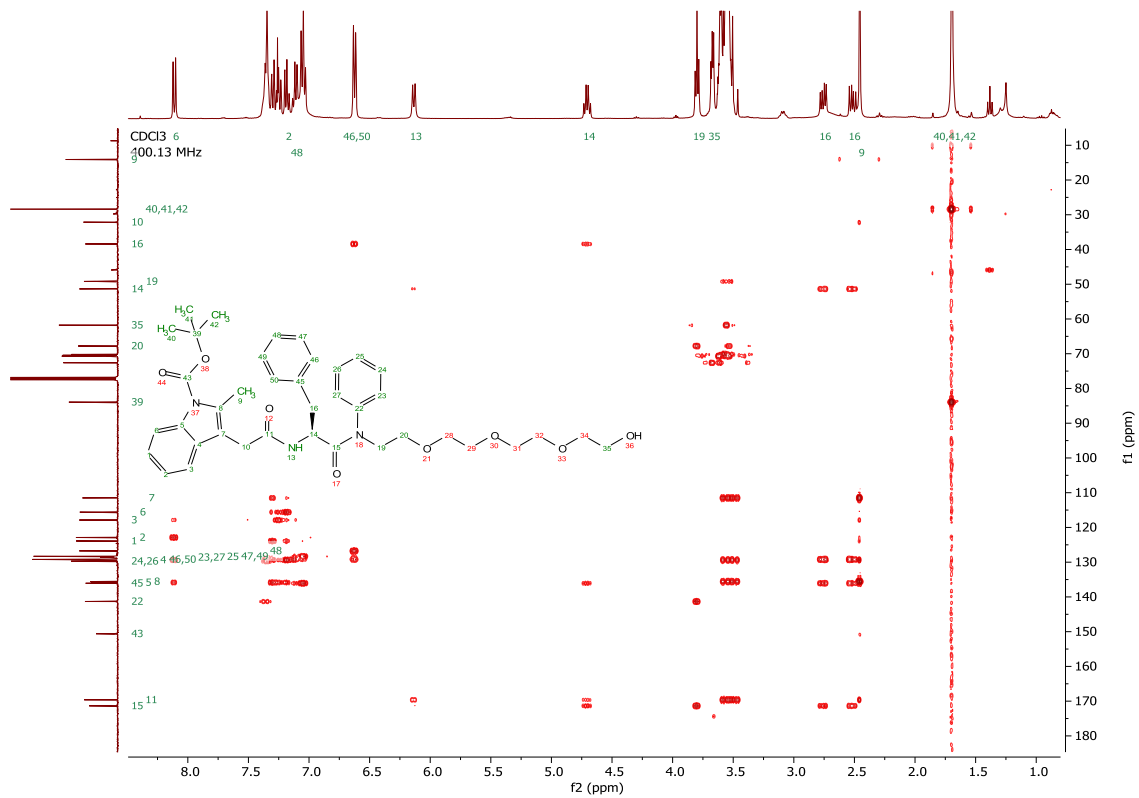




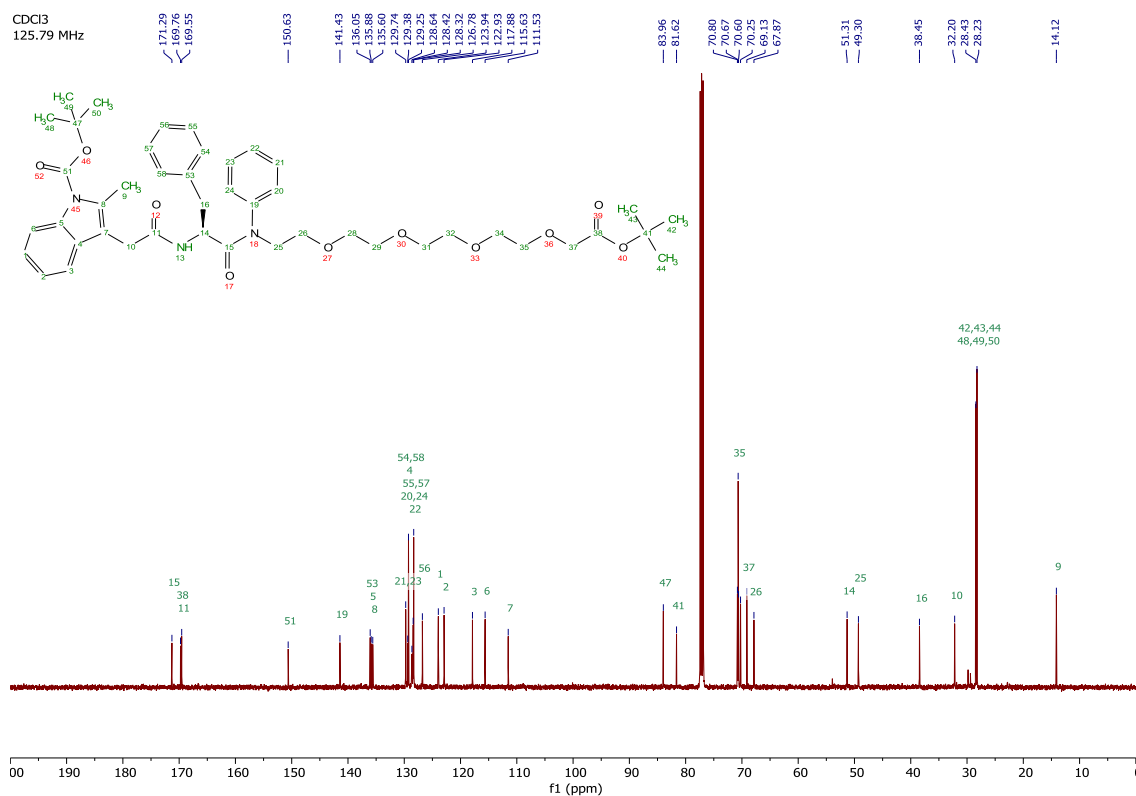
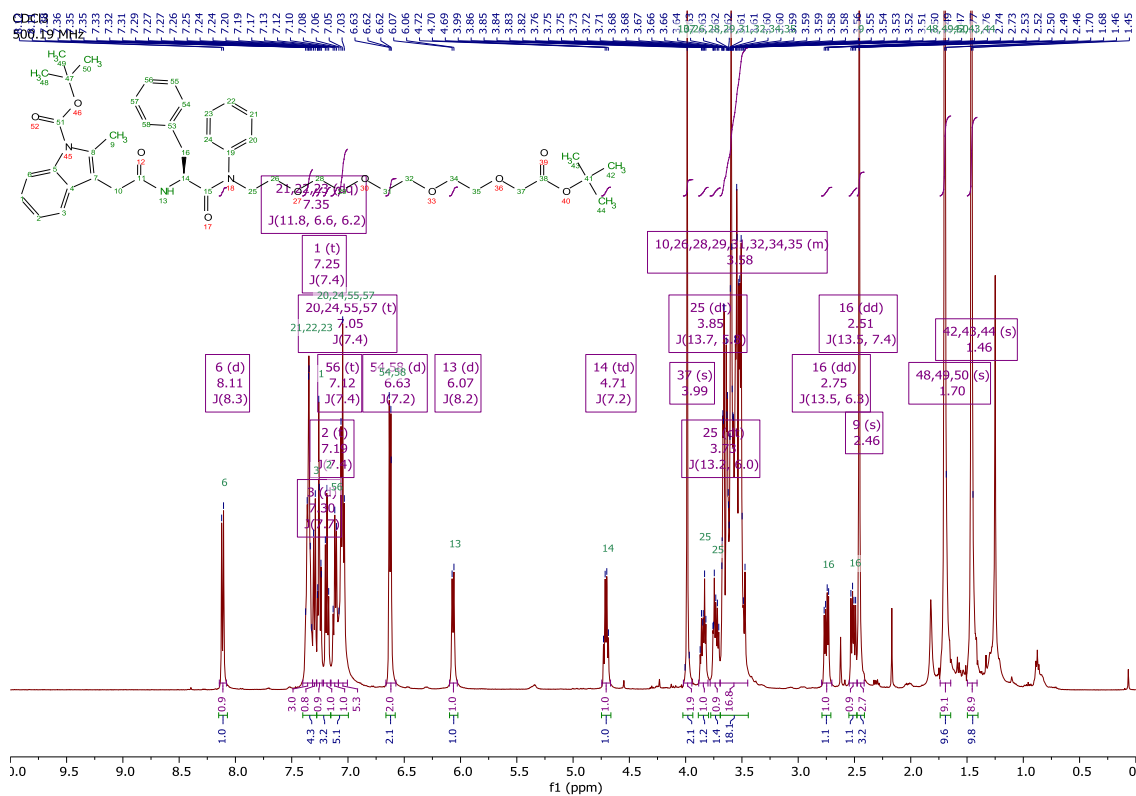
$^1\text{H}$ ,  $^{13}\text{C}$ , COSY HSQC and HMBC NMR spectra of alcohol **2.56**.

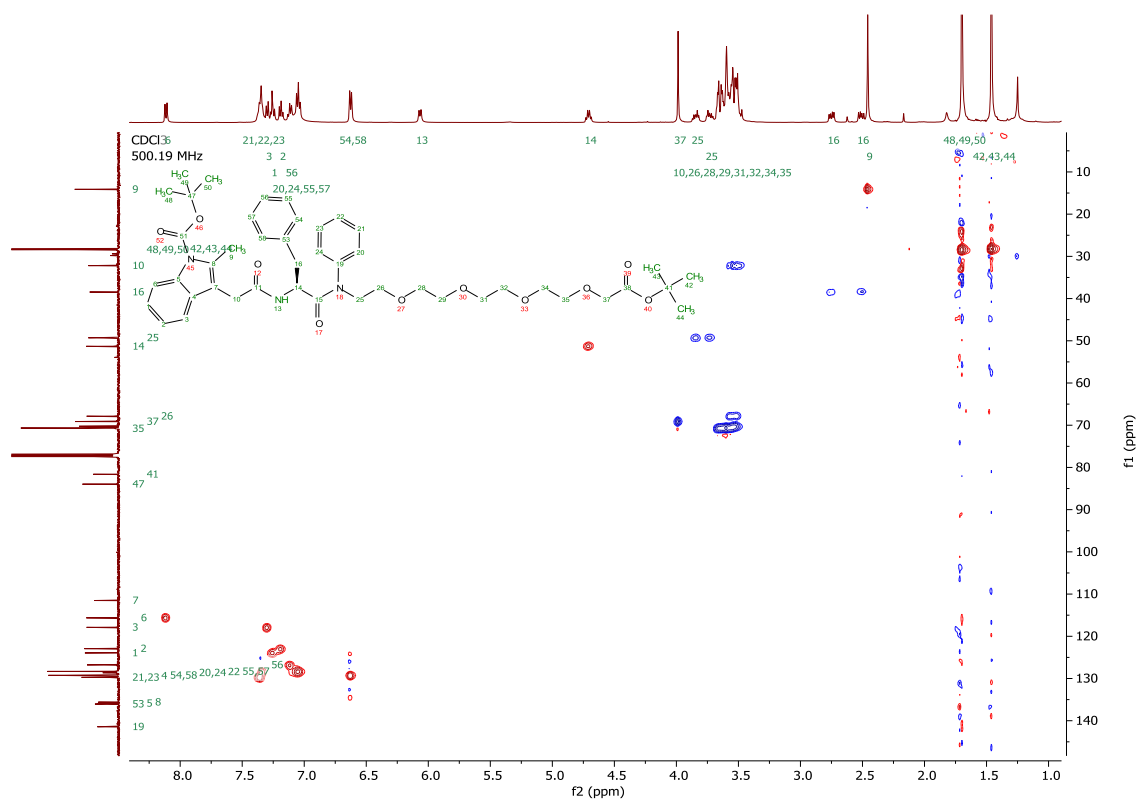
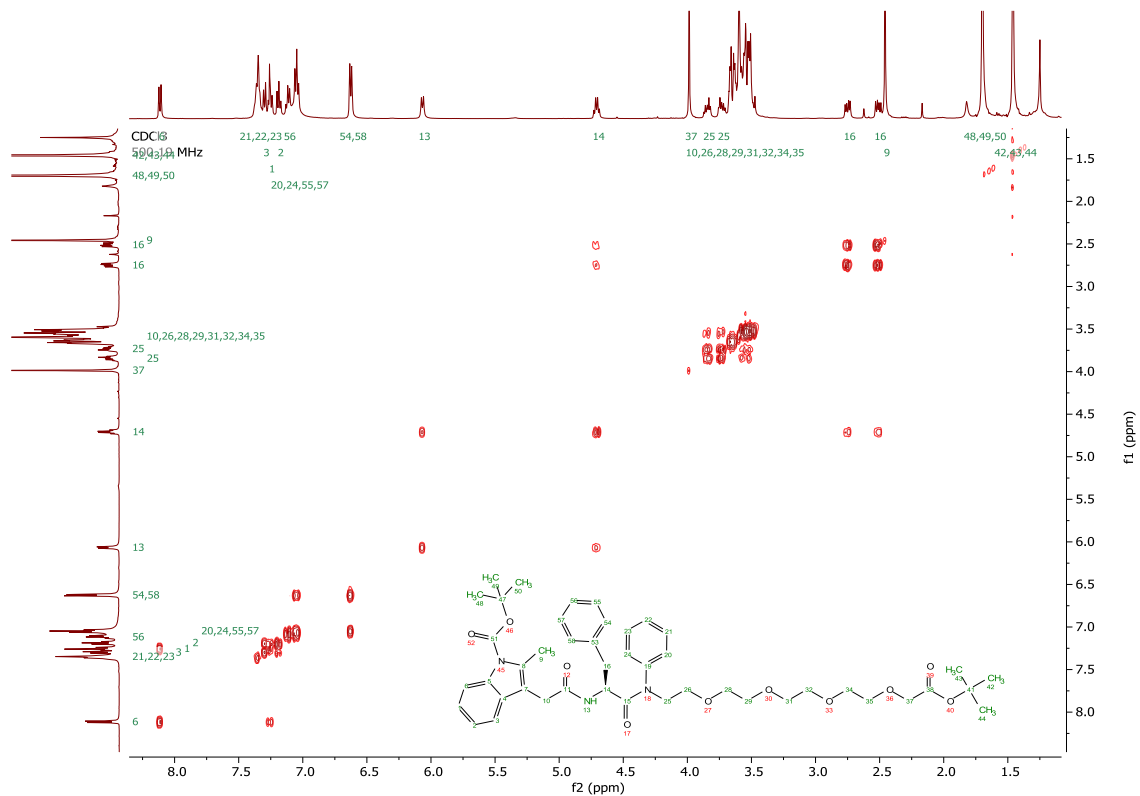


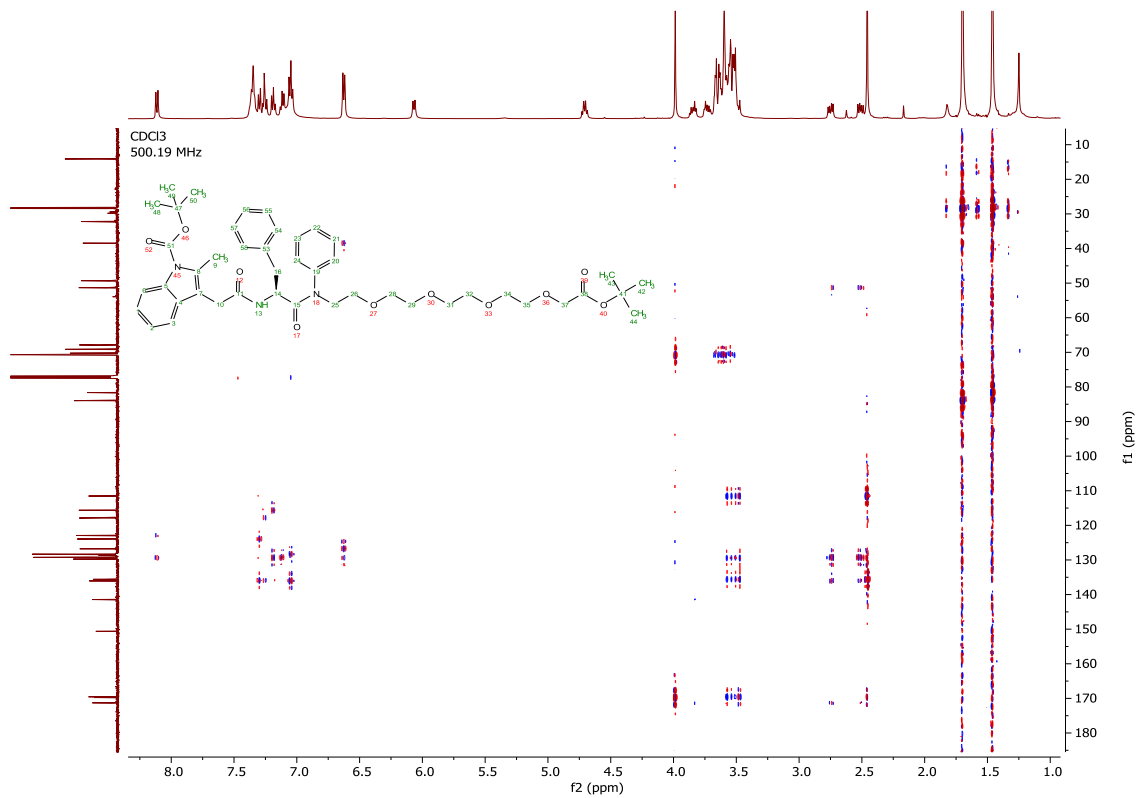




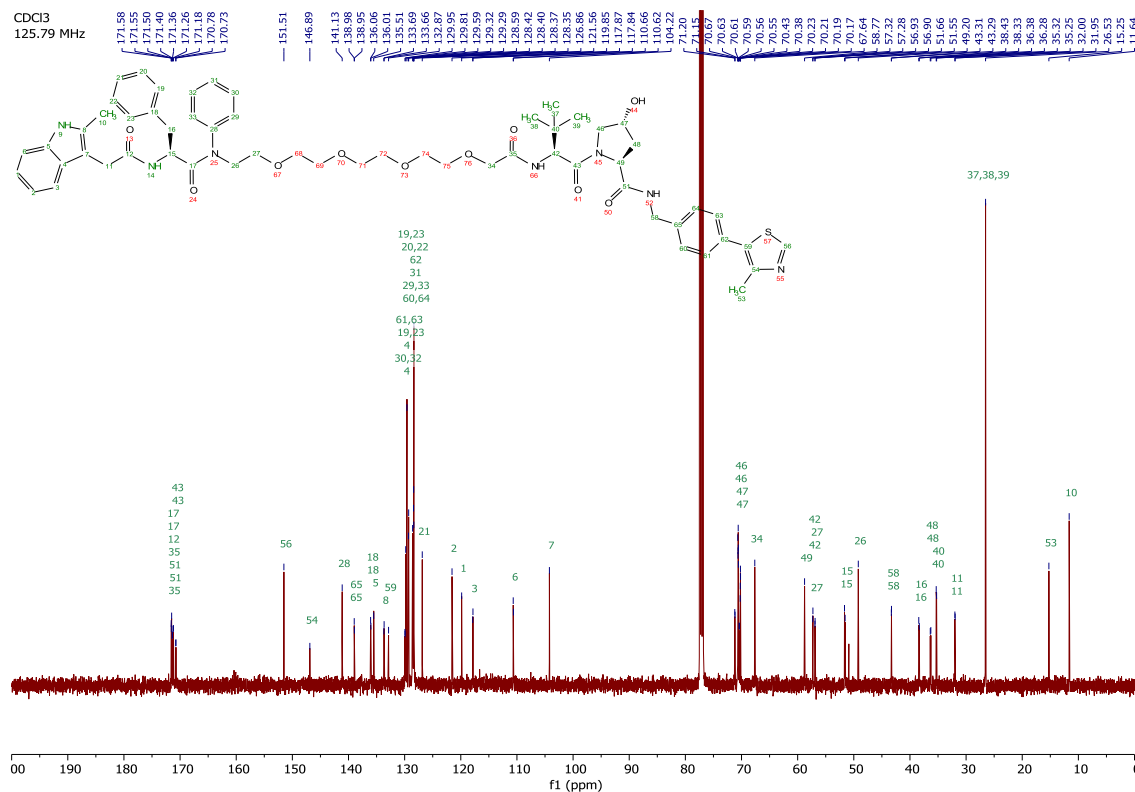
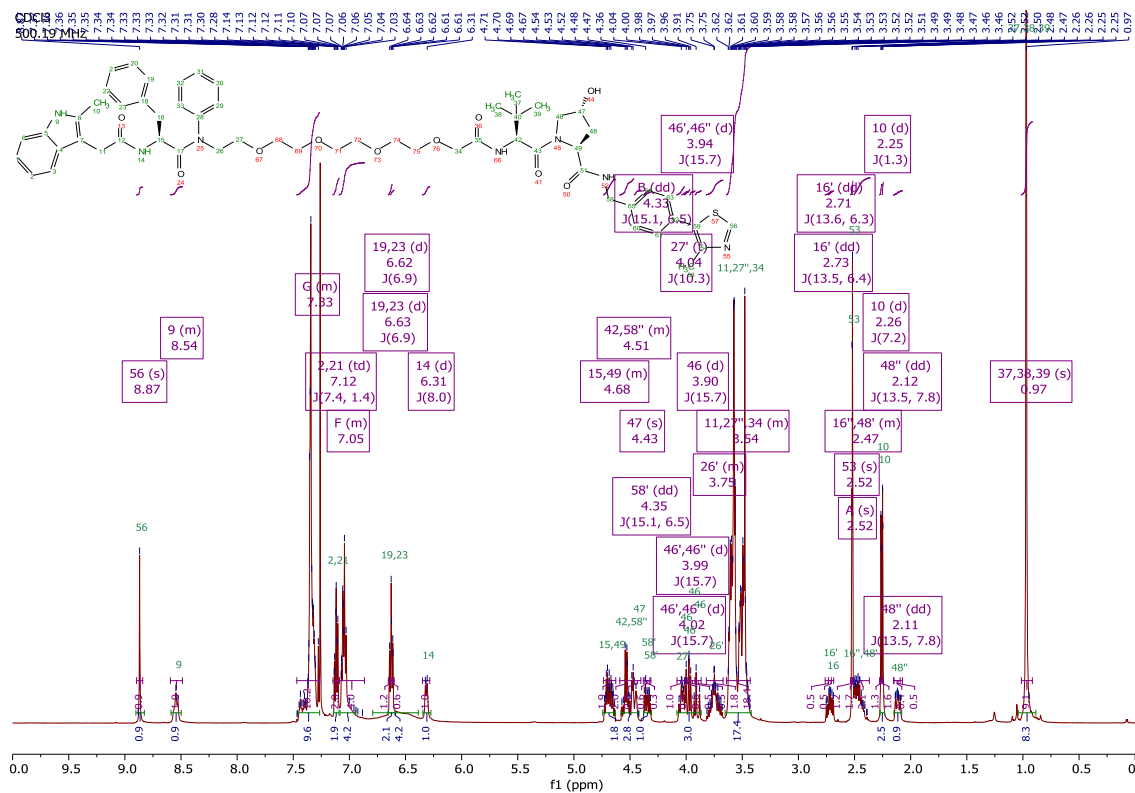
$^1\text{H}$ ,  $^{13}\text{C}$ , COSY HSQC and HMBC NMR spectra of *tert*-butyl ester **2.57**.

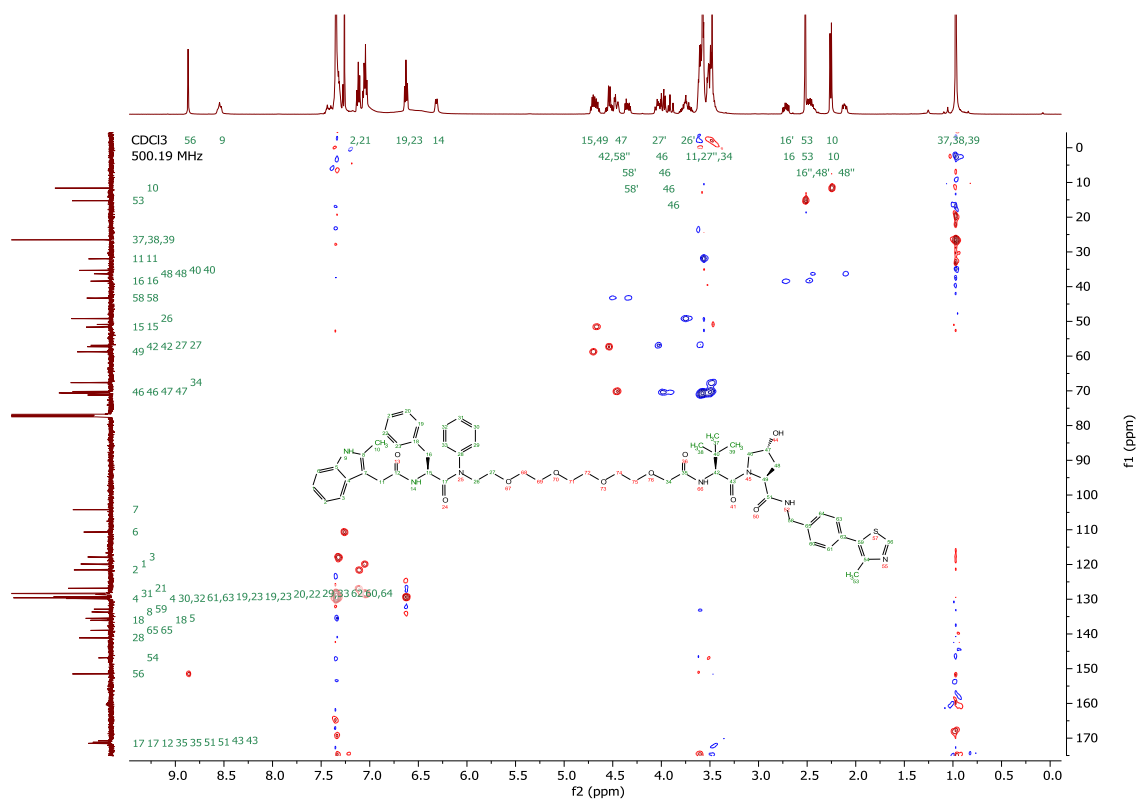
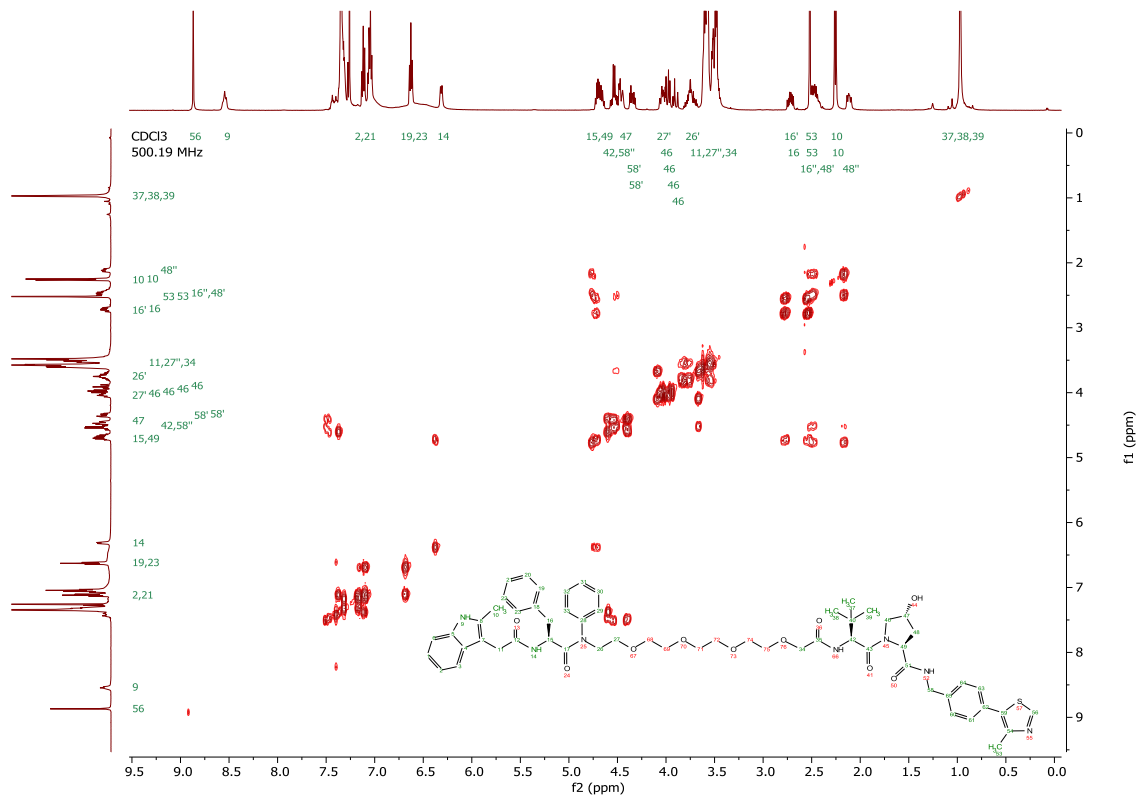


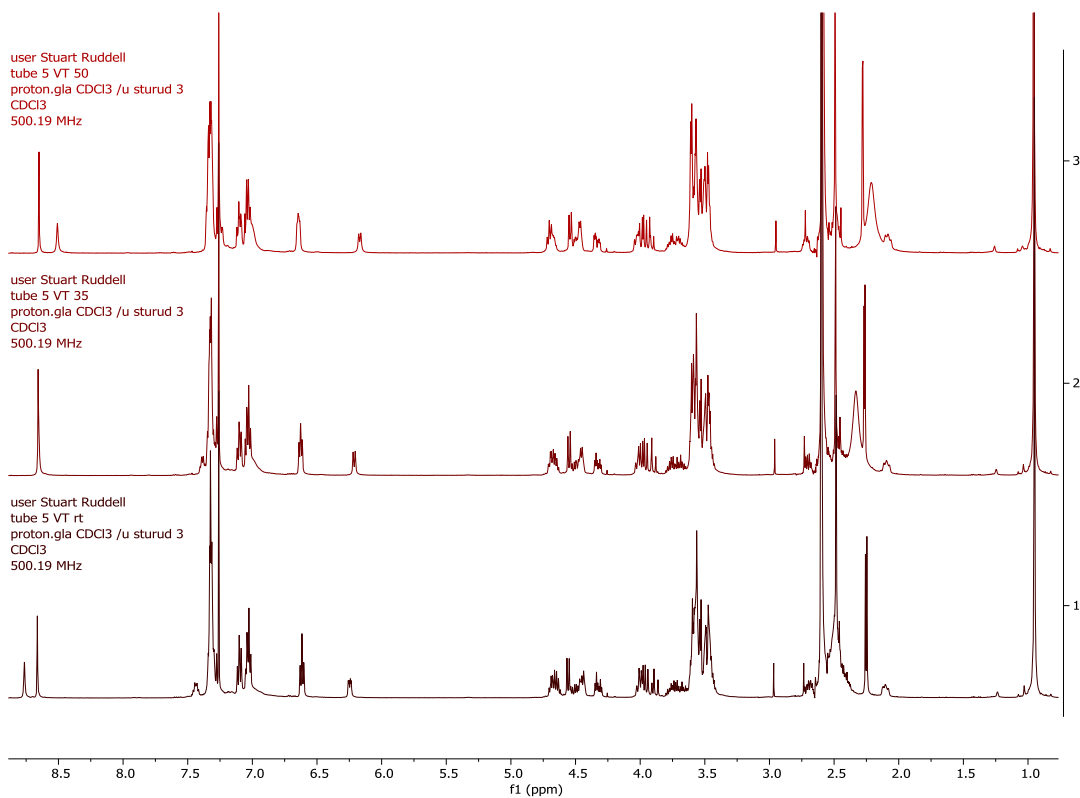
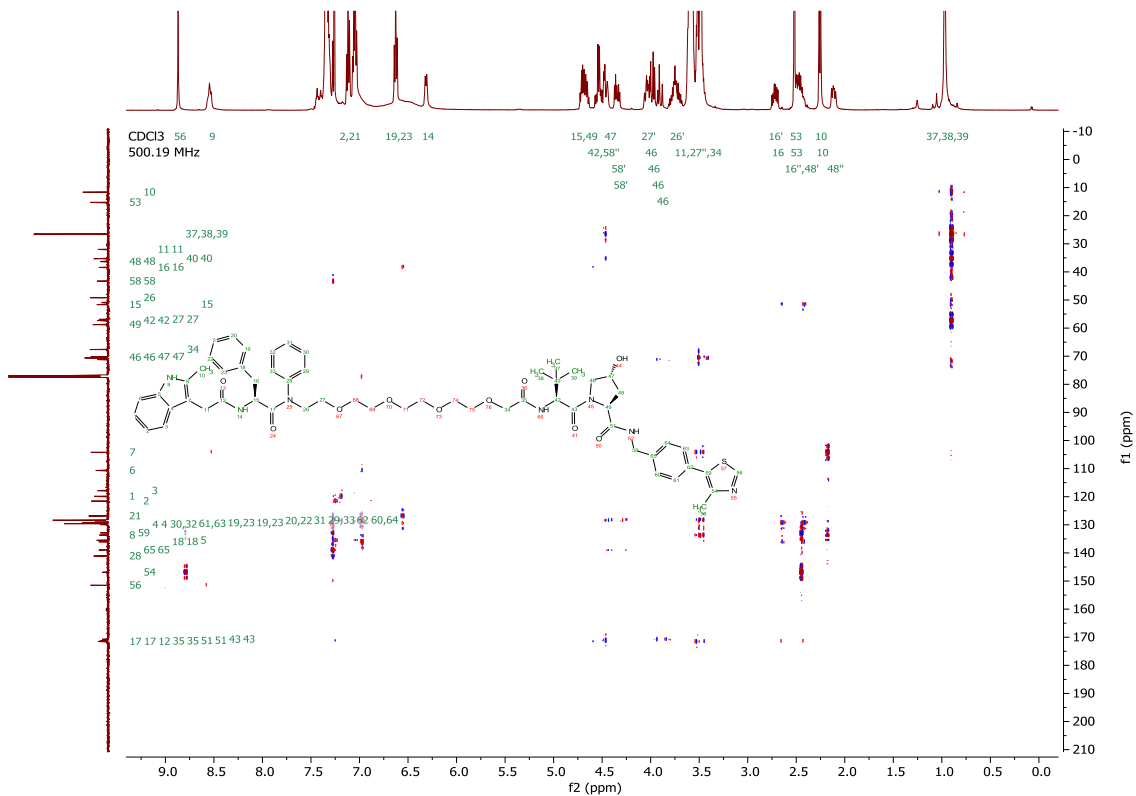




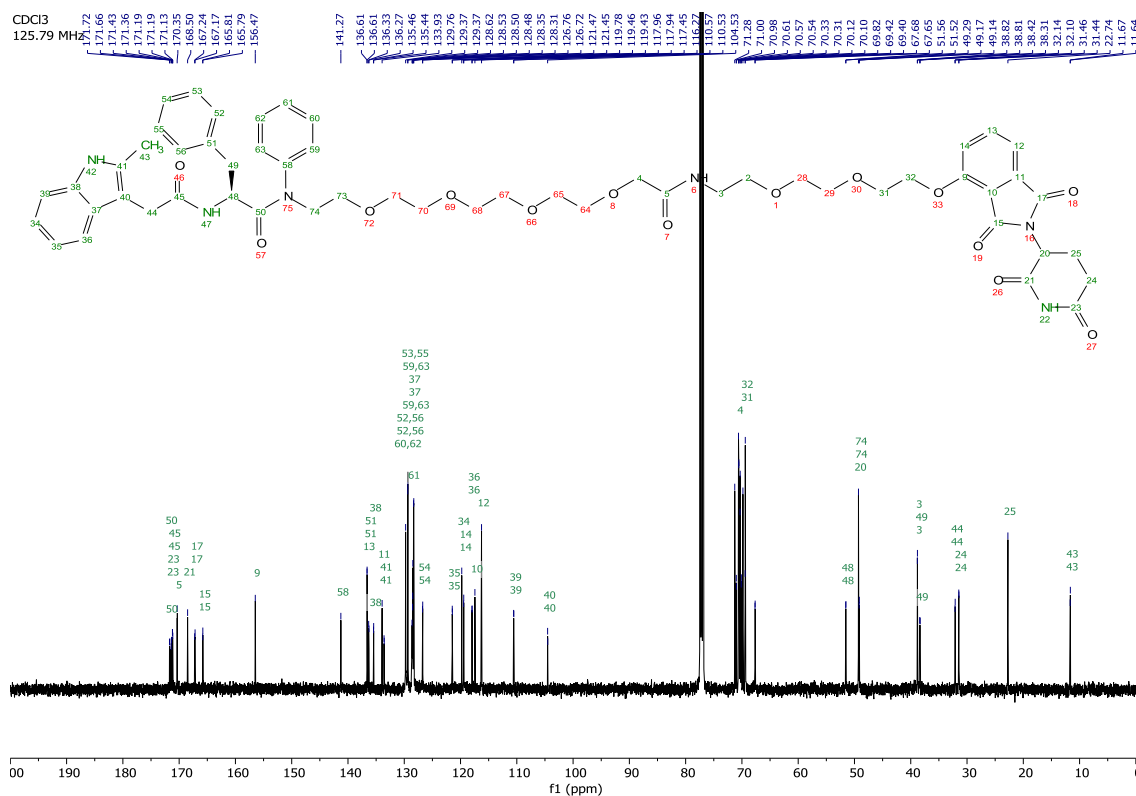
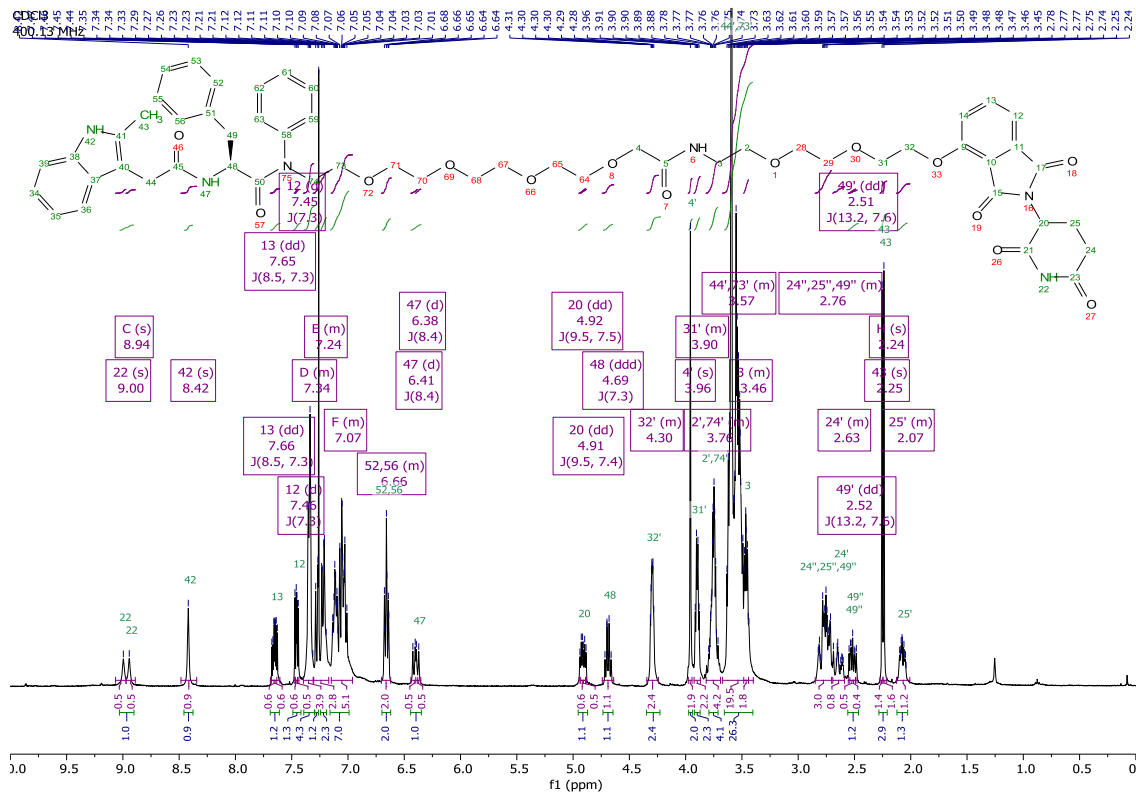
<sup>1</sup>H, <sup>13</sup>C, COSY, HSQC, HMBC and VT (rt, 35 °C, 50 °C) NMR spectra of PROTAC VHL-13.

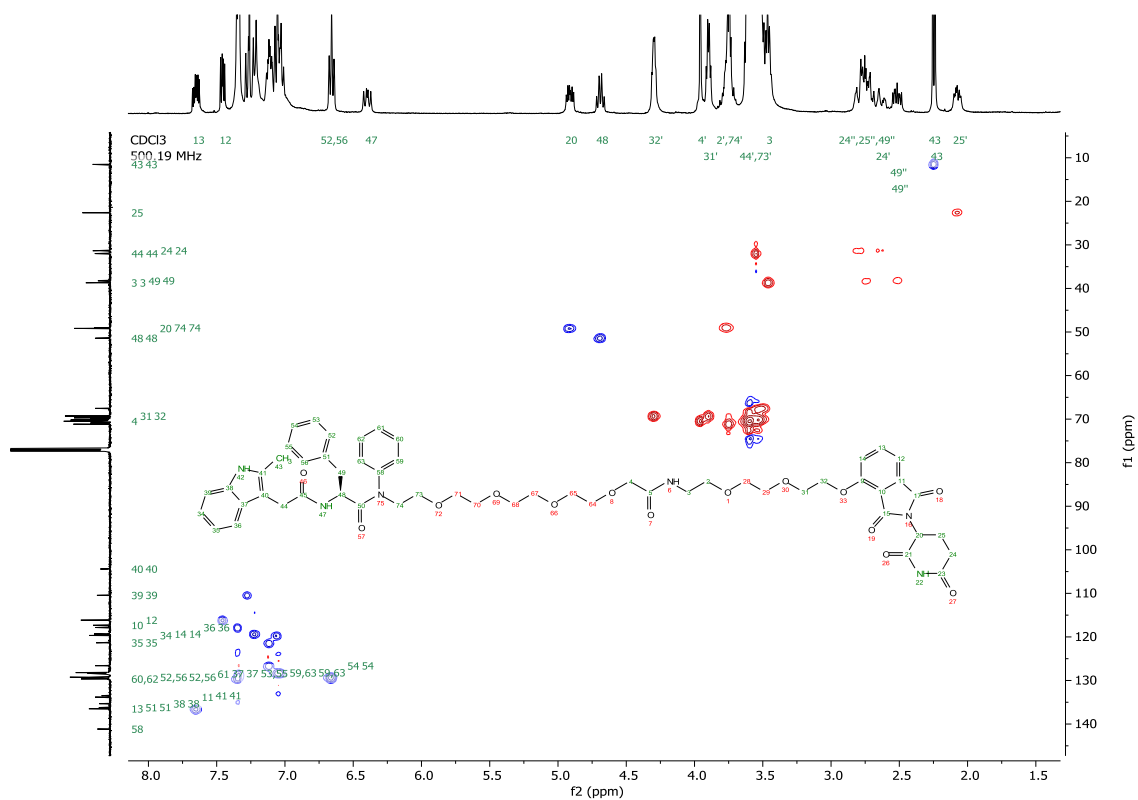
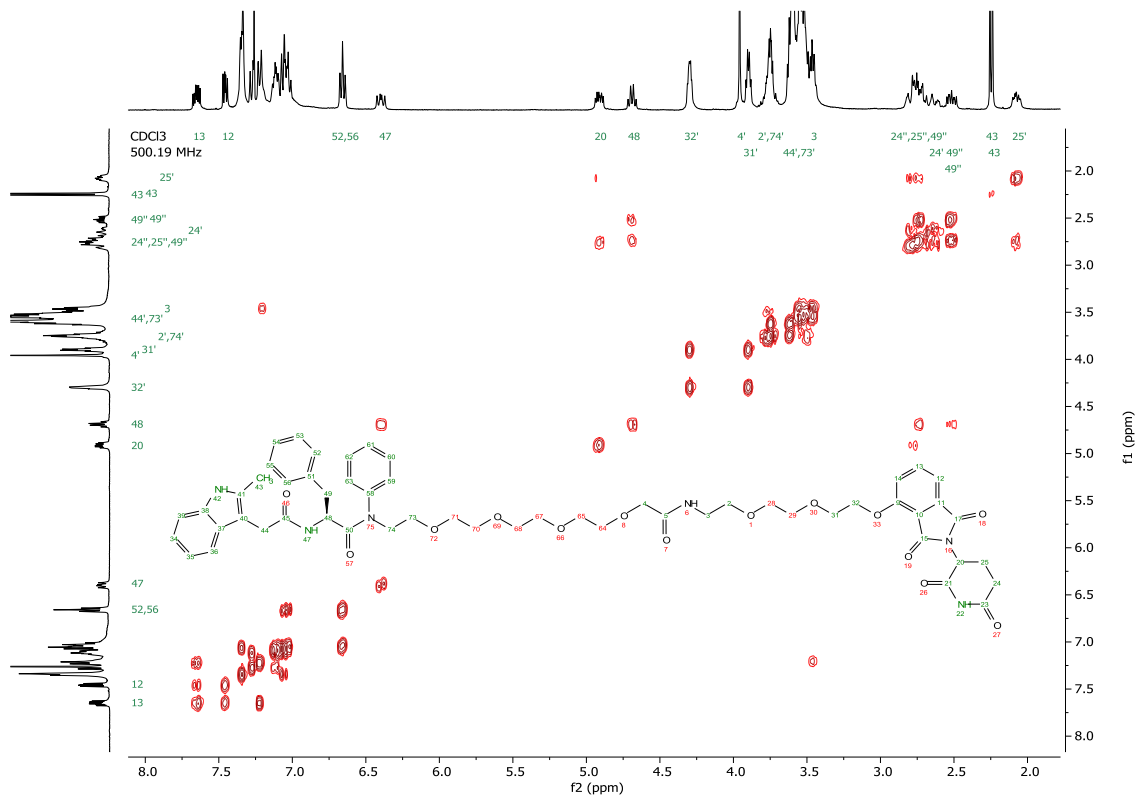


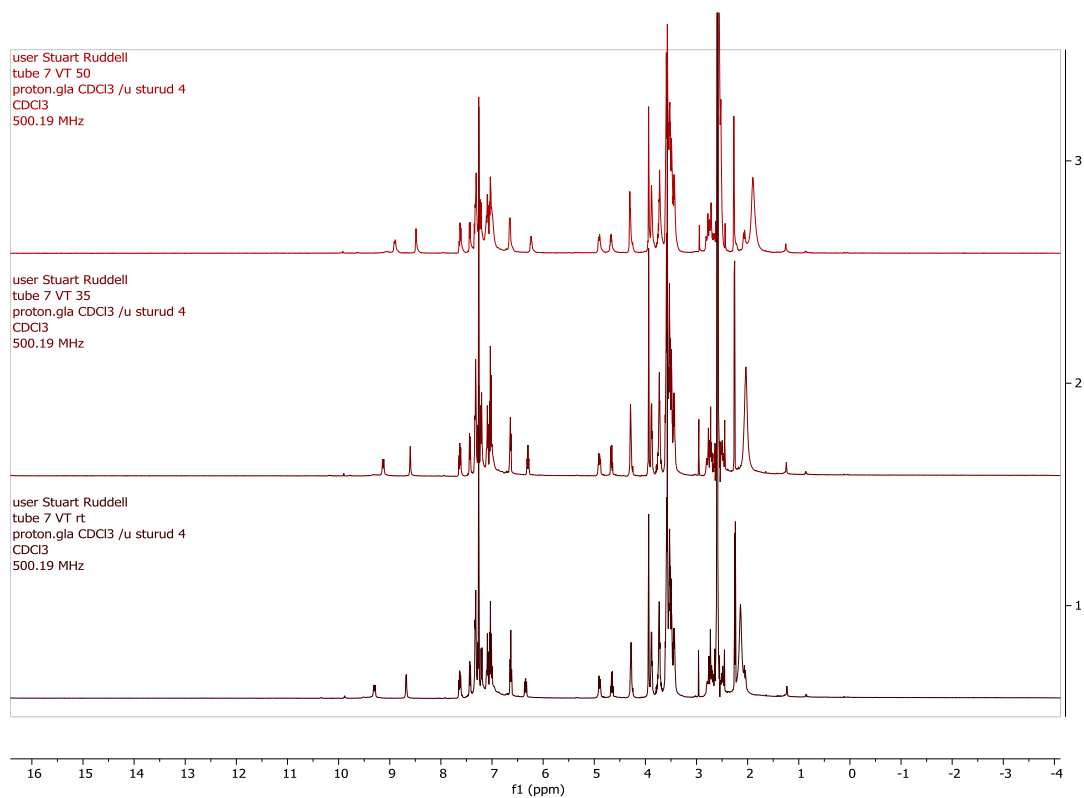
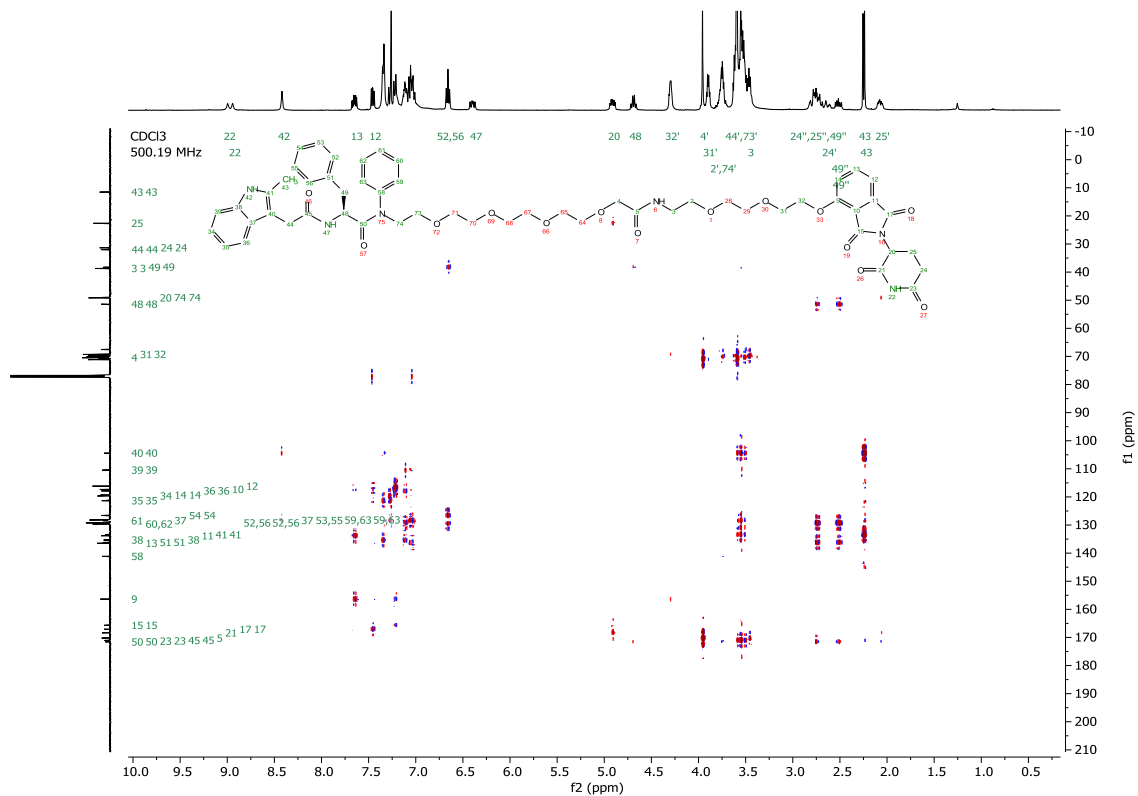




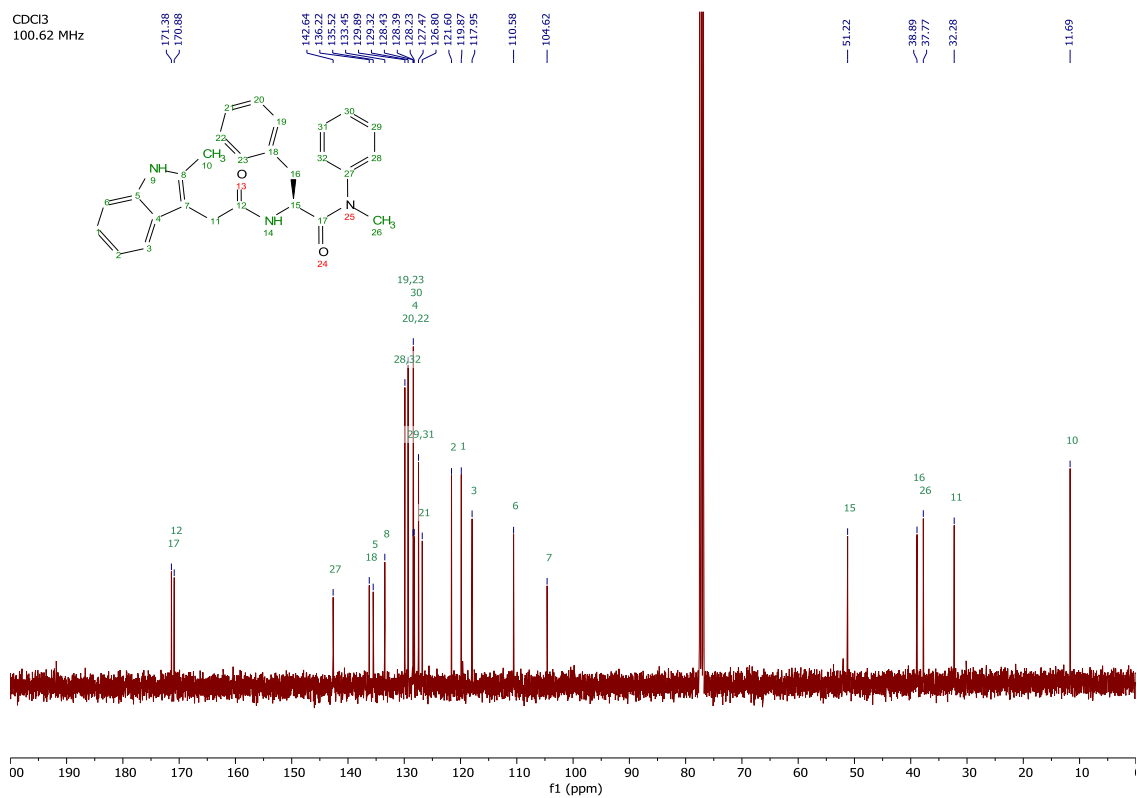
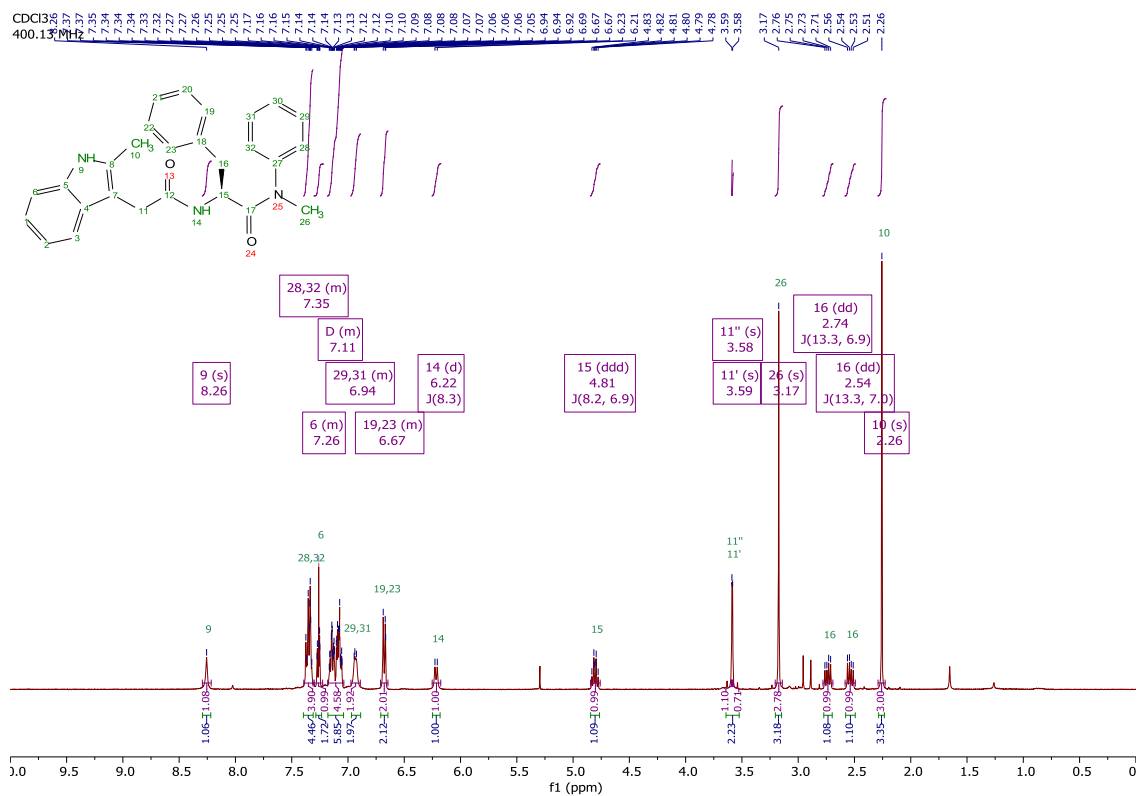
<sup>1</sup>H, <sup>13</sup>C, COSY, HSQC, HMBC and VT (rt, 35 °C, 50 °C) NMR spectra of PROTAC CRBN-O22.

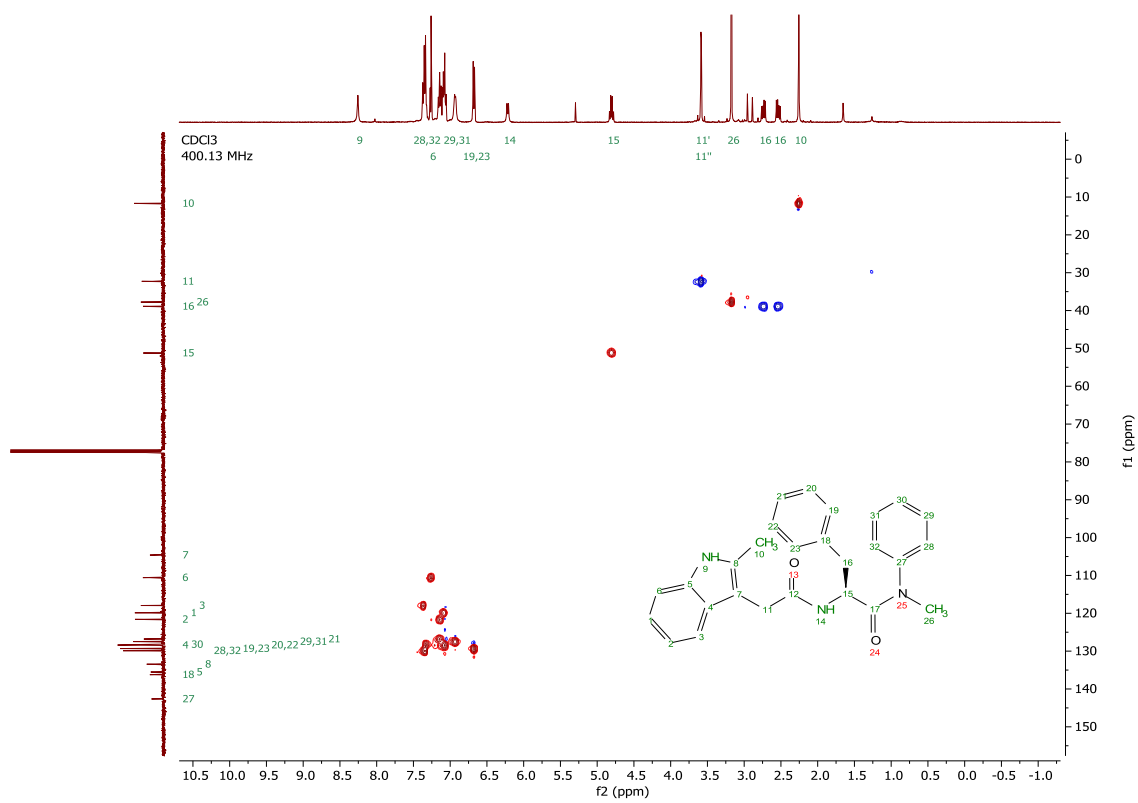
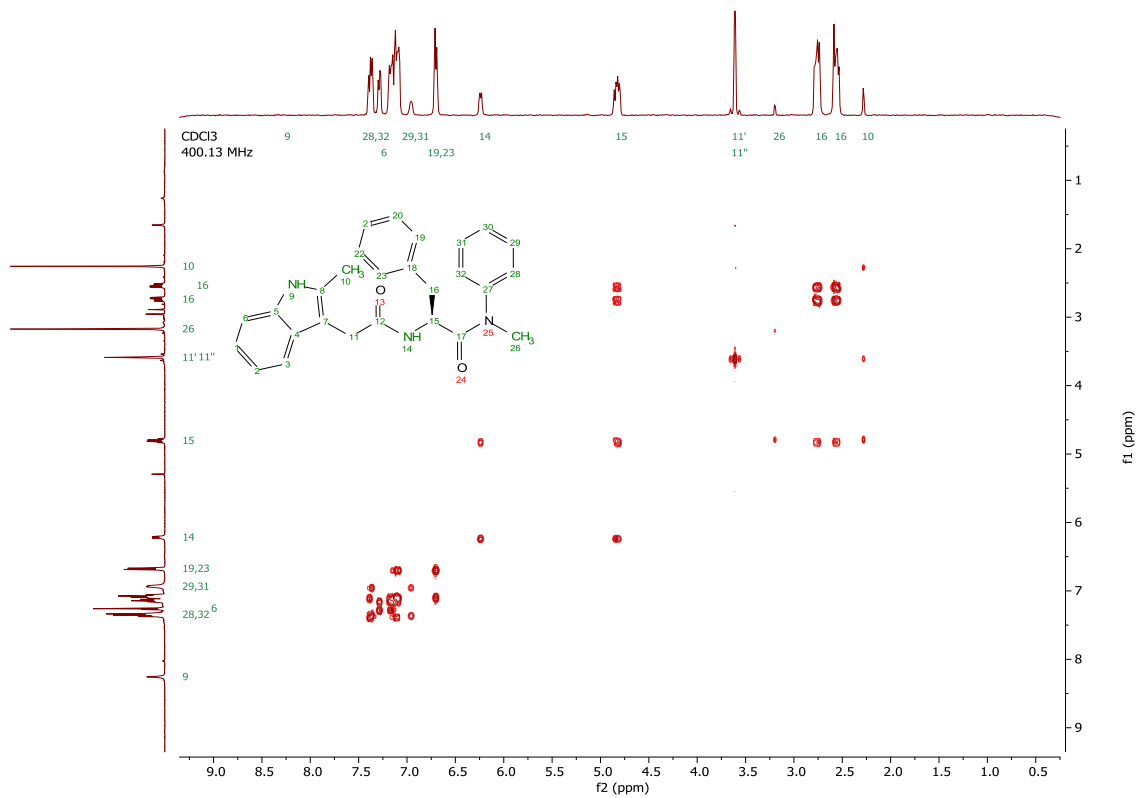


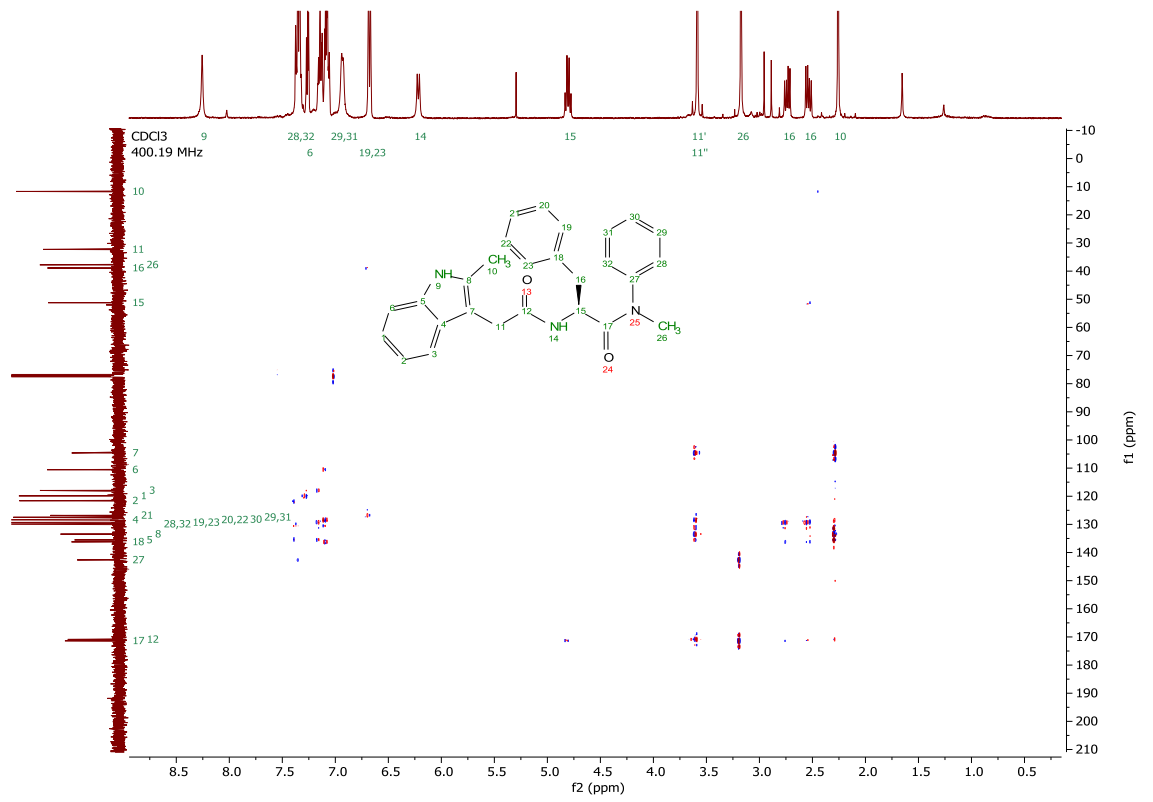




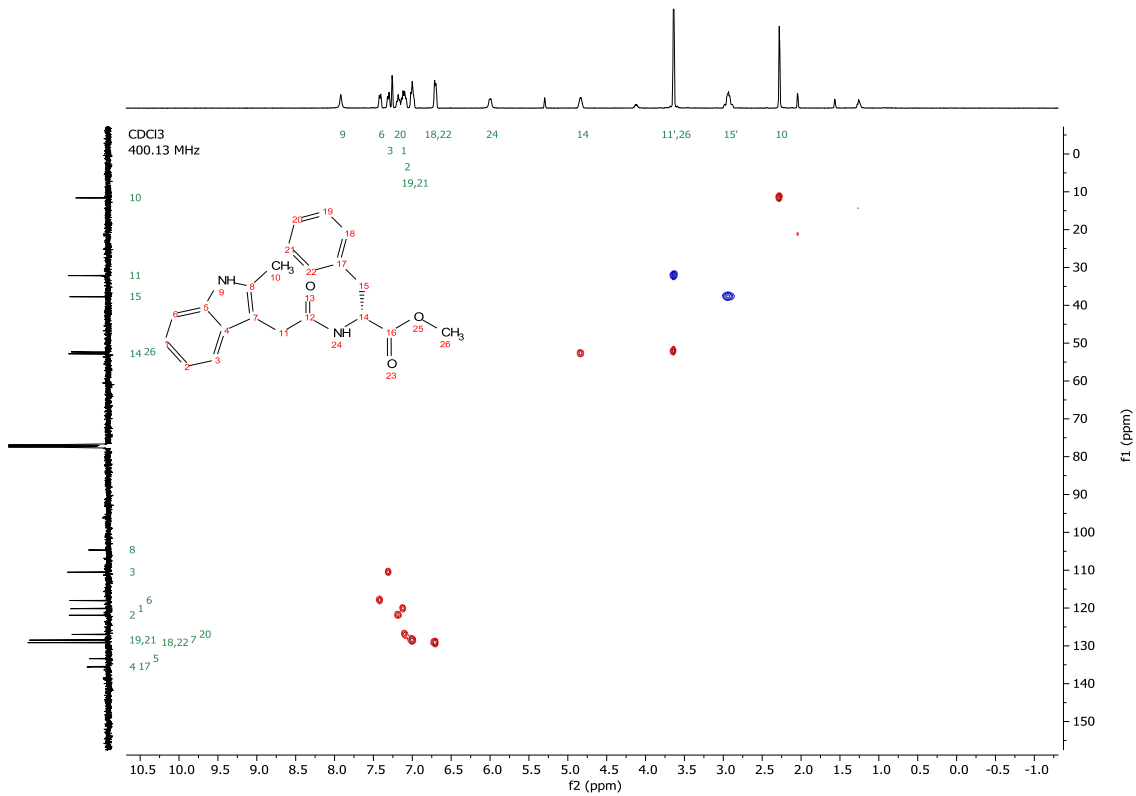
<sup>1</sup>H, <sup>13</sup>C, COSY, HSQC, and HMBC NMR spectra of Natural **PF74**.



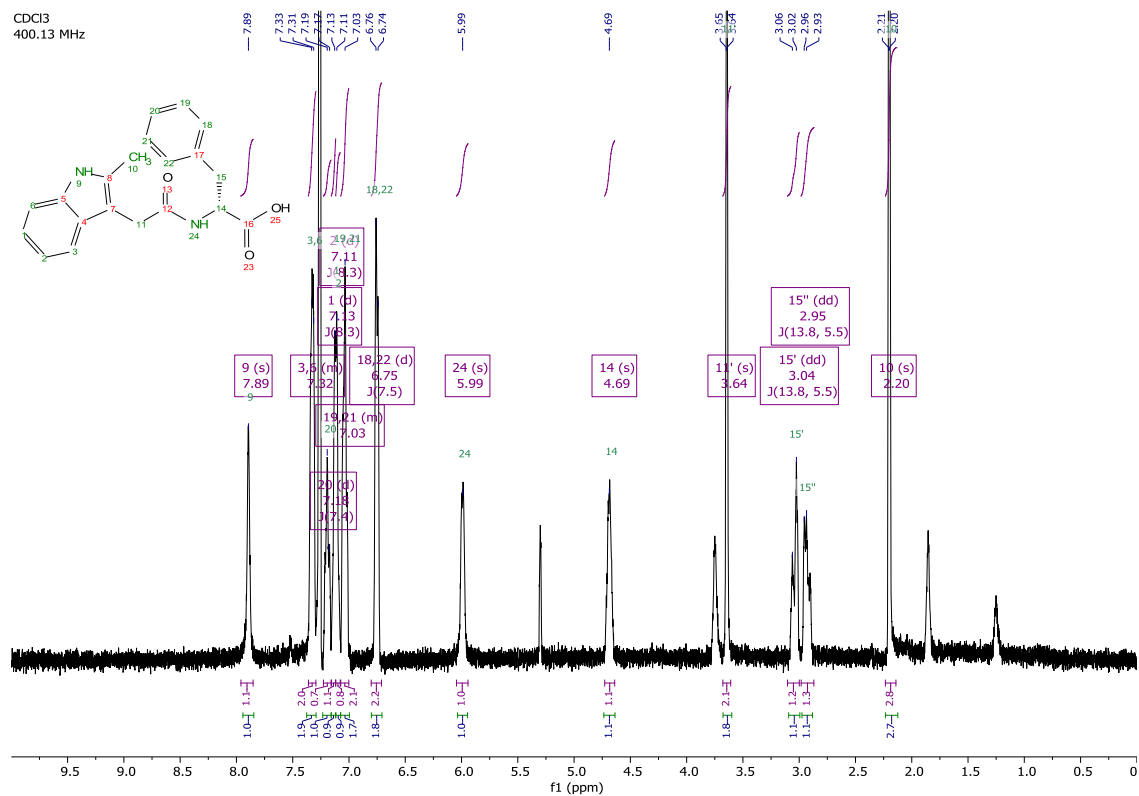




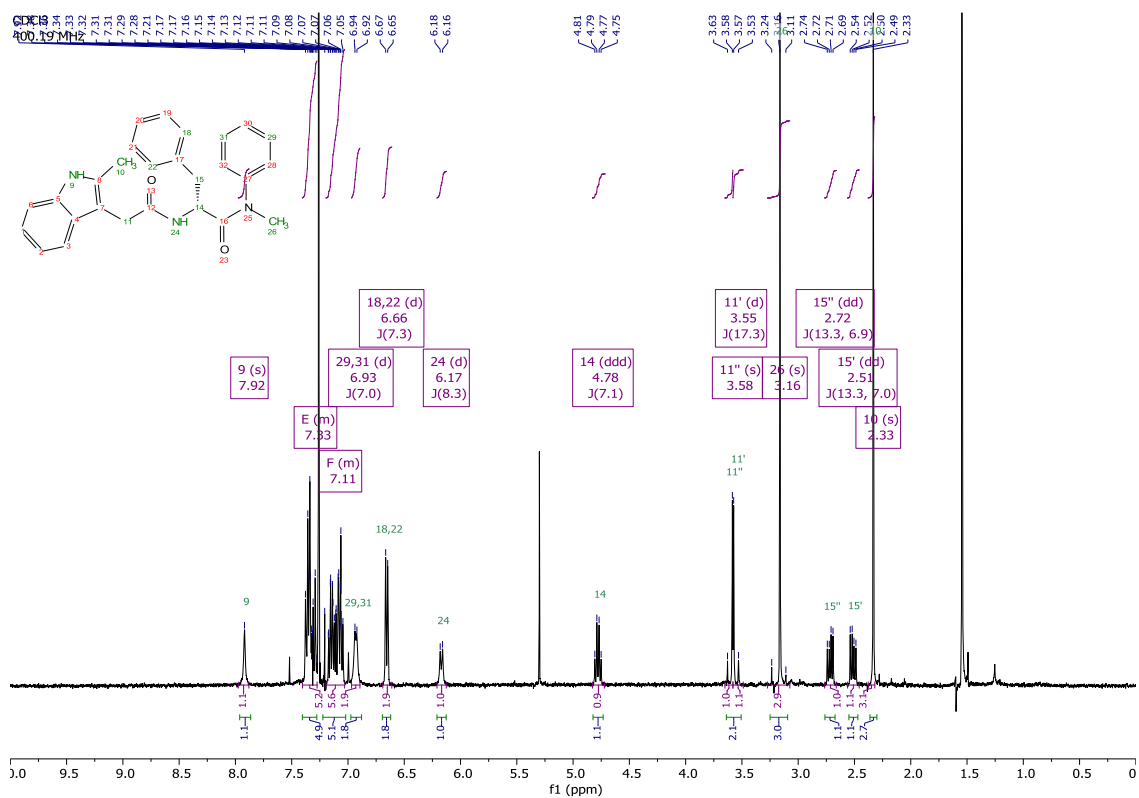




<sup>1</sup>H NMR spectrum of acid *Epi-2.11*.

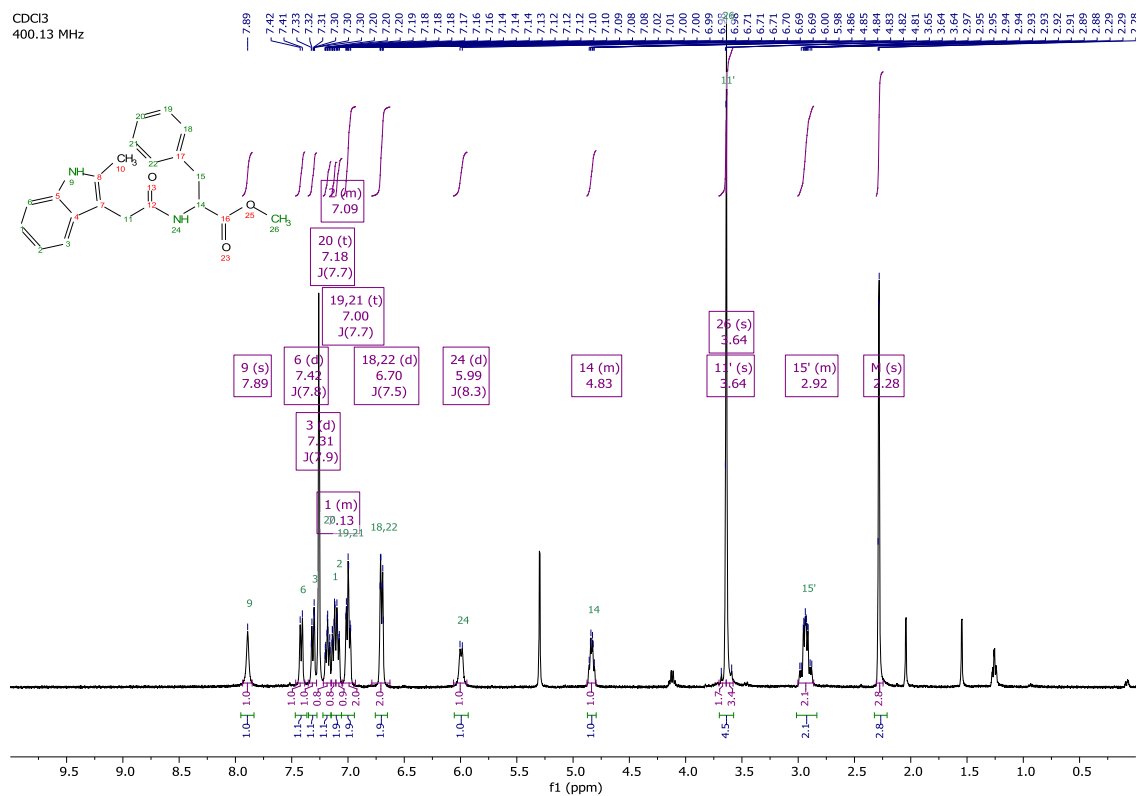


<sup>1</sup>H NMR spectrum of Unnatural PF74.

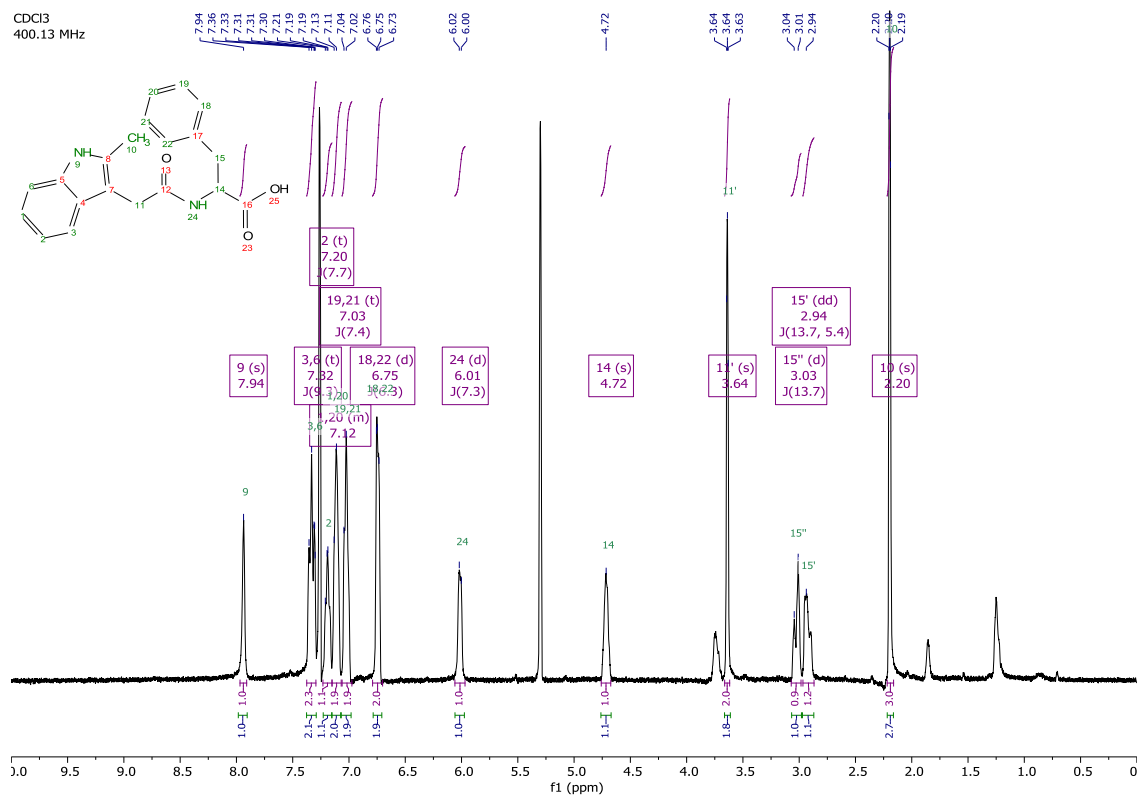


# <sup>1</sup>H NMR spectrum of methyl ester *Rac-2.10*.

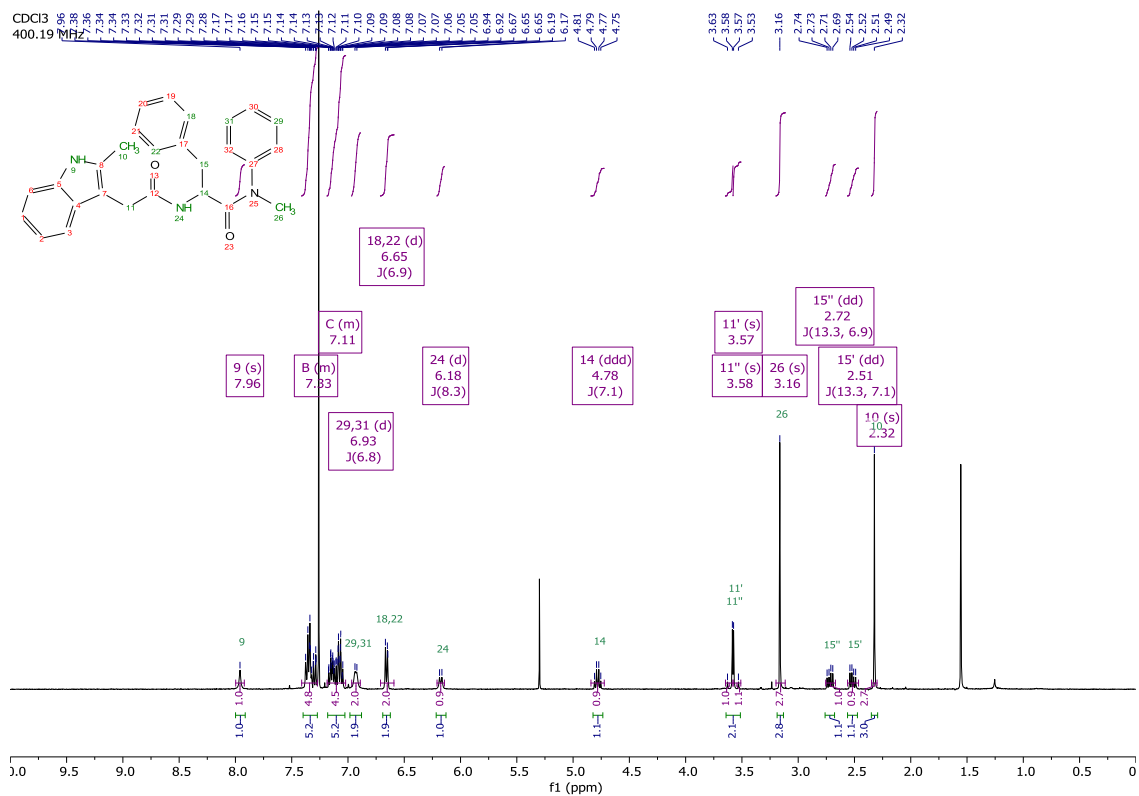
CDCl<sub>3</sub>  
400.13 MHz



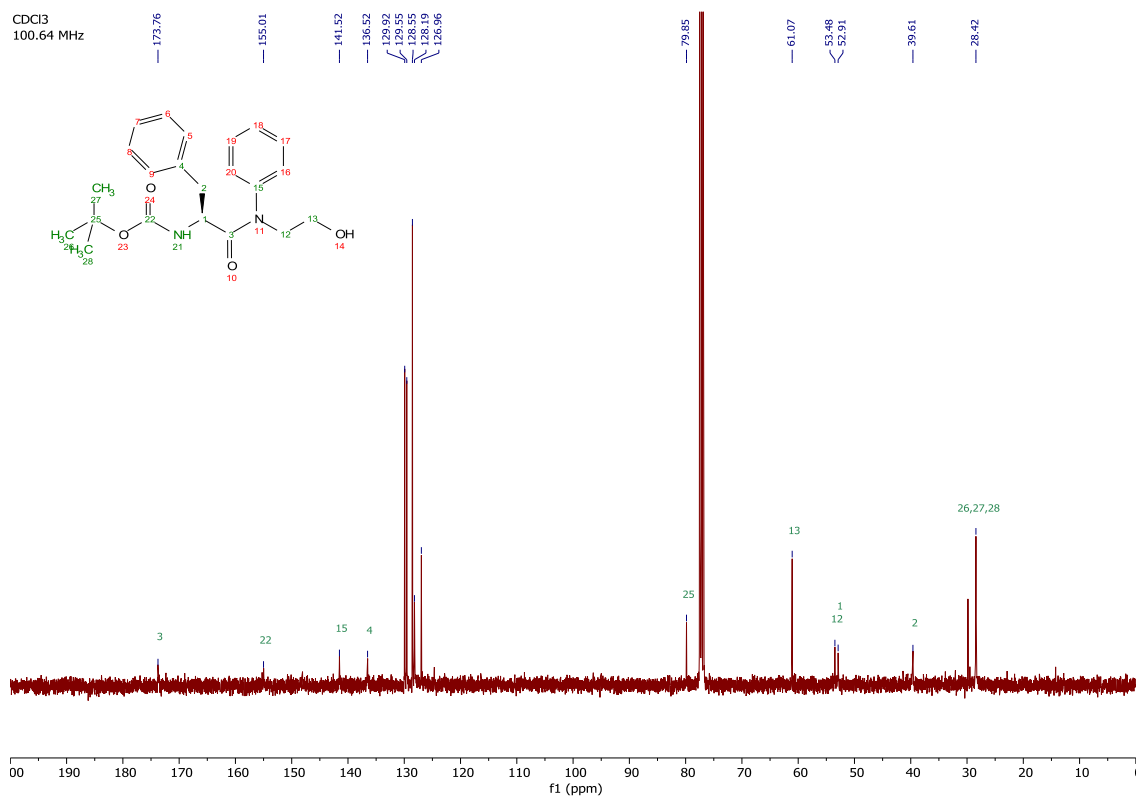
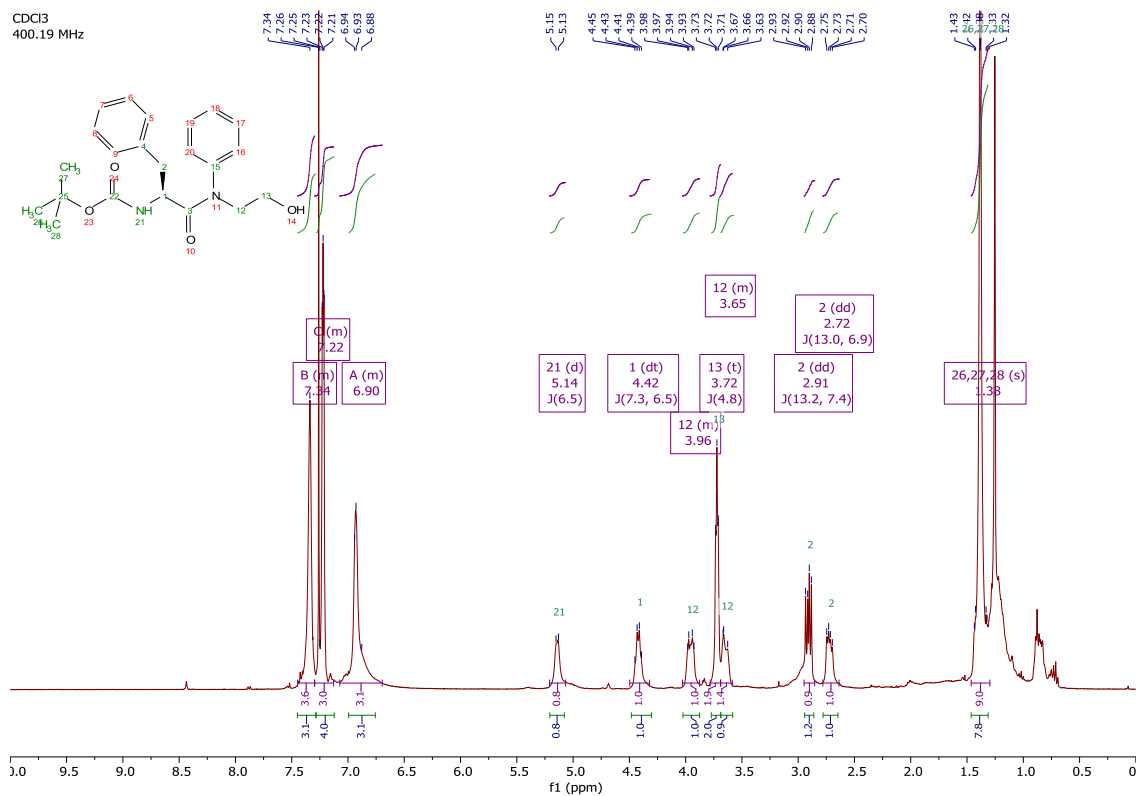
<sup>1</sup>H NMR spectrum of acid *Rac-2.11*.



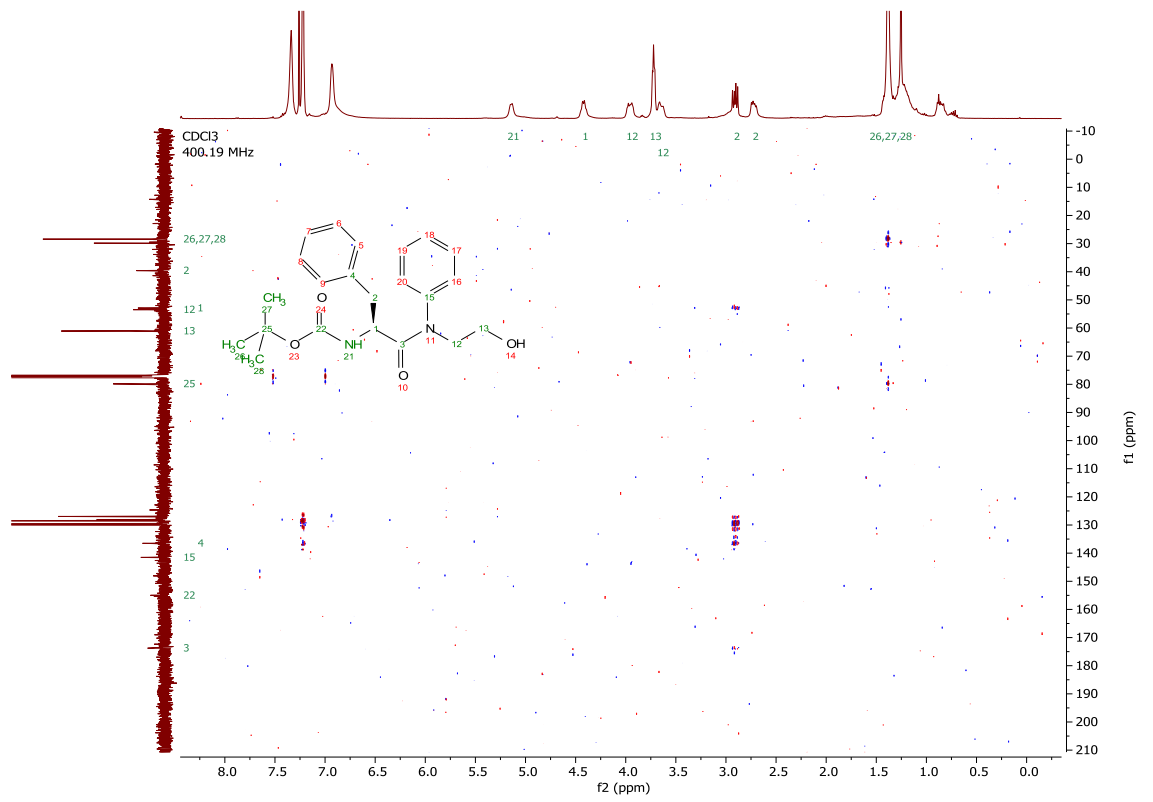
<sup>1</sup>H NMR spectrum of Racemic PF74.



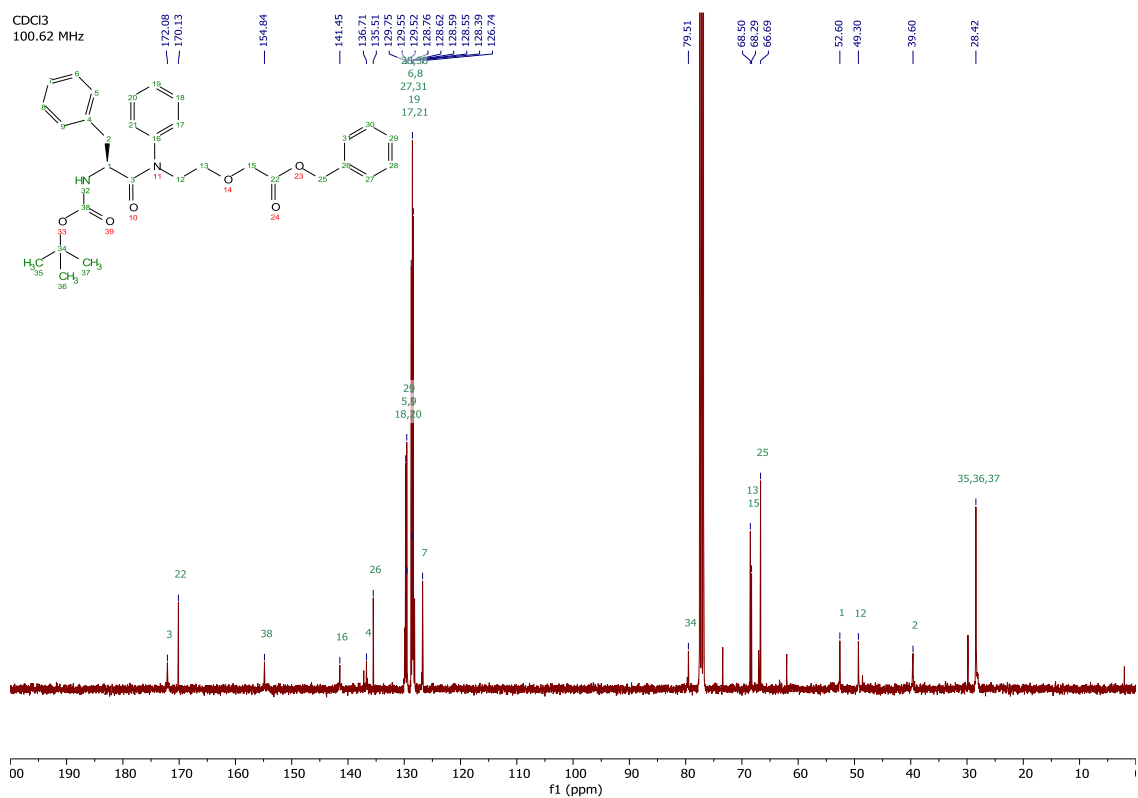
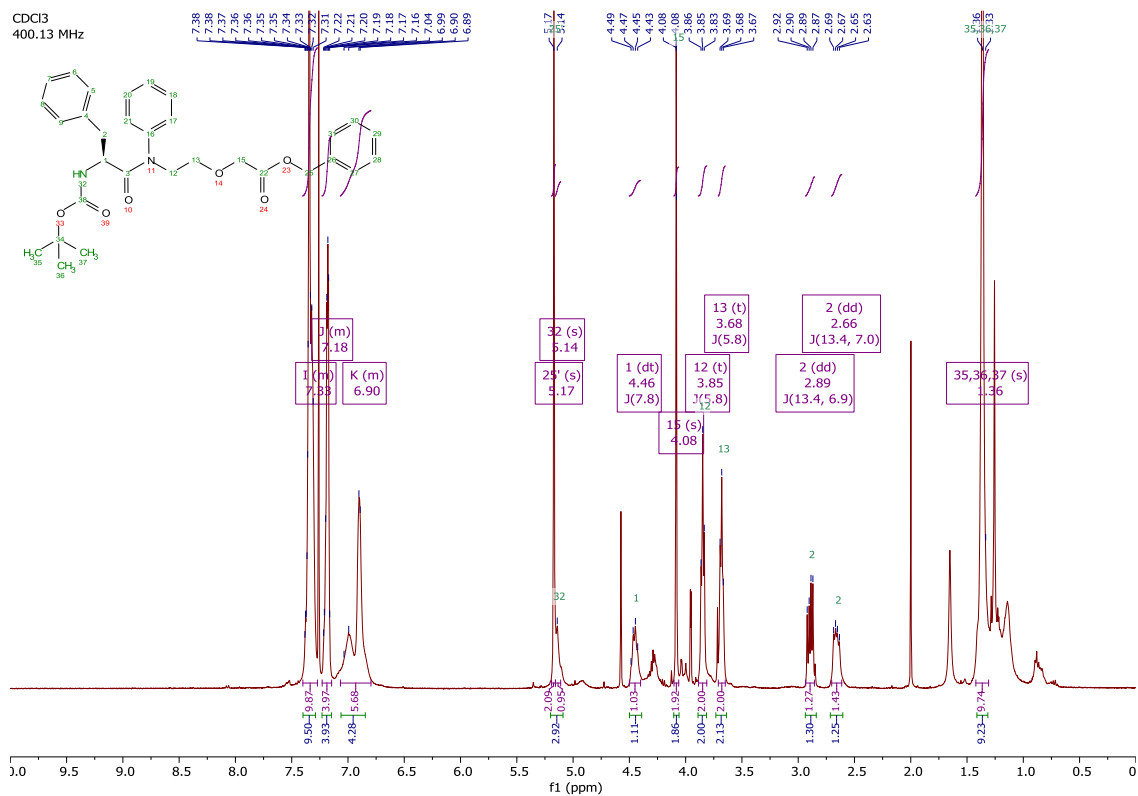
$^1\text{H}$ ,  $^{13}\text{C}$ , COSY, HSQC and HMBC NMR spectra of alcohol **2.35**.

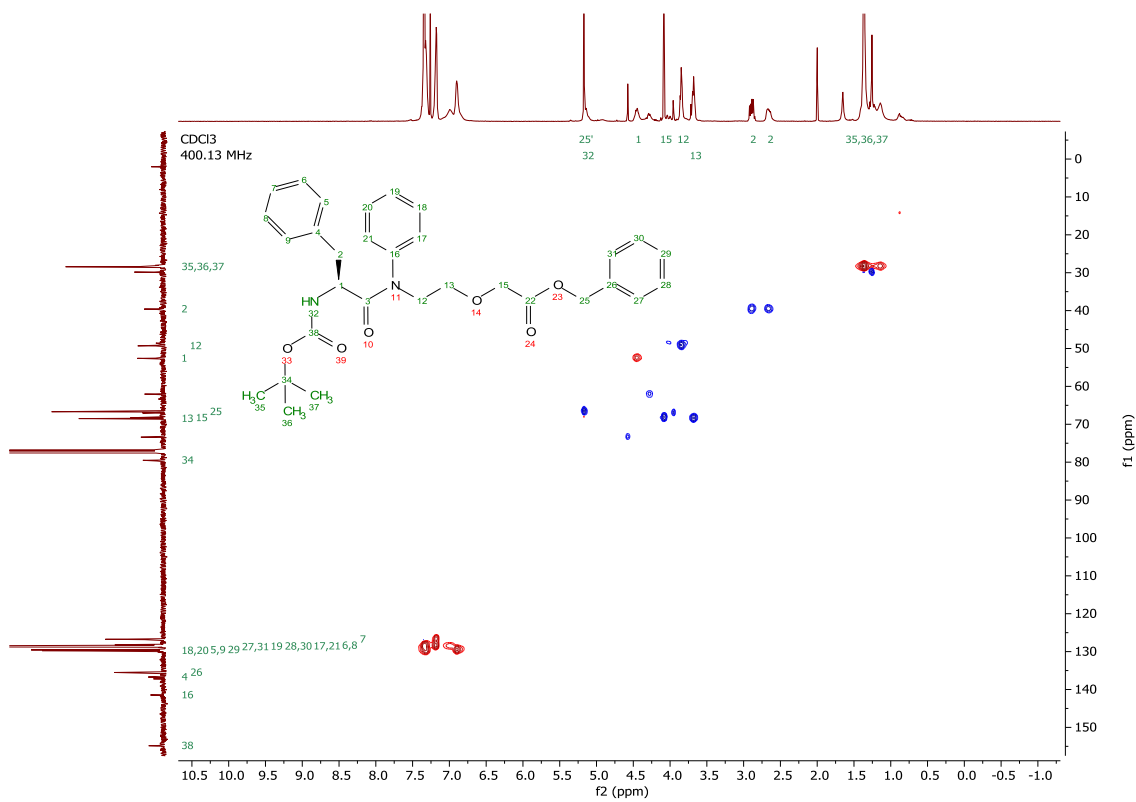
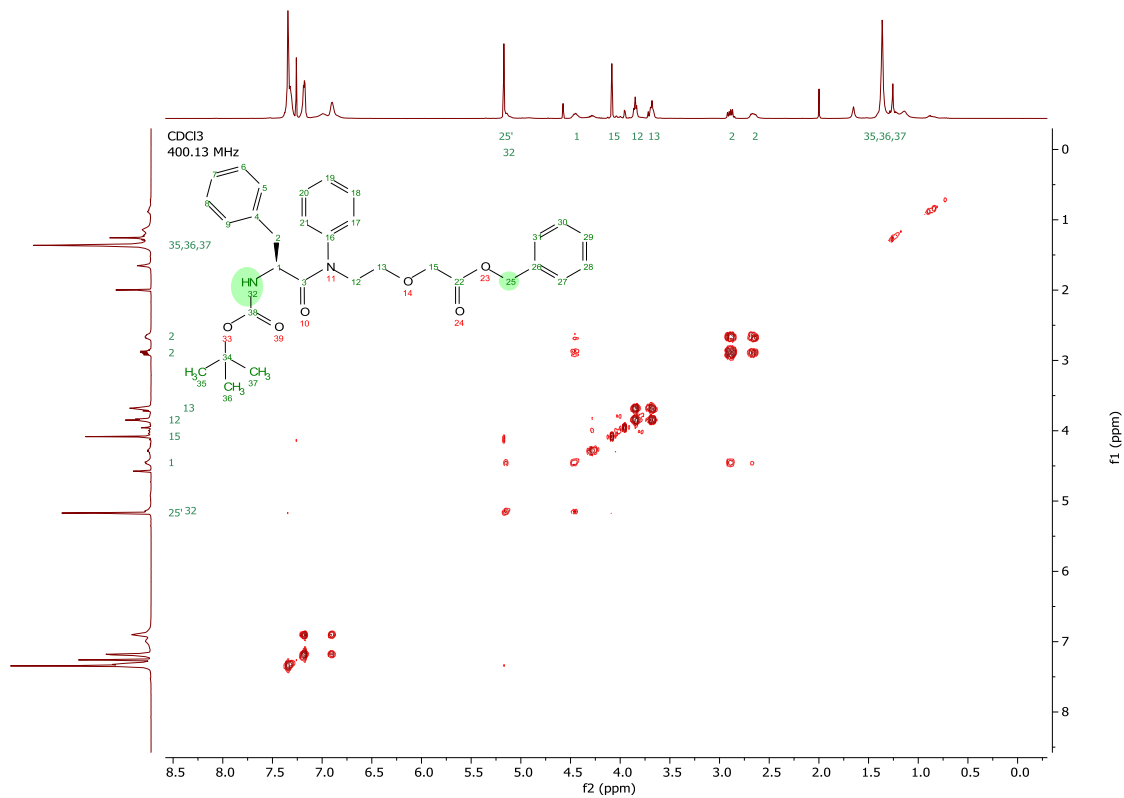


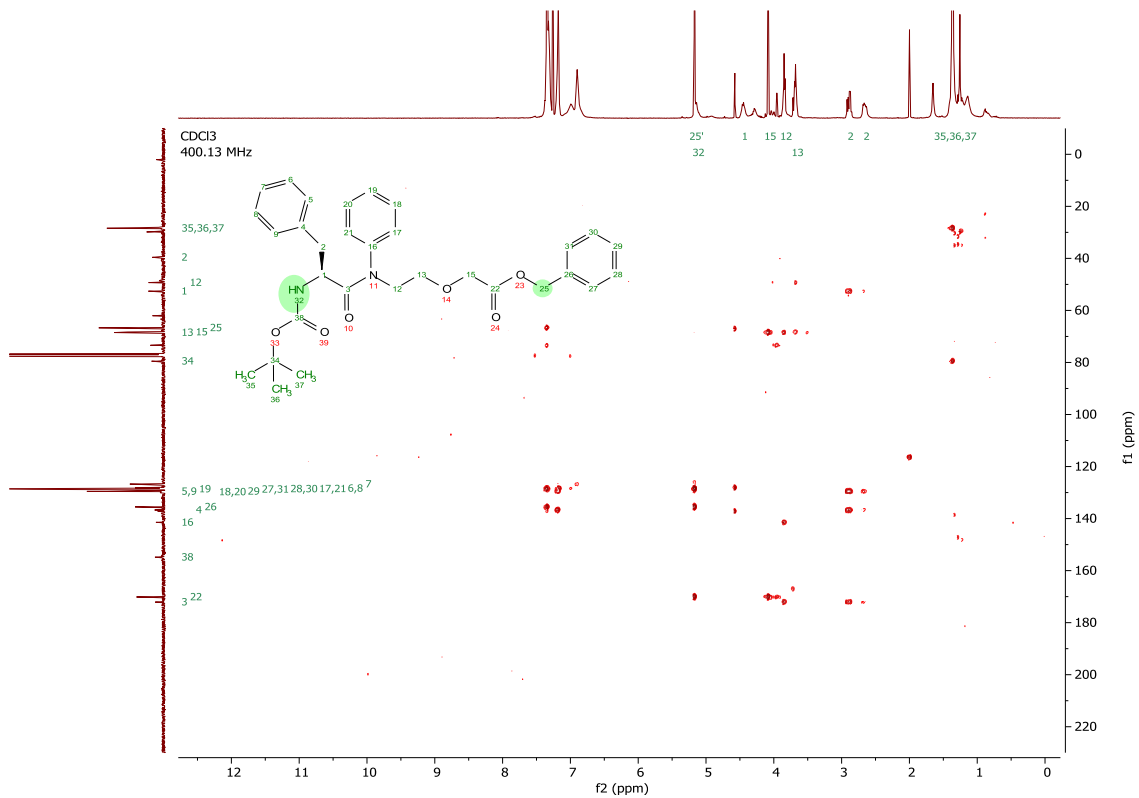




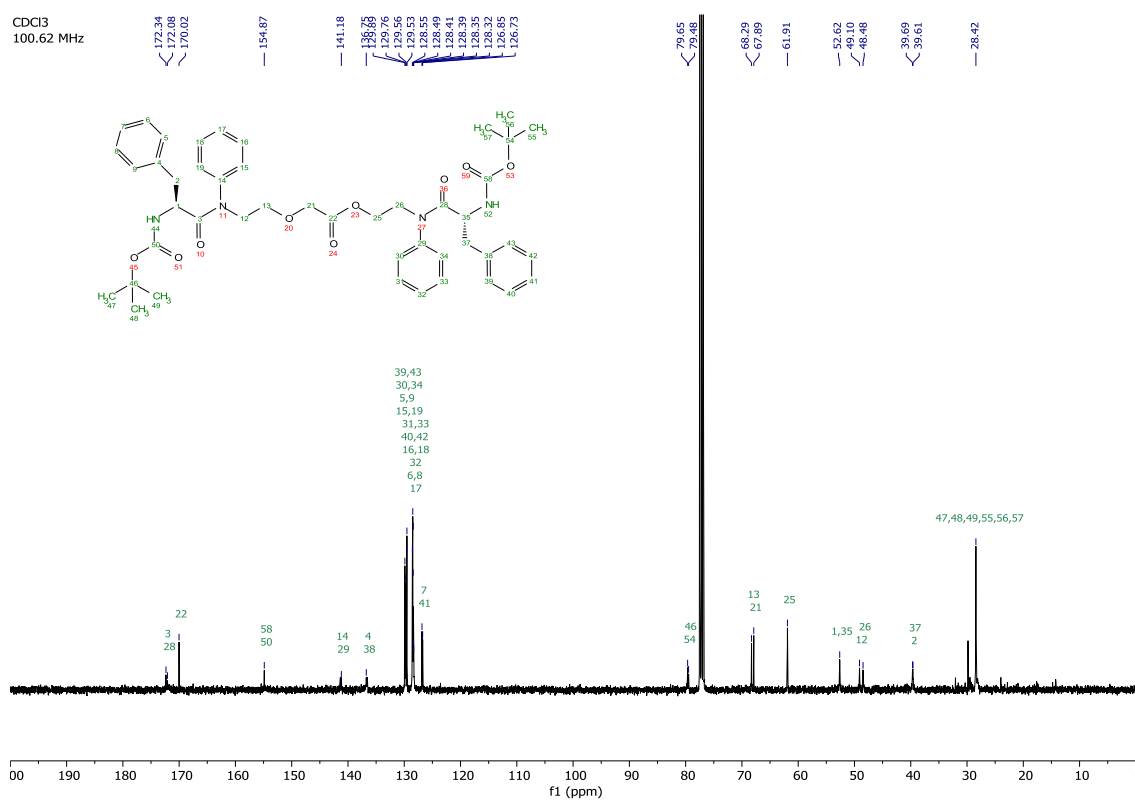
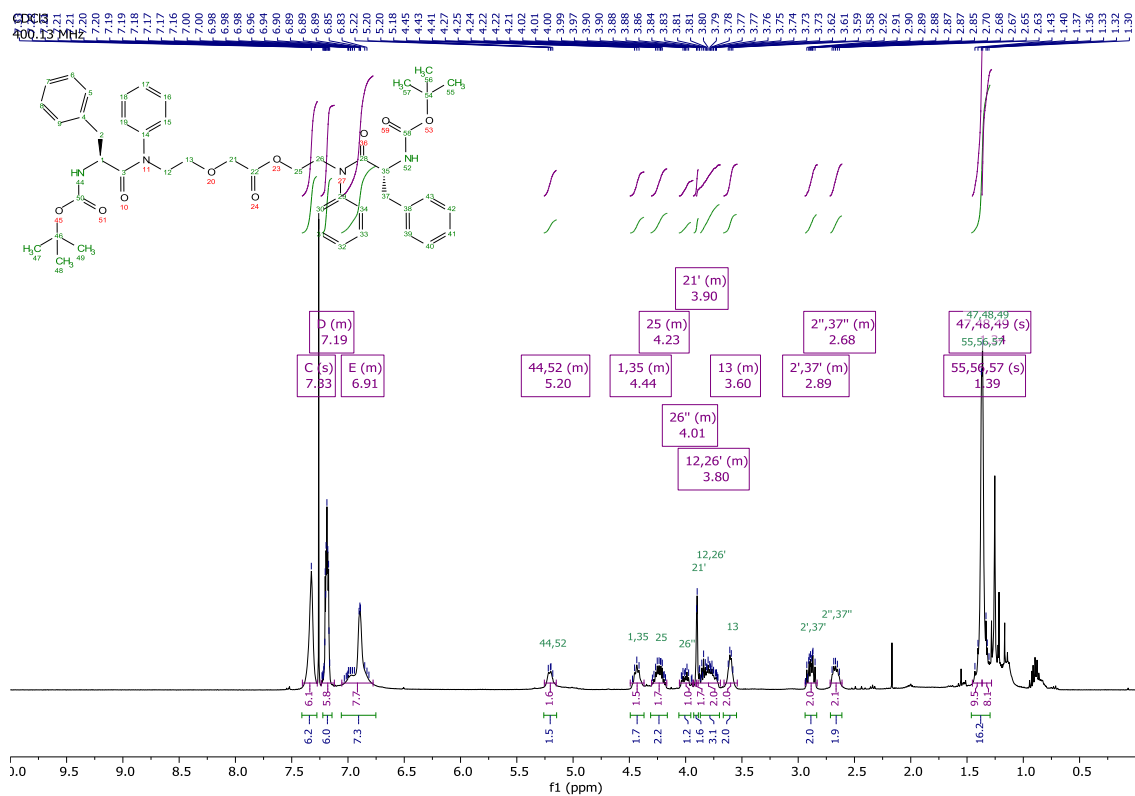
$^1\text{H}$ ,  $^{13}\text{C}$ , COSY, HSQC and HMBC NMR spectra of *tert*-butyl ester **2.38**.

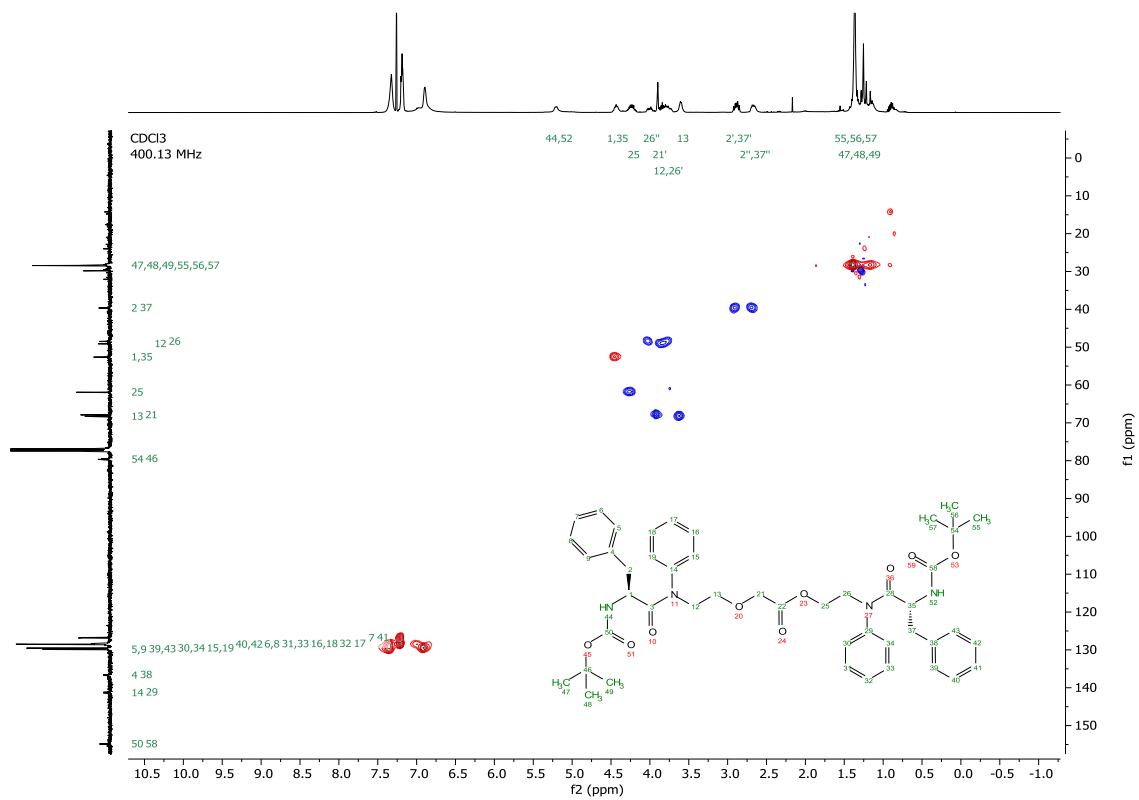
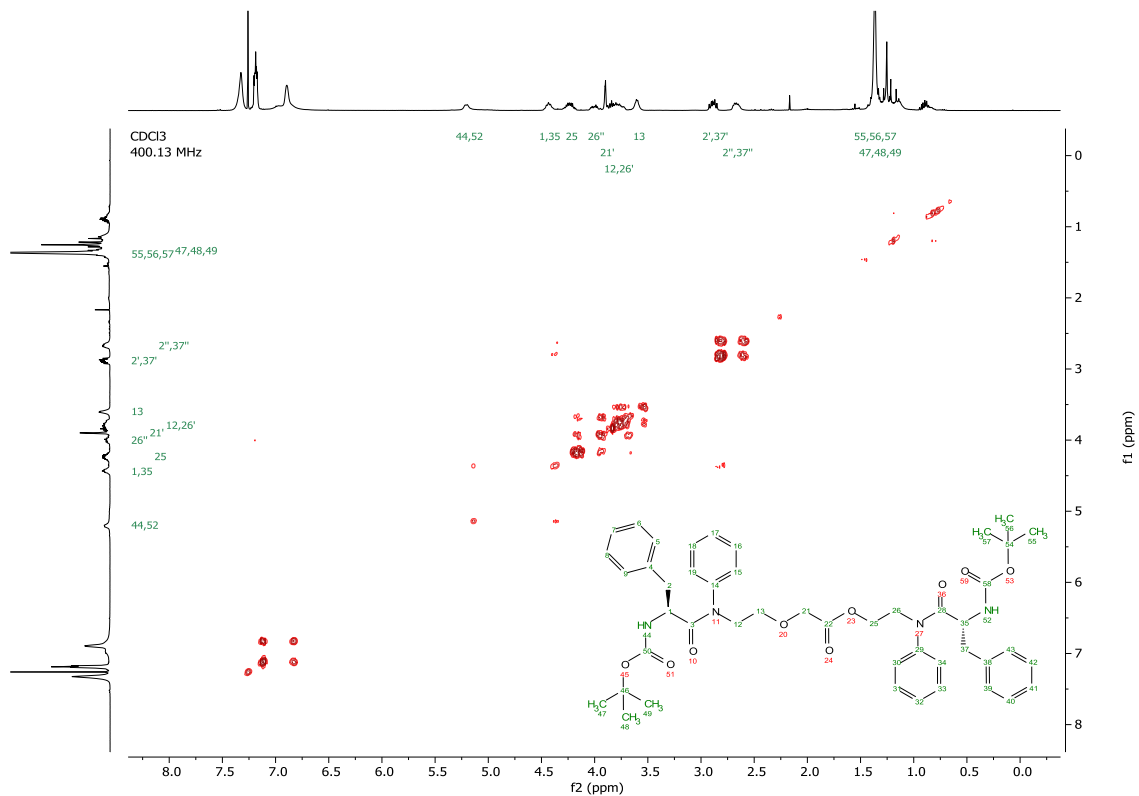


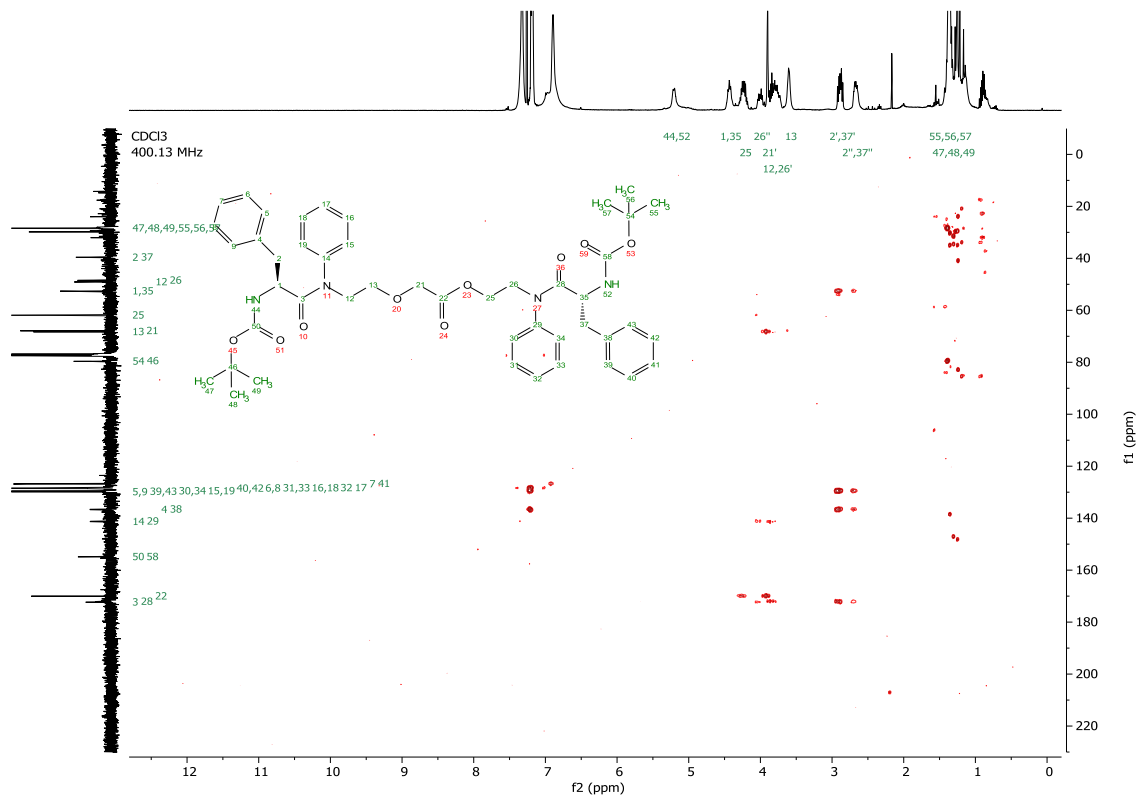




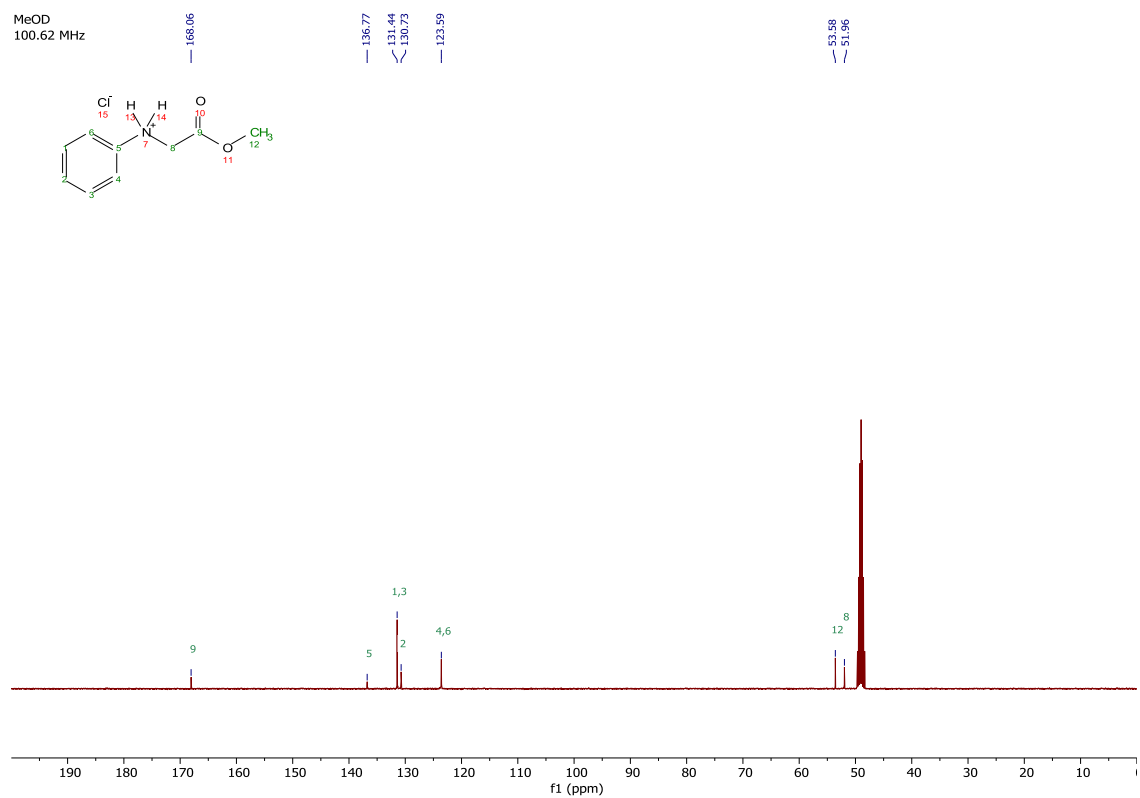
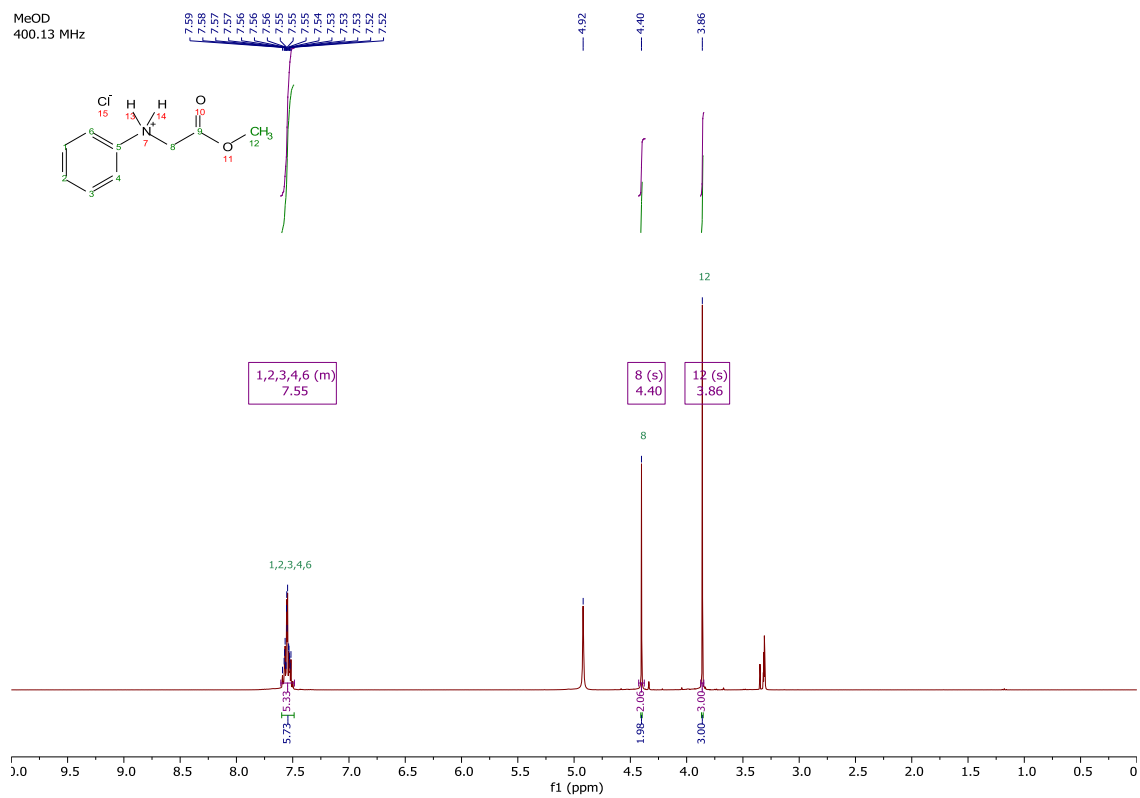
$^1\text{H}$ ,  $^{13}\text{C}$ , COSY, HSQC and HMBC NMR spectra of *tert*-butyl ester **2.39**.



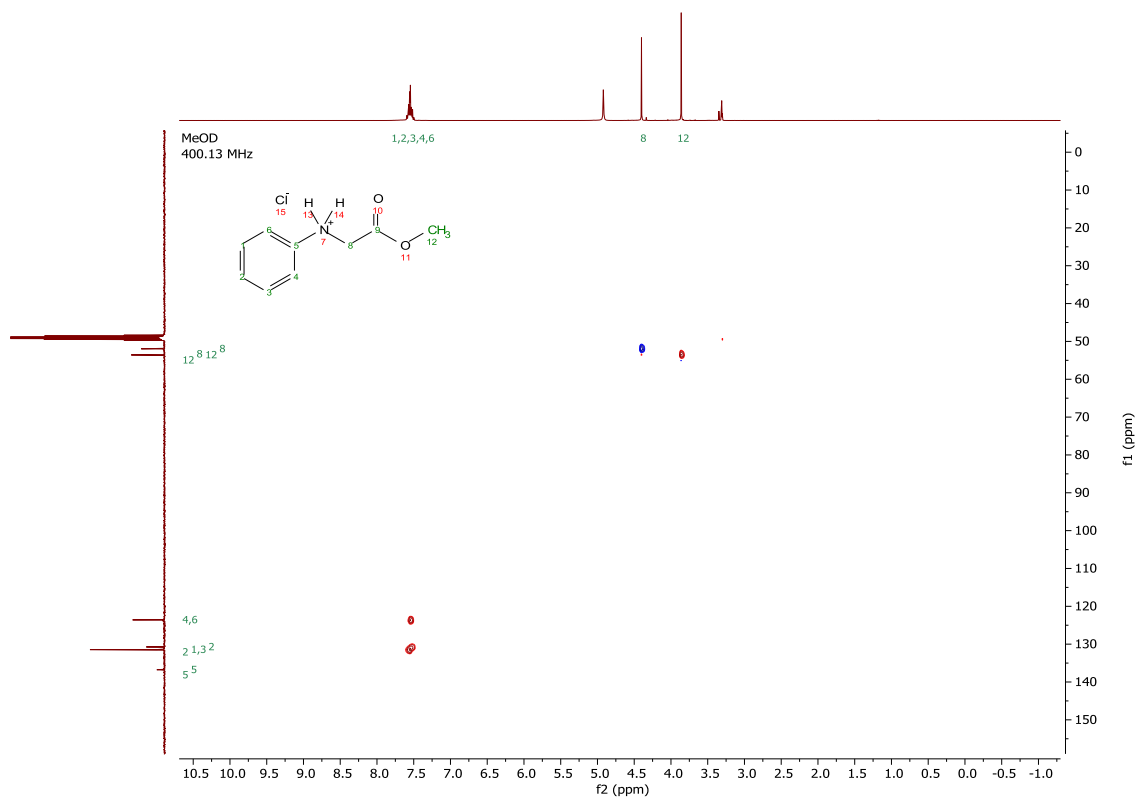
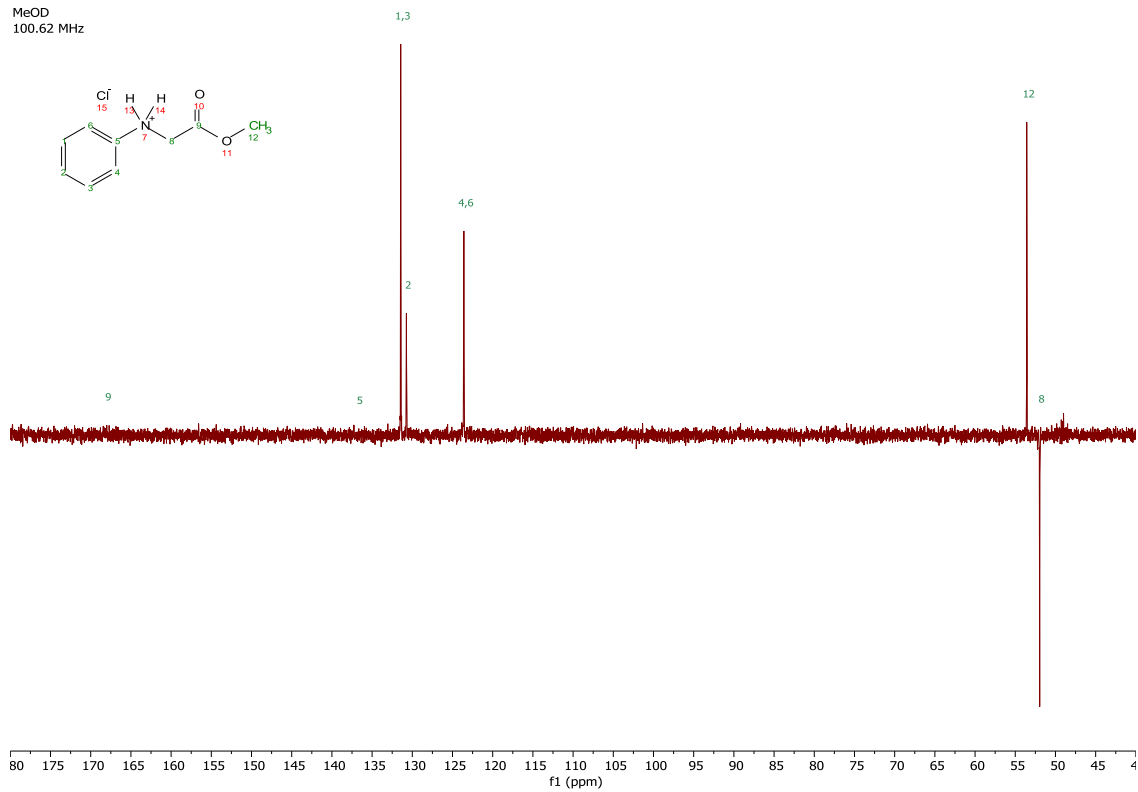
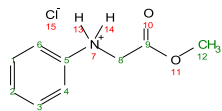


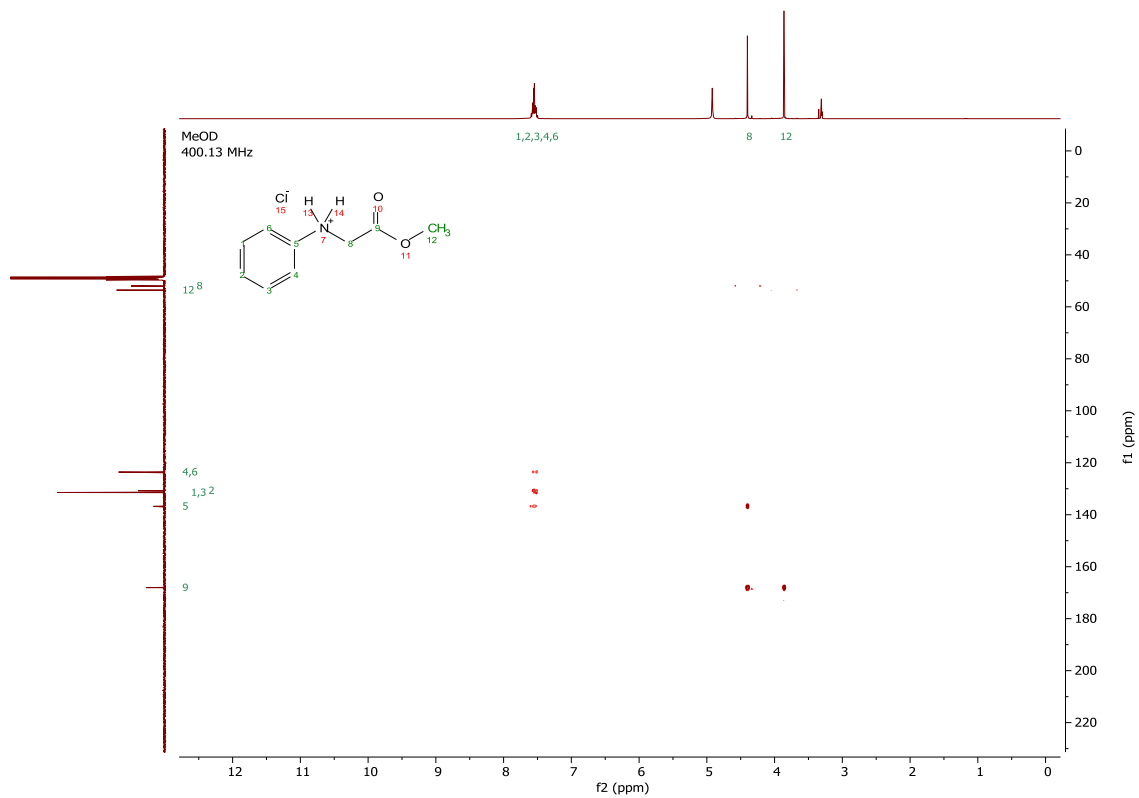


$^1\text{H}$ ,  $^{13}\text{C}$ , DEPT-135, HSQC and HMBC NMR spectra of methyl ester **2.25**.



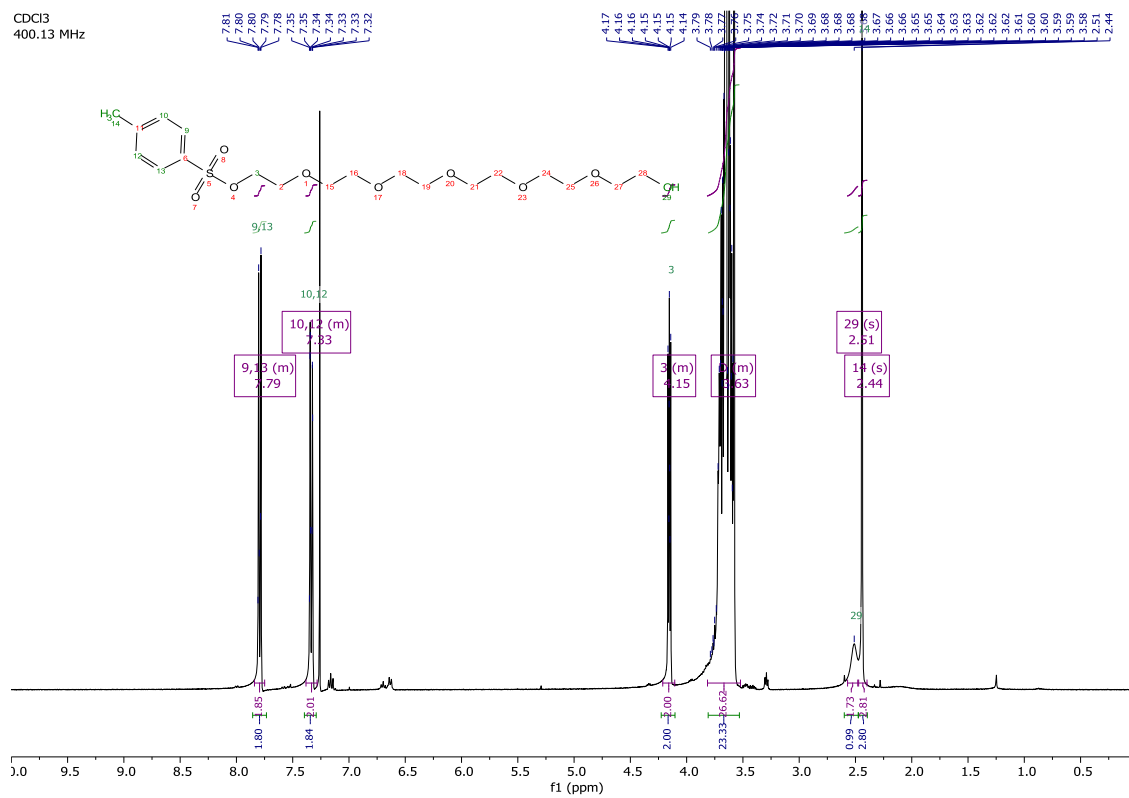
MeOD  
100.62 MHz





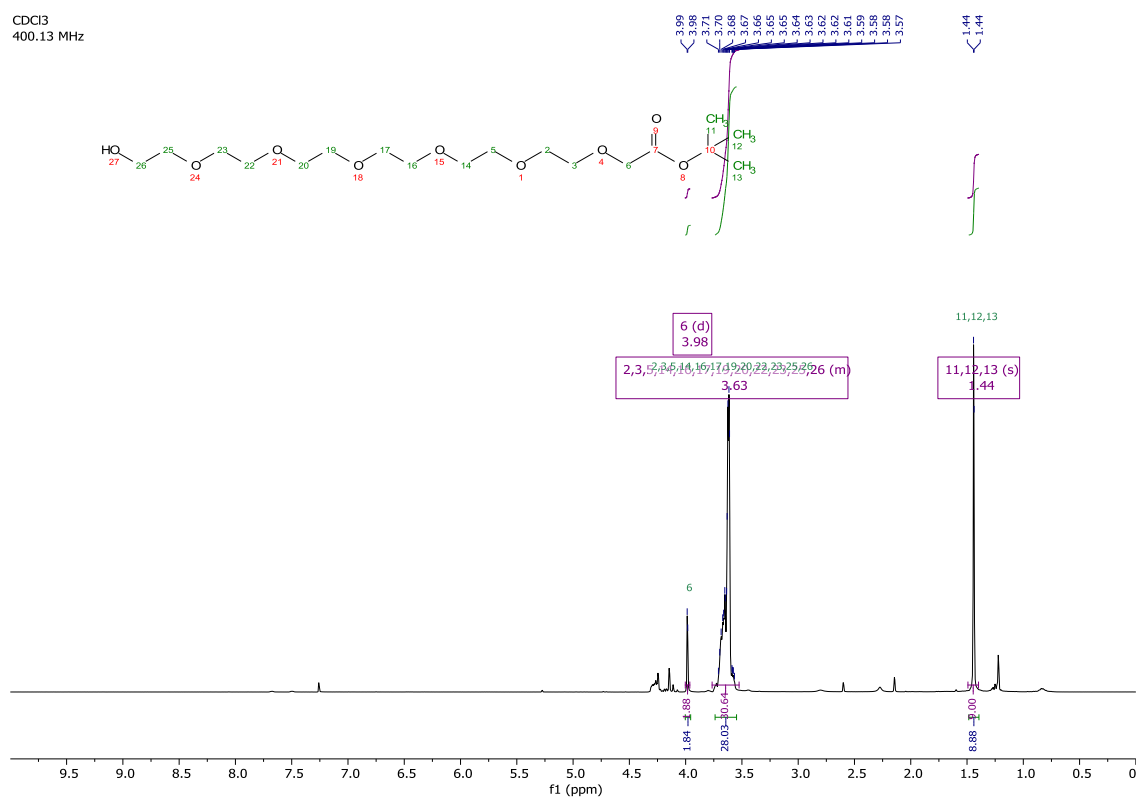
# <sup>1</sup>H NMR spectrum of tosylate 2.6.

CDCl<sub>3</sub>  
400.13 MHz



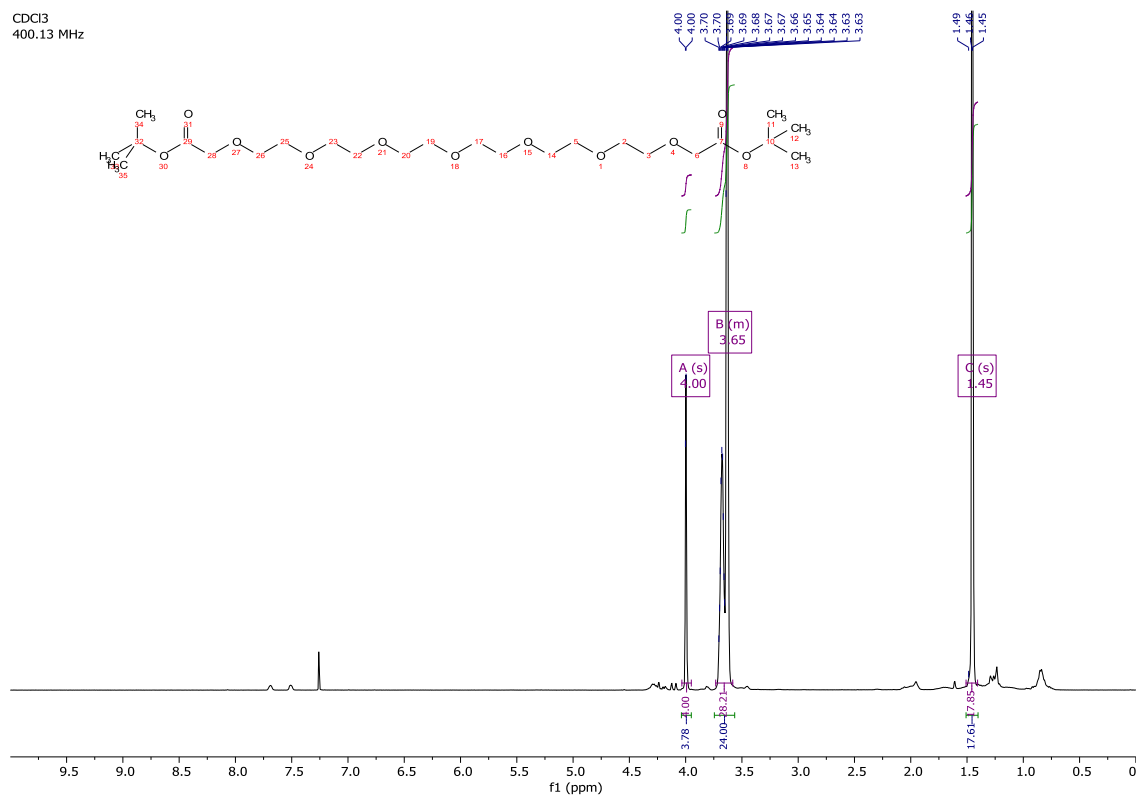
# <sup>1</sup>H NMR spectrum of *tert*-butyl ester **2.4**.

CDCl<sub>3</sub>  
400.13 MHz



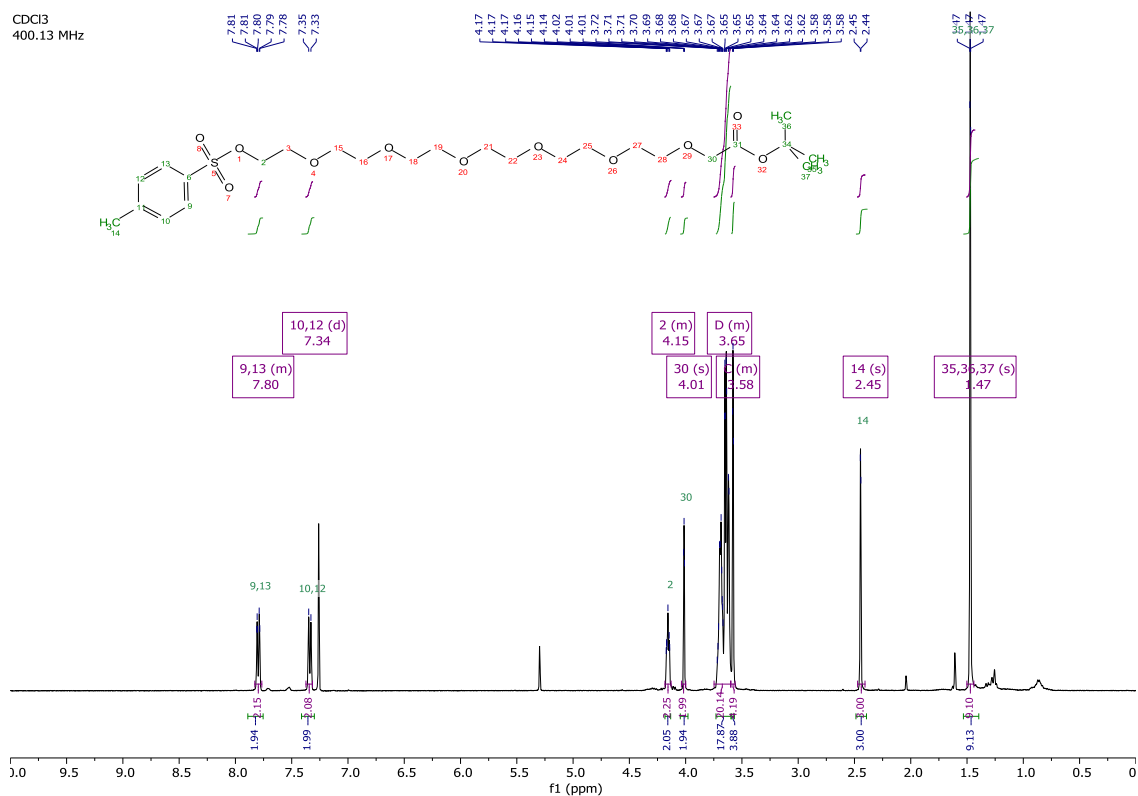
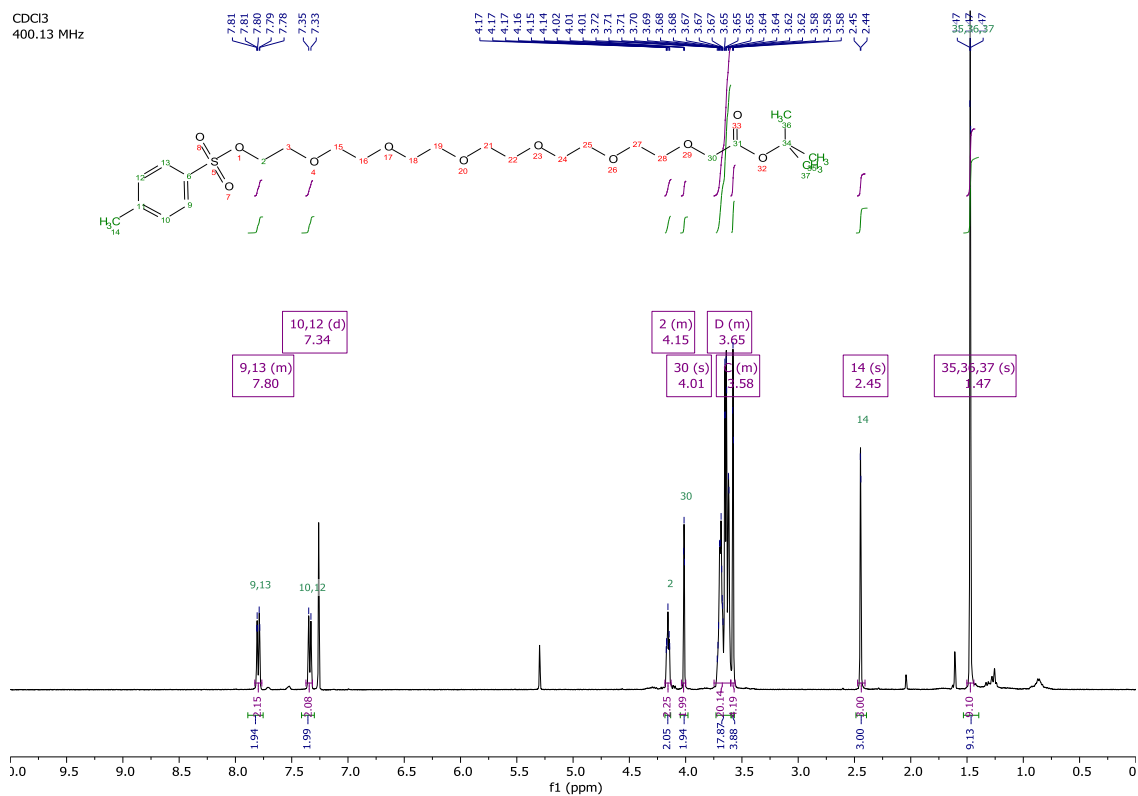
# $^1\text{H}$ NMR spectrum of *tert*-butyl ester **2.4b**.

CDCl<sub>3</sub>  
400.13 MHz



# $^1\text{H}$ and $^{13}\text{C}$ NMR spectra of *tert*-butyl ester 2.5.

CDCl<sub>3</sub>  
400.13 MHz



## Chapter 2 Biology

### PF74 and PROTAC Assay Data

Graph 2.2.

CSGW+VSVg (mL)	DMSO 1 %			No DMSO		
50.000000	98.392770	99.075360	98.011950	98.403920	98.793530	98.522470
16.666670	87.891520	86.759850	86.036620	86.800450	86.836810	87.435150
5.555556	51.990970	54.212940	50.234380	53.184630	52.562680	51.118050
1.851852	21.589440	21.525690	22.574260	23.621660	22.803760	23.097210
0.617284	7.987106	7.683891	6.880040	8.303516	7.390329	7.734807
0.205761	2.500893	2.537403	2.368056	2.769842	2.582798	2.564741
0.068600	0.745562	0.779442	1.009977	0.881659	0.885950	0.955494
0.022900	0.300661	0.219834	0.264550	0.236260	0.322261	0.319725
0.007620	0.200803	0.036581	0.126791	0.108893	0.037351	0.111996
0.002540	0.047910	0.097111	0.074710	0.036527	0.000000	0.049462
0.000847	0.000000	0.024172	0.012220	0.012271	0.024585	0.012352
0.000000	0.023491	0.000000	0.000000	0.012197	0.024041	0.012136

CSGW+VSVg (mL)	PF74 10 $\mu$ M			No Compound		
50.000000	20.992520	18.127600	18.816970	98.269480	98.529600	98.811460
16.666670	5.764315	6.832634	6.608479	87.265140	86.654760	88.008230
5.555556	1.612702	2.606476	1.827454	51.622570	50.408160	49.750500
1.851852	0.670058	0.596580	0.405481	20.412900	19.972010	21.683180
0.617284	0.274966	0.324675	0.124138	6.336053	7.189045	7.473935
0.205761	0.074991	0.122951	0.070671	2.313820	2.136266	2.038723
0.068600	0.025253	0.026613	0.013776	0.633553	0.663858	0.773365
0.022900	0.000000	0.040263	0.013583	0.203071	0.278129	0.277998
0.007620	0.012618	0.000000	0.000000	0.077952	0.050923	0.052459
0.002540	0.000000	0.000000	0.000000	0.026392	0.025897	0.064683
0.000847	0.012762	0.000000	0.000000	0.000000	0.024888	0.000000
0.000000	0.012719	0.000000	0.013620	0.000000	0.050524	0.051520

Graph 2.3.

Compound Concentration ( $\mu\text{M}$ )	PF74 Purchased	PF74 Synth Natural	PF74 Synth unnatural
100.000000	0.02470051	0.392638	0.01233502
25.000000	0.01297017	0.02574665	0.02021427
6.250000	1.612903	1.670146	1.880431
1.562500	1.680564	1.767088	1.895793
0.390625	11.615390	10.830280	12.613940
0.09765625	15.796180	15.522640	16.346860
0.02441406	17.899910	15.507370	16.467210
0.00610352	17.541470	15.998100	15.480860
0.00152588	18.094270	15.739290	17.193240
0.00038147	17.184580	16.775060	17.442710
0.000095367	17.012240	15.971710	15.622710

## Graph 2.4.

### Virus titration

( $\mu\text{L}$ )	PF74 Synth natural		PF74 natural HPLC		PF74 unnatural HPLC		1% DMSO	
50.000000	30.852990	28.498340	37.256810	33.662240	97.742190	97.587900	98.570850	97.845700
16.666670	10.550580	9.128788	15.321510	13.446210	81.484370	81.242550	85.687950	86.583250
5.555556	3.352644	3.461296	5.231100	4.868729	46.404900	46.364940	52.578800	51.539670
1.851852	1.130856	1.042945	1.506703	1.329027	18.926260	18.488060	21.843220	19.688080
0.617284	0.397614	0.348086	0.6512657	0.4692011	6.835836	6.023771	8.002645	7.604208
0.205761	0.098790	0.122730	0.1328984	0.2071655	2.149437	2.585541	2.570395	
0.068600	0.037000	0.060990	0.08397313	0.07451565	0.4301075	0.5393317	0.8826584	
0.022900	0.000000	0.012346	0.03690491	0.000000	0.206852	0.2142475	0.2710727	0.2155172
0.007620	0.000000	0.012539	0.04898959	0.03669725	0.01284027	0.06595436	0.1818654	0.1218357
0.002540	0.012416	0.024594	0.01218324	0.000000	0.0388249	0.03938042	0.01306506	0.03994674
0.000847	0.012285	0.012427	0.000000	0.000000	0.02577652	0.01299883	0.0129199	0.05285412
0.000000	2.593486	1.000366	0.01188778	0.000000	0.000000	0.01278772	0.01287001	0.000000

## Graph 2.5.

### Concentration

nM

PF74 natural

PF74 unnatural

80.00000000	0.01870441	0.02638696	0.00000000	1.24698800	1.47417200	1.32005300
40.00000000	0.07584856	0.09908184	0.05377790	3.50662700	3.00157000	2.76214800
20.00000000	0.65683480	0.66411240	0.58224170	8.86051000	9.17569000	8.18059100
10.00000000	0.84240300	0.79645450	0.72289160	12.93217000	14.32376000	13.87006000
5.00000000	1.22054900	1.00186200	1.16301700	16.35303000	16.56745000	15.02223000
2.50000000	5.25615500	4.34866000	4.48713800	17.39930000	17.23571000	16.25933000
1.25000000	10.43679000	10.16471000	9.79564000	17.34089000	18.01613000	18.04260000
0.62500000	16.36967000	16.15547000	15.28016000	18.17944000	18.20436000	17.60394000
0.31250000	18.01269000	17.52320000	15.54325000	18.77847000	18.98207000	17.48279000
0.15625000	18.22168000	16.99035000	16.30507000	18.10652000	18.42089000	17.90247000

## Graph 2.6.

Virus titration

( $\mu$ L)	PF74 Synth natural	CRBN-O13	CRBN-O22	VHL-4				
50.000000	30.852990	28.498340	94.450850	94.071960	97.496670	97.537010	4.848901	5.440742
16.666670	10.550580	9.128788	73.974000	71.040960	80.335700	78.063730	2.628755	3.570463
5.555556	3.352644	3.461296	35.344940	33.370540	42.296490	40.553850	1.494690	1.626126
1.851852	1.130856	1.042945	13.766850	12.986180	16.003570	15.932750	0.505185	0.506869
0.617284	0.397614	0.348086	5.243779	5.380995	5.536913	5.605078	0.131648	0.188857
0.205761	0.098790	0.122730	1.697707	1.280228	1.713415	1.680783	0.078278	0.108006
0.068600	0.037000	0.060990	0.518135	0.618318	0.542245	0.557621	0.039557	0.066260
0.022900	0.000000	0.012346	0.254033	0.215983	0.220264	0.304595	0.013530	0.026781
0.007620	0.000000	0.012539	0.063203	0.038139	0.012927	0.040967	0.040225	0.000000
0.002540	0.012416	0.024594	0.099552	0.025621	0.012602	0.040431	0.000000	0.013534
0.000847	0.012285	0.012427	0.000000	0.012506	0.025523	0.000000	0.026929	0.013631
0.000000	2.593486	1.000366	0.025192	0.012347	0.025078	0.025723	0.026236	0.051606

Virus titration

( $\mu$ L)	VHL-13	258	1% DMSO			
50.000000	54.371760	52.803980	99.986760	99.960650	98.570850	97.845700
16.666670	25.395260	23.616100	99.973630	99.986890	85.687950	86.583250
5.555556	10.473060	9.314654	99.960520	99.961410	52.578800	51.539670
1.851852	3.149606	3.071672	99.922150	99.935950	21.843220	19.688080

0.617284	1.054067	0.939732	99.974090	99.923310	8.002645	7.604208
0.205761	0.406855	0.217252	99.960410	99.909770	2.570395	
0.068600	0.110619	0.063735	99.934620	99.948730	0.8826584	
0.022900	0.012217	0.051001	99.922090	99.974450	0.2710727	0.2155172
0.007620	0.024737	0.025013	99.987020	99.974240	0.1818654	0.1218357
0.002540	0.000000	0.012492	99.857810	99.897590	0.01306506	0.03994674
0.000847	0.024795	0.012762	99.921670	99.899300	0.0129199	0.05285412
0.000000	0.048420	0.012376	0.075940	0.050314	0.01287001	0.000000

## Graph 2.7.

Compound	PF74	PF74 Synth	PF74 Synth	CRBN-	CRBN-		
Concentration (µM)	Purchased	Natural	unnatural	O13	O22	VHL-4	VHL-13
100.000000	0.02470051	0.392638	0.01233502	1.169401	0.472879	0.597213	0.3959276
25.000000	0.01297017	0.02574665	0.02021427	3.935275	6.112665	0.01786352	0.3293988
6.250000	1.612903	1.670146	1.880431	11.777140	12.645400	1.763578	3.882263
1.562500	1.680564	1.767088	1.895793	14.892570	16.350090	15.532380	16.738890
0.390625	11.615390	10.830280	12.613940	17.649990	16.989510	17.441290	17.368290
0.09765625	15.796180	15.522640	16.346860	16.411330	16.213860	18.048370	17.367320
0.02441406	17.899910	15.507370	16.467210	17.132780	17.639780	16.214180	17.450070
0.00610352	17.541470	15.998100	15.480860	17.130090	17.449500	17.981070	17.888010
0.00152588	18.094270	15.739290	17.193240	16.324810	17.410320	17.317320	16.505960
0.00038147	17.184580	16.775060	17.442710	16.850800	17.138950	17.541690	17.115410
0.000095367	17.012240	15.971710	15.622710	17.336260	16.870140	16.944790	17.121930

## Graph 2.8.

Virus titration (µL)	PF74 Synthetic	Natural	CRBN-O13	CRBN-O22		
50.000000	24.386690	19.808090	23.139290	21.501750	22.814530	19.244980
16.666670	8.505532	8.247846	8.746006	8.360634	9.121932	8.347919
5.555556	2.811881	2.442586	3.107455	2.493862	2.701997	2.604167
1.851852	1.162319	1.053058	0.9793814	0.9137188	1.050720	0.8970909
0.617284	0.3533569	0.3697346	0.2719855	0.4049112	0.3249708	0.300575
0.205761	0.1178628	0.06636581	0.1049318	0.1428386	0.1545595	0.0524109

0.068600	0.0259538	0.01338867	0.0920205	0.000000	0.06539367	0.05310674
0.022900	0.02587992	0.01351534	0.05294507	0.06452446	0.02588327	0.02666667
0.007620	0.000000	0.0131406	0.01293326	0.01312164	0.03942699	0.02643055
0.002540	0.000000	0.01338509	0.01328551	0.01295505	0.000000	0.02642008
0.000847	0.02639915	0.000000	0.03869969	0.02577984	0.02586318	0.000000
0.000000	0.01313888	0.02671297	0.01281887	0.01270971	0.03834846	0.0129584

Virus titration ( $\mu\text{L}$ )	VHL-4		VHL-13	
50.000000	20.981550	17.337980	19.860360	16.704110
16.666670	8.282934	7.734960	6.745516	5.798817
5.555556	2.634366	2.366127	2.430953	2.058143
1.851852	1.028695	1.094939	0.664577	0.728218
0.617284	0.3626595	0.2311667	0.328823	0.230710
0.205761	0.1202084	0.1607932	0.062964	0.102749
0.068600	0.01319784	0.04014989	0.000000	0.063824
0.022900	0.02684204	0.02673439	0.025233	0.012887
0.007620	0.04005875	0.04076641	0.012845	0.000000
0.002540	0.01328727	0.000000	0.000000	0.000000
0.000847	0.000000	0.013611	0.012847	0.000000
0.000000	0.000000	0.000000	0.000000	0.000000

## Graph 2.9.

Compound Concentration ( $\mu\text{M}$ )	PF74 Purchased	PF74	PF74	CRBN-O13	CRBN-O22	VHL-4	VHL-13
		Natural	unnatural				
100.000000	0.249258	0.843631	0.109025	3.712153	1.713120	1.822079	0.978593
25.000000	3.634021	3.283540	2.527517	3.010610	3.100775	2.705362	1.567797
6.250000	3.625453	3.678708	3.643832	3.001464	3.522936	2.948217	3.452970
1.562500	3.562855	3.749836	3.266902	3.526570	3.604042	3.284487	2.982541
0.390625	3.547590	3.125400	3.342514	3.296970	3.191748	2.936139	3.504701
0.09765625	3.380246	2.997449	3.057714	3.355949	3.620731	3.456883	3.057992
0.02441406	3.299333	3.351016	3.488372	3.437949	3.366524	3.258359	3.429952

0.006103516	3.302064	3.093319	3.426752	3.241686	3.552376	3.621205	3.192386
0.001525879	3.820451	3.206465	3.380917	3.376998	2.821657	3.613861	3.587935
0.00038147	3.639798	3.533931	3.360615	3.482099	3.558548	3.001331	3.503109
0.0000953674	3.949708	3.281027	2.977978	3.179957	3.454523	3.390663	3.292978

**Graph 2.10.**

Virus titration (μL)	PF74 Synthetic Natural		CRBN-O13		CRBN-O22	
50.000000	41.130810	42.188150	98.197340	98.333550	98.530200	98.359990
16.666670	16.433070	16.374510	83.255000	82.864070	87.041040	83.007330
5.555556	5.958517	5.925731	46.978630	45.100620	52.849670	49.953510
1.851852	2.067151	1.992630	20.117320	19.286740	20.130040	21.324630
0.617284	0.770299	0.518962	6.945346	6.670154	8.019683	7.506988
0.205761	0.201334	0.092999	2.432575	2.418833	2.955021	2.508582
0.068600	0.062712	0.080917	0.826555	0.704501	0.894855	0.926672
0.022900	0.024759	0.013396	0.287507	0.273438	0.388450	0.253198
0.007620	0.037688	0.000000	0.040027	0.120401	0.091027	0.201830
0.002540	0.000000	0.000000	0.039257	0.039505	0.039411	0.026599
0.000847	0.000000	0.000000	0.012850	0.000000	0.026466	0.013224
0.000000	0.012137	0.000000	0.000000	0.012425	0.000000	0.000000

Virus titration (μL)	VHL-13		VHL-4		258	
50.000000	67.574600	69.167580	4.111798	5.786692	99.971590	99.916690
16.666670	36.342500	37.644220	1.324764	1.567703	99.971960	99.916500
5.555556	15.002640	15.441080	0.444270	0.526956	99.917630	99.918670
1.851852	5.510644	5.605232	0.209424	0.119095	99.891630	99.959280
0.617284	1.945786	1.615487	0.000000	0.054208	99.946160	99.919730
0.205761	0.656340	0.684472	0.026216	0.013435	99.946210	99.959810
0.068600	0.228035	0.308849	0.012987	0.013548	99.931890	99.973180
0.022900	0.093771	0.066702	0.000000	0.013630	99.932100	99.876860
0.007620	0.000000	0.053684	0.000000	0.000000	99.889140	99.850030
0.002540	0.026501	0.000000	0.013120	0.000000	99.918070	99.972360
0.000847	0.000000	0.013242	0.000000	0.000000	99.934050	99.919720

	0.000000	0.012601	0.000000	0.000000	0.000000	0.012893	0.000000
Virus titration (μL)	1% DMSO		No compound				
50.000000	98.838620	98.862700	99.109550	99.117730			
16.666670	92.222220	91.612460	91.574220	91.383010			
5.555556	59.500670	59.002500	60.163850	59.829830			
1.851852	25.966330	24.731480	27.878020	26.248070			
0.617284	9.869298	8.891929	10.005140	9.996085			
0.205761	3.148547	3.197832	3.404694	3.379696			
0.068600	1.252694	0.878141	1.189553	1.022257			
0.022900	0.493794	0.192228	0.474116	0.363967			
0.007620	0.146667	0.244731	0.128601	0.104275			
0.002540	0.053655	0.066881	0.013011	0.012980			
0.000847	0.081422	0.041197	0.025546	0.000000			
0.000000	0.038546	0.000000	0.012665	0.012658			

**Graph 2.11.**

Virus titration (μL)	PF74 Synthetic Natural		CRBN-O13		CRBN-O22	
50.000000	78.650220	77.864160	98.338110	98.420280	98.789570	98.493690
16.666670	46.978640	42.457300	82.293120	84.674740	85.507630	85.447460
5.555556	19.708830	19.337250	45.957590	47.167100	49.756990	47.499330
1.851852	7.615939	7.037918		18.980350	19.026320	19.485540
0.617284	2.427251	2.255846	6.785666	6.081794	7.010634	6.419098
0.205761	0.900651	0.872214	1.846722	1.973425	2.129617	2.470120
0.068600	0.292154	0.210556	0.870630	0.796033	0.756068	0.643259
0.022900	0.136073	0.056883	0.203611	0.157708	0.250924	0.216714
0.007620	0.013778	0.099263	0.067033	0.106895	0.157957	0.054742
0.002540	0.013691	0.041294	0.013497	0.040371	0.039604	0.040661
0.000847	0.027813	0.014112	0.040128	0.026354	0.013353	0.053727
0.000000	0.000000	0.013287	0.013130	0.000000	0.000000	0.013184

Virus titration (μL)	VHL-13		VHL-4		258	
50.000000	94.798630	94.260580	67.156730	65.348430	99.944660	99.932370

16.666670	71.082700	71.914130	37.048520	32.096160	99.904320	99.945290
5.555556	35.590230	37.237640	14.136260	14.447110	99.945760	99.932200
1.851852	14.138070	13.938980	5.478737	4.962105	99.958640	99.973150
0.617284	5.010776	5.029708	1.998422	1.457351	99.919080	99.946840
0.205761	1.502117	1.363884	0.640774	0.472779	99.959760	99.973610
0.068600	0.561413	0.422920	0.196850	0.131100	99.972690	99.973730
0.022900	0.041351	0.189779	0.039401	0.071644	99.932570	99.946200
0.007620	0.067322	0.095799	0.000000	0.014507	99.946020	99.946670
0.002540	0.040811	0.041448	0.013300	0.000000	99.958720	99.880050
0.000847	0.000000	0.000000	0.000000	0.000000	99.906300	99.904650
0.000000	0.000000	0.013108	0.000000	0.000000	0.051921	0.025381

Virus titration ( $\mu$ L)	1% DMSO		No compound	
50.000000	98.608840	98.905460	99.032260	98.465170
16.666670	86.124730	84.767300	89.612280	88.274680
5.555556	49.381720	48.906480	54.754720	53.209080
1.851852	20.634500	20.218650	23.780250	23.677130
0.617284	6.841687	7.845799	8.014595	8.500130
0.205761	2.484144	2.508711	3.238242	2.794463
0.068600	0.766486	0.831572	0.997223	0.899492
0.022900	0.300222	0.237298	0.380035	0.379747
0.007620	0.121196	0.100157	0.088889	0.088911
0.002540	0.000000	0.054735	0.025439	0.038221
0.000847	0.013240	0.000000	0.025631	0.012649
0.000000	0.000000	0.012816	0.013034	0.051447

## Graph 2.12.

E3 Ligase Ligand Conc ( $\mu$ M)	PF-74	PF-74 no Ligase control	CRBN-O13
267.000000	1.804577	1.675563	1.798466
66.750000	1.478035	1.779613	1.724599
16.687500	1.352068	1.690141	1.741486

4.171875	1.621115	1.640226	1.654629	1.645237	20.529450	20.176250
1.042969	1.660247	1.595816	1.714731	1.935309	19.949160	21.158220
0.260742	1.606856	1.577883	1.651400	1.670061	21.225970	20.408700
0.065186	1.476159	1.580710	1.963048	1.535930	19.866400	20.087390
0.016296	1.618165	1.628276	2.129570	1.720549	19.644750	20.357620
0.004074	1.620980	1.573427	1.724588	2.149230	20.391320	20.212770
0.001019	1.302845	1.416656	1.620126	2.121622	20.167060	20.194710
0.000255	1.686363	1.455722	1.865414	1.954928	19.915370	20.656600
0.000000	0.000000	0.000000	0.026171	0.013546	0.000000	0.026785
E3 Ligase Ligand Conc ( $\mu$ M)	CRBN-O13 no Ligase control		CRBN-O22		CRBN-O22 noLigase control	
267.000000	24.839900	23.652780	24.087810	24.134250	24.804290	25.452800
66.750000	24.253630	21.941750	22.219100	23.847130	24.053790	24.066910
16.687500	21.524780	21.799120	22.759260	23.806330	23.857530	24.257160
4.171875	21.966360	22.246340	21.789050	22.891570	22.826810	24.331370
1.042969	22.100920	21.247480	22.018350	22.378670	24.351050	24.353890
0.260742	21.245030	22.183780	21.866520	21.849190	23.282490	23.313640
0.065186	21.769510	22.139770	21.079010	22.482400	23.287110	23.912750
0.016296	22.720020	21.733240	21.648800	21.231850	23.681660	25.324140
0.004074	21.058270	22.237050	19.914750	22.183340	24.715490	24.030050
0.001019	21.736820	20.881200	21.542410	23.032110	23.762910	24.822600
0.000255	22.089590	22.314050	20.975940	22.619840	23.073750	24.446580
0.000000	0.013503	0.000000	0.013364	0.027289	0.054690	0.027111
E3 Ligase Ligand Conc ( $\mu$ M)	CRBN (Ligase control)		1% DMSO			
267.000000	28.247390	30.114770	28.943760	28.504990		
66.750000	30.110300	29.589630	28.473080	29.150360		
16.687500	29.336770	29.830050	28.813340	28.112980		
4.171875	28.930230	29.618850	27.283750	27.568890		
1.042969	29.277410	29.494840	27.181480	27.742540		
0.260742	28.544190	27.803420	27.111700	27.476130		

0.065186	29.440940	29.898310	29.173250	26.818680
0.016296	28.731240	29.541460	28.054540	28.745760
0.004074	28.720980	27.238250	27.963330	28.081080
0.001019	27.374080	29.361530	27.912490	29.534030
0.000255	29.299970	28.555830	28.375380	27.584810
0.000000	0.027972	0.043091	0.000000	0.000000

**Graph 2.13.**

E3 Ligase Ligand Conc ( $\mu$ M)	PF-74		PF-74 no Ligase control		VHL-13	
267.000000	1.555911	1.580565	1.798466	1.731844	4.513064	4.547564
66.750000	1.388316	1.149103	1.724599	1.810643	4.086171	4.267688
16.687500	1.664264	1.583387	1.741486	1.708117	3.720299	4.036476
4.171875	1.273223	1.333856	1.654629	1.645237	4.263932	4.388208
1.042969	1.439219	1.237525	1.714731	1.935309	4.291963	4.337284
0.260742	1.456058	1.451906	1.651400	1.670061	4.136617	4.735564
0.065186	1.041804	1.587302	1.963048	1.535930	4.233518	4.299320
0.016296	1.469072	1.240150	2.129570	1.720549	4.078894	4.346087
0.004074	1.254753	1.629591	1.724588	2.149230	4.099581	4.193416
0.001019	1.599688	1.181102	1.620126	2.121622	3.992447	4.188338
0.000255	1.144343	1.515745	1.865414	1.954928	3.654661	3.921042
0.000000	0.012389	0.000000	0.026171	0.013546	0.000000	0.000000

E3 Ligase Ligand Conc ( $\mu$ M)	VHL-13 no Ligase control		VHL-4		VHL-4 no Ligase control	
267.000000	4.680736	4.488458	0.287443	0.389864	0.359521	0.240487
66.750000	4.840484	4.267366	0.167131	0.305100	0.220036	0.323852
16.687500	4.249025	4.226508	0.230165	0.233132	0.177552	0.272814
4.171875	4.746709	4.850389	0.269578	0.275596	0.296698	0.312542
1.042969	4.443283	4.172367	0.145792	0.385781	0.283798	0.316151
0.260742	4.340921	5.130661	0.208932	0.409445	0.316122	0.162977
0.065186	4.431138	4.251817	0.157874	0.257383	0.179326	0.202867
0.016296	4.463475	3.925417	0.249737	0.248859	0.167375	0.221545

0.004074	4.135993	4.137931	0.227974	0.277228	0.208714	0.381731
0.001019	4.208844	5.183347	0.197550	0.217569	0.236624	0.365903
0.000255	4.441489	5.278155	0.253030	0.214736	0.197785	0.325777
0.000000	0.013033	0.000000	0.000000	0.013120	0.012628	0.000000

E3 Ligase Ligand Conc

( $\mu$ M)	VHL (Ligase control)		1% DMSO	
267.000000	27.276750	28.094870	28.943760	28.504990
66.750000	28.998150	30.143210	28.473080	29.150360
16.687500	28.564000	30.349230	28.813340	28.112980
4.171875	28.240980	30.038270	27.283750	27.568890
1.042969	26.966150	29.411000	27.181480	27.742540
0.260742	27.914190	27.556820	27.111700	27.476130
0.065186	27.332990	27.965320	29.173250	26.818680
0.016296	27.827080	28.198740	28.054540	28.745760
0.004074	26.086960	27.801050	27.963330	28.081080
0.001019	26.688670	28.322130	27.912490	29.534030
0.000255	27.238660	27.562200	28.375380	27.584810
0.000000	0.079872	0.013528	0.000000	0.000000